PHYTOCHEMICAL AND PHARMACOLOGICAL EVALUATION OF SOME SELECTED MEDICINAL PLANTS OF KERALA

THESIS SUBMITTED TO THE UNIVERSITY OF KERALA FOR THE AWARD OF THE

DEGREE OF DOCTOR OF PHILOSOPHY IN CHEMISTRY

UNDER THE FACULTY OF SCIENCE

By

PRABHA B

Under the guidance of

Dr. K. V. RADHAKRISHNAN

Organic Chemistry Section
Chemical Sciences and Technology Division
CSIR–National Institute for Interdisciplinary Science and Technology (NIIST)
Thiruvananthapuram-695 019, Kerala

2018

Dedicated to my beloved mother…

Declaration

I hereby declare that the Ph.D. thesis entitled "**Phytochemical and pharmacological evaluation of some selected medicinal plants of Kerala**" is an independent work carried out by me under the guidance of Dr. K. V. Radhakrishnan at the Organic Chemistry Section, Chemical Sciences and Technology Division, Council of Scientific and Industrial Research-National Institute for Interdisciplinary Science and Technology (CSIR-NIIST), Thiruvananthapuram and it has not been submitted anywhere else for any other degree or diploma.

Prabha B

Thiruvananthapuram

November, 2018

NATIONAL INSTITUTE FOR INTERDISCIPLINARY SCIENCE & TECHNOLOGY

Council of Scientific & Industrial Research

GOVERNMENT OF INDIA

Trivandrum-695 019, India

Dr. K. V. Radhakrishnan

Organic Chemistry Section

Chemical Sciences and Technology Division

Telephone: 91-471-2515420

Fax: 91-471-2491712

CERTIFICATE

This is to certify that the work embodied in the thesis entitled "***Phytochemical and pharmacological evaluation of some selected medicinal plants of Kerala***" has been carried out by **Mrs. Prabha B.** under my supervision and guidance at the Organic Chemistry Section of National Institute for Interdisciplinary Science and Technology (CSIR), Trivandrum and the same has not been submitted elsewhere for any other degree.

K. V. Radhakrishnan

(Thesis Supervisor)

Thiruvananthapuram

November, 2018

Email: ***radhu2005@gmail.com***

Acknowledgements

The work embodied in this thesis is the result of countless effort and help from a number of dedicated people, to whom I would like to express my profound acknowledgement.

With great happiness and respect, I would like express my deep sense of gratitude to my thesis supervisor ***Dr. K. V. Radhakrishnan*** *for introducing me to the attractive area of Natural products and also for his excellent guidance, parental care, constant encouragement, patience, constructive criticism and wholehearted help that led to the successful completion of this work.*

I am grateful to Dr. A. Ajayaghosh, Director, CSIR-NIIST and former Directors Dr. Suresh Das and Dr. Gangan Prathap for allowing me to avail the infrastructure facilities to carry out the research work.

I would like to acknowledge Dr. R. Luxmi Varma, APC coordinator at CSIR-NIIST for her timely help, care, support and advice for the academic procedures.

I am thankful to Dr. R. Luxmi Varma, Dr. K. R. Gopidas and Dr. D. Ramaiah, Present and Former Heads, Chemical Sciences and Technology Division for their help, support and inspiration throughout my Ph. D. period.

I am grateful to Dr. G. Vijay Nair, Emeritus Scientist, Organic Chemistry Section, for his inspiring presence and motivation.

I would like to acknowledge Dr. Mangalam S. Nair, Dr. Kaustabh Kumar Maiti, Dr. B. S. Sasidhar, Dr. L. Ravi Shankar and Dr. Sunil Varughese, Scientists of Organic Chemistry Section, for their encouragement and support.

I also wish to record my heartfelt thanks to Dr. Jubi John for his constant help, care, support and motivation and also extend my sincere thanks to Dr. Ganesh Chandra Nandi, for the encouragement and support.

With great happiness and respect, I am grateful to Dr. P Nisha and Dr. P. Jayamurthy, Agroprocessing and Technology Division, CSIR-NIIST, Thiruvananthapuram for biological studies; Dr. Anil Kumar and V. V. Sivan (MSSRF, Wayanad), Dr. Pradeep Kumar (University of Calicut) and Dr. K B Ramesh Kumar and Dr. Mathew Dan (JNTBRI, Palode) for collaboration in this area; Dr. T. K. Manojkumar, IIITM-K, Thiruvananthapuram for molecular simulation studies.

I am grateful to Dr. Sunil Varughese for single crystal-X ray analysis. Mrs. Saumini Mathew, Mr. Saran P. Raveendran, Mr. Syam and Mr. Rakesh Gokul are acknowledged

for recording NMR spectra. Thanks are also due to Mrs. S. Viji and Ms. S. Aathira for mass spectral analysis.

I would like to thank Dr. K. G. Raghu, Dr. Dileep Kumar B. S Scientists of Agroprocessing and Technology Division, for their help, encouragement and support.

All the biological and computational work reported here would have been virtually impossible without the help of Dr. Sini S. Ms. Lekhmi Krishnan M, Ms. Reshmita T. R (Biological work), Dr. Sherin D. R (molecular simulation studies) and I specially acknowledge them for constant support and valuable help rendered in conducting many of the experiments mentioned in the thesis.

I am grateful to Dr. P. S. Aparna for her emphatic help and great support during all stages of my doctoral studies. Also, stating special thanks to Mr. Madhukrishnan M for his help and support.

I am grateful to: My seniors- Dr. Praveen Prakash, Dr. E. Jiji, Dr. K. R. Ajish, Dr. T. V. Baiju, Dr. P. Preethanuj, Dr. S. Saranya, Dr. Ajesh Vijayan, Dr. M. Shimi, Dr. P. V. Santhini, Dr. R. J. Maya, Dr. Nayana Joseph, V. S. Suchithra and Dr. S. Anu Priya; and my colleagues- Mr. P. Sasikumar, Ms. Greeshma Gopalan, Ms. P. Sharathna, Ms. P. R. Nitha, Ms. K. T. Ashitha, Ms. S. Neethu, Ms. M. Aswathy, Ms. V. Jiitha, Mr. V. Praveen Kumar, Ms. Irfana Jesim, Mr. Vishnu K. Omanakkuttan, Ms. P. R. Rajimol, Mrs. Athira Krishna, Mrs. C. T. Fathimath Salfeena, Mr. K. K. Rajeev, Mr. K. Jayakrishnan, Ms. Remya Raj, Ms. P. Sreedevi, Ms. S. Santhi, and Mrs. Jyothi B. Nair, Ms. Alisha Valsan C; for their assistance, consideration, companionship and massive support.

I am thankful to Dr. Vandana Siva, Mrs. Sithara Thomas, Mr. Billu Abraham and all friends in Agroprocessing and Technology Division for their help, support and companionship.

I wish to thank Dr. C. R. Sinu, Dr. Rony Rajan Paul, Dr. K. Sajin Francis, Dr. S. R. Dhanya, Dr. K. C. Seetha Lakshmi, Mr. K. Jagadeesh, Ms. Mayadevi and all other present and former members of Organic Chemistry Section, for their friendship and creative inspirations. I am penning and remembering with lot of thanks some of our internship fellows, Ms. Ummu Jumaila C. P, Ms. Dibi Mol and Ms. Anjali N. J for their togetherness and intimacy.

I take this opportunity to sincerely thank all my teachers from St. Roch's Convent H. S (Thope), St. Mary's H. S .S (Vettucadu), All Saints College (TVM), Department of Chemistry, University of Kerala, Kariavattom, Kerala University Teacher Education Centre (Kariavattom) and to those at CSIR-NIIST (Thiruvananthapuram) who motivated

and blessed me throughout my academic carrier, and have helped me in becoming the person that I am today.

I am grateful to Council of Scientific and Industrial Research (CSIR) and Department of Science and Technology (DST) New Delhi, for the financial assistance.

For her unwavering strength and encouragement to pursue my dreams, I am profoundly grateful to my mother Mrs. Leela B. I am also obliged to my beloved brother Mr. Baburaj B, my husband Mr. Mirash George and all other family members (especially Mr. Joseph Sebastian, Mr. & Mrs. Lucy Nelson, Mr. & Mrs. Treasa Anson, Mr. Nigil Nelson and Mr. & Mrs. Esabel George) for their help, support, encouragement, unconditional love and care throughout my thesis work and my life. Without them, the successful completion of this thesis would have been practically impossible.

Above all, I thank the ***Almighty*** *for giving me the opportunity, strength, skills, and being with me throughout my life and giving all these people to help and encourage me, for the successful completion of the work.*

Prabha B

Contents

Pages

Declaration -1-

Certificate -2-

Acknowledgements -3-

Contents -4-

List of Tables -20-

List of Figures -23-

List of Abbreviations -45-

Preface -52-

Chapter 1 Plant Derived Natural Products: An Overview

1.1. Introduction 1

1.2. Historical outline of plant derived natural products 5

1.3. Antidiabetic drugs from plants 8

1.4. Anti-inflammatory drugs from plants 9

1.5. Cardiovascular drugs from plants 10

1.6. Biosynthetic pathway 11

1.6.1. Biosynthetic pathway of quassinoids 12

1.6.2. Biosynthetic pathway of triterpenoids 14

1.6.3. Biosynthetic pathway of resveratrol 14

1.6.4. Biosynthetic pathway of acylphenols 16

1.7. Outline and organisation of the thesis 16

Chapter 2A Isolation, Characterization and Antidiabetic Potential of Quassinoids from the Seeds of *Quassia indica* (Gaertn.) Noot.

2A.1.		Simaroubaceae	19
2A.2.		*Quassia* genus	20
	2A.2.1.	*Quassia africana*	20
	2A.2.2.	*Quassia amara*	21
	2A.2.3.	*Quassia undulate*	23
2A.3.		Aim and scope of the present investigation	23
2A.4.		Plant material collection, extraction, bioguided isolation and characterization of compounds from *Quassia indica* seed	26
	2A.4.1.	Plant material	26
	2A.4.2.	Extraction, bio guided isolation and characterization of compounds	26
2A.5.		Antidiabetic property of phytochemicals isolated from *Quassia indica*	67
	2A.5.1.	α-Amylase inhibitory activity	67
	2A.5.2.	α -Glucosidase inhibitory activity	67
	2A.5.3.	Antiglycation property	68
	2A.5.4.	Molecular simulation studies	69
	2A.5.5.	Pharmacophore modelling	74
	2A.5.6.	Glucose uptake in L6 myotubes	75
2A.6.		Conclusion	77

2A.7. Experimental 77

2A.7.1. General experimental procedures and chemicals 77

2A.7.2. Plant material collection and isolation of phytochemicals 78

2A.7.2.1. Isolation of compound **1** 79

2A.7.2.2. Isolation of compound **2** 80

2A.7.2.3. Isolation of compound **3** 81

2A.7.2.4. Isolation of compound **4** 82

2A.7.2.5. Isolation of compound **5** 83

2A.7.2.6. Isolation of compound **6** 84

2A.7.2.7. Isolation of compound **7** 85

2A.7.2.8. Isolation of compound **8** 86

2A.7.3. α -Amylase inhibitory activity 86

2A.7.4. α -Glucosidase inhibitiory activity 86

2A.7.5. Antiglycation property 87

2A.7.6. *In silico* studies 87

2A.7.7. Cell culture and treatment conditions 88

2A.7.8. Cell viability assay 88

2A.7.9. Glucose uptake assay 88

Chapter 2B Isolation, Characterization and Antidiabetic Potential of Phytochemicals from the Stem Bark of *Quassia indica*

2B.1. Extraction and extract level antidiabetic studies 89

2B.2. Activity oriented isolation and characterization of 89

phytochemicals

2B.3. *In vitro* and *in silico* studies of lupenone (9), 18α-olean-19α -ol-3-one (**12**), ferulic acid (**13**) and scopoletin (**14**) with carbohydrate digestive enzymes 100

2B.4. Antiglycation property 102

2B.5. Molecular docking studies 103

2B.6. Conclusion 107

2B.7. Experimental 107

2B.7.1. Collection of plant material, extraction, isolation and characterization of phytochemicals from the stem bark of *Quassia indica* 107

2B.7.1.1. Isolation of compound **9** 108

2B.7.1.2. Isolation of compound **10** and compound **11** 109

2B.7.1.3. Isolation of compound **12** 111

2B.7.1.4. Isolation of compound **13** 112

2B.7.1.5. Isolation of compound **14** 113

2B.7.1.6. Isolation of compound **15** 114

2B.7.1.7. Isolation of compound **16** and **17** 114

2B.7.1.8. Isolation of compound **18** 114

2B.7.1.9. Isolation of compound **19** 114

Chapter 3 Isolation, Characterization and Anti-inflammatory Activity of Phytochemicals from the Stem Bark of *Ailanthus excelsa* Roxb.

3.1.		*Ailanthus* genus	115
	3.1.1.	*Ailanthus altissima*	116
	3.1.2.	*Ailanthus triphysa*	120
3.2.		Aim and scope of the present investigation	120
3.3.		Extraction, isolation and characterization of compounds from *Ailanthus excelsa* stem bark	124
	3.3.1.	Plant material	124
	3.3.2.	Extraction, isolation and characterization of secondary metabolites	124
3.4.		Antiinflammatory activity of phytochemicals isolated from *Ailanthus excelsa*	143
	3.4.1.	Cytotoxic effects of compounds 1-3 on RAW 264.7 macrophages	144
	3.4.2.	NO production in LPS-stimulated RAW 264.7 macrophages	144
	3.4.3.	TNF-α, IL-6, LOX-1, COX-2 and IL10 production in LPS-stimulated RAW 264.7 cell lines	146
	3.4.4.	Compound 3 inhibited NF-κB expression in LPS-stimulated RAW 264.7 macrophages	147
3.5.		Conclusion	148
3.6.		Experimental	149
	3.6.1.	General experimental procedures and chemicals	149
	3.6.2.	Plant material, extraction and isolation procedure	149

3.6.2.1. Isolation of compound **22** 150

3.6.3. Cell culture and treatment conditions 151

3.6.4. Cytotoxicity assay 151

3.6.5. Determination of nitric oxide (NO) production 152

3.6.6. ELISA of TNF-α, IL-6, LOX-1, COX-2 and IL-10 152

Chapter 4A Isolation and characterization of phytochemicals from *Vatica chinensis* L. and their ameliorative effect on H_2O_2 induced oxidative stress in H9c2 cardiomyoblasts

4A.1. Dipterocarpaceae 153

4A.2. *Vatica* genus 153

4A.2.1. *Vatica affinis* 156

4A.2.2. *Vatica bantamensis* 157

4A.2.3. *Vatica cinerea* 158

4A.2.4. *Vatica diospyroides* 159

4A.2.5. *Vatica mangachapoi* 159

4A.2.6. *Vatica odorata* 162

4A.2.7. *Vatica pauciflora* 163

4A.2.8. *Vatica parvifolia* 165

4A.2.9. *Vatica rassak* 165

4A.2.10. *Vatica umbonata* 166

4A.3. Aim and scope of the present investigation 166

4A.4. Extraction, activity-oriented isolation and characterization of compounds 168

	4A.4.1.	Plant material	168
	4A.4.2.	Extraction and extract level antioxidant activity	168
	4A.4.3.	Activity-oriented isolation and characterization of compounds	169
4A.5.		Biosynthetic pathway of (-)-ε-viniferin, (-)-ampelopsin F and vaticaphenol A	201
4A.6.		Antioxidant activity of isolated phytochemicals	202
4A.7.		Cell viability	203
4A.8.		Intracellular ROS production	204
4A.9.		Effect on antioxidant enzyme system	205
4A.10.		Mitochondrial membrane potential ($\Delta\Psi m$) reduction	207
4A.11.		ATP level by HPLC analysis	208
4A.12.		Conclusion	208
4A.13.		Experimental section	210
	4A.13.1.	General experimental procedure	210
	4A.13.2.	Plant material	210
	4A.13.3.	Extraction and isolation	210
	4A.13.3.1.	Isolation of compound **27** and **28**	211
	4A.13.3.2.	Isolation of compound **29**	213
	4A.13.3.3.	Isolation of compound **30**	213
	4A.13.3.4.	Isolation of compound **31**	214
	4A.13.3.5.	Isolation of compound **32** and **33**	214

4A.13.4.	Chemicals and reagents	216
4A.13.5.	Evaluation of total phenolic content	216
4A.13.6.	DPPH radical scavenging activity	216
4A.13.7.	ABTS radical cation scavenging assay	217
4A.13.8.	Cell line and culture conditions	217
4A.13.9.	Cell viability assay	217
4A.13.10.	Intracellular reactive oxygen species (ROS) levels	218
4A.13.11.	Activities of antioxidant enzymes	218
4A.13.12.	Rhodamine 123 staining	219
4A.13.13.	Adenosine Triphosphate (ATP) production by HPLC analysis	219
4A.13.14.	Statistical analysis	219

Chapter 4B Antidiabetic Effects of Resveratrol Oligomers from the Stem Bark of *Vatica chinensis*

4B.1.	Introduction	221
4B.2.	Aim and scope of the present work	221
4B.3.	Extract level *in vitro* antidiabetic activity	222
4B.4.	α-Amylase inhibitory activity	223
4B.5.	α-Glucosidase inhibitory activity	224
4B.6.	Antiglycation property	224
4B.7.	Molecular simulation studies	225
4B.8.	2-NBDG uptake in L6 myoblasts	227

4B.9. Conclusion 229

4B.10. Experimental 229

Chapter 5A Isolation, Characterization and Antidiabetic Potential of Phytochemicals from the Stem Bark of *Hopea parviflora*

5A.1. *Hopea* Genus 231

5A.1.1. *Hopea exalata* 235

5A.1.2. *Hopea chinensis* 235

5A.1.3. *Hopea hainanensis* 237

5A.1.4. *Hopea malibato* 238

5A.2. Aim and scope of the present investigation 238

5A.3. Plant material collection, extraction, bio guided isolation and characterization of compounds from the stem bark of *Hopea parviflora* Bedd. 240

5A.3.1. Plant material 240

5A.3.2. Extraction, bio-guided isolation and characterization of secondary metabolites 241

5A.4. Biosynthetic pathway of (-) – hopeaphenol 262

5A.5. Antidiabetic property of phytochemicals isolated from *Hopea parviflora* 263

5A.5.1. α-Amylase inhibitory activity 264

5A.5.2. α-Glucosidase inhibitory activity 264

5A.5.3. Antiglycation property 264

5A.6. Molecular simulation studies 265

5A.7. Glucose uptake in L6 myotubes 268

5A.8. Conclusion 269

5A.9. Experimental 270

5A.9.1. General experimental procedures and chemicals 270

5A.9.2. Plant material and extraction 270

5A.9.2.1. Isolation of compound **34** 271

5A.9.2.2. Isolation of compound **35** 272

5A.9.2.3. Isolation of compound **36** 273

5A.9.2.4. Isolation of compound **37** 273

5A.9.2.5. Isolation of compound **38** 274

5A.9.2.6. Isolation of compound **39** 274

5A.9.2.7. Isolation of compound **40** 275

5A.9.2.8. Isolation of compound **41** 276

5A.9.2.9. Isolation of compound **42** 277

Chapter 5B **Anti-inflammatory Effects and Mechanisms of Action of Ellagic acid-3, 3', 4-trimethoxy 4'-*O*-*α*-L-rhamnopyranoside Isolated from *Hopea parviflora* Bedd. in Lipopolysaccharide-Stimulated RAW 264.7 Macrophages**

5B.1. Introduction 279

5B.2. Cytotoxic effects of compounds 1-5 in RAW 264.7 macrophages 280

5B.3. NO production in LPS-stimulated RAW 264.7 macrophages 281

5B.4.		TNF- α, IL-6, LOX-1, COX-2 and IL10 production in LPS-stimulated RAW 264.7 macrophages	282
5B.5.		Compound **5** inhibited NF-kB expression in LPS-stimulated RAW 264.7 cell lines	284
5B.6.		Conclusion	284
5B.7.		Experimental	285
	5B.7.1.	Cell culture and treatment conditions	285
	5B.7.2.	Cytotoxicity assay	285
5B.7.3.		Determination of nitric oxide (NO) production	285
	5B.7.4.	ELISA of TNF-α, IL 6, LOX-1 , COX-2 and IL-10	286
	5B.7.5.	Western blot for the expression of NF-κB in RAW cells	286

Chapter 6A Isolation, Characterization and Antidiabetic Potential of Phytochemicals from the Stem Bark of *Myristica fatua* Houtt.

6A.1.		Myristicaceae	287
6A.2.		*Myristica* Genus	288
6A.3.		*Myristica* species found in Kerala	292
	6A.3.1.	*Myristica fragrans* Houtt.	292
	6A.3.2.	*Myristica malabarica* Lam.	292
6A.4.		Aim and scope of the present investigation	294
6A.5.		Isolation and characterization of compounds from	296

Myristica fatua stem bark

6A.5.1. Plant material 296

6A.5.2. Isolation and characterization of secondary metabolites 296

6A.6. Biosynthetic pathway of malabaricones 311

6A.7. Antidiabetic property of phytochemicals isolated from *M. fatua* Houtt. 311

6A.7.1. α-Amylase inhibitory activity 312

6A.7.2. α -Glucosidase inhibitory activity 313

6A.7.3. Antiglycation property 314

6A.7.4. Molecular simulation studies 314

6A.7.5. Pharmacophore modelling 318

6A.7.6. Cytotoxicity in L6 cell line 318

6A.7.7. Glucose uptake in L6 myotubes 319

6A.8. Conclusion 320

6A.9. Experimental 321

6A.9.1. General experimental procedures and chemicals 321

6A.9.2. Plant material and isolation procedure 322

6A.9.2.1. Isolation of compound 43 323

6A.9.2.2. Isolation of compound 44 324

6A.9.2.3. Isolation of compound 45 324

6A.9.2.4. Isolation of compound 46 325

6A.9.2.5. Isolation of compound 47 326

6A.9.2.6. Isolation of compound 48 327

6A.9.2.7. Isolation of compound 49 328

6A.9.3. α -Amylase inhibitory activity 329

6A.9.4. α -Glucosidase inhibitiory activity 329

6A.9.5. Antiglycation property 330

6A.9.6. *In silico* studies 330

6A.9.7. Cell culture and treatment conditions 330

6A.9.8. Cytotoxicity assay 331

6A.9.9. Glucose uptake assay 331

6A.9.10. Statistical analysis 331

Chapter 6B Dactyloidin and Promalabaricone B from *Myristica fatua* Houtt. Seeds Exhibit Antidiabetic Effects via AMPK Pathway in L6 Myotubes

6B.1. Aim and scope of the present work 333

6B.2. Plant material collection, isolation and characterization of compounds from *Myristica fatua* Houtt. seeds 335

6B.2.1. Plant material 335

6B.2.2. Isolation and characterization of secondary metabolites 335

6B.3. Antidiabetic property of dactyloidin (**55**) and promalabaricone B (**56**) 344

6B.3.1. Effect on digestive enzymes 344

6B.3.2. Antiglycation property 344

	6B.3.3.	Molecular simulation studies	345
	6B.3.4.	Cell toxicity	348
	6B.3.5.	2-NBDG uptake	348
	6B.3.6.	GLUT4 translocation	349
	6B.3.7.	AMPK signalling	350
6B.4.		Conclusion	351
6B.5.		Experimental	352
	6B.5.1.	General experimental procedures and chemicals used	352
	6B.5.2.	Plant material	352
	6B.5.3.	Extraction, isolation and characterization of secondary metabolites	352
	6B.5.3.1.	Isolation of compound **55**	353
	6B.5.3.2.	Isolation of compound **56**	354
	6B.5.4.	α -Amylase inhibitory activity, α -glucosidase inhibitiory activity, antiglycation property, *In silico* studies, cell culture and treatment conditions, cytotoxicity assay and fluorescence analysis of 2-NBDG uptake by flow cytometry	356
	6B.5.5.	Western blot for the expression of AMPK and GLUT4 in L6 myotubes	356
	6B.5.6.	Statistical analysis	356
Summary and conclusions			357
Bibliography and references			367
List of Publications			387

List of Tables *Pages*

Table 1.1.	FDA approved plant derived drugs launched during 2005-2015	6
Table 2A.1.	Different genus of Simaroubaceae family	19
Table 2A.2.	*Quassia* species and their distribution	20
Table 2A.3	Scientific classification of *Quassia indica*	24
Table 2A.4.	Extract level *in vitro* antidiabetic studies of the seeds of *Quassia indica*	26
Table 2A.5.	^{1}H (500 MHz) and ^{13}C (125 MHz) NMR data of compound **6** in Acetone-d_6	53
Table 2A.6.	^{1}H (500 MHz) and ^{13}C (125 MHz) NMR data of compound **8** in Acetone-d_6	66
Table 2A.7.	Porcine pancreatic α-amylase inhibitory activity and *Saccharomyces cervease* α-glucosidase inhibitory activity and antiglycation property of quassinoids isolated from *Quassia indica*	68
Table 2A.8.	ADME/T properties of compound **1-8**	69
Table 2A.9.	G-Score/D-Score of isolated compounds with human pancreatic α-amylase (**3A4A**) and human maltase glucoamylase (*N*- terminal, **2QMJ**; *C*- terminal, **3TOP**)	73
Table 2B. 1.	Extract level *in vitro* antidiabetic activity of the stem bark of *Quassia indica*	90
Table 2B.2.	Inhibitory activities of α-amylase enzyme, α-glucosidase enzyme and protein glycation property of compounds isolated from the stem bark of *Quassia indica*	102
Table 2B.3.	G-/D-score of isolated compounds with porcine pancreatic α-amylase (**3AJ7**) and isomaltase from *Saccharomyces cerevisiae* (**3A4A**)	102

Table 2B.4.	ADME/T properties of compound	103
Table 2B. 5.	G-Score/D-Score of isolated compounds with human pancreatic α-amylase (**4GQQ**) and human maltase glucoamylase (*N*- terminal, **2QMJ**; *C*- terminal, **3TOP**)	104
Table. 3.1.	*Ailanthus* species and their distribution	115
Table 3.2.	Scientific classification of *Ailanthus excelsa* Roxb.	121
Table 3.3.	^{1}H (500 MHz) and ^{13}C (125 MHz) NMR data of compound **23** in $CDCl_3$	135
Table 3.4.	^{1}H (500 MHz) and ^{13}C (125 MHz) NMR data of compound **24** in $CDCl_3$	142
Table 4A.1.	Different genus of Dipterocarpaceae family	154
Table 4A.2.	*Vatica* species and their distribution	154
Table 4A.3.	Scientific classification of *Vatica chinensis*	167
Table 4A.4.	TPC and DPPH radical scavenging activity of different extracts	168
Table 4A.5.	The 1D and 2D NMR spectra of vaticanol R (Acetone-d_6)	175
Table 4A.6.	The ^{1}H and^{13}C NMR data of vaticaphenol A (Acetone-d_6)	187
Table 4A.7.	Antioxidant activities of isolated compounds (**27-33**)	188
Table 4B.1.	Extract level antidiabetic activity of the stem bark of *Vatica chinensis*	223
Table 4B.2	Molecular level antidiabetic activity of compound **27-33**	224
Table 4B.3.	ADME/T properties of compound **27-33**	226
Table 4B.4.	G-score/D-score of isolated compounds with human pancreatic α-amylase (**4GQQ**) and human maltase glucoamylase (*N*-terminal, **2QMJ**; *C*- terminal, **3TOP**)	227
Table 5A.1.	*Hopea* species and their distribution	231

Table 5A.2.	Scientific classification of *Hopea parviflora*	239
Table 5A.3.	Extract level *in vitro* antidiabetic activity of *Hopea parviflora*	241
Table 5A.4.	^{1}H and ^{13}C NMR spectra of (-)-hopeaphenol in Acetone $-d_6$	254
Table 5A.5.	α-Amylase, α-glucosidase and protein glycation inhibitory activities of compounds isolated from *Hopea parviflora*	265
Table 5A.6.	ADME/T properties of compounds	266
Table 5A.7.	G-Score/D-Score of isolated compounds with human pancreatic α-amylase (**4GQQ**) and human maltase glucoamylase (*N*- terminal, **2QMJ**; *C*- terminal, **3TOP**)	267
Table. 6A.1.	Different genus of Myristicaeceae family	287
Table.6A.2	*Myristica* species and their distribution	288
Table 6A.3.	Scientific classification of *Myristica fatua*	295
Table 6A.4.	Porcein pancreatic α-amylase inhibitory activity, rat intestinal α-glucosidase inhibitory activity and antiglycation property of compounds isolated from *Myristica fatua*	313
Table 6A.5.	ADME/T properties of compound**s**	315
Table 6A.6.	G-Score/D-Score of isolated compounds with human pancreatic α-amylase (**4GQQ**) and human maltase glucoamylase (*N*- terminal, **2QMJ**; *C*- terminal, **3TOP**)	316
Table 6B.1.	ADME/T properties of compound **55** and **56**	345

List of Figures *Pages*

Figure 1.1.	Traditionally important medicinal plants and structure of the derived drugs	2
Figure 1.2.	Microbial derived drugs	3
Figure 1.3.	Marine derived natural products	4
Figure 1.4.	Animal derived natural products	4
Figure 1.5.	(B) Biological macromolecule, (N) Unaltered natural product, (NB) Botanical drug (defined mixture), (ND) Natural product derivative, (S) Synthetic drug, (S*) Synthetic drug (NP pharmacophore), (V) Vaccine, (S/NM) Mimic of natural product	6
Figure 1.6.	Structures of FDA approved plant drugs launched during 2005-2015	7
Figure 1.7.	Plant derived antidiabetic drugs	9
Figure 1.8.	Plant derived anti-inflammatory compounds	10
Figure 1.9.	Plant derived cardiovascular drugs	11
Figure 1.10.	Biosynthetic pathways and precursors for the major classes of secondary metabolites	12
Figure 1.11.	Different types of quassinoids	13
Figure 1.12.	Biosynthetic pathway of quassinoids	13
Figure 1.13.	Biosynthetic pathway of triterpenoids	14
Figure 1.14.	Biosynthetic pathway of resveratrol	15
Figure 1.15.	Modifications of resveratrol	15
Figure 1.16.	Biosynthetic pathway of acylphenols	16

Figure 2A.1.	Compounds isolated from *Quassia africana*	21
Figure 2A.2.	Compounds isolated from *Quassia amara*	22
Figure 2A.3.	Compounds isolated from *Quassia undulate*	23
Figure 2A.4.	*Quassia indica (*Gaertn.*)* Nooteboom	24
Figure 2A.5.	Compounds isolated from *Quassia indica*	25
Figure 2A.6.	^{1}H NMR spectrum (500 MHz, $CDCl_3$) of samaderin A (**1**)	28
Figure 2A.7.	^{13}C NMR spectrum (125 MHz, $CDCl_3$)of samaderin A (**1**)	28
Figure 2A.8.	^{1}H-^{1}H COSY NMR spectrum (500 MHz, $CDCl_3$) of samaderin A (**1**)	29
Figure 2A.9.	HMQC NMR spectrum (500 MHz, $CDCl_3$) of samaderin A (**1**)	29
Figure 2A.10.	HMBC spectrum (500 MHz, $CDCl_3$) of samaderin A (**1**)	30
Figure 2A.11.	DEPT 135 spectrum (500 MHz, $CDCl_3$) of samaderin A (**1**)	30
Figure 2A.12.	Single crystal X-ray analysis of samaderin A (**1**)	31
Figure 2A.13.	^{1}H NMR spectrum (500 MHz, DMSO-d_6) of samaderin B (**2**)	32
Figure 2A.14.	^{13}C NMR spectrum (125 MHz, DMSO-d_6) of samaderin B (**2**)	33
Figure 2A.15.	^{1}H-^{1}H COSY NMR spectrum (500 MHz, DMSO-d_6) of samaderin B (**2**)	33
Figure 2A.16.	HMQC NMR spectrum (500 MHz, DMSO-d_6) of samaderin B (**2**)	34

Figure 2A.17.	DEPT 135 spectrum (500 MHz, DMSO-d_6) of samaderin B (**2**)	34
Figure 2A.18.	Single crystal X-ray analysis of samaderin B (**2**)	35
Figure 2A.19.	^{1}H NMR spectrum (500 MHz, $CDCl_3$) of dihydrosamaderin B (**3**)	36
Figure 2A.20.	^{13}C NMR spectrum (125 MHz, $CDCl_3$) of dihydrosamaderin B (**3**)	37
Figure 2A.21.	^{1}H-^{1}H COSY NMR spectrum (500 MHz, $CDCl_3$) of dihydrosamaderin B (**3**)	37
Figure 2A.22.	HMQC NMR spectrum (500 MHz, $CDCl_3$) of dihydrosamaderin B (**3**)	38
Figure 2A.23.	HMBC spectrum (500 MHz, $CDCl_3$) of dihydrosamaderin B (**3**)	38
Figure 2A.24.	DEPT 135 spectrum (500 MHz, $CDCl_3$) of dihydrosamaderin B (**3**)	39
Figure 2A.25.	NOESY spectrum (500 MHz, $CDCl_3$) of dihydrosamaderin B (**3**)	39
Figure 2A.26.	Single crystal X-ray analysis of dihydrosamaderin B (**3**)	40
Figure 2A.27.	^{1}H NMR spectrum (500 MHz, DMSO-d_6) of samaderin C (**4**)	41
Figure 2A.28.	^{13}C NMR spectrum (500 MHz, DMSO-d_6) of samaderin C (**4**)	42
Figure 2A.29.	^{1}H-^{1}H COSY NMR spectrum (500 MHz, DMSO-d_6) of samaderin C (**4**)	42
Figure 2A.30.	HMQC NMR spectrum (500 MHz, DMSO-d_6) of samaderin C (**4**)	43

Figure 2A.31.	HMBC spectrum (500 MHz, DMSO-d_6) of samaderin C (**4**)	43
Figure 2A.32.	Single crystal X-ray analysis of samaderin C (**4**)	44
Figure 2A.33.	^{1}H NMR spectrum (500 MHz, DMSO-d_6) of cedronin (**5**)	45
Figure 2A.34.	^{13}C NMR spectrum (125 MHz, DMSO-d_6) of cedronin (**5**)	46
Figure 2A.35.	^{1}H-^{1}H COSY NMR spectrum (500 MHz, DMSO-d_6) of cedronin (**5**)	46
Figure 2A.36.	HMQC NMR spectrum (500 MHz, DMSO-d_6) of cedronin (**5**)	47
Figure 2A.37.	HMBC NMR spectrum (125 MHz, DMSO-d_6) of cedronin (**5**)	47
Figure 2A.38.	Single crystal X-ray analysis of cedronin (**5**)	48
Figure 2A.39.	^{1}H NMR spectrum (500 MHz, DMSO-d_6) of novel compound (**6**)	49
Figure 2A.40.	^{13}C NMR spectrum (125 MHz, DMSO-d_6) of novel compound (**6**)	50
Figure 2A.41.	^{1}H-^{1}H COSY NMR spectrum (500 MHz, DMSO-d_6) of novel compound (**6**)	50
Figure 2A.42.	HMQC NMR spectrum (500 MHz, DMSO-d_6) of novel compound (**6**)	51
Figure 2A.43.	HMBC spectrum (500 MHz, DMSO-d_6) of novel compound (**6**)	51
Figure 2A.44.	DEPT 135 spectrum (500 MHz, DMSO-d_6) of novel compound (**6**)	52
Figure 2A.45.	NOESY spectrum (500 MHz, DMSO-d_6) of novel	52

compound (**6**)

Figure 2A.46. HRESIMS spectrum of novel compound (**6**) 53

Figure 2A.47. The key HMBC and NOESY correlations of novel compound **(6)** 54

Figure 2A.48. Single crystal X-ray analysis of novel compound (**6**) 55

Figure 2A.49. ^{1}H NMR spectrum (500 MHz, DMSO-d_6) of brucein D (**7**) 56

Figure 2A.50. ^{13}C NMR spectrum (125 MHz, DMSO-d_6) of brucein D (**7**) 57

Figure 2A.51. ^{1}H-^{1}H COSY NMR spectrum (500 MHz, DMSO-d_6) of brucein D (**7**) 57

Figure 2A.52. HMQC NMR spectrum (500 MHz, DMSO-d_6) of brucein D (**7**) 58

Figure 2A.53. HMBC spectrum (500 MHz, DMSO-d_6) of brucein D (**7**) 58

Figure 2A.54. DEPT 135 spectrum (500 MHz, DMSO-d_6) of brucein D (**7**) 59

Figure 2A.55. NOESY spectrum (500 MHz, DMSO-d_6) of brucein D (**7**) 59

Figure 2A.56. ^{1}H NMR spectrum (500 MHz, DMSO-d_6) of novel compound (**8**) 61

Figure 2A.57. ^{13}C NMR spectrum (125 MHz, DMSO-d_6) of novel compound (**8**) 62

Figure 2A.58. ^{1}H-^{1}H COSY NMR spectrum (500 MHz, DMSO-d_6) of novel compound (**8**) 62

Figure 2A.59. HMQC NMR spectrum (500 MHz, DMSO-d_6) of novel compound (**8**) 63

Figure 2A.60.	HMBC spectrum (500 MHz, DMSO-d_6) of novel compound (**8**)	63
Figure 2A.61.	DEPT 135 spectrum (500 MHz, DMSO-d_6) of novel compound (**8**)	64
Figure 2A.62.	NOESY spectrum (500 MHz, DMSO-d_6) of novel compound (**8**)	64
Figure 2A.63.	HRESIMS spectrum of novel compound (**8**)	65
Figure 2A.64.	The key HMBC and NOESY correlations of novel compound (**8**)	65
Figure 2A.65.	2D interaction diagram of cedronin (**5**), novel compound (**6**), brucein D (**7**) and novel compound (**8**) with the protein **3A4A**	71
Figure 2A.66.	2D interaction diagram of novel compound (**6**) and novel compound (**8**) with the protein **4GQQ**	72
Figure 2A.67.	2D interaction diagram of novel compound (**8**) with the protein **2QMJ**	74
Figure 2A.68.	Pharmacophore model generated for quassinoids	75
Figure 2A.69.	Cytotoxicity in L6 cell lines (**1-8**)	76
Figure 2A.70.	2-NBDG uptake in differentiated L6 myotubes	76
Figure 2A.71.	Schematic representation of isolation of quassinoids from the stem bark of *Quassia indica*	78
Figure 2B.1.	^{1}H NMR spectrum (500 MHz, $CDCl_3$) of lupenone (**9**)	91
Figure 2B.2.	^{13}C NMR spectrum (125 MHz, $CDCl_3$) of lupenone (**9**)	91
Figure 2B.3.	Structure of β-sitosterol (**10**) and stigmasterol (**11**)	92
Figure 2B.4.	^{1}H NMR spectrum (500 MHz, $CDCl_3$) of 18α-olean-19α -	93

	ol-3-one (**12**)	
Figure 2B.5.	^{13}C NMR spectrum (125 MHz, $CDCl_3$) of 18*α*-olean-19*α* -ol-3-one (**12**)	93
Figure 2B.6.	^{1}H-^{1}H COSY NMR spectrum (500 MHz, $CDCl_3$) of 18*α*-olean-19*α* -ol-3-one (**12**)	94
Figure 2B.7.	HMQC NMR spectrum (125 MHz, $CDCl_3$) of 18*α*-olean-19*α*-ol-3-one (**12**)	94
Figure 2B.8.	HMBC spectrum (125 MHz, $CDCl_3$) of 18*α*-olean-19*α*-ol-3-one (**12**)	95
Figure 2B.9.	DEPT 135 spectrum (125 MHz, CDCl3) of 18α-olean-19α-ol-3-one (12)	95
Figure 2B.10.	NOESY spectrum (500 MHz, $CDCl_3$) of 18*α*-olean-19*α*-ol-3-one (**12**)	96
Figure 2B.11.	Single crystal X-ray analysis of 18*α*-olean-19*α*-ol-3-one (**12**)	96
Figure 2B.12.	^{1}H NMR spectrum (500 MHz, $CDCl_3$) of ferulic acid (**13**)	97
Figure 2B.13.	^{13}C NMR spectrum (125 MHz, $CDCl_3$) of ferulic acid (**13**)	98
Figure 2B.14.	^{1}H NMR spectrum (500 MHz, $CDCl_3$) of scopoletin (**14**)	99
Figure 2B.15.	^{13}C NMR spectrum (125 MHz, $CDCl_3$) of scopoletin (**14**)	99
Figure 2B.16.	Structures of compound **15-19**	100
Figure 2B.17.	2D interaction diagram of ferulic acid and scopoletin with (A & B) **3AJ7** and (C & D) **3A4A**	105
Figure 2B.18.	2D interaction diagram of ferulic acid and scopoletin with (A & B) **4GQQ;** (C & D) **2QMJ** and (E & F) **3TOP**	106

Figure 2B.19.	The schematic representation of the extraction and isolation of phytochemicals from the stem bark of *Quassia indica.*	108
Figure 3.1.	Compounds isolated from *Ailanthus altissima*	120
Figure 3.2.	Compounds isolated from from *Ailanthus triphysa*	121
Figure 3.3.	*Ailanthus excelsa* -Tree, flower and leaves	122
Figure 3.4.	Compounds isolated from *Ailanthus excelsa*	123
Figure 3.5.	Structure of *β*-sitosterol and stigmasterol	124
Figure 3.6.	^{1}H NMR spectrum (500 MHz, $CDCl_3$) of ocotillone (**22**)	125
Figure 3.7.	^{13}C NMR spectrum (125 MHz, $CDCl_3$) of ocotillone (**22**)	126
Figure 3.8.	^{1}H-^{1}H COSY NMR spectrum (500 MHz, CDCl3) of ocotillone (**22**)	126
Figure 3.9.	HMQC NMR spectrum (125 MHz, CDCl3) of ocotillone (**22**)	127
Figure 3.10.	HMBC spectrum (125 MHz, $CDCl_3$) of ocotillone (**22**)	127
Figure 3.11.	DEPT 135 spectrum (125 MHz, $CDCl_3$) of ocotillone (**22**)	128
Figure 3.12.	^{1}H NMR spectrum (500 MHz, $CDCl_3$) of novel compound (**23**)	130
Figure 3.13.	^{13}C NMR spectrum (125 MHz, $CDCl_3$) of novel compound (**23**)	130
Figure 3.14.	^{1}H-^{1}H COSY NMR spectrum (500 MHz, $CDCl_3$) of novel compound (**23**)	131
Figure 3.15.	HMQC NMR spectrum (125 MHz, $CDCl_3$) of novel compound (**23**)	131

Figure 3.16.	HMBC NMR spectrum (125 MHz, $CDCl_3$) of novel compound (**23**)	132
Figure 3.17.	NOESY spectrum (500 MHz, $CDCl_3$) of novel compound (**23**)	132
Figure 3.18.	DEPT 135 spectrum (125 MHz, $CDCl_3$) of novel compound (**23**)	133
Figure 3.19.	HRESIMS spectrum of novel compound (**23**)	133
Figure 3.20.	Single crystal X-ray analysis of novel compound (**23**)	134
Figure 3.21.	The key HMBC and NOESY correlations of novel compound (**23**)	134
Figure 3.22.	^{1}H NMR spectrum (500 MHz, $CDCl_3$) of novel compound (**24**)	137
Figure 3.23.	^{13}C NMR spectrum (125 MHz, $CDCl_3$) of novel compound (**24**)	138
Figure 3.24.	^{1}H-^{1}H COSY NMR spectrum (500 MHz, $CDCl_3$) of novel compound (**24)**	138
Figure 3.25.	HMQC NMR spectrum (125 MHz, $CDCl_3$) of novel compound (**24**)	139
Figure 3.26.	HMBC spectrum (125 MHz, $CDCl_3$) of novel compound (**24**)	139
Figure 3.27.	NOESY spectrum (500 MHz, $CDCl_3$) of novel compound (**24**)	140
Figure 3.28.	DEPT 135 spectrum (125 MHz, CDCl3) of novel compound (**24**)	140
Figure 3.29.	HRESIMS spectrum of novel compound (**24**)	141
Figure 3.30.	Single crystal X-ray analysis of novel compound (**23**)	141

Figure 3. 31.	The compounds chosen for anti-inflammatory study	144
Figure 3. 32.	The compounds chosen for anti-inflammatory study	144
Figure 3.33.	Effect of 2.5 μM and 10 μM concentrations of compound **3** on NO production in LPS-stimulated RAW 264.7 cell lines.	145
Figure 3.34.	Effect of 2.5 μM and 10 μM concentrations of compound **3** on TNF-α, IL-6, LOX-1, COX-2 and IL10 production in LPS-stimulated RAW 264.7 cell lines	147
Figure 3.35.	Expression level of 2.5 μM and 10 μM concentrations of compound **3** on NF-κB production	148
Figure 3.36.	The schematic representation of extraction and isolation procedure of stem bark of *Ailanthus excelsa*	150
Figure 4A.1.	The structures of some of the compounds isolated from *Vatica affinis*	156
Figure 4A.2.	The structures of the compounds isolated from *Vatica bantamensis*	157
Figure 4A.3.	The structures of the compounds isolated from *Vatica cinerea*	158
Figure 4A.4.	The structures of the compounds isolated from *Vatica diospyroides*	159
Figure 4A.5.	The structures of the compounds isolated from *Vatica mangachapoi*	162
Figure 4A.6.	The structures of the compounds isolated from *Vatica odorata*	162
Figure 4A.7.	The structures of the compounds isolated from *Vatica pauciflora*	164

Figure 4A.8.	The structure of vatiparol isolated from *Vatica parvifolia*	165
Figure 4A.9.	The structure of vaticanol D isolated from *Vatica rassak*	165
Figure 4A.10.	*Vatica chinensis* L.	166
Figure 4A.11.	Compounds previously isolated from *Vatica chinensis*	167
Figure 4A.12.	^{1}H NMR spectrum (500 MHz, Acetone-d_6) of (-) - ε-viniferin (**27**)	170
Figure 4A.13.	^{13}C NMR spectrum (125 MHz, Acetone-d_6) of (-) - ε-viniferin (**27**)	170
Figure 4A.14.	^{1}H NMR spectrum (500 MHz, Acetone-d_6) of (-) - ampelopsin F (**28**)	172
Figure 4A.15.	^{13}C NMR spectrum (500 MHz, Acetone-d_6) of (-) - ampelopsin F (**28**)	172
Figure 4A.16.	Structure and key HMBC correlations of vaticanol R (**29**)	174
Figure 4A.17.	^{1}H NMR spectrum (500 MHz, Acetone-d_6) of vaticanol R (**29**)	177
Figure 4A.18.	^{13}C NMR spectrum (125 MHz, Acetone-d_6) of vaticanol R (**29**)	177
Figure 4A.19.	DQF COSY NMR spectrum (500 MHz, Acetone-d_6) of vaticanol R (**29**)	178
Figure 4A.20.	HMQC NMR spectrum (125 MHz, Acetone-d_6) of vaticanol R (**29)**	178
Figure 4A.21.	HMBC NMR spectrum (125 MHz, Acetone-d_6) of vaticanol R (**3**)	179
Figure 4A.22.	DEPT 135 NMR spectrum (125 MHz, Acetone-d_6) of vaticanol R (**3**)	179

Figure 4A.23.	NOESY spectrum (500 MHz, Acetone-d_6) of vaticanol R (**3**)	180
Figure 4A.24.	HRESIMS spectrum of vaticanol R (**29**)	180
Figure 4A.25.	CD spectrum of vaticanol R (**blue**) and (-)- ampelopsin F (**Orange**)	181
Figure 4A.26.	^{1}H NMR spectrum (500 MHz, Acetone-d_6) of vaticaphenol A (**30**)	183
Figure 4A.27.	^{13}C NMR spectrum (125 MHz, Acetone-d_6) of vaticaphenol A (**30**)	183
Figure 4A.28.	^{1}H-^{1}H COSY NMR spectrum (500 MHz, Acetone-d_6) of vaticaphenol A (**30**)	184
Figure 4A.29.	HMQC NMR spectrum (125 MHz, Acetone-d_6) of vaticaphenol A (**30**)	184
Figure 4A.30.	HMBC NMR spectrum (125 MHz, Acetone-d_6) of vaticaphenol A (**30**)	185
Figure 4A.31.	NOESY NMR spectrum (500 MHz, Acetone-d_6) of vaticaphenol A (**30**)	185
Figure 4A.32.	DEPT 135 NMR spectrum (125 MHz, Acetone-d_6) of vaticaphenol A (**30**)	186
Figure 4A.33.	Key ^{1}H-^{1}H COSY, HMBC and NOESY correlations of vaticaphenol A (**30**)	186
Figure 4A.34.	^{1}H NMR spectrum (500 MHz, Acetone-d_6) of vaticanol M (**31**)	189
Figure 4A.35.	^{13}C NMR spectrum (125 MHz, Acetone-d_6) of vaticanol M (**31**)	190
Figure 4A.36.	^{1}H-^{1}H COSY NMR spectrum (500 MHz, Acetone-d_6) of	190

vaticanol M (**31**)

Figure 4A.37. HMQC NMR spectrum (125 MHz, Acetone-d_6) of vaticanol M (**31**) 191

Figure 4A.38. HMBC NMR spectrum (125 MHz, Acetone-d_6) of vaticanol M (**31**) 191

Figure 4A.39. DEPT 135 spectrum (125 MHz, Acetone-d_6) of vaticanol M (**31**) 192

Figure 4A.40. NOESY NMR spectrum (500 MHz, Acetone-d_6) of vaticanol M (**31**) 192

Figure 4A.41. ^{1}H NMR spectrum (500 MHz, DMSO-d_6) of bergenin (**32**) 194

Figure 4A.42. ^{13}C NMR spectrum (125 MHz, DMSO-d_6) of bergenin (**32**) 194

Figure 4A.43. ^{1}H-^{1}H NMR spectrum (500 MHz, DMSO-d_6) of bergenin (**32**) 195

Figure 4A.44. HMQC NMR spectrum (125 MHz, DMSO-d_6) of bergenin (**32**) 195

Figure 4A.45. HMBC NMR spectrum (125 MHz, DMSO-d_6) of bergenin (**32**) 196

Figure 4A.46. DEPT 135 NMR spectrum (125 MHz, DMSO-d_6) of bergenin (**32**) 196

Figure 4A.47. ^{1}H NMR spectrum (500 MHz, DMSO-d_6) of methoxybergenin (**33**) 197

Figure 4A.48. ^{13}C NMR spectrum (125 MHz, DMSO-d_6) of methoxybergenin (**33**) 198

Figure 4A.49. ^{1}H-^{1}H COSY NMR spectrum (500 MHz, DMSO-d_6) of 198

	methoxybergenin (**33**)	
Figure 4A.50.	HMQC NMR spectrum (125 MHz, DMSO-d_6) of methoxybergenin (**33**)	199
Figure 4A.51.	HMBC NMR spectrum (125 MHz, DMSO-d_6) of methoxybergenin (**33**)	199
Figure 4A.52.	DEPT 135 NMR spectrum (125 MHz, DMSO-d_6) of methoxybergenin (**33**)	200
Figure 4A.53.	NOESY NMR spectrum (500 MHz, DMSO-d_6) of methoxybergenin (**33**)	200
Figure 4A.54.	Biosynthetic pathway of (-)-ε-viniferin and (-)-ampelopsin F	201
Figure 4A.55.	Biosynthetic pathway of vaticaphenol A	201
Figure 4A.56.	The effect of compounds **(27-33)**), H_2O_2 and 100 μM H_2O_2 pretreatment of cells with compounds (**27-33**), on H9c2 cell viability by MTT assay.	204
Figure 4A.57.	Measurement of ROS production in H9c2 cells were analysed by DCFH-DA dye.	206
Figure 4A.58.	Effect of compound, **27-33** on SOD and CAT activity in H9c2 cells treated with 100 μM H_2O_2.	207
Figure 4A.59.	Quantification of Mitochondrial membrane potential by Rhodamine 123 staining and ATP level by staining method.	209
Figure 4A.60.	Schematic representation of the isolation procedure of the acetone extract of the stem bark of *Vatica chinensis*	211
Figure 4B.1.	Structures of the compounds for antidiabetic studies	222
Figure 4B.2.	2D interaction diagram of bergenin **(32)** with **4GQQ (A)**,	227

2QMJ (B) and **3TOP (B)**

Figure 4B.3.	% of cytotoxicity in L6 cell line (**27**-**33**)	228
Figure 4B.4.	Fluorescence analysis of 2-NBDG uptake by flow cytometry.	228
Figure 5A.1.	Phytochemicals isolated from *Hopea exalata*	236
Figure 5A.2.	Phytochemicals isolated from *Hopea chinensis*	236
Figure 5A.3.	Phytochemicals isolated from *Hopea hainanensis*	237
Figure 5A.4.	Phytochemicals isolated from *Hopea malibato*	238
Figure 5A.5.	*Hopea parviflora* Bedd.	239
Figure 5A.6.	Compounds previously isolated from *Hopea parviflora*	240
Figure 5A.7.	^{1}H NMR spectrum (500 MHz, $CDCl_3$) of friedelin (**34**)	243
Figure 5A.8.	^{13}C NMR spectrum (125 MHz, $CDCl_3$) of friedelin (**34**)	243
Figure 5A.9.	^{1}H NMR spectrum (500 MHz, $CDCl_3$) of friedelan-3β-ol (**35**)	245
Figure 5A.10.	^{13}C NMR spectrum (125 MHz, $CDCl_3$) of friedelan-3β-ol (**35**)	245
Figure 5A.11.	^{1}H NMR spectrum (500 MHz, Acetone-d_6) of **(-)-** ampelopsin A (**37**)	247
Figure 5A.12.	^{13}C NMR spectrum (125 MHz, Acetone-d_6) of **(-)-** ampelopsin A (**37**)	248
Figure 5A.13.	^{1}H-^{1}H COSY NMR spectrum (500 MHz, Acetone-d_6) of **(-)-**ampelopsin A (**37**)	248
Figure 5A.14.	HMQC NMR spectrum (125 MHz, Acetone-d_6) of **(-)-** ampelopsin A (**37**)	249
Figure 5A.15.	DEPT 135 spectrum (125 MHz, Acetone-d_6) of **(-)-**	249

ampelopsin A (**37**)

Figure 5A.16. ^{1}H NMR spectrum (500 MHz, Acetone-d_6) of (-)-hopeaphenol (**38**) 251

Figure 5A.17. ^{13}C NMR spectrum (125 MHz, Acetone-d_6) of (-)-hopeaphenol (**38**) 251

Figure 5A.18. ^{1}H-^{1}H COSY NMR spectrum (500 MHz, Acetone-d_6) of (-)-hopeaphenol (**38**) 252

Figure 5A.19. HMQC NMR spectrum (125 MHz, Acetone-d_6) of (-)-hopeaphenol (**38**) 252

Figure 5A.20. DEPT 135 spectrum (125 MHz, Acetone-d_6) of (-)-hopeaphenol (**38**) 253

Figure 5A.21. NOESY NMR spectrum (500 MHz, Acetone-d_6) of (-)-hopeaphenol (**38**) 253

Figure 5A.22. ^{1}H NMR spectrum (500 MHz, Acetone-d_6) of 2, 4, 8-trihydroxyphenanthrene-2-*O*-glucoside (**40**) 256

Figure 5A.23. ^{13}C NMR spectrum (125 MHz, Acetone-d_6) of 2, 4, 8-trihydroxyphenanthrene-2-*O*-glucoside (**40**) 257

Figure 5A.24. ^{1}H-^{1}H COSY NMR spectrum (500 MHz, Acetone-d_6) of 2, 4, 8-trihydroxyphenanthrene-2-*O*-glucoside (**40**) 257

Figure 5A.25. HMQC NMR spectrum (125 MHz, Acetone-d_6) of 2, 4, 8-trihydroxyphenanthrene-2-*O*-glucoside (**40**) 258

Figure 5A.26. ^{1}H NMR spectrum (500 MHz, DMSO-d_6) of ellagic acid-3,3', 4-trimethoxy-4'-*O*-α-L-rhamnopyranoside (**41**) 259

Figure 5A.27. ^{13}C NMR spectrum (125 MHz, DMSO-d_6) of ellagic acid-3,3', 4-trimethoxy-4'-*O*-α-L-rhamnopyranoside (**41**) 260

Figure 5A.28. ^{1}H-^{1}H COSY NMR spectrum (500 MHz, DMSO-d_6) of ellagic acid-3,3', 4-trimethoxy-4'-*O*-α-L- 260

rhamnopyranoside (**41**)

Figure 5A.29. HMQC NMR spectrum (125 MHz, DMSO-d_6) of ellagic acid-3,3', 4-trimethoxy-4'-*O*-α-L-rhamnopyranoside (**41**) 261

Figure 5A.30. HMBC spectrum (125 MHz, DMSO-d_6) of ellagic acid-3,3', 4-trimethoxy-4'-*O*-α-L-rhamnopyranoside (**41**) 261

Figure 5A.31. DEPT 135 spectrum (125 MHz, DMSO-d_6) of ellagic acid-3,3', 4-trimethoxy-4'-*O*-α-L-rhamnopyranoside (**41**) 262

Figure 5A.32. Biosynthetic pathway of (-) – hopeaphenol 263

Figure 5A.33. 2D interaction diagram of (-)-ampelopsin A (**37**) with **(A) 4GQQ, (B) 2QMJ** and **(C) 3TOP** 267

Figure 5A.34. 2D interaction diagram of ellagic acid 3, 3', 4-trimethoxy-4'-*O*-α-L-rhamnopyranoside (**41**) with **(A) 4GQQ** and **(B) 2QMJ** 268

Figure 5A.35. Cytotoxicity of compounds 269

Figure 5A.36. 2-NBDG assay by flow cytometry in L6 myotubes. 269

Figure 5A.37. Schematic representation of isolation procedure of the acetone extract of the stem bark of *Hopea parviflora* 271

Figure 5B.1. Isolated compounds for anti-inflammatory study 280

Figure 5B.2. Cytotoxic effect of compounds 1-5 in RAW 264.7 macrophages 281

Figure 5B.3. Effect of 1 μM and 5 μM concentrations of compound **5** on NO production in LPS-stimulated RAW 264.7 cell lines. 282

Figure 5B.4. Effect of 1 μM and 5 μM concentrations of compound 5 on TNF-α, IL-6 and IL10 production in LPS-stimulated RAW 264.7 cell lines. 283

Figure 5B.5.	Expression level of 1 μM and 5 μM concentrations of compound **5** on NF-κB production	284
Figure 6A.1.	Phytochemicals isolated from *Myristica fragrans*	293
Figure 6A.2.	Phytochemicals isolated from *Myristica malabarica*	294
Figure 6A.3.	*Myristica fatua* Houtt. var. *magnifica* (Bedd.) Sinclair	295
Figure 6A.4.	Compounds previously isolated from *Myristica fatua* Houtt.	296
Figure 6A.5.	^{1}H NMR spectrum (500 MHz, $CDCl_3$) of 3-tridecanoylbenzoic acid (**43**)	297
Figure 6A.6.	^{13}C NMR spectrum (125 MHz, $CDCl_3$) of 3-tridecanoylbenzoic acid (**43**)	298
Figure 6A.7.	^{1}H- ^{1}H COSY spectrum (500 MHz, $CDCl_3$) of 3-tridecanoylbenzoic acid (**43**)	298
Figure 6A.8.	HMQC spectrum (125 MHz, $CDCl_3$) of 3-tridecanoylbenzoic acid (**43**)	299
Figure 6A.9.	HMBC spectrum (125 MHz, $CDCl_3$) of 3-tridecanoylbenzoic acid (**43**)	299
Figure 6A.10.	DEPT 135 spectrum (125 MHz, $CDCl_3$) of 3-tridecanoylbenzoic acid (**43**)	300
Figure 6A.11.	HRESIMS spectrum of 3-tridecanoylbenzoic acid (**43**)	300
Figure 6A.12.	^{1}H NMR spectrum (500 MHz, $CDCl_3$) of 1-(2-methoxy-6-hydroxyphenyl)tetradecan-l-one (**44**)	302
Figure 6A.13.	^{13}CNMR spectrum (125 MHz, $CDCl_3$) of 1-(2-methoxy-6-hydroxyphenyl)tetradecan-l-one (**44**)	302
Figure 6A.14.	^{1}H NMR spectrum (500 MHz, $CDCl_3$) of 1-(2, 6-dihydroxyphenyl) tetradecan-1-one (**45**)	303

Figure 6A.15.	^{13}C NMR spectrum (125 MHz, $CDCl_3$) of 1-(2, 6-dihydroxyphenyl) tetradecan-1-one (**45**)	304
Figure 6A.16.	^{1}H NMR spectrum (500 MHz, Acetone-d_6) of malabaricone A (**46)**	305
Figure 6A.17.	^{13}C NMR spectrum (125 MHz, Acetone-d_6) of malabaricone A (**46)**	305
Figure 6A.18.	^{1}H NMR spectrum (500 MHz, $CDCl_3$) of 1-(2-hydroxy-6-methoxyphenyl)-9-(4-hydroxy phenyl)nonan-one (**47**)	307
Figure 6A.19.	^{13}C NMR spectrum (125 MHz, $CDCl_3$) of 1-(2-hydroxy-6-methoxyphenyl)-9-(4-hydroxy phenyl)nonan-1-one (**47**)	307
Figure 6A.20.	^{1}H NMR spectrum (500 MHz, $CDCl_3$) of malabaricone B (**48)**	308
Figure 6A.21.	^{13}C NMR spectrum (125 MHz, $CDCl_3$) of malabaricone B (**48)**	309
Figure 6A.22.	^{1}H NMR spectrum (500 MHz, Acetone-d_6) of malabaricone C (**49**)	310
Figure 6A.23.	^{13}C NMR spectrum (125 MHz, Acetone-d_6) of malabaricone C (**49**)	310
Figure 6A.24.	Hypothetical pathway for malabaricones biosynthesis	311
Figure 6A.25.	2D interaction diagram of malabaricone C with **(A) 4GQQ, (B) 2QMJ,** and **(C) 3TOP**	316
Figure 6A.26.	(A) Root mean square deviation of **2QMJ** with malabaricone C and (B) **2QMJ**- Malabaricone C contacts	317
Figure 6A.27.	Pharmacophore modelling	318
Figure 6A.28.	Cytotoxicity of compounds **43-49** in L6 cell line.	319

Figure 6A.29.	Fluorescence analysis of 2-NBDG uptake by flow cytometry.	320
Figure 6A.30.	Schematic representation of the extraction and isolation of phytochemicals from the stem bark of *Myristica fatua* Houtt.	322
Figure 6B.1.	Schematic representation of AMPK pathway	334
Figure 6B.2.	Structures of the compounds isolated from the seeds of *Myristica fatua*	336
Figure 6B.3.	^{1}H NMR spectrum (500 MHz, Acetone-d_6) of dactyloidin (**55**)	337
Figure 6B.4.	^{13}C NMR spectrum (125 MHz, Acetone-d_6) of dactyloidin (**55**)	337
Figure 6B.5.	DEPT 13 NMR spectrum (125 MHz, Acetone-d_6) of dactyloidin (**55**)	338
Figure 6B.6.	^{1}H-^{1}H COSY NMR spectrum (500 MHz, Acetone-d_6) of dactyloidin (**55**)	338
Figure 6B.7.	HMQC NMR spectrum (125 MHz, Acetone-d_6) of dactyloidin (**55**)	339
Figure 6B.8.	HMBC NMR spectrum (125 MHz, Acetone-d_6) of dactyloidin (**55**)	339
Figure 6B.9.	Single X-ray of dactyloidin (**55**)	340
Figure 6B.10.	^{1}H NMR spectrum (500 MHz, Acetone-d_6) of promalabaricone B (**56**)	341
Figure 6B.11.	^{13}C NMR spectrum (125 MHz, Acetone-d_6) of promalabaricone B (**56**)	341
Figure 6B.12.	DEPT 135 NMR spectrum (125 MHz, Acetone-d_6) of	342

	promalabaricone B (**56**)	
Figure 6B.13.	HOMOCOSY NMR spectrum (500 MHz, Acetone-d_6) of promalabaricone B (**56**)	342
Figure 6B.14.	HMQC NMR spectrum (125 MHz, Acetone-d_6) of promalabaricone B (**56**)	343
Figure 6B.15.	HMBC NMR spectrum (125 MHz, Acetone-d_6) of promalabaricone B (**56**)	343
Figure 6B.16.	2D interaction diagram of dactyloidin with **4GQQ** (A)**, 2QMJ** (B) and **3TOP** (C) and promalabaricone B with **4GQQ** (D), **2QMJ** (E) and **3TOP** (F)	347
Figure 6B.17.	(A) Root mean square deviation of **3TOP** with promalabaricone B and (B) **3TOP** - promalabaricone B contacts	348
Figure 6B.18.	Cytotoxicity of dactyloidin (**6**) and promalabaricone B (**7)** was evaluated in L6 myoblast at varying concentrations.	348
Figure 6B. 19.	2-NBDG uptake in L6 skeletal myotubes.	349
Figure 6B.20.	Western blot analysis for the expression of GLUT4 expression in L6 myotubes.	350
Figure 6B.21.	Western blot analysis for the expression of AMPK in L6 myotubes.	351
Figure 6B.22.	Schematic representation of the extraction and isolation of phytochemicals from the seeds of *Myristica fatua* Houtt.	353
Figure 1.	Schematic representation of phytochemical investigation and antidiabetic potential of quassinoids isolated from the seeds of *Quassia indica*	358

Figure 2.	Schematic representation of phytochemical investigation and antidiabetic potential of compounds isolated from the stem bark of *Quassia indica*	359
Figure 3.	Schematic representation of phytochemical investigation and anti-inflammatory potential of compounds from the stem bark of *Ailanthus excelsa*	360
Figure 4.	Schematic representation of phytochemical investigation and their ameliorative effect on H_2O_2 induced oxidative stress in H9c2 cardiomyoblasts	361
Figure 5.	Schematic representation of antidiabetic potential of compounds isolated from the stem bark of *Vatica chinensis*	362
Figure 6.	Schematic representation of antidiabetic potential of compounds isolated from the stem bark of *Hopea parviflora*	363
Figure 7.	Schematic representation of anti-inflammatory activity of compounds isolated from the stem bark of *Hopea parviflora*	364
Figure 8.	Schematic representation of phytochemical and antidiabetic potential of compounds isolated from the stem bark of *Myristica fatua*	365
Figure 9.	Schematic representation of phytochemical and antidiabetic potential of compounds isolated from the seeds of *Myristica fatua*	366

List of Abbreviations

υ_{max}	-Absorption maximum
α	-Alpha
&	-And
β	-Beta
δ	-Delta
ε	-Epsilon
γ	-Gamma
κ	-Kappa
μM	-Micromolar
$\Delta\Psi m$	- Mitochondrial membrane potential
%	-Percent
Π	-Pi
μM	-Micromolar
1D/2D	-One or two dimensional
	- Percent human oral bbsorption
A_0	-Absorbance of control
As	-Absorbance of sample
ABTS	- 2,2'-Azino-bis(3-ethylbenzothiazoline-6-sulphonic acid)
AChE	- Acetylcholinesterase
A.D	-Anno domini
ADME/T	- Adsorption, distribution, metabolism and

	excretion/toxicity
AGEs	- Advanced glycation end products
AGS	- Human gastric ademocarcinoma
AKT	- Protein kinase B
AMPK	-5'- Adenosine monophosphate activated protein kinase
ATP	- Adenosine triphosphate
B.C	-Before christ
BGC-803	- Human gastric cancer
br	-broad
brs	-Broad singlet
BSA	-Bovin serum albumin
^{13}C	-Carbon-13
CADD	- Computer aided drug design
CAT	- Catalase
CC	-Column chromatography
CD	-Circular dichorism
$CDCl_3$	-Deuterated chloroform
$CHCl_3$	-Chloroform
4CL	-4-coumarate-CoA ligase
cm	-centimetre
CNS	- Central nervous System
CO_2	-Carbon dioxide

CoA	- Coenzyme A
COX	- Cyclooxygenase
d	-doublet
dd	-doublet of doublet
D-Score	-Dock score
DCFH-DA	- Dichloro-dihydro-fluorescein diacetate
DCM	-Dichloromethane
DEPT	-Distortionless enhancement by polarization transfer
DMEM	- Dulbecco's modified eagle's medium
DMSO-d_6	- Deuterated dimethyl sulfoxide
DNA	-Deoxyribonucleic acid
DQF COSY	-Double quantum filtrated correlation spectroscopy
ELISA	- Enzyme-linked immune sorbent assay
EtOH	-Ethanol
EtOAc	-Ethyl acetate
FACS	- Fluorescence Activated Cell Sorting
FBS	-Fetal bovin serum
FDA	-Food and drug administration
FISA	- Hydrophilic component of total solvent accessable area
FTIR	-Fourier transform infrared

g	-Gram
G-Score	-Glide score
GAE	-Gallic acid equivalent
GLUT4	- Glucose transporter 4
h	-Hour
^{1}H NMR	-Proton nuclear magnetic resonance spectroscopy
^{1}H-^{1}H COSY	-Homonuclear correlation spectroscopy
HBA	- Hydrogen bond acceptor
HBD	- Hydrogen bond donor
HeLa	- Helen Lane or Helen Larson
HMBC	-Heterouclear multiple bond correlation
HMQC	- Heterouclear multiple quantum correlation
HOA	- Human oral absorption
H_2O_2	-Hydrogen peroxide
HREIMS	-High resolution electron impact mass spectroscopy
HRP	- Horse radish peroxidase
HTS	- High throughput screening
Hz	-Hertz
IκB	- Inhibitory protein
IC_{50}	-Inhibitory concentration for 50 %
IFN-γ	- Interferon gamma
IL	- Interleukin

IPP	- Isopentenyl diphosphate
J	- Coupling constant
JAK	- Janus kinase
kcal	-Killo calorie
KB	- Human nasopharynyeal epidermoid tumor
KBr	-Potassium bromide
kg	-Kilogram
L	-Litre
LPS	- Lipopolysaccharide
LOX-1	- Lectin-like, oxidized low-density lipoprotein receptor-1
m	-Multiplet
m/z	- Mass-to-charge ratio
MAPK	- Mitogen activated protein kinase
MD	- Molecular dynamics
MeOH	-Methanol
MHz	-Mega hertz
mg	-Milligram
min	-Minute
mL	-Milliliter
mM	-Millimolar
Mp	-Melting point
Mol	-Mole

mol %	-Mole percent
MTT	-3-(4,5-Dimethylthiazal-2-yl)-2,5-diphenyl terazolium
M.W.	-Molecular weight
n	-normal
2-NBDG	-(2-(N-(7-Nitrobenz-2-oxa-1,3-diazol-4-yl)Amino)-2-Deoxyglucose)
NCCS	-National centre for cell sciences
NF-κB	-Nuclear factor kappa-light-chain-enhancer of activated B cells
NMR	-Nuclear magnetic resonance
NPs	- Natural products
NO	- Nitric oxide
NOE	-Nuclear Overhauser effect
NOESY	- Nuclear Overhauser effect spectroscopy
NSAIDs	-Non-steroidal anti-inflammatory drugs
p	*-para*
PDB	- Protein data bank
PGE_2	- Prostaglandin E_2
P-L	- Protein ligand
PPARγ	- Peroxisome proliferator-activated receptors
PVDF	- Polyvinylidene difluoride
RCSB	- Research collaboratory for structural bioinformatics

RMSD	- Root mean square deviation
RNA	-Ribonucleic acid
Ro5	- Number of violations of Lipinski's rule of five
ROS	-Reactive oxygen species
RSA	-Radical scavenging activity
rt	-Room temperature
s	-Singlet
SASA	- Total solvent accessible surface area in square angstroms
SD	-Standard deviation
SGLT-2	- Sodium glucose co-transporters-2
SOD	- Superoxide dismutase
STAT	-Signal transducers and activators of transcription
SW1116	- Human colon cancer
t	-*Tertiary*
T2DM	- Type II diabetes mellitus
TLC	-Thin layer chromatography
TMS	- Tetramethylsilane
TNF-α	-Tumour necrosis factor alpha
TMV	- Tobacco mosaic virus
WHO	-World health organization
UV	-Ultraviolet

Preface

Plants can be considered as the master craftsman of molecules as they can synthesise a variety of secondary metabolites with structural complexity. Majority of the drugs in the current market are derived from plants, mostly based on traditional knowledge. Kerala, "God's own country" is well known for its prosperity of plant diversity and also for Ayurveda. However, the active ingredients in many Ayurvedic medicines and their mechanism of action are poorly understood. Scientific validation of Ayurvedic medicines is still a big challenge to the scientific community. Therefore, we have embarked on a study involving the isolation, characterization and pharmacological evaluation of phytochemicals from five plant species of Simaroubaceae, Dipterocarpaceae and Myristicaceae family, found in the Western Ghats of Kerala.

Chapter **1** gives a brief account of plant derived natural products with special emphasis on antidiabetic, anti-inflammatory and cardiovascular drugs.

Second chapter deals with the phytochemical investigation and antidiabetic potential of *Quassia indica* Gaertn (synonym: *Samadera indica* Gaertn). In first part of this chapter, the isolation, characterization and antidiabetic activity of quassinoids from the seeds of *Quassia indica* is described. Two novel quassinoids were also isolated from the seeds of *Quassia indica*. Part B of the second chapter outlines the isolation, characterization and antidiabetic activity of phytochemicals from *Quassia indica* stem bark.

Chapter **3** describes the phytochemical exploration and anti-inflammatory activity of the stem bark of *Ailanthus excelsa* Roxb. The phytochemical investigation on the stem bark of *Ailanthus excelsa* led to the isolation of **7** compounds including two novel molecules. Moreover, we evaluated the anti-inflammatory activity of the isolated compounds.

Chapter **4** of the thesis is divided into two parts. Part A deals with the isolation, characterization and H_2O_2 induced oxidative stress (in H9c2 cell lines) of resveratrol oligomers from the stem bark of *Vatica chinensis* L. One novel resveratrol tetramer named as, vaticanol R was also isolated from this species. The second part of this chapter deals with the antidiabetic potential of all the isolates.

Phytochemical investigation and antidiabetic studies of the medicinal plant *Hopea parviflora* Bedd. is the subject matter of first part of chapter **5**. The second part of this Chapter deals with anti-inflammatory effects and mechanisms of action of ellagic acid-3,

3',4-trimethoxy-4'-*O*-*α*-L-rhamnopyranoside isolated from *Hopea parviflora* Bedd. in lipopolysaccharide-stimulated RAW 264.7 macrophages.

Chapter **6** of the thesis is also divided into two parts. First part of chapter **6** deals with antidiabetic effect of acyl phenols isolated from the stem bark of *Myristica fatua* Houtt. One novel molecule named as, 3-tridecanoylbenzoic acid was also isolated. In the second part, we describe the phytochemical investigation of the seeds of *Myristica fatua*. Among the isolated molecules, dactylodin and promalabaricone B displayed promising 2-NBDG uptake in L6 myotubes and this prompted us to investigate the molecular mechanism of the improved glucose uptake in L6 skeletal muscle cells *via* AMPK pathway.

CHAPTER 1

Plant Derived Natural Products: An Overview

1.1. Introduction

Kerala, "God's Own Country" is the harbour of diversity in biological resources, culture, tradition and indigenous knowledge practices; lies along the windward side of the Western Ghats of Indian peninsula. Our Western Ghats is recognized as one of the world's eight "hottest hotspots" of biological diversity, which hosts an enormous variety of flora and fauna that are being used for the welfare of common man. Among the states located within the Western Ghats region, Kerala is the richest of all three levels of biodiversity such as ecosystem, species and genetic diversity and is an abode of nearly 7,500 plant species with excellent therapeutic properties which is being used in different traditional health care systems.

Nature produces a variety of natural products with highly diverse structures. These natural products are commonly termed "secondary metabolites" in contrast to the "primary metabolites" which are essential for normal growth, development or reproduction of an organism. In addition to their physiological function, natural products also have a strong impact on human culture/tradition. Secondary metabolites were previously regarded as "waste products" without physiological function for an organism. Based on source/origin**,** natural products are broadly divided into four; plant derived, microbial derived, marine derived and animal derived natural products (NPs).

Plants are the best natural laboratories as they synthesize innumerable structurally diverse motifs that can be used for the treatment of various diseases. According to the World Health Organization (WHO) reports, 80 % of people in the developing countries still rely on plant based therapy for their primary health care [Belay *et al*., **2016**]. Nowadays, the scientific world gives an evergreen recognition to traditional medicinal plants for the discovery of novel drug leads. Some of the traditionally important medicinal plants and the structure of the plant drugs are shown in **Figure 1.1**.

Artemisia annua (Asteraceae), also known as sweet worm wood/qinghao is a traditional Chinese medicinal plant used for the treatment of malaria. It yields endoperoxide sesquiterpene lactone, artemisinin that is effective against multidrug-

resistant malaria including *Plasmodium falciparum* [Tu *et al*., **1981**]. In 2015, Tu Youyou shared the Nobel Prize for the development of the antimalarial drug, artemisinin. *Cinchona officinalis* (Rubiaceae) is a medicinal plant used for the production of antimalarial and anti-fever agent quinine [Sudhanshu *et al*., **2003**]. *Papaver somniferum* (Papaveraceae); commonly known as opium poppy or bread seed is the commercial source for the narcotic analgesics such as morphine and codeine [Da *et al*., **2015**]. *Catharanthus roseus* (Apocynaceae); commonly known as Madagascar periwinkle, rose periwinkle, or rosy periwinkle, which is endemic to Madagascar is a source of anticancer drugs vincristine and vinblastine [Cragg *et al*., **2005**].

Artemisia annua

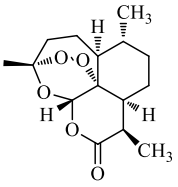

Artemisinin

Papaver somnif erum

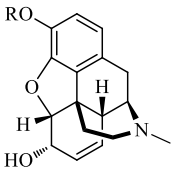

R=H, Morphine
R=CH_3, Codeine

Cinchona of f icinalis

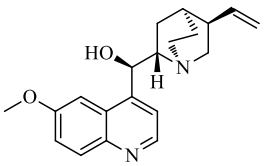

Quinine

Catharanthus roseus

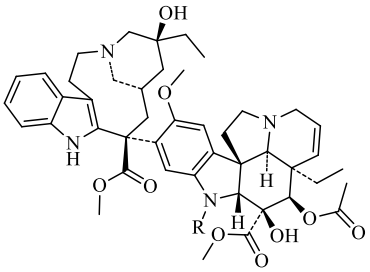

R=CH_3, Vinblastine
R=CHO, Vincristine

Figure 1.1. Traditionally important medicinal plants and structure of the derived drugs

Microorganisms such as viruses, bacteria, algae, fungi and protozoa have been invaluable to discover drugs and drug leads. Nearly, 50,000 natural products have been isolated from microorganisms, of these 10,000 are reported to have biological activity, among them, 100 natural products are used as antibiotics, antitumor agents and agrochemicals. Penicillin is the first antibiotic accidentally discovered from *Penicillium notatum* by Alexander Fleming in 1928 (**Figure 1.2**). This antibiotic discovery led to drug research especially from microorganisms [Arnold, **2014**]. Lovastatin is a fungal metabolite (*Aspergillus terreus*), used as a lead compound in the synthesis of a series of drugs that lower blood cholesterol level [Ganellin, **2013**] (**Figure 1.2**).

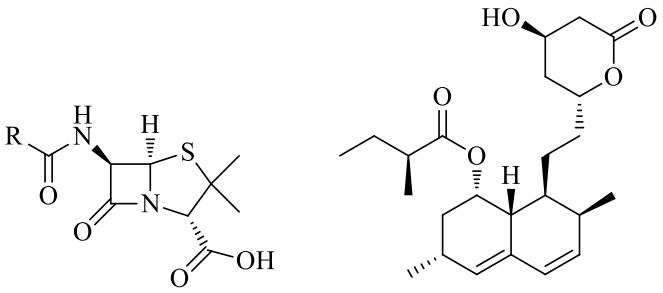

Pencillin core **Lovastatin**

Figure 1.2. Microbial derived drugs

Drug discovery from marine secondary metabolites has enjoyed a renaissance in the last few years. The first bioactive natural products isolated from marine species were spongouridine and spongothymidine from the Carribean sponge '*Cryptothya crypta'* in 1950 and they showed promising anticancer and antiviral activities. Ziconotide, a peptide compound used for the treatment of pain, was isolated from tropical cone snail [Sarfaraj *et al*., **2012**]. Trabectedin, first marine anticancer drug isolated from sea squirt called *Ecteinascidia turbinate* [Tadeusz *et al*., **2009**]. Among all the marine organisms investigated, marine sponges (Porifera) are recognized as the richest sources of bioactive drug leads (**Figure 1.3**).

Terrestrial animals have also been a source of many bioactive compounds that can be used as drugs. Venoms and toxins from animals have played a significant role in the drug discovery process. Epibatidine, obtained from the skin of an Ecuadorian poison frog (*Ameerega bilinguis),* is ten times more potent than morphine [John *et al*., **2000**]. Teprotide, extracted from a Brazilian pit viper (*Bothrops jararaca*), has led to the development of cilazapril and captopril, which are effective against hypertension [Alan,

2014]. In contrast to plants and microorganisms, the structural diversity of natural products from animals seems to be very limited (**Figure 1.4**).

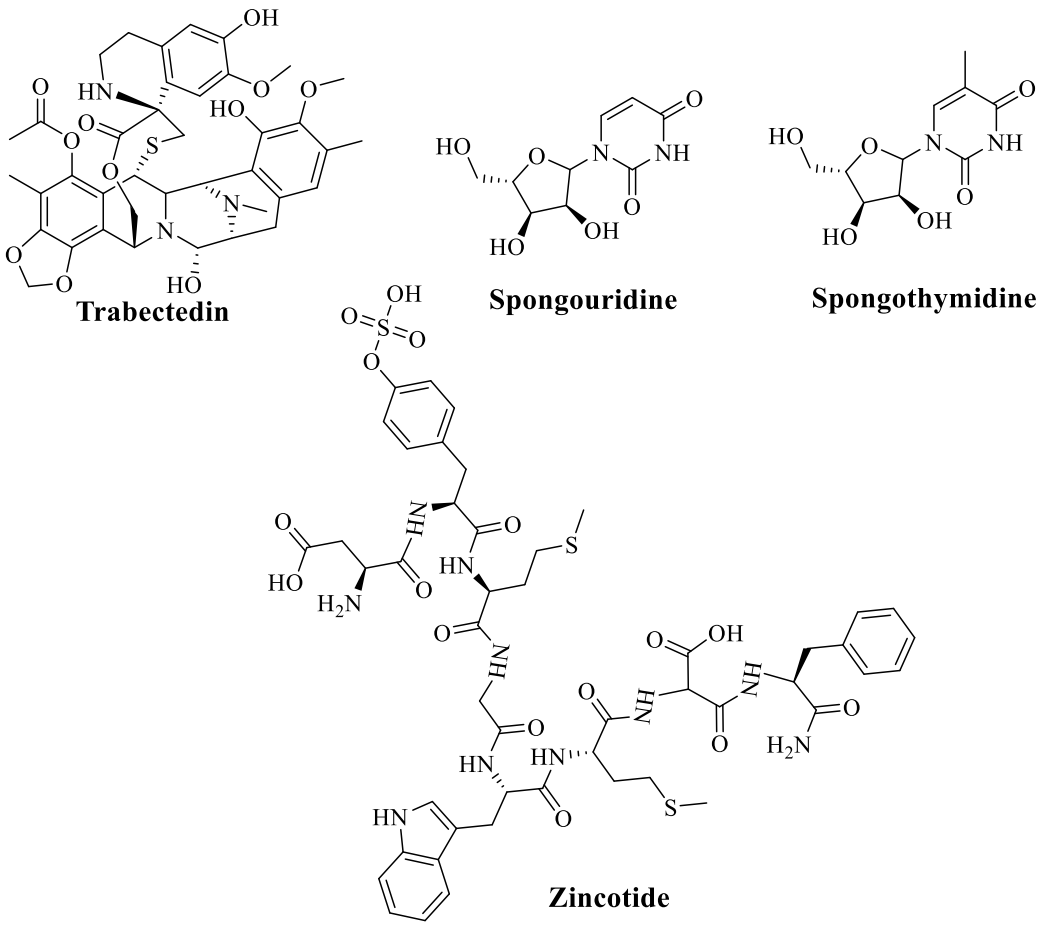

Figure 1.3. Marine derived natural products

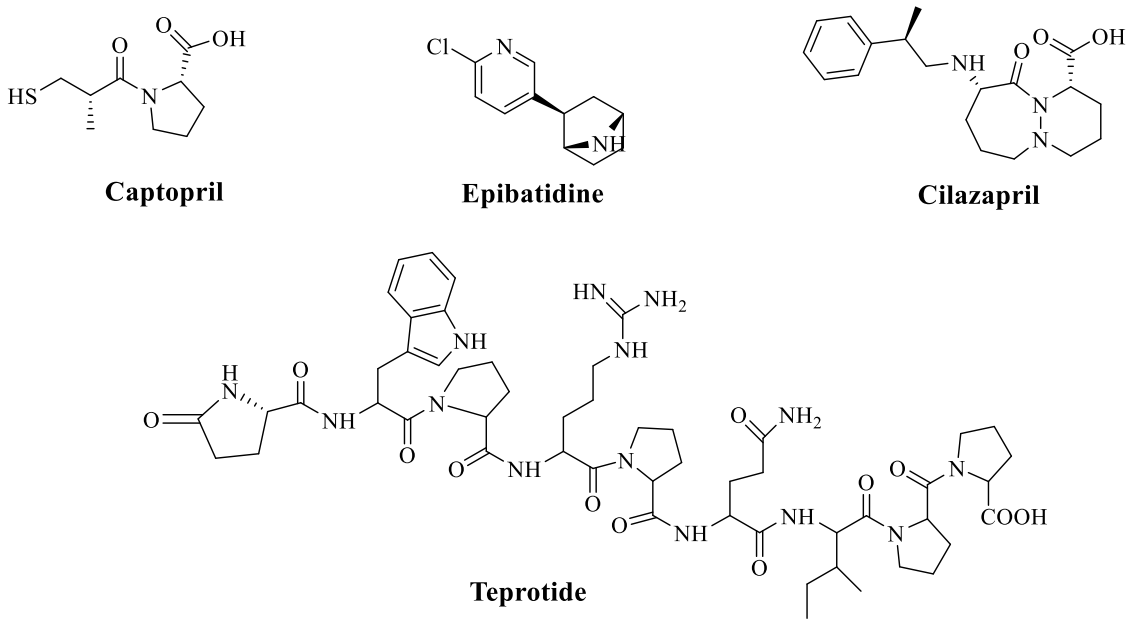

Figure 1.4. Animal derived natural products

1.2. Historical outline of plant derived natural products

Since the time immemorial, plants have been used in folklore for the treatment of many life threatening diseases. Nowadays, plants have been the most successful source of potential drug lead. But, only 10 % of the world's biodiversity has been examined for potential biological activity, many other drugs leads are still awaiting for drug discovery process. The first records of plant derived natural products dates back to B.C. 2600 from Mesopotamia on clay tablets. The oils from *Cupressus sempervirens* and *Commiphora* species are now used today to treat coughs, colds and inflammation [Cragg *et al*., **2005**]. The 'Ebers Papyrus' (Egyptian pharmaceutical record, B.C. 2900) has documented more than 700 plant-based drugs ranging from gargles, pills, infusions to ointments. The Chinese Materia Medica (B.C.1100) recorded 52 prescriptions of drugs. In nearly B. C. 100, the Shennong Herbal documented 365 drugs and the Tang Herbal (659 A.D.) documented 850 drugs from natural products. Dioscorides (Greek physician, A.D.100) and Theophrastus (Greek philosopher and natural scientist, B.C. 300) also recorded the collection, storage and the uses of medicinal herbs [Daniel *et al*., **2012**].

Plants play an essential role in primary healthcare and their use has been extensively documented by different cultures. The WHO-Traditional Medicine Centre's reports point out that, of 122 pure compounds identified from plants, 80 % used were derived from 94 plant species based on traditional knowledge. For example, khellin isolated from *Ammi visnaga* (L) Lamk., which led to the development of cromolyn (bronchodilator) and galegine, verapamil derived from papaverine used in the treatment of hypertension. Some of the best examples of ethnomedicine's role in guiding drug discovery and development is that of the antimalarial drugs, particularly quinine and artemisinin; the antihypertensive agent, reserpine; ephedrine, anti-asthma agent; salbutamol and salmeterol, the muscle relaxant [Cragg *et al*., **2013**].

Recently, Newman and co-workers published an article that highlighted the significance of natural product and/or natural product structures in the drug discovery and development process. Of the 1562 drugs approved in recent years; 422 drugs from the synthetic origin, 101 drugs were vaccines, 320 were natural products derivative, 67 were unaltered natural products, 9 were botanical drugs. The schematic representation of all the new drugs approved between the years 1985-2014 is shown in **Figure 1.5**. In this chapter, we have mainly emphasized on plant derived drugs. Some of the FDA approved plant

derived NP inspired/derived drugs launched in between 2005-2015 are given in **Table 1.1.** and structures are shown in **Figure 1.6** [Newman *et al*., **2016**].

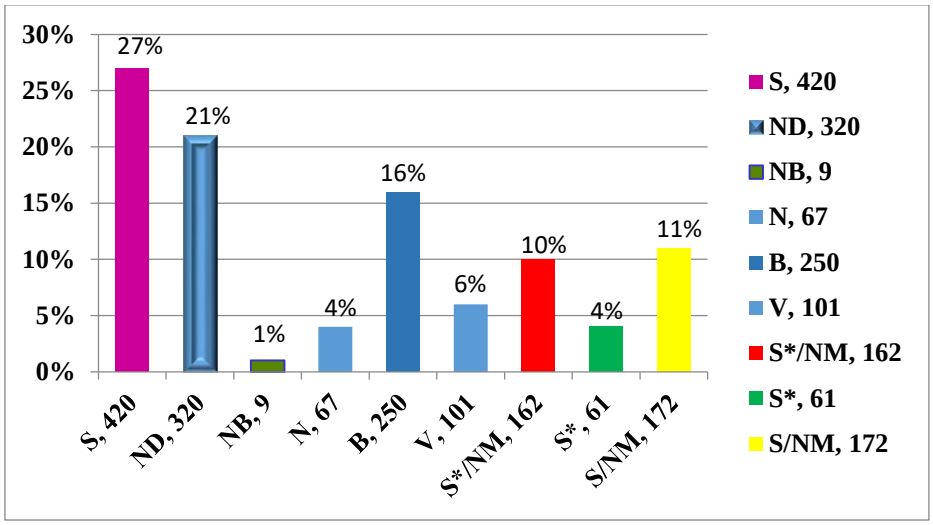

Figure 1.5. (B) Biological macromolecule, (N) Unaltered natural product, (NB) Botanical drug (defined mixture), (ND) Natural product derivative, (S) Synthetic drug, (S*) Synthetic drug (NP pharmacophore), (V) Vaccine, (S/NM) Mimic of natural product

Table 1.1. FDA approved plant derived drugs launched during 2005-2015

Sl. No	Year	Generic name	Lead compound	Disease area/Use
1	2005	Tamibarotene	Retinoic acid	Myelogenous leukemia
2	2005	Abraxane	Paclitaxel	Breast cancer
3	2006	Hycamtin	Camptothecin	Cervical cancer
4	2006	Varenicline	Cytisine	Nicotine dependence
5	2006	Cesamet	Tetrahydrocannabinol	Chemotherapy & nausea
6	2007	Lisdexamfetamine	Amphetamine	ADHD
7	2008	Methylnaltrexone	Morphine	Opioid-induced constipation
8	2009	Vinflunine	Vinblastine	Cancer
9	2009	Nalfurafine	Morphine	Pruritus
10	2010	Cabazitaxel	Paclitaxel	Cancer

11	2010	Zucapsaicin	Capsaicin	Pain
12	2012	Arterolane	Artemisinin	Antimalarial
13	2012	Dapagliflozin	Phlorizin	Diabetes
14	2013	Canagliflozin	Phlorizin	Diabetes
15	2013	Trastuzumab, emtansine	Maytansine	Cancer
16	2014	Naloxigol	Thebaine (paramorphine)	Opioid-induced constipation
17	2014	Empagliflozin	Phlorizin	Diabetes
18	2014	Vorapaxar	Himbacine	To reduce the risk of heart attack

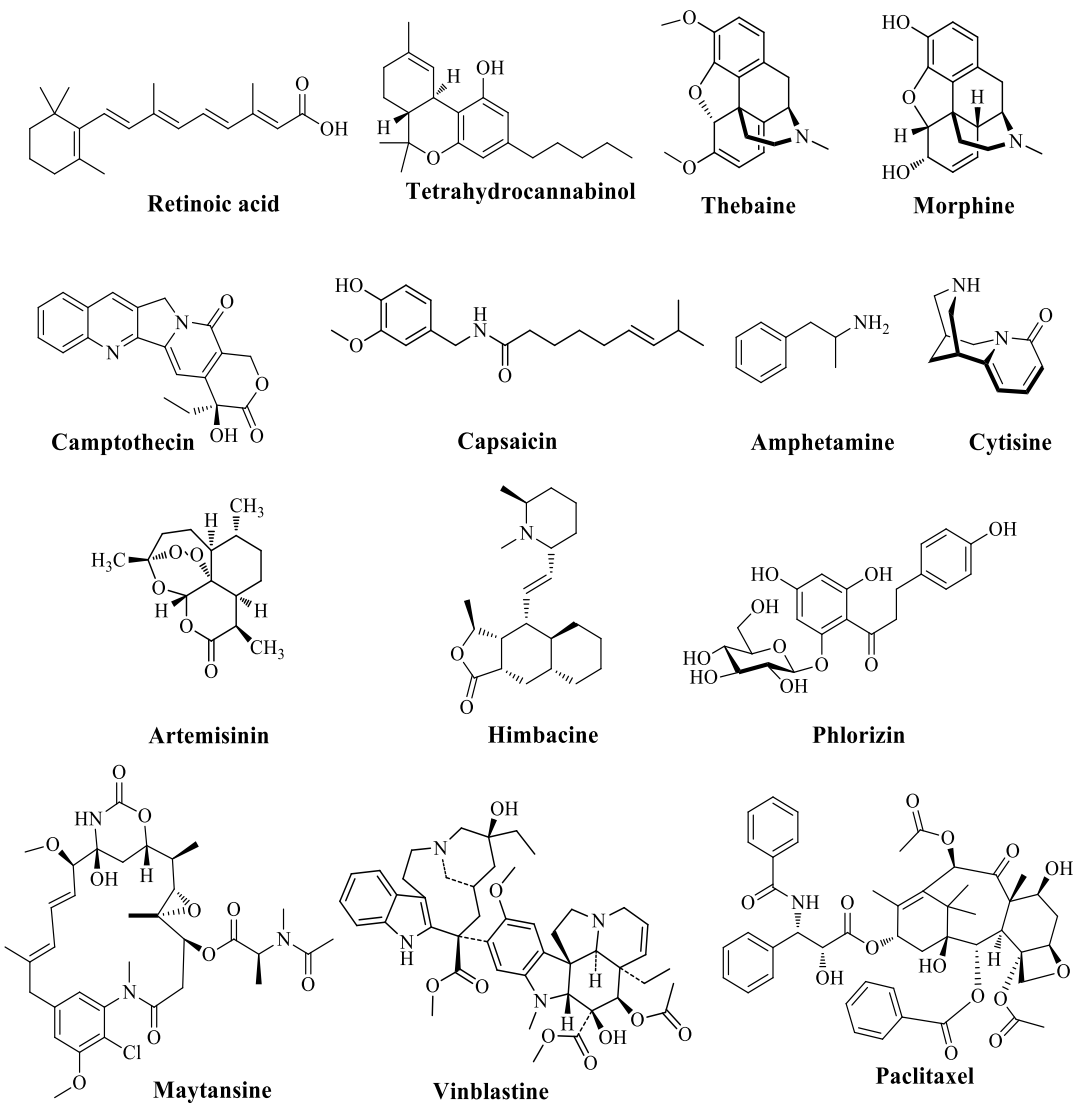

Figure 1.6. Structures of FDA approved plant drugs launched during 2005-2015

1.3. Antidiabetic drugs from plants

Diabetes or diabetes mellitus is a group of metabolic diseases in which the person has high blood glucose (blood sugar), either because insulin production is inadequate, or because the body's cells do not respond properly to insulin or both. There are three types of diabetes; type I, type II and gestational diabetes. Type I diabetes, insulin-dependent diabetes, juvenile diabetes or early-onset diabetes results from the body's failure to produce insulin. The daily insulin injections and proper diet are essential for maintaining health of people with type 1 diabetes. Type II diabetes arises due to the inability of the cells to properly use insulin or the body does not produce enough insulin for proper function. Approximately 90 % of all cases of diabetes in worldwide are of type II diabetes. Proper diet, physical exercise oral medication/ insulin are necessary to control blood glucose level. Gestational diabetes affects females during pregnancy and can be controlled by exercise and diet. The common diabetes symptoms include frequent urination, intense thirst and hunger, weight gain, unusual weight loss, fatigue, cuts and bruises that do not heal, male sexual dysfunction, numbness and tingling in hands and feet [American Diabetics Association, **2012**].

The common antidiabetic agents are α-glucosidase inhibitors (acarbose, miglitol), amylin analogs (pramlintide), dipeptidyl peptidase 4 inhibitors (alogliptan, linagliptan, saxagliptin, sitagliptin), incretin mimetics (albiglutide, dulaglutide, exenatide, liraglutide, lixisenatide), insulin, meglitinides (nateglinide, repaglinide), non-sulfonylureas (metformin), SGLT-2 inhibitors (canagliflozin, dapagliflozin, empagliflozin), sulfonylureas (chlorpropamide, glimepiride, glipizide, glyburide, tolazamide, tolbutamide) and thiazolidinediones (rosiglitazone, pioglitazone)[Abdulfatai *et al*., **2012**].

Metformin (dimethyl-biguanide), one of the most widely used oral antidiabetic agent was developed from the natural compound galegine (isoamylene guanidine) of *Galega officinalis* [Zhang *et al*., **2016**]. Phlorizin, a dihydrochalcone glycoside isolated from the bark *of Malus domestica* (Rosaceae family) lowers glucose plasma levels and improves insulin resistance levels through inhibition of sodium glucose co-transporters (SGLT-2) [Ehrenkranz *et al*., **2005**]. Canagliflozin and empagliflozin are phlorizin analogs which acts as SGLT-2 inhibitors [Ashley *et al*., **2017**]. Some of the plant derived antidiabetic drugs are shown in **Figure 1.7**. Apart from individual drugs or its combinations, traditional medicine has also played a significant role in managing diabetes in developing countries. For example, Glucosol (an extract from the leaves of

Lagerstroemia speciosa standardized to 1 % corosolic acid) and BGR-34 are used to manage type II diabetes [Jung *et al*., **2006**].

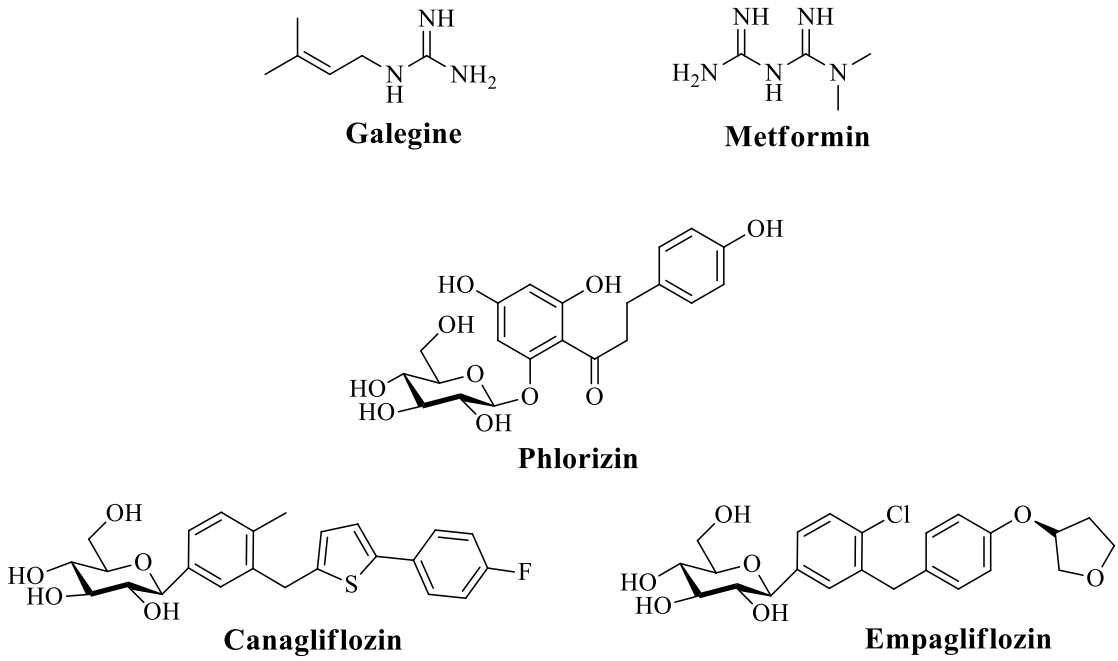

Figure 1.7. Plant derived antidiabetic drugs

1.4. Anti-inflammatory drugs from plants

Inflammation is a complex phenomenon that occurs when tissues are infected or injured by harmful stimuli. Immune cells, blood vessels, and molecular mediators are mainly involved in this process. The word 'inflammation' derived from the Latin 'inflammare' which means to set on fire. The main purpose of inflammation is to limit and eliminate the causes of cellular damage, clear and/or absorb necrotic cells and tissues, and initiate tissue repair. They are two forms of inflammation, acute and chronic. Acute inflammation is self-limiting and beneficial to the host, but chronic inflammation resulted in many chronic diseases and its associated complications. The first step in the inflammatory process is to activate the mast cells, monocytes, macrophages, lymphocytes, and other immune cells. After that, the cells are migrated to the site of injury, which resulted in the generation of reactive oxygen species (ROS) that damages various macromolecules. The inflammatory cells also produce large amounts of inflammatory mediators like cytokines, chemokines, and prostaglandins and these mediators' further recruit macrophages to localized sites of inflammation and directly activate multiple signal transduction cascades and transcription factors associated with inflammation. The NF-κB (nuclear factor kappa B), MAPK (mitogen-activated protein

kinase), and JAK (Janus kinase), STAT (signal transducers and activators of transcription) signaling pathways are involved in the development of the pathway of inflammation [Syed *et al*., **2017**].

Natural products play a noticeable role in the discovery of anti-inflammatory drugs. The drugs used for the treatment of inflammation are called non-steroidal anti-inflammatory drugs (NSAIDs). Some of the NSAIDs are aspirin, celecoxib, ibuprofen, indomethacin, oxaprozin, piroxicam *etc*. The NSAIDs block COX-1 and COX-2 enzyme activity. The COX enzyme mainly promotes the production of prostaglandin. The prolonged use of NSAIDs drugs causes many adverse side effects, which includes gastric lesions, cardiovascular, renal failure and gastrointestinal damage *etc*. Curcumin, isolated from the rhizomes of *Curcuma longa* L. traditionally has been used for the treatment of inflammatory disorders. Silymarins (Silibinin A and Silibinin B) from the ripe seeds of *Silybum marianum* exhibited anti-inflammatory activity. Colchicine isolated from *Colchicum autumnale* is used as an anti-inflammatory agent for the treatment of gout [Fürst *et al*., **2014**]. The structures of some of the plant derived anti-inflammatory compounds are shown in **Figure 1.8**.

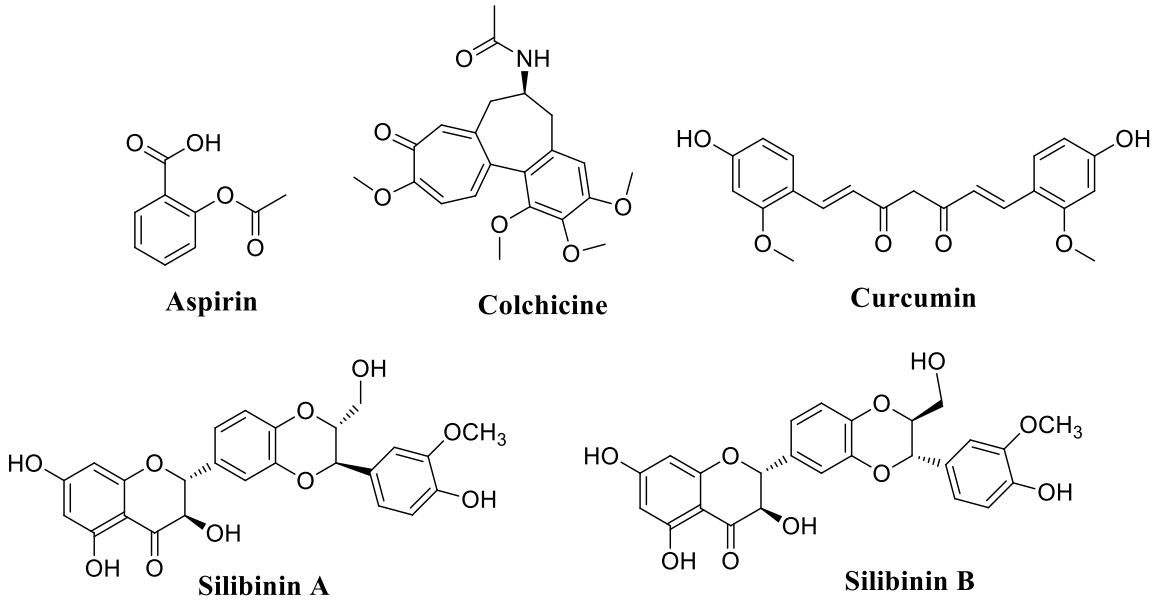

Figure 1.8. Plant derived anti-inflammatory compounds

1.5. Cardiovascular drugs from plants

The cardiac glycoside digoxin from the foxglove plant *Digitalis lanata* (Plantaginaceae family) is used for the treatment of mild to moderate heart failures in adults Another cardiac glycosides are digitoxin from *Digitalis purpurea* and ouabain

from the seeds of *Strophanthus gratus* (Apocynaceae family) [Belz *et al*., **1981;** Schoner, **2002;** De Souza *et al*., **2007**]. Vorapaxar is synthesised from himbacine (*Galbulimi mabaccata*; Himantandraceae family) which decrease the risk of heart attack, stroke, and to restore the blood flow to the heart in patients with a previous heart attack [Loretta, **2015**]. Reserpine, an indole alkaloid isolated from the dried roots of *Rauwolfia serpentine* (Indian snakeroot; Apocynaceae family) is used as a medication to treat high blood pressure [Douglas**, 2015**]. The structures of some of the plant derived anti-inflammatory compounds are shown in **Figure 1.9**.

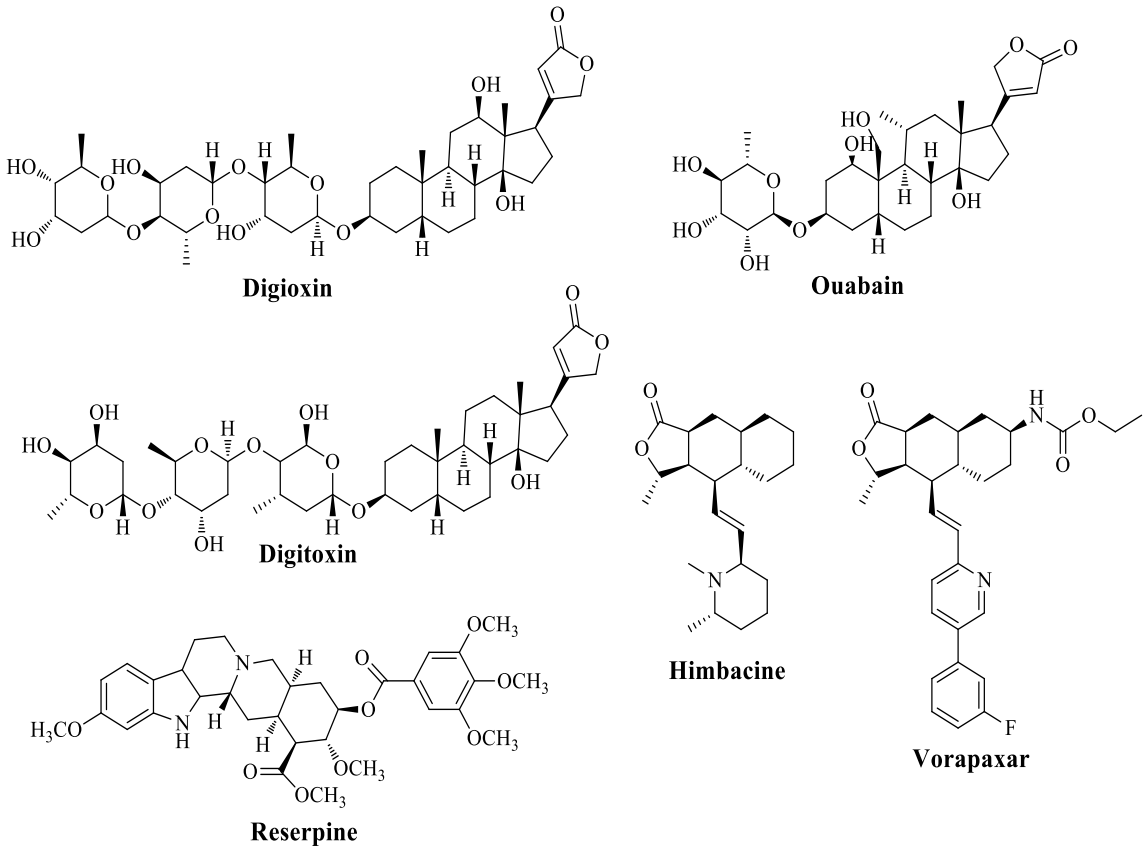

Figure 1.9. Plant derived cardiovascular drugs

1.6. Biosynthetic pathway

Biosynthesis is a multi-step, enzyme-catalyzed process where substrates are converted into more complex products. The major essential elements for biosynthesis are precursor compounds, chemical energy, and catalytic enzymes. The primary precursors are derived from protein (amino acids), DNA/RNA (amino acid and sugar), carbohydrate (sugars) and lipid (fatty acid) metabolism. The nitrogen-containing compounds, alkaloids are biosynthesized from amino acids. The shikimate pathway provides the precursors for phenolic derivatives, flavonoids and organic acids in plants. All terpenoids (isoprenoids)

including both primary and more than 25,000 secondary metabolites are derived from the five-carbon precursor called isopentenyl diphosphate (IPP). Some of the major biosynthetic pathways are given in **Figure 1.10** [Gutzeit *et al*., **2014;** Jones *et al*., **2015;** www.cengage.com]**.**

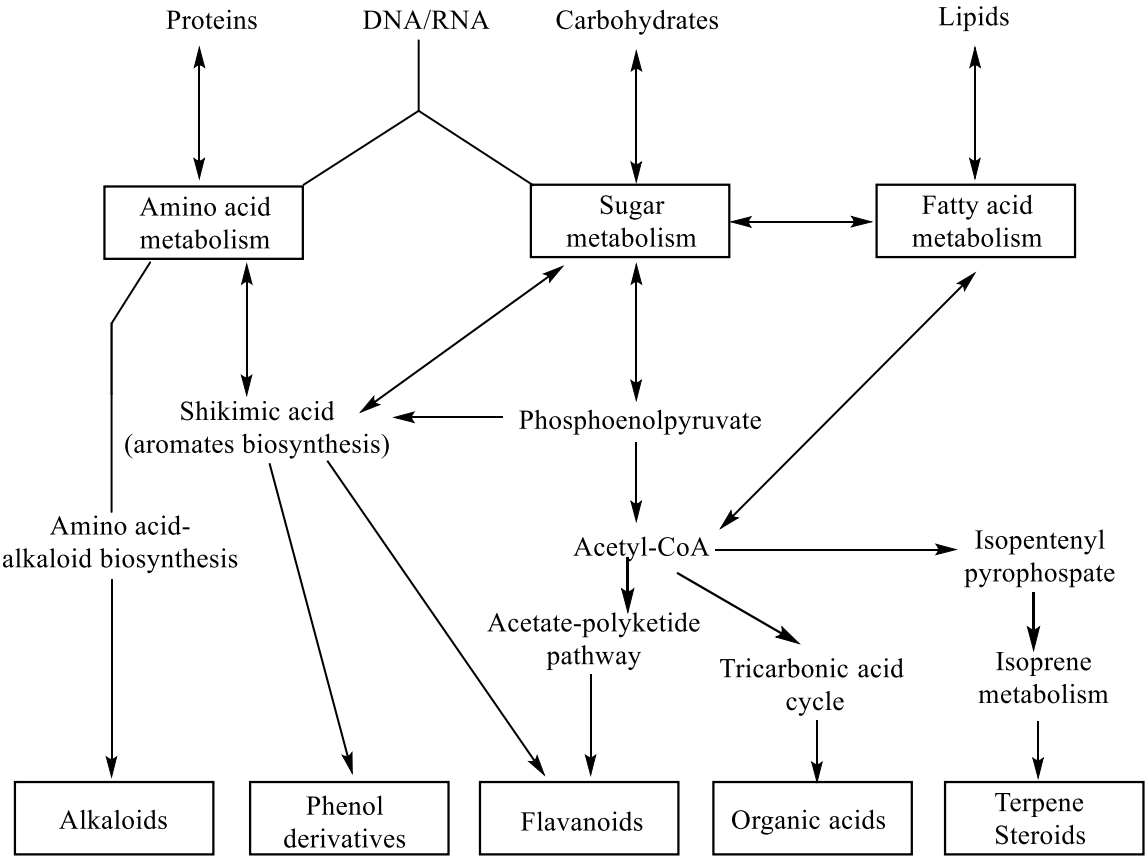

Figure 1.10. Biosynthetic pathways and precursors for the major classes of secondary metabolites

1.6.1. Biosynthetic pathway of quassinoids

Quassinoids are highly oxygenated degraded triterpenes, the marker compounds of the Simaroubaceae family. According to their basic skeleton, quassinoids are categorized into five groups, C-18, C-19, C-20, C-22 and C-25 types (**Figure 1.11**). All quassinoids are believed to be biosynthesized through the common triterpenoid biogenetic pathway. The biosynthetic process begins with the degradation of triterpenes including the loss of a methyl group at C-4 and the four carbon atoms at the end of the side chain. A Bayer-Villiger-type oxidation leads to the cleavage of the bond between C-16 and C-17, it helps to form a δ-lactone ring through the C-16 carbonyl with the 7α-hydroxy group, the common moiety in most of the C-20 quassinoids. Additional introduction of an oxygen

atom allows the cleavage of the C-13/C-17 bond, resulting in the formation of most C-20 and C-19 quassinoids (**Figure 1.12**) [Guo *et al*., **2005**].

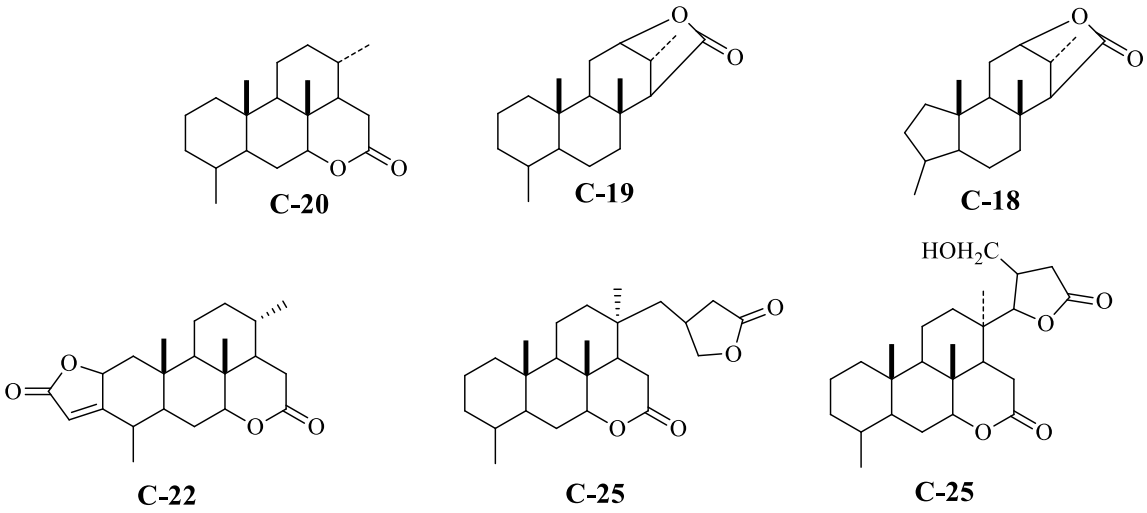

Figure 1.11. Different types of quassinoids

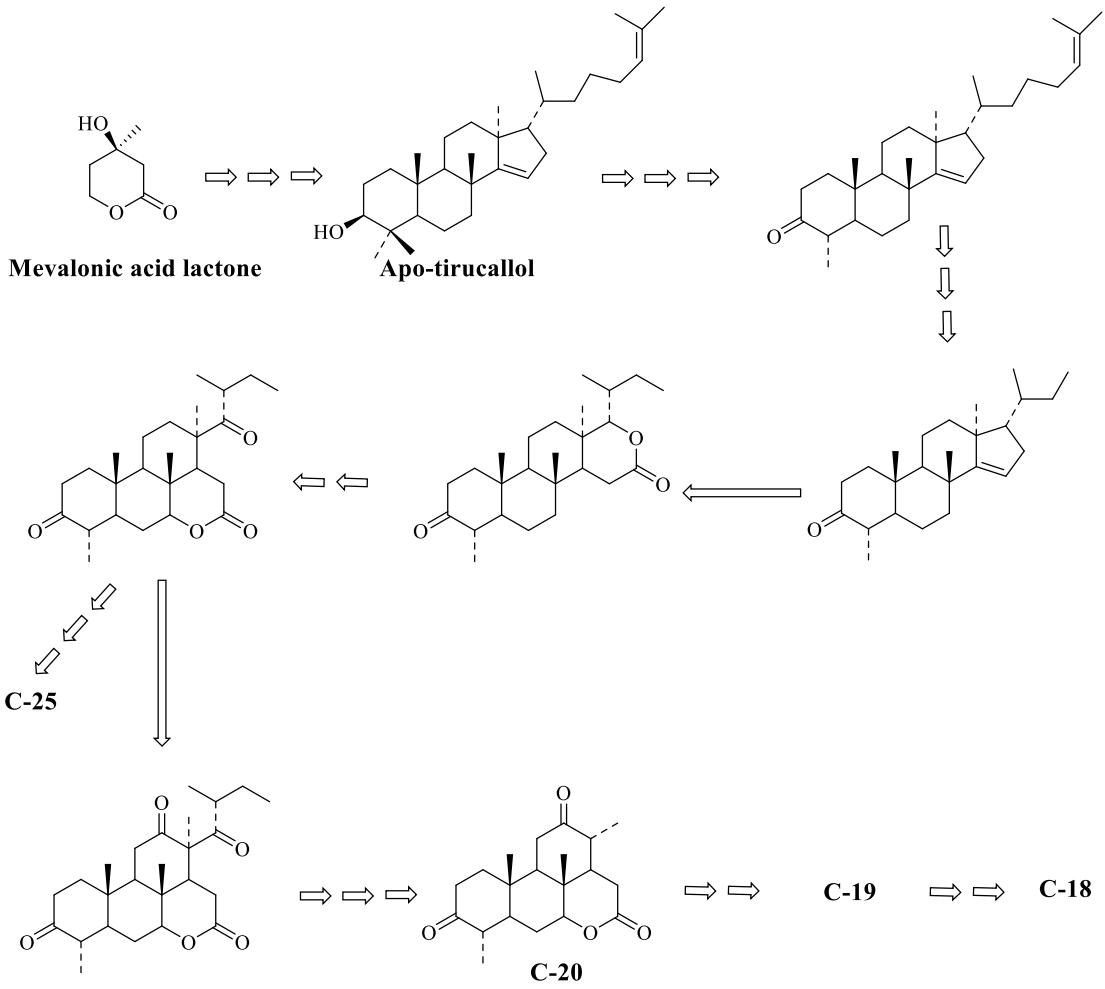

Figure 1.12. Biosynthetic pathway of quassinoids

1.6.2. Biosynthetic pathway of triterpenoids

Pentacyclic triterpenoids such as oleanane, lupane and related skeletons are derived from oxidosqualene. *β*-amyrin is biosynthesized from (3*S*)-2,3-oxidosqualene by the enzyme *β*-amyrinsynthase. The opening of the epoxide ring of oxidosqualene and followed by a series of electrophilic reactions produces the dammarenyl cation. Dammarenyl cation is then quenched with water to produce dammaren diol. Further, the reaction proceeds to expand the fourth ring, here lupenyl cation can be quenched by proton removal to form lupeol. Then, the expansion of the fifth ring will produce the six-membered oleanyl cation, which gives rise to *β*–amyrin (**Figure 1.13**) [John, **2005**].

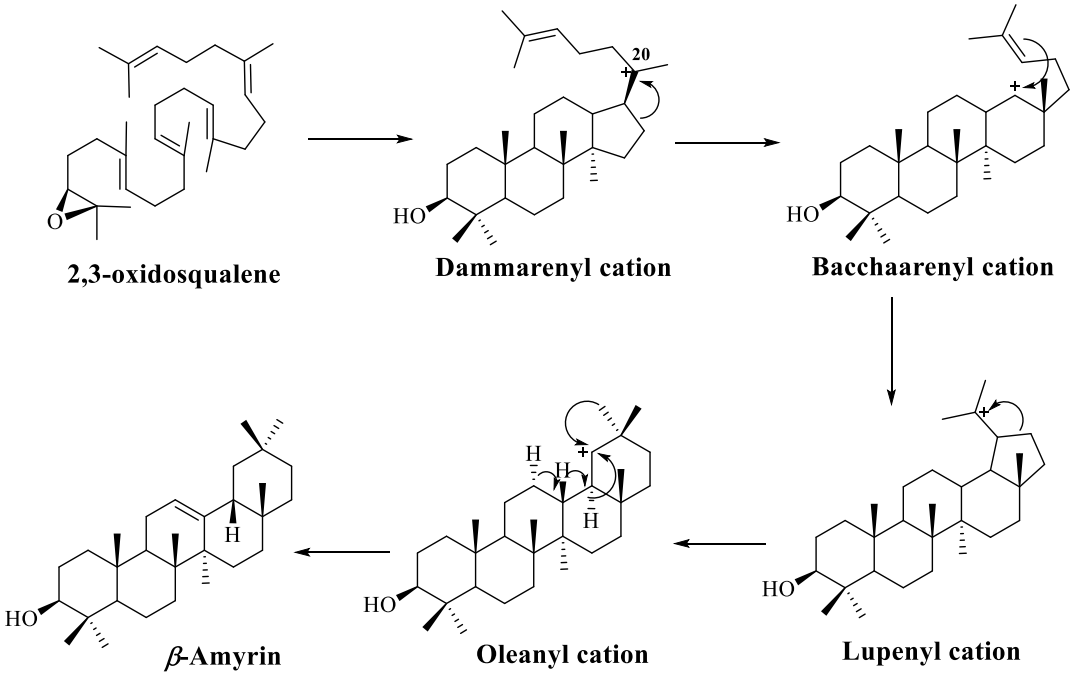

Figure 1.13. Biosynthetic pathway of triterpenoids

1.6.3. Biosynthetic pathway of resveratrol

Resveratrol is a naturally occurring phytoalexin with a stilbene moiety distributed in the plant families including Vitaceae, Dipterocarpaceae, Gnetaceae, Cyperaceae, and Leguminosae. The stilbene moiety is built on a 14-carbon skeleton composed of two phenyl rings linked by an ethylene bridge. Stilbenes are synthesised from the general phenylpropanoid pathway, starting from phenylalanine. Biosynthesis of resveratrol starts by the coupling of *p*-coumaric acid to CoA by the 4CL (CoA ligase) enzyme. Consequently, coumaroyl-CoA is converted into resveratrol by sequential addition of three malonyl-CoA units with the release of CO_2 (**Figure 1.14**). Further modifications such as glycosylation, methylation, oligomerization, isomerization and isoprenylation,

generate various resveratrol derivatives with fascinating chemical diversity (**Figure 1.15**) [Shan *et al.*, **2013**].

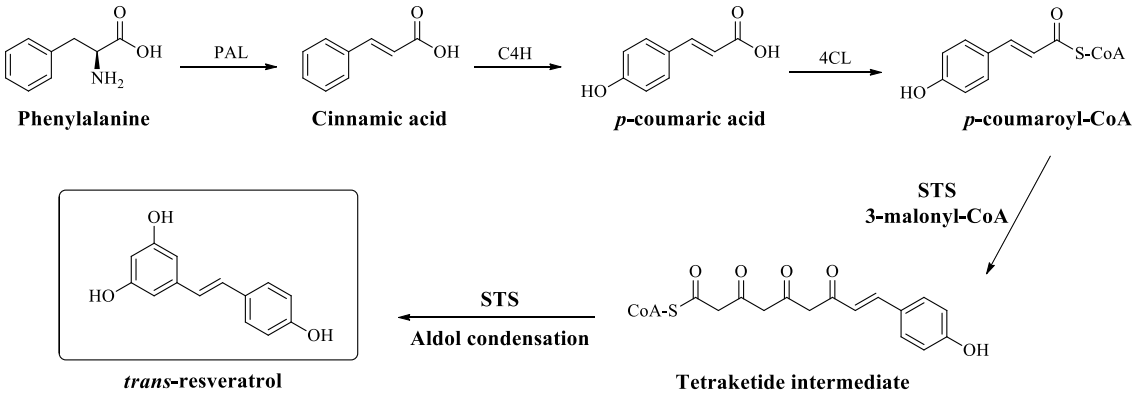

Figure 1.14. Biosynthetic pathway of resveratrol

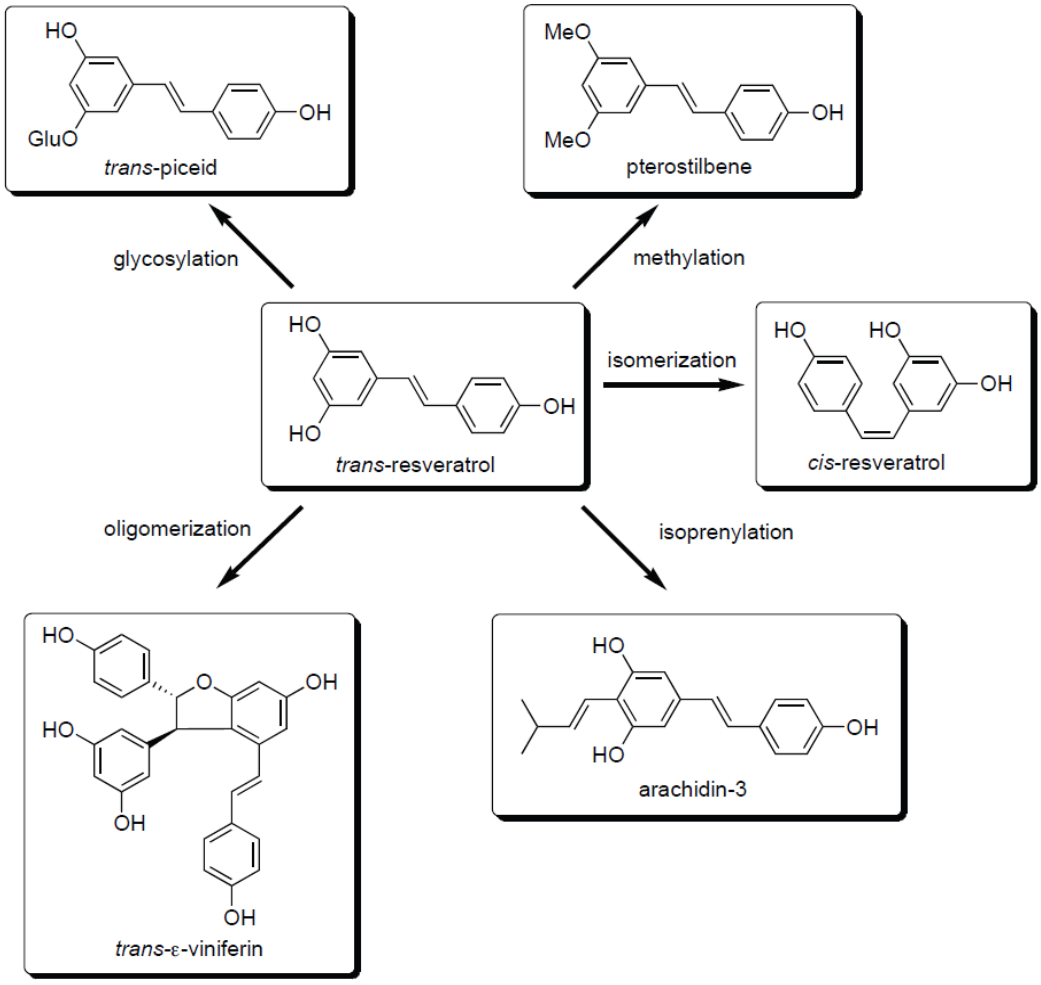

Figure 1.15. Modifications of resveratrol

1.6.4. Biosynthetic pathway of acyl phenols

Acyl phenols were biosynthesised from the same precursors as those used by chalcone synthase in the flavonoid biosynthetic pathway, starting from a cinnamoyl CoA derivative (originating from shikimic acid) and elongated with six acetyl- CoA unit. The cyclization of last three acetyl units of the polyketide intermediate yields a phloroglucinol type aromatic ring. The cinnamoyl polyketide undergoes reduction of the carbonyl at 9, 11, 13 into -CH_2- groups, and of carbonyl-3 into secondary alcohol group to yield prepromalabaricones and finally, the ring closure, dehydration of the secondary alcohol and enolization leads to malabaricones (**Figure 1.16**) [Van *et al*., **2002**].

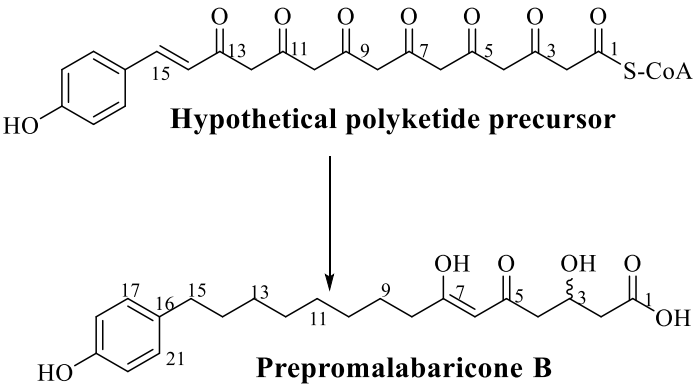

Figure 1.16. Biosynthetic pathway of acylphenols

1.7. Outline and organisation of the thesis

Natural products and its derivatives are widely used as drugs for the treatment of various life threatening diseases. A large percentage of drugs in the market are derived from plants, mainly based on traditional knowledge. Moreover, the natural product inspired designs and synthesis results in the discovery of many modern medicines. Thus, it is very important and urgent to discover the lead molecules that give medicinal value to a particular plant. India has rich biodiversity as a source of the next generation of medicines. It is therefore very important to develop models of bio-prospecting, assaying, development and marketing of drugs for providing affordable health care to the Indian population. India, with its richest biodiversity is one of the mega-biodiversity centres of the world. The Western Ghats, the Eastern Ghats and the North Eastern hills are the main biodiversity hot spots of India. Among this, the Western Ghats represents one of the eight 'hottest hot spots' of world bio-diversity and is considered to be a vast repository of rare, endemic and threatened flora and fauna. Our investigations were focused on the isolation,

characterization and pharmacological activities of phytochemicals from five plant species of Simaroubaceae, Dipterocarpaceae and Myristicaceae family, found in the Western Ghats of Kerala.

Chapter **1** gives an overview of plant derived natural products with special emphasis on antidiabetic, anti-inflammatory and cardiovascular drugs.

The isolation, characterization and antidiabetic activity of quassinoids isolated from the seeds of *Quassia indica* (Gaertn.) Noot. is the subject matter of the first part of chapter 2. *Quassia indica* Gaertn. (Synonym: *Samadera indica* Gaertn.) commonly recognized as "Niepa bark tree" or " Lokhanadi" or "Karinjotta" belonging to the Simaroubaceae family. The ethanol extract of the seeds of *Quassia indica* exhibited significant antidiabetic potential; which encouraged us to isolate compounds from ethanol extract. The ethanol extract was subjected to repeated column chromatographic purification resulting in the isolation of **8** quassinoids. It includes two novel molecules. All quassinoids were tested for their *in vitro* and *in silico* antidiabetic activity. The second part of chapter **2** deals with the phytochemical and antidiabetic activity of the stem bark of *Quassia indica,* which resulted in the isolation of **11** compounds, of which two of them; scopoletin and ferulic acid are isolated for the first time from this species.

Chapter **3** gives the phytochemical investigation and anti-inflammatory activity of the stem bark of *Ailanthus excelsa* Roxb. It is commonly known as"plant of heaven" or "Indian tree of heaven" which is a deciduous tree also belonging Simaroubaceae family. The phytochemical investigation on the stem bark of *Ailanthus excelsa* led to the isolation of **7** compounds including two novel molecules. Moreover, we checked the anti-inflammatory activity of isolated compounds.

Chapter **4** of the thesis is divided into two parts. Part A deals with the isolation, characterization and H_2O_2 induced oxidative stress in H9c2 cell lines of resveratrol oligomers from the stem bark of *Vatica chinensis* L. It is commonly known as “Adakkapine”, “Cherupiney”, “Payinipasa” belonging to the family Dipterocarpaceae, native to India and Sri Lanka. The acetone extract of the stem bark of *Vatica chinensis* exhibited highest TPC, DPPH radical scavenging activity and antidiabetic property. Therefore, further isolation and purifications were focused on the acetone extract, which resulted in the isolation of **7** compounds. A novel non-heterocyclic resveratrol tetramer was also isolated from the stem bark of *Vatica chinensis*. All the compounds were tested for their antioxidant activity using DPPH and ABTS radical scavenging assay. Besides,

we checked the hydrogen peroxide-induced oxidative stress in H9c2 cell lines. In the second part of chapter 4 deals with the antidiabetic potential of all the isolates. All the compounds displayed significant α-glucosidase inhibitory activity and antiglycation property and moderate α- amylase inhibition. Moreover, we have evaluated the glucose uptake in presence of these phytomolecules in L6 myotubes.

Phytochemical investigation and antidiabetic studies on the medicinal plant *Hopea parviflora* Bedd. is the subject matter of first part of chapter **5**. *Hopea parviflora* also belongs to Dipterocarpaceae family distributed in Southeast Asia and locally known as Thambagam or Irimpakam. The stem bark of *Hopea parviflora* resulted in the isolation of **9** compounds, of which **5** of them are isolated for the first time from this species. We have also analysed the antidiabetic property of isolated molecules. The second part of Chapter **5** deals with anti-inflammatory effects and mechanisms of action of ellagic acid-3, 3', 4-trimethoxy 4'-*O*-α-L-rhamnopyranoside isolated from *Hopea parviflora* Bedd. in lipopolysaccharide-stimulated RAW 264.7 macrophages.

Chapter **6** of the thesis is also divided into two parts. The first part of chapter **6** deals with the antidiabetic effect of acyl phenols isolated from the stem bark of *Myristica fatua* Houtt. *Myristica fatua* Houtt.; the wild relative of nutmeg, (*Myristica fragrans*) is native to evergreen forests of Western Ghats of Kerala. Phytochemical investigation on the stem bark of *Myristica fatua* led to the isolation of a novel compound (3-tridecanoylbenzoic acid), along with six known acyl phenols. All the compounds displayed moderate α-amylase and significant α-glucosidase inhibition and antiglycation property. We have evaluated the 2-NBDG uptake in L6 myotubes in the presence of the above molecules. In the second part, we carried out the phytochemical investigation of the seeds of *Myristica fatua*, which resulted in the isolation of **7** major compounds. Dactylodin and promalabaricone B displayed promising 2-NBDG uptake in L6 myotubes which prompted us to investigate the molecular mechanism of the improved glucose uptake in L6 skeletal muscle cells *via* AMPK pathway.

Isolation, Characterization and Antidiabetic Potential of Quassinoids from the Seeds of *Quassia indica* (Gaertn.) Noot.

Traditional medicinal plants are now enjoying the evergreen attention to the scientific community and common man because of their less toxicity, minimal side effects, and the higher chance of bioavailability and containing numerous novel bio-active drug leads. Simaroubaceae family is of great importance and relevance in the ethnopharmacological framework since many of its species are widely used in the folk medicine practice of many countries. One such plant species which has a great reputation in traditional systems of medicine all over the world is *Quassia indica* (Gaertn.) Noot. In the first part of this chapter, we have focused on the isolation, characterization and antidiabetic activity of phytochemicals present in the seeds of *Quassia indica*.

2A.1. Simaroubaceae

The Simaroubaceae family includes 16 genera (**Table 2A.1**) and 102 accepted plant species of trees and brushes of pantropical distribution [www.theplantlist.org]. The main distribution hotspots are located in tropical areas of America, Africa, Madagascar and Australia. This family is characterized by the presence of quassinoids and it can be considered as a taxonomic marker of the Simaroubaceae family. Quassinoids possess a wide spectrum of biological activities such as antitumor, antimalarial, antiviral, insecticide, feeding deterrent, ameobicide, antiparasitic and herbicidal. Alkaloids, triterpenes, steroids, coumarins, anthraquinones and flavonoids are other phytochemicals present in this family [Iasmine *et al*., **2014**].

Table 2A.1. Different genus of Simaroubaceae family

• *Ailanthus* • *Amaroria* • *Brucea* • *Castela* • *Eurycoma*	• *Gymnostemon* • *Hannoa* • *Iridosma* • *Leitneria* • *Odyendyea* • *Picrasma*	• *Picrolemma* • *Pierreodendron* • ***Quassia*** • *Simaba* • *Simarouba*

2A.2. *Quassia* genus

Quassia is a flora genus in the family Simaroubaceae and the genus was named after a former slave from Graman Quassi, a Surinamese healer and botanist in the eighteenth century. Some of the known *Quassia* species are listed in **Table 2A.2**. A detailed literature survey of some of the *Quassia* species for example; *Quassia africana*, *Quassia amara* and *Quassia undulata* are discussed in the following sections.

Table 2A.2. *Quassia* species and their distribution

Sl. No	*Quassia* species	Distribution
1	*Quassia africana*	Africa
2	*Quassia amara*	America
3	*Quassia baileyana*	Oceania
4	*Quassia baileyana*	Oceania
5	*Quassia borneensis*	Asia
6	*Quassia crustacea*	America
7	*Quassia cuneata*	America
8	*Quassia cuspidata*	America
9	*Quassia ferruginea*	Africa
10	*Quassia gabonensis*	Africa
11	*Quassia grandifolia*	Africa
12	*Quassia harmandiana*	Asia
13	*Quassia indica*	Asia
14	*Quassia laevis*	America
15	*Quassia obovata*	America
16	*Quassia schweinfurthii*	Africa
17	*Quassia tulae*	America
18	*Quassia undulata*	Africa
19	*Quassia versicolor*	America

2A.2.1. *Quassia africana*

Quassia africana, a shrub growing 1.2 - 4 metres tall and mainly found in Africa. The leaves and root are bitter in taste and are used as a tonic, appetizer and vermifuge. The different extracts of this plant showed pronounced antiviral activity against Herpes simplex, Semliki forest, Coxsackie and Vesicular stomatitis viruses. In 1985, Luyengi *et*

al., reported the isolation of canthin-6-one, 4,5-dimethoxycanthin-6-one, *β*-carboline- 1-propionic acid and quassin from the roots of *Quassia africana* [Luyengi *et al*.,**1985**]. In 2002, Sandra *et al*., reported the isolation of quassin and simalikalactone D from the root bark of *Quassia africana*. The simalikalactone D also showed promising antiviral activity [Sandra *et al*., **2002**]. **Figure 2A.1** represents the compound isolated from *Quassia africana*.

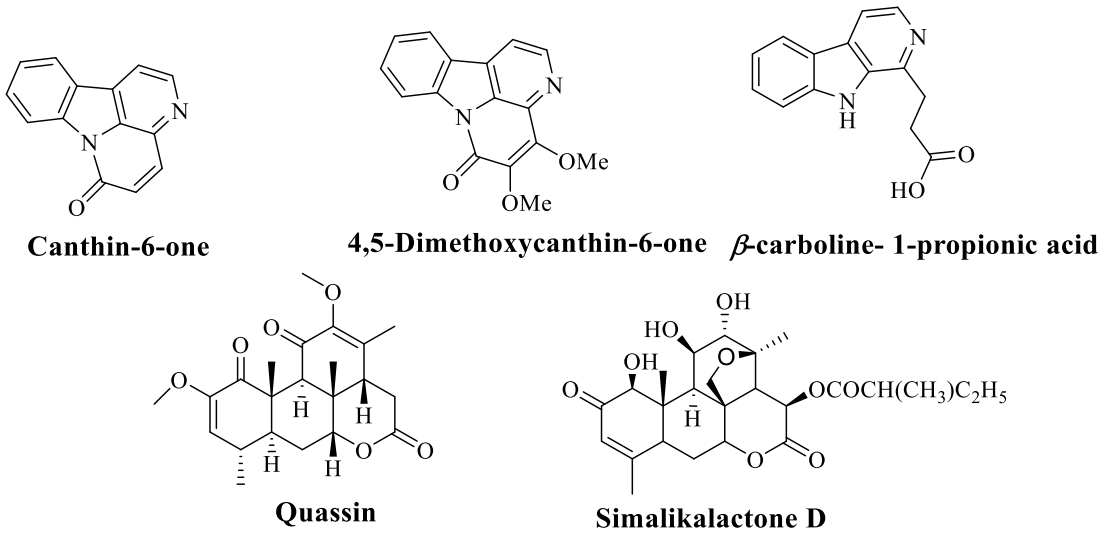

Figure 2A.1. Compounds isolated from *Quassia africana*

2A.2.2. *Quassia amara*

Quassia amara, also known as amargo, bitter-ash, bitter-wood, or hombre grande; mainly found in Americas. Traditionally, plant is used in digestive problems, fever, and hair parasites (lice, fleas) and mosquito larvae in ponds. It is also used as an insecticide and additive in the food industry. Based on the literature reports, the journey of *Quassia amara* started in the year 1976 by Kupchan *et al*. They reported the isolation of antileukemic quassinoid; quassimarin and the companion quassinoid, simalikalactone D from the sap of *Quassia amara* [Kupchan *et al*., **1976**]. Graddlini *et al*., reported the isolation of dihydronor-neoquassin**,** paraine, isoparaine and 4-methoxy-5-hydroxycantin-6-one from the wood of *Quassia amara*. [Graddlini*et al*., **1987**]. Same year, Barbetti *et al*., isolated three *β*-carboline alkaloids namely, 1-vinyl-4,8-dimethoxy- *β* -carboline , 1-methoxycarbonyl- *β*-carboline, and 3-methylcantin-2,6-dione from the wood of *Quassia amara* [Barbetti *et al*., **1987**]. Same group also reported three canthin-6-one alkaloids [3-methyl-4-methoxy-5-hydroxycanthin-2, 6-dione, 4-methoxy-5-hydroxycanthin-6-one-3-*N*-oxide and 3-methylcanthin-5, 6-dione] from the wood of *Quassia amara* [Barbetti *et*

al., **1990**]. Barbetti *et al*., also isolated five quassinoids [11-*α*-*O*-(*β*-D-glucopyranosyl)-16-*α*-*O*-methylneoquassin, 1*α*-*O*-methylneoquassin, 12*α*-hydroxy-13, 18-dehydroparain, 16-*α*-*O*-methylneoquassin and 11-acetylparain] from *Quassia amara* wood [Barbetti *et al*., **1993**]. Vincent *et al*., isolated 2-methoxycanthin-6-one and quassin from the stem

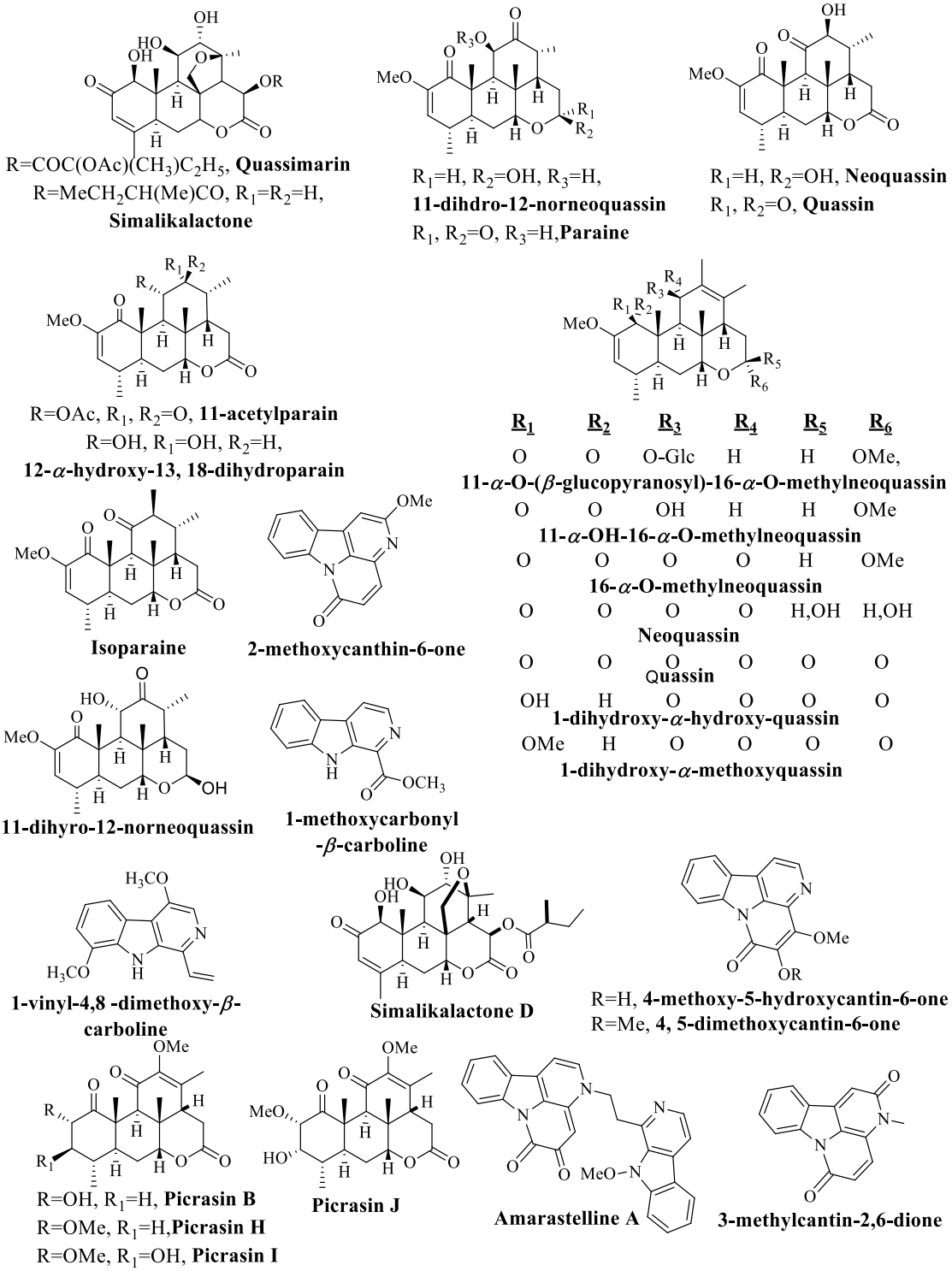

Figure 2A.2. Compounds isolated from *Quassia amara*

wood of *Quassia amara* [Vincent *et al*., **1993**]. In 2009, Emeline *et al*., isolated simalikalactone D, picrasin B, picrasin H, neoquassin, quassin, picrasin and picrasin J from the leaves of *Quassia amara* [Emeline *et al*., **2009**]. Gulam and coworkers reported the antidiabetic activity of standardized extract of *Quassia amara* in Nicotinamide-Streptozotocin-induced diabetic rats [Gulam *et al.,* **2011**]. Amarastelline A, a fluorescent alkaloid was isolated from *Quassia amara* and it exhibited fluorescent properties in the HeLa cell line [Kaori *et al*., **2012**]. The structures of compounds isolated from *Quassia amara* are shown in **Figure 2A.2.**

2A.2.3. *Quassia undulate*

Quassia undulate, commonly known as "Mjoho" and found in tropical Africa. In 2009, Adesanwo *et al*., reported antimicrobial and cytotoxic activity of the stem and root bark extracts of *Quassia undulata* and isolated scopoletin, glaucarubinone and 15-desacetylundulatone from root and stem bark. Eniotorin was found only in root bark [Adesanwo *et al*., **2009**] (**Figure 2A.3**).

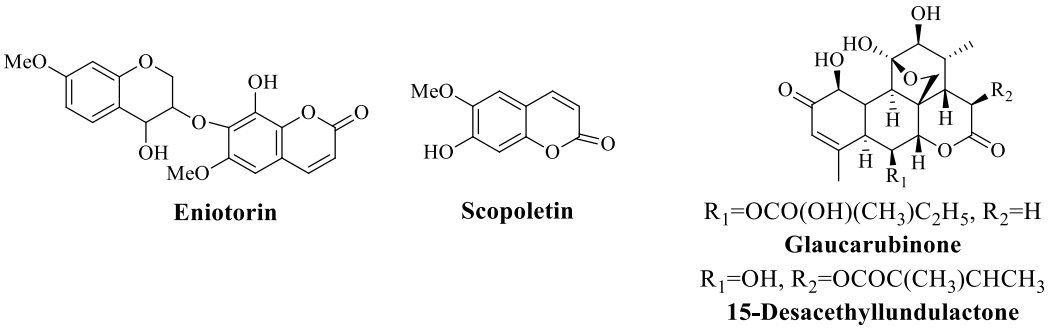

Figure 2A.3. Compounds isolated from *Quassia undulate*

2A.3. Aim and scope of the present investigation

Quassia indica (Gaertn.) Noot. (Synonym: *Samadera indica* Gaetrn.) (**Figure 2A.4**) is a bitter plant, distributed in India. The bitterness is due to the presence of a class of triterpenoids called quassinoids. It belongs to the family Simaroubaceae family the genus *Quassia*. The taxonomic classification of *Quassia indica* is shown in **Table 2A.3**. It is commonly recognized as "Niepia Bark Tree" (English), "Lokhanadi" (Hindi) and "Karinjotta" or "Karinjotta" (Malayalam). It exhibits antitumor, insect antifeedant and growth regulating [Govindachari *et al*., **2005]**, antibacterial [Viswanad *et al*., **2010]**, and antioxidant [Sindhu *et al*., **2015]** activities. In 2003, Kazuo *et al*. reported the isolation of indaquassins A-F, samaderines B-E, dihydrosamaderin B, brucein D, soulameolide, cedronin and canthin-2,6-dione from the bark of *Quassia indica* [Kazuo *et al*., **1993**; Kazuo *et al*.,**1994**]. Later in 1996, Isao *et al.* isolated samaderines X- Z, indaquassin X, 2-

O-glucosylsamaderine C, samaderine B, C and E, indaquassin C and simarinolide from the stems of *Quassia indica*. Samaderines X, Z, E and B have exhibited significant growth-inhibitory activity against the cultured malarial parasite, *Plasmodium falciparum* and some of the compounds also demonstrated *in vitro* cytotoxicity against KB cell lines. Samaderines X, B and C as well as indaquassin X exhibited inhibitory activity on *in vitro* endothelial cell-neutrophil leukocyte adhesion assay, whereas samaderines X and B have exhibited significant anti-inflammatory activity [Isao *et al*., **1996**] (**Figure 2A.5)**. To the best of our knowledge, there are no other reports on the phytochemical and pharmacological evaluation of *Quassia indica* (Gaertn.) Noot. Therefore, it appeared suitable and relevant to carry out the phytochemical and pharmacological investigation of *Quassia indica.* So as part of this Ph.D. program, a detailed phytochemical investigation of *Quassia indica* stem bark and seed was carried out. In the first part of this chapter, the ethanol extract of *Quassia indica* was subjected to repeated column chromatographic purification, which led to the isolation of eight quassinoids. It included two novel compounds with no previous reports from any natural resources along with six known quassinoids. All quassinoids were tested for their *in vitro* and *in silico* inhibitory activities on digestive enzymes (α-amylase and α-glucosidase), delaying of AGEs formation and glucose uptake in L6 myotubes.

Figure 2A.4. *Quassia indica* (Gaertn.) Nooteboom

Table 2A.3. Scientific classification of *Quassia indica*

Kingdom	Plantae
Order	Magnoliopsida
Family	Simaroubaceae
Genus	*Quassia*
Species	*Q. indica*
Binomial name	*Quassia indica* (Gaertn.) Nooteboom

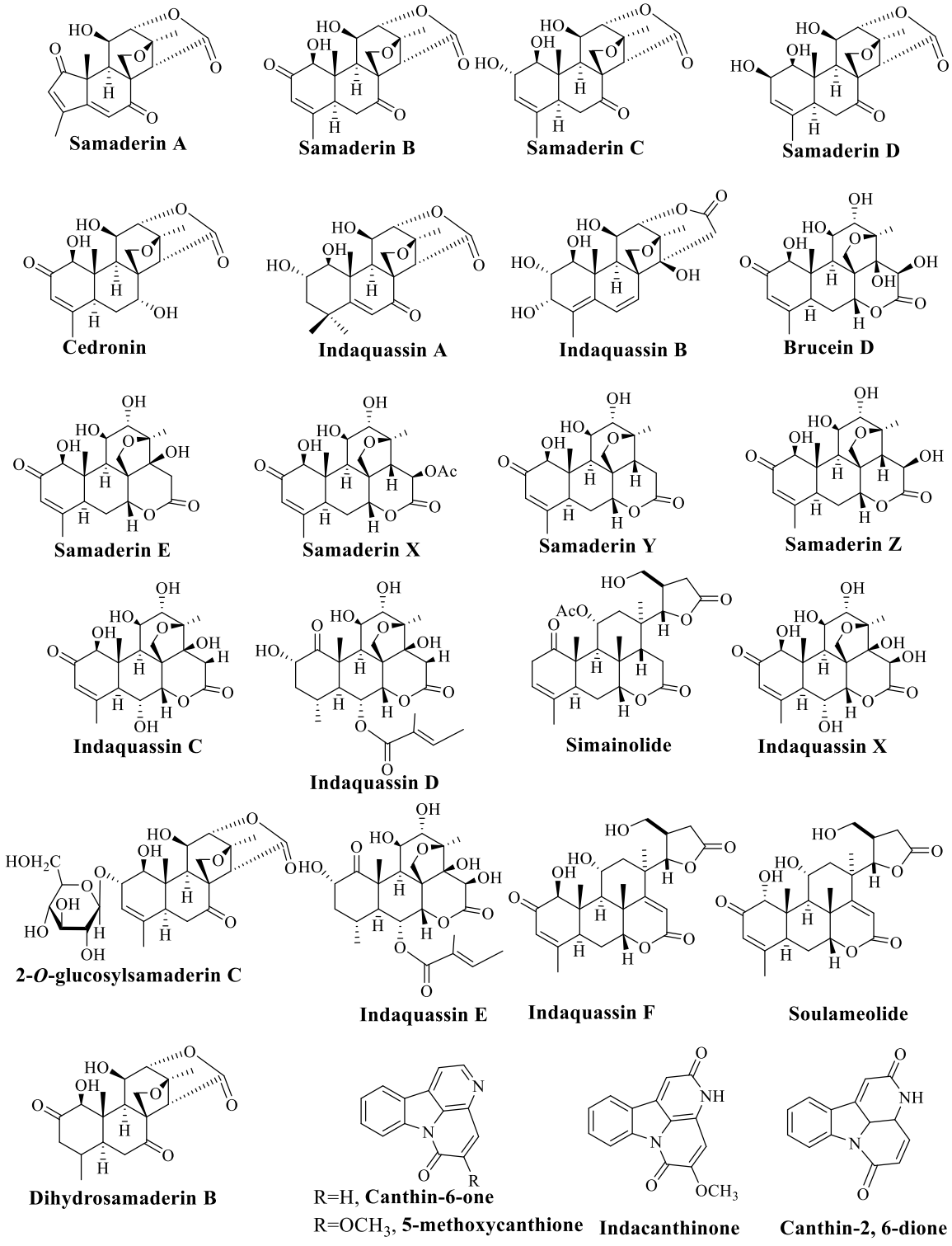

Figure 2A.5. Compounds isolated from *Quassia indica*

2A.4. Plant material collection, extraction, bio guided isolation and characterization of compounds from *Quassia indica* seed

2A.4.1. Plant material

The seeds of *Quassia indica* (300 g) were collected from Alappuzha district, Kerala, India in October 2017, and identified by plant taxonomist of Jawaharlal Nehru Tropical Botanic Garden and Research Institute, Palode, Kerala, India and a voucher specimen (**TBGT 81765**) is deposited in the Herbarium of repository of Jawaharlal Nehru Tropical Botanic Garden and Research Institute, Palode, Kerala, India.

2A.4.2. Extraction, bio guided isolation and characterization of compounds

Air and oven-dried seeds of *Quassia indica* (300 g) were milled and extracted successively with *n*-hexane (1 L x 48 h x 3 times; 65 g), acetone (1 L x 48 h x 3 times; 35 g), EtOH (1 L x 48 h x 3 times; 28 g) and water (1 L x 48 h x 3 times; 12 g). All extracts were checked for their *in vitro* antidiabetic activities on digestive enzymes as well as for their antiglycation properties. The results were shown in **Table 2A.4**. The ethanol extract has promising inhibitory activity on carbohydrate hydrolyzing enzyme and antiglycation property. Therefore, further isolation and purification were focused on ethanol extract.

Table 2A.4. Extract level *in vitro* antidiabetic studies of the seeds of *Quassia indica*

Extracts	*α*-Amylase (*μ*g/mL)	*α*-Glucosidase (*μ*g/mL)	Antiglycation (*μ*g/mL)
Hexane	196.44 ± 0.453	45.14 ± 0.353	274.13 ± 0.567
Acetone	208.73 ± 0.231	48.51 ± 0.487	309.67 ± 0.478
Ethanol	**160.03 ± 0.435**	**15.65 ± 0.699**	**279.04 ± 0.126**
Water	563.34 ± 0.146	41.02 ± 0.765	373.75 ± 0.654
Acarbose	5.53 ± 0.367	45.37 ± 0.681	-
Ascorbic acid	-	-	48 ± 0.876

Each value represents mean ± SD (standard deviation) from triplicate measurements

An aliquot of ethanol extract (25 g) was subjected to column chromatographic separation on 100-200 mesh sized silica gel and eluted with the increasing order of *n*-hexane, *n*-hexane/ethyl acetate, ethyl acetate and ethyl acetate/methanol polarity mixtures resulted in 18 fraction pools after analysing the thin layer chromatography (TLC).

The fraction pool 6 was again subjected to column chromatographic separation using 100-200 mesh sized silica gel with *n*-hexane/ethyl acetate polarities resulting in the isolation of compound **1**. It was obtained as a colourless solid and showed a molecular ion peak at m/z 331.1191 $[M+H]^+$ (calcd. for $C_{18}H_{19}O_6$, 331.1182) in the HRESIMS, and the molecular formula was established as $C_{18}H_{18}O_6$. IR absorptions at 3410 and 1760 cm^{-1} revealed the presence of hydroxyl and lactone moieties, respectively. The 1D and 2D NMR spectra are shown in **Figure 2A.6-11**. The ^1H NMR spectrum of compound **1** displayed the presence of three methyl groups at δ_H 1.60 (s), 1.73 (s) and 2.23 (d, J = 1.5 Hz) ppm, oxymethine proton signals at δ_H 4.82 ppm [H-11 and H-30b resonances are superimposed; the H-11 multiplicity could not be determined], oxymethylene proton at δ_H 4.82 (d, J = 9 Hz, 1H) and 4.16 (dd, J_1 = 9 Hz, J_2 = 1.5 Hz, 1H) ppm, olefinic proton at δ_H 6.24 (d, J = 1 Hz, 1H) and 6.02 (s, 1H) ppm. The ^{13}C NMR spectrum of compound **1** displayed the presence of 18 carbon atoms was ascertained with the carbon signals at δ_C 203.5 and 193.8 ppm assigned to two carbonyl groups, δ_C 171.1 ppm to a lactone, δ_C 134.1 (CH), 163.3 (C); δ_C 116.8 (CH) and 168.8 (C) ppm to two trisubstituted double bonds, δ_C 76.1 ppm to an oxymethylene, δ_C 69.0 and 81.8 ppm to two oxymethine, δ_C 89.2 ppm to a fully substituted carbon and δ_C 21.4, 20.9 and 13.7 ppm to three methyl groups. In comparison with previously reported spectroscopic data [Philip *et al*., **2005**] and single crystal X-ray analysis (**Figure 2A.12**) the compound **1** was confirmed as C18 type quassinoid, samaderin A. The structure of the same is shown below.

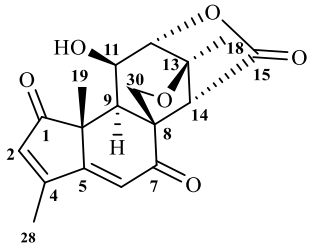

Samaderin A (1)

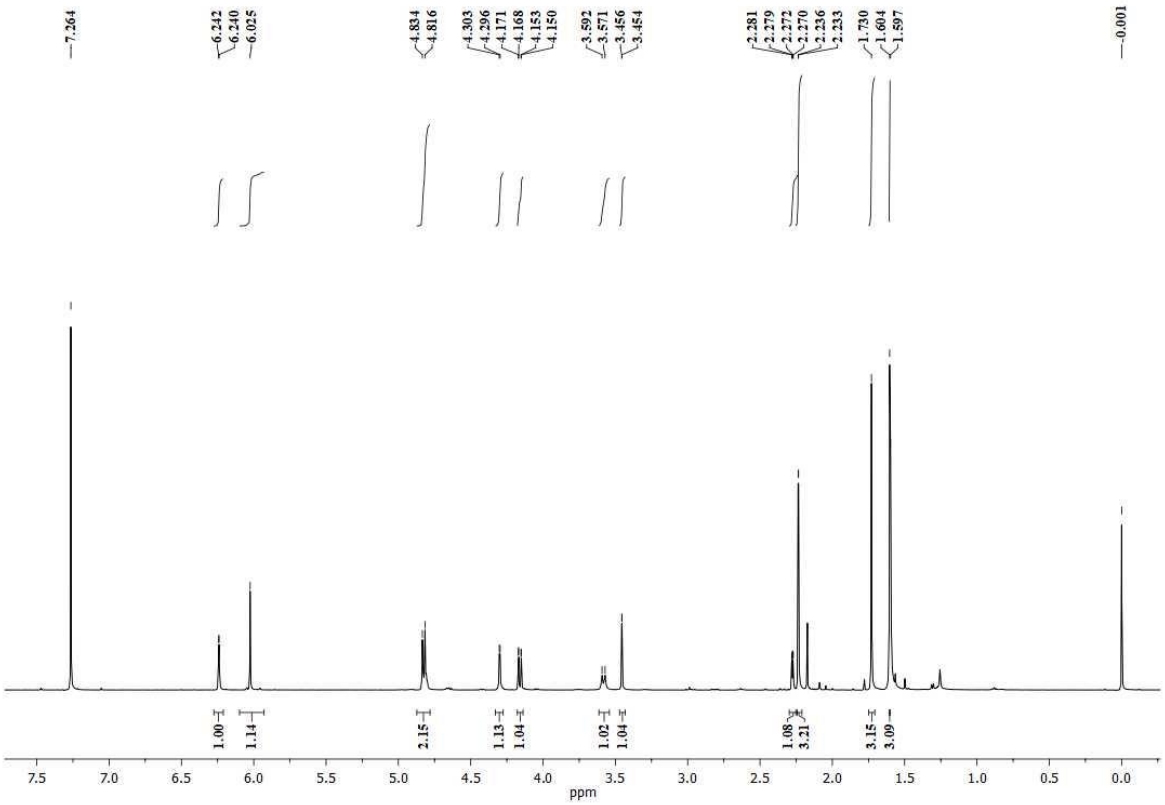

Figure 2A.6. ^{1}H NMR spectrum (500 MHz, $CDCl_3$) of samaderin A (**1**)

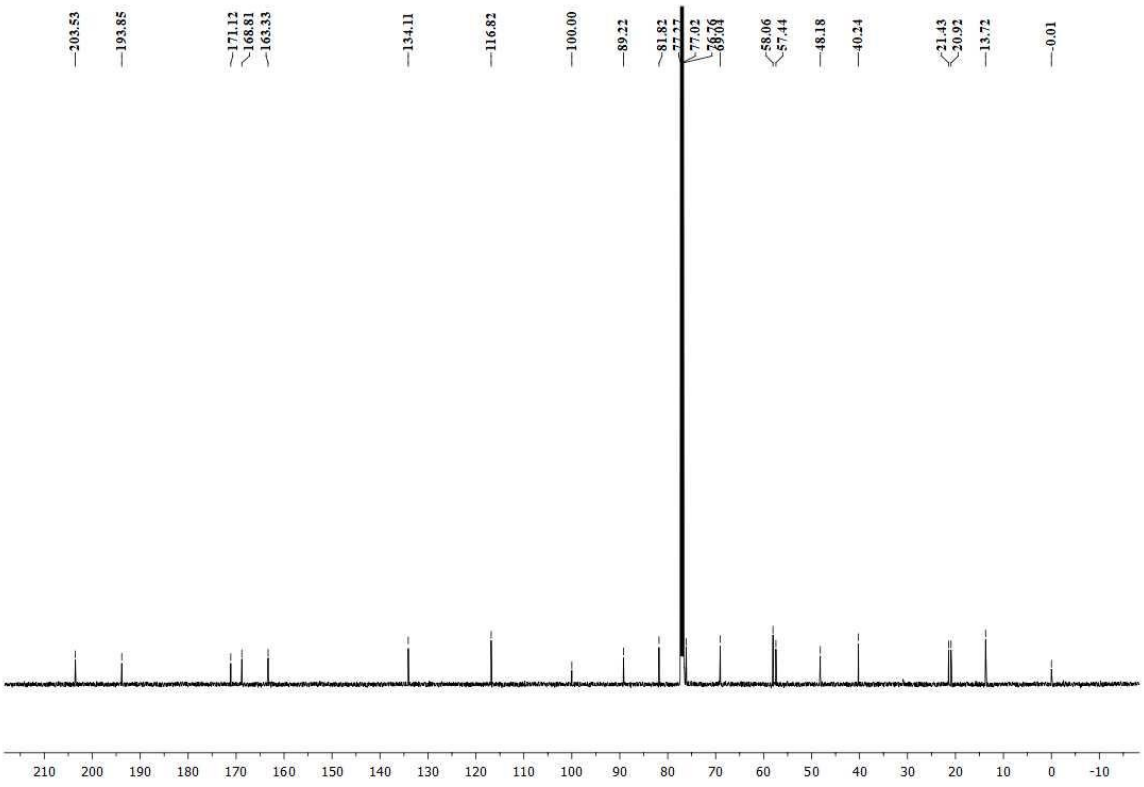

Figure 2A.7. ^{13}C NMR spectrum (125 MHz, $CDCl_3$) of samaderin A (**1**)

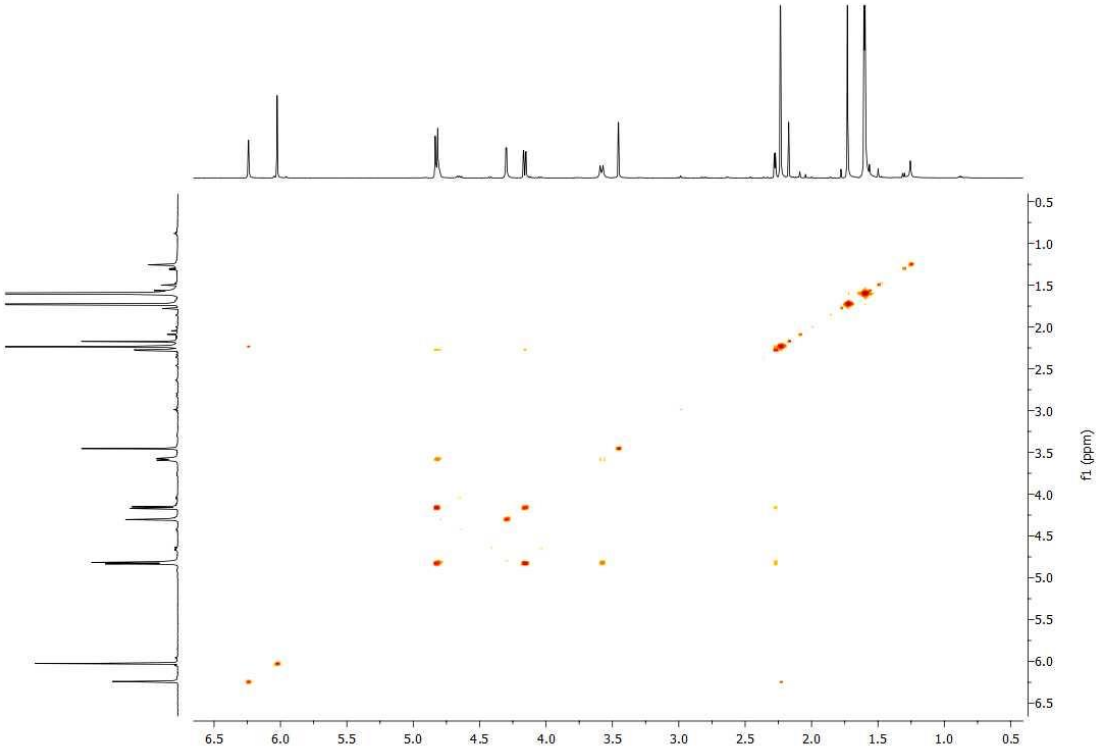

Figure 2A.8. ^{1}H-^{1}H COSY NMR spectrum (500 MHz, $CDCl_3$) of samaderin A (**1**)

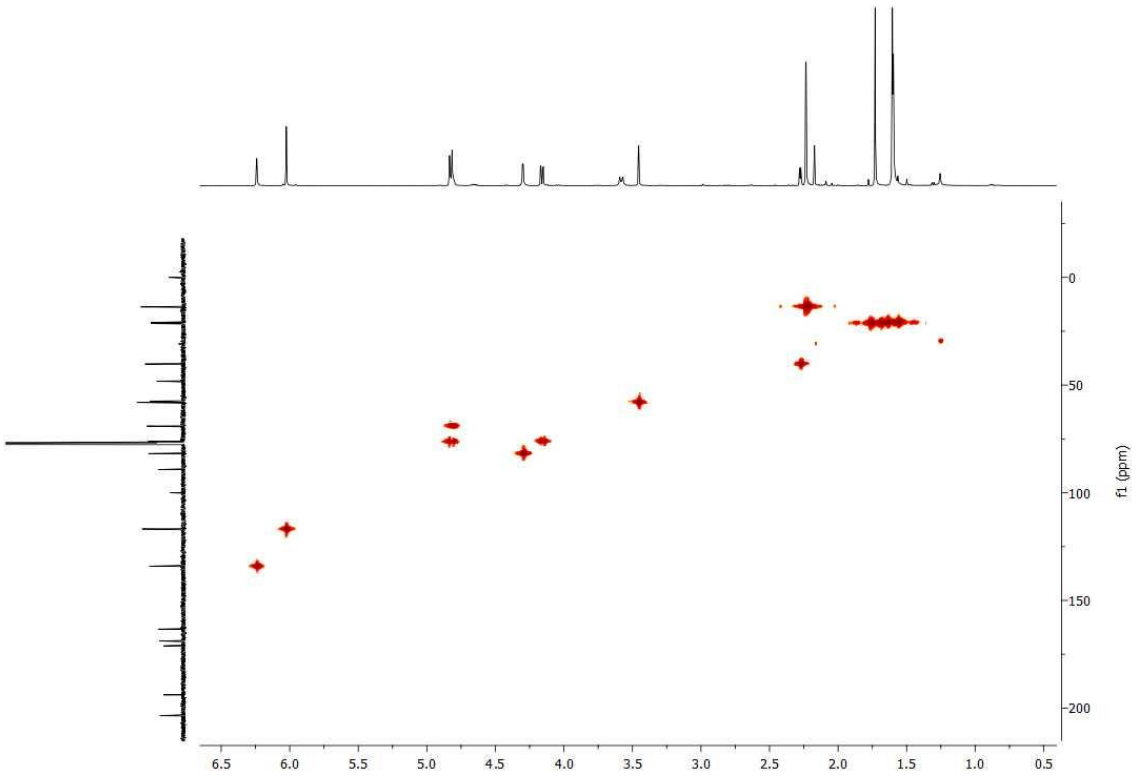

Figure 2A.9. HMQC NMR spectrum (125 MHz, $CDCl_3$) of samaderin A (**1**)

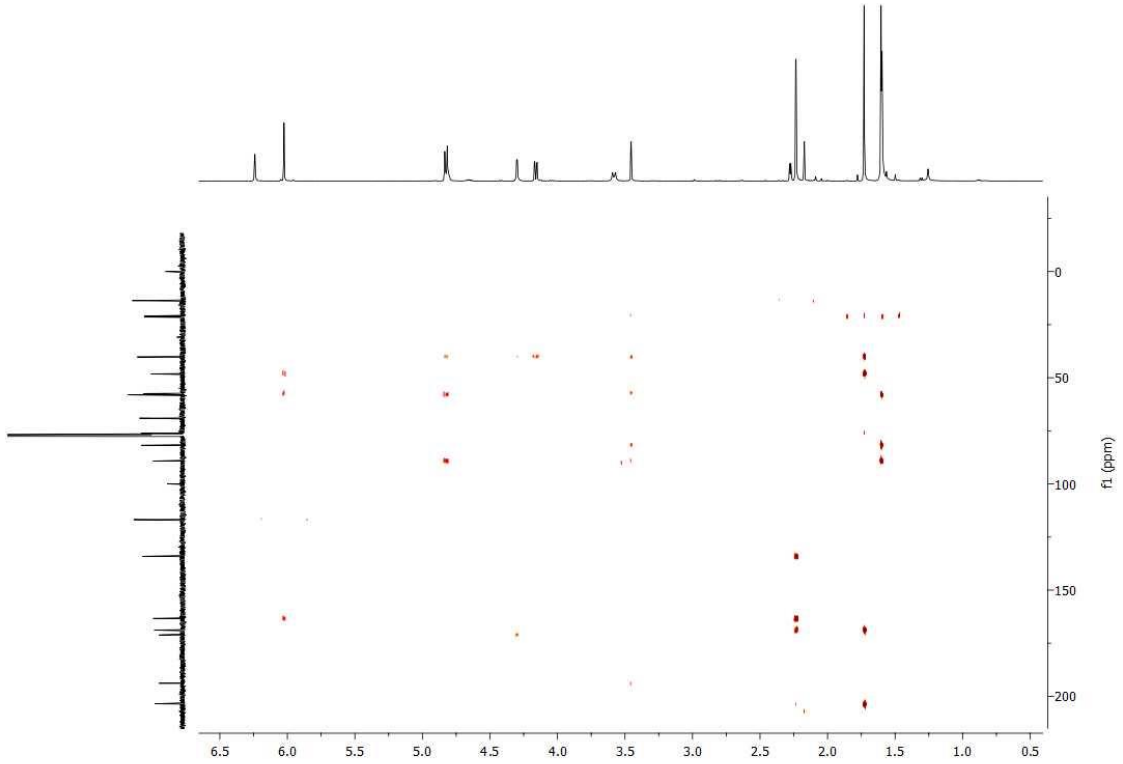

Figure 2A.10. HMBC spectrum (125 MHz, $CDCl_3$) of samaderin A (**1**)

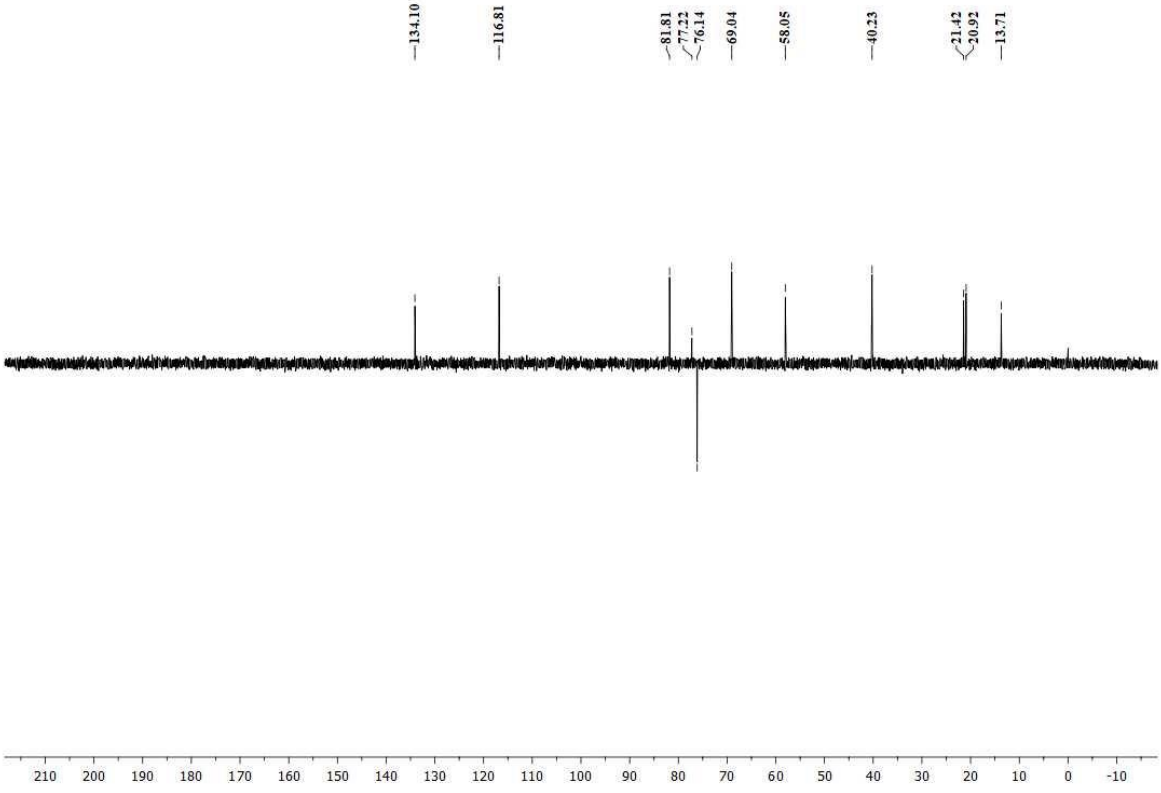

Figure 2A.11. DEPT 135 spectrum (125 MHz, $CDCl_3$) of samaderin A (**1**)

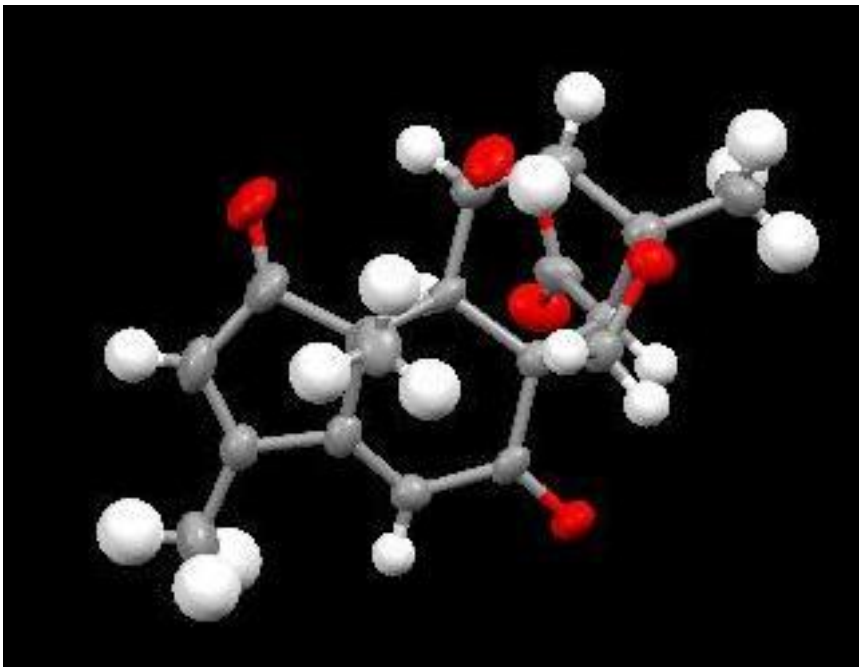

Figure 2A.12. Single crystal X-ray analysis of samaderin A (**1**)

Fraction pool 8 was subjected to column chromatographic separation using 100-200 mesh sized silica gel with *n*-hexane-ethyl acetate polarities resulting in the isolation of compound **2**. Compound **2** was obtained as colourless crystalline solid and showed a molecular ion peak at m/z 363.1448 $[M+H]^+$ (calcd. for $C_{19}H_{23}O_7$, 363.1444) in the HRESIMS, and the molecular formula was established as $C_{19}H_{22}O_7$. IR absorptions at 3380 and 1768 cm^{-1} revealed the presence of a hydroxyl and a carbonyl lactone, respectively. The 1D and 2D NMR spectra are shown in **Figure 2A.13-17**. The ^1H NMR spectrum of compound **2** exhibited the presence of olefinic proton signals at δ_H 5.99 (d, J = 1 Hz) ppm, three oxymethine proton signals at δ_H 4.63 (m), 4.27 (d, J = 3.5 Hz) and 4.23 (d, J = 2.5 Hz) ppm, a oxymethylene proton at δ_H 4.82 (d, J = 9 Hz) and 4.16 (dd, J_1 = 9 Hz, J_2 = 1.5 Hz) ppm, three methine signals at δ_H 3.47 (d, J = 1 Hz), 3.07 (d, J = 3.5 Hz) and 2.12 (d, J = 3.5 Hz) ppm and three methyl singlets at δ_H 1.9, 1.4 and 1.2 ppm. From the ^{13}C NMR spectrum of compound **2**, the presence of 19 carbon atoms was ascertained with the carbon signals at δ_C 83.6, 80.9 and 69.5 ppm assigned to three oxymethines, δ_C 55.3, 48.5 and 46.3 ppm to three sp^3 methines, δ_C 124.2 ppm to sp^2 methines, δ_C 205.0 ppm to carbonyl group, δ_C 197.7 ppm to α, β-unsaturated carbonyl moiety, δ_C 171.9 ppm to a lactone carbonyl, δ_C 74.6 ppm to an oxygenated quaternary carbon, δ_C 60.4 and 46.7 ppm to two sp^3 quaternary carbons, and δ_C 21.4, 20.4 and 9.9 ppm to three methyls. In comparison with previously reported spectroscopic data [Philip

et al., **2005**] and single crystal X-ray analysis (**Figure 2A.18**) the compound **2** was identified as a C19 type quassinoid, samaderin B. The structure of samaderin B is shown below.

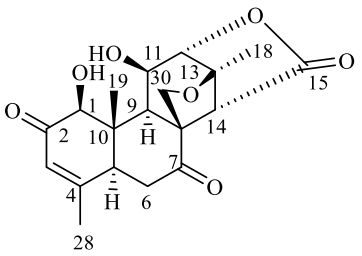

Samaderin B (2)

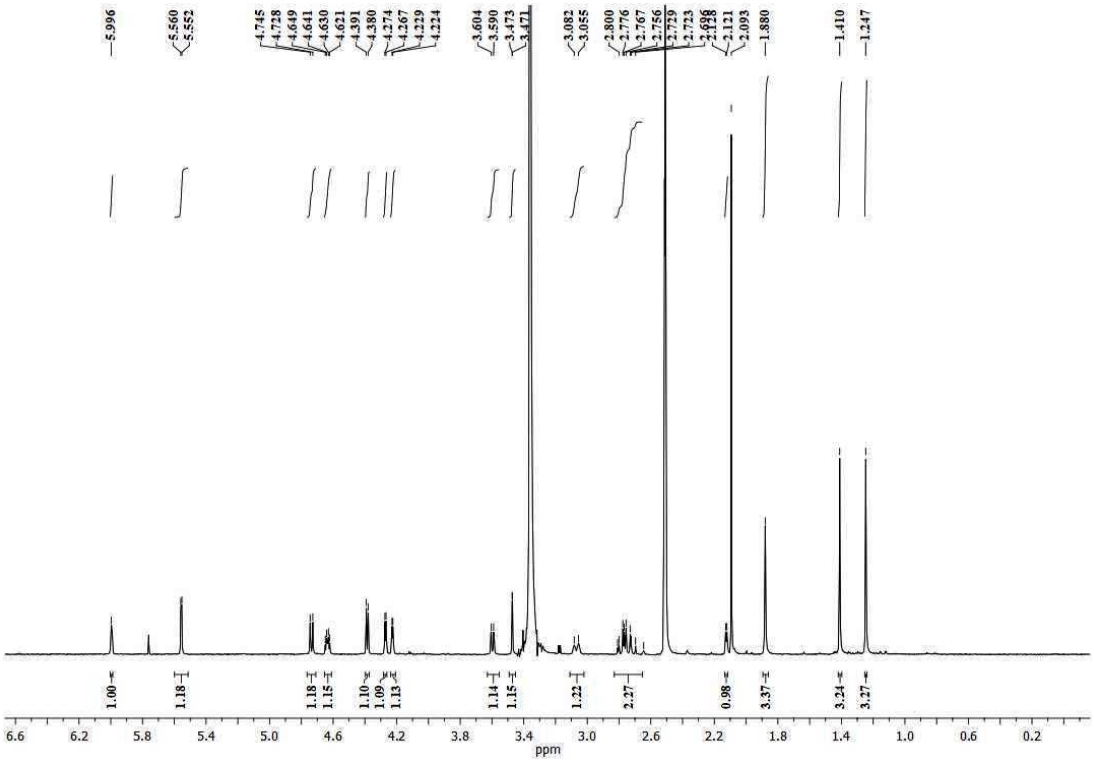

Figure 2A.13. ^{1}H NMR spectrum (500 MHz, DMSO-d_6) of samaderin B (**2**)

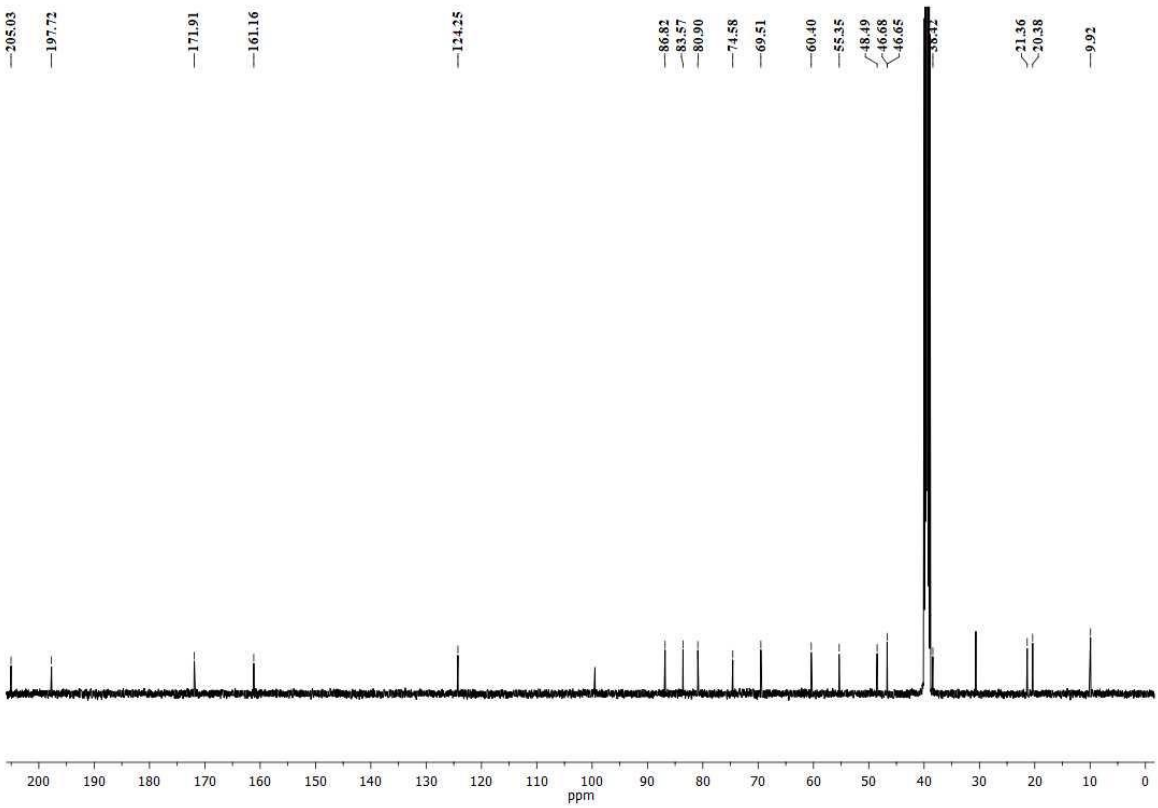

Figure 2A.14. ^{13}C NMR spectrum (125 MHz, DMSO-d_6) of samaderin B (**2**)

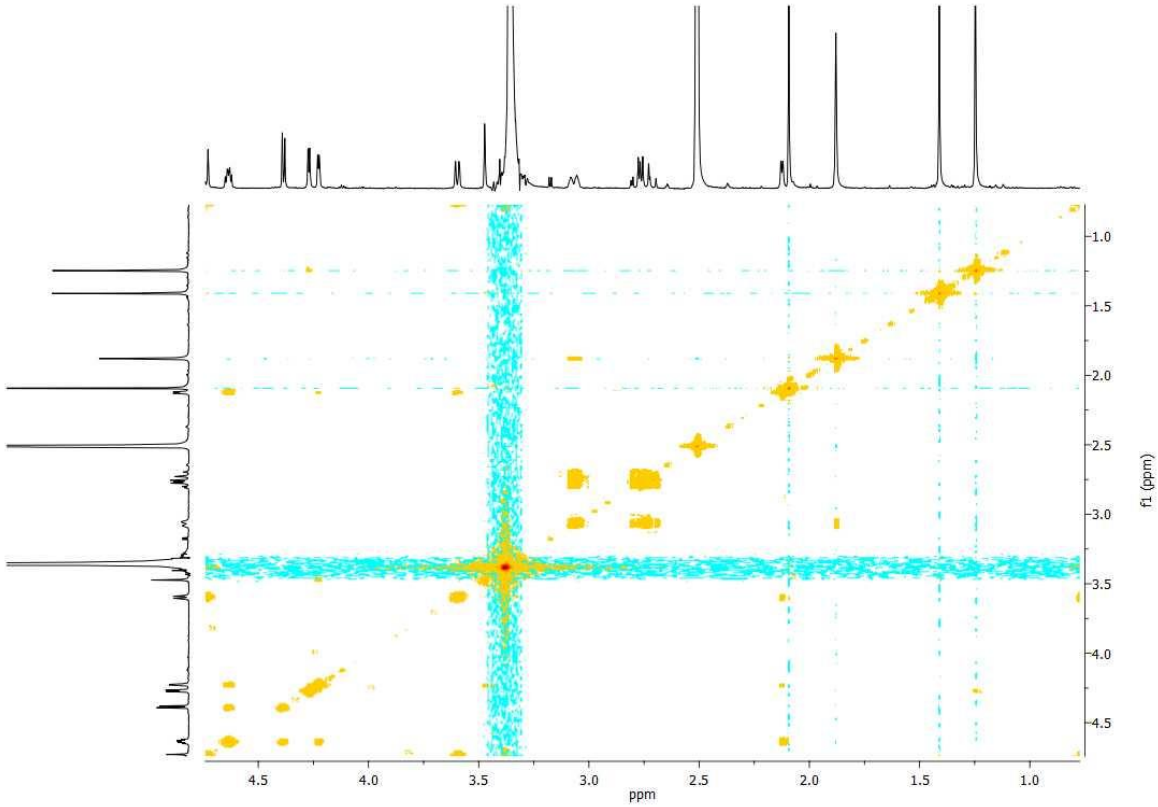

Figure 2A.15. ^{1}H-^{1}H COSY NMR spectrum (500 MHz, DMSO-d_6) of samaderin B (**2**)

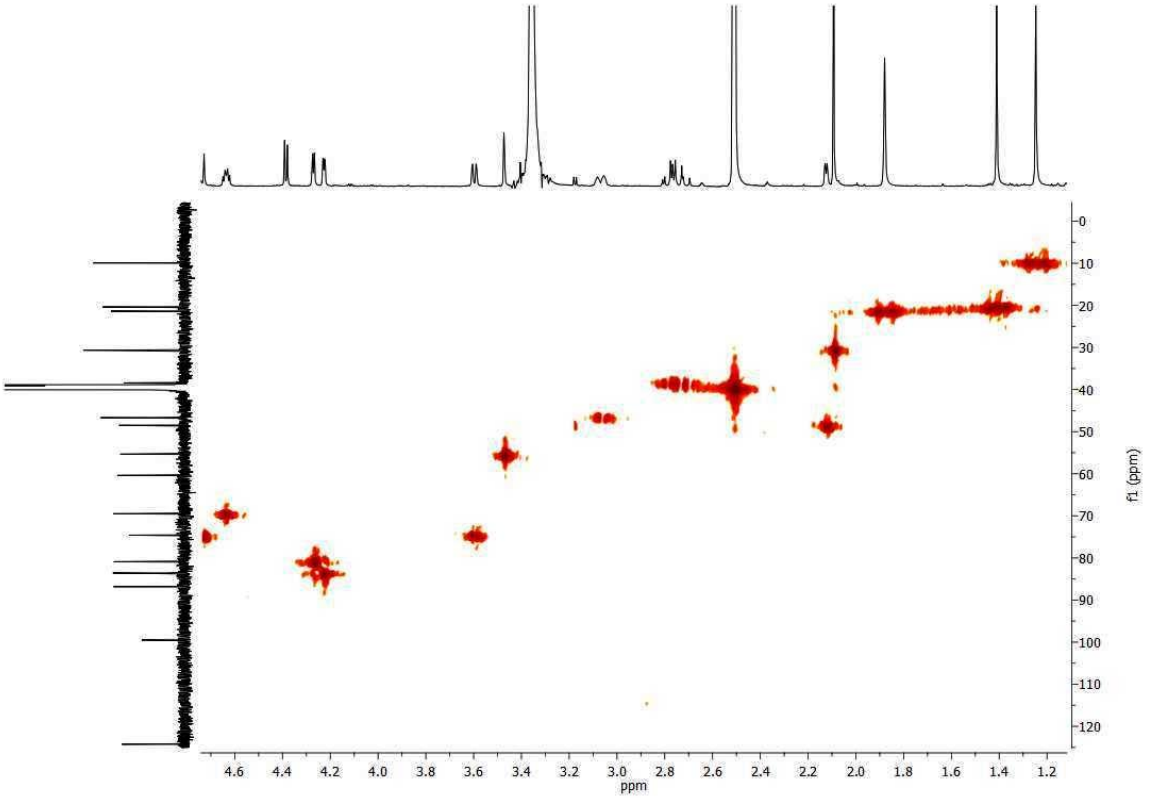

Figure 2A.16. HMQC NMR spectrum (125 MHz, DMSO-d_6) of samaderin B (**2**)

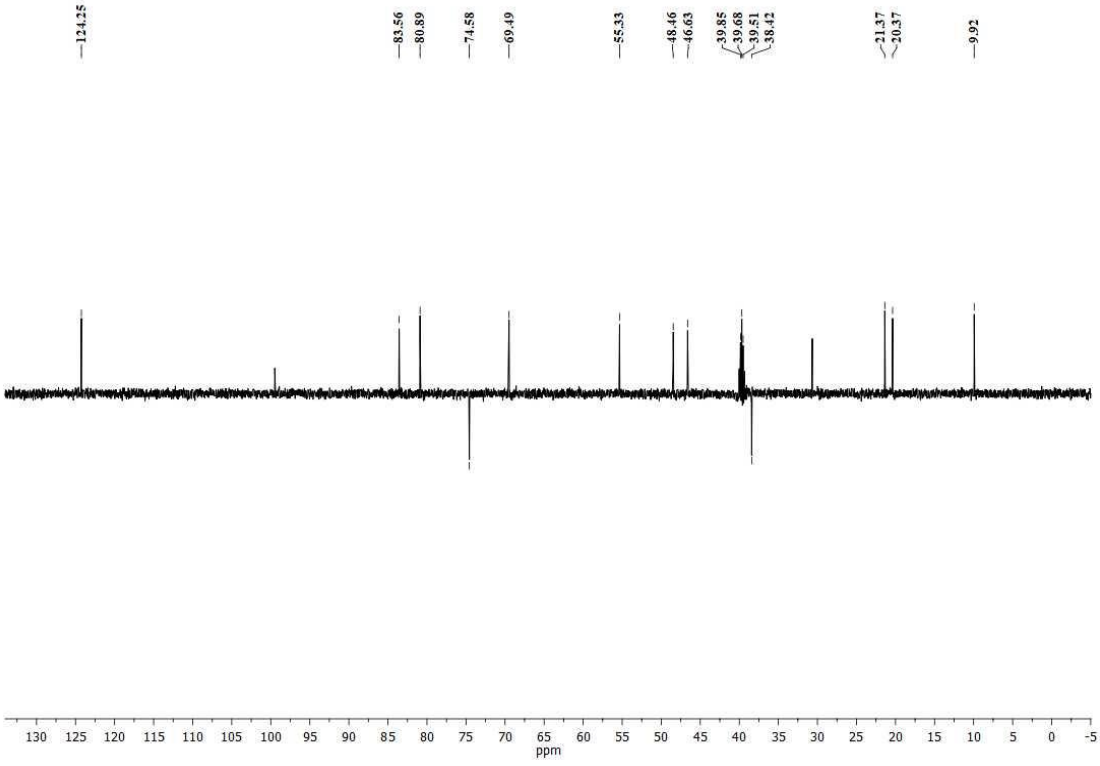

Figure 2A.17. DEPT 135spectrum (125 MHz, DMSO-d_6) of samaderin B (**2**)

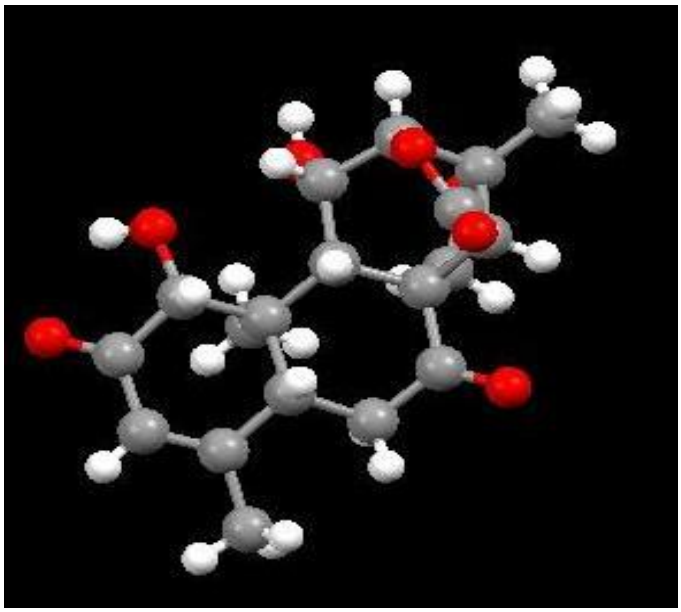

Figure 2A.18. Single crystal X-ray analysis of samaderin B (**2**)

The fraction pool 10 was subjected to column chromatographic separation using 100-200 mesh sized silica gel with *n*-hexane-ethyl acetate polarities resulted in the isolation of compound **3** and compound **4**. The compound **3** was obtained as a colourless crystalline solid and showed a molecular ion peak at m/z 365.1670 $[M+H]^+$ (calcd. for $C_{19}H_{25}O_7$, 365.1600) in the HRESIMS, and the molecular formula was established as $C_{19}H_{24}O_7$. IR absorptions at 3415 and 1770 cm^{-1} revealed the presence of a hydroxyl and a carbonyl lactone, respectively. The 1D and 2D NMR spectra are shown in **Figure 2A.19-25**. The ^1H NMR spectrum of compound **3** displayed the presence of hydroxyl group at δ_H 4.35 (d, J = 3.5 Hz) and 3.65 (brs) ppm, three oxymethine proton signals at δ_H 4.64 (dd, J_1 = 10 Hz, J_2 = 7 Hz), 4.30 (dd, J_1 = 3.5 Hz, J_2 = 1 Hz) and 4.13 (d, J = 2.5 Hz), oxymethylene proton at δ_H 3.77 (dd, J_1 = 8.5 Hz, J_2 = 1.5 Hz) and 4.72 (d, J = 8 Hz) ppm, four methine signals at δ_H 3.64 (d, J = 1 Hz), 2.44 (m), 2.34 (m) and 2.02 (dd, J_1 = 4.5 Hz, J_2 = 1 Hz) ppm and three methyl signals at δ_H 1.56 (s), 1.36 (s) and 0.97 (d, J = 8 Hz) ppm. From the ^{13}C NMR spectrum of compound **3**, the presence of 19 carbon atoms was ascertained with the carbon signals at δ_C 83.7, 81.9 and 70.3 ppm to three oxymethines, δ_C 74.4 ppm to oxymethylene carbon, δ_C 55.6, 50.6, 45.1 and 35.7 ppm to four sp^3 methines, δ_C 208.6 and 204.0 ppm to carbonyl group, δ_C 171.9 ppm to a lactone carbonyl, δ_C 74.4 ppm to an oxygenated quaternary carbon, δ_C 87.6 and 60.7 ppm to two sp^3 quaternary carbons, and δ_C 20.8, 15.4 and 13.9 ppm to three methyls. By comparison with previously reported spectroscopic data [Kazuo *et al.*,**1994**] and single crystal X-ray

analysis (**Figure 2A.26**) the compound **3** was C19 type quassinoid, dihydrosamaderin B. The structure of dihydrosamaderin B is shown below.

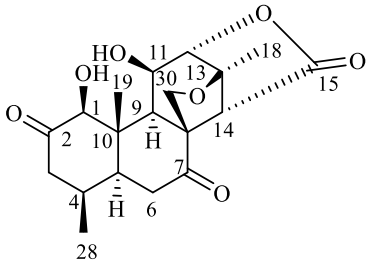

Dihydrosamaderin B (3)

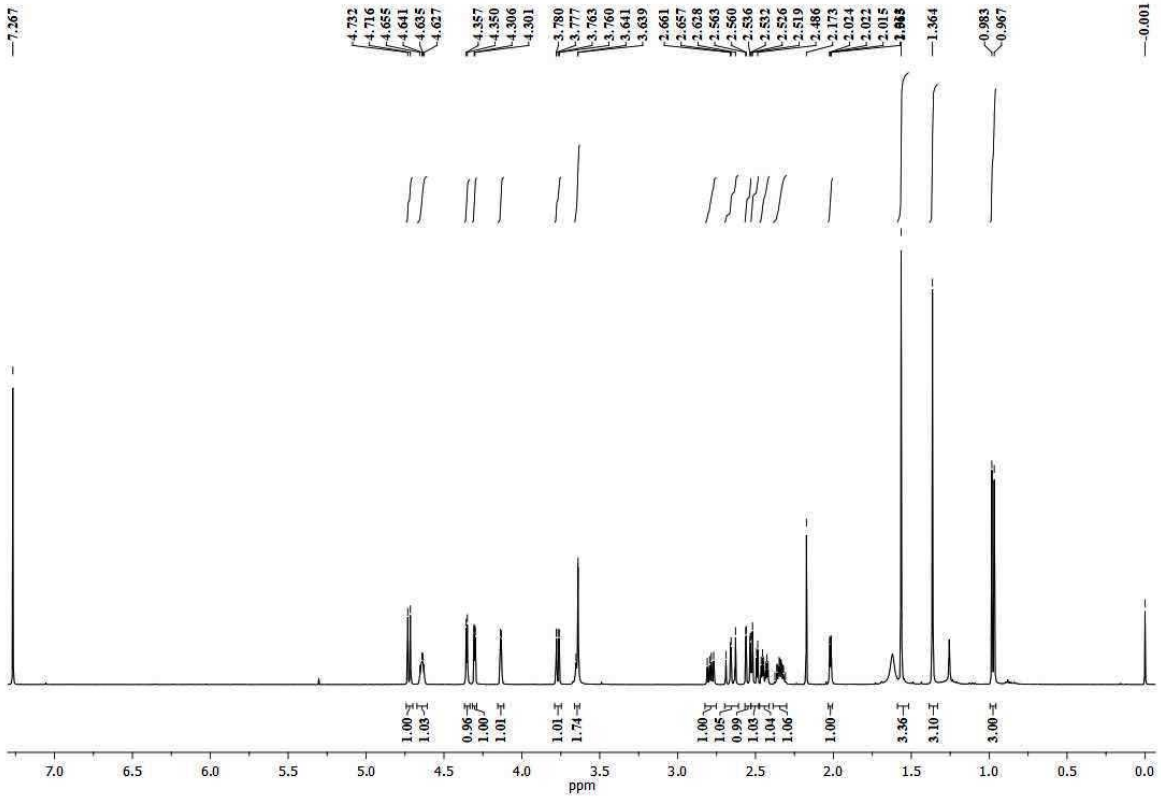

Figure 2A.19. ^{1}H NMR spectrum (500 MHz, $CDCl_3$) of dihydrosamaderin B (**3**)

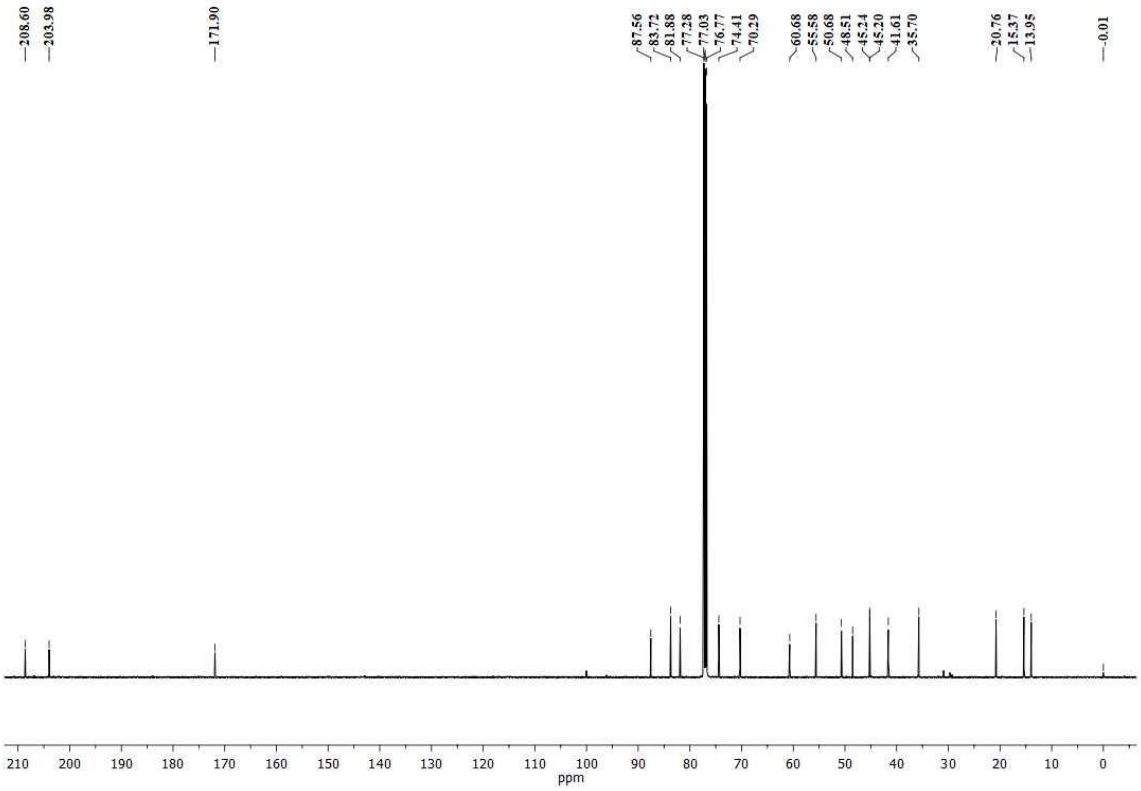

Figure 2A.20. ^{13}C NMR spectrum (125 MHz, $CDCl_3$) of dihydrosamaderin B (**3**)

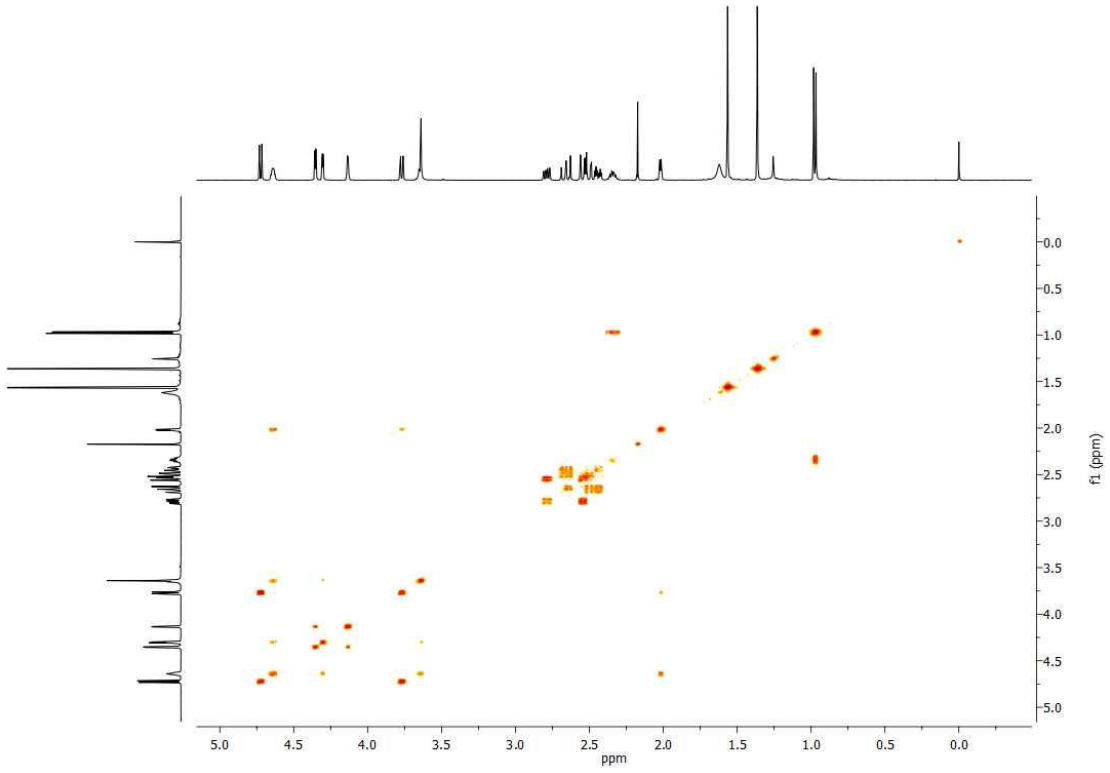

Figure 2A.21. ^{1}H-^{1}H COSY NMR spectrum (500 MHz, $CDCl_3$) of dihydrosamaderin B (**3**)

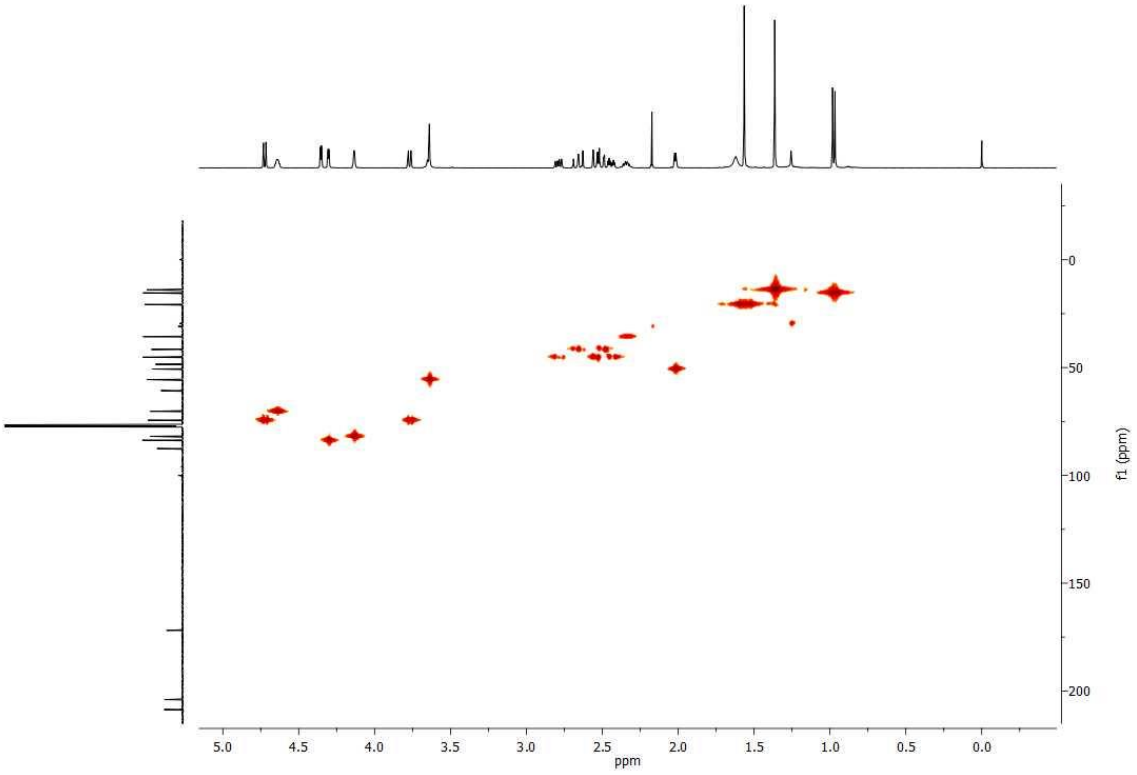

Figure 2A.22. HMQC NMR spectrum (125 MHz, $CDCl_3$) of dihydrosamaderin B (**3**)

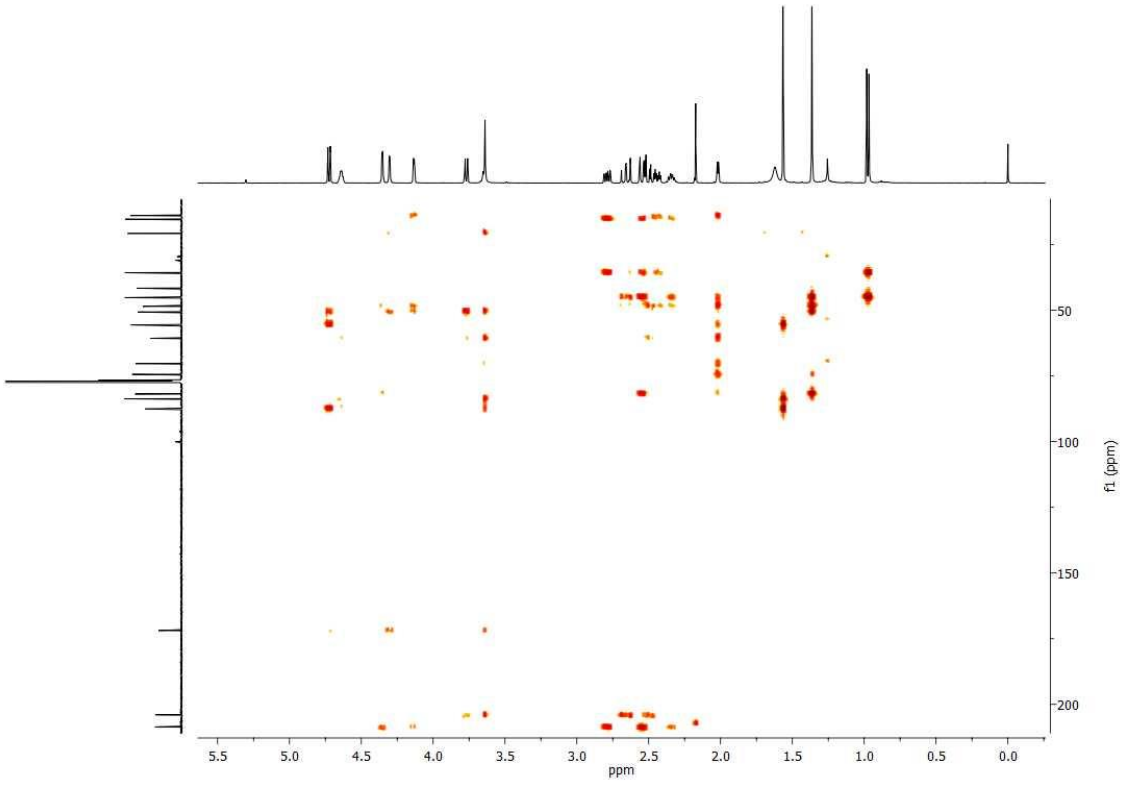

Figure 2A.23. HMBC spectrum (125 MHz, $CDCl_3$) of dihydrosamaderin B (**3**)

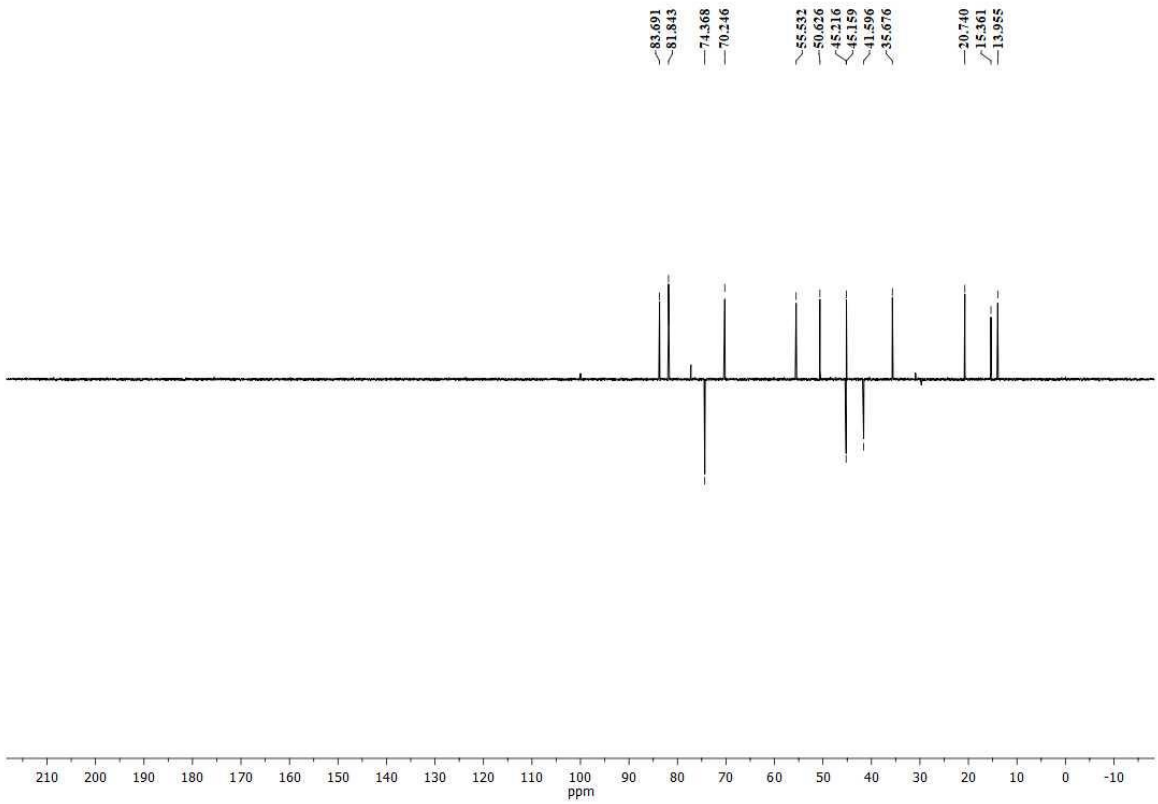

Figure 2A.24. DEPT 135 spectrum (125 MHz, $CDCl_3$) of dihydrosamaderin B (**3**)

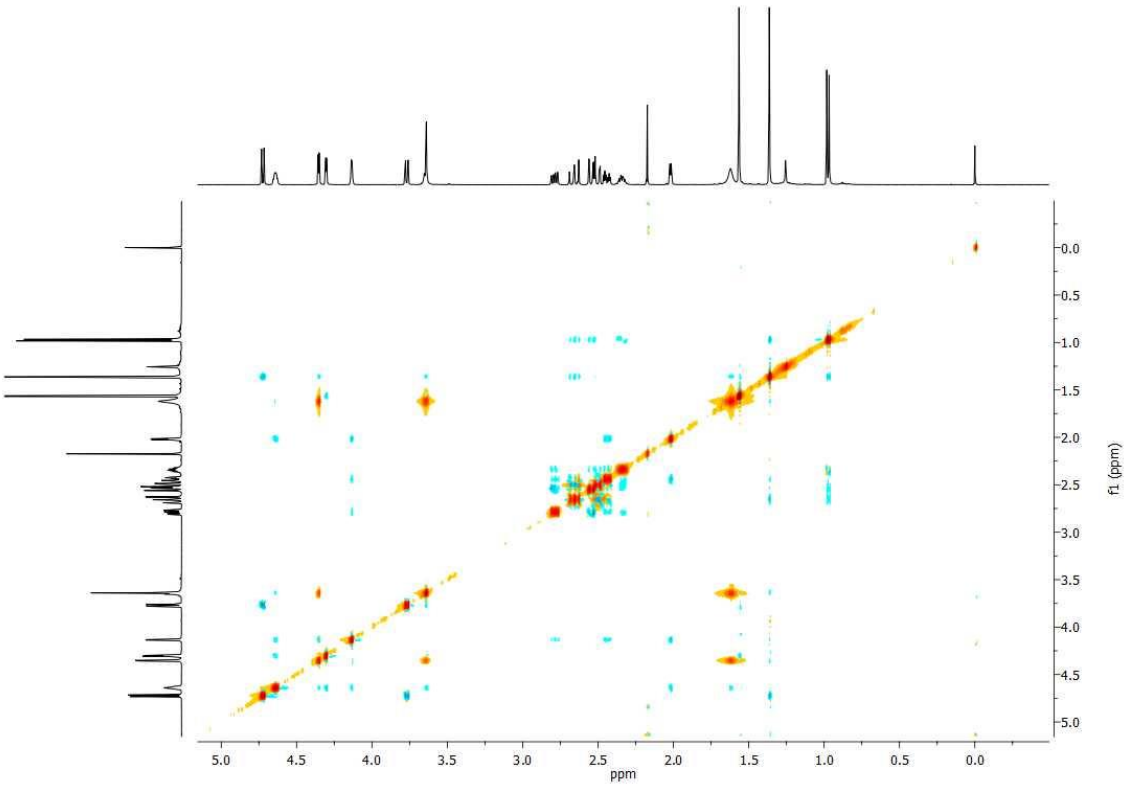

Figure 2A.25. NOESY spectrum (500 MHz, $CDCl_3$) of dihydrosamaderin B (**3**)

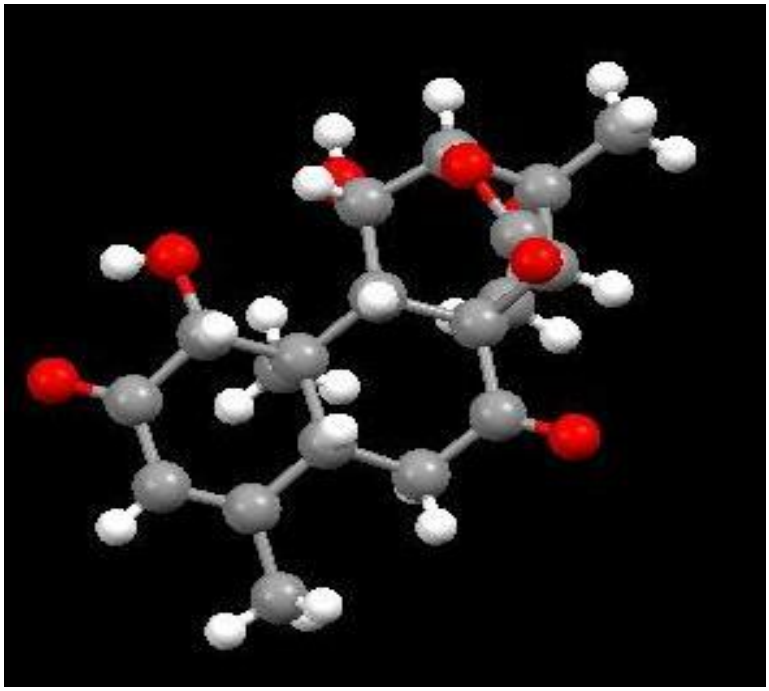

Figure 2A.26. Single crystal X-ray analysis of dihydrosamaderin B (**3**)

Compound **4** was also obtained as a colourless crystalline solid and displayed a molecular ion peak at m/z 365.1610 $[M+H]^+$ (calcd. for $C_{19}H_{25}O_7$, 367.1600) in the HRESIMS, and the molecular formula was established as $C_{19}H_{24}O_7$. IR absorptions at 3400 and 1771 cm^{-1} revealed the presence of a hydroxyl and carbonyl lactone moieties. The 1D and 2D NMR spectra are shown in **Figure 2A.27-31**. The ^1H NMR spectrum of compound **4** exhibited the presence of olefinic proton signal at δ_H 5.67 (d, J = 4.5 Hz) ppm, a oxymethylene proton signals at δ_H 4.66 (dd, J_1 = 9 Hz, J_2 = 5 Hz) and 3.59 (d, J = 8.5 Hz) ppm, three methine signals at δ_H 3.43 (s), 2.55 (t, J = 4.5 Hz), 2.35 (d, J = 13 Hz) ppm and three methyl singlets at δ_H 1.5, 1.4 and 1.3 ppm. From the ^{13}C NMR spectrum of compound **4**, the presence of 19 carbon atoms was established with the carbon signals at δ_C 73.6, 67.4, 76.1, 76.0 and 87.0 ppm assigned to five oxymethines, δ_C 56.0, 43.2, 52.1 and 27.8 ppm to four sp^3 methines, δ_C 125.7 and 132.4 ppm to two sp^2 methines, δ_C 172.2 ppm to lactone moiety and δ_C 20.4, 20.1 and 10.3 ppm to three methyls. By comparison with previously reported spectroscopic data [Isao *et al*., **1996**] and single crystal X-ray analysis (**Figure 2A.32**) the compound **4** was samaderin C. Samaderin C is also C19 type quassinoid and the structure is shown below.

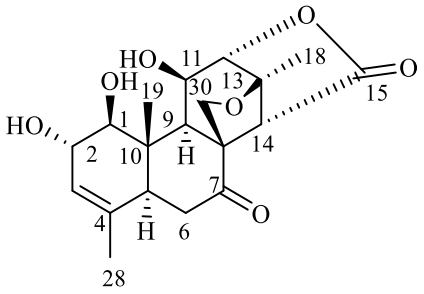

Samaderin C (4)

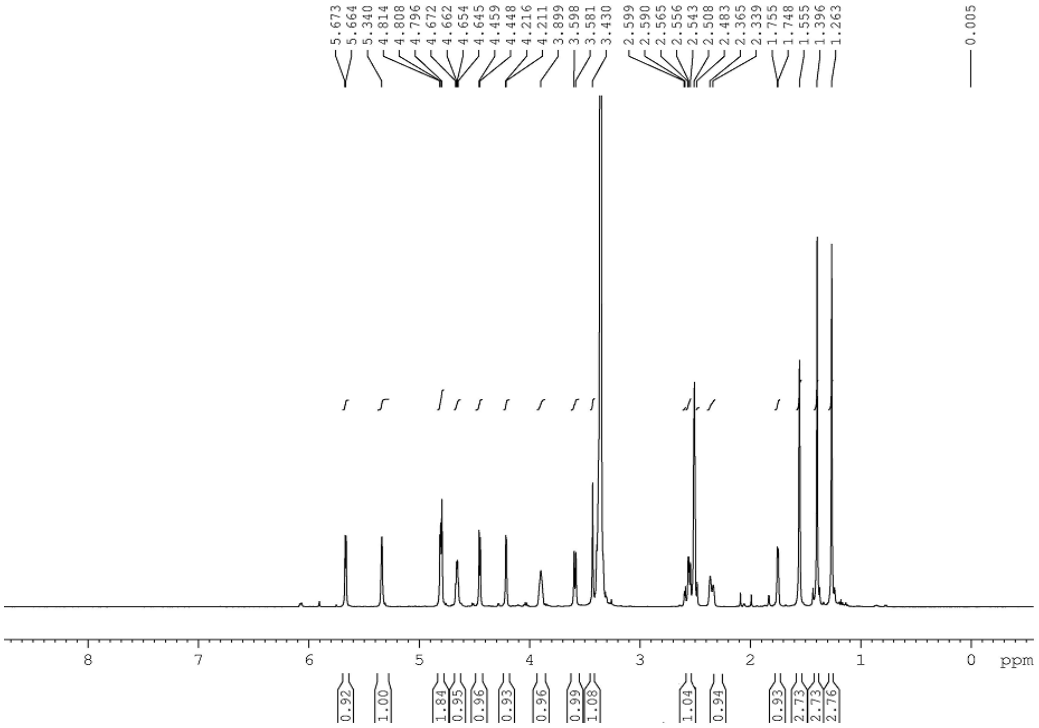

Figure 2A.27. ^{1}H NMR spectrum (500 MHz, DMSO-d_6) of samaderin C (**4**)

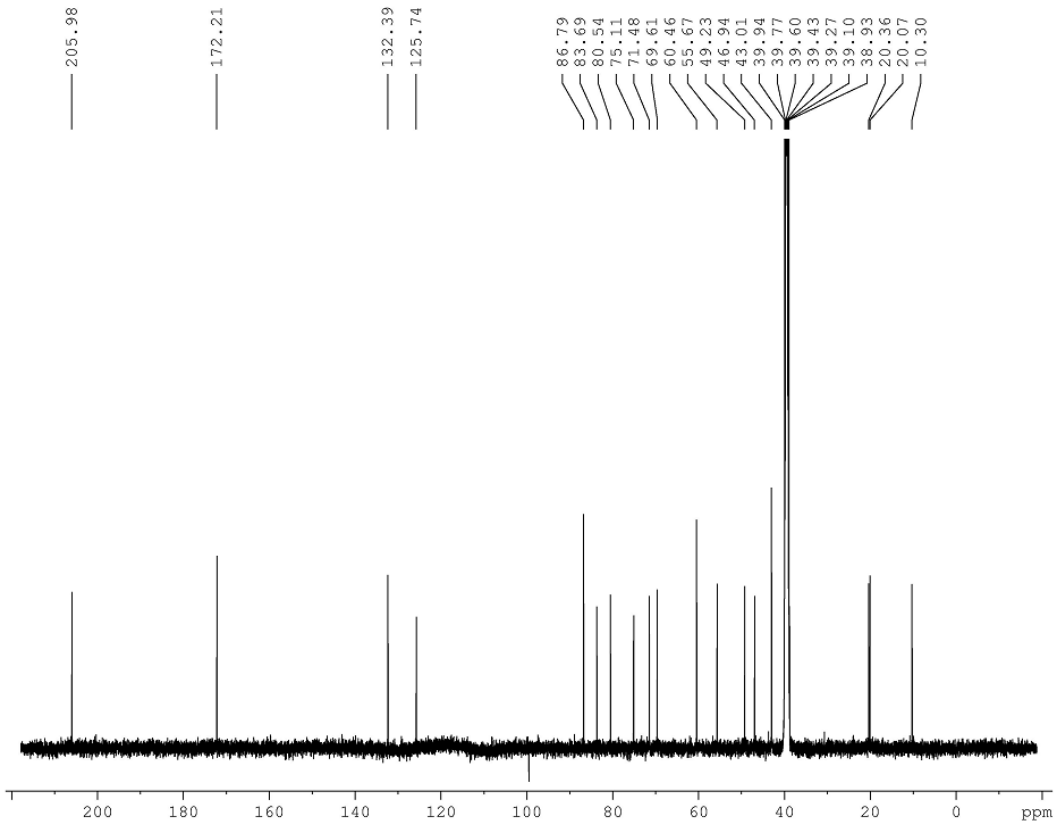

Figure 2A.28. ^{13}C NMR spectrum (125 MHz, DMSO-d_6) of samaderin C (**4**)

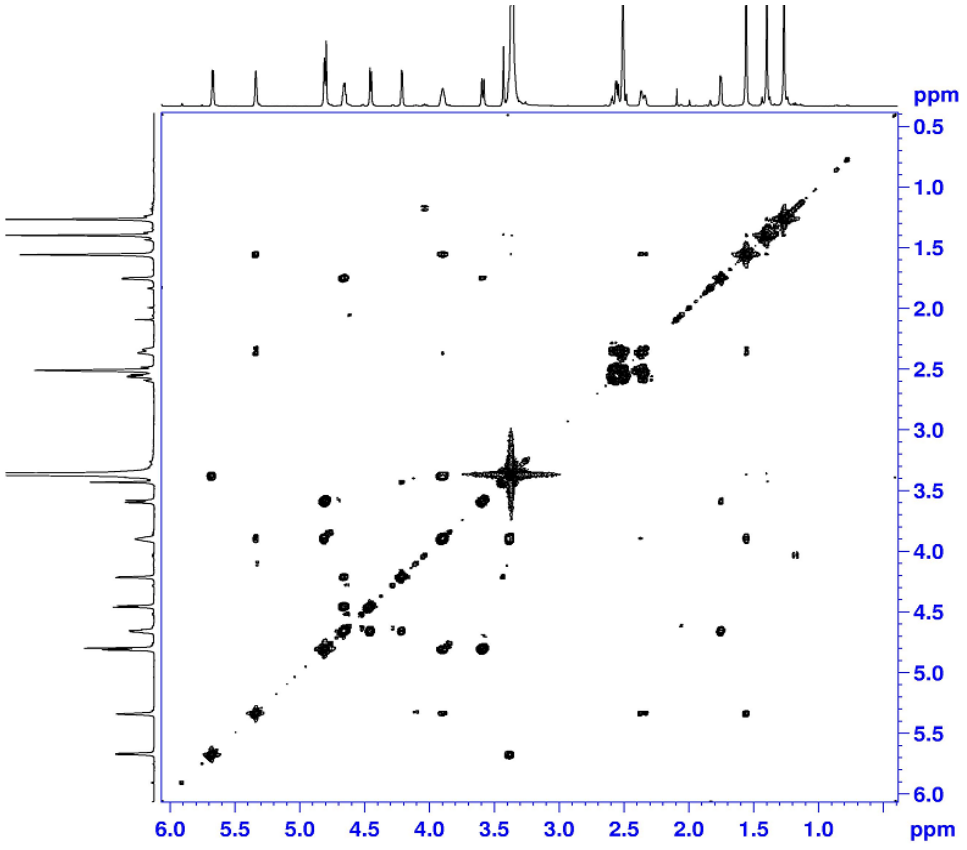

Figure 2A.29. ^{1}H-^{1}H COSY NMR spectrum (500 MHz, DMSO-d_6) of samaderin C (**4**)

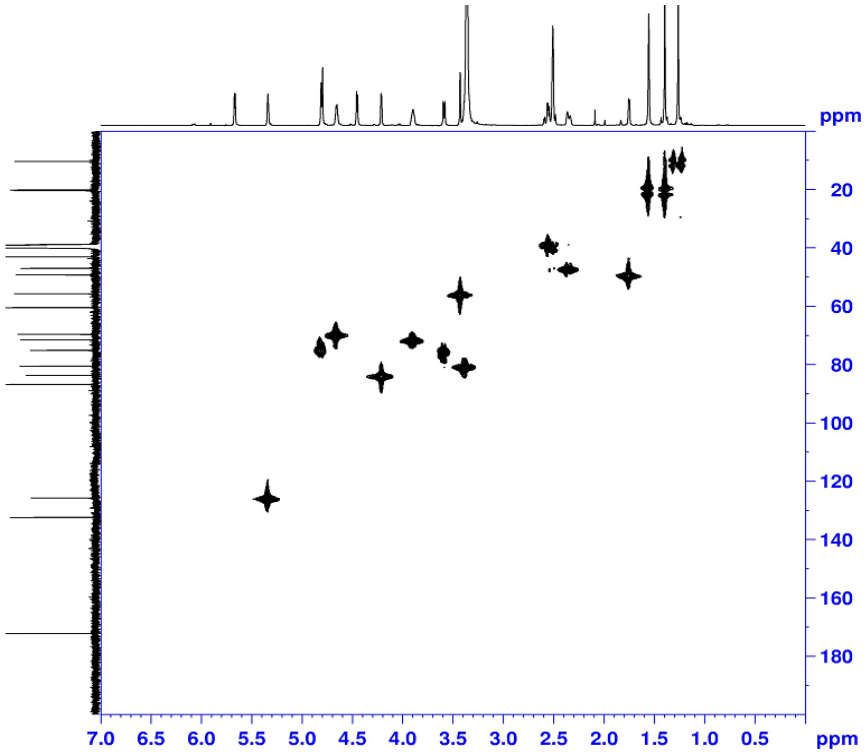

Figure 2A.30. HMQC NMR spectrum (125MHz, DMSO-d_6) of samaderin C (**4**)

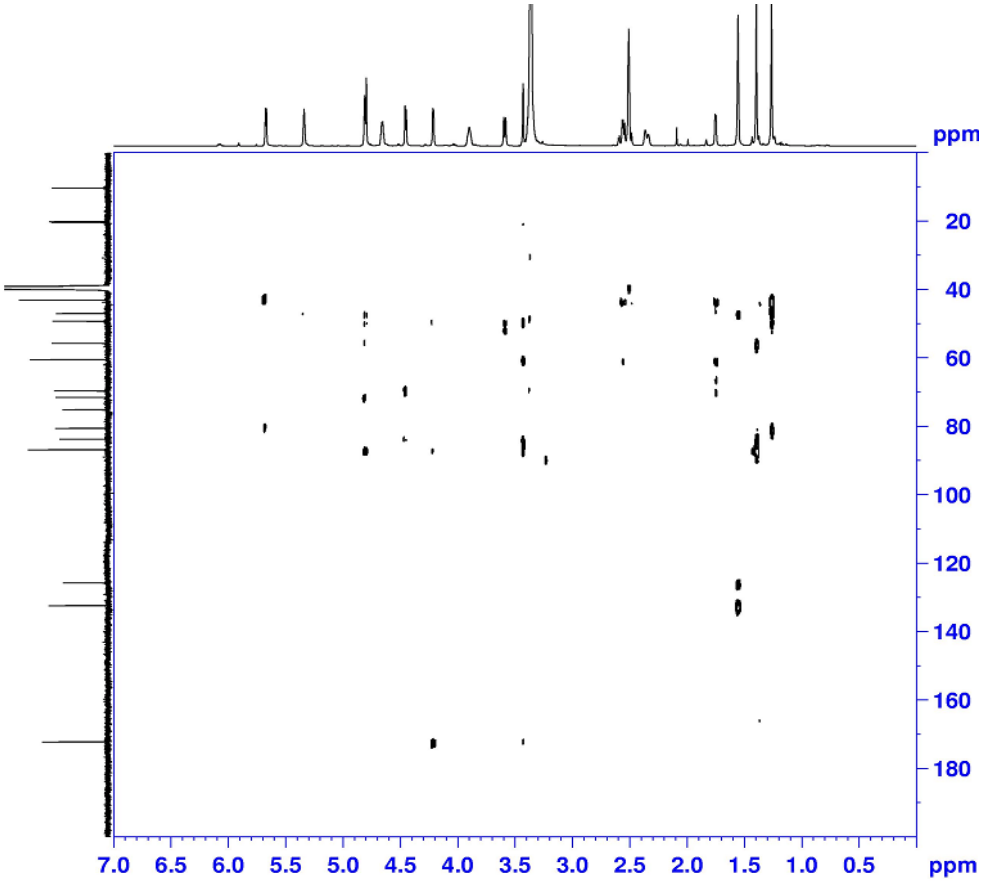

Figure 2A.31. HMBC spectrum (125 MHz, DMSO-d_6) of samaderin C (**4**)

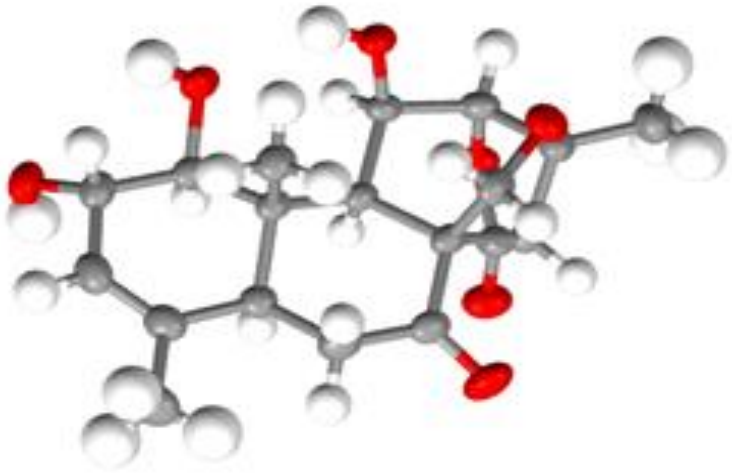

Figure 2A.32. Single crystal X-ray analysis of samaderin C (**4**)

Fraction pool **11** was subjected to column chromatographic separation using 100-200 mesh sized silica gel with *n*-hexane-ethyl acetate polarities leading to the isolation of compound **5**. It was obtained as a colourless crystalline solid and showed a molecular ion peak at m/z 365.1617 $[M+H]^+$ (calcd. for $C_{19}H_{25}O_7$, 365.1600) in the HRESIMS, and the molecular formula was established as $C_{19}H_{24}O_7$. IR absorptions at 3410 and 1760 cm^{-1} revealed the presence of a hydroxyl and a carbonyl lactone, respectively. The 1D and 2D NMR spectra are shown in **Figure 2A.33-37**. The ^1H NMR spectrum of compound **5** exhibited the presence of olefinic proton signals at δ_H 5.96 (d, J = 1.5 Hz) ppm, three oxymethine proton signals at δ_H 4.69 (t, J = 3 Hz), 4.04 (d, J = 3.5 Hz), 3.73 (s) and 3.06 (d, J = 12.5 Hz) ppm, oxymethylene proton at δ_H 4.47 (d, J = 8 Hz) and 3.60 (d, J = 8.5 Hz) ppm, three methine signals at δ_H 2.70 (s), 2.09 (t, J = 4.5 Hz) and 1.91 (m) and three methyl singlets at δ_H 1.9, 1.3 and 1.1 ppm. From the ^{13}C NMR spectrum of compound **5**, the presence of 19 carbon atoms was ascertained with the carbon signals at δ_C 83.1, 69.8, 69.4 and 42.1 ppm assigned to four oxymethines, δ_C 58.6, 44.0 and 29.1 ppm to three sp^3 methines, δ_C 124.0 ppm to sp^2 methines, δ_C 198.3 ppm to α, β-unsaturated carbonyl moiety, δ_C 172.1 ppm to a lactone carbonyl, δ_C 74.4 ppm to an oxygenated quaternary carbon and δ_C 22.1, 20.7 and 10.4 ppm to three methyls. By comparison with previously reported spectroscopic data [Philip *et al*., **2005**] and single crystal X-ray analysis (**Figure 2A.38**) the compound **5** was C19 type quassinoid cedronin.

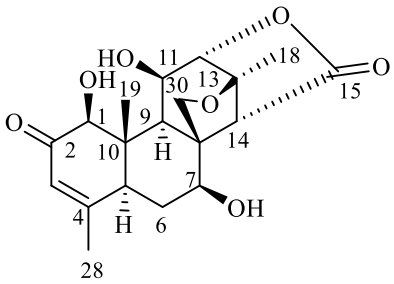

Cedronin (5)

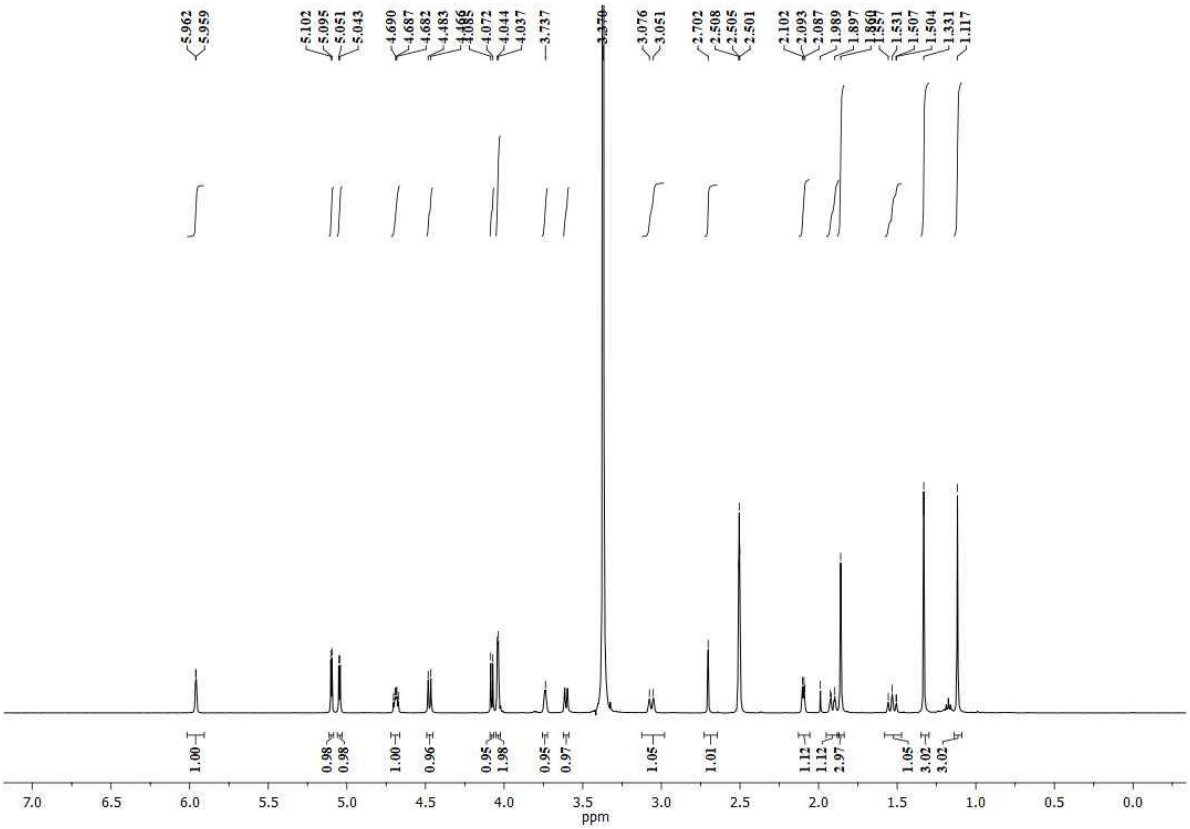

Figure 2A.33. ^{1}H NMR spectrum (500 MHz, DMSO-d_6) of cedronin (**5**)

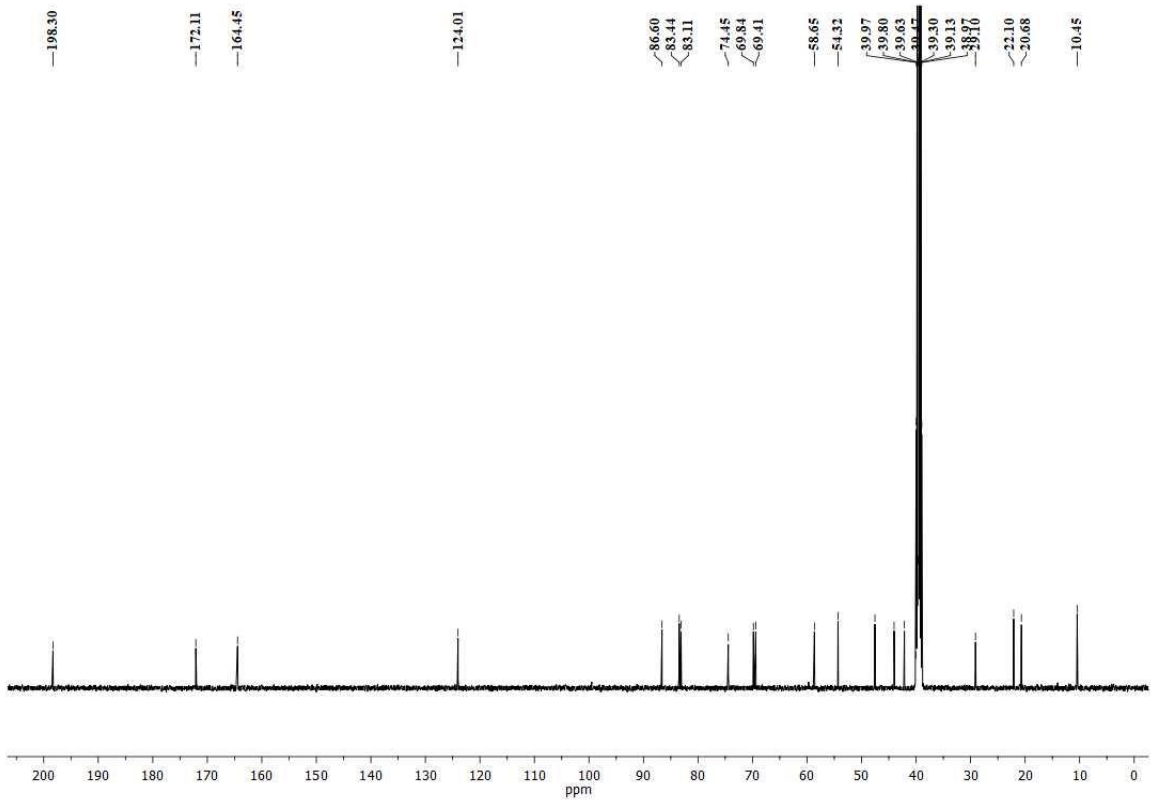

Figure 2A.34. ^{13}C NMR spectrum (125 MHz, DMSO-d_6) of cedronin (**5**)

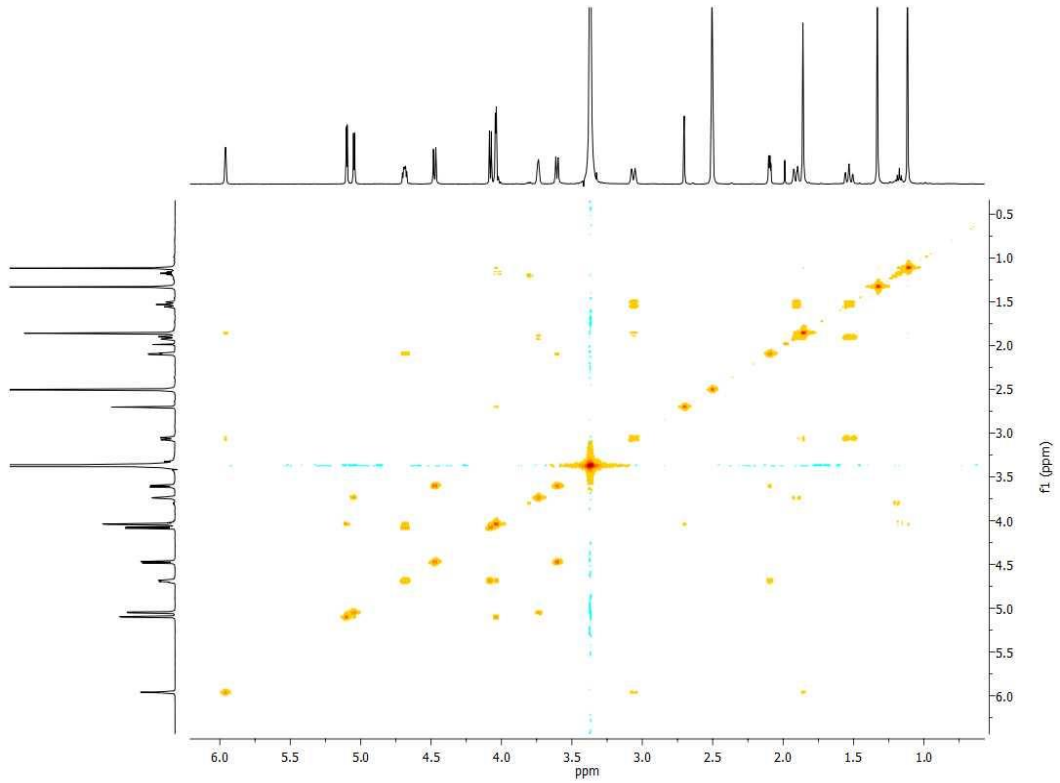

Figure 2A.35. ^{1}H-^{1}H COSY NMR spectrum (500 MHz, DMSO-d_6) of cedronin (**5**)

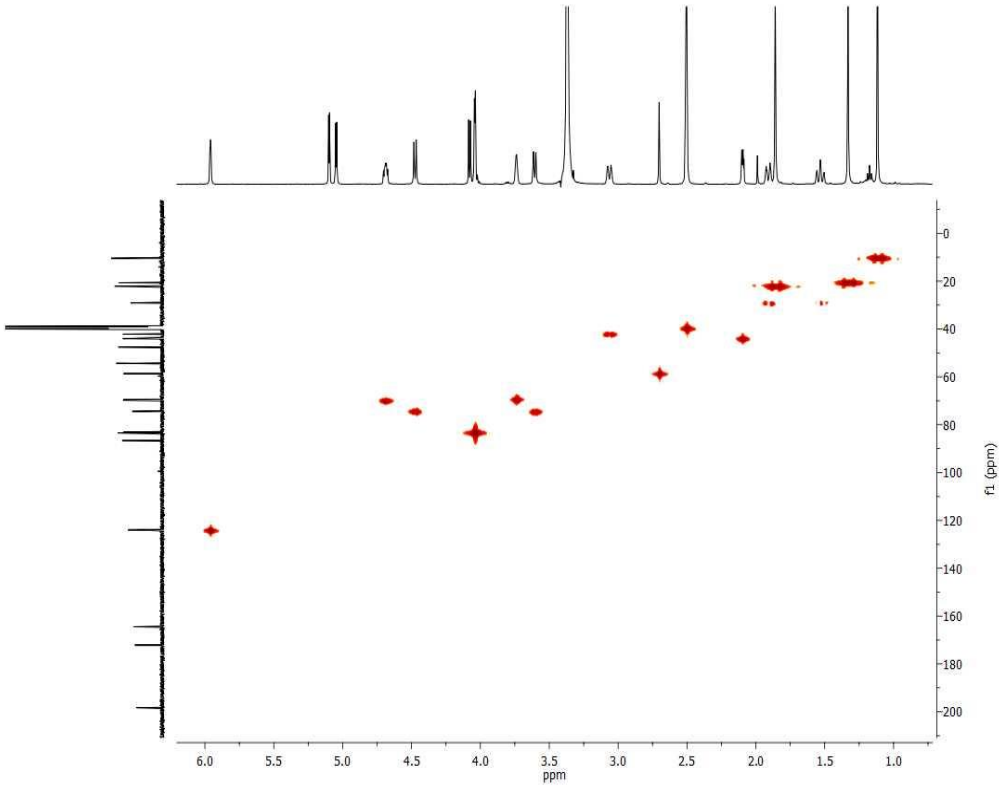

Figure 2A.36. HMQC NMR spectrum (125 MHz, DMSO-d_6) of cedronin (**5**)

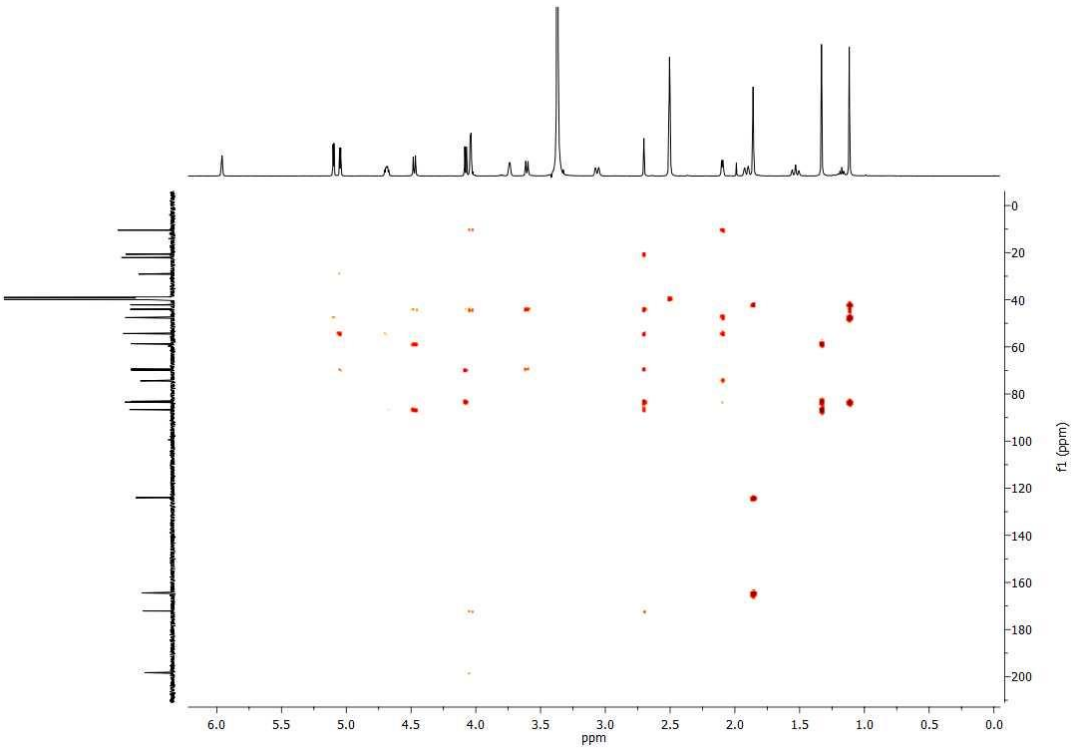

Figure 2A.37. HMBC NMR spectrum (125 MHz, DMSO-d_6) of cedronin (**5**)

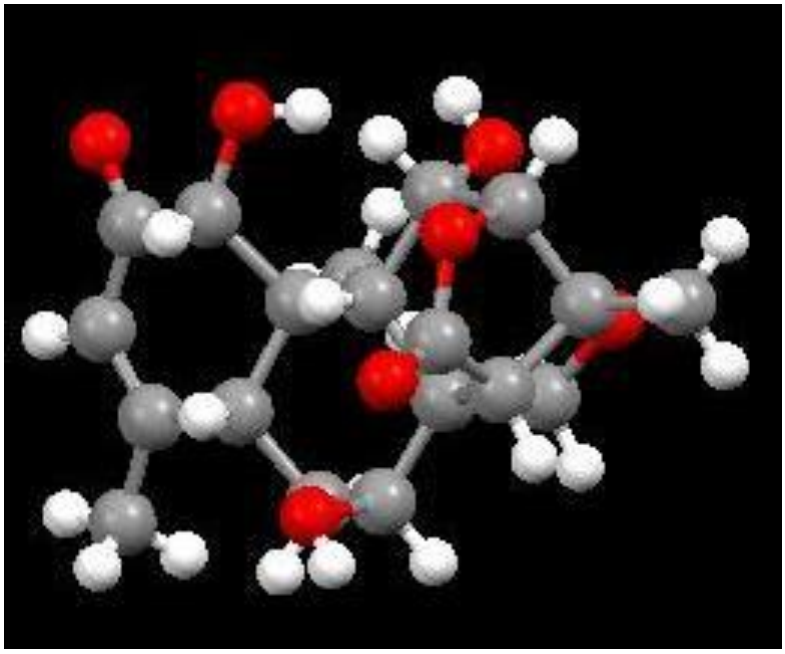

Figure 2A.38. Single crystal X-ray analysis of cedronin (**5**)

Compound **6** was obtained as colourless crystalline solid (Mp: 271-273 ^{o}C). The HRESIMS spectrum displayed a molecular ion at m/z 435.1631 $[M+Na]^{+}$ (calcd. for $C_{20}H_{28}O_9Na$, 435.1631) consistent with the chemical formula $C_{20}H_{28}O_9$ (**Figure 2A.46**). The IR spectra suggested the presence of hydroxyl (3410 cm^{-1}) and a γ-carbonyl lactone (1762 cm^{-1}) of a C20-type quassinoid. The compound **6** exhibited specific rotation at $[\alpha]^{25}_{D}$ +63.1 ^{o} (*c* 0.3, MeOH). The 1D and 2D NMR spectra are shown in **Figure 2A.39-45.** The ^{1}H NMR spectrum of compound **6** exhibited a signals corresponding to an oxymethylene [δ_H 4.45 and 3.80 ppm], four oxymethines [δ_H 4.73, 4.63-4.57, 4.38-4.35 and 3.75 ppm], two tertiary methyl groups [δ_H 1.18 and 1.62 ppm], and a secondary methyl groups [δ_H 1.14 (d, J = 6 Hz) ppm]. The ^{13}C NMR spectrum of **6** revealed 20 signals including those for carbonyl groups [δ_C 215.5 ppm], a γ- lactone carbonyl carbon [δ_C 169.2 ppm], seven oxygen substituted carbons [δ_C 84.2, 81.8, 81.3, 73.5 and 71.0 ppm] and methylene carbon [δ_C 50.0 and 37.6 ppm]. This is consistent with ^{1}H-^{1}H COSY, HMQC, HMBC and DEPT 135 experiments (**Table 2A.5**). The presence of the γ-carbonyl lactone function at C-16 was established by the HMBC experiment with correlations from H-15 (**Figure 2A.47**). The stereochemistry of compound **6** was determined by NOESY spectrum. Furthermore, the correlations observed between H-5 and H-9, and H-11 indicated that, these protons are in α-orientation. The correlations between H-6 and H-7 in the NOESY spectrum with small coupling constant revealed that

the protons are in *β*-orientation (**Figure 2A.47**). To the best of our knowledge, this is a new quassinoid molecule and the structure of the compound was further unambiguously confirmed from its single crystal X-ray analysis (**Figure 2A.48**).

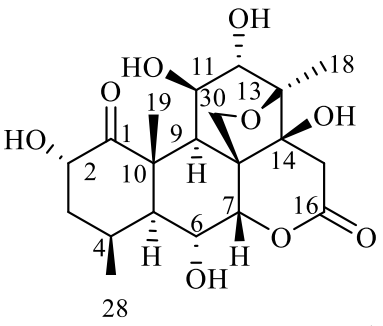

Novel compound (6)

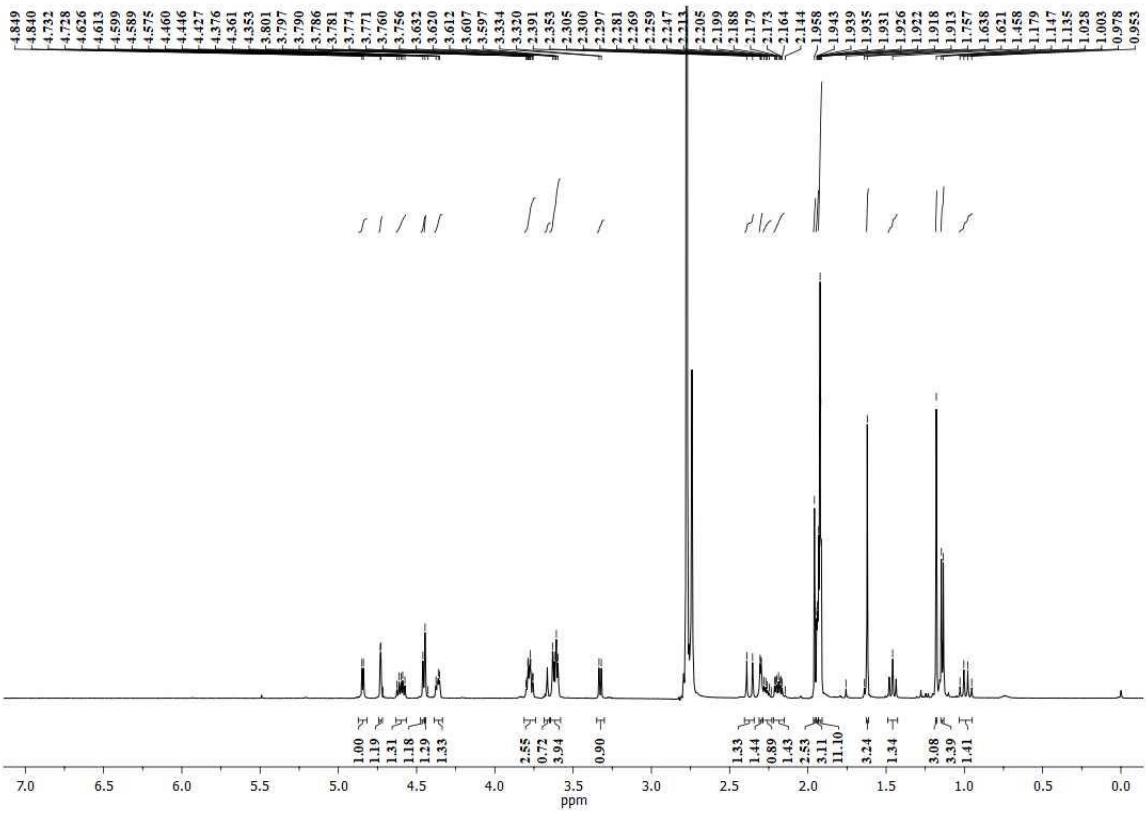

Figure 2A.39. ^{1}H NMR spectrum (500 MHz, Acetone-d_6) of novel compound (**6**)

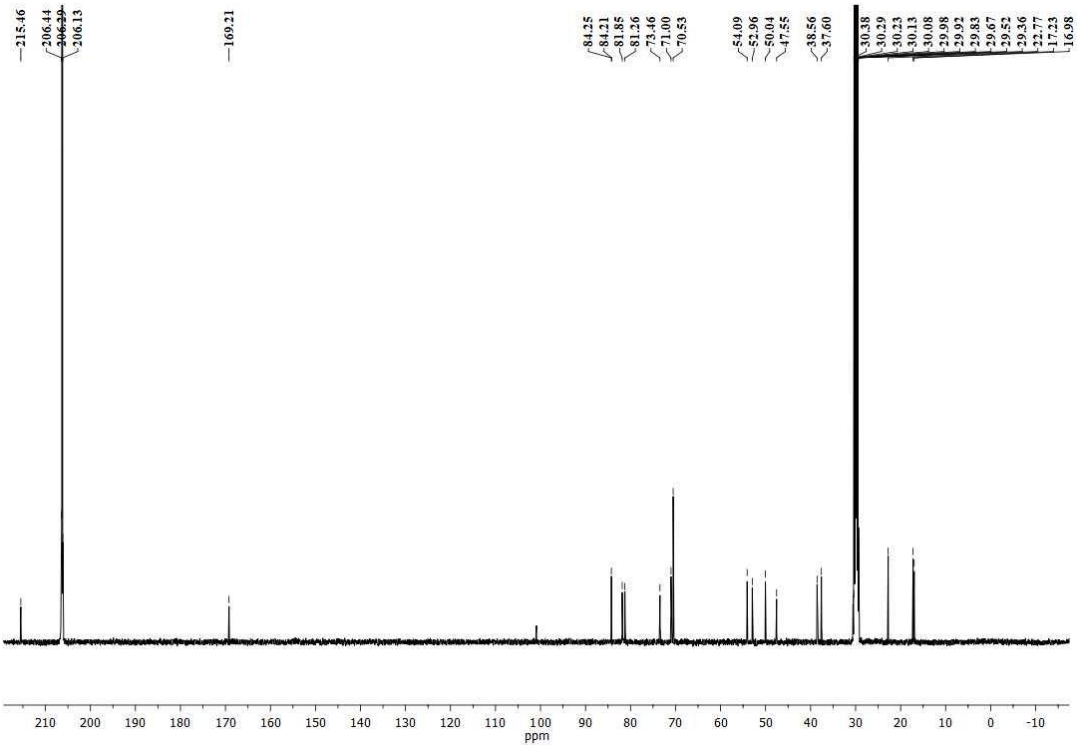

Figure 2A.40. ^{13}C NMR spectrum (125 MHz, Acetone-d_6) of novel compound (**6**)

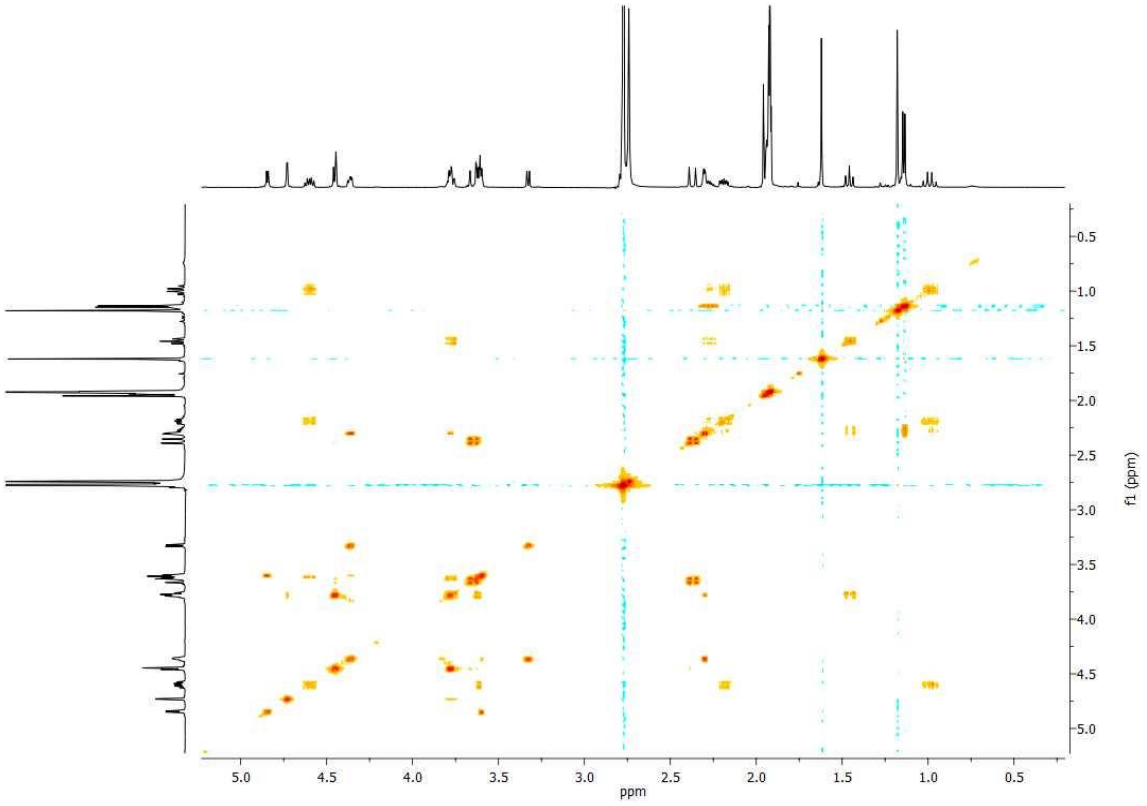

Figure 2A.41. ^{1}H-^{1}H COSY NMR spectrum (500 MHz, Acetone-d_6) of novel compound (**6**)

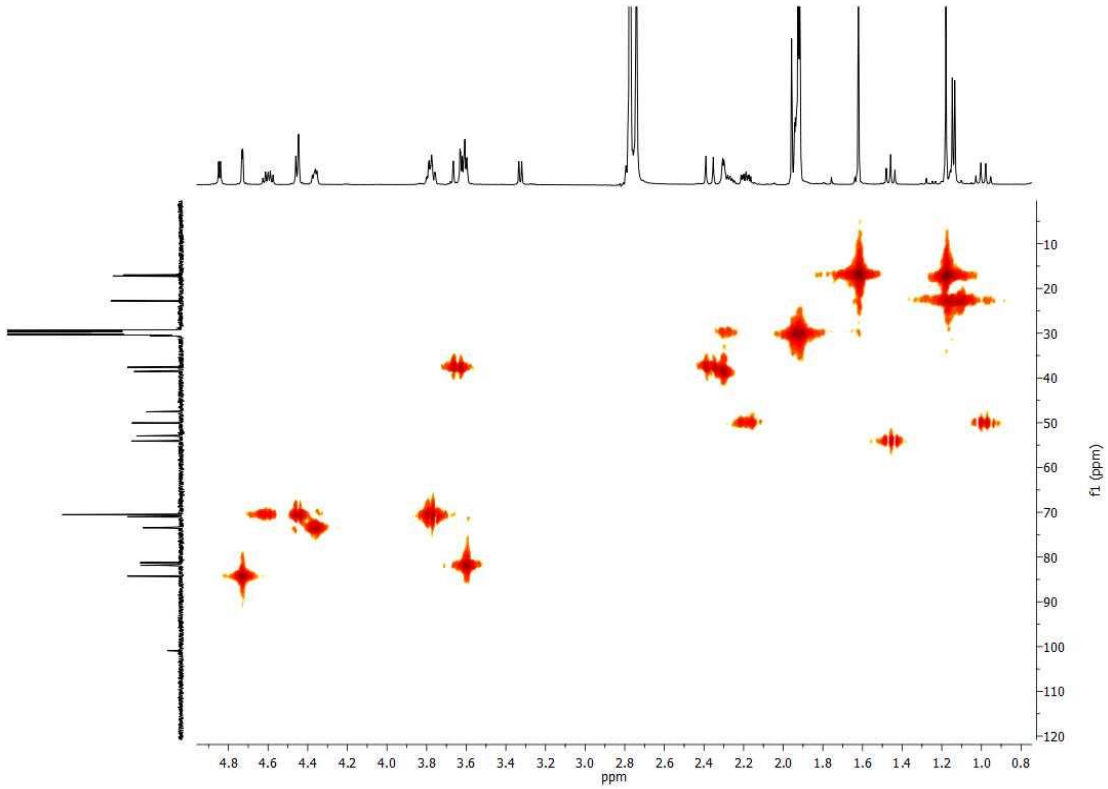

Figure 2A.42. HMQC NMR spectrum (125 MHz, Acetone-d_6) of novel compound (**6**)

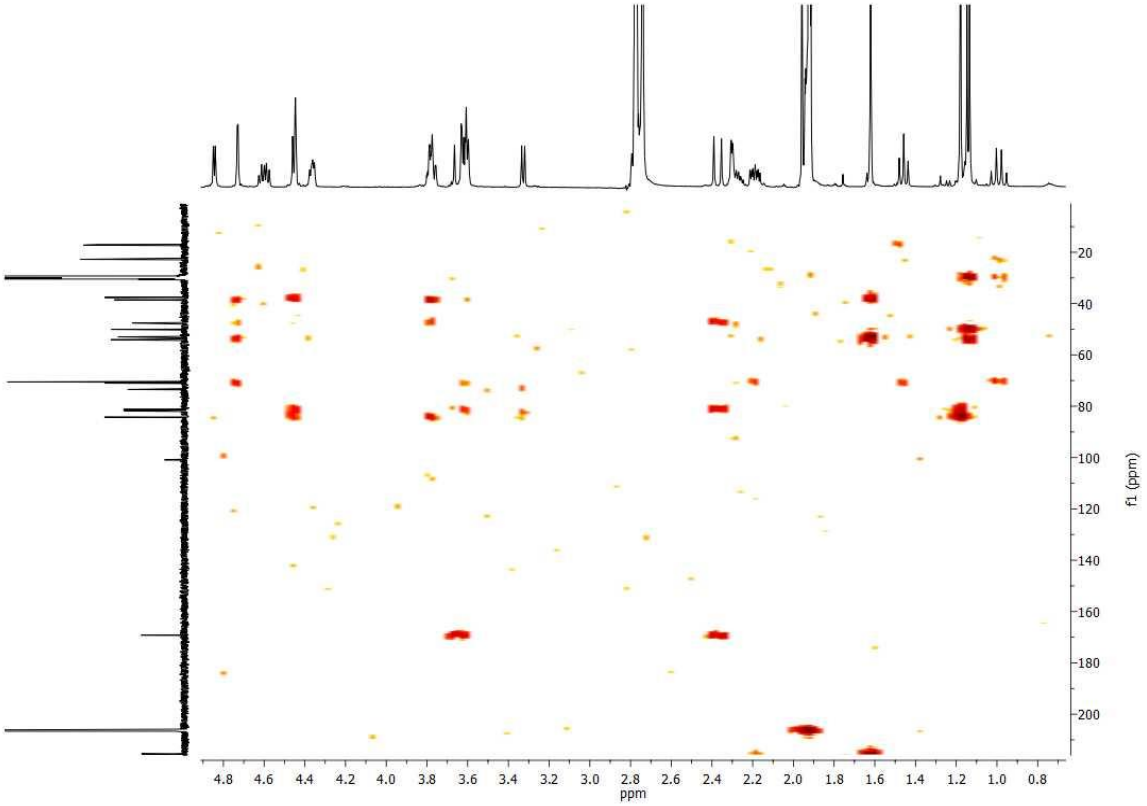

Figure 2A.43. HMBC spectrum (125 MHz, Acetone-d_6) of novel compound (**6**)

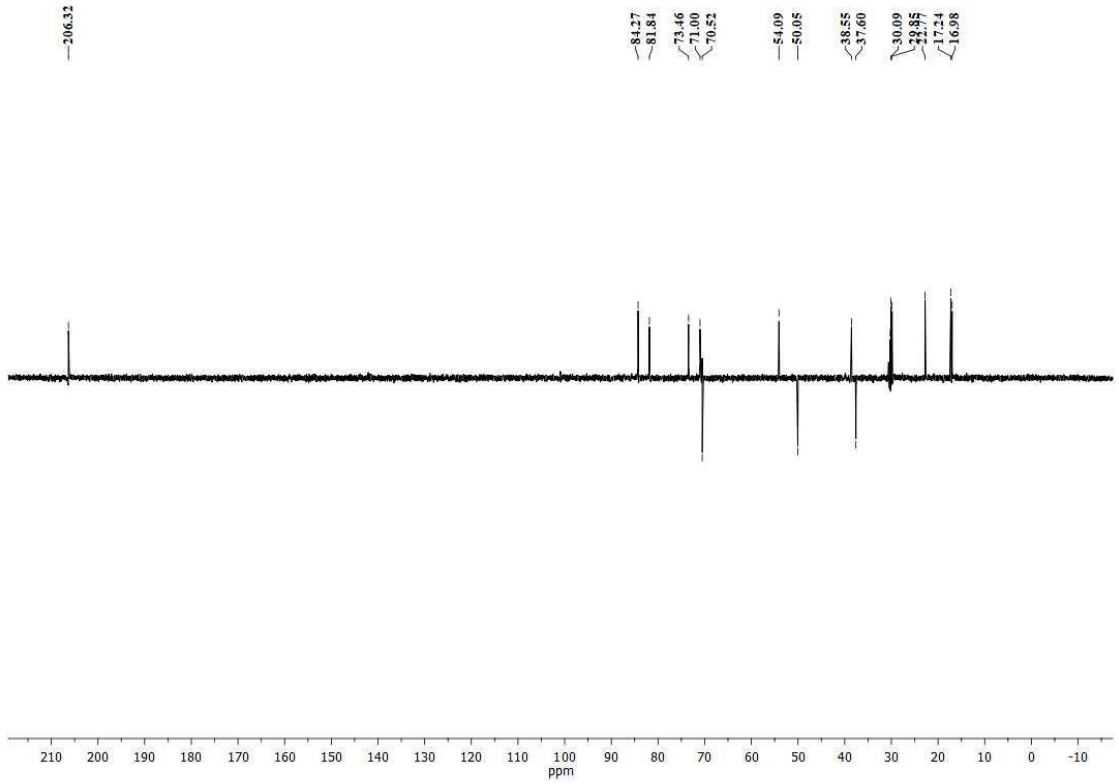

Figure 2A.44. DEPT 135 spectrum (125 MHz, Acetone-d_6) of novel compound (**6**)

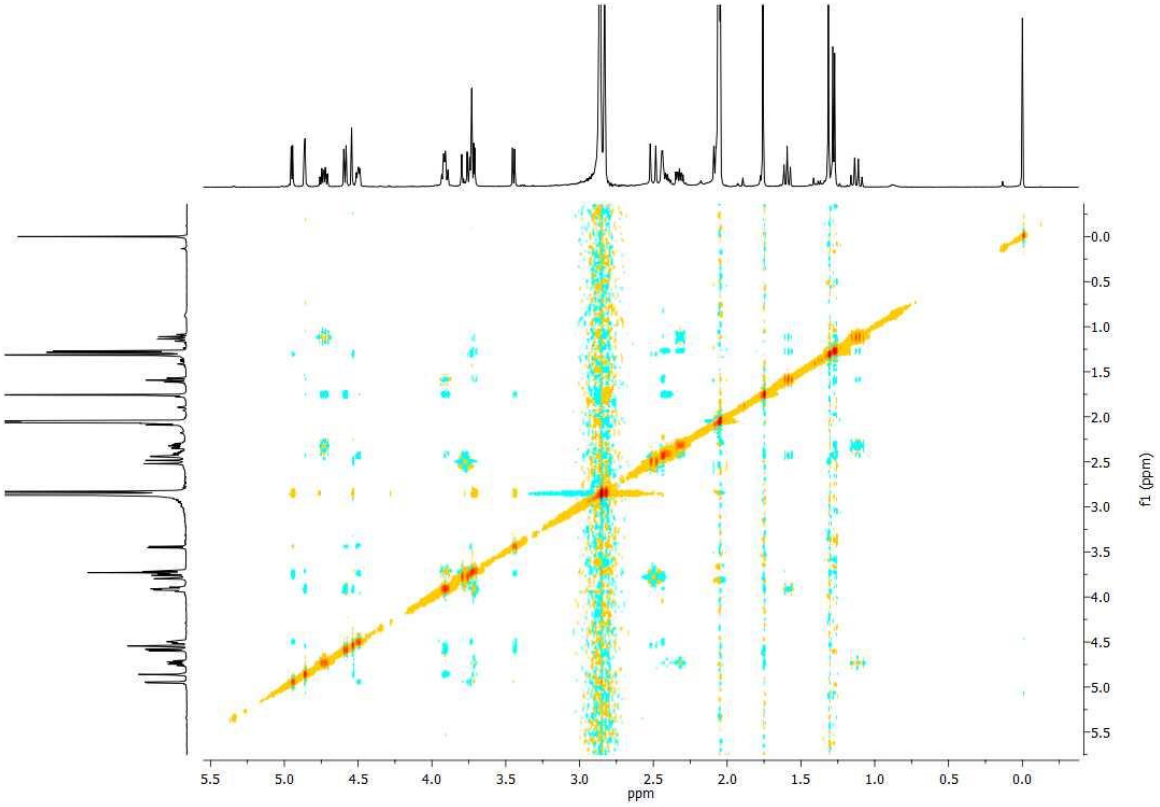

Figure 2A.45. NOESY spectrum (500 MHz, Acetone-d_6) of novel compound (**6**)

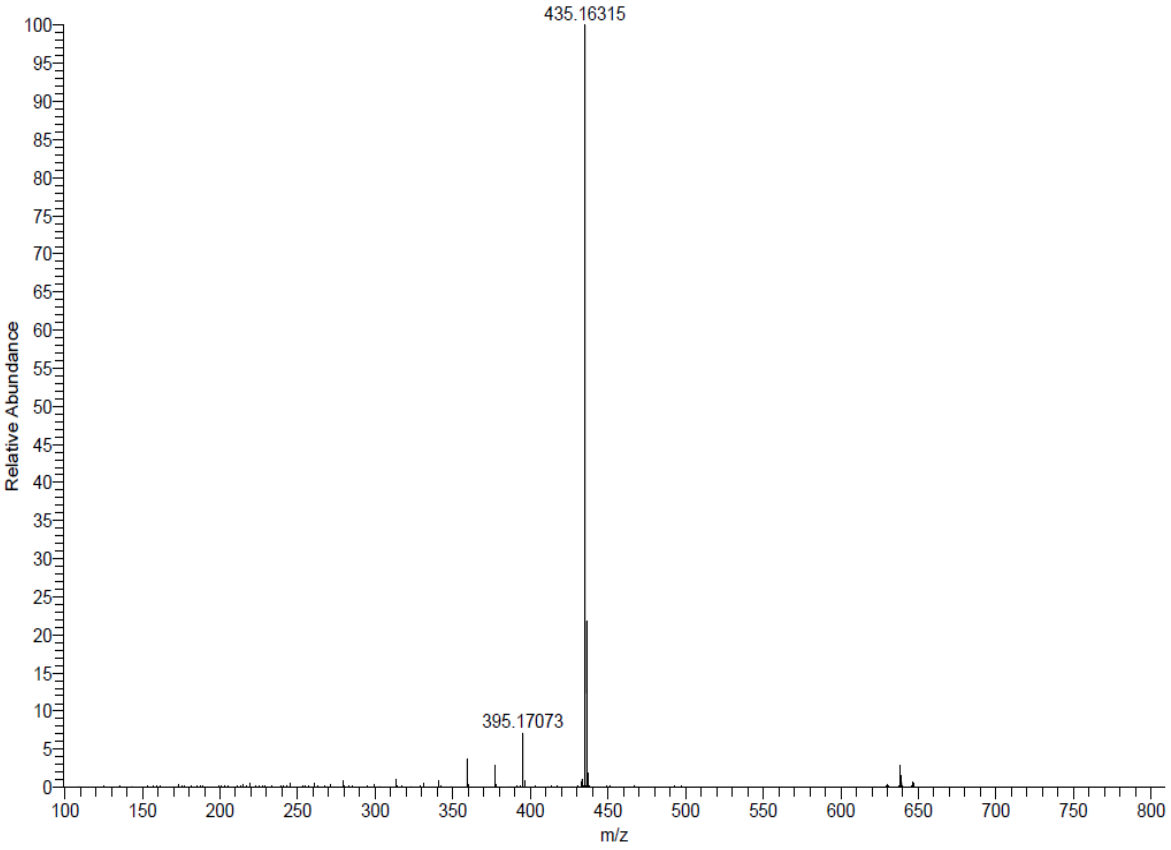

Figure 2A.46. HRESIMS spectrum of novel compound (**6**)

Table 2A.5. ^{1}H (500 MHz) and ^{13}C (125 MHz) NMR data of compound **6** in Acetone-d_6

Position	**^{1}H NMR**	**^{13}C NMR**
1	-	215.5
2	3.61 (brs, 1H)	81.8
3	2.21-2.14 (m, 1H) 1.03-0.95 (m, 1H)	50.0
4	2.28-2.23 (m, 1H)	30.6
5	1.14 (t, *J* = 11 Hz and 10.5 Hz, 1H)	54.1
6	3.80 - 3.76 (m, 1H, mergered with H-30)	71.0
7	4.73 (d, *J* = 2 Hz, 1H)	84.3
8	-	47.5
9	2.31-2.30 (m, 1H)	38.6

10	-	53.0
11	4.38-4.35 (m, 1H)	73.5
12	4.46 (s, 1H)	71.1
13	-	81.3
14	-	84.2
15	3.63-3.62 (m, 1H) 2.37 (d, *J* = 19 Hz, 1H)	37.6
16	-	169.2
18	1.18 (s, 3H)	17.9
19	1.62 (s, 3H)	16.5
28	1.14 (d, *J* = 6 Hz, 3H)	22.9
30	4.45 (s, 1H) 3.80 (m, 1H)	70.5

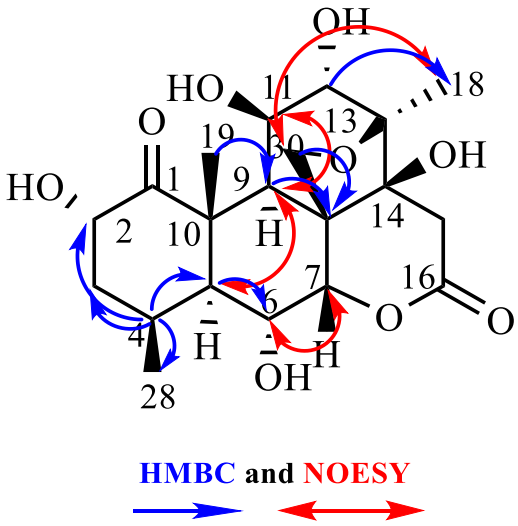

Figure 2A.47. The key HMBC and NOESY correlations of novel compound (**6**)

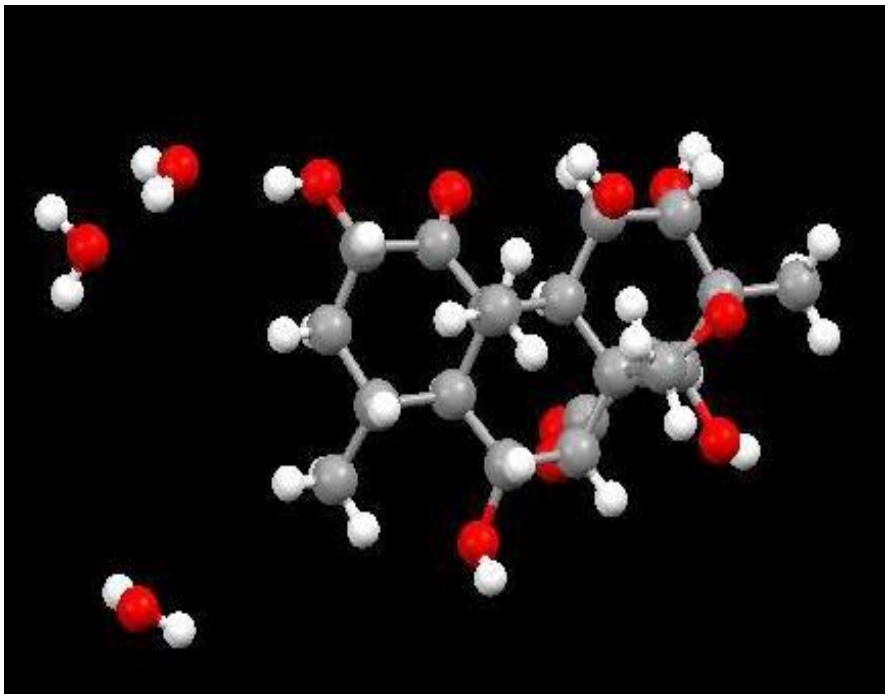

Figure 2A.48. Single crystal X-ray analysis of novel compound (**6**)

Chromatographic purification of fraction pool 11 using 100-200 mesh sized silica gel with *n*-hexane-ethyl acetate polarities resulted in the isolation of compound **5**. Compound **5** was obtained as a colourless amorphous solid and showed a molecular ion peak at m/z 433.1480 $[M+Na]^+$ (calcd. for $C_{20}H_{26}O_9Na$, 433.1475) in the HRESIMS, and the molecular formula was established as $C_{20}H_{26}O_9$. IR absorptions at 3410 and 1760 cm^{-1} revealed the presence of a hydroxyl and a carbonyl lactone, respectively. The 1D and 2D NMR spectra are shown in **Figure 2A.49-55**. The ^1H NMR spectrum of compound **5** displayed the signals corresponding to; olefinic proton at δ_H 5.98 (s), five hydroxyl protons at δ_H 5.48 (d, J = 5 Hz), 5.31 (s), 5.25 (s), 5.04 (d, J = 7.5 Hz) and 2.9 (brs) ppm, oxymethine protons at 4.83 (brs), 4.42 (t, J_1 = 5.5 Hz or J_1 = 4.5 Hz) and 4.20 (brs) ppm, δ_H oxymethylene protons at δ_H 4.35 (d, J = 7 Hz) and 3.64 (d, J = 7.5 Hz) ppm, three methine signals at δ_H 2.70 (s), 2.09 (t, J = 4.5 Hz) and 1.91 (m) ppm and three methyl singlets at δ_H 2.20,1.15 and 1.12 ppm. From the ^{13}C NMR spectrum of compound **5**, the presence of 21 carbon atoms was ascertained with the carbon signals at δ_C 82.4, 82.2 and 80.6 ppm assigned to three oxymethines, δ_C 68.7 ppm to oxymethyne carbon, δ_C 58.6, 44.0 and 29.1 ppm to three sp^3 methines, δ_C 124.0 ppm to sp^2 methines, δ_C 198.3 ppm to α, β-unsaturated carbonyl moiety, δ_C 169.9 ppm to a lactone carbonyl, δ_C 83.4 and 80.0 ppm to an oxygenated quaternary carbon, δ_C 68.7 and 37.1 ppm to methylene carbon and δ_C 27.0, 17.4 and 12.4 ppm to three methyls. Finally, in comparison with previous reports

spectroscopic data [Yaeko *et al*., **1989**] confirmed as a C20 type quassinoid, brucein D, and the structure of the compound is shown below.

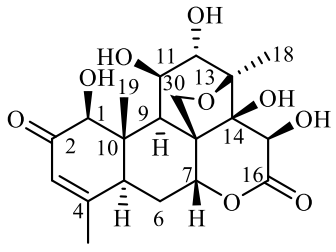

Brucein D (7)

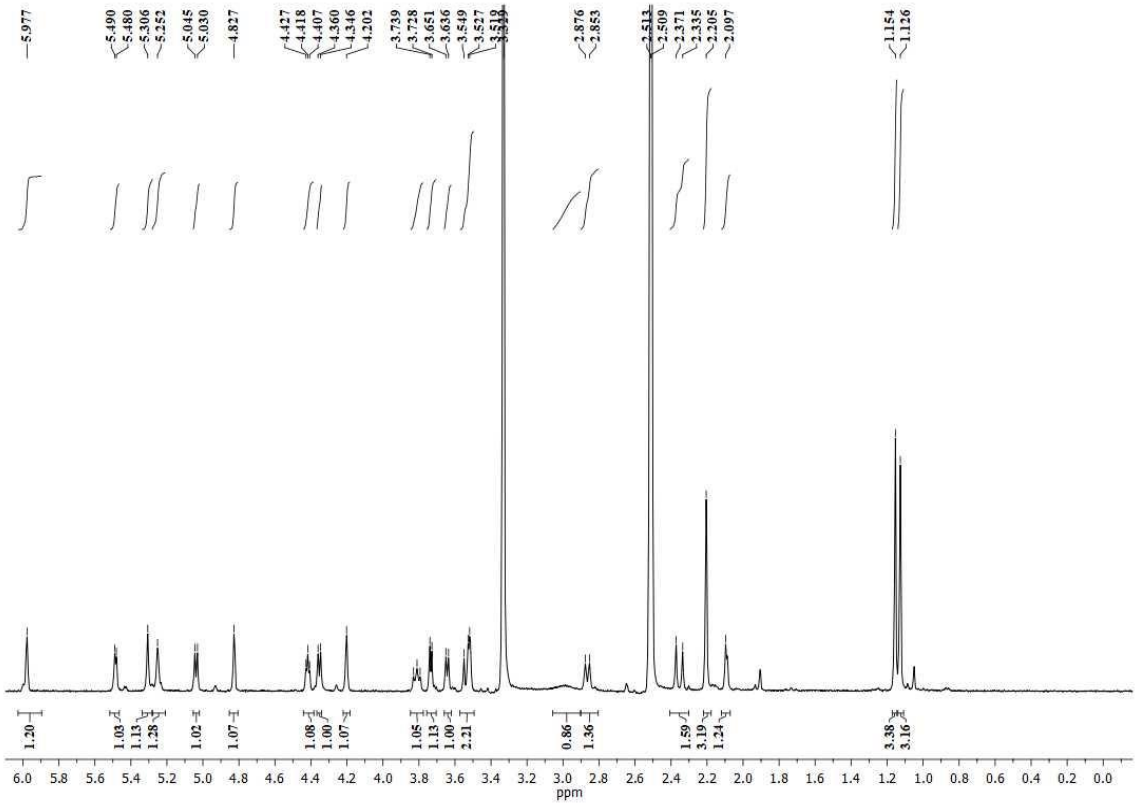

Figure 2A.49. ^{1}H NMR spectrum (500 MHz, DMSO-d_6) of brucein D (**7**)

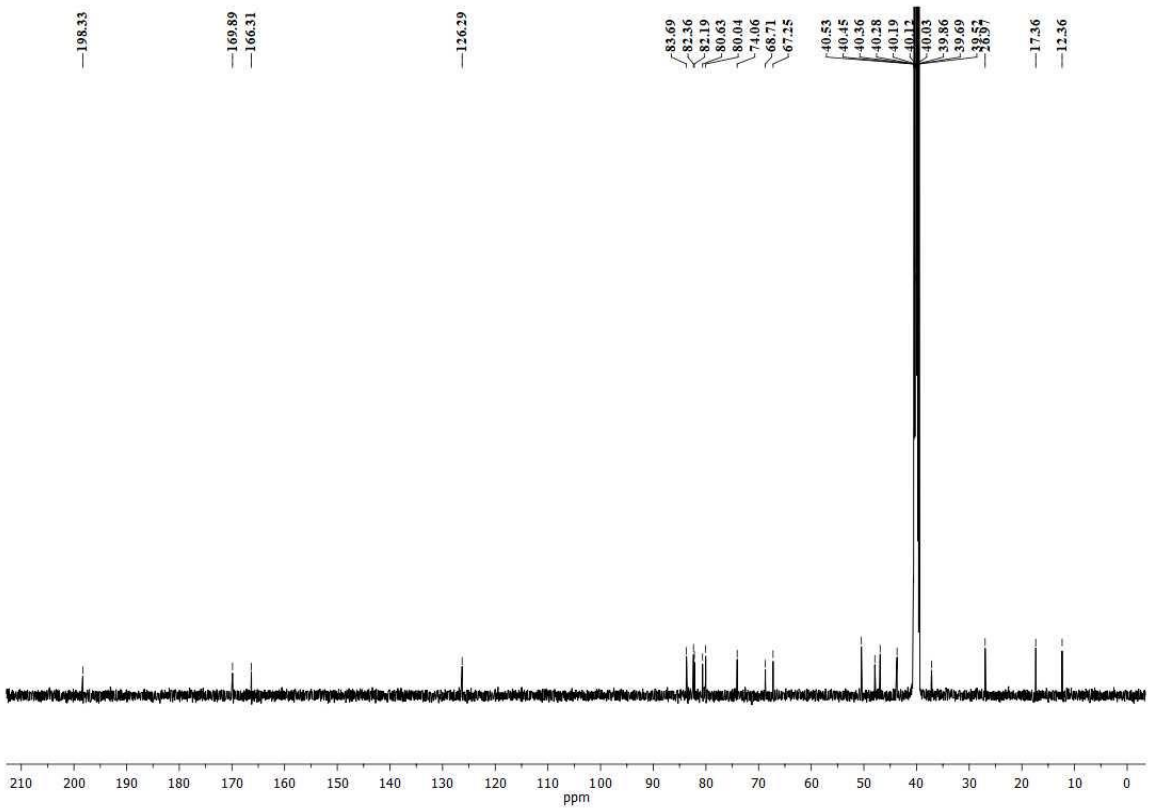

Figure 2A.50. ^{13}C NMR spectrum (125 MHz, DMSO-d_6) of brucein D (**7**)

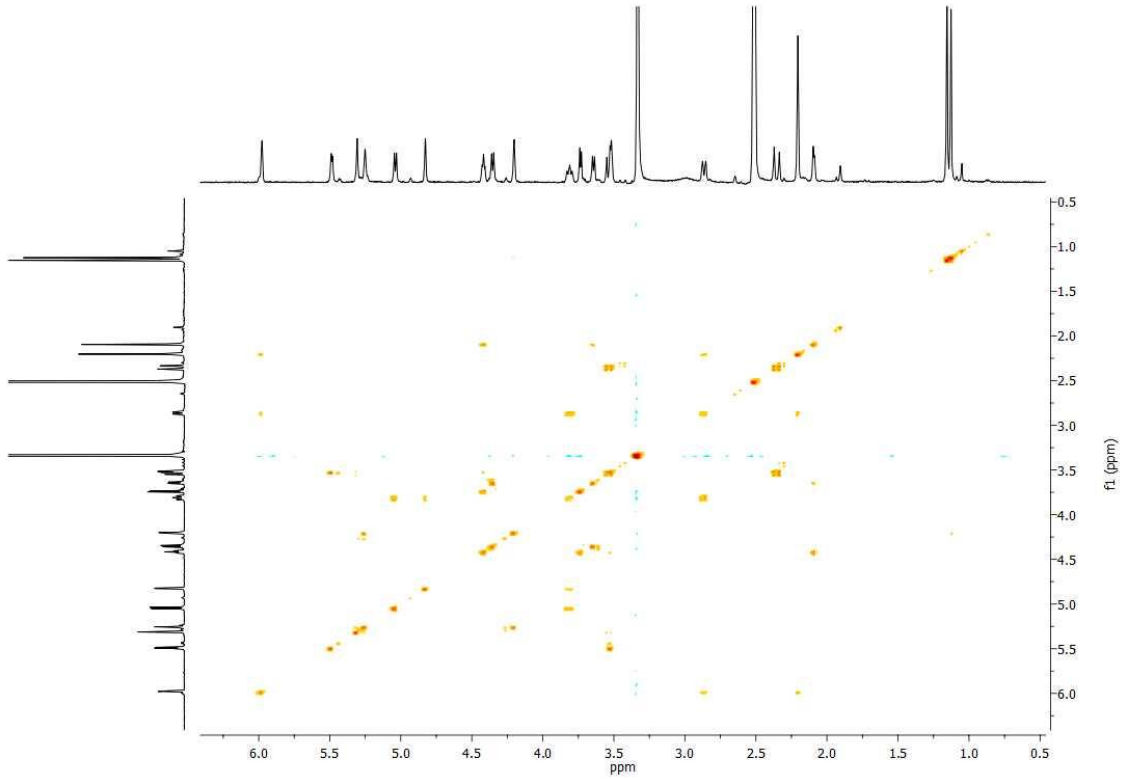

Figure 2A.51. ^{1}H-^{1}H COSY NMR spectrum (500 MHz, DMSO-d_6) of brucein D (**7**)

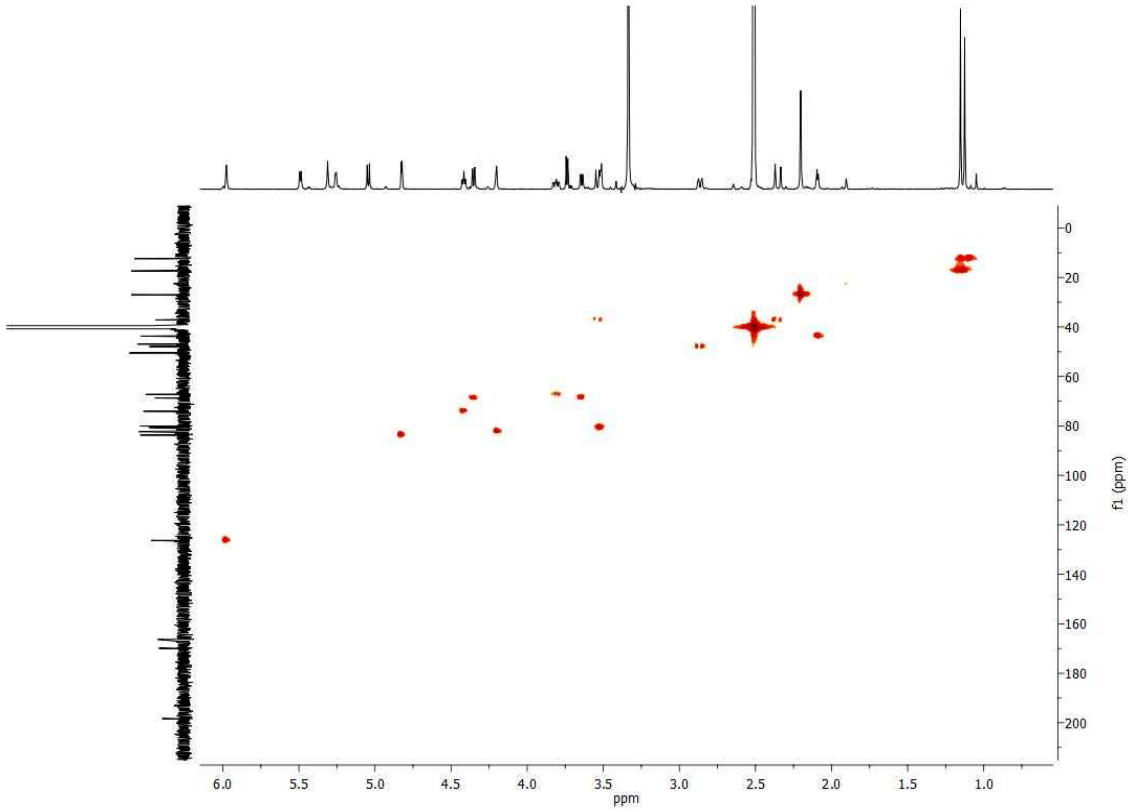

Figure 2A.52. HMQC NMR spectrum (125 MHz, DMSO-d_6) of brucein D (**7**)

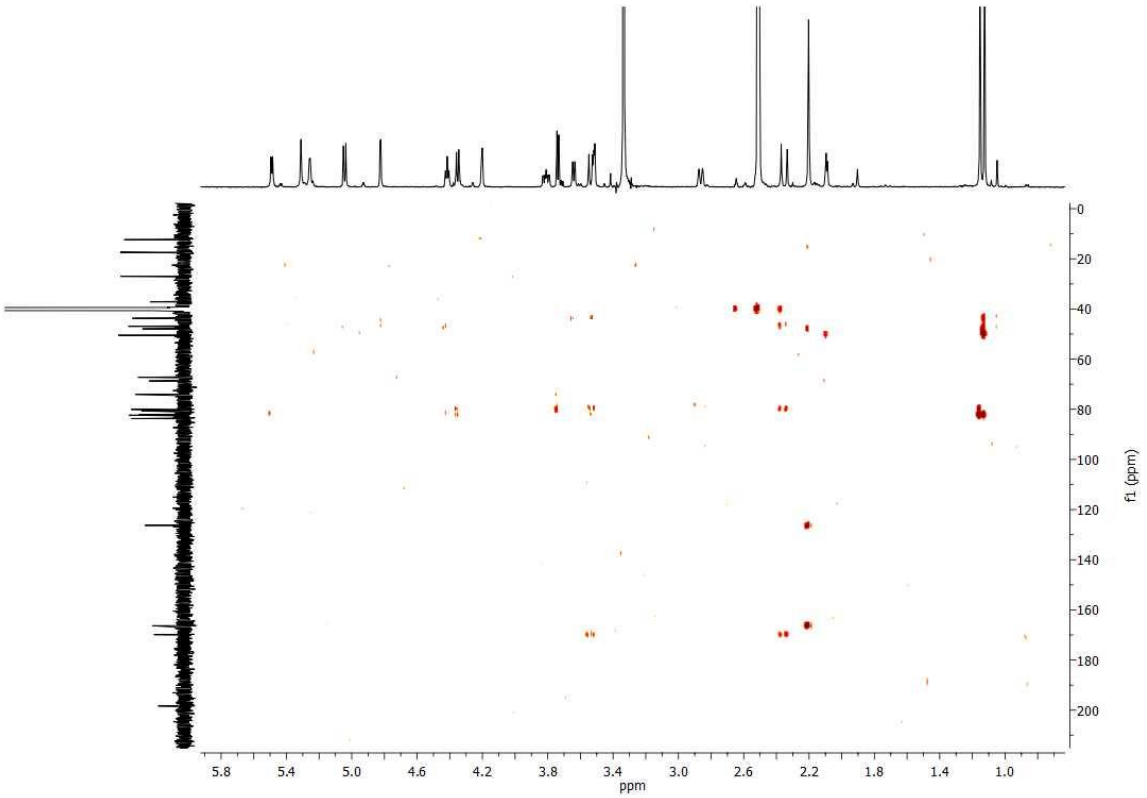

Figure 2A.53. HMBC spectrum (125 MHz, DMSO-d_6) of brucein D (**7**)

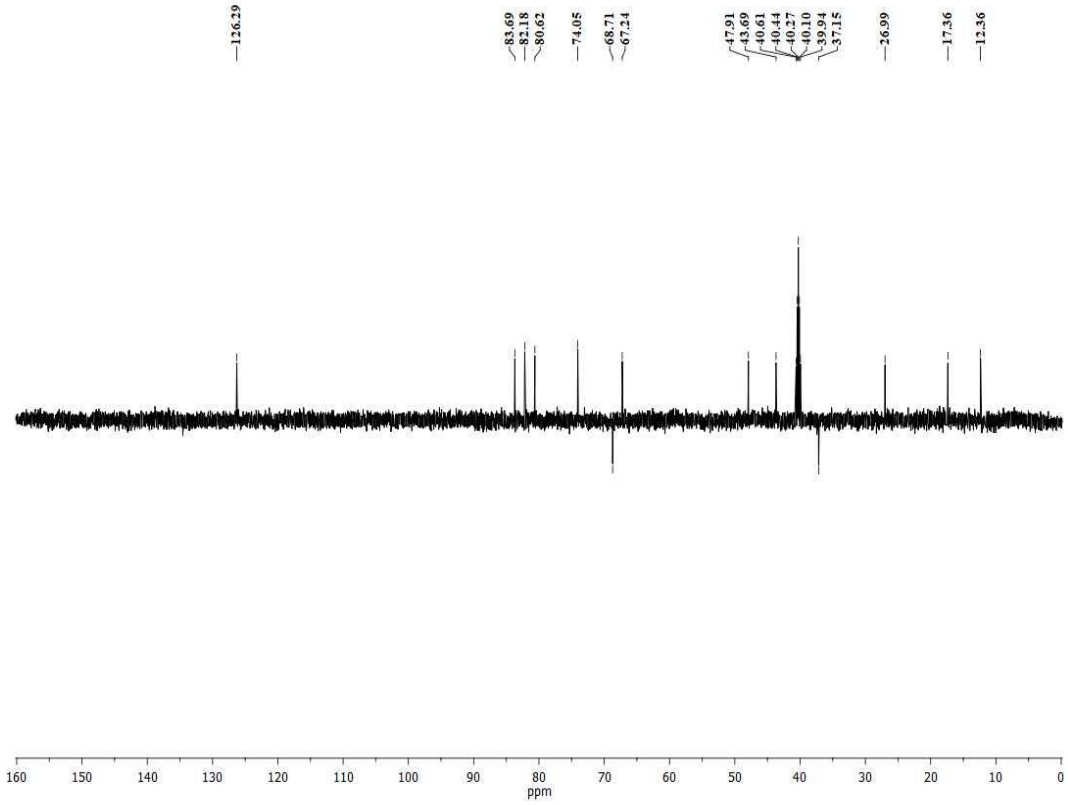

Figure 2A.54. DEPT 135 spectrum (125 MHz, DMSO-d_6) of brucein D (**7**)

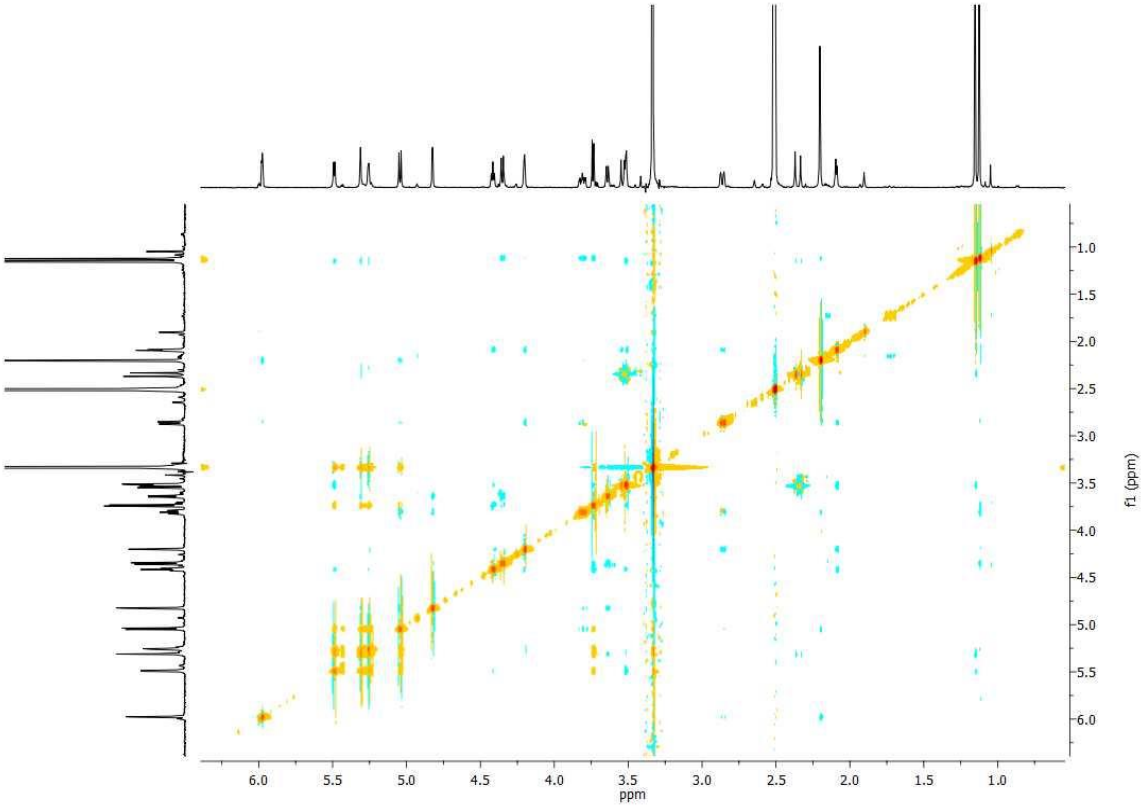

Figure 2A.55. NOESY spectrum (500 MHz, DMSO-d_6) of brucein D (**7**)

Compound **8** was isolated as a colourless amorphous solid (Mp: 232-234 ^{o}C), whose molecular formula was established as $C_{26}H_{38}O_{14}$ by HRESIMS (m/z, 597.2157 $[M+Na]^{+}$; calcd. for $C_{26}H_{38}O_{14}Na$, 597.22) (**Figure 2A.63**). Its IR spectrum displayed absorption bands, corresponding to hydroxyl (3421 cm^{-1}), δ-lactone (1723 cm^{-1}), and double bond (1662 cm^{-1}) moieties. The compound **8** exhibited specific rotation at $[\alpha]^{25}_{D}$ +70 ^{o} (*c* 0.4, DMSO).The 1D and 2D NMR spectra are shown in **Figure 2A.56-62** and ^{1}H and ^{13}C NMR are depicted in **Table 2A.6.** The ^{1}H NMR and heteronuclear quantum correlation (HMQC) spectra of compound 8 exhibited signals of an olefinic proton [δ_H 5.53 (1H, s, H-3)], five oxymethines [δ_H 4.47 (t, J_1 = 6 Hz and J_2 = 5.5 Hz, 1H, H-11), 3.90 (d, J = 5.5 Hz, 1H, H-6, H-12), 3.60-3.59 (dd, J_1= 7 Hz and J_2 = 4 Hz, 1H, H-1) and 3.47-3.42 (m, 2H, H-6 and H-7)], an oxymethylene [δ_H 4.43 and 3.63 (d, J = 7 Hz, each 1H, H-20)], one methylene [δ_H 3.47 and 2.34 (s, 1H each, H-15)], three methyl groups [δ_H 1.87 (s, 3H, H3-18), 1.19 (s, 3H, H3-19) and1.14 (s, 3H, H3-21)] and signals for a characteristic glucopranosyl moiety [δ_H 4.34 (d, J = 7.5 Hz, 1H, H-1'), 3.71-3.65 (m, 1H, H-6'), 3.47-3.40 (m, 1H, H-6'), 3.17-3.03 (m, 1H, H-3'), 3.07-3.02 (m, 1H, overlap, H-4'), 2.97 (td, J_1 = 8 Hz and J_2 = 3.5 Hz, 2')]. The ^{13}C NMR and distortionless enhancement by polarization transfer (DEPT) spectra exhibited 26 carbon signals, including one carbonyl, one olefinic, three methyls, one methylene, three methines, four quaternary, and six saccharide-type carbons. The HMBC correlation between the anomeric proton H-1' and C-2 and between H-2 and C-1' confirmed that the glucopyranosyl unit was attached at the C-2 position and must be a β-anomer, as suggested by the coupling constant (7.5 Hz) of the anomeric proton. The nuclear Overhauser effect spectroscopy (NOESY) cross peaks of H-2/H3-19, H-6/H3-19, H-7/H-14, H-7/Ha-20, H3-19/Ha-20, H-13/Hb-20, and H-14/Hb-20 indicated that H-2, H-6, H-7, H-13, H-14, and Me-19 are cofacial and assigned as β-orientations, while the NOESY of H-1/H-5, H-1/H-9, and H-5/H-9 showed that these protons are α-oriented. The key HMBC and NOESY correlations are shown in **Figure 2A.64.** To the best of our knowledge, this is a new quassinoid glucoside and structure of compound **8** is shown below.

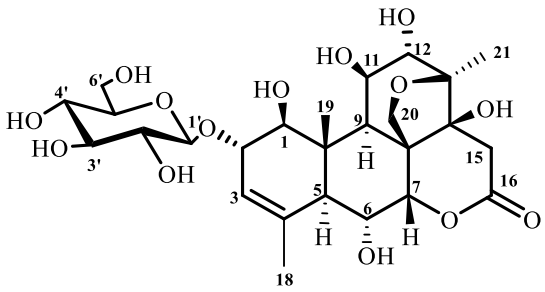

Novel compound (8)

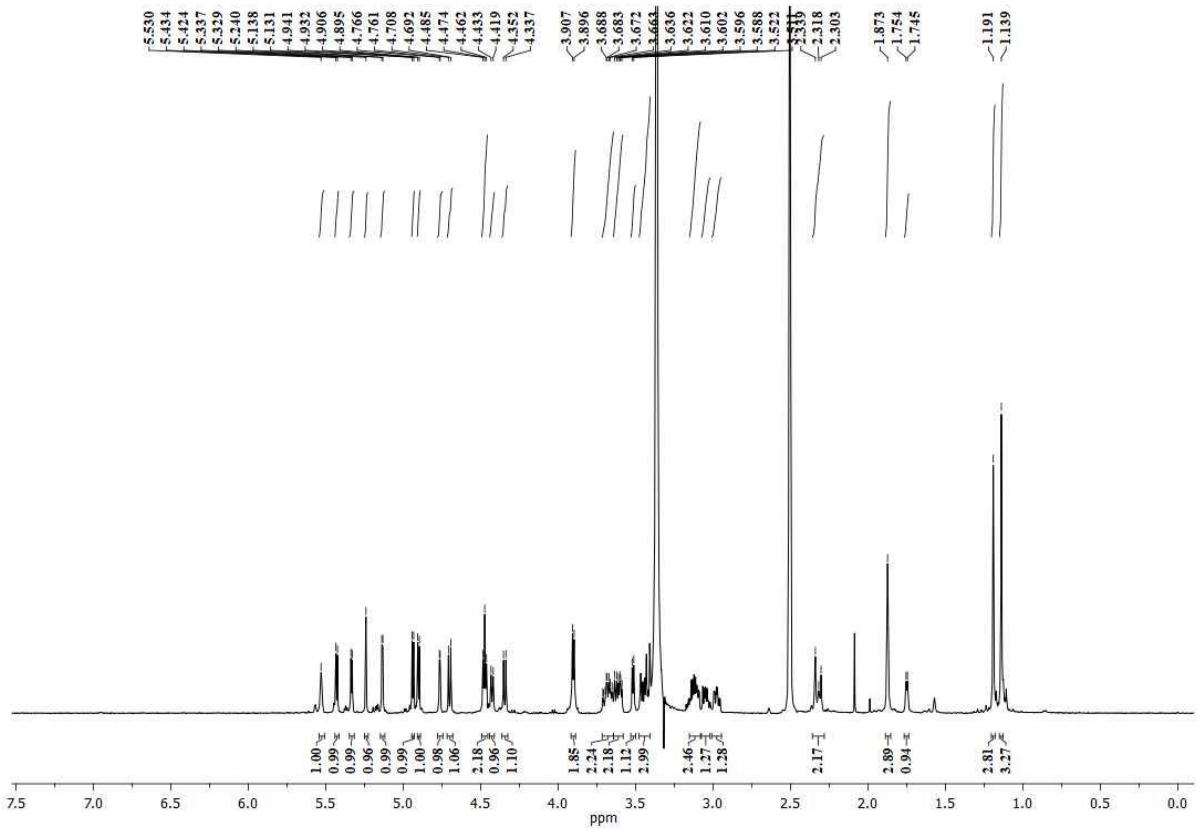

Figure 2A.56. ^{1}H NMR spectrum (500 MHz, DMSO-d_6) of novel compound (**8**)

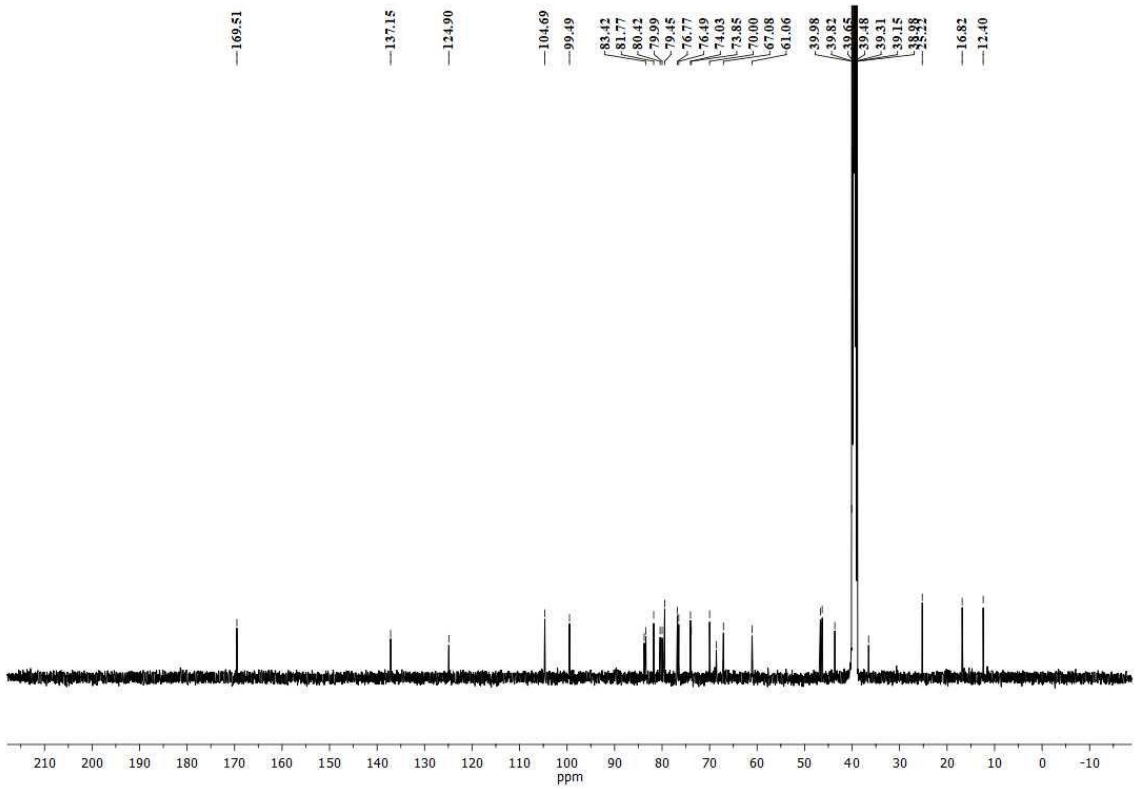

Figure 2A.57. ^{13}C NMR spectrum (125 MHz, DMSO-d_6) of novel compound (**8**)

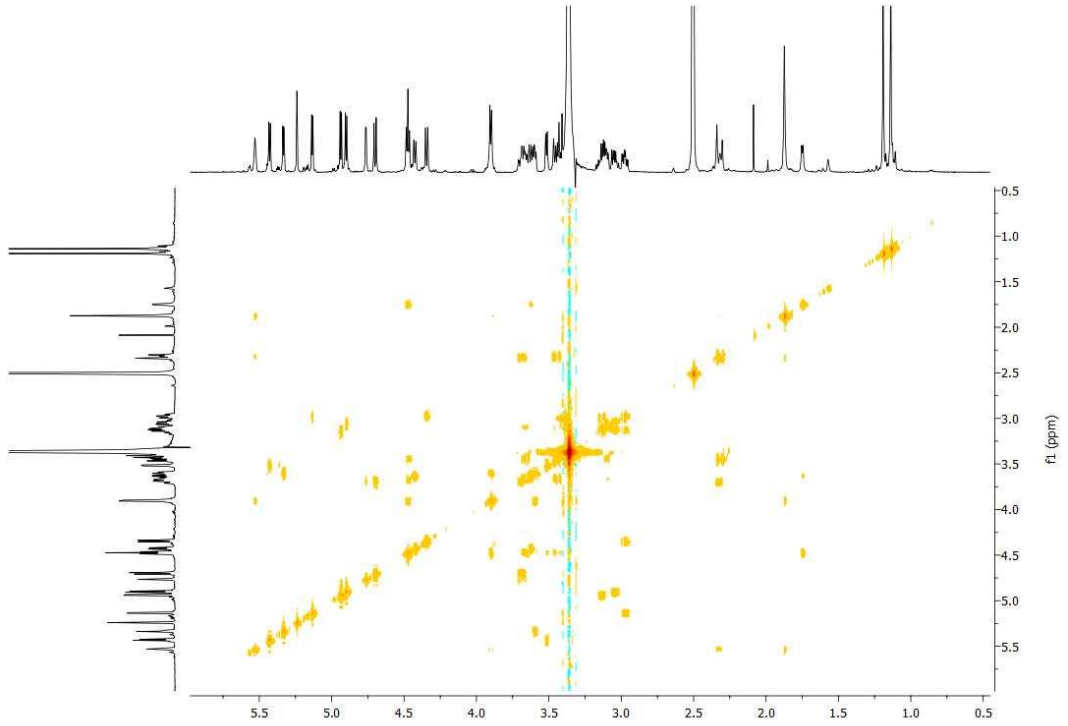

Figure 2A.58. ^{1}H-^{1}H COSY NMR spectrum (500 MHz, DMSO-d_6) of novel compound (**8**)

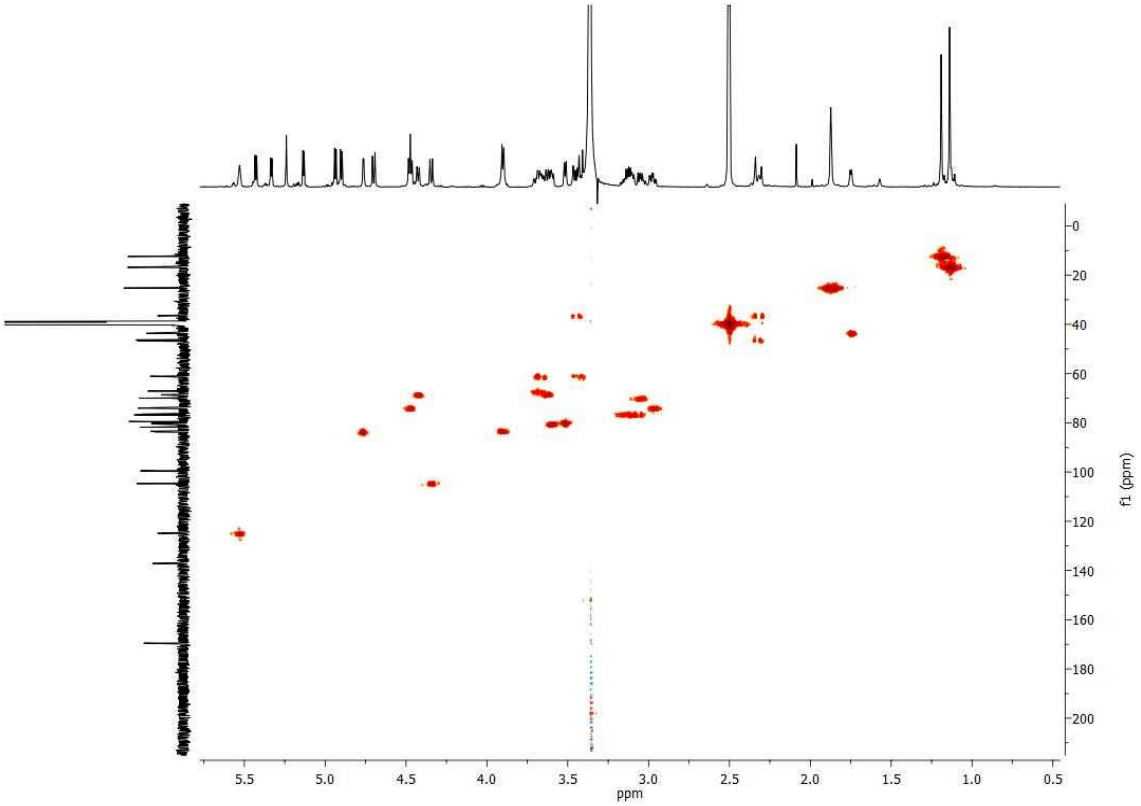

Figure 2A.59. HMQC NMR spectrum (125 MHz, DMSO-d_6) of novel compound (**8**)

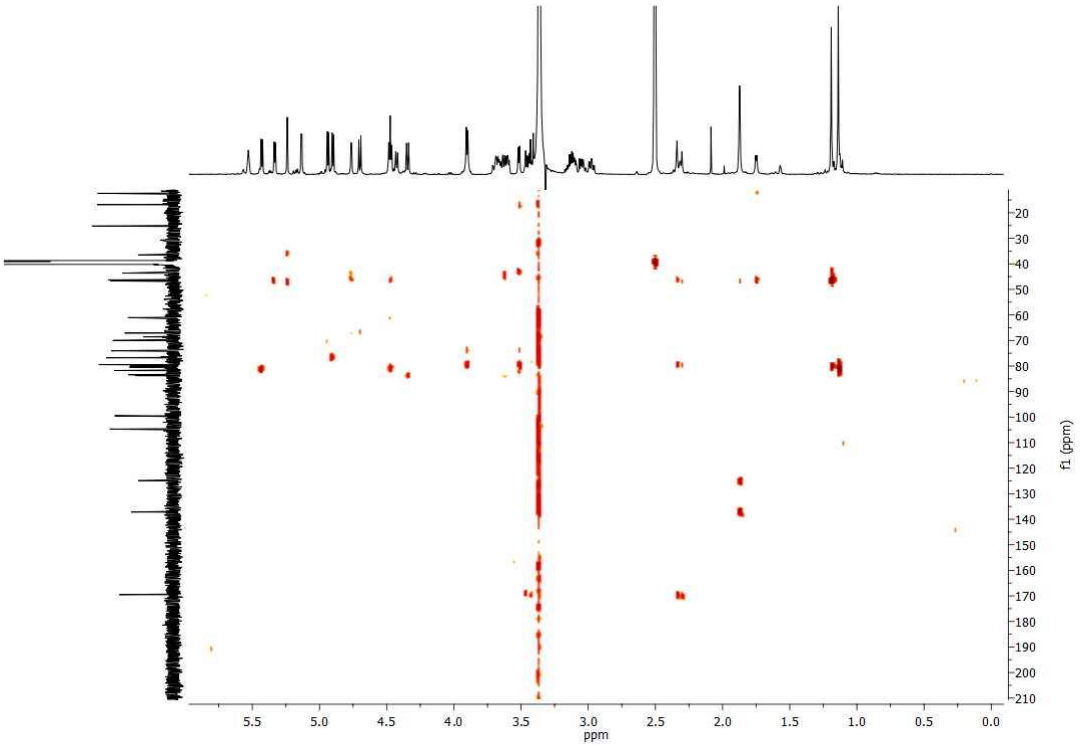

Figure 2A.60. HMBC spectrum (125 MHz, DMSO-d_6) of novel compound (**8**)

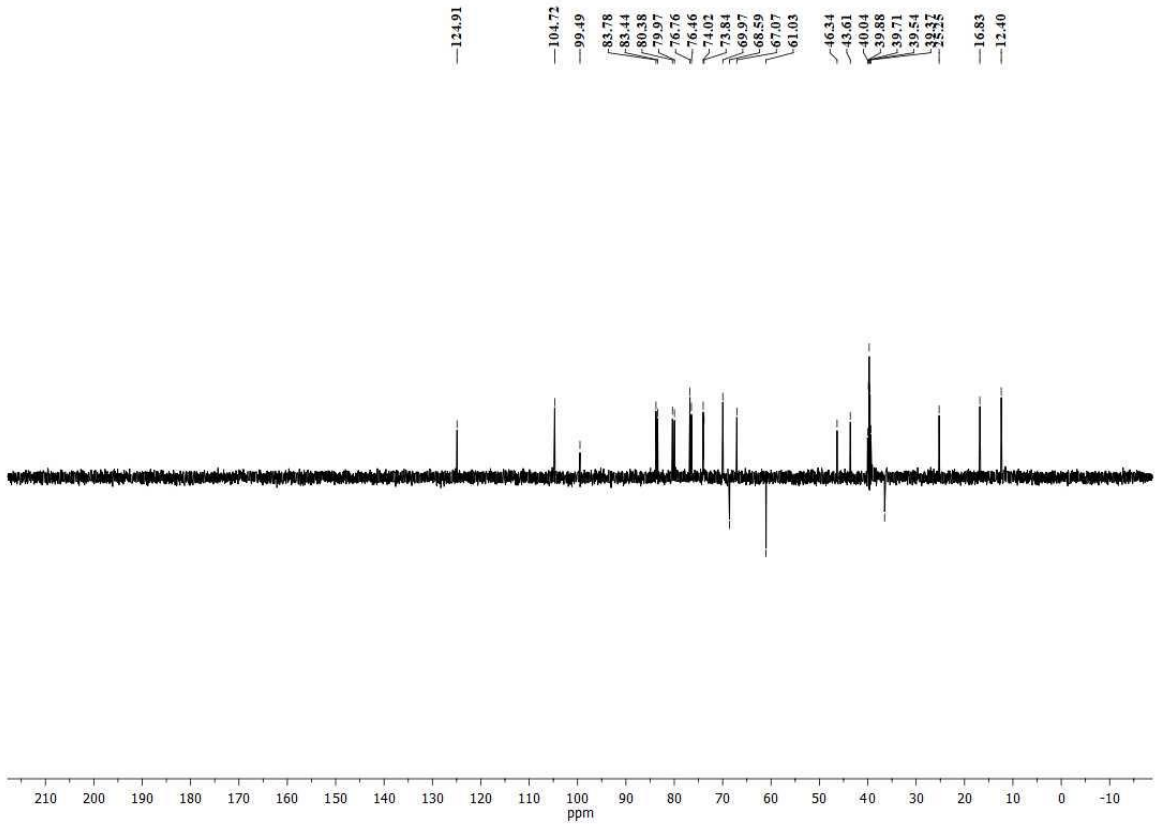

Figure 2A.61. DEPT 135 spectrum (125 MHz, DMSO-d_6) of novel compound (**8**)

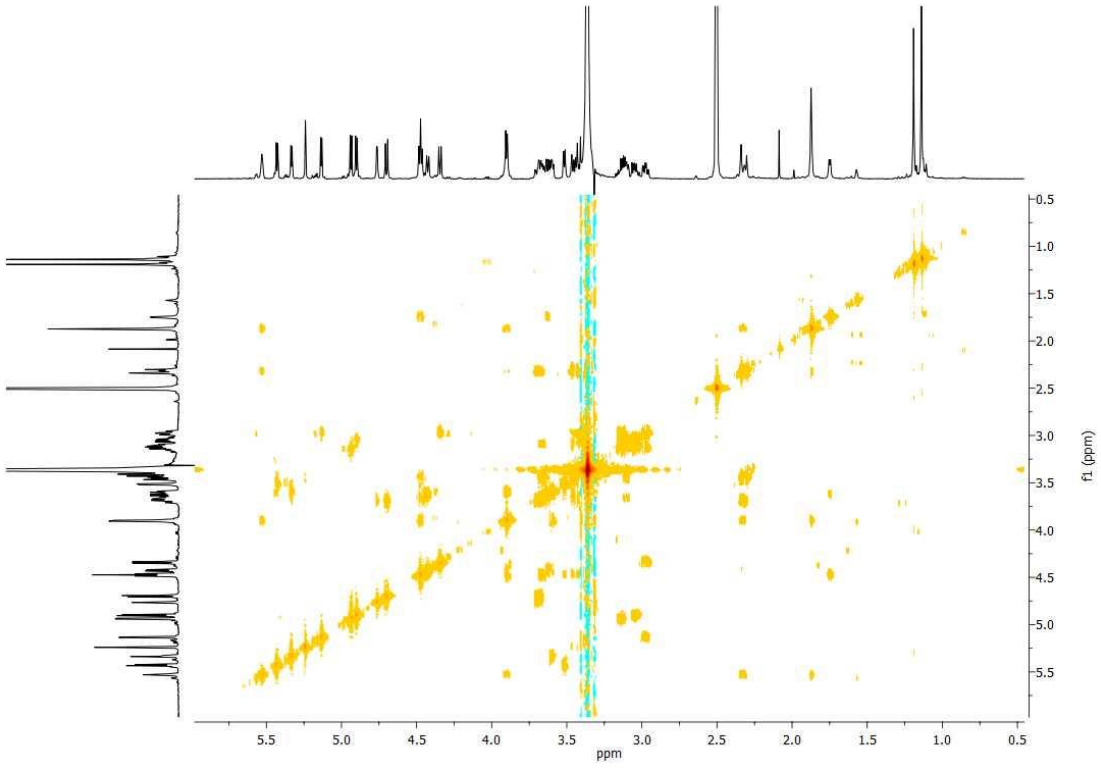

Figure 2A.62. NOESY spectrum (500 MHz, DMSO-d_6) of novel compound (**8**)

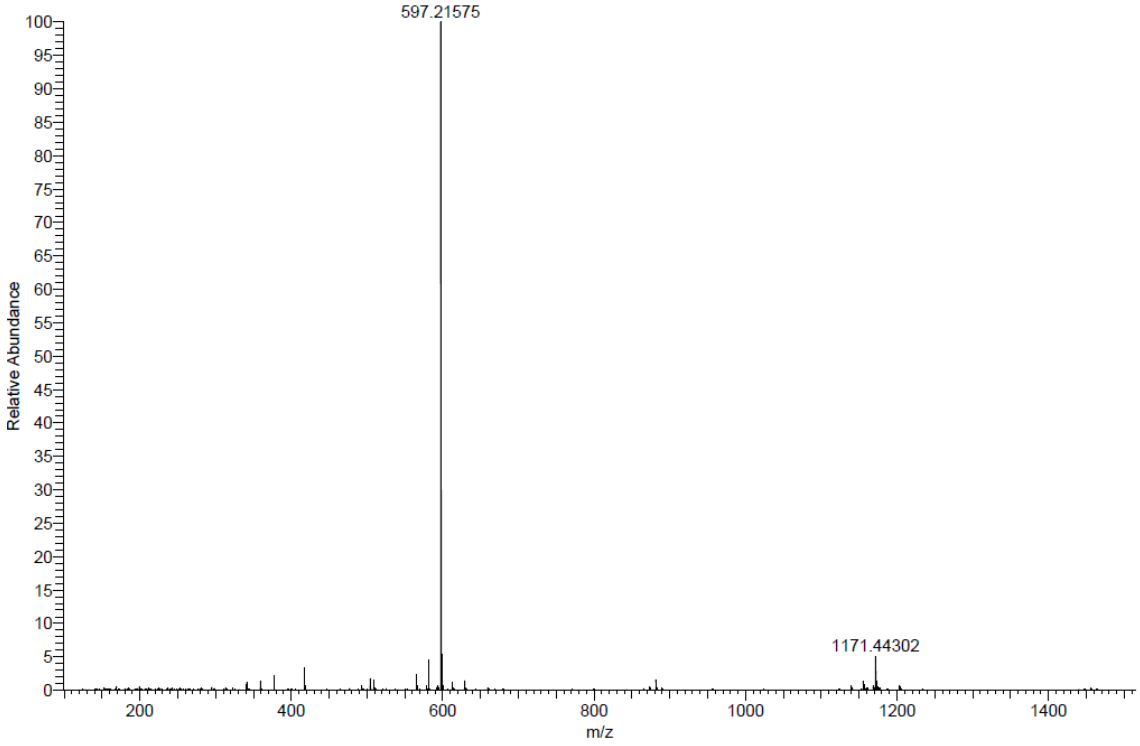

Figure 2A.63. HRESIMS spectrum of novel compound (**8**)

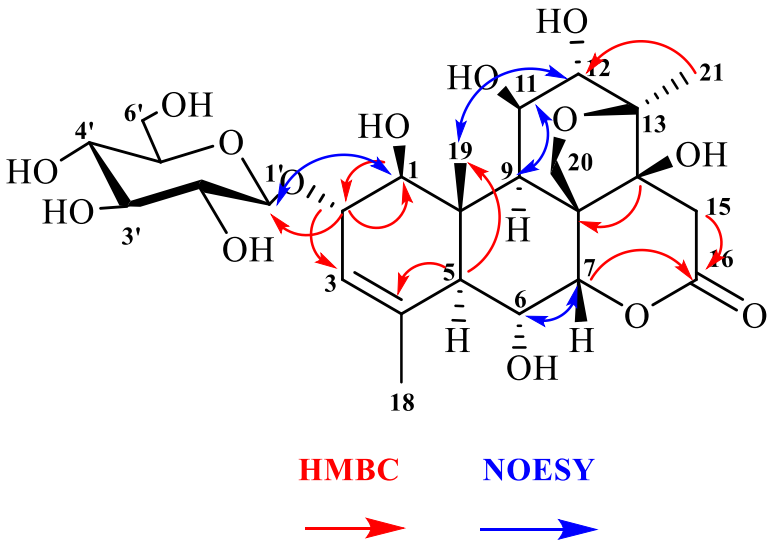

Figure 2A.64. The key HMBC and NOESY correlations of novel compound (**8**)

Table 2A.6. ^{1}H (500 MHz) and ^{13}C (125 MHz) NMR data of compound **8** in Acetone-d_6

Position	**^{1}H NMR**	**^{13}C NMR**
1	3.60-3.59 (dd, J_1 = 7 Hz and J_2 = 4 Hz)	80.4
2	3.90 (d, J = 5.5 Hz, 1H)	83.4
3	5.30 (s, 1H)	124.9
4	-	137.1
5	2.31 (d, J = 15 Hz, 1H)	46.4
6	3.47-3.40 (m, 1H)	61.1
7	3.47-3.40 (m, 1H)	80.2
8	-	46.7
9	1.75 (d, J = 4.5 Hz, 1H)	43.6
10	-	46.4
11	4.47 (t, J = 6 and 5.5 Hz, 1H)	74.03
12	3.90 (d, J = 5.5 Hz, 1H)	83.4
13	-	81.7
14	-	79.4
15	3.47-3.40 (m, 1H) 2.34 (s, 1H)	36.5
16	-	169.5
18	1.87 (s, 1H)	25.2
19	1.19 (s, 1H)	12.4
20	1.14 (s, 1H)	16.8
21	4.43 (d, J = 7 Hz, 1H) 3.63 (d, J = 7 Hz, 1H)	82.0
1’	4.34 (d, J = 7.5 Hz, 1H)	104.7
2’	2.97 (td, J_1 = 8 Hz and J_2 = 3.5 Hz, 1H)	73.8
3’	3.10 (m, 1H)	76.8
4’	3.05 (dd, J_1 = 9 Hz and J_2 = 5.5 Hz, 1H)	70.1
5’	3.10-3.09 (m, 1H)	76.7
6’	3.71-3.65 3.47-3.40	61.1

2A.5. Antidiabetic property of phytochemicals isolated from *Quassia indica*

Type II diabetes mellitus (T2DM) is a chronic metabolic disease, characterized by high glucose level because of the impairment in insulin secretion and resistance to the action of insulin on the targeted tissues [Ross *et al*., **2004**]. Nowadays, more than 422 million people live with diabetes due to environmental and hereditary factors, energy-rich diet and sedentary lifestyle [WHO Reports, **2016**]. Proper diet and exercise, inhibition of carbohydrate hydrolysing enzymes such as α-amylase and α-glucosidase, delaying of advanced glycated end products (AGEs) formation and enhancing the glucose uptake in muscle cells and adipose tissue are the main strategies for the prevention and control of T2DM [Trapero *et al*., **2012**; Yonemoto *et al*., **2014**; Riya *et al*., **2015**; Patel *et al*., **2016**; Prabhakar *et al*., **2011**]. Even though the currently available drugs are blessing to the patients, they possess some adverse side effects including hepatotoxicity, weight gain and cardiovascular problems [Victor *et al.*, **2006**; Hollander *et al.*, **2007**; Nissen *et al.*, **2007**]. Nature has gifted numerous structurally diverse and biologically active scaffolds that are now enjoying significant recognition by the scientific community because of their low toxicity, high bioavailability, and food additive properties. Hence, search for new antidiabetic leads from natural sources are on-going all over the world. Thus, as part of our continuing interest in this area, we have checked the antidiabetic property of phytochemicals isolated from *Quassia indica*.

2A.5.1. α-Amylase inhibitory activity

α-Amylase enzyme present in saliva and pancreatic juice helps to hydrolyse α-1, 4- starch to glucose and maltose. Here, porcine pancreatic α-amylase is used as a model for human pancreatic α -amylase, because it contains 496 amino acid residues and it has 83 % homology with human pancreatic α-amylase [Sui *et al*., **2016**; Sun *et al*., **2016**]. All quassinoids were evaluated for their porcine pancreatic α-amylase inhibitory activity. In the present, standard α-amylase inhibitor acarbose was used as a positive control. The IC_{50} values of the compounds are shown in **Table 2A.7**. All quassinoids displayed an IC_{50} value >100 μM.

2A.5.2. α-Glucosidase inhibitory activity

α-Glucosidase inhibitors are commonly used as oral antidiabetic agents for preventing the early-onset of diabetic problems by inhibiting postprandial hyperglycemia. They suppress the action of α-glucosidase enzymes found in small intestine and delay the release of glucose from polysaccharides. A considerable body of literature reports

suggested that traditional medicinal plants and plant derived constituents have been known to exhibit significant α-glucosidase inhibitory activity. Recently, Abdulwali, *et al*. reported the antidiabetic effects of *Brucea javanica* seeds in type 2 diabetic rats. In that paper, the authors reported the α-glucosidase inhibitory activity of Brucein D [Abdulwali, *et al*., **2017**]. To the best of our knowledge, there is no other report on α-glucosidase inhibitory activity of quassinoids. As shown in **Table 2A.7**; all quassinoids exhibited moderate to significant inhibition of α-glucosidase compared to the standard α-glucosidase inhibitor, acarbose. Among them, cedronin (**5**), novel molecule (**6**), brucein D (**7**) and novel molecule (**8**) exhibited significant α-glucosidase inhibitory activity than other compounds with IC_{50} value of 28.03 ± 0.231, 59.96 ± 0.690, 66.39 ± 0.129 and 58.5 ± 0.871 μM, respectively.

Table 2A.7. Porcine pancreatic α-amylase inhibitory activity and *Saccharomyces cervease* α-glucosidase inhibitory activity and antiglycation property of quassinoids isolated from *Quassia indica*

Compounds	α-Amylase (μM)	α-Glucosidase (μM)	Antiglycation (μM)
Samaderin A (1)	>100	80.70 ± 0.532	350.73 ± 0.812
Samaderin B (2)	>100	123.70 ± 0.654	573.08 ± 0.231
Dihydrosamaderin B (3)	>100	259.01 ± 0.911	354.75 ± 0.344
Samaderin C (4)	>100	352.69 ± 0.785	235.58 ± 0.442
Cedronin (5)	>100	28.03 ± 0.231	415.96 ± 0.701
Novel Molecule (6)	>100	59.96 ± 0.690	309.55 ± 0.487
Brucein D (7)	>100	66.39 ± 0.129	246.36 ± 0.711
Novel Molecule (8)	>100	58.5 ± 0.871	250.73 ± 0.619
Acarbose	8.93 ± 0.48	52.87 ± 0.224	-
Ascorbic acid	-		154.63 ± 0.497

Each value represents mean ± SD (standard deviation) from triplicate measurements

2A.5.3. Antiglycation property

Advanced glycated end products (AGEs) represent a heterogeneous group of molecules formed by the non-enzymatic reaction of reducing sugars with proteins, lipids and nucleic acids. The formation and accumulation of AGEs are mainly responsible for the secondary complications such as retinopathy, nephropathy, or atherosclerosis in

diabetic patients [Adrover *et al*., **2014**]. Several studies proved that natural products and its derivatives exhibit significant antiglycation property. Inspired with these observations, we examined the antiglycation property of the isolated quassinoids, (**Table 2A.7**). Of them, samaderin C (**4**), brucein D (**7**) and novel compound (**8**) showed significant ability to inhibit advanced glycated end products formation with IC_{50} value of 235.58 ± 0.442, 246.36 ± 0.711 and 250.73 ± 0.619 μM respectively.

2A.5.4. Molecular simulation studies

In order to check the druggability of quassinoids from *Quassia indica*, we carried out the QikProp anlaysis (**Table 2A.8**) and it was found that all the compounds are more drug like with few #stars value. The molecular weights of all of them are below 575 with acceptable number of non-trivial and non-hindered rotatable bonds (#rotor, 0-15). All are less toxic to central nervous system and having appreciable range of hydrogen bond donors and acceptors. The solvent accessible surface area (SASA) and its hydrophilic component (FISA) show the binding ability of the ligands and their acceptance as drugs. The human oral absorption value indicates their oral absorptivity and binding to human serum albumin (QPlogKhsa, -1.5 to 1.5) increases its bioavailability, which is further confirmed by octanol/water partition coefficient, QPlogPo/w (-2.0 to 6.50) and aqueous solubility, QPlogS (-6.5 to 0.5). All the eight compounds are predicted as good candidates for antidiabetic drug development based on acceptable ADME/T with minimum violation from Lipinski's rule of five (Ro5).

Table 2A.8. ADME/T properties of compound **1-8**

Sl. No	1	2	3	4	5	6	7	8
M.W	330.337	362.379	364.394	364.394	364.394	412.436	408.447	574.578
#stars	0	1	1	0	0	0	0	8
#rotor	1	2	2	3	3	5	4	12
CNS	-1	-2	-2	-2	-1	-2	-2	-2
SASA	497.304	515.284	512.036	517.716	507.991	547.745	561.038	740.658
FISA	143.266	189.026	187.6	177.822	168.164	218.532	203.599	352.292
HBA	9.45	11.15	11.15	10.85	10.85	13.3	11.6	21.5
HBD	1	2	2	3	3	5	4	9
QPlogKhsa	-0.645	-0.669	-0.645	-0.541	-0.546	-0.638	-0.469	-1.294
HOA	3	2	3	2	2	2	2	1
% HOA	75.925	64.572	64.933	67.863	69.614	56.356	63.578	0
QPlogPo/w	0.303	-0.309	-0.289	-0.072	-0.053	-0.857	-0.056	-2.916

QPlogS	-2.028	-2.074	-2.032	-2.282	-2.728	-2.238	-2.651	-2.132
R Of Five	0	0	0	0	0	0	0	3

M.W. (Molecular Weight):130.0 to 725.0; #stars (few stars-more drug-like): 0 to 5; #rotor (Number of non-trivial and non-hindered rotatable bonds):0 to 15; CNS (Central Nervous System activity): -2 to +2; SASA (Total solvent accessible surface area in square angstroms): 300.0 to 1000.0 FISA (Hydrophilic component of total solvent accessable area): 7.0 to 333.0; HBA (Hydrogen bond acceptor): 2.0 to 20.0; HBD (hydrogen bond donor): 0.0 to 6.0; QPlogKhsa (binding to human serum albumin): -1.5 to 1.5; HOA (Human Oral Absorption): 1, 2, or 3 for low medium, and high; % HOA (Percent Human Oral Absorption): >80 % is high, <25 % is poor; QPlogPo/w (octanol/water partition coefficient): -2.0 to 6.5; QPlogS (Aqueous solubility): -6.5 to 0.5; Ro5 (Number of violations of Lipinski's rule of five): maximum is 4.

To visualize the probable binding modes of quassinoids on *α*-glucosidase enzymes, we carried out flexible docking simulations of selected receptors with isolated ligands. The crystal structures of isomaltase from *Saccharomyces cerevisiae* (PDB ID: **3A4A**) and the *N*-terminal and *C*-terminal of human maltase glucoamylase (PDB ID: **2QMJ** and **3TOP** respectively) were retrieved from RCSB PDB (Research Collaboratory for Structural Bioinformatics Protein Data Bank). Initially, we carried out the docking simulations of all the eight quassinoids against **3A4A** and it was found that compound **8** shows better binding affinity with D-score and G-score of -8.88 kcal/mol (**Table 2A.9**). Three other compounds- **7, 6** and **5** were also showed better binding with scores less than -6.00 kcal/mol. The quassinoids generally exhibit strong hydrogen bond interaction with the protein **3A4A** due to the presence of hydroxyl groups and these hydroxyl groups are act as H-bond donors as shown in interaction diagrams (**Figure 2A.65**). In addition, in compound **7** the pyranose-*O* act as H-bond acceptor while in the novel quassinoids (**8**) oxygen from glucose ring act as the donor and stabilizes the complex. In **3A4A** of compound **8-**, there are strong H-bonds formed with TYR 158 (2.12 Å), PRO 312 (1.84 Å) and SER 240 (2.28 Å) whereas compound **7** interacts with ASP 242 (1.46 and 2.79 Å), PRO 312 (1.87 Å) and ARG 315 (2.06 Å). Compound **4** also forms strong H-bond interaction with hydrophobic PRO 312 (1.65 Å) in addition to the interaction with LEU 313 (2.13 Å). In compound **5** -protein complex, interaction with TYR 158 (2.05 Å), ASP 242 (2.39 Å) and ASP 307 (1.59 Å) are the stabilizing factors. These findings are in good

agreement with experimental results and hence we decided to check the interaction of these compounds with human maltase-glucoamylase.

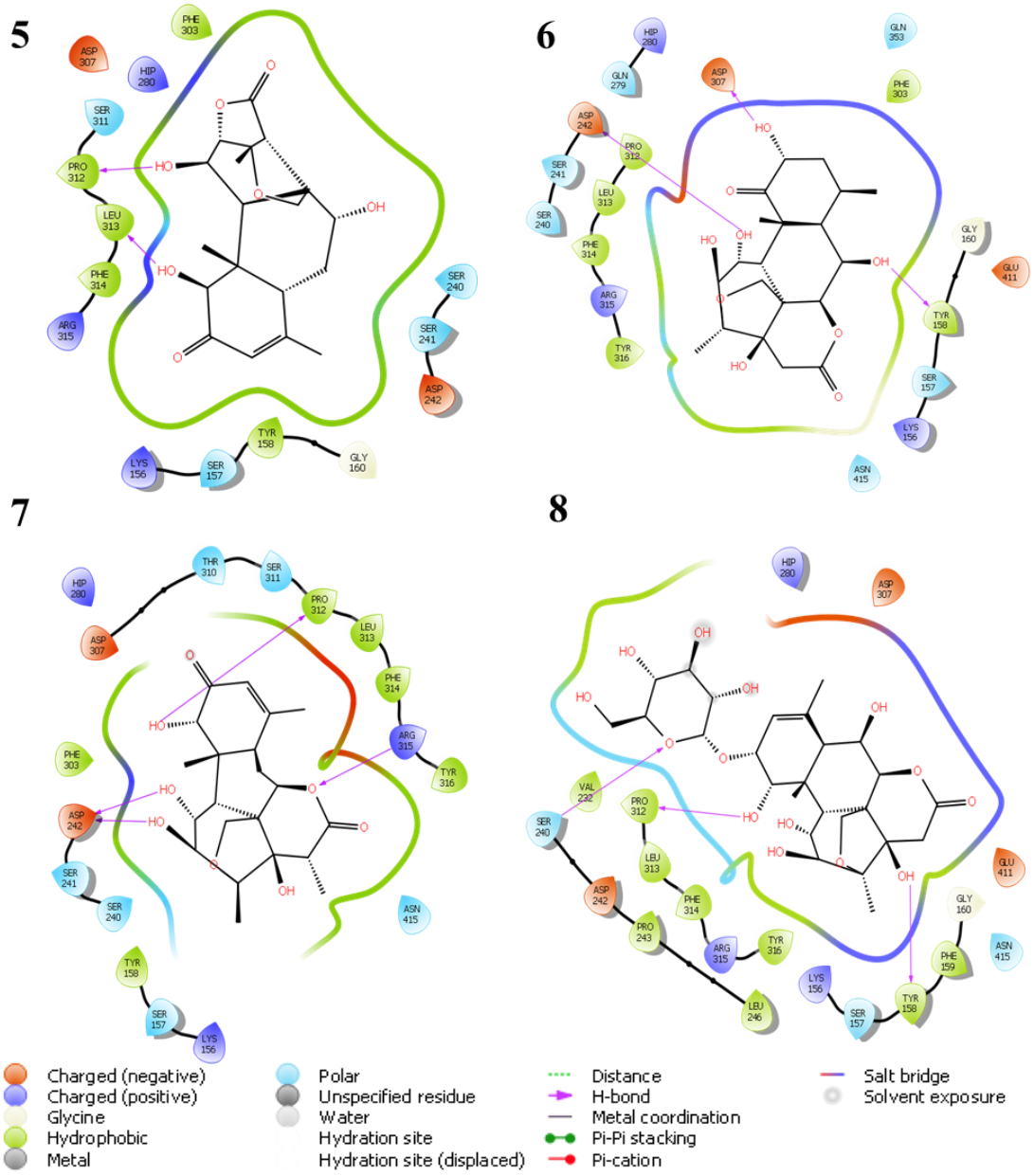

Figure 2A.65. 2D interaction diagram of cedronin (**5**), novel compound (**6**), brucein D (**7**) and novel compound (**8**) with the protein **3A4A**

Consequently, we checked whether these quassinoids interacts with *N*- and *C*-terminal of human maltase-glucoamylase (**2QMJ** and **3TOP** respectively**)**. Novel molecule (**8**) [-8.07 kcal/mol] effectively binds with **2QMJ**, while others are not. Meanwhile, the C-terminal catalytic domains of human maltase glucoamylase (**3TOP**) show better interaction with novel molecule (**8**, G-Score/D-Score of -8.19 kcal/mol),

followed by **7** (G-score and D-score of -7.08 kcal/mol). These results suggested that quassinoids (compounds **5-8**) can act as a promising target for the treatment of T2DM. Further it was more clear from docking data that the *C*-terminal provides the better binding pocket for the quassinoids in general. The 2D interaction diagrams are shown in **Figure 2A.66 (3TOP) and Figure 2A.67 (2QMJ),** and the G/D-score of all the isolates are shown in **Table 2A.8.**

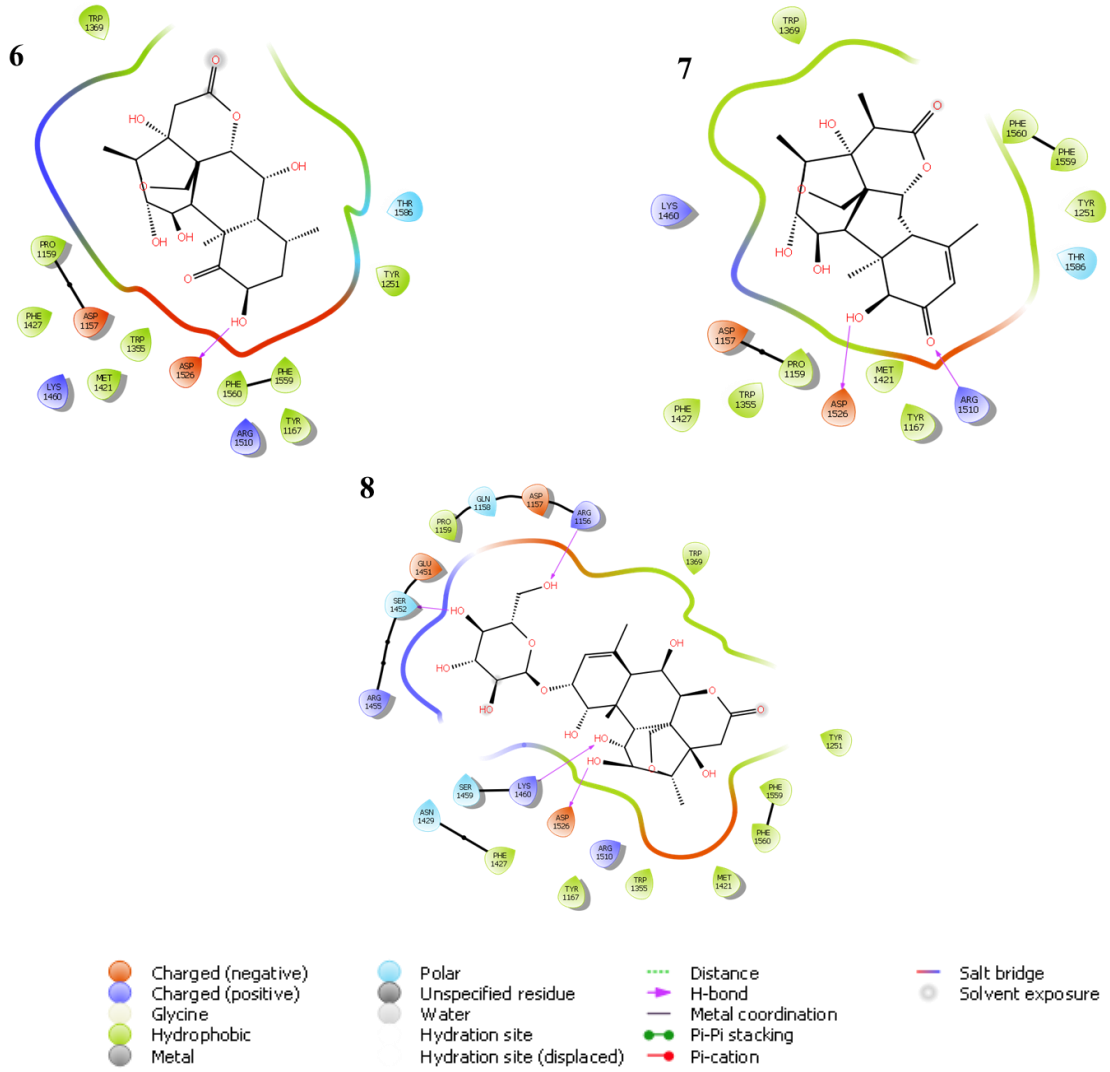

Figure 2A.66. 2D interaction diagram of novel compound (**6**) brucein D (**7**) and novel compound (**8**) with the protein **3TOP**

Compound **8** show exceptional H-bond interactions due to the presence of hydroxyl groups from glucose ring. In the case of interaction with **2QMJ**, the two hydroxyl groups from the ring form H-bond with negatively charged ASP 327 (1.58 and 1.78 Å) while that from -CH_2OH acts as H-bond donor and acceptor by forming bond with positively charged ARG 526 (2.26 Å) and negatively charged ASP 542 (1.88 Å).

There is an additional H-bond of hydroxyl group with ASP 203 (1.97 Å). At the same time with **3TOP**, the hydroxyl group of glucose moiety form H-bond with SER 1452 (1.90 Å) and glucosyl -CH_2OH interact with ARG 1156 (1.96 Å). In addition, two hydroxyl groups form H-bond with LYS 1460 (2.30 Å) and ASP 1526 (2.51 Å). Compound **8** show better affinity due to the well packing of the compound inside the binding pocket compared to the others. Moreover, it is very clear that the *C*-terminal gives the suitable binding pocket for all the compounds, whereas compound **8** is suitably fit into *N*-terminal also. The carbonyl oxygen from cyclohexenyl ring of compound **7** form H-bond with positively charge ASP 1510 (1.84 Å) while the hydroxyl group from the same ring forms bond with negatively charged ASP 1526 (2.04 Å). The hydroxyl group of cyclohexyl ring from compound **6** interact with ASP 1526 (1.59 Å) results in the lesser affinity with **3TOP** (G-score and D-score of -5.88 kcal/mol). The positive results from docking simulations indicate the need for the generation of a pharmacophore model based on seven point hypothesis.

Table 2A.9. G-Score/D-Score of isolated compounds with human pancreatic α-amylase (**3A4A**) and human maltase glucoamylase (*N*- terminal, **2QMJ**; *C*- terminal, **3TOP**)

Compounds	**3A4A** (kcal/mol)		**2QMJ** (kcal/mol)		**3TOP** (kcal/mol)	
	G-Score	D-Score	G-Score	D-Score	G-Score	D-Score
Samaderin A (**1**)	-4.16	-4.16	-3.05	-3.05	-3.83	-3.83
Samaderin B (**2**)	-5.11	-5.11	-2.26	-2.26	-5.3	-5.3
Dihydrosamaderin B (**3**)	-4.81	-4.81	-2.33	-2.33	-5.1	-5.1
Samaderin C (**4**)	-5.61	-5.61	-4.36	-4.36	-5.2	-5.2
Cedronin (**5**)	-6.88	-6.88	-3.38	-3.38	-4.79	-4.79
Novel Molecule (**6**)	-6.65	-6.65	4.07	4.07	-5.88	-5.88
Brucein D (**7**)	-7.62	-7.62	-3.89	-3.89	-7.08	-7.08
Novel Molecule (**8**)	-8.88	-8.88	-8.07	-8.07	-8.19	-8.19

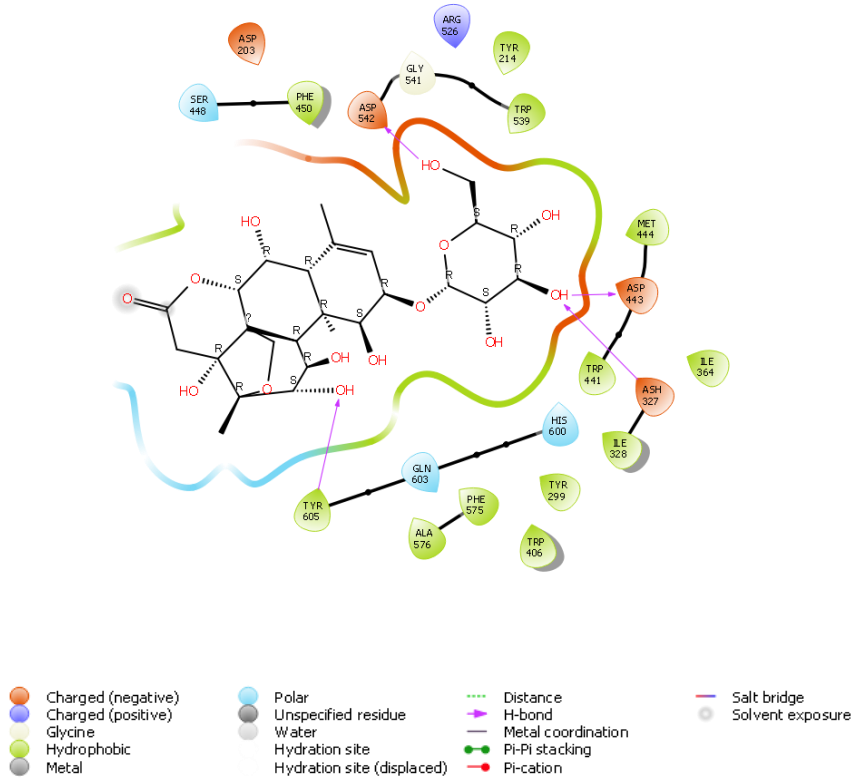

Figure 2A.67. 2D interaction diagram of novel compound (**8**) with the protein **2QMJ**

2A.5.5. Pharmacophore modelling

Pharmacophore modelling is an integral part of computer aided drug design (CADD), which has become one of the major tools in hit identification, lead optimization, and rational design of novel drugs. A pharmacophore modelling is the assembly of familiar steric and electronic features that are essential to make certain the optimal molecular interactions with a precise biological target and to trigger or block its biological response. It can be used to characterize molecules on 3D level by identifying the essential properties of molecular recognition. Every type of atom or group in a compound can be reduced to a pharmacophore fingerprint. These molecular patterns would be labelled by a number of chemical properties, such as hydrogen bond donors or acceptors, aromatic, cationic, *etc*, which can be used to analyze the resemblance among a library of small molecules and identify the key causal features to the biological function **(Figure 2A.68).** The spatial arrangements of chemical features that interact with the receptor are three acceptors, one donor and three hydrophobic centers, which comprises the pharmacophore for quassinoids with hypothesis score of 1.35.

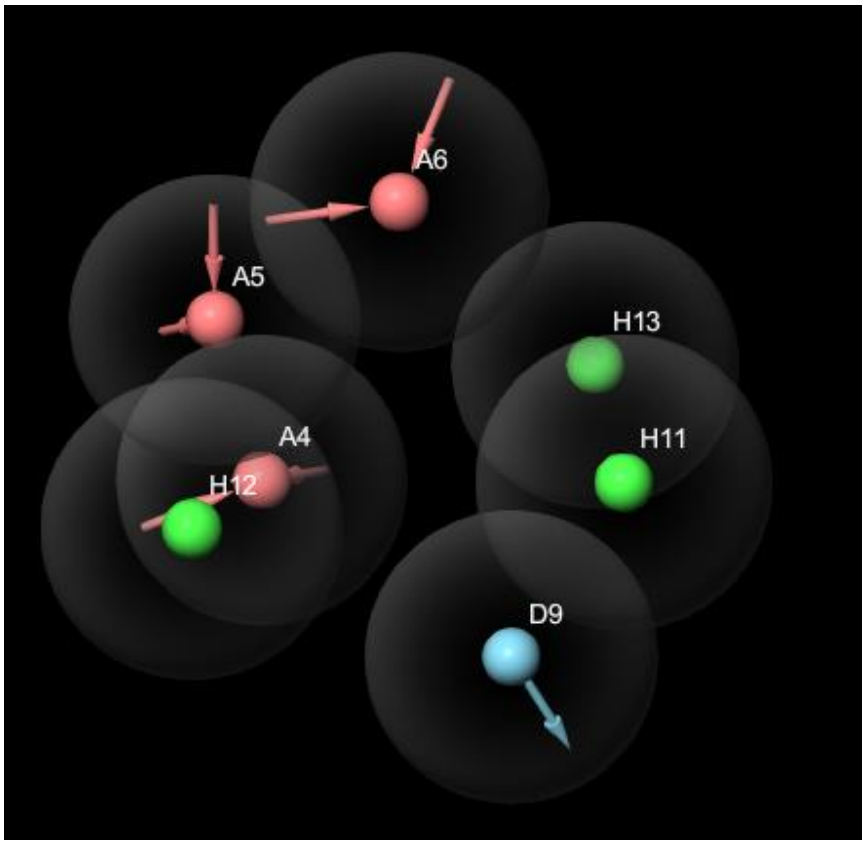

Figure 2A.68. Pharmacophore model generated for quassinoids

2A.5.6. Glucose uptake in L6 myotubes

Muscle cells and adipose tissues are the key player of glucose consumption in our body and majority of insulin stimulated glucose uptake occurs here. The imbalance of glucose homeostasis leads to T2DM. The effect of quassinoids on glucose uptake was assessed in differentiated skeletal myotubes. In order to find out the working concentrations of quassinoid, the cell viability was examined in L6 cell line by MTT assay. The cell viability decreased significantly in a dose-dependent manner. A concentration of 15 μM caused cell viability to decrease by about 45 %. Therefore, 5μM and 10 μM concentrations of quassinoids were selected for cellular glucose uptake experiments (**Figure 2A.69**). It was monitored using the fluorescently labeled glucose analogue, 2-NBDG (10 μM) after the pre-treatment of the differentiated L6 myotubes with 5 and 10 μM concentrations of quassinoids. All quassinoids shows moderate 2-NBDG uptake in L6 myotubes (**Figure 2A.70**).

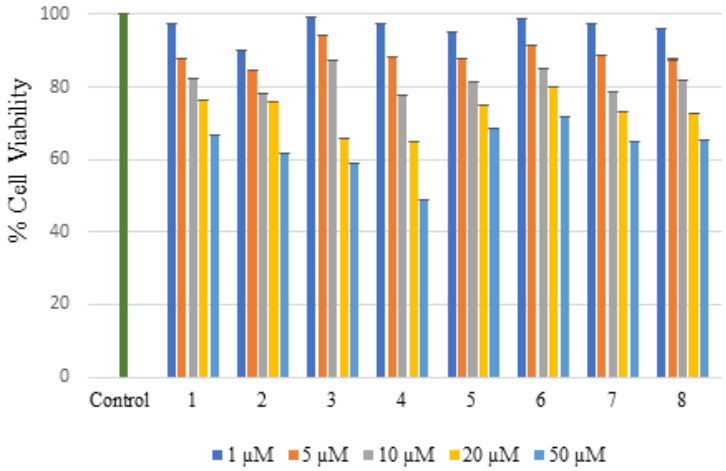

Figure 2A.69. Cytotoxicity in L6 cell lines (**1-8**)

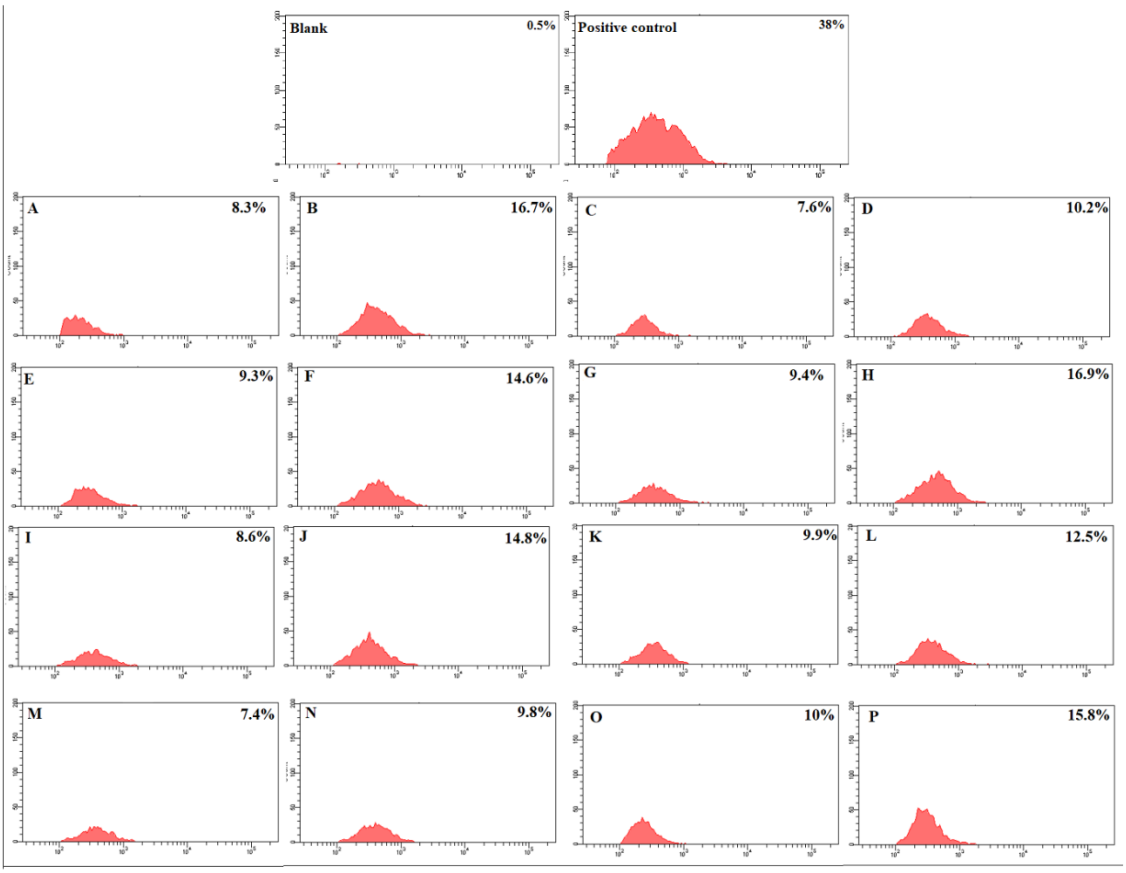

Figure 2A.70. 2-NBDG uptake in differentiated L6 myotubes was assessed by the uptake of control cells (Blank), 100 nM Rosiglitazone treated cells (Positive control), 5 μM and 10 μM samaderin A (A and B), 5 μM and 10 μM samaderin B (C and D), 5 μM and 10 μM dihydrosamaderin B (E and F), 5 μM and 10 μM samaderin C (G and H), 5 μM and 10 μM cedronin (I and J), 5 μM and 10 μM novel compound (K and L), 5 μM and 10 μM brucein D (M and N) and 5 μM and 10 μM novel compound (O and P) treated with cells

2A.6. Conclusion

In conclusion, phytochemical investigation of the seeds of *Quassia indica* led to the isolation of two novel compound (**6**) and (**8**) along with six known quassinoids [samaderin A (**1**), samaderin B (**2**), dihydrosamaderin B (**3**), samaderin C (**4**), cedronin (**5**) and brucein D (**7**)]. All quassinoids exhibited moderate α-amylase inhibitory activity and moderate to significant α-glucosidase inhibitory activity. Cedronin (**5**) exhibited promising α-glucosidase inhibitory activity with IC_{50} value of 28.03 ± 0.231 μM. The molecular simulation studies indicated that novel compound (**8**) effectively binds the pocket of isomaltase from *Saccharomyces cerverce* (**3A4A**) and *N*- (**2QMJ**) and *C*- (**3TOP**) terminal human maltase glucoamylase. All quassinoids showed moderate antiglycation property. *In vitro* antidiabetic activity in L6 myotubes revealed these compounds moderately stimulates the glucose uptake in a dose dependant manner. Further studies are in progress to establish the therapeutic efficacy and safety of compounds as promising α-glucosidase inhibitors from *Quassia indica.*

2A.7. Experimental

2A.7.1. General experimental procedures and chemicals

The melting points were performed on a Buchi melting point apparatus. The FTIR spectra were achieved using Bruker FTIR spectrometer, and values are acquired in cm^{-1}. NMR spectra was acquired from Bruker Avance 500 MHz, using $CDCl_3$ and acetone-d_6 as solvents and the chemical shifts are expressed in δ (ppm) relative to the tetramethylsilane peak. The multiplicities of NMR signals were assigned as singlet (s), doublet (d), triplet (t), multiplet (m), and broad singlet (brs). The HRESIMS data was recorded at 60,000 resolution using Thermo Scientific Exactive mass spectrometer. Column chromatography was done using silica gel (100−200 and 230−400 mesh; Merck, Darmstadt, Germany). Merck precoated silica gel F_{254} plates were used for thin-layer chromatography (TLC). Spots were detected on TLC under UV light or by heating after spraying samples with anisaldehyde-sulfuric acid.

Porcine pancreatic α-amylase, α-glucosidase from *Saccharomyces cerevesae*, acarbose, bovine serum albumin (BSA), α-D-glucose, ascorbic acid, metformin, 4-nitrophenyl α-D-glucopyranoside (*p*-NPG), Dulbecco's modified Eagle's media (DMEM), fetal bovine serum (FBS), antibiotic-antimycotic solution (Pencillin–streptomycin–amphotericin B mix) and 3-(4,5-dimethylthiazol -2-yl)-2,5-diphenyl tetrazolium bromide (MTT) were procured from M/s Sigma–Aldrich Chemicals (St.

Louis, MO, **USA**). 2-(N-(7-nitrobenz-2-oxa-1, 3-diazol-4-yl)amino)-2-deoxy glucose (2-NBDG) was obtained from molecular probe (Invitrogen Life Technologies, Carlsbad, CA, **USA**).

2A.7.2. Plant material collection and isolation of phytochemicals

The seeds of *Quassia indica*were collected from Alappuzha district, Kerala, India. The seeds were cleaned, air dried and then dried in drier maintained at 50 ^{o}C and powdered. The powdered seed (300 g) was subjected to extraction using *n*-hexane, acetone, ethanol and water (1 L x 3 times) at room temperature. After extraction, the solvent was removed under reduced pressure using Büchi rotary evaporator. The crude extract (28 g) was subjected to silica gel (100-200 mesh) column chromatography using *n*-hexane, *n*-hexane-EtOAc gradient and EtOAc. Eighteen fractions of 200 mL each were collected and concentrated under reduced pressure. The schematic representation of extraction and isolation procedure was shown in **Figure 2A.71.**

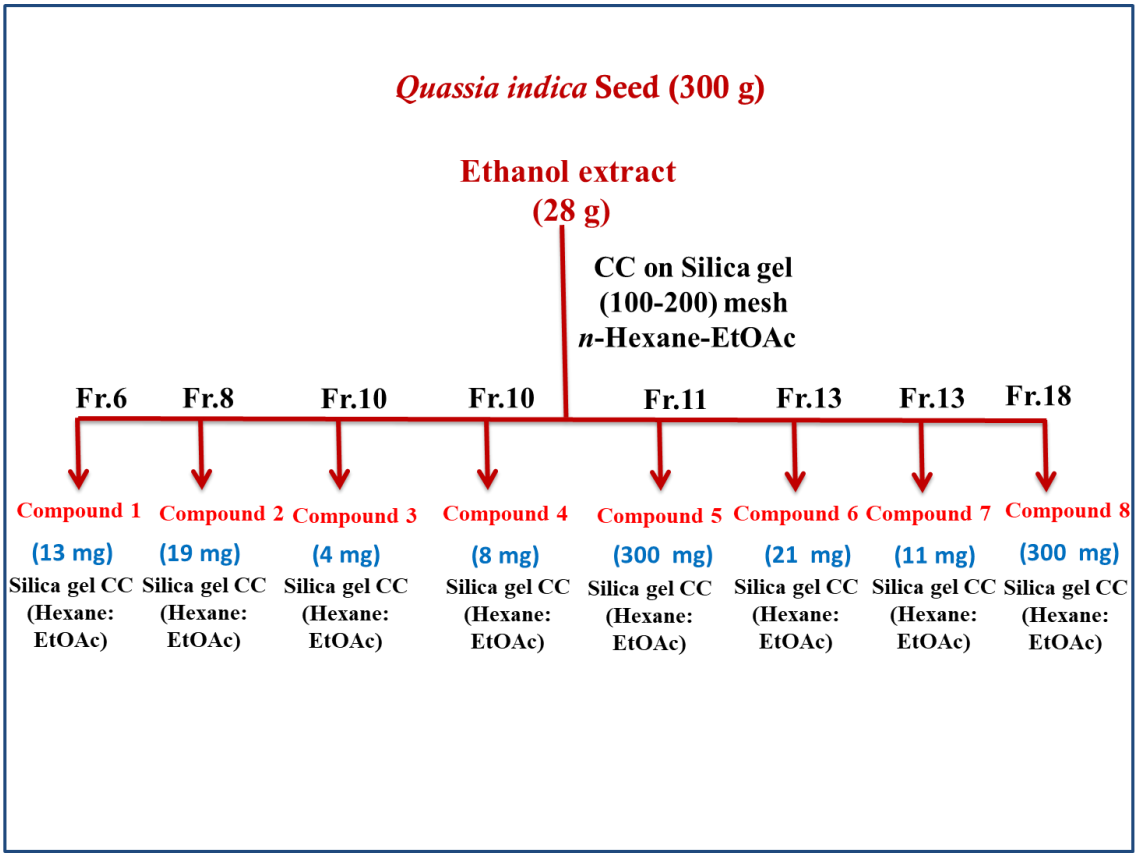

Figure 2A.71. Schematic representation of isolation of quassinoids from the stem bark of *Quassia indica*

2A.7.2.1. Isolation of compound 1

The isolation procedure of compound **1** is represented in **Figure 2A.71.** Compound **1** (13 mg) was obtained as a colourless solid from the fraction pool 6, on eluting the column (silica gel 100-200 mesh) with 40 % EtOAc in *n*-hexane. The detailed analysis of IR, ^{1}H, ^{13}C, ^{1}H-^{1}H COSY, HMQC, DEPT 135, HMBC NMR spectra, single crystal XRD and HRESIMS gave compound **1** as samaderin A.

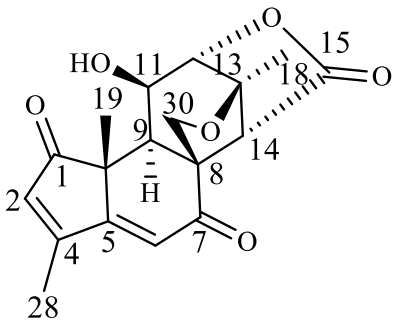

Nature	Colourless crystalline solid
Melting Point	254-256 °C
Specific rotation ($[\alpha]^{D}_{25}$)	-30° (*c* 0.1, MeOH)
FTIR (KBr, υ_{max})	3420, 2980, 1760, 1625, 1590 and 1480 cm^{-1}.
^{1}H NMR (500 MHz, $CDCl_3$)	δ 6.24 (d, *J* = 1 Hz, 1H, H-2), 6.02 (s, 1H, H-6), 4.82 (d, *J* = 9 Hz, 2H, H-11 and H-30), 4.30 (d, *J* = 3.5 Hz, 1H, H-12), 4.16 (dd, J_1 = 9 Hz, J_2 = 1.5 Hz, 1H, H-30), 3.58 (d, *J* = 10.5 Hz, 1H, H-11,-OH), 3.45 (d, *J* = 1 Hz, 1H, H-14), 2.27 (dd, J_1 = 1 Hz, J_2 = 4.5 Hz, 1H, H-9), 2.23 (d, *J* = 1.5 Hz, 3H, H-28), 1.73 (s, 3H, H-19), 1.60 (s, 3H, H-18) ppm.
^{13}C NMR (125 MHz, $CDCl_3$)	δ 203.5 (C-1), 193.8 (C-7), 171.1 (C-15), 168.8 (C-5), 163.3 (C-4), 134.1 (C-2), 116.8 (C-6), 89.2 (C-13),

	81.8 (C-12), 76.1 (C-30), 69.0 (C-11), 58.1 (C-14), 57.4 (C-8), 48.2 (C-10), 40.2 (C-9), 21.4 (C-19), 20.9 (C-18), 13.7 (C-28) ppm.
HRESIMS (m/z)	331.1211 $[M+H]^+$

2A.7.2.2. Isolation of compound 2

Fraction pool 8 on column chromatographic purification (silica gel 100-200 mesh) using 50 % EtOAc/*n*-hexane as eluent afforded compound **2** (19 mg) as colourless crystalline solid. The detailed analysis of FTIR, ^{1}H, ^{13}C, ^{1}H-^{1}H COSY, HMQC, DEPT 135 and HMBC NMR spectra, HRESIMS and single crystal XRD gave compound **2** as samaderin B.

Nature	Colourless crystalline solid
Melting Point	237-239 °C
Specific rotation ($[\alpha]^{D}_{25}$)	-61° (*c* 0.2, MeOH)
FTIR (KBr, υ_{max})	3415, 2983, 1765, 1625, 1521 1461, 1230, 1140 and 980 cm^{-1}.
^{1}H NMR (500 MHz, DMSO-d_6)	δ 5.99 (d, *J* = 1 Hz, 1H, H-4), 5.55 (brs, 1H, -OH), 4.74 (d, *J* = 8.5 Hz, 1H, H-30), 4.63 (s, 1H), 4.38 (d, *J* = 4.5 Hz, 1H) 4.27 (d, *J* = 3.5 Hz, 1H), 4.23 (d, *J* = 2.5 Hz, 1H), 3.60 (d, *J* = 7 Hz, 1H, H-30), 3.42 (d, *J* = 1 Hz, 1H), 3.07 (d, *J* = 13.5 Hz, 1H), 2.75 (m, 2H),

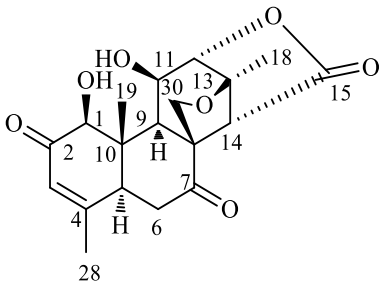

Samaderin B

	2.12 (d, *J* = 3.5 Hz, 1H), 1.88 (s, 3H, H-28), 1.41 (s, 3H, H-18), 1.24 (s, 3H, H-19) ppm.
^{13}C NMR (125 MHz, DMSO-d_6)	δ 205.3 (C-7), 197.7 (C-2), 171.9 (C-15), 161.2 (C-4), 124.2 (C-3), 86.8, 83.6, 80.9, 74.6 (C-30), 69.5, 60.4, 55.3, 48.5, 46.7, 46.6, 38.4 (C-6), 21.4 (C-21), 20.4 (C-18), 9.9 (C-19) ppm.
HRESIMS (m/z)	385.12671 $[M+Na]^+$

2A.7.2.3. Isolation of compound 3

Compound **3** (4 mg) was obtained as a colourless crystalline solid from the fraction pool 10, on eluting the column (silica gel 100-200 mesh) with 55 % EtOAc in *n*-hexane. The detailed analysis of IR, ^{1}H, ^{13}C, ^{1}H-^{1}H COSY, HMQC, DEPT 135, HMBC NMR spectra, single crystal XRD and HRESIMS gave compound **3** as dihydrosamaderin B.

Nature	Colourless crystalline solid
Melting Point	135-137 ^{o}C
Specific rotation ($[\alpha]^D_{25}$)	-45° (*c* 0.3, MeOH)
FT-IR (KBr, υ_{max})	3380, 2970, 1760, 1615, 1530 1475, 1240, 1150 and 960 cm^{-1}.
^{1}H NMR (500 MHz, $CDCl_3$)	δ 4.72 (d, *J* = 8 Hz, 1H, C-30), 4.64 (dd, J_1 = 10 Hz, J_2 = 7 Hz, 1H, C-11), 4.35 (d, *J* = 3.5 Hz, 1H, -OH), 4.30 (dd, J_1 = 3.5 Hz, J_2 = 1 Hz, 1H, C-1), 4.13 (d, *J* =

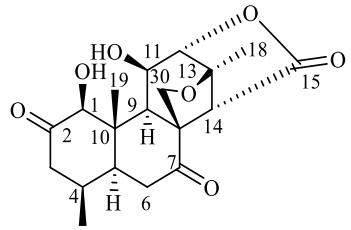

Dihydrosamaderin B

	2.5 Hz, 1H, C-13), 3.77 (dd, J_1 = 8.5 Hz, J_2 = 1.5 Hz, 1H, C-30), 3.64 (d, J = 1 Hz, 2H), 2.79 (q, J_1 = 13 Hz, J_2 = 8 Hz, 1H), 2.66 (dd, J_1 = 16.5 Hz, J_2 = 14.5 Hz, 1H, C-6), 2.55 (dd, J_1 = 13.5 Hz, J_2 = 1.5 Hz, 1H, C-3), 2.51 (dd, J_1 = 16.5 Hz, J_2 = 3.5 Hz, 1H, C-6), 2.44 (m, 1H, C-3), 2.34 (m, 1H), 2.02 (dd, J_1 = 4.5 Hz, J_2 = 1 Hz, 1H), 1.56 (s, 3H, C-18), 1.36 (s, 3H, C-19), 0.97 (d, J= 8 Hz, 3H, C-28) ppm.
^{13}C NMR (125 MHz, $CDCl_3$)	δ 208.6 (C-7), 204.0 (C-2), 171.9 (C-15), 87.6 (C-13), 83.7 (C-1), 81.9 (C-13), 74.4 (C-30), 70.3 (C-11), 60.7 (C-15), 55.6, 50.7, 48.5 (C-14), 45.2 (C-3), 45.2, 41.6 (C-6), 35.7, 20.8 (C-18), 15.4 (C-28), 13.9 (C-19) ppm.
HRESIMS (m/z)	365.1760 $[M+H]^+$

2A.7.2.4. Isolation of compound 4

Compound **4** (8 mg) was also obtained as a colourless crystalline solid from the fraction pool 10, on eluting the column (silica gel 100-200 mesh) with 55 % EtOAc in *n*-hexane. The detailed analysis of FTIR, ^{1}H, ^{13}C, ^{1}H-^{1}H COSY, HMQC, DEPT 135, HMBC NMR spectrum, single crystal XRD and HRESIMS gave compound **4** as samaderin C.

Nature	Colourless crystalline solid
Melting Point	266-268 ^{o}C
Specific rotation ($[\alpha]^D_{25}$)	-71° (*c* 0.2, MeOH)

FTIR (KBr, υ_{max})	3340, 2960, 1741, 1530 1450, 1225, 1050 and 938 cm^{-1}.
^{1}H NMR (500 MHz, $CDCl_3$)	δ 5.67 (d, *J* = 4.5 Hz, 1H, -OH), 5.34 (s, 1H), 4.80 (t, *J* = 3 Hz, 2H), 4.66 (dd, J_1 = 9 Hz, J_2 = 5 Hz, 1H), 4.45 (d, *J* = 5.5 Hz, 1H, -OH), 4.21 (d, *J* = 5 Hz, 1H), 3.90 (s, 1H), 3.59 (d, *J* = 8.5 Hz, 1H), 3.43 (s, 1H), 2.55 (t, *J* = 4.5 Hz, 1H), 2.35 (d, *J* = 13 Hz, 1H), 1.75 (d, *J* = 3.5 Hz, 1H), 1.55 (s, 3H, C-28), 1.40 (s, 3H, C-18), 1.26 (s, 3H, C-19) ppm.
^{13}C NMR (125 MHz, $CDCl_3$)	δ 206.0 (C-1), 172.2 (C-15), 132.4 (C-4), 125.7 (C-3), 86.8 (C-13), 83.7 (C-1), 80.5, 75.1 (C-30), 71.5, 69.6, 60.5 (C-15), 55.7, 49.2, 47.5, 46.9, 43.0, 20.4 (C-28), 20.1 (C-19), 10.3 (C-18) ppm.
HRESIMS (m/z)	365.1610 $[M+H]^+$

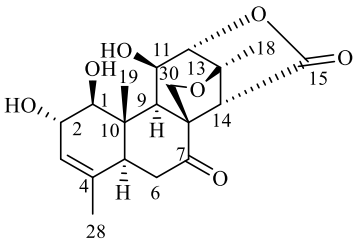

Samaderin C

2A.7.2.5. Isolation of compound 5

Compound **5** (300 mg) was obtained as a colorless crystalline solid from the fraction pool 11, on eluting the column (silica gel 100-200 mesh) with 60 % EtOAc in *n*-hexane. The detailed analysis of FTIR, ^{1}H NMR, ^{13}C, ^{1}H-^{1}H COSY, HMQC, DEPT 135, HMBC NMR spectrum, single crystal XRD and HRESIMS gave compound **5** as cedronin.

Nature	Colourless crystalline solid
Melting Point	161-163 ^{o}C

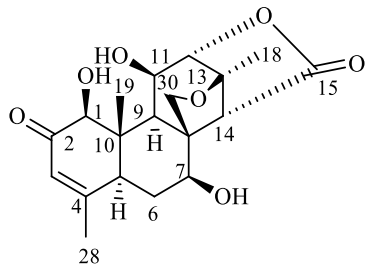

Cedronin

Specific rotation ($[\alpha]^{D}_{25}$)	-47° (*c* 0.1, MeOH)
FTIR (KBr, υ_{max})	3400, 1760, 1570, 1230, 1065 and 920 cm^{-1}.
^{1}H NMR (500 MHz, $CDCl_3$)	δ 5.96 (d, *J* = 1.5 Hz, 1H, H-3), 5.10 (d, *J* = 3.5 Hz, 1H, -OH), 5.05 (d, *J* = 4 Hz, 1H, -OH), 4.69 (t, *J* = 3 Hz, 1H, H-11), 4.47 (d, *J* = 8 Hz, 1H, H-30), 4.08 (d, *J* = 6.5 Hz, 1H, H-12), 4.04 (d, *J* = 3.5 Hz, 2H, H-1), 3.73 (s, 1H, H-30), 3.60 (d, *J* = 8.5 Hz, 1H, H-), 3.06 (d, *J* = 12.5 Hz, 1H), 2.70 (s, 1H, H-14), 2.09 (t, *J* = 4.5 Hz, 1H), 1.91 (m, 1H), 1.86 (s, 3H, H-28), 1.53 (t, *J* = 13 Hz, 1H), 1.33 (s, 3H, H-18), 1.12 (s, 3H, H-19) ppm.
^{13}C NMR (125 MHz,$CDCl_3$)	δ 198.3 (C-2), 172.1 (C-15), 164.4 (C-4), 124.0 (C-3), 86.6 (C-13), 83.4 (C-12), 83.1 (C-1), 74.4 (C-30), 69.8 (C-11), 69.4 (C-7), 58.6 (C-14), 54.3 (C-8), 47.5 (C-10), 44.0 (C-9), 42.1 (C-5), 29.1 (C-6), 22.1 (C-28), 20.7 (C-19), 10.4 (C-18) ppm.
HRESIMS (m/z)	365.1610 $[M+H]^{+}$

2A.7.2.6. Isolation of compound 6

Compound **6** (21 mg) was obtained as a colourless crystalline solid from the fraction pool 13, on eluting the column (silica gel 100-200 mesh) with 65 % EtOAc in *n*-hexane. The detailed analysis of FTIR, ^{1}H NMR, ^{13}C, ^{1}H-^{1}H COSY HMQC, DEPT 135, HMBC NMR spectrum, single crystal XRD and HRESIMS gave compound **6** as novel compound.

2A.7.2.7. Isolation of compound 7

Compound **7** (11 mg) also was obtained as a colourless amorphous solid from the fraction pool 13, on eluting the column (silica gel 100-200 mesh) with 65 % EtOAc in *n*-hexane. The detailed analysis of FTIR, ^{1}H NMR, ^{13}C, ^{1}H-^{1}H COSY, HMQC, DEPT 135, HMBC NMR spectrum, and HRESIMS gave compound **7** as brucein D.

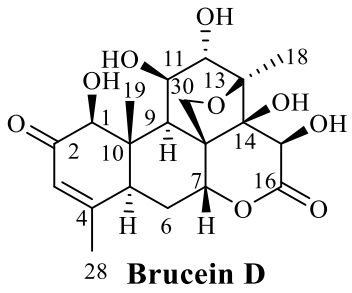

Brucein D

Nature	Colourless amorphous solid
Melting Point	289-291 ^{o}C
Specific rotation $[\alpha]^{D}_{25}$	-9° (*c* 0.1, MeOH)
FTIR (KBr, υ_{max})	3380, 1710, 1655 and 1620 cm^{-1}.
^{1}H NMR (500 MHz, DMSO-d_6)	δ 5.98 (s, 1H, C-3), 5.48 (d, J = 5 Hz, 1H, -OH), 5.31 (s, 1H, -OH), 5.25 (s, 1H, -OH), 5.04 (d, J = 7.5 Hz, 1H, -OH), 4.83 (brs, 1H), 4.42 (t, J_1 = 5.5 Hz or J_1= 4.5 Hz, 1H), 4.35 (d, J = 7 Hz, 1H), 4.20 (brs, 1H), 3.73 (d, J = 5.5 Hz, 1H), 3.64 (d, J = 7.5 Hz, 1H), 3.55 (s, 1H), 2.9 (brs, 1H, -OH), 2.35 (d, J = 18 Hz, 2H), 2.20 (s, 3H, C-28), 2.10 (m, 1H), 1.15 (s, 3H, H-18), 1.12 (s, 3H, H-19) ppm.
^{13}C NMR (125 MHz, DMSO-d_6)	δ 198.3 (C-2), 169.9 (C-16), 166.3 (C-4), 126.3 (C-3), 83.7, 82.4, 82.2, 80.6, 80.0, 74.1 (C-1), 68.7 (C-1), 67.2, 50.5, 47.9, 46.9, 43.7, 37.1, 27.0 (C-28), 17.4 (C-18), 12.4 (C-19) ppm.
HRESIMS (m/z)	433.1480 $[M+Na]^{+}$

2A.7.2.8. Isolation of compound 8

The isolation procedure of compound **8** is represented in **Figure 2A.71.** Compound **8** (300 mg) was obtained as a colourless amprphous solid from the fraction pool 18, on eluting the column (silica gel 100-200 mesh) with 80 % EtOAc in *n*-hexane. The detailed analysis of FTIR, ^{1}H, ^{13}C, ^{1}H-^{1}H COSY, HMQC, DEPT 135, HMBC NMR spectra and HRESIMS gave compound **8** as glucoside of C20 quassinoid and considered as a novel compound.

2A.7.3. α-Amylase inhibitory activity

α-Amylase inhibitory activity was analyzed based on the starch-iodine test [Xio *et al*., **2006**]. Starch containing α-amylase solution, ($1UmL^{-1}$) along with different concentrations of compounds (**1-8**) were incubated at 50 ^{o}C for 30 min. After incubation, the reaction was terminated with 1 M HCl. Then, 100 μL of iodine reagent was added to the reaction mixture. Enzymatic activity was quantified by measuring absorbance at 580 nm using Synergy 4 Biotek multimode reader (USA). The results were expressed in terms of IC_{50}, which is defined as the concentration of α-amylase inhibitor that inhibited 50% of enzyme activity. Acarbose was used as a positive control and the percentage of inhibition was calculated using following equation,

$$\% \text{ of inhibition} = \frac{\text{Absorbance of control - Absorbance of sample}}{\text{Absorbance of control}} \times 100$$

2A.7.4. α-Glucosidase inhibitiory activity

α-Glucosidase inhibitory activity was determined using a previous method with slight modification [Apostolidis *et al*., **2007**]. Different concentrations of compounds 1-7 and 100 μL of rat intestinal α-glucosidase solution (1.0 U/mL) in 0.1 M phosphate buffer (pH 6.9) were incubated at 25 ^{o}C for 10 min. After that, 50 μL of 5 mM *p*-nitrophenyl-α-D-glucopyranoside (250 μL) solution in 0.1 M phosphate buffer (pH 6.9) was added and the mixture was again incubated at 37 ^{o}C for 20 min. Enzymatic activity was quantified by measuring absorbance at 405 nm using Synergy 4 Biotek multimode reader (USA) and the percentage of inhibition (IC_{50}) was calculated using the above equation. The standard drug, acarbose was used as a positive control.

$$\% \text{ of inhibition} = \frac{\text{Absorbance of control - Absorbance of sample}}{\text{Absorbance of control}} \times 100$$

2A.7.5. Antiglycation property

Antiglycation property was measured as previously reported with slight modifications [Jedsadayanmata *et al*., **2005**]. Briefly, 1 mg/mL of BSA was incubated with 400 μL of α-D-glucose (500 mM) and different concentrations of compounds **1-8** in 0.2 M potassium phosphate buffered saline at 60 ^{o}C for 24 h. The reaction was terminated by adding 100 % trichloroacetic acid (TCA) and kept at 4 ^{o}C for 10 min. Further, the compounds were subjected to centrifugation (10,000 *x*g) and the precipitate was again dissolved in alkaline PBS. The fluorescence of the glycated end products was measured by excitation at 370 nm and emission at 440 nm using Synergy 4 Biotek multimode reader (USA). Ascorbic acid serves as a positive control. The AGEs formation was calculated using the following equation,

$$\text{AGEs formation} = \frac{\text{Fluorescence of control - Fluorescence of sample}}{\text{Fluorescence of control}} \times 100$$

2A.7.6. *In silico* studies

The preparation of the receptor and the ligands for docking, prediction of ADME/T (Absorption, Distribution, Metabolism, Excretion and Toxicity) properties, molecular docking and dynamics simulation studies were done by Schrodinger suite 2018-2. All the conformers of the eight quassinoids (**1-8**) were generated by LigPrep tool, then used for QikProp analysis to verify the pharmacokinetic parameters in order to predict the ADME/T properties. The values are compared with the range obtained from QikProp manual. The crystal structures of isomaltase from *Saccharomyces cerevisiae* (PDB ID: **3A4A**) and the *N*-terminal and *C*-terminal of human maltase glucoamylase (PDB ID: **2QMJ** and **3TOP** respectively) were retrieved from RCSB PDB (Protein Data Bank) [Yamamoto *et al*., **2010**; Sim *et al*., **2008**; Ren *et al*., **2011**]. The prepared PDB files were further used for grid generation around the centroid of the workspace ligand 'acarbose'. Molecular docking of ligands with the receptors were carried out using Glide programme of Schrodinger suite [Friesner *et al*., **2006**; Halgren *et al*., **2004**]. The binding affinity of the ligands were predicted on the basis of scoring functions- G-score (Glide score) and D-score (Dock score) using XP-visualizer.

2A.7.7. Cell culture and treatment conditions

L6 cell lines were purchased from National Centre for Cell Sciences (NCCS), Pune, India and were cultured in DMEM supplemented with 10 % FBS and 0.5 % antibiotic-antimycotic (penicillin-streptomycin-amphotericin B mix) solution at 37 ^{o}C, in a humidified atmosphere containing 5 % CO_2. The medium was replaced for every 2 days.Cell lines at above 80 % confluence were used for all the experiments.

2A.7.8. Cell viability assay

Cell viability was determined using MTT assay. Cultures were maintained at 37 ^{o}C in 5 % CO_2 incubator. The cells were trypsinized and seeded in 24 well plates (1 x 10^4 cells per well). Cells after attaining above 80 % of confluency, were treated with different concentrations [5 μM, 10 μM, 50 μM, 100 μM and 200 μM] of quassinoid for 24 h. After the incubation, cells were treated with MTT reagent (0.5 g/L) for 4 h. Mitochondrial dehydrogenase enzyme is active only in live cells that reduce the yellow dye, MTT to purple formazan crystals. The formazan crystals were dissolved in 200 μL DMSO and the absorbance was read at 570 nm using Synergy 4 Biotek multimode reader. The untreated cells were used as a control and the percentage of cell viability was calculated as,

$$\% \text{ of cell viability} = \frac{\text{Absorbance of test}}{\text{Absorbance of control}} \times 100$$

2A.7.9. Glucose uptake assay

Differentiated myotubes were pre-treated with 5 and 10 μM concentration of quassinoids **1-8** for 24 h. After removal of the culture medium, the cells were washed twice with pre-cooled PBS. The cells were then treated with the fluorescent analog of glucose, 2- NBDG and incubated for 30 min. The uptake of 2-NBDG by the cells, was stopped by removing the incubation medium, and the cells were then washed twice with PBS. Following incubation, the cells were washed twice with PBS, trypsinized and subsequently resuspended in 1 mL PBS. For each measurement, data from 10,000 single cell events were collected using Fluorescence Activated Cell Sorting (BD FACS Aria II, BD Bioscience, **USA**) and BD FACS Diva software. Rosiglitazone (100 μM) was served as positive control [Somwar *et al*., **1998**; Tamrakar *et al*., **2011**].

Isolation, Characterization and Antidiabetic Potential of Phytochemicals from the Stem Bark of *Quassia indica*

As mentioned in the first part of chapter 2, antidiabetic activity of *Quassia indica* has not been explored anywhere. Hence in this chapter, we are describing the isolation, characterization and antidiabetic activity of phytochemicals isolated from the stem bark of *Quassia indica*.

2B.1. Extraction and extract level antidiabetic studies

The stem bark of *Quassia indica* (1.25 kg) was collected from Alappuzha district, Kerala, India in April 2017, and identified by a plant taxonomist of Jawaharlal Nehru Tropical Botanic Garden and Research Institute, Palode, Kerala, India and a voucher specimen (**TBGT 81765**) was deposited in the Herbarium of repository of the same institute.

The air and oven-dried stem bark of *Quassia indica* (1.25 kg) was grounded and extracted successively with *n*-hexane (3 L x 48 h x 3 times; 11 g), acetone (3 L x 48 h x 3 times; 14 g), EtOH (3 L x 48 h x 3 times; 9.5 g) and water (3 L x 48 h x 3 times; 12 g). All extracts were checked for their *in vitro* inhibitory activities on carbohydrate hydrolyzing enzymes such as α-amylase and α-glucosidase as well as for their antiglycation properties. The results were shown in **Table 2B.1**. The acetone extract has promising inhibitory activity on α-amylase α-glucosidase and protein glycation with IC_{50} value of 14.53 ± 0.629, 17.60 ± 0.261 and 82.34 ± 0.781 μg/mL. Therefore, we further focussed on the acetone extract for the isolation and purification.

2B.2. Activity oriented isolation and characterization of phytochemicals

An aliquot of acetone extract (13.5 g) was subjected to column chromatographic separation on 100-200 mesh sized silica gel and eluted with the increasing order of *n*-hexane, *n*-hexane-ethyl acetate, ethyl acetate and ethyl acetate-methanol polarity mixtures resulted in 25 fraction pools by analysing the TLC.

Table 2B.1. Extract level *in vitro* antidiabetic activity of the stem bark of *Quassia indica*

Extracts	*α*-Amylase (*μ*g/mL)	*α*-Glucosidase (*μ*g/mL)	Antiglycation (*μ*g/mL)
Hexane	43.67 ± 0.205	26.11 ± 0.007	274 ± 0.669
Acetone	**14.53 ± 0.629**	**17.60 ± 0.261**	**82.34 ± 0.781**
Ethanol	49.54 ± 0.664	20.55 ± 0.558	134.04 ± 0.912
Water	366.41 ± 0.523	218.27 ± 1.004	381.57 ± 0..887
Acarbose	5.71 ± 0.282	45.37 ± 0.681	-
Ascorbic acid	-	-	48 ± 0.876

Each value represents mean ± SD (standard deviation) from triplicate measurements

Compound **9** (120 mg) was isolated as colourless crystalline solid from the fraction pool 2. The HRESIMS gave a molecular ion peak at m/z 425.3778 corresponding to its $(M+H)^+$ ion suggesting the molecular formula as $C_{30}H_{48}O$, which was supported by the ^{13}C NMR spectral data. The ^{1}H and ^{13}C NMR spectra are shown in **Figure 2B.1-2**. The ^{1}H NMR spectra of compound **9** displayed the presence of seven methyl singlets at δ_H 0.8, 0.9, 0.9, 1.0, 1.1, 1.1 and 1.7 ppm. The presence of two exocyclic double bonded protons appeared at δ_H 4.55 (d, J_1 = 2.5 Hz, J_2 = 1.5 Hz) and 4.47 (d, J = 2 Hz) ppm. In the ^{13}C NMR spectrum, saturated carbonyl group appeared at δ_C 217.4 ppm, the alkene carbons at δ_C 150.6 and 109.6 ppm and seven methyl moieties at δ_C 26.7, 21.0, 19.3, 18.1, 16.0, 15.8 and 15.8 ppm. All these spectral data suggested the presence of a lupane triterpene having a carbonyl group. Thus, the structure of compound **9** was assigned as the known compound lupenone, which was confirmed by the physical and spectral data reported in the literature [Chaturvedula *et al*., **2012**]. The structure of lupenone is shown below.

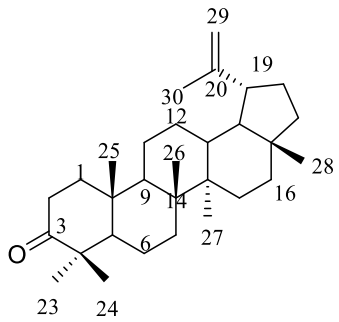

Lupenone (9)

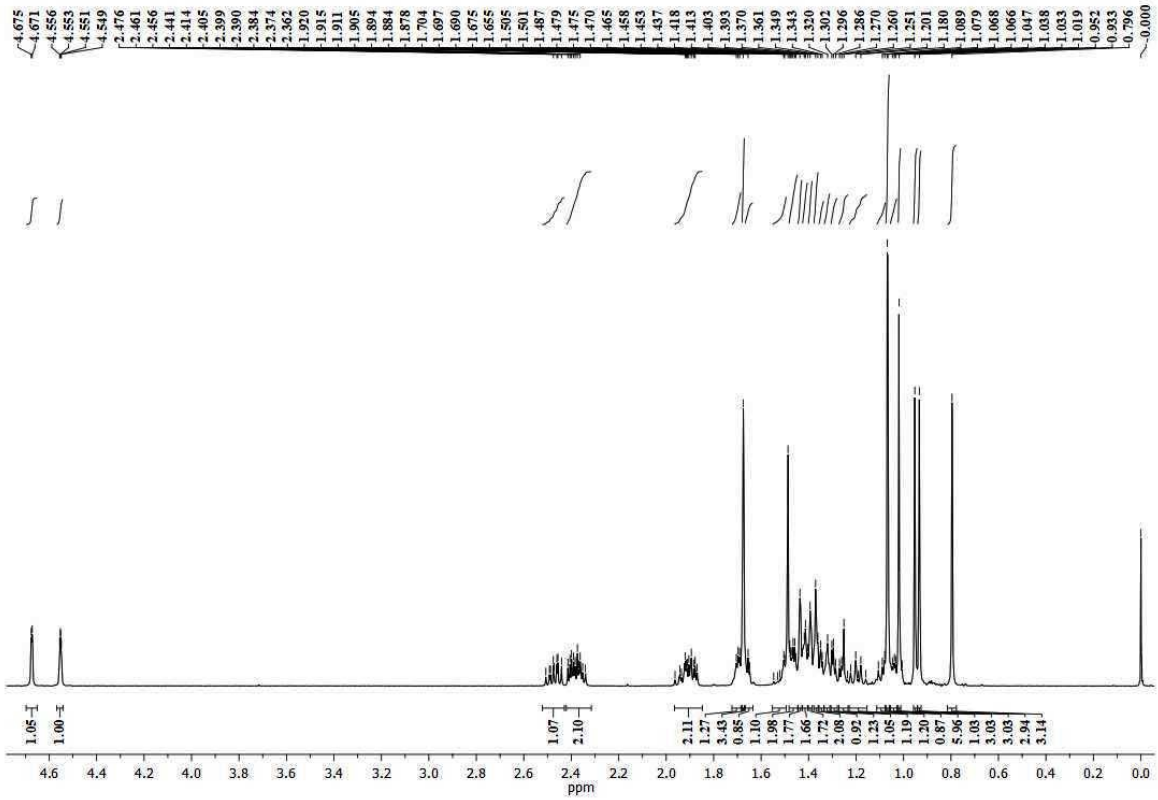

Figure 2B.1. ^{1}H NMR spectrum (500 MHz, $CDCl_3$) of lupenone (**9**)

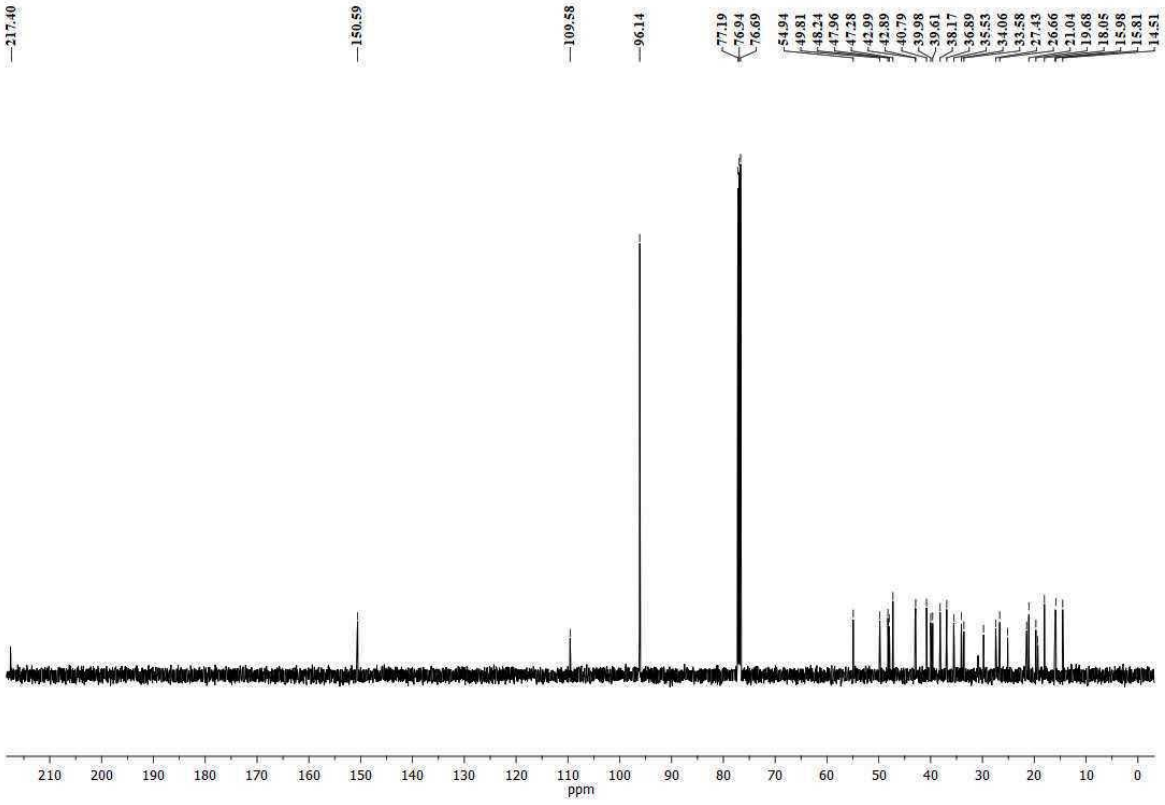

Figure 2B.2. ^{13}C NMR spectrum (125 MHz, $CDCl_3$) of lupenone (**9**)

From the fraction pool 3, compound **10** and **11** was isolated in 28 and 16 mg as a UV inactive colourless solid. From the physical parameters, ^{1}H and ^{13}C NMR spectra, the isolated compounds were identified as *β*-sitosterol and stigmasterol. The structures of the compound are shown in **Figure 2B.3.**

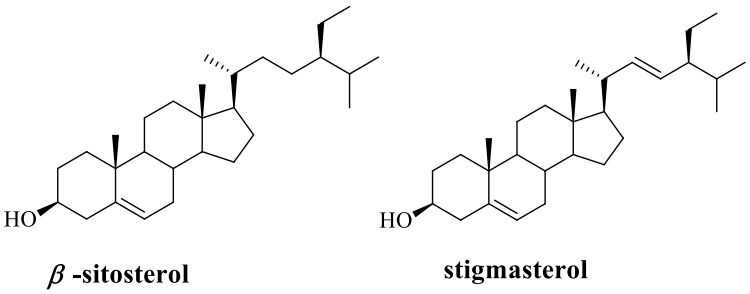

***β* -sitosterol** **stigmasterol**

Figure 2B.3. Structure of *β*-sitosterol (**10**) and stigmasterol (**11**)

Compound **12** (70 mg) was obtained as a colourless crystalline solid from the fraction pool **6**, while eluting the column with 7 % ethyl acetate in *n*-hexane. The IR spectrum of the compound showed absorption bands at 3320 and 1720 cm^{-1} suggesting the presence of hydroxyl as well as carbonyl groups. Compound **12** exhibited a molecular ion peak at m/z 465.3727 $[M+Na]^{+}$ (calcd. for $C_{30}H_{50}NaO_2$, 465.3709) in the HRESIMS, and the molecular formula was established as $C_{30}H_{50}O_2$. The 1D and 2D NMR spectra are shown in **Figure 2B.4-10**. In the ^{1}H NMR spectrum, the oxymethine proton resonated as a doublet at δ_H 3.30 (J = 10.5 Hz) ppm. The eight methyl groups appeared as singlet at δ_H 1.10, 1.07, 1.03, 0.98, 0.97, 0.94, 0.89 and 0.85 ppm. In the ^{13}C NMR spectrum, the -CH_3 groups resonated at δ_C 30.0, 26.7, 21.0, 19.8, 18.2, 16.0, 15.8 and 14.5 ppm. The -CH_2- carbons resonated at δ_C 39.5, 38.1, 37.8, 34.8, 34.1, 33.5, 28.1, 26.5, 21.8 and 19.7 ppm. The -CH- carbons resonated at δ_C 78.1, 54.8, 49.1, 45.9 and 38.0 ppm. The quaternary carbons resonated at δ_C 47.3, 42.9, 41.1, 37.5 and 36.7 ppm. The structure of the compound was finally confirmed by single crystal X-ray analysis (**Figure 2B.11**) and the compound **12** was an olean type triterpenoid, 18*α*-olean-19*α* -ol-3-one. The structure of 18*α*-olean-19*α* -ol-3-one is shown below.

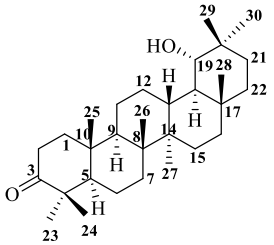

18*α*-Olean-19*a* -ol-3-one (12)

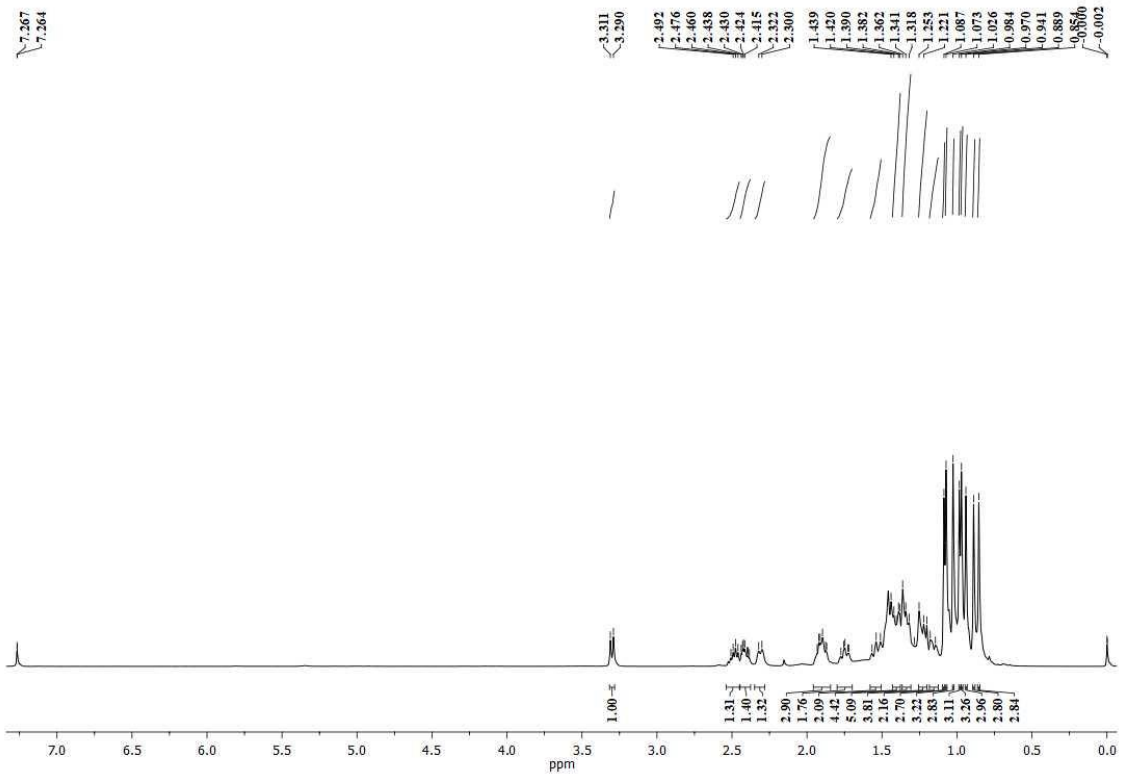

Figure 2B.4. ^{1}H NMR spectrum (500 MHz, $CDCl_3$) of 18*α*-olean-19*α* -ol-3-one (**12**)

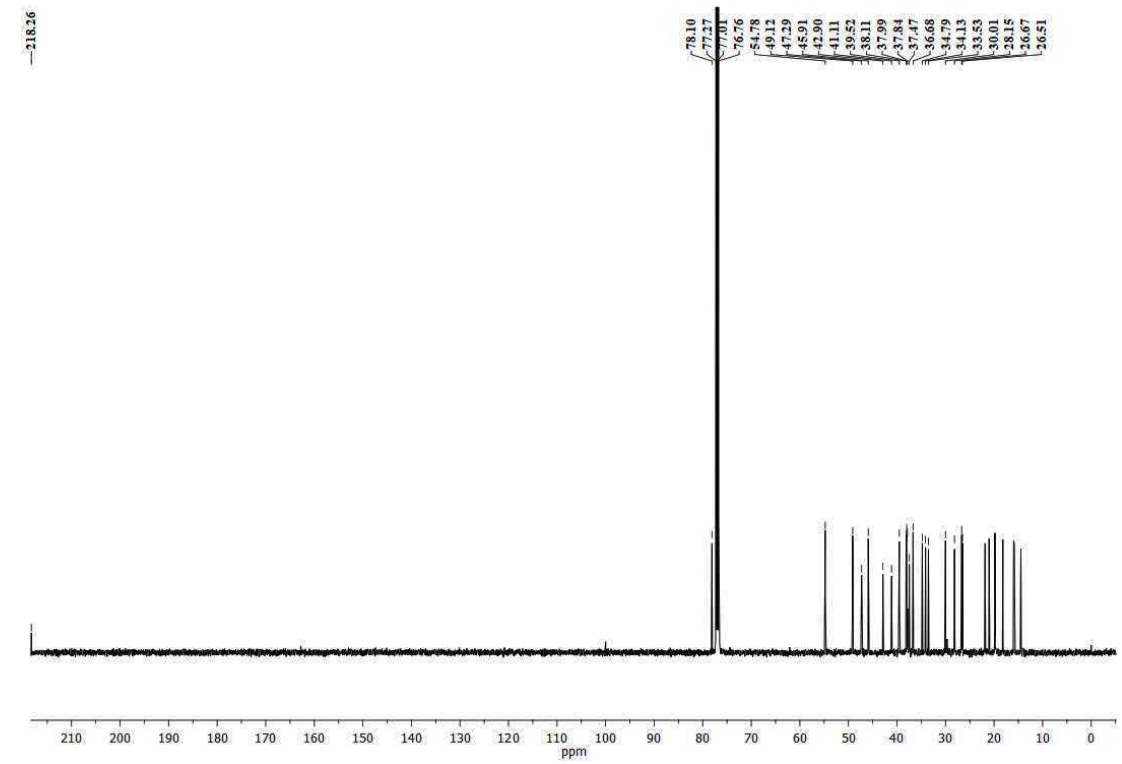

Figure 2B.5. ^{13}C NMR spectrum (125 MHz, $CDCl_3$) of 18*α*-olean-19*α* -ol-3-one (**12**)

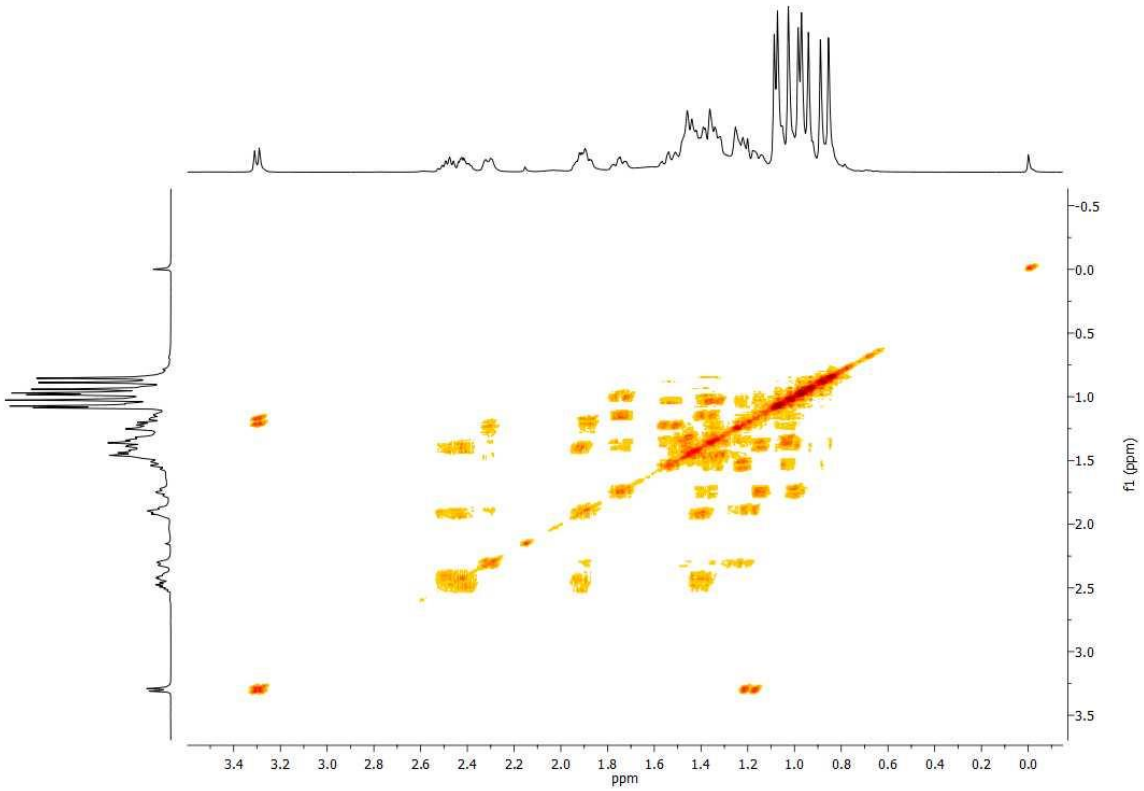

Figure 2B.6. ^{1}H-^{1}H COSY NMR spectrum (500 MHz, $CDCl_3$) of 18α-olean-19α -ol-3-one (**12**)

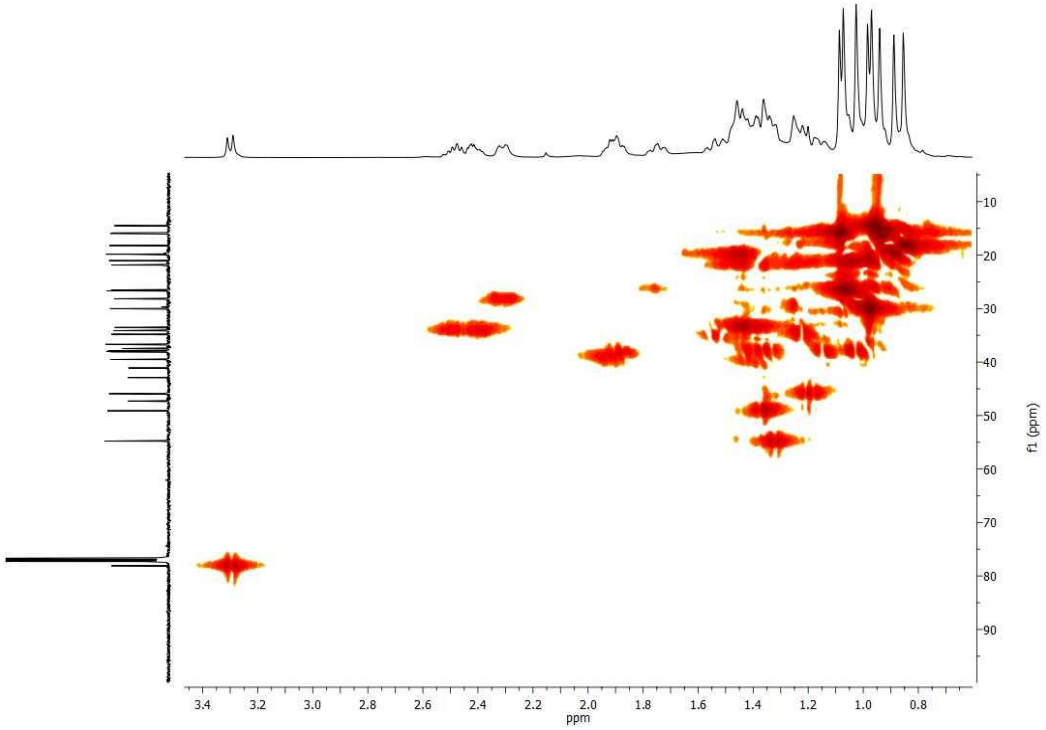

Figure 2B.7. HMQC NMR spectrum (125 MHz, $CDCl_3$) of 18α-olean-19α-ol-3-one (**12**)

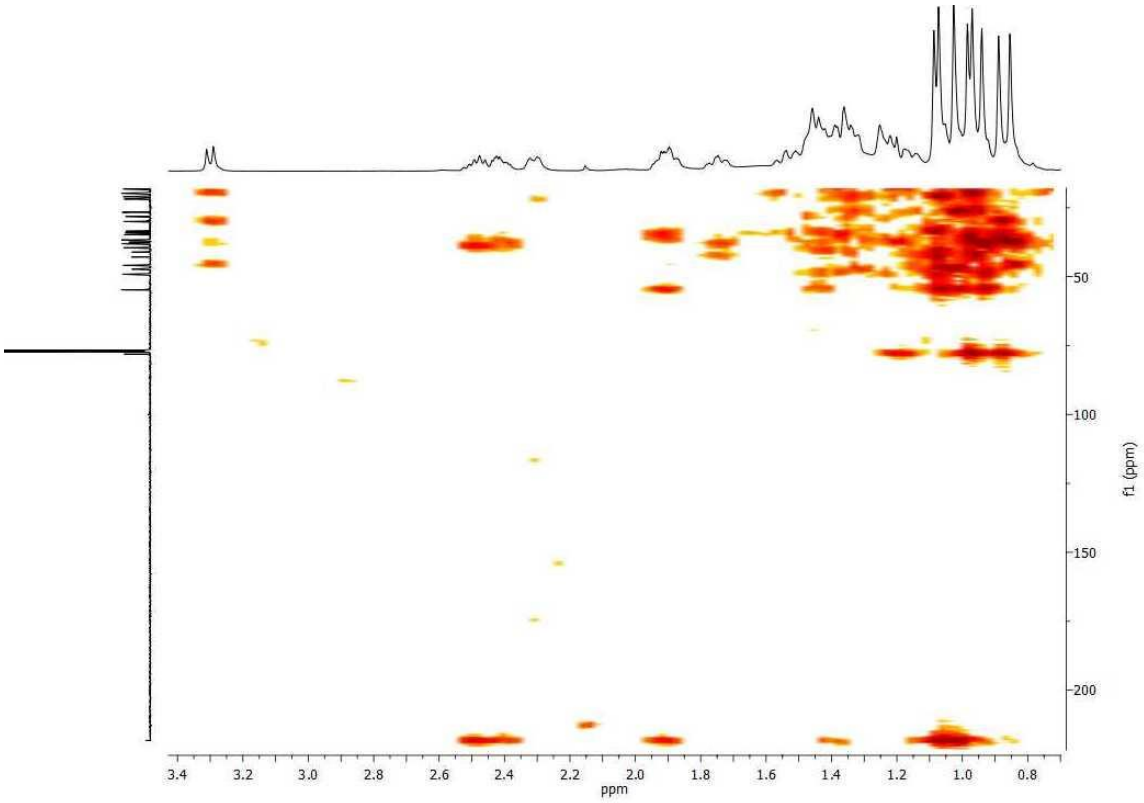

Figure 2B.8. HMBC spectrum (125 MHz, $CDCl_3$) of 18α-olean-19α-ol-3-one (**12**)

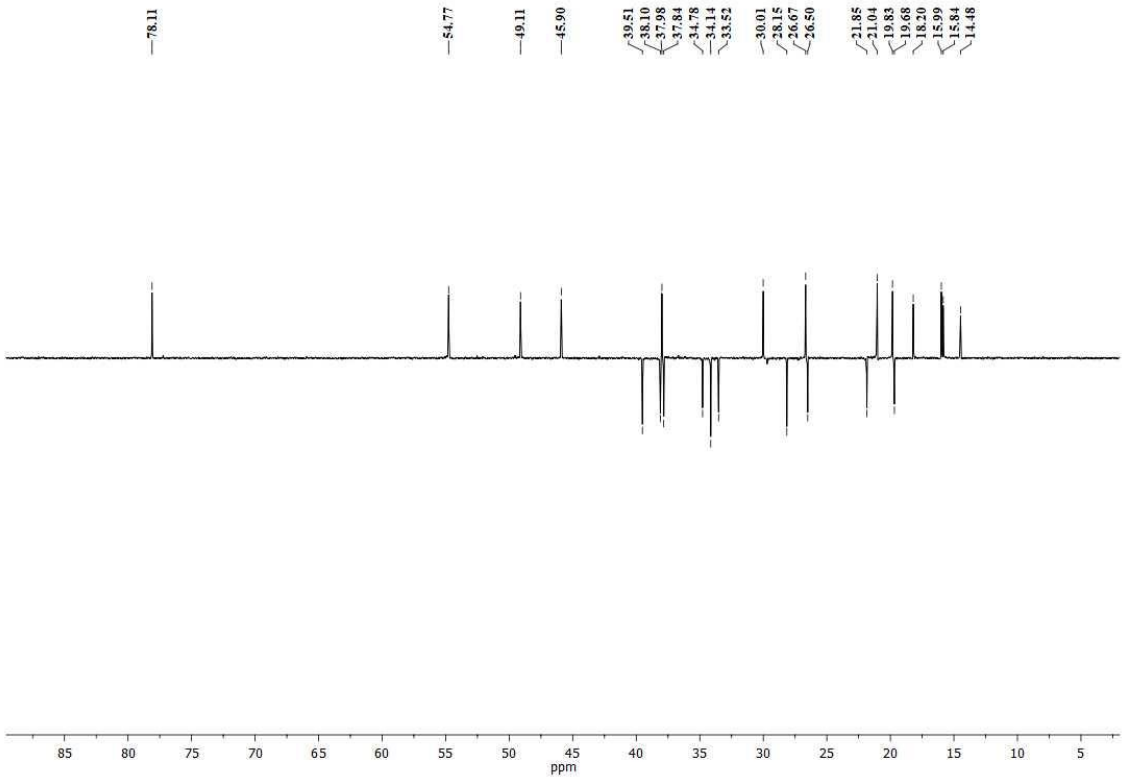

Figure 2B.9. DEPT 135 spectrum (125 MHz, $CDCl_3$) of 18α-olean-19α-ol-3-one (**12**)

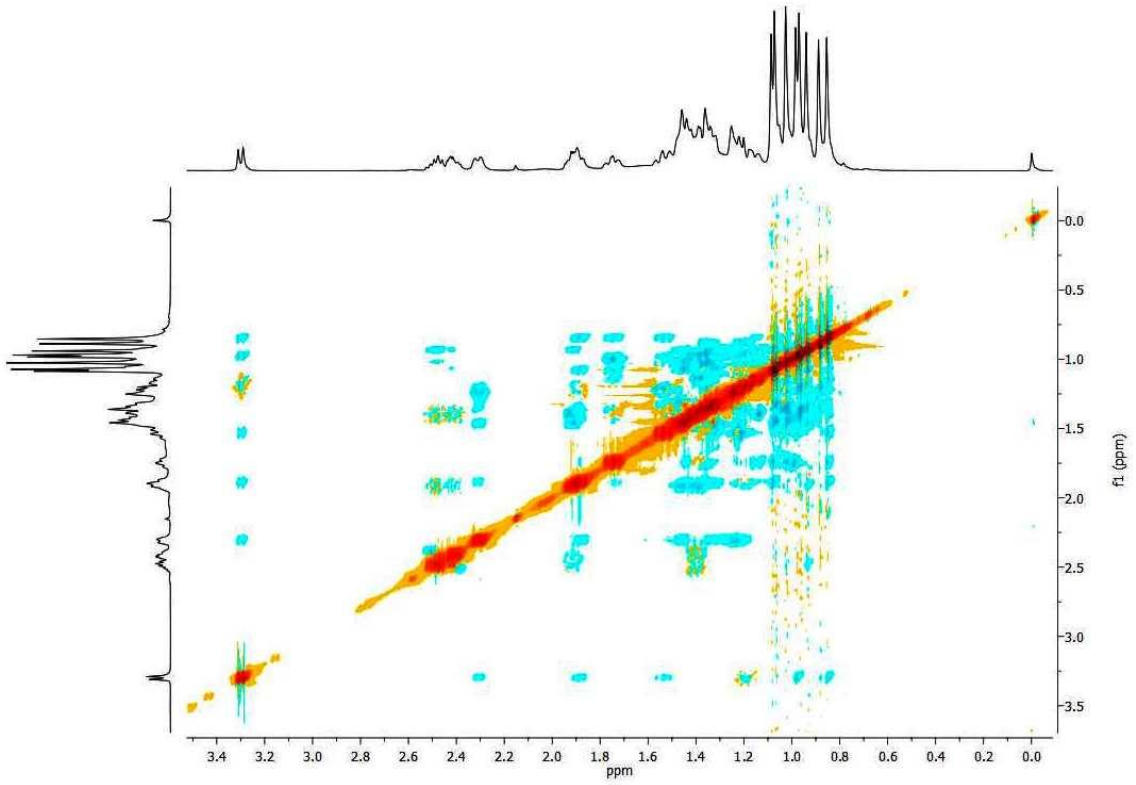

Figure 2B.10. NOESY spectrum (500 MHz, $CDCl_3$) of 18α-olean-19α-ol-3-one (**12**)

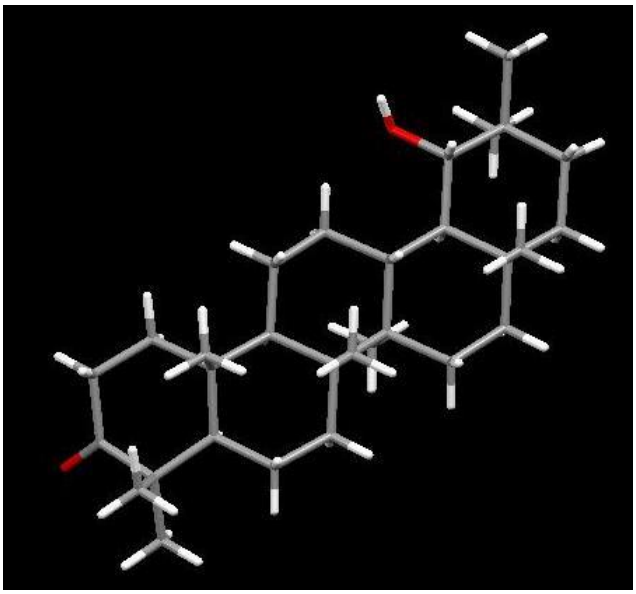

Figure 2B.11. Single crystal X-ray analysis of 18α-olean-19α-ol-3-one (**12**)

Compound **13** (11 mg) was isolated from fraction pool 9 as UV active pale yellow solid with a molecular ion peak at 193.07607 corresponding to $(M-H)^+$ ion. The FTIR spectrum gave -OH stretching of carboxylic acid at 3450 cm^{-1}, carboxylic acid C=O stretching at 1690 cm^{-1}, carboxylic acid C-O stretching at 1275 and 1510 cm^{-1} and

aromatic C=C stretching at 1605 cm^{-1}. The ^{1}H and ^{13}C NMR spectra are shown in **Figure 2B. 12-13**. ^{1}H NMR spectrum showed characteristic signal for a methoxy proton at δ_H 3.94 ppm. The three protons of the aromatic part of the compound H-6, H-5 and H-3 resonated at δ_H 6.94 (d, J = 8 Hz), 7.12 (dd, J_1 = 8 Hz and J_2 = 2 Hz) and 7.06 (d, J = 1.5 Hz) respectively. The presence of further two proton doublets with J = 16 Hz at δ_H 6.30 and 7.71 ppm were indicated the presence of H-2' and H-1' of the olefinic respectively. The ^{13}C NMR spectrum displayed the presence of 10 signals, δ_C 147.1, 146.8, 126.7, 123.6, 114.4 and 109.5 ppm for six aromatic carbon, δ_C 146.8 and 114.8 ppm for olefinic carbon, δ_C 56.0 ppm for methoxy carbon and δ_C 171.3 ppm for acid carbonyl carbon [Seyed *et al*., **2012**]. The structure of the compound is given below.

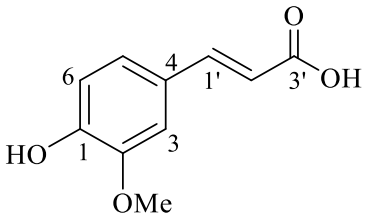

Ferulic acid

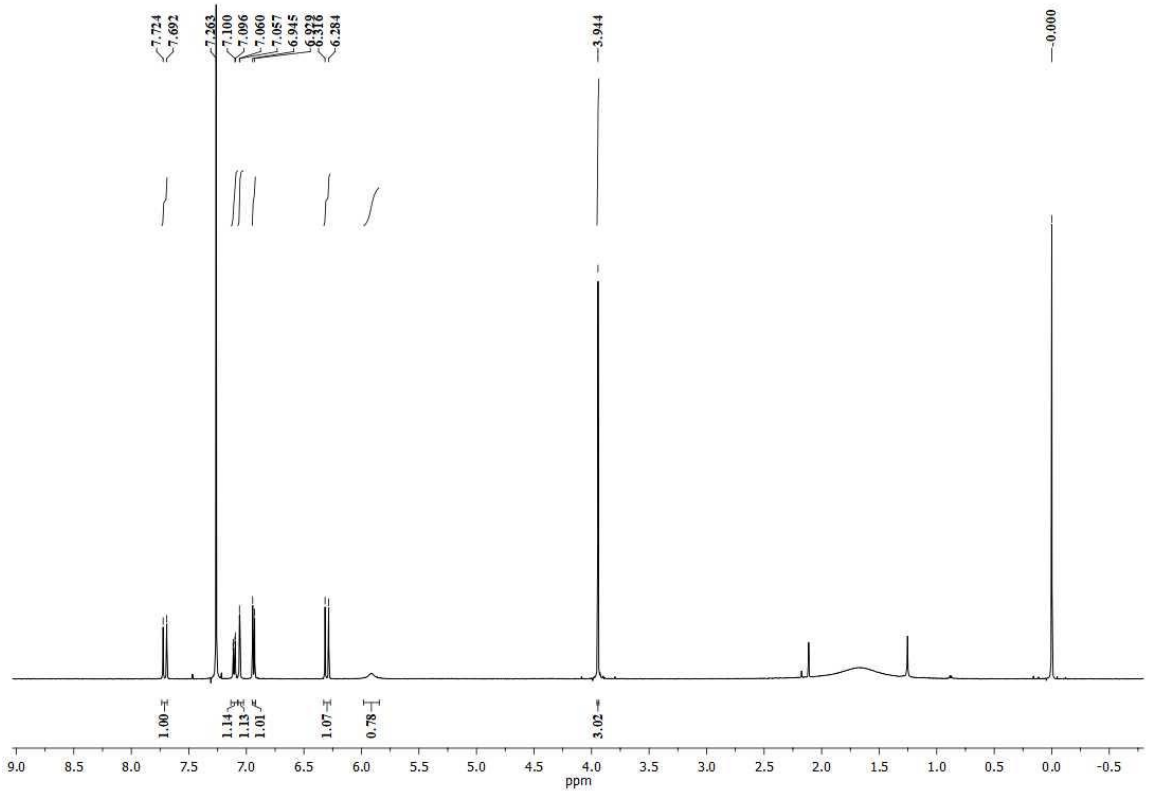

Figure 2B.12. ^{1}H NMR spectrum (500 MHz, $CDCl_3$) of ferulic acid (**13**)

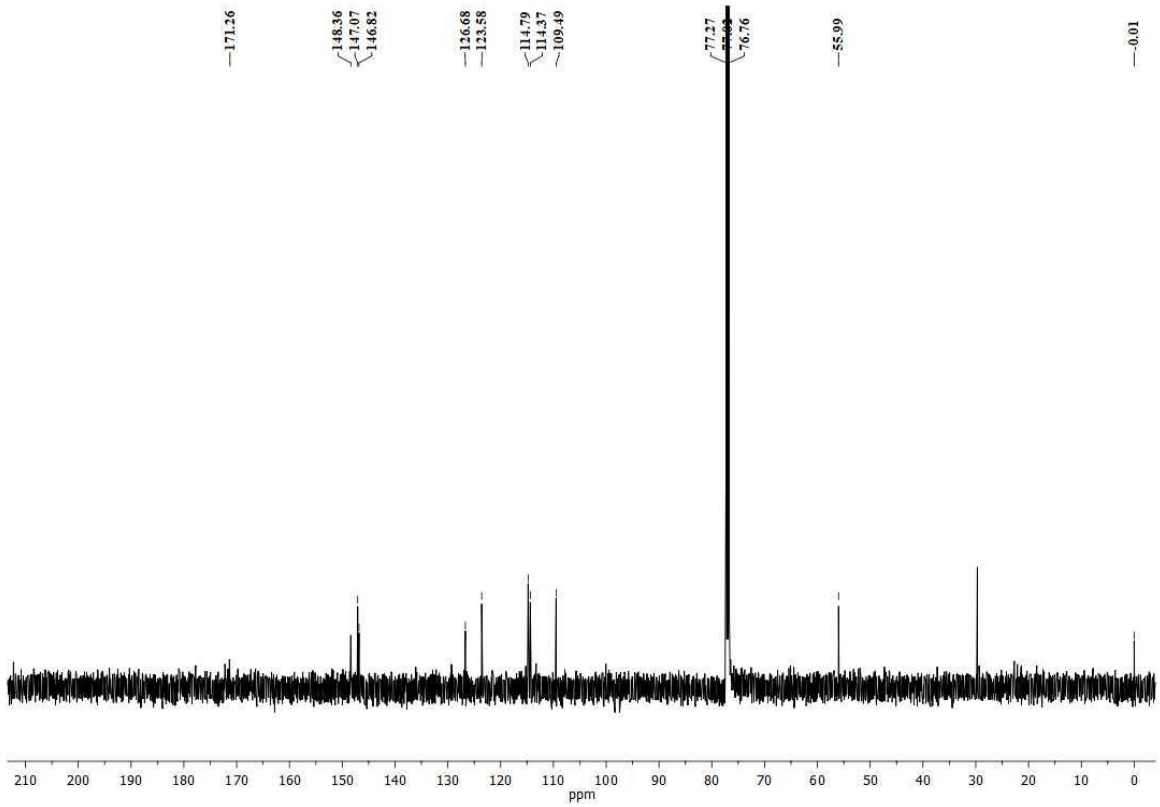

Figure 2B.13. ^{13}C NMR spectrum (125 MHz, $CDCl_3$) of ferulic acid (**13**)

Compound **14** was obtained in 8 mg as a colourless amorphous solid. It showed an intense blue colour in short UV. The HRESIMS displayed a molecular ion peak at m/z 193.0101 corresponding to $[M+H]^+$ peak. The ^1H NMR spectrum exhibited four aromatic protons [δ_H 7.57 (d, J = 9.5 Hz, 1H), 6.91 (s, 1H), 6.82 (s, 1H), 6.26 (d, J = 9.5 Hz, 1H) and 6.10 (s, 1H) ppm] and one methoxy group [δ_H 3.96 ppm]. The ^{13}C NMR spectrum displayed 10 signals; δ_C 160.8 ppm for δ-lactone, δ_C 150.3, 149.7, 143.9, 143.0, 138.3, 113.5, 111.4, 107.3 and 103.3 ppm for aromatic carbons and δ_C 56.3 ppm for methoxy carbon. In comparison with previously reported spectroscopic data [Akhmad, *et al*., **2012**], compound **14** was confirmed as scopoletin. The structure of scopoletin is shown below.

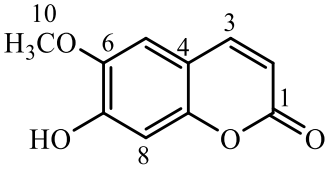

Scopoletin (14)

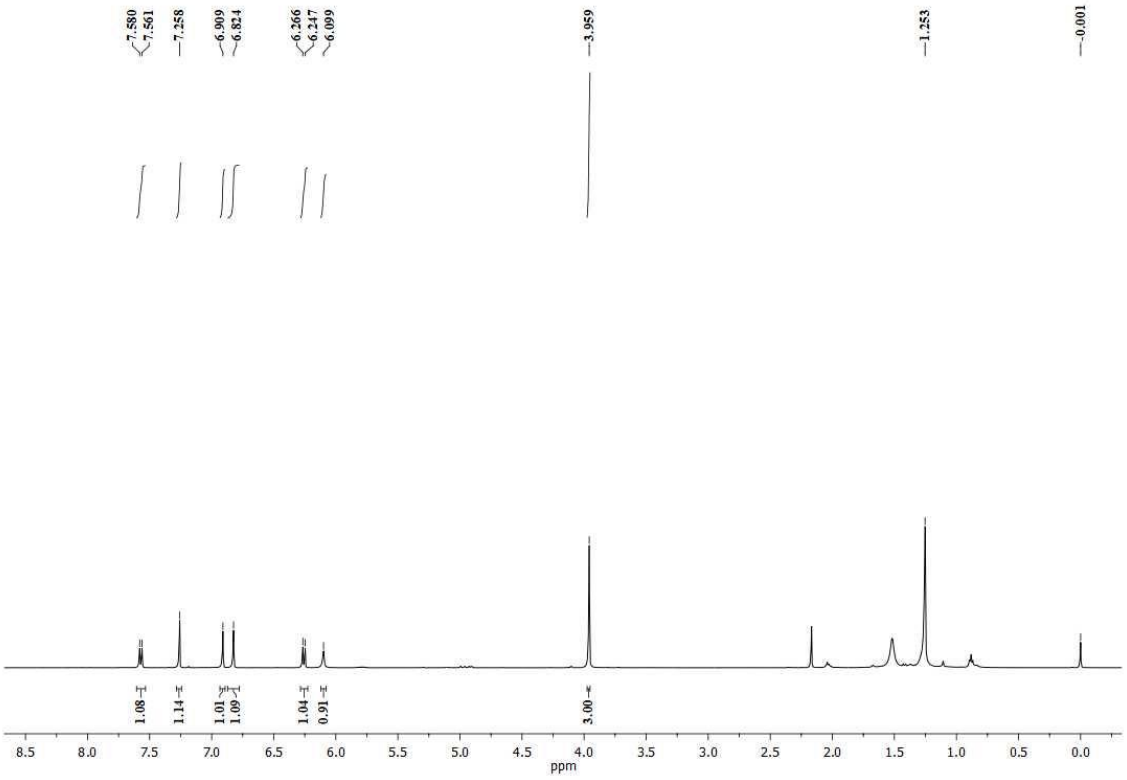

Figure 2B.14. ^{1}H NMR spectrum (500 MHz, $CDCl_3$) of scopoletin (**14**)

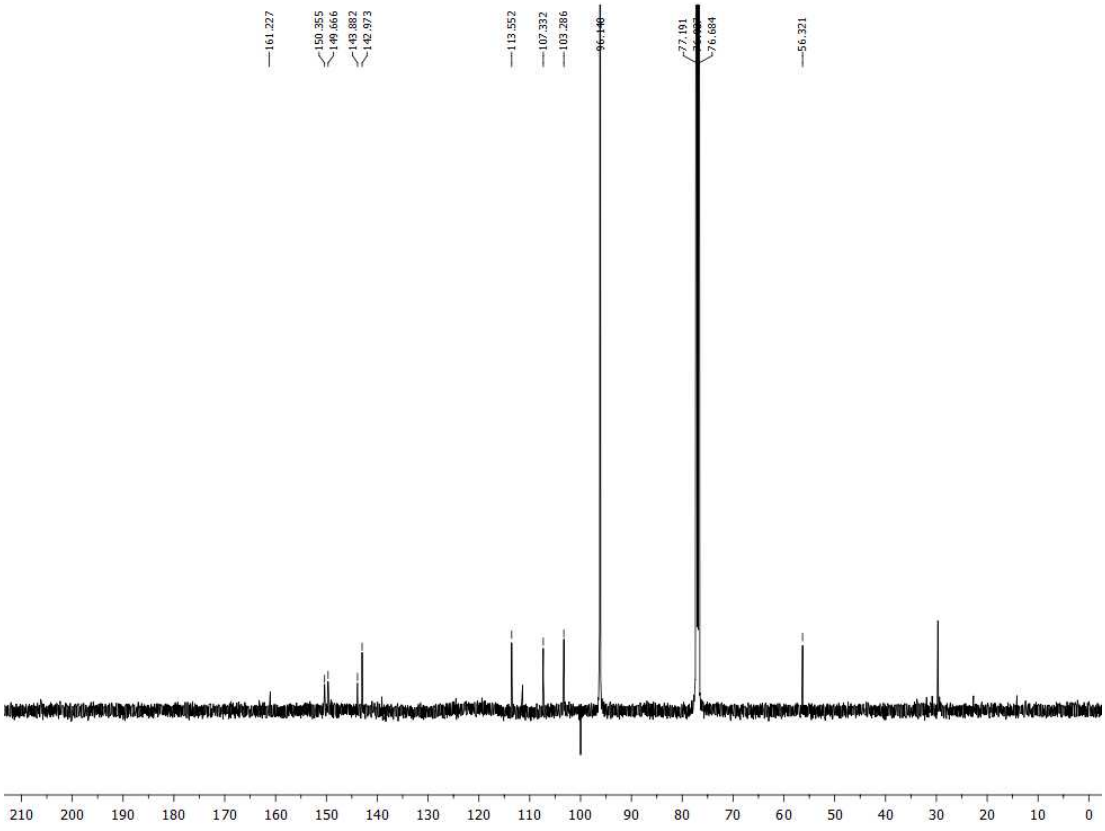

Figure 2B.15. ^{13}C NMR spectrum (125 MHz, $CDCl_3$) of scopoletin (**14**)

Compound **15** (34 mg) was isolated from fraction pool 12. Compound **15** was as UV active colourless crystalline solid with a molecular ion peak at 331.1211 corresponding to $(M+H)^+$. From the NMR analysis, the structure of the compound was identified as samaderin A [Philip *et al*., **2005**]. Compound **16** (127 mg) and compound **17** (7 mg) were obtained as colourless crystalline solid from the fraction pool 14. Compounds 1**6** and **17** were samaderin B [Philip *et al*., **2001**] and dihydrosamaderin B [Kazuo *et al*., **1994**]. Compound **18** (250 mg) was obtained as a colourless crystalline solid from fraction pool 16, while eluting the column with 70 % ethyl acetate in *n*-hexane. From the fraction pool 20, compound **19** (18 mg) was precipitated as colourless amorphous solid [Isao *et al*., **1996**]. The structures of compound **15-19** are shown in Figure **2B.16.**

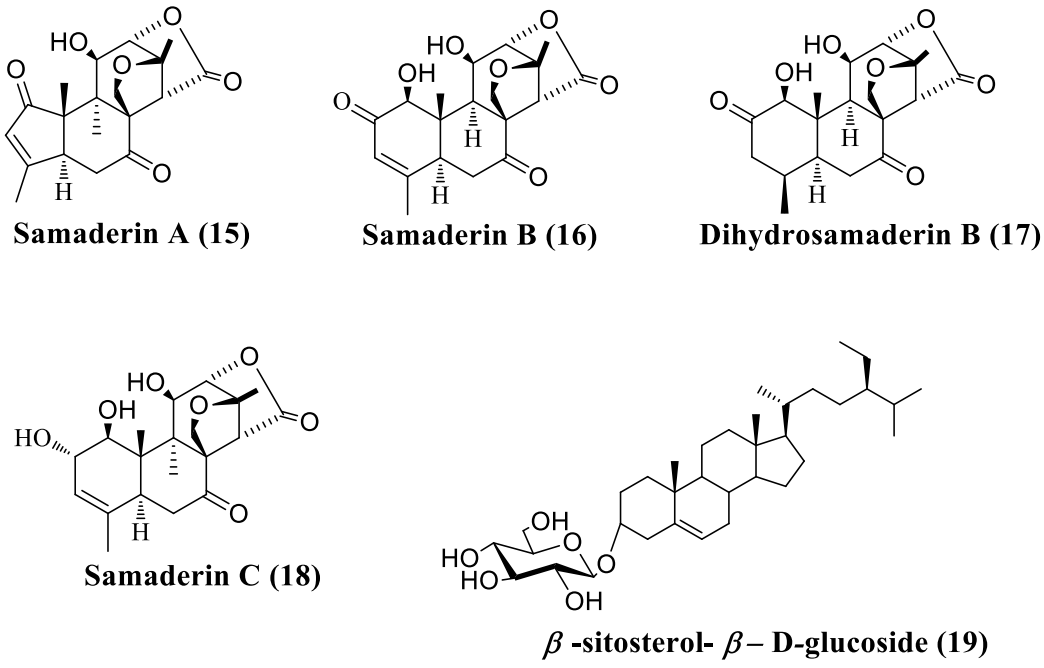

Figure 2B.16. Structures of compound **15-19**

2B.3. *In vitro* and *in silico* studies of lupenone (9), 18*α*-olean-19*α* -ol-3-one (12), ferulic acid (13) and scopoletin (14) with carbohydrate digestive enzymes

Diabetes is a chronic metabolic disease, characterized by increase in blood glucose level due to the breakdown of polysaccharides into simple sugars. Currently available antidiabetic drugs (*α*-amylase and *α*-glucosidase inhibitors) often exhibit many side effects. So, it is highly desirable to find out a natural way to cure diabetes and these facts guided us to check the carbohydrate digestive enzymes inhibitory activity of lupenone (**9**), 18*α*-olean-19*α* -ol-3-one (**12**), ferulic acid (**13**) and scopoletin (**14**).

Lupenone (**9**) displayed significant α-amylase inhibitory activity, with IC_{50} value of 7.35 ± 0.255 μM, better than the positive control acarbose (8.93 ± 0.48 μM), while the compound lupenone (**9**) exhibited moderate α-glucosidase inhibitory activity, with IC_{50} value of 117.48 ± 0.793 μM. The molecular docking studies were carried out in **3AJ7** [porcine pancreatic α-amylase] and **3A4A** enzyme [isomaltase from *Saccharomyces cerevisiae*]. Lupenone binds the catalytic domain of **3A4A** enzyme with G-/D-score of -1.45 kcal/mol. In the case of olean type triterpenoid, 18α-olean-19α -ol-3-one (**12**) exhibited porcine pancreatic α-amylase inhibitory activity with IC_{50} value of 14.88 ± 0.42 μM, whereas in the case of α-glucosidase enzyme 18α-olean-19α -ol-3-one (**12**) displayed an IC_{50} value of 135.71±1.541 μM. 18α-olean-19α -ol-3-one (**12**) binds **3AJ7** and **3A4A** enzyme with G-/D-score of -2.69 and -1.45 kcal/mol.

Ferulic acid (**13**) and scopoletin (**14**) showed moderate inhibitory activity on α-amylase enzyme with IC_{50} value of 53.92 ± 0.541 μM and 44.53 ± 0.781 μM, respectively. The molecular docking results envisaged that ferulic acid (**13**) and scopoletin (**14**) binds in a site different from the catalytic domain of **3AJ7** enzyme with G-/D-score of -3.94/-3.35 and -4.4/-4.39 kcal/mol, respectively. Results from molecular docking studies revealed that ferulic acid has interactions with **3AJ7** and is mainly composed by Π-cation and hydrogen bond acceptor interactions.

Ferulic acid (**13**) and scopoletin (**14**) showed significant inhibitory activity on α-glucosidase enzyme with IC_{50} value of 54.87 ± 0.734 μM and 51.44 ± 1.278 μM, respectively. The molecular docking results predicted that ferulic acid (**13**) and scopoletin (**14**) binds **3A4A** enzyme with G-Score/D-Score of -4.4/-4.39 and -5.32/-5.31 kcal/mol, respectively. The 2D interaction diagram is shown in **Figure 2B.17**. Results from molecular docking studies showed that ferulic acid has good interactions with **3A4A,** which is mainly composed by Π- Π stacking interaction with PHE 303 and hydrogen bond donor interactions with ASH 215 and AGR 442. Scopoletin interact with **3A4A** enzyme by Π- Π stacking interaction with TYR 158 and hydrogen bond donor interaction with ASP 248 and acceptor interaction with AGR 315.

In detailed pharmacokinetic studies, lupenone (**9**), 18α-olean-19α -ol-3-one (**12**), ferulic acid (**13**) and scopoletin (**14**) showed promising ADME/T properties. The compound is nontoxic to central nervous system, octanol-water partition coefficient, hydrophilicity, hydrophobicity and satisfy Lipinski's rule of five; which proves that this compounds can act as a promising drug candidate (**Table 2B.4**).

Table 2B.2. Inhibitory activities of α-amylase enzyme, α-glucosidase enzyme and protein glycation property of compounds isolated from the stem bark of *Quassia indica*

Compounds	α-Amylase (μM)	α-Glucosidase (μM)	Antiglycation (μM)
Lupenone	7.35 ± 0.255	117.48 ± 0.793	237.84 ± 0.912
18α-olean-19α -ol-3-one	14.88 ± 0.42	135.71 ± 1.541	249.34 ± 0.641
Ferrulic acid	53.92 ± 0.541	54.87 ± 0.734	174.87 ± 0.569
Scopoletin	44.53 ± 0.781	51.44 ± 1.278	164.32 ± 0.711
Acarbose	8.93 ± 0.48	66.57 ± 0.982	-
Ascorbic acid	-	-	155.38 ± 0.547

Each value represents mean ± SD (standard deviation) from triplicate measurements

Table 2B.3. G-/D-score of isolated compounds with porcine pancreatic α-amylase (**3AJ7**) and isomaltase from *Saccharomyces cerevisiae* (**3A4A**)

Compounds	3AJ7 kcal/mol		3A4A kcal/mol	
	G-Score	D-Score	G-Score	D-Score
Lupenone	-	-	-1.45	-1.45
18α-olean-19α -ol-3-one	-2.69	-2.69	-1.45	-1.45
Ferulic acid	-3.94	-3.35	-4.18	-4.18
Scopoletin	-4.4	-4.39	-5.32	-5.31

2B.4. Antiglycation property

The formation and accumulations of advanced glycation end products (AGEs) resulted in the pathogenesis of several diabetic associated complications. Many studies suggested that natural products can effectively inhibit the protein glycation. This encouraged us to carry out the antiglycation properties of lupenone (**9**), 18α-olean-19α -ol-3-one (**12**), ferulic acid (**13**) and scopoletin (**14**). The molecules moderately inhibited the formation and accumulation of AGEs with IC_{50} value of 237.84 ± 0.912, 249.34 ± 0.641, 174.87 ± 0.569 and 164.32 ± 0.711 μM, respectively.

Table 2B.4. ADME/T properties of compound

Sl. No	Lupenone	18*α*-olean-19*α* -ol-3-one	Ferulic acid	Scopoletin
M.W	424.709	442.724	194.187	192.171
#stars	4	2	0	0
#rotor	1	1	5	2
CNS	1	0	-2	0
SASA	674.479	681.808	415.186	382.95
FISA	37.014	64.547	165.782	123.689
HBA	2	3.7	3.5	4
HBD	0	1	2	1
QPlogKhsa	1.981	1.638	-0.614	-0.483
HOA	1	1	3	3
% HOA	100	100	67.74	82.518
QPlogPo/w	6.939	5.98	1.381	0.862
QPlogS	-7.789	-7.178	-1.827	-1.709
R Of Five	1	1	0	0

M.W. (Molecular Weight):130.0 to 725.0; #stars (few stars-more drug-like): 0 to 5; #rotor (Number of non-trivial and non-hindered rotatable bonds):0 to 15; CNS (Central Nervous System activity): -2 to +2; SASA (Total solvent accessible surface area in square angstroms): 300.0 to 1000.0 FISA (Hydrophilic component of total solvent accessable area): 7.0 to 333.0; HBA (Hydrogen bond acceptor): 2.0 to 20.0; HBD (hydrogen bond donor): 0.0 to 6.0; QPlogKhsa (binding to human serum albumin): -1.5 to 1.5; HOA (Human Oral Absorption): 1, 2, or 3 for low medium, and high; % HOA (Percent Human Oral Absorption): >80 % is high, <25 % is poor; QPlogPo/w (octanol/water partition coefficient): -2.0 to 6.5; QPlogS (Aqueous solubility): -6.5 to 0.5; Ro5 (Number of violations of Lipinski's rule of five): maximum is 4.

2B.5. Molecular docking studies

In order to predict the presumed binding modes of lupenone (**9**), 18*α*-olean-19*α* -ol-3-one (**12**), ferulic acid (**13**) and scopoletin (**14**) on digestive enzymes present in our body, we selected human pancreatic *α*- amylase (**4GQQ**), human maltase-glucoamylase *C*-terminal (**2QMJ**) and *N*-terminal (**3TOP**) for *in silico* studies. From **Table 2B.7**, we

can clearly see that, ferulic acid (**13**) and scopoletin (**14**) showed comparatively better binding affinity than lupenone (**9**), 18*α*-olean-19*α* -ol-3-one (**12**). Ferulic acid effectively interacts with **4GQQ, 2QMJ** and **3TOP** with G-/D-score of -3.35/-3.35, -4.63/-4.63, -5.24/-5.24 kcal/mol, respectively. In human pancreatic *α*-amylase enzyme, scopoletin exhibited G-Score/D-Score of -3.62/-3.61 kcal/mol. The *N*-terminal and *C*- terminal human maltase glucoamylase (**2QMJ**) showed G-/D-score of -3.94/-5.03 and -5.43/-5.42 kcal/mol, respectively. Results from molecular docking studies revealed that scopoletin interacts with **4GQQ,** which is mainly composed by hydrogen bond donor interaction with ASP 236 (-OH) and hydrogen bond acceptor interactions with LYS 257 (-OCH_3). The hydroxyl group of scopoletin forms hydrogen bond donor interaction with ASP 327 amino acid residue of **2QMJ.** In the case of **3TOP** enzyme, scopoletin forms a three Π- Π stacking interaction with TRP 1355 and PHE 1559. The carbonyl group of scopoletin also forms strong hydrogen bond acceptor interactions with HIE 1584 amino acid residue. The 2D interaction diagram of ferulic acid (**13**) and scopoletin (**14**) with **4GQQ**, **2QMJ** and **3TOP** are shown in **Figure 2B.18.**

Table 2B.5. G-Score/D-Score of isolated compounds with human pancreatic *α*-amylase (**4GQQ**) and human maltase glucoamylase (*N*- terminal, **2QMJ**; *C*- terminal, **3TOP**)

Compounds	**4GQQ** (kcal/mol)		**2QMJ** (kcal/mol)		**3TOP** (kcal/mol)	
	G-Score	D-Score	G-Score	D-Score	G-Score	D-Score
Lupenone	-1.54	-1.54	-1.24	-1.24	-	-
18*α*-olean-19*α* -ol-3-one	-1.74	-1.74	-1.87	-1.87	-3.87	-3.87
Ferulic acid	-3.35	-3.35	-4.63	-4.63	-5.24	-5.24
Scopoletin	-3.62	-3.61	-3.94	-5.03	-5.43	-5.42

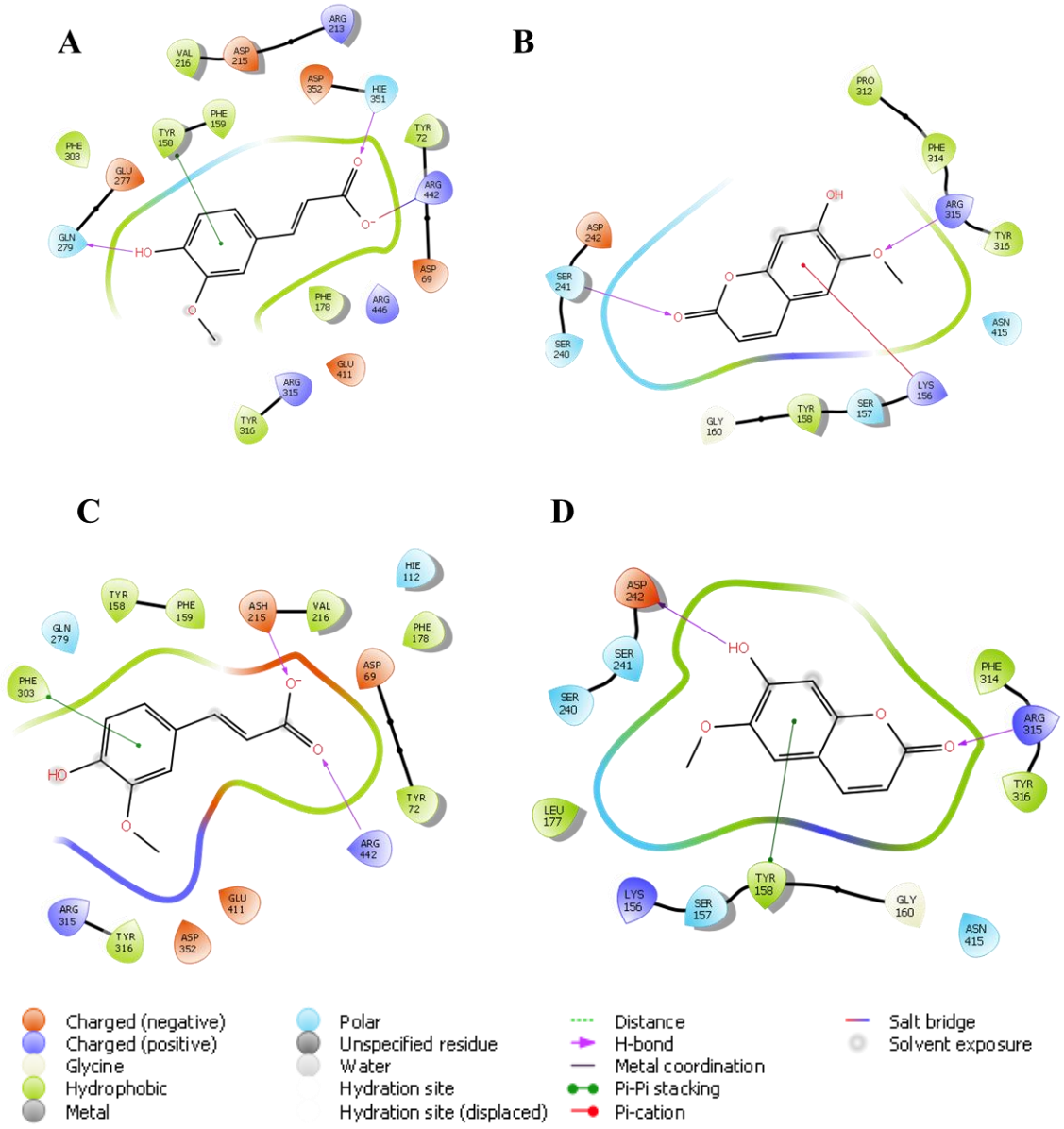

Figure 2B.17. 2D interaction diagram of ferulic acid and scopoletin with (A & B) **3AJ7** and (C & D) **3A4A**

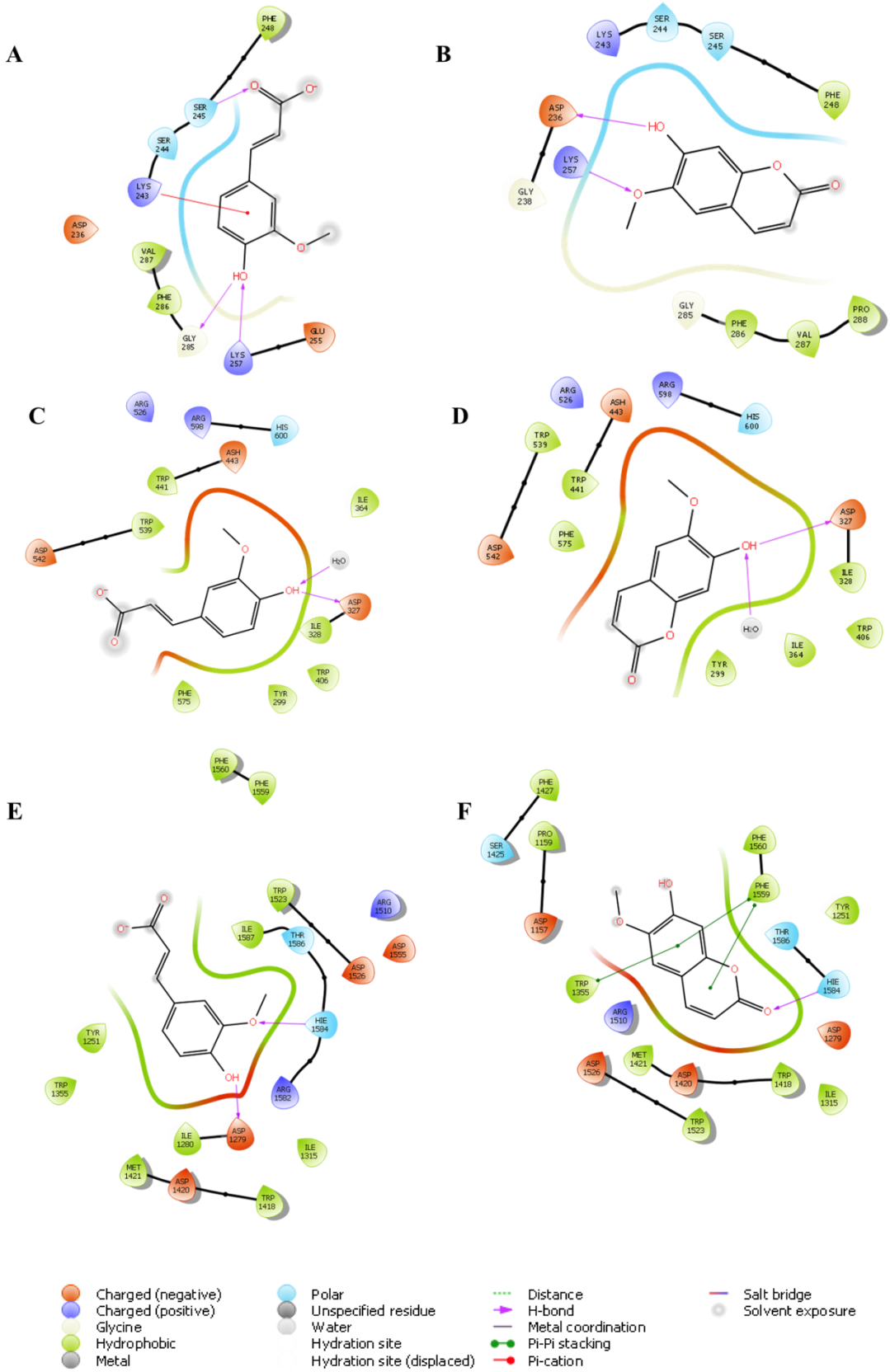

Figure 2B.18. 2D interaction diagram of ferulic acid and scopoletin with (A & B) **4GQQ**; (C & D) **2QMJ** and (E & F) **3TOP**

2B.6. Conclusion

In conclusion, the acetone extract of the stem bark of *Quassia indica* exhibited significant inhibitory activities on carbohydrate hydrolyzing enzyme and protein glycation. Inspired with this result, we isolated phytochemicals from the stem bark of *Quassia indica*, which resulted in the isolation of 11 compounds. It includes lupenone (**9**), *β*-sitosterol (**10**), stigmasterol (**11**), 18*α*-olean-19*α* -ol-3-one (**12**), ferulic acid (**13**), scopoletin (**14**), samaderin A (**15**), samaderin B (**16**), dihydrosamaderin B (**17**), samaderin C (**18**) and *β*-sitosterol- *β*-D-glucoside (**19)**. Ferulic acid (**13**) and scopoletin (**14**) were isolated from the stem bark of *Quassia indica* for the first time. We have tested the *in vitro* antidiabetic activity of lupenone (**9**), 18*α*-olean-19*α* -ol-3-one (**12**), ferulic acid (**13**) and scopoletin (**14**). Lupenone (**9**) and 18*α*-olean-19*α* -ol-3-one (**12**) exhibited significant inhibitory activity on *α*-amylase with IC_{50} value of 7.35 ± 0.255 and 14.88 ± 0.42 μM. In the case of *α*-glucosidase enzyme, ferulic acid (**13**) and scopoletin (**14**) displayed significant inhibitory activity with IC_{50} value of 54.87 ± 0.734 and 51.44 ± 1.278 μM. We have also carried out molecular docking studies with porcine pancreatic *α*-amylase (**3AJ7**), isomaltase from *Saccharomyces cerevisiae* (**3A4A**), human pancreatic *α*- amylase (**4GQQ**), human maltase-glucoamylase *C*-terminal (**2QMJ**) and *N*-terminal (**3TOP**). Further studies are necessary to establish the therapeutic potential of the stem bark of *Quassia indica*.

2B.7. Experimental

General experimental procedures and chemicals used were described in section **2A.14** of Chapter **2** Part **A**.

2B.7.1. Collection of plant material, extraction, isolation and characterization of phytochemicals from the stem bark of *Quassia indica*

The stem bark of *Quassia indica* was collected from Alappuzha district, Kerala, India. The stem bark was thoroughly cleaned, cut into small pieces, air dried and then dried in drier maintained at 50 ^{o}C and powdered. The powdered stem bark (1.25 kg) was subjected to extraction using *n*-hexane (3 L x 48 h x 3 times; 11 g), acetone (3 L x 48 h x 3 times; 14 g), EtOH (3 L x 48 h x 3 times; 9.5 g) and water (3 L x 48 h x 3 times; 12 g). All the extracts were checked for their *in vitro* inhibitory activities on carbohydrate hydrolyzing enzymes such as *α*-amylase and *α*-glucosidase as well as for their antiglycation properties. The acetone extract has promising inhibitory activity on *α*-amylase *α*-

glucosidase and protein glycation. Therefore, further isolation and purification was focussed on acetone extract. The crude acetone extract (13.5 g) was subjected to silica gel (100-200 mesh) column chromatography using *n*-hexane, *n*-hexane-EtOAc gradient and EtOAc. Twenty fractions of 200 mL each were collected and concentrated under reduced pressure. The schematic representation of the entire isolation procedures are shown in **Figure 2B.19.**

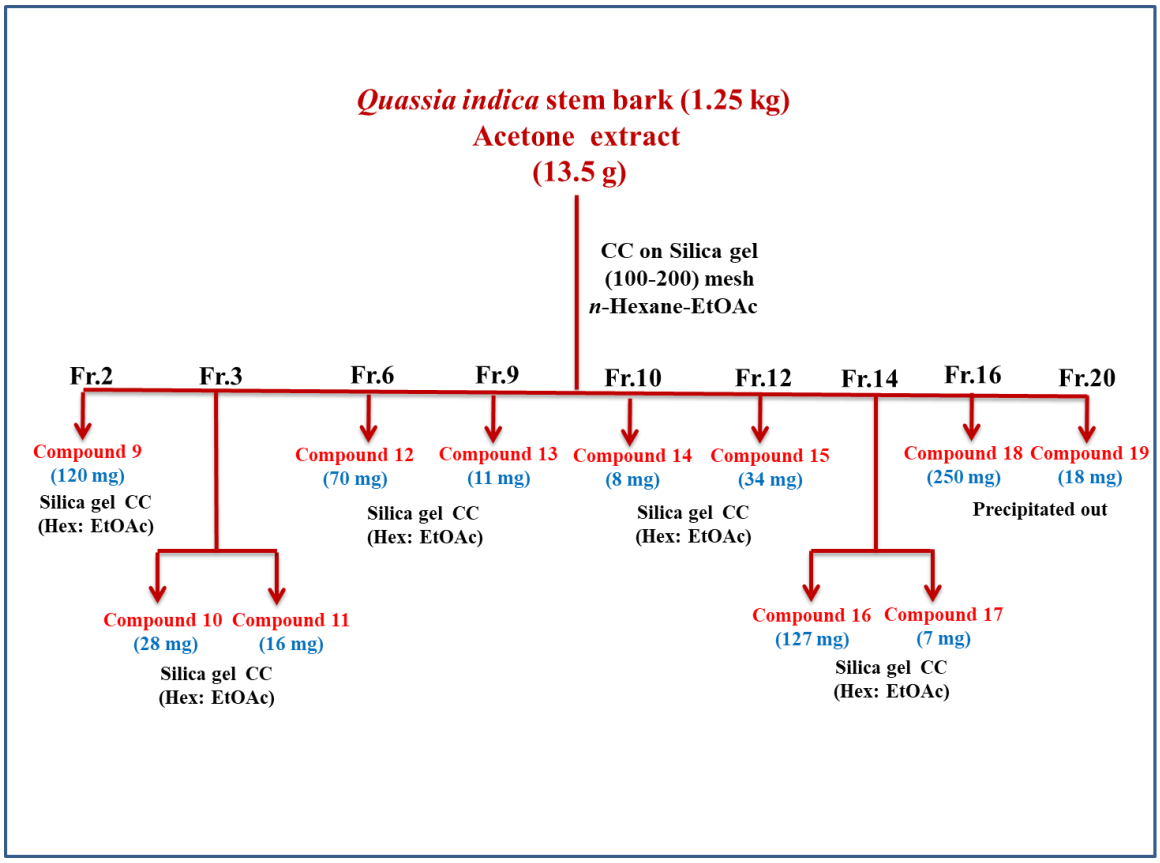

Figure 2B.19. The schematic representation of the extraction and isolation of phytochemicals from the stem bark of *Quassia indica*

2B.7.1.1. Isolation of compound 9

The isolation procedure of compound **9** is represented in **Figure 2B.19.** Compound **1** (120 mg, fraction pool 2) was obtained as a white crystalline solid, on eluting the column (silica gel 100-200 mesh) with 3 % EtOAc in *n*-hexane. From the detailed analysis of various spectroscopic data, the structure of the compound was analysed as lupenone.

Nature	Colourless crystalline solid
Melting point	168-170 ºC

FTIR (KBr, υ_{max}, cm^{-1})	2927, 2860, 1708, 1459, 1382.
^1H NMR (500 MHz, $CDCl_3$)	δ 0.80 (s, 3H, H-28), 0.90 (s, 3H, H-25), 0.93 (s, 3H, H-27), 1.00 (s, 3H, H-24), 1.1 (s, 3H, H-23), 1.1 (s, 3H, H-26), 1.7 (s, 3H, H-30), 1.87-1.96 (m, H-21), 2.34-2.42 (m, H-19), 2.45-2.51 (m, H-19), 4.55 (d, J_1 = 1.5 Hz, J_2 = 2.5 Hz, H-29) and 4.47 (d, J = 2 Hz, H-29) ppm.
^{13}C NMR (125 MHz,$CDCl_3$)	δ 14.5 (C-27), 15.8 (C-26), 16.0 (C-25), 18.0 (C-28), 19.3 (C-6), 19.7 (C-30), 21.0 (C-24), 21.5 (C-11), 25.1 (C-12), 26.7 (C-23), 27.4 (C-15), 29.8 (C-21), 33.6 (C-7), 34.1 (C-2), 35.5 (C-16), 36.9 (C-10), 38.2 (C-13), 39.6 (C-1), 40.0 (C-22), 40.8 (C-8), 42.9 (C-14), 43.0 (C-17), 47.3 (C-4), 48.0 (C-19), 48.2 (C-18), 49.8 (C-9), 54.9 (C-5), 109.6 (C-29), 150.6 (C-20), 217.7 (C-3) ppm.
HRESIMS (m/z)	425.37788 $(M+H)^+$

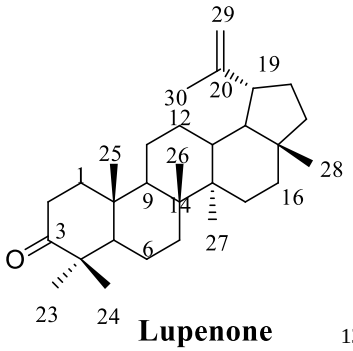

Lupenone

2B.7.1.2. Isolation of compound 10 and compound 11

Fraction pool 3 on column chromatographic separation using silica gel 100-200 mesh, afforded two compounds, β- sitosterol (**10**) and stigmasterol (**11**) which showed blue intense spot while charring the TLC in Mc Gill solution. From spectroscopic analysis the compound was identified as β- sitosterol. Signals at 5.37 ppm in ^1H NMR and 121.7 ppm in ^{13}C NMR indicated the presence of olefinic proton. The oxymethine proton resonated as a multiplet between δ_H 3.53-3.54 ppm, and it is one of the characteristic peaks. DEPT experiment reveals that the compound contains eleven -CH_2- and six -CH_3 groups. The mass spectra showed molecular ion peak at 415.1097 $(M+H)^+$.

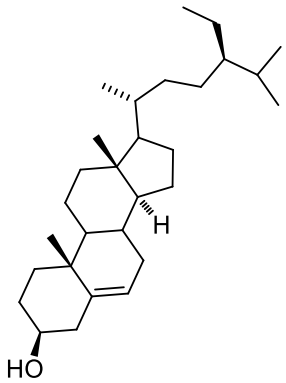

***β*- sitosterol**

Nature	Colourless crystalline solid
Melting point	128-130 ^{o}C
FTIR (KBr, υ_{max}, cm^{-1})	3408, 2935, 2863, 1459, 1374, 1316, 1257, 1190, 1099, 1054, 1024, 958, 802.
^{1}H NMR (500 MHz, $CDCl_3$)	δ 5.37 (d, J = 5 Hz, 1H), 3.53-3.54 (m, 1H), 2.30-2.29 (m, 2H), 2.04-1.87 (m, 2H), 1.87-1.84 (m, 3H),1.68-1.66 (m, 2H), 1.60-1.45 (m, 7H), 1.32-1.23 (m, 6H), 1.20-1.10 (m, 3H), 1.09-1.96 (m, 3H), 1.02 (s, 5H), 0.94- 0.93 (m, 3H), 0.87-0.71 (m, 9H), 0.69 (s, 3H) ppm.
^{13}C NMR (125 MHz,$CDCl_3$)	δ 140.8, 121.7, 71.8, 56.8, 56.0, 50.1, 45.8, 42.3, 42.3, 39.8, 37.2, 36.5, 36.2, 33.9, 31.9, 31.7, 29.1, 28.3, 26.0, 24.3, 23.0, 21.1, 19.8, 19.4, 19.0, 18.8, 11.9, 11.9 ppm.
HRESIMS (m/z)	415.3940 $[M+H]^{+}$

NMR spectra of compound **11** are almost similar to that of compound **10**. In the ^{1}H NMR spectrum of compound **11,** the olefinic proton at 20 resonated as a doublet of doublet at δ_H 5.15 ppm with coupling of constant 15.5 and 11 Hz. Similarly the olefinic proton at 21 resonated as a doublet of doublet at δ_H 5.02 ppm with coupling constant of 15.0 Hz and 13.5 Hz. And in ^{13}C NMR spectrum, the peak at δ_C 132.4 and 129.4 ppm indicating the presence of *trans* double bond. The mass spectra showed a molecular ion peak at 413.6917 $[M+H]^{+}$.

Nature	Colourless crystalline solid
Melting point	162-165 ^{o}C
FTIR(KBr, υ_{max},	3408, 3272, 2935, 2863, 1645, 1459,

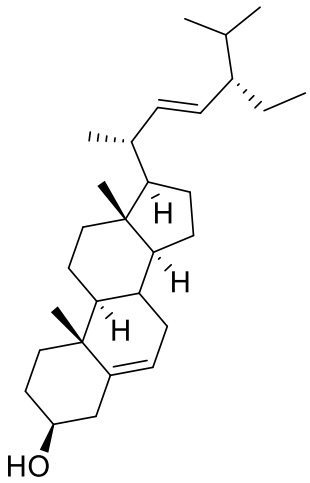

Stigmasterol

cm^{-1})	1374, 1316, 1257, 1190, 1099, 1054, 1024 cm^{-1}
^{1}H NMR (500 MHz, $CDCl_3$)	δ 5.35 (d, J = 2 Hz, 1H), 5.15 (dd, J_1 = 15.5 Hz and J_2 = 11 Hz, 1H), 5.02 (dd, J_1=15 Hz and J_2 =13.5 Hz, 1H), 3.53-3.52 (m, 1H), 2.29-2.00 (m, 2H), 1.99-1.83 (m, 3H), 1.57-1.55 (m, 2H), 1.54-1.25 (m, 12H), 1.8-1.14 (m, 7H), 1.10-1.04 (m, 7H), 1.03-1.00 (m, 2H), 0.85-0.82 (m, 3H), 0.80-0.70 (m, 5H), 0.68 (s, 3H) ppm.
^{13}C NMR (125 MHz,$CDCl_3$)	δ 140.8, 138.428, 129.4, 121.7, 71.8, 56.8, 56.0, 50.1, 45.8, 42.3, 42.3, 39.7, 37.2, 36.5, 36.2, 33.9, 31.9, 29.11, 28.6, 26.0, 24.3, 23.0, 21.1, 19.8, 19.4, 19.0, 18.8, 11.98, 11.7 ppm.
HRESIMS (m/z)	413.6917 $[M+H]^+$

2B.7.1.3. Isolation of compound 12

Fraction pool 6 on column chromatographic purification (silica gel 100-200 mesh) using 7 % EtOAc/*n*-hexane as eluent afforded compound **12** as a colourless crystalline solid.

Nature	Colourless crystalline solid
Melting point	127-129 ºC
FTIR (KBr, υ_{max})	3450, 2945, 2866, 1712, 1460, 1385, 1363 and 1009 cm^{-1}.
^{1}H NMR (500 MHz, $CDCl_3$)	δ 3.30 (d, J = 10.5 Hz, 1H, C-19), 2.50-2.46 (m, 1H, C-2a), 2.44-2.41 (m, 1H, C-2b), [2.31 (d, J = 11 Hz, 1H), 1.93-1.87 (m, 3H),

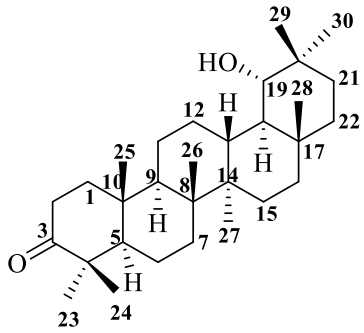

18α-Olean-19α-ol-3-one

	1.77-1.72 (m, 2H), 1.54 - 1.51 (m, 2H), 1.46-1.38 (m, 4H), 1.36-1.32 (m, 6H), 1.25-1.20 (m, 5H), 1.14 (m, 2H) other aliphatic protons], 1.1 (s, 3H, Me), 1.07 (s, 3H, Me), 1.03 (s, 3H, Me), 0.98 (s, 3H, Me), 0.97 (s, 3H, Me), 0.94 (s, 3H, Me), 0.89 (s, 3H, Me), 0.85 (s, 3H, Me) ppm.
^{13}C NMR (125 MHz,$CDCl_3$)	δ 218.3 (C-3), 78.1 (C-19), [54.8, 49.1, 47.3, 45.9, 42.9, 41.1, 39.5, 38.1, 38.0, 37.8, 37.5, 36.7, 34.8, 34.1, 33.5, 30.0, 28.1, 26.7, 26.5 (other aliphatic carbons)], 21.8 (Me), 21.0 (Me), 19.8 (Me), 19.7 (Me), 18.2 (Me), 16.0 (Me), 15.8 (Me), 14.5 (Me) ppm.
HRESIMS (m/z)	465.37276 $(M+Na)^+$

NMR spectral assignments were made on the basis of ^{1}H-^{1}H COSY, HMQC, DEPT 135 and HMBC analysis.

2B.7.1.4. Isolation of compound 13

Fraction pool 9 on column chromatographic separation (silica gel 100-200 mesh) using 35 % EtOAc/*n*-hexane as eluent afforded compound **13** (11 mg) as pale yellow solid. NMR spectral assignments were made on the basis of ^{1}H-^{1}H COSY, HMQC, DEPT 135 and HMBC analysis and in comparison with the literature reports.

Nature	Pale yellow solid
Melting point	167-169 ^{o}C
FTIR (KBr, υ_{max})	3450, 1690, 1605, 1275, 1510 cm^{-1}.
^{1}H NMR	δ 7.71 (d, J = 16 Hz, 1H, H-

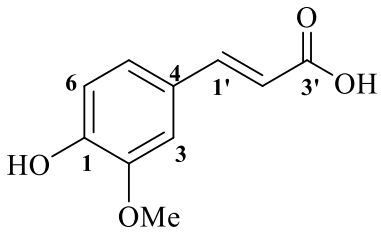

Ferulic acid

(500 MHz, $CDCl_3$)	1'), 7.17 (dd, J_1 = 8, J_2 = 8 Hz, 1H), 7.06 (d, J = 1.5 Hz, 1H, H-3), 6.94 (d, J = 8 Hz, 1H, H-6), 6.30 (d, J = 16 Hz, 1H, H-2'), 5.91 (brs, 1H, OH), 3.94 (s, 3H, OMe) ppm.
^{13}C NMR (125 MHz,$CDCl_3$)	δ 171.3 (3'), 148.4 (C-2), 147.1 (C-1), 146.8 (C-1'), 126.7 (C-4), 123.6 (C-5), 114.8 (C-2'), 114.4 (C-6), 109.5 (C-3), 56.0 (-OCH_3) ppm.
HRESIMS (m/z)	193.07607 $(M-H)^+$

2B.7.1.5. Isolation of compound 14

Fraction pool **10** on column chromatographic separation (silica gel 100-200 mesh) using 40 % EtOAc/*n*-hexane as eluent gave compound **6** (8 mg) as colourless amorphous solid.

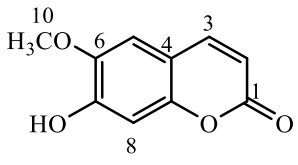

Scopoletin

Nature	Colourless amorphous solid
Melting point	138-140 ^oC
FTIR (KBr, υ_{max})	3338, 3320, 2990, 2950, 1702, 1698, 1608, 1565, 1567 1510 cm^{-1}.
^{1}H NMR (500 MHz, $CDCl_3$)	δ 7.57 (d, J = 9.5 Hz, 1H, H-3), 6.91 (s, 1H, H-5), 6.82 (s, 1H, H-8), 6.26 (d, J = 9.5 Hz, 1H, H-1), 6.10 (s, 1H, H-8), 3.96 (s, 3H, H-10) ppm.
^{13}C NMR (125 MHz,$CDCl_3$)	δ 160.8 (C-1), 150.3 (C-9), 149.7 (C-7), 143.9 (C-6),

	143.0, 138.3, 113.5 (C-1), 111.4 (C-4), 107.3 (C-6), 103.3 (C-8), 56.3 (C-10) ppm.
HRESIMS (m/z)	193.0101 $(M+H)^+$

NMR spectral assignments were made on the basis of HOMOCOSY, HMQC, DEPT 135 and HMBC analysis and in comparison with the literature reports.

2B.7.1.6. Isolation of compound 15

The isolation procedure of compound **15** is represented in **Figure 2B.19.** Compound **15** (34 mg, fraction pool 12) was obtained as a colourless crystalline solid, on eluting the column (silica gel 100-200 mesh) with 45 % EtOAc in *n*-hexane. From the detailed analysis of various spectroscopic data, the structure of the compound was identified as samaderin A, previously isolated from the seeds of *Quassia indica*.

2B.7.1.7. Isolation of compound 16 and 17

Fraction pool **14** on column chromatographic separation (silica gel 100-200 mesh) using 55 % EtOAc/*n*-hexane as eluent gave compound **16** (127 mg) and compound **17** (7 mg) as colourless crystalline solid. From the detailed analysis of various spectroscopic data, the structures of the compounds were analysed as samaderin B and dihydrosamaderin B. Both the compounds are previously isolated from the seeds of *Quassia indica*.

2B.7.1.8. Isolation of compound 18

The isolation procedure of compound **18** is depicted in **Figure 2B.19.** Compound **18** (120 mg, fraction pool 2) was obtained as a colourless crystalline solid, on eluting the column (silica gel 100-200 mesh) with 65 % EtOAc in *n*-hexane. From the detailed analysis of various spectroscopic data, the structure of the compound was analysed as samaderin C.

2B.7.1.9. Isolation of compound 19

Compound **19** was isolated from fraction pool 20 in 18 mg as colourless amorphous solid. The structural characterization of this molecule showed that it is *β*-sitosterol- *β*-*D*-glucoside.

Isolation, Characterization and Anti-inflammatory Activity of Phytochemicals from the Stem Bark of *Ailanthus excelsa* Roxb.

Medicinal plants have historically proven their value as a source of structurally diverse molecules with potent therapeutic potential, and nowadays still represent an important tool for the identification of novel drug leads for various ailments. In the past few decades, the pharmaceutical industry and medicinal chemists were mainly focused on libraries of synthetic compounds as the source of drug discovery. They are comparably easy to synthesise and resupply, and demonstrate good compatibility with established high throughput screening (HTS) platforms. However, at the same time, there has been a declining trend in the number of new drugs reaching the market, raising renewed scientific interest in drug discovery from natural sources, despite of its known challenges. We herein report a snapshot of the isolation, characterization and antiinflammatory activity of phytochemicals from the stem bark of *Ailanthus excelsa* Roxb.

3.1. *Ailanthus* genus

Ailanthus; an Ambonese word ‘ailanto’ which means "tree of the gods" or "tree of heaven". This genus belongs to Simaroubaceae family and native to Asia and Australasia. They are fast-growing deciduous trees growing upto 25-45 m tall, small yellows to greenish flowers and male flowers have a strong odour. Ailanthus species are used as crude drugs or as traditional medicine in Indian villages. Some of the Ailanthus species and their distribution are shown in **Table 3.1.**

Table. 3.1. *Ailanthus* species and their distribution

Sl. No	*Ailanthus* species	Distribution
1	*Ailanthus altissima*	China, Taiwan, America, Britain & Australia
2	*Ailanthus excelsa*	India & Sri Lanka
3	*Ailanthus fordii*	China
4	*Ailanthus integrifolia*	New Guinea, Queensland & Australia
5	*Ailanthus triphysa*	India, Southeast Asia &Australia
6	*Ailanthus vietnamensis*	Vietnam

3.1.1. *Ailanthus altissima*

Ailanthus altissima is a deciduous tree up to 45 m tall, distributed over North Australia and Asia. Plants from this genus are widely used for a number of therapeutic applications including anthelmintic, antispasmodic, bronchitis, diarrhea, epilepsy, nervous diseases, and hypertension, and contain various natural product classes such as alkaloids, coumarins, flavonoids, phenolic glycosides, terpenoids, and steroids. In 1996, Kengo *et al*., reported the isolation of ailantinols A and B, shinjudilactone, ailanthone, shinjulactone A, amaloride, amaloride-11-acetate, shinjulactone K, $\Delta^{13(18)}$-dehydroglaucarubinone, $\Delta^{13(18)}$-dehydroglaucarubolone, shinjulactone B, and shinjulactone C from the stem bark of *Ailanthus excelsa* [Kengo *et al*., **1996**]. Same group also reported the ailantinol C, ailantinol D, shinjulactone A and shinjudilactone from the stem bark of *Ailanthus excelsa* [Kengo *et al*., **1996**]. The chloroform extract of the seeds of *Ailanthus altissima*, gave two new sterols, named ailanthusterol A and ailanthusterol B [Ansari *et al*., **2003**]. In 2003, Sadaaki *et al.*, reported the isolation of ailantinol E, ailantinol F, ailantinol G from *Ailanthus excelsa* [Sadaaki *et al.*, **2003**]. In 2006, same group also reported the isolation of ailantinol H from aerial parts of *Ailanthus altissima* [Sadaaki *et al.*, **2006**]. In 2007, Zhang *et al*., reported the isolation of two new alkaloidal glycosides, ailantcanthinosides A and B from the root bark of *Ailanthus altissima* [Zhang *et al*., **2007**]. Trong-Tuan *et al*., reported the isolation of four new terpenylated coumarins (Altissimacoumarin C-F) from the stem bark of *Ailanthus altissima* [Trong-Tuan *et al*., **2012**]. Same year, Qing-Wei *et al*., reported the isolation of nine *seco*-neolignan glycosides namely, *seco*-dehydrodiconiferyl alcohol-4-*O*-*β*-D-glucopyranoside, dehydro-diconiferyl alcohol-4-*O*-*β*-D-glucopyranoside, dihydrodehydrodiconiferyl alcohol, dihydrodehydro diconiferyl alcohol-4-*O*-*β*-D-glucopyranoside, 7, 9, 9'-trihydroxy-3, 3', 5'-trimethoxy-8-*O*-4'-neolignan-4-*O*-*β*-D-glucopyranoside, sonchifolignan B, citrusin B, gallic acid and 4-*O*-*β*-D-glucopyranosyl-3,5-dimethoxygallic acid from the root bark of *Ailanthus altissima* [Qing-Wei *et al*., **2012**]. In 2013, Zhi-Lai *et al*., reported altissimanins A-E, terpenylated coumarin (altissimacoumarin G), (24*S*)-24, 25-dihydroxy tirucall-7-en-3-one, niloticin, piscidinol A, bourjotinolone B, (23*E*)-3*β*, 25-dihydroxy tirucalla-7, 23-diene, isofouquierone, (20*S*)-hydroxy-25-methoxy-dammar-23-en-3-one, 24,25-dihydroxy dammar-20-en-3-one, cabralealactone, betulafol ienediolone, altissimacoumarin B, (20*S*, 24*R*)-12*β*,25-dihydroxy-20, 24-epoxydamaran-3-one, altissimacoumarin D and shinjudilactone and 7*β* -hydroxysitosterol, respectively [Zhi-Lai

et al., **2013**]. Same year, Yan *et al*., reported the isolation of 14 quassinoids namely; altissinol A, altissinol B, ailanthone, 13, 18-dehydroglaucarubinone, (-)-chaparrinone, 6*α*-tigloyloxychaparrinone, shinjulactone A, 6 *α*-tigloyloxychaparrin, glaucarubin, amarolide, 11-acetylamarolide, chaparrolide, shinjulactone C and shinjulactone B [Yan *et al*., **2013**]. In 2014, Xiao-Lin *et al*., isolated shinjulactone O, shinjulactone M, isoailanthone, ailanthone, chaparrinone, shinjulactone C shinjulactone A, and 6*α*-, including a new tigloyloxychaparrin from the root bark of *Ailanthus altissima* [Xiao-Lin *et al*., **2014**]. In 2016, Hye *et al*., reported the isolation and anti-inflammatory activity of six canthinone-type alkaloids [(*R*)-5-(1-hydroxyethyl)-canthine-6-one, canthin-6-one, 4-hydroxycanthin-6-one, 10-hydroxy- canthin-6-one, 9-hydroxycanthin-6-one, 11-hydroxycanthin-6-one and *trans*-4(*R*)-hydroxy-2-nonenoic acid], four phenyl propanoids [dihydroconiferyl alcohol, epoxyconiferyl alcohol, sinapaldehyde, scopoletin], two lignans [*erythro*-guaiacyl glycerol-*β*-*O*-4′-coniferyl ether and ficusesquilignan B], two triterpenoids [20(*R*)-24, 25-trihydroxy-dammaran-3-one and hispidol B] and a fatty acid [*trans*-4(*R*)-hydroxy-2-nonenoic acid] [Hye *et al*., **2016**]. Same year, Ruxing *et al*., reported the antitumour activity of 2-dihydroailanthone from the bark of *Ailanthus altissima* against U251 [Ruxing *et al*., **2016**]. In 2017, Jian-Cheng *et al*., reported the isolation and anti-tobacco mosaic virus (TMV) activity of 2-hydroxy-N-[(2-*O*-*β*-D-glucopyranosyl) phenyl] propionamide, 2-hydroxy-*N*-[(2-*O*-*β*-D-glucopyranosyl-(1→6)-*β*-D-glucopyran osyl) phenyl]propionamide, 2-hydroxy-*N*-(2-hydroxyphenyl) propion amide, 2*β*-carboxyl-piperidine-4*β*-acetic acid methyl ester, 4-hydroxyphenyl-1-*O*-[6-(hydrogen-3-hydroxy-3-methylpentanedioate)]-*β*-D-glucopyranoside, arbutin, *β*-D-glucopyranosyl-(1→6)-arbutin, hydroquinone, 2-(4-hydroxyphenyl)propane-1,3-diol, 4-methoxy phenylacetic acid, 4-hydroxybenzoic acid, protocatechuic acid, vanillic acid, gallic acid, methyl gallate, 1-*O*-galloyl-*β*-D-glucose, 3, 4, 8, 9,10-pentahydroxydibenzo [*b, d*]pyran-6-one, corilagin, astragalin, kaempferol 3-*O*-rutinoside, kaempferol 3-*O*-(2′′-*O*-galloyl)-rutinoside, quercetin, isoquercitrin, quercitrin, quercetin 3-*O*-(2′′-*O*-galloyl)-*β*-D-glucopyranoside, quercetin 3-*O*-(6′′-*O*-galloyl)-*β*-D-glucopyranoside, rutin and quercetin-3-*O*-(2′′-*O*-galloyl)-rutinoside from the fruit of *Ailanthus altissima* [Jian-Cheng *et al*., **2017**]. In 2017, Ru-Xing *et al*., reported the isolation and antitumor activity of isoailanthone, shinjudilactone, 2-dihydroailanthone, shinjulactone B, ailanthone and 12-dihydroisoailanthone from the bark of *Ailanthus altissima* [Ru-Xing *et al*., **2017**]. Seung-Kye and coworkers reported the anti-inflammatory activity of canthin-6-one

alkaloids from *Ailanthus altissima* [Seung-Kye *et al*., **2017**]. Recently, Jian-Cheng and coworker reported the isolation and antiviral effect against Tobacco mosaic virus (TMV) of 4-hydroxyphenol-1-O-[6-*O*-(E)-feruloyl-*β*-D-glucopyranosyl]-(1→6)-*β*-D-glucopyran oside and a new terpenylated coumarin (altissimacoumarin H) along with, esculetin, scopoletin, methyl chlorogenate, 5-*O*-caffeoyl quinic acid butyl ester, syringine, *p*-coumaric acid, caffeic acid, 3-hydroxy-1-(4-hydroxyphenyl)-1-propanone, *ω*-hydroxypropioguaiacone and *threo*-1-(4-hydroxyphenyl)-1-methoxy-2,3-propanediol from the fruit of *Ailanthus altissima* [Jian-Cheng *et al*., **2018**]. In 2018, Qing-Wei *et al*., reported the isolation and anti-tobacco mosaic virus activity of chuglycosides A−I, chaparrinone, glaucarubinone and ailanthone, shinjuglycoside A, shinjuglycoside B, glaucarubolone, ailanthinone, $\Delta^{13(18)}$- glaucarubolone and dehydroailanthinone from the samara of *Ailanthus altissima* [Qing-Wei *et al*., **2018**]. Structures of some of the phytochemicals isolated from *Ailanthus altissima* species are shown in **Figure 3.1.**

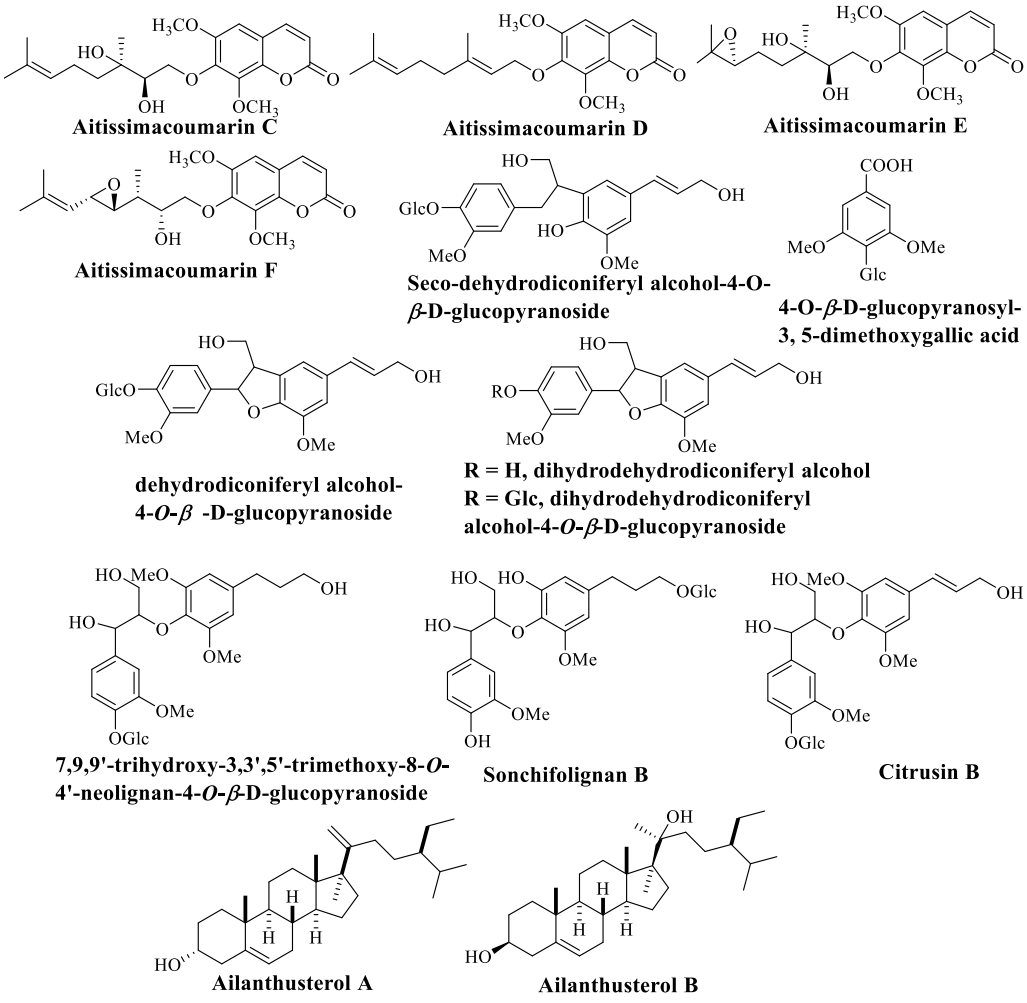

Continued…

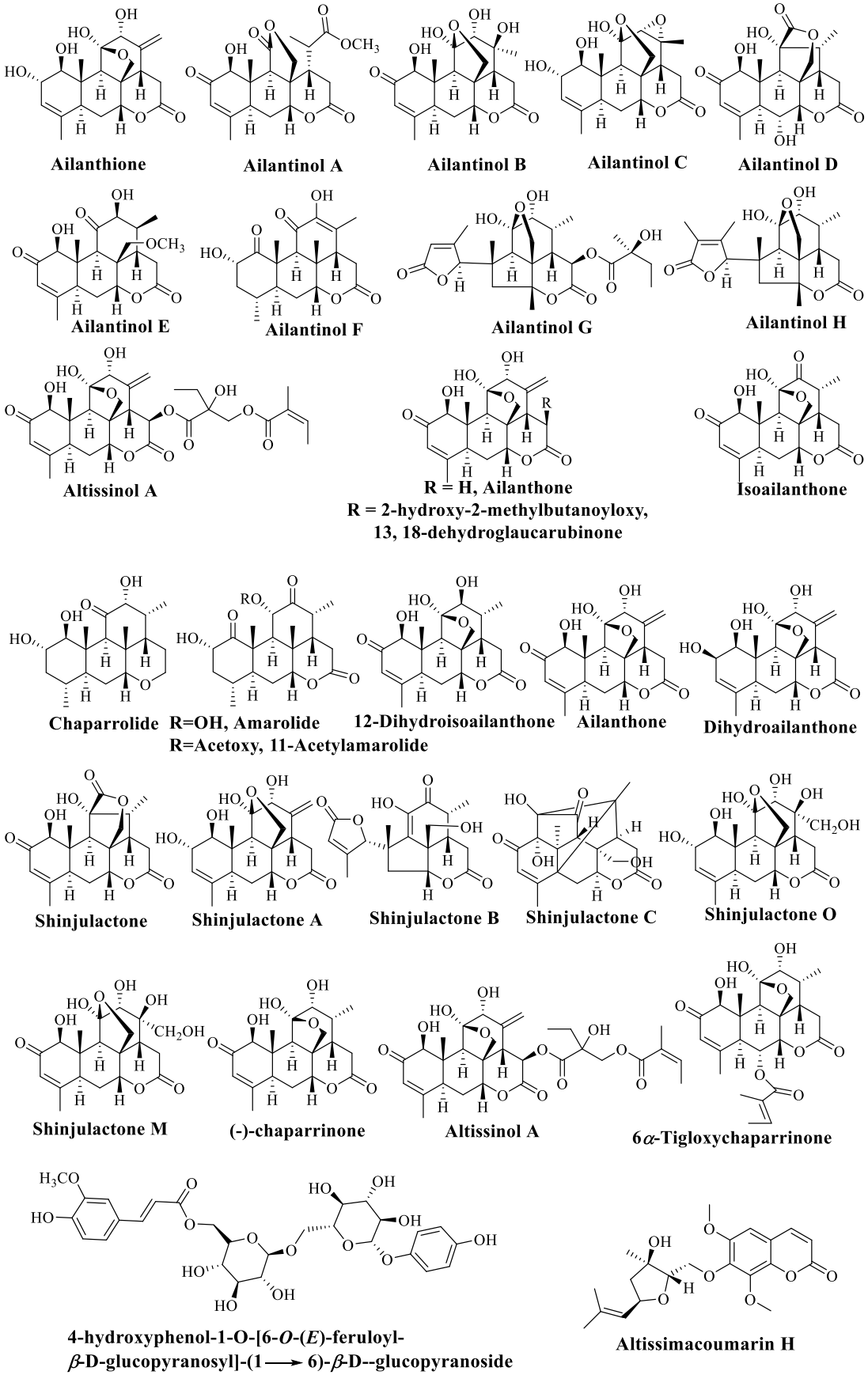

Figure 3.1. Compounds isolated from *Ailanthus altissima*

3.1.2. *Ailanthus triphysa*

Ailanthus triphysa is a deciduous tree, distributed over North Australia and Asia. The plant has been used for the treatment of dyspepsia, bronchitis, ophthalmia and snake bite. The stem and stem barks of *A. triphysa* exhibited good inhibition against four human cancer cell lines (HepG2, HuCCA-1, A549, and MOLT-3). Phytochemical investigation of *Ailanthus triphysa* led to the isolation of cycloapotirucallane-type derivatives, malabaricane-type derivatives, phyllocladane and nor-lupane triterpenoid [Shu-Hua *et al*., **2003**; Sanit *et al*., **2016**].

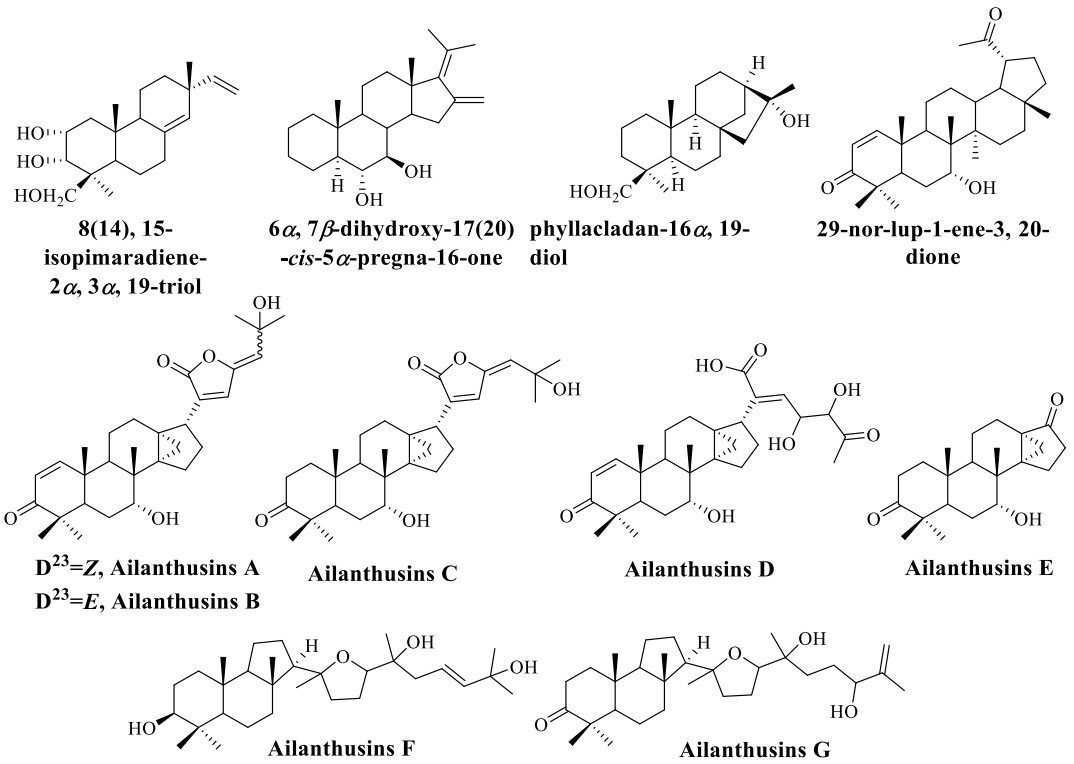

Figure 3.2. Compounds isolated from *Ailanthus triphysa*

3.2. Aim and scope of the present investigation

Ailanthus excelsa (**Figure 3.3, Table 3.2**) or "Plant of Heaven" is a decidous tree belonging to Simaroubaceae family and commonly known as “Mahanimba” due to its resemblance with the neem tree (*Azadirachita indica*) and “Maharukha” due to its large size. The traditional claims, phytochemical investigations, and pharmacological evaluation and some ayurvedic formulations provide the backbone to make this tree as a plant of Heaven. The name ‘*Ailanthus excelsa*’ derived from two words; *Ailanthus* and *excelsa*. The word *ailanto* which means 'tree of heaven' and *excelsa* means 'tall'. *Ailanthus excelsa* is a fast growing tree extensively cultivated in many parts of India towards the vicinity of villages. The tree is indigenous to southern and central India and distributed in

western peninsula, Rajasthan, Bihar, Orissa, Madhya Pradesh, Gujarat, in dry deciduous forests of Maharastra, scrace in Deccan and Karnataka and the forest of Tamil Nadu. It is often planted along the road sides and the plant is known for its high economic and commercial importance. In Chinese system of Medicine, barks of *A. excelsa* is used to treat diarrhea and dysentery, especially when there is blood in the stool. The bark has been used in Asian and Australian traditional medicine to counteract worms, excessive vaginal discharge, malaria and asthma. In Africa, the plant is used to treat cramps, gonorrhea, epilepsy, tape worm infestation and high blood pressure. In Bombay, the bark and leaves are of great repute as a tonic especially in debility after child birth. They are used in dyspepsia, bronchitis and asthma. It is also used to cure wounds and skin eruptions. The plant is used as a natural antifertility agent by the Irula women in Mavanahalla region of the Nilgiri district in Tamil Nadu. The bark is used as bitter, refrigerant, astringent, appetizer, anthelmintic, febrifuge, in dysentery, earache, skin disease, troubles of the rectum and fever due to tridosha and allay thirst. It is also used in gout and rheumatism. In Ayurveda, it is used to remove the bad taste of mouth. The bark is a good substitute for kurchi, holarrhena antidysenterica. The plant serves as one of the hosts for silkworms. In France, the tree is cultivated for its leaves, on which the caterpillar of the silk spinning Ailanthus moth and cheaper than mulberry silk.

Figure 3.3. *Ailanthus excelsa* -Tree, flower and leaves

Table 3.2. Scientific classification of *Ailanthus excelsa* Roxb.

Kingdom	Plantae
Order	Sapindale
Family	Simaroubaceae
Genus	*Ailanthus*
Species	*A. excelsa*
Binomial name	*Ailanthus excelsa* Roxb.

According to the literature survey, the journey of *Ailanthus excelsa* started in the year, 1971 by Kapoor *et al*. They isolated *β*-sitosterol and vitexin from the leaves of *Ailanthus excelsa* [Kapoor *et al*., **1971]**. After that, Surror *et al*., isolated 13,18-dehydroexcelsin and glaucarubol from the bark of *Ailanthus excelsa* [Surror *et al*., **1980**]. Same year, Mary *et al*., isolated 3*S*, 24*S*, 25-trihydroxytirucall-7-ene from the root barks of *Ailanthus excelsa* [Mary *et al*., **1980**]. In 1993, Arun *et al*., isolated excelsin from the stem bark of *Ailanthus excelsa* and it showed antifeedant activity against *Spilosoma obliqua* [Arun *et al*., **1993**]. In 2003, Bipin *et al*., isolated three new quassinoids, 4-dihydroexcelsin, excelsin, glaucarubine, ailanthinone, glaucarubinone and glaucarubolone from the stem bark of *Ailanthus excelsa* [Bipin *et al*., **2003]**. In 2004, Anuj Pandey and coworkers, reported the *in vitro* antimalarial activity of excelsin and they isolated two new molecules from the stem bark of *Ailanthus excelsa*. In 2006, Pullela *et al*., isolated two new dammarane-type triterpenes, ailexcelone and ailexcelol, together with ocotillone, malabaricol, epoxymalabaricol, lupeol, and sitosterol-3-*O*-*β*-D-glucoside from the heartwood of *Ailanthus excelsa* [Pullela *et al*., **2006**]. Manish and coworkers reported the anticancer activity of novel triterpenoid from the root bark of *Ailanthus excelsa* [Manish *et al*., 2009]. Furthermore, Ataa *et al*., reported the antioxidant and antiproliferative activities of *Ailanthus excelsa* and they isolated flavones and flavanols namely, apigenin, apigenin 7-*O*-*β*-glucoside, luteolin, luteolin-7-*O*-*β*-glucoside, kaempferol, kaempferol-3-*O*-*α*-arabinoside, kaempferol-3-*O*-*β*-galactoside, quercetin, quercetin-3-*O*-*α*-arabinoside, quercetin-3-*O*-*β*-galactoside and quercetin-3-*O*-rutinoside from the leaves of *Ailanthus excelsa* [Ataa *et al.*, **2010**]. In 2011, Dinesh *et al*., reported antiasthmatic and antiallergic potential of methanolic extract of leaves of *Ailanthus excelsa* [Dinesh *et al*., **2011**]. Recently, Xia reported the protective effects of *Ailanthus excelsa* in myocardial infraction post mesenchymal stem cell transplantation [Xia, **2016**]. Apart from these, there is no report on the phytochemical investigation of this plant. We herein report the anti-inflammatory activity of phytochemicals isolated from the stem bark of *Ailanthus excelsa* Roxb.

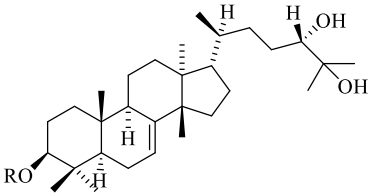

3*S*, 24*S*, 25-trihydroxytirucall-7-ene

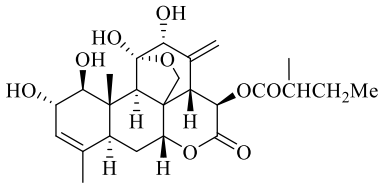

13,18-dehydroexcelsin

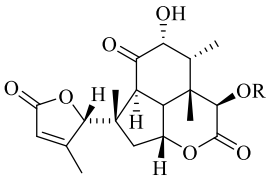

R = $COCH(CH_3)CH_2CH_3$, Ailanex A
R = $COC(CH_3)(OH)CH_2CH_3$, Ailanex B
R = H, Polyandrol

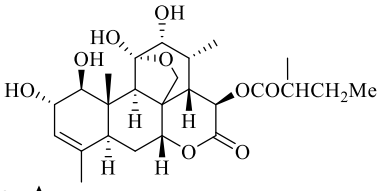

Excelsin

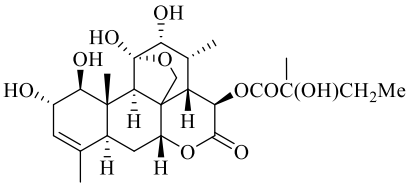

Glaucarubin

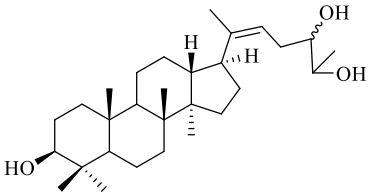

Ailexcelol

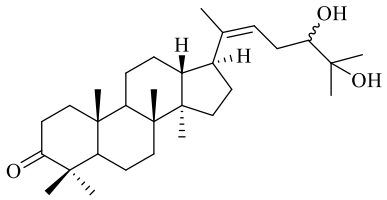

Ailexcelone

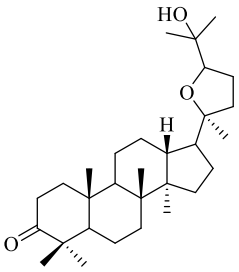

Ocotillone

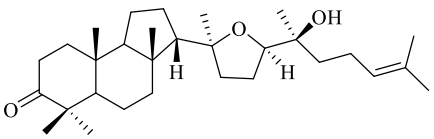

Malabaricol

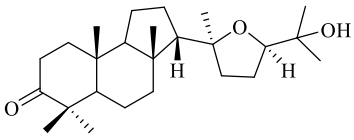

Epoxymalabaricol

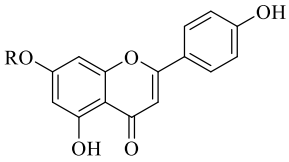

R = H, Apigenin
R = Glucose, Apigenin-7-O-*b*-glucoside

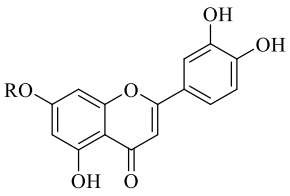

R = H, Luteolin
R = Glucose, Luteolin-7-O-β-glucoside

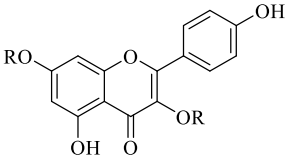

R = H, Kampferol
R = Arabinose, Kampferol-3-*O*-α-arabinoside
R = Galactose, Kampferol-3-*O*-β-galactoside

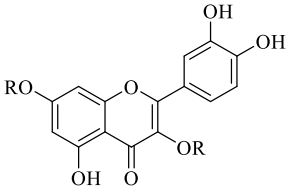

R = H, Quercetin
R = Arabinose, Quercetin-3-*O*-α-arabinoside
R = Galactose, Quercetin-3-*O*-β-galactoside
R = Rutinose, Quercetin-3-*O*-rutinoside

Figure 3.4. Compounds isolated from *Ailanthus excelsa*

3.3. Extraction, isolation and characterization of compounds from *Ailanthus excelsa* stem bark

3.3.1. Plant material

The stem bark of *Ailanthus excelsa* (5 kg) was collected from Eranakulam district, Kerala, India in March 2017, and identified by the plant taxonomist of MSSRF, Wayanad, Kerala, India and a voucher specimen was deposited in the Herbarium repository of M. S. Swaminadhan Research Foundation, Wayanad, Kerala, India.

3.3.2. Extraction, isolation and characterization of secondary metabolites

The air and oven-dried stem bark of *Ailanthus excelsa* (5 kg) were milled and extracted with ethanol (12 L x 4 times x 72 h) to give 11 g of ethanol extract. Ethanol extract (11 g) was subjected to column chromatographic separation on 100-200 mesh sized silica gel and eluted with the increasing order of *n*-hexane, *n*-hexane- ethyl acetate polarities, ethyl acetate and ethyl acetate-methanol polarity mixtures resulted in 12 fraction pools by analyzing the TLC.

The fraction pool 2 was subjected to column chromatographic separation using 100-200 mesh sized silica gel with *n*-hexane-ethyl acetate polarities resulted in the isolation of compound **20** and compound **21** as colorless amorphous solid. Based on the physical properties and complete analysis of ^{1}H and ^{13}C NMR spectrum, the compound **20** and **21** was identified as *β*-sitosterol and stigmasterol. The structures are shown below.

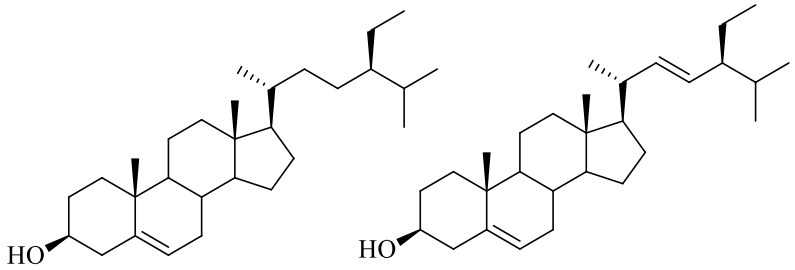

β -Sitosterol **Stigmasterol**

Figure 3.5. Structure of *β*-sitosterol and stigmasterol

The fraction pool 3 was subjected to column chromatographic separation using 100-200 mesh sized silica gel with *n*-hexane-ethyl acetate polarities and again subjected to column chromatographic separation using $CHCl_3$-MeOH polarities resulting in the isolation of compound **22**. Compound **22** was obtained as a colourless amorphous solid and showed a molecular ion peak at m/z 481.3651 $[M+Na]^+$ (calcd. for $C_{31}H_{54}NaO_2$, 481.3658) in the HRESIMS, and the molecular formula was established as $C_{31}H_{54}O_2$. The IR absorptions at 3410 cm^{-1} revealed the presence of a hydroxyl moiety. The ^{1}H NMR

spectrum exhibited eight quaternary methyl signals as singlets at δ_H 1.21, 1.14, 1.12, 1.08, 1.04, 0.99, 0.94 and 0.88 ppm. It further displayed a 1-*H* triplet at δ_H 3.73 (J = 7.5 Hz) ppm indicating the presence of a -OH group attached to the carbon atom (oxymethine). A multiplet integrated for 1H each at δ_H 2.53 - 2.47 ppm and δ_H 2.45 - 2.40 ppm is due to the presence of a -CH_2- group adjacent to –C (-OH)- group. The ^{13}C NMR spectrum of compound **22** displayed the presence of 30 carbon atoms. The DEPT 135 experiment showed the presence of eight -CH_3, ten -CH_2-, and five -CH- groups, and seven quaternary C-atoms. The signal at δ_C 217.1 ppm is due to the presence of -C=O atom. Further the comparision with literature reports [Thanesuan *et al*., **2011**] and the complete analysis of 1D and 2D NMR spectra (**Figure 3.6-11**) the structure of the compound is shown below.

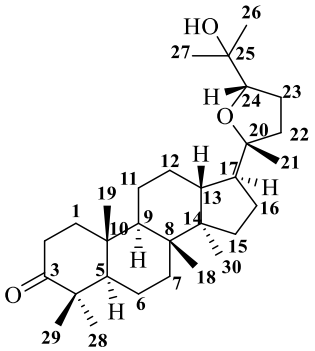

Ocotillone (22)

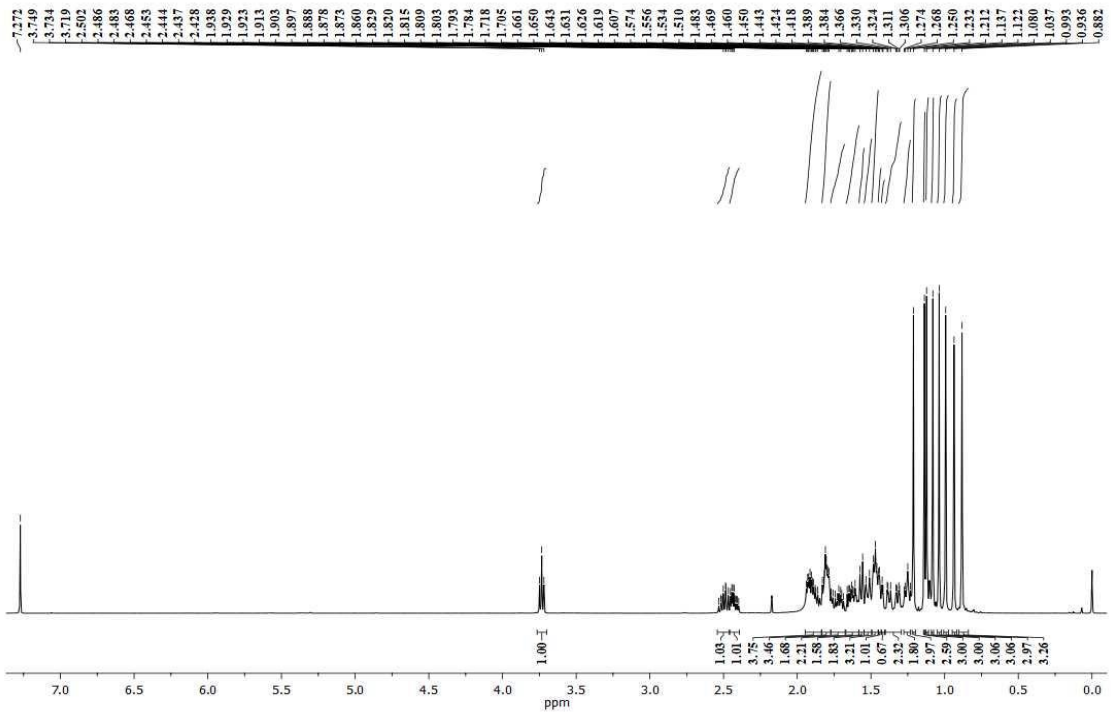

Figure 3.6. ^{1}H NMR spectrum (500 MHz, $CDCl_3$) of ocotillone (**22**)

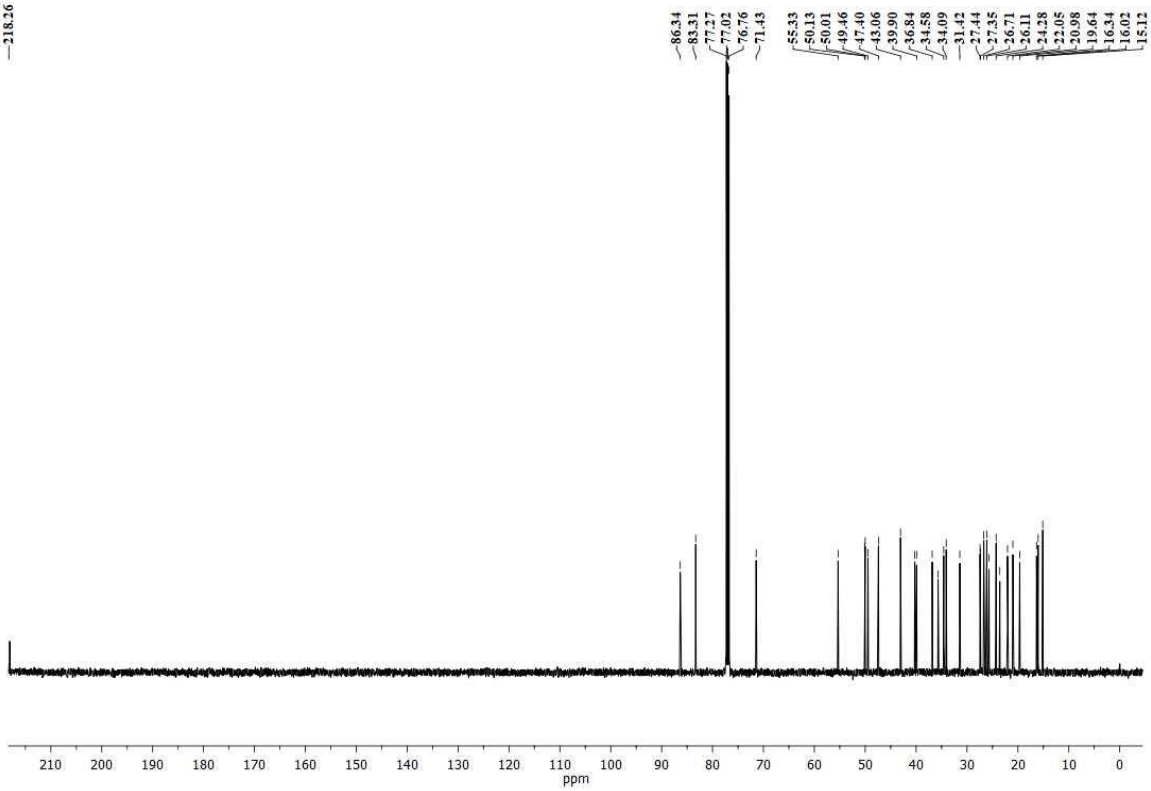

Figure 3.7. ^{13}C NMR spectrum (125 MHz, $CDCl_3$) of ocotillone (**22**)

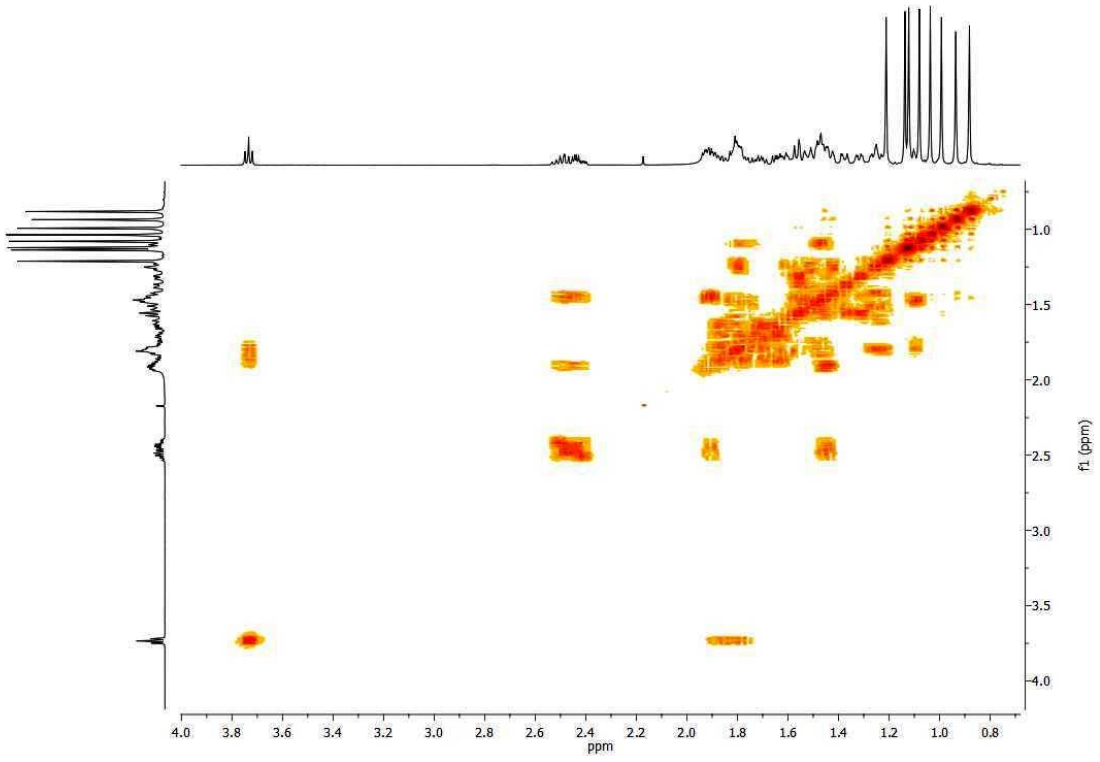

Figure 3.8. ^{1}H-^{1}H COSY NMR spectrum (500 MHz, $CDCl_3$) of ocotillone (**22**)

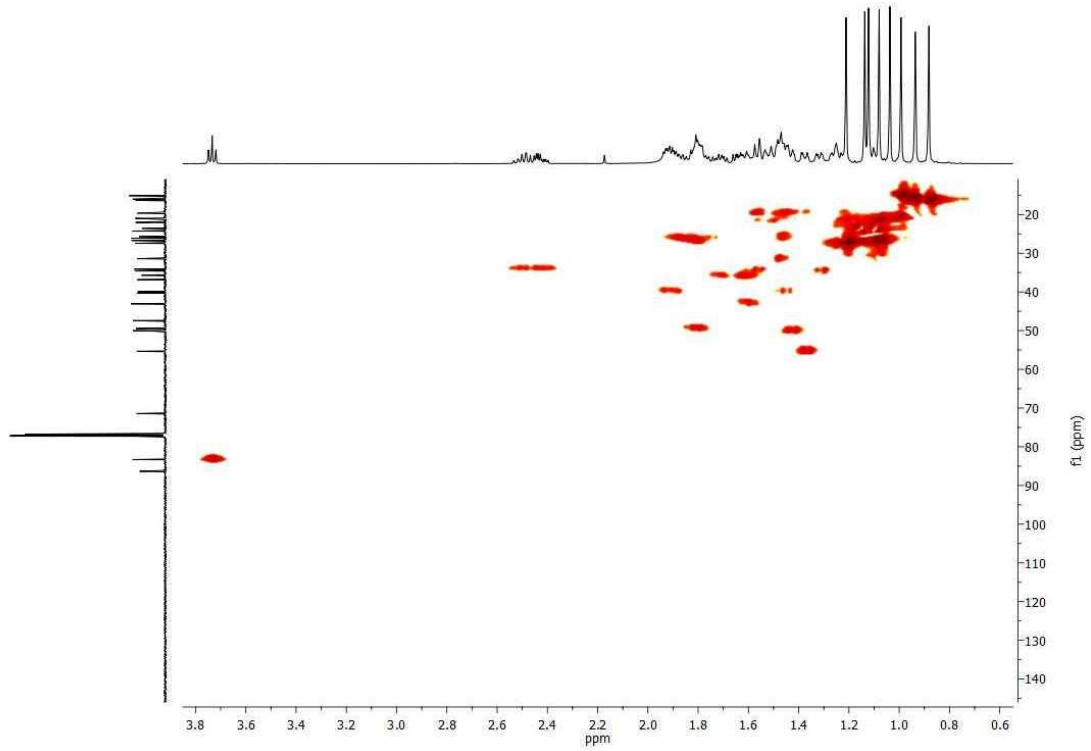

Figure 3.9. HMQC NMR spectrum (125 MHz, $CDCl_3$) of ocotillone (**22**)

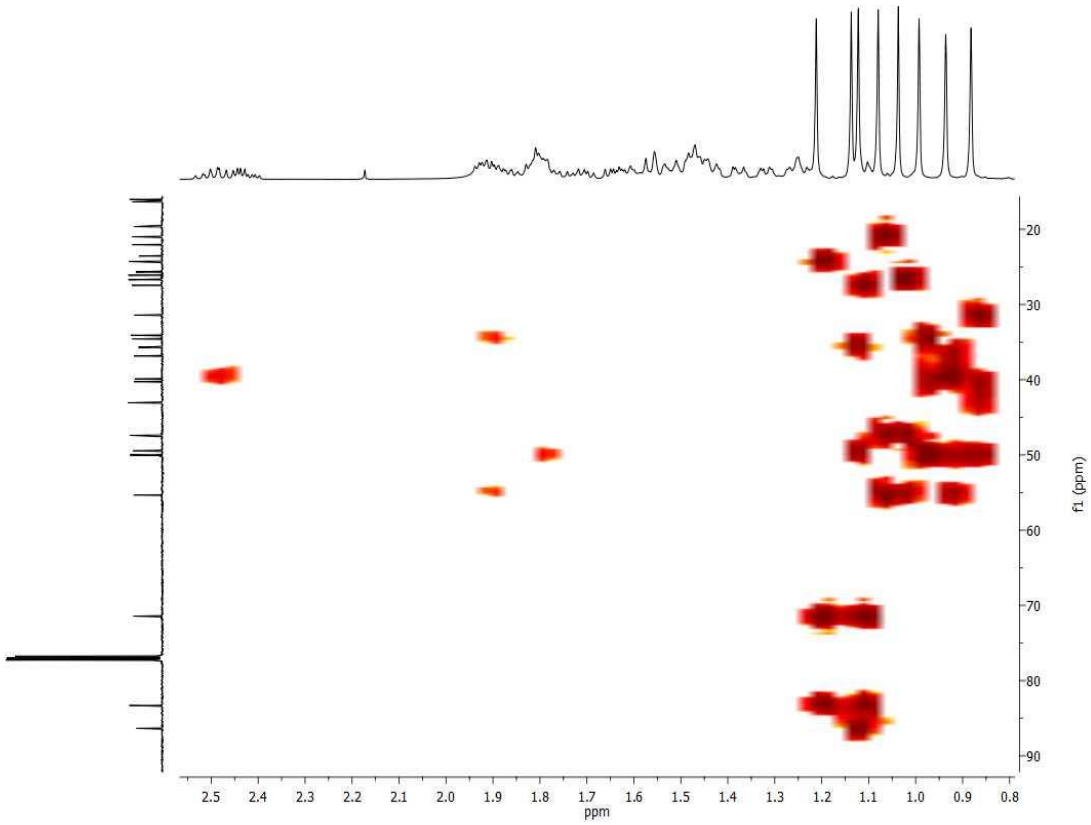

Figure 3.10. HMBC NMR spectrum (125 MHz, $CDCl_3$) of ocotillone (**22**)

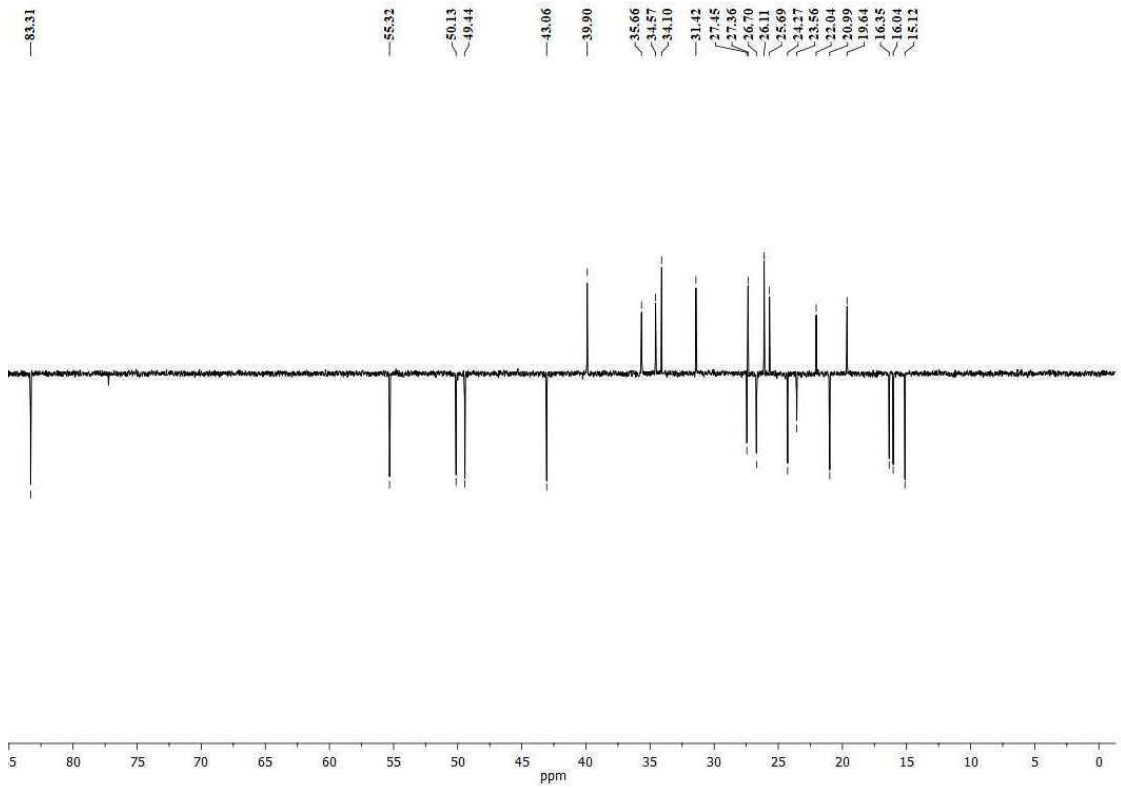

Figure 3.11. DEPT 135 NMR spectrum (125 MHz, $CDCl_3$) of ocotillone (**22**)

Fraction pool 6 was subjected to column chromatographic separation using 100-200 mesh sized silica gel with *n*-hexane-ethyl acetate polarities and again subjected to column chromatographic separation (100-200 mesh) using $CHCl_3$-MeOH polarities leading to the isolation of compound **23**. Compound **23** was obtained as colourless crystals (Mp: 208-210 ^oC). HRESIMS (**Figure 3.19**) indicated a molecular formula of $C_{30}H_{46}O_5$ from the $[M+H]^+$ ion peak at m/z 487.3403 (calcd 487.3423 for $C_{30}H_{47}O_5$),. The IR absorptions at 3325 cm^{-1} revealed the presence of a hydroxyl moiety. The 1D and 2D NMR spectra are shown in **Figure 3.12-18 (Table 3.3).** The ^1H NMR spectrum of compound **23** had resonances due to six methyl groups [δ_H 1.31, 1.25, 1.18, 1.15, 1.13 and 1.09 (s, each 3H) ppm], a cyclopropane ring [δ_H 0.67 (d, J = 4.5 Hz, 1H, H-18a) and 0.54 (d, J = 4.5 Hz, 1H, H-18b) ppm], two olefinic protons conjugated with a carbonyl group [δ_H 7.02 (d, J = 10.5 Hz, 1H, H-1) and 5.81 (d, J = 10 Hz, 1H, H-2) ppm], the oximethine protons [δ_H 3.85 (d, J = 2.5 Hz, 1H, H-7), 3.83-3.81 (m, 1H, H-25) and 3.44 (dd, J_1 = 9 Hz and J_2 = 4 Hz, 1H, H-24) ppm] and the oxymethylene group [δ_H 3.59 (m, 2H, H-21) ppm]. The ^{13}C and DEPT 135 NMR spectra exhibited 30 carbon signals, including one carbonyl [δ_C 205.5 (C-3) ppm], one olefinic carbon [δ_C 159.5 (C-1) and 125.4 (C-2) ppm], six methyls [δ_C 29.7, 27.5, 26.4, 22.3, 21.5 and 20.6 ppm], eight methylenes [δ_C 64.9, 36.9, 27.1, 27.0,

26.2, 24.8, 17.2 and 14.9 ppm], four methines and five quaternary carbons. The key HMBC and NOESY correlations are shown in **Figure 3. 21.** The stereochemistry of compound **23** was determined by analysis of the NOESY spectrum. Furthermore, the correlations between H-9 and H-5, and H-9 and H_2-18 indicated an α-orientation of the cyclopropane ring. The 7-OH moiety was also α-oriented, as confirmed from the NOESY correlations between H-7 and H3-30 and the small coupling constant ($J_{6,7}$ = 2.5 Hz) between H-6 and H-7. The absence of correlation between the proton at H-17 and H-20 indicated that both the protons are in *trans* configuration. Also, the absence of correlation between the proton at H-24 and H-25 in the NOESY spectrum and the higher coupling constant confirmed that both the protons are in *trans* configuration. Finally, X-ray crystallographic analysis (**Figure 3.20**) unambiguously confirmed the structure of compound **23** are shown below. The absolute configuration of compound **23** was established on the basis of optical activity with the value of $[\alpha]^{2}_{5D}$ + 31.6 ^{o}(c, 0.2 DMSO). To the best of our knowledge, there is no reports on this compound and the compound is considered as novel.

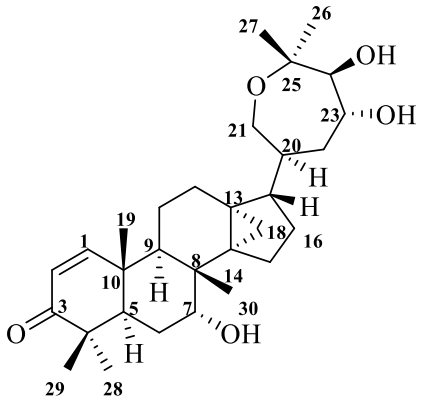

Novel compound (23)

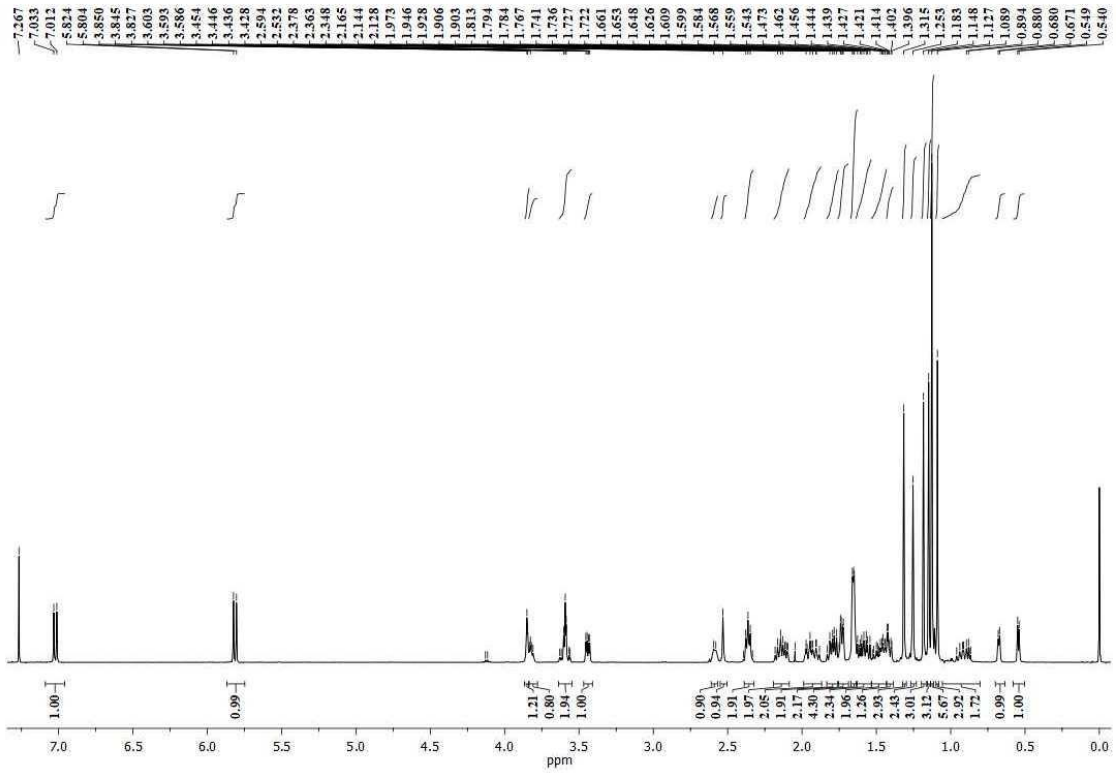

Figure 3.12. ^{1}H NMR spectrum (500 MHz, $CDCl_3$) of novel compound (**23**)

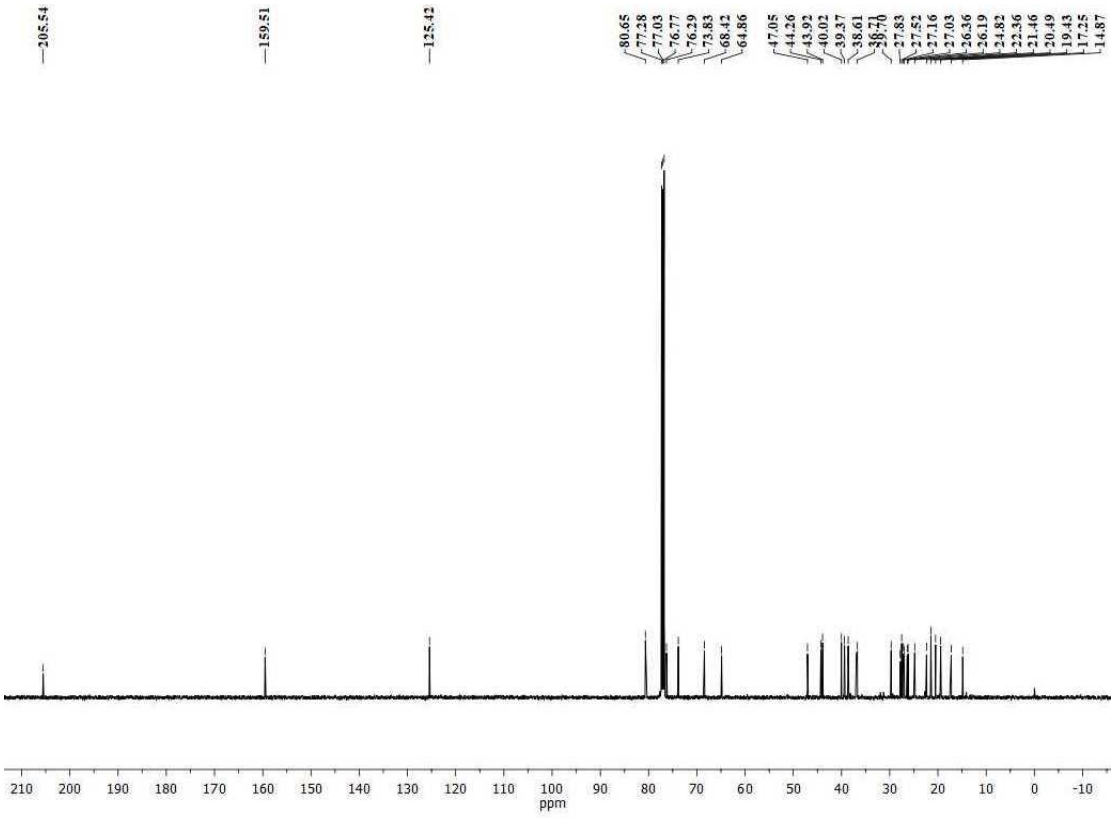

Figure 3.13. ^{13}C NMR spectrum (125 MHz, $CDCl_3$) of novel compound (**23**)

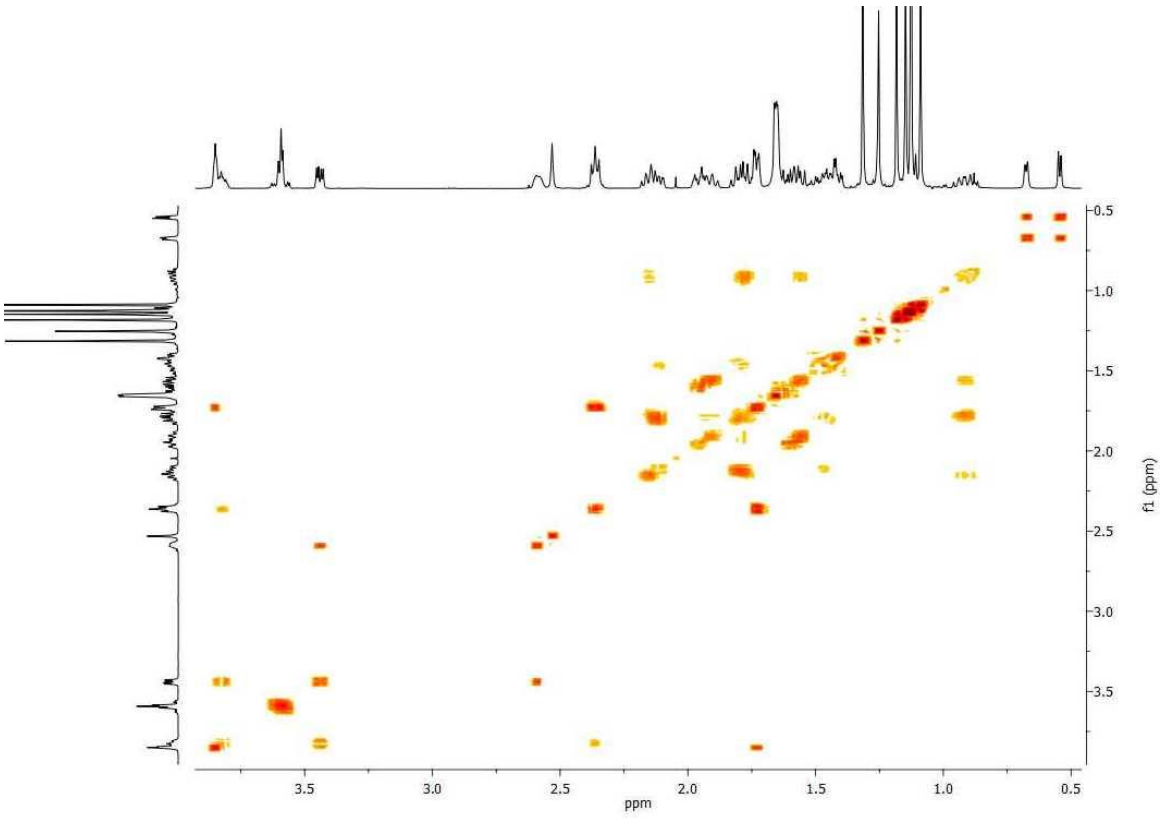

Figure 3.14. ^{1}H-^{1}H COSY NMR spectrum (500 MHz, $CDCl_3$) of novel compound (**23**)

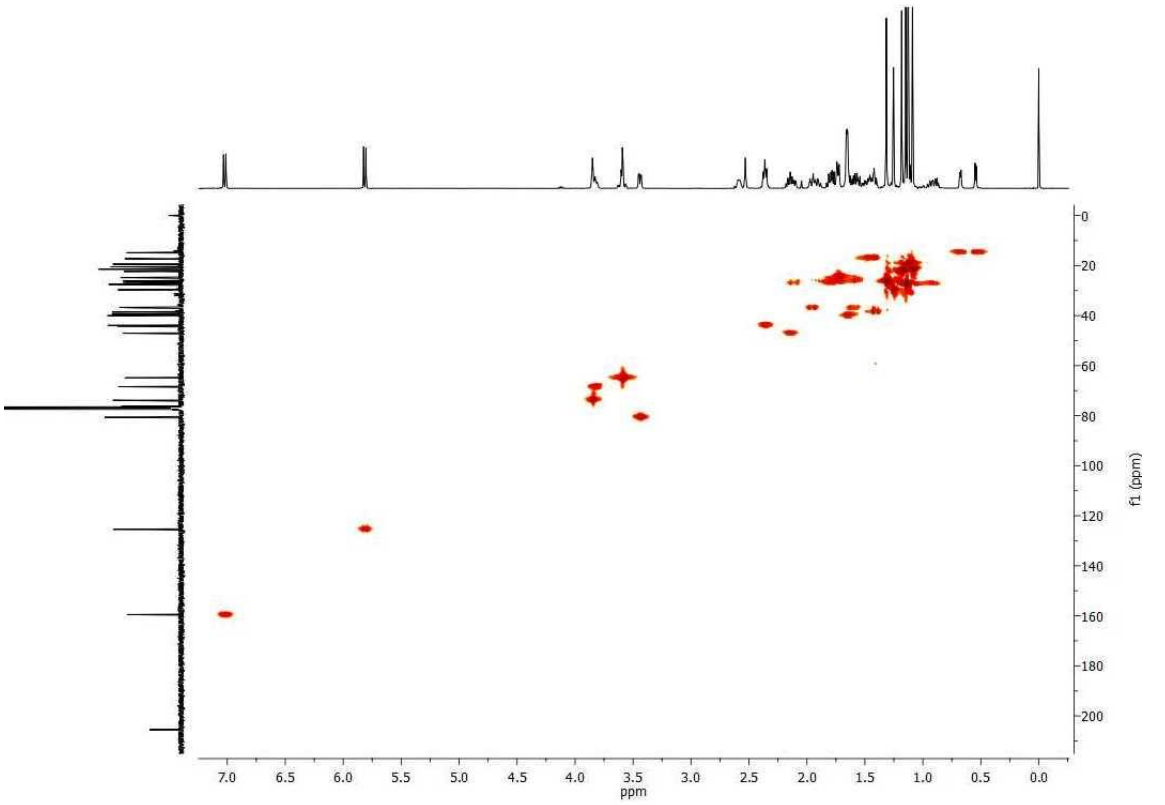

Figure 3.15. HMQC NMR spectrum (125 MHz, $CDCl_3$) of novel compound (**23**)

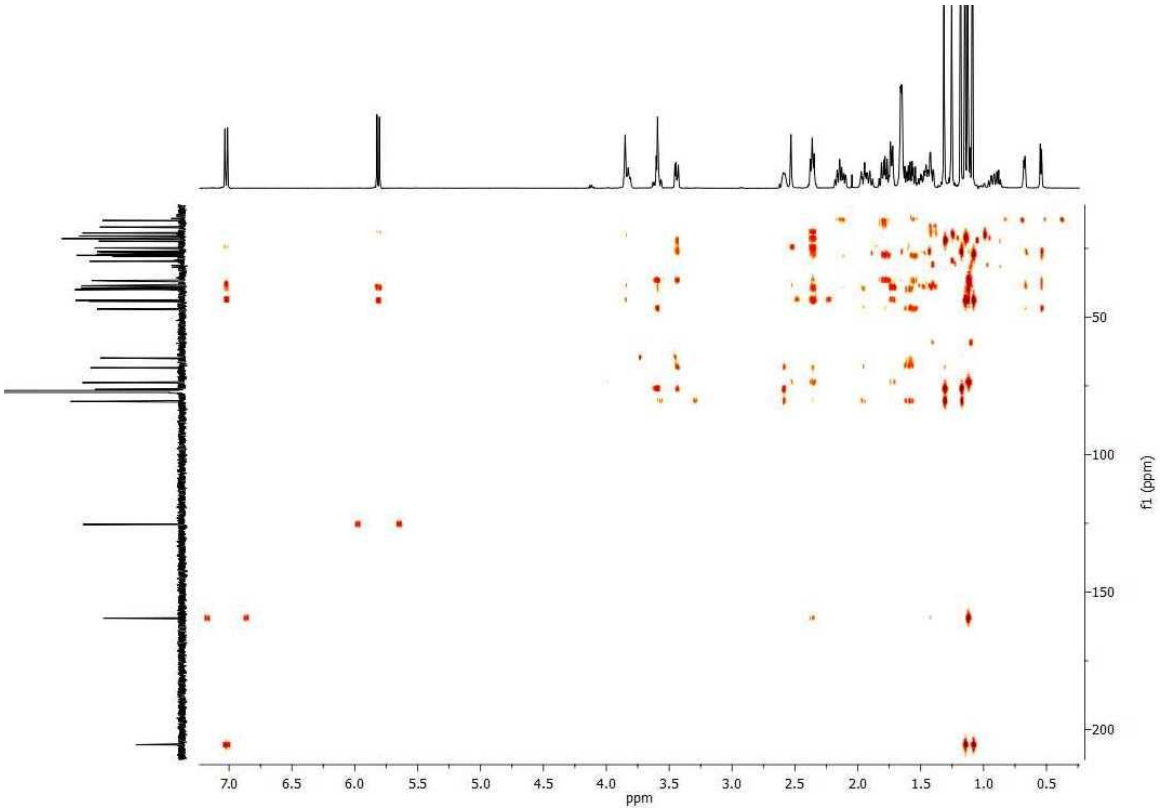

Figure 3.16. HMBC NMR spectrum (125 MHz, $CDCl_3$) of novel compound (**23**)

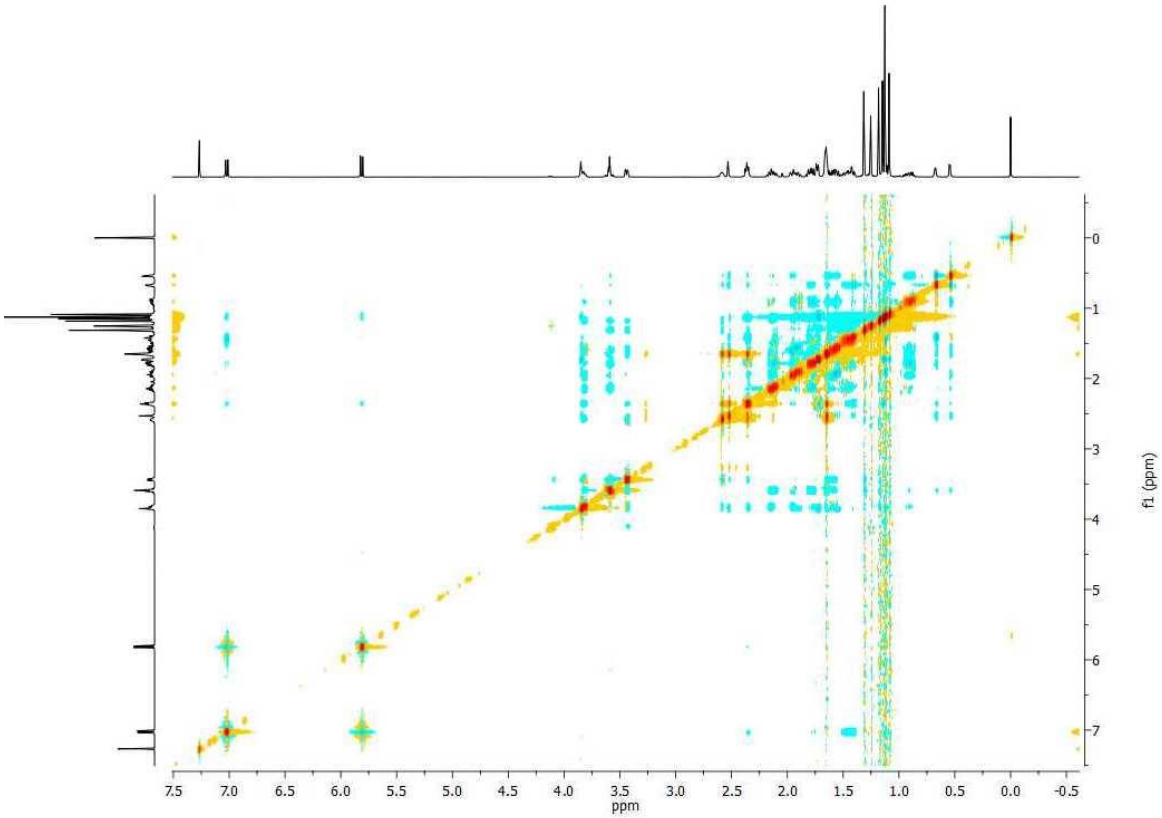

Figure 3.17. NOESY spectrum (500 MHz, $CDCl_3$) of novel compound (**23**)

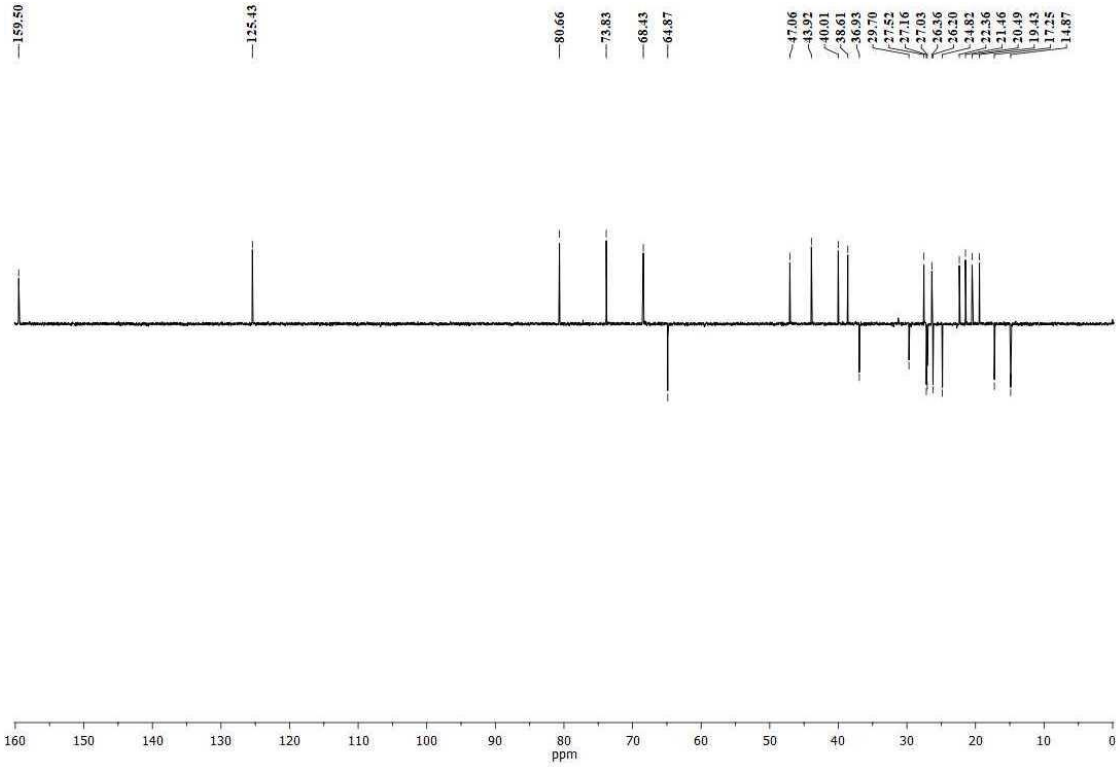

Figure 3.18. DEPT 135 spectrum (125 MHz, $CDCl_3$) of novel compound (**23**)

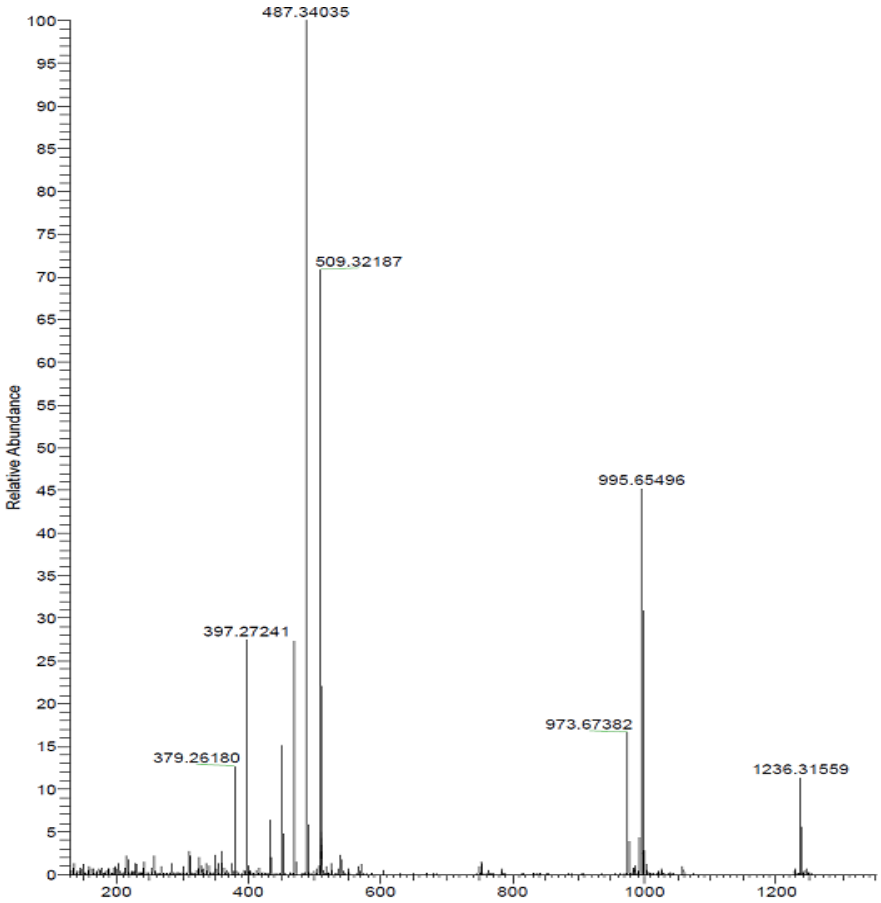

Figure 3.19. HRESIMS spectrum of novel compound (**23**)

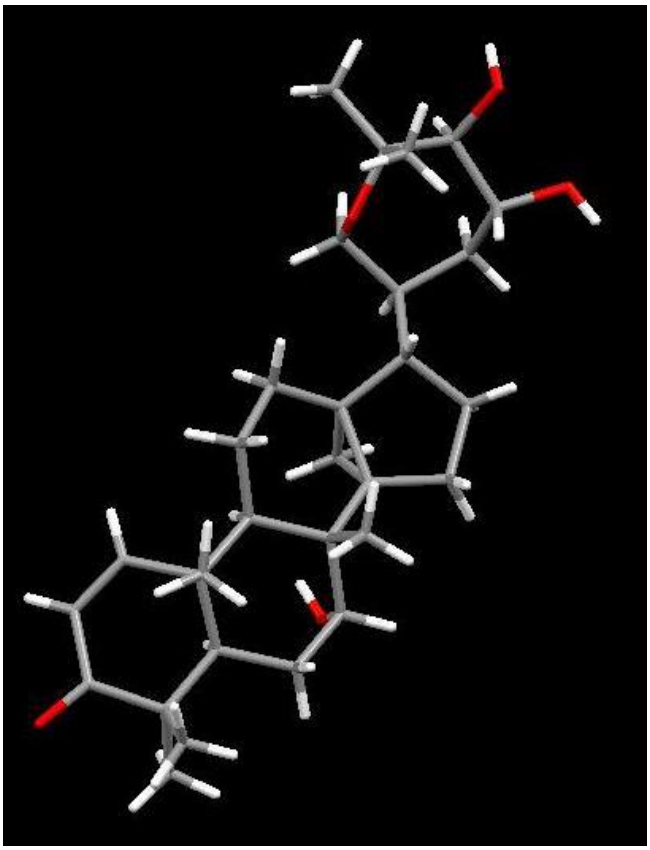

Figure 3.20. Single crystal X-ray analysis of novel compound (**23**)

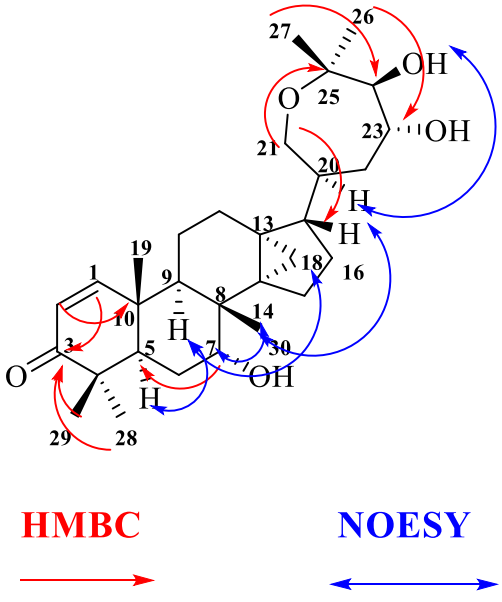

Figure 3.21. The key HMBC and NOESY correlations of novel compound (**23**)

Table 3.3 ^{1}H (500 MHz) and ^{13}C (125 MHz) NMR data of compound **23** in $CDCl_3$

Position	**^{1}H NMR**	**^{13}C NMR**
1	7.02 (d, *J* = 10.5 Hz, 1H)	159.5
2	5.81 (d, *J* = 10.5 Hz, 1H)	125.4
3	-	205.5
4	-	44.3
5	2.36 (t, *J* = 7.5 Hz, 1H)	43.6
6	1.83-1.75 (m, 2H)	24.8
7	3.85 (d, *J* = 2.5 Hz, 1H)	73.8
8	-	39.5
9	1.43-1.40 (m, 1H)	38.6
10	-	39.4
11	1.52-1.44 (m, 2H)	17.3
12	1.83-1.75 (m, 2H)	26.2
13	-	27.8
14	-	36.7
15	2.18-2.09 (m, 2H)	27.0
16	0.96-0.87 (m, 2H)	27.2
17	1.63-1.60 (m, 1H)	26.4
18	0.67 (d, *J* = 4.5 Hz, 1H) 0.54 (d, *J* = 4.5 Hz, 1H)	14.9
19	1.13 (s, 3H)	20.6
20	1.65 (m, 1H)	40.02
21	3.63-3.56 (m, 2H)	64.9
22	1.97-1.88 (m, 2H)	36.9
23	3.44 (dd, J_1 = 9 Hz, J_2 = 4 Hz, IH)	80.6
24	3.83-3.81 (m, 1H)	68.4
25	-	76.3
26	1.31 (s, 3H)	26.4
27	1.25 (s, 3H)	29.7
28	1.15 (s, 3H)	27.5
29	1.09 (s, 3H)	21.5

30	1.13 (s, 3H)	20.6

The fraction pool 6 was subjected to various column chromatographic separation using 100-200 mesh sized silica gel with *n*-hexane-ethyl acetate and $CHCl_3$-MeOH polarities afforded compound **24**. Compound **24** was obtained as colourless amorphous solid (Mp: 222-224 ^oC). The HRESIMS (**Figure 3.29**) data indicated a molecular formula of $C_{30}H_{46}O_5$ from the $[M+H]^+$ ion peak at m/z 487.3403 (calcd 487.3423 for $C_{30}H_{47}O_5$) as same as that of compound **23.** The IR absorptions at 3412 cm^{-1} revealed the presence of a hydroxyl moiety and 1721 cm^{-1} indicated the presence of carbonyl moety. The 1D and 2D NMR spectra are shown in **Figure 3.22-28 (Table 3.4).** The ^1H NMR spectrum of compound **24** exhibited the presence of six methyl groups [δ_H 1.34, 1.31, 1.16, 1.15, 1.13 and 1.09 (s, each 3H) ppm], a cyclopropane ring [δ_H 0.69 ppm (d, J = 5 Hz, 1H, H-18a) and 0.51 (d, J = 5 Hz, 1H, H-18b) ppm], two olefinic protons conjugated with a carbonyl group [δ_H 7.02 (d, J = 10.5 Hz, 1H, H-1) and 5.82 (d, J = 10 Hz, 1H, H-2)], the oximethine protons [δ_H 3.88 (m, 1H, H-7), 3.86 (m, 1H, H-25) and 3.21 (d, J = 2.5 Hz, 1H, H-24) ppm] and the oxymethylene group [δ_H 4.10 (d, J = 12 Hz, 1H) and 3.44 (dd, J_1 = 12 Hz and J_2 = 2 Hz) ppm]. The ^{13}C and DEPT 135 NMR spectra exhibited 30 carbon signals, including one carbonyl [δ_C 205.5 (C-3) ppm], one olefinic carbon [δ_C 159.4 (C-1) and 125.5 (C-2) ppm], six methyls [δ_C 28.7, 28.3, 27.5, 26.2, 24.0 and 21.5 ppm], eight methylenes [δ_C 70.7, 36.4, 28.2(2), 26.2, 24.8, 17.3 and 14.7 ppm], four methines and five quaternary carbons. The key HMBC and NOESY correlations are shown in **Figure 3.30**. The stereochemistry of compound **24** was established with the help of the NOESY spectrum. Moreover, the correlations between H-9 and H-5, and H-9 and H_2-18 indicated an α-orientation of the cyclopropane ring. The 7-OH group was also α-oriented, as deduced from the NOESY correlations between H-7 and H3-30 and the small coupling constant ($J_{6,7}$= 2.5 Hz) between H-6 and H-7. The absence of correlation between the proton at H-17 and H-20 indicated that both the protons are in *trans* configuration. Also, the absence of correlation between the proton at H-24 and H-25 in the NOESY spectrum and the higher coupling constant confirmed that both the protons are in *trans* configuration. The noticeable differences of compound **23** from compound **24** is the position of oxymethylene group. In compound **23**, the oxymethylene group is in position C-23 and in compound **24**, the oxymethylene group is in position C-25. The absolute configuration of compound **24** was established on the basis of optical activity with the

value of $[\alpha]^{2}_{5D}$ + 11.3 ^{o}(c, 0.2 DMSO).This was confirmed from the 1D and 2D NMR spectra. To the best of our knowledge, there is no report on this compound and the compound **24** is also considered as a novel molecule and the structure of compound **24** is shown below.

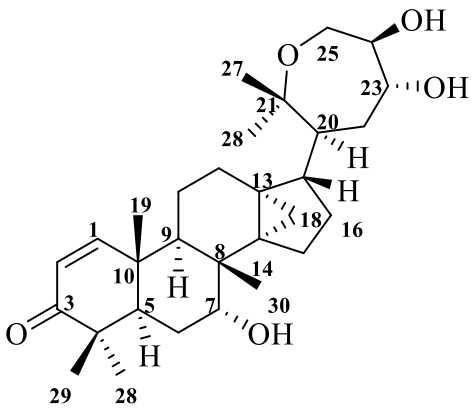

Novel compound (24)

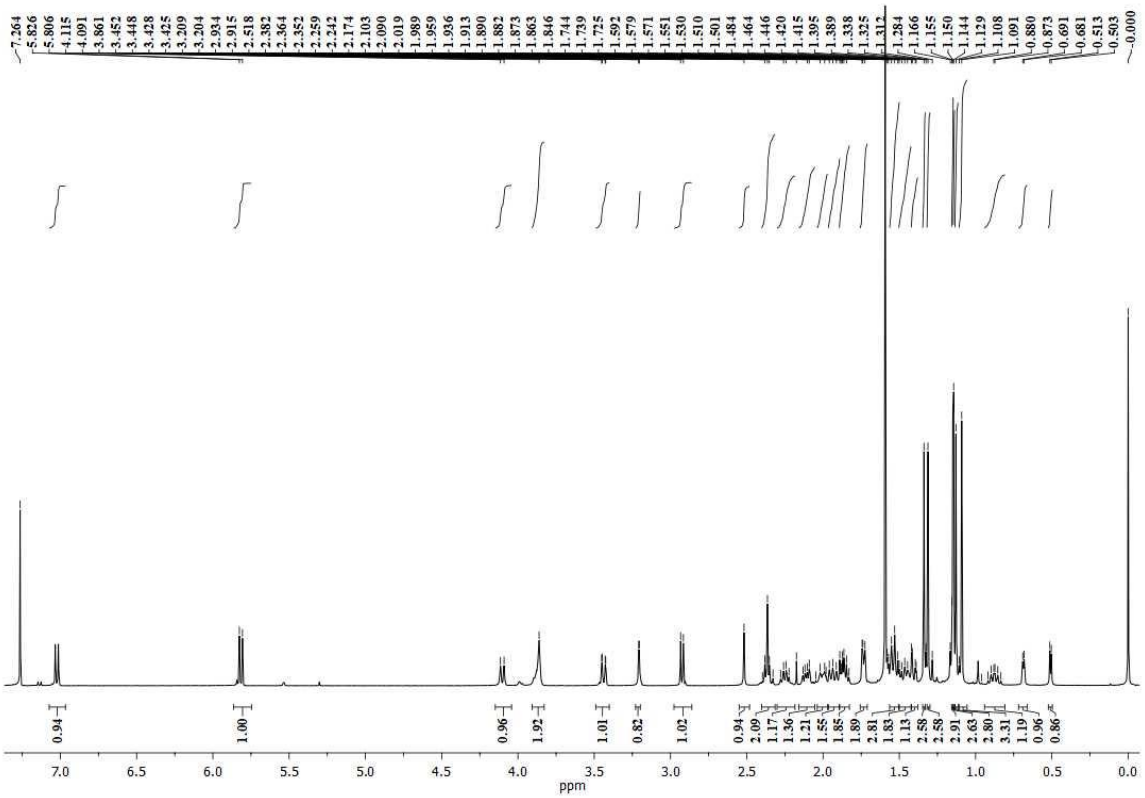

Figure 3.22. ^{1}H NMR spectrum (500 MHz, $CDCl_3$) of novel compound (**24**)

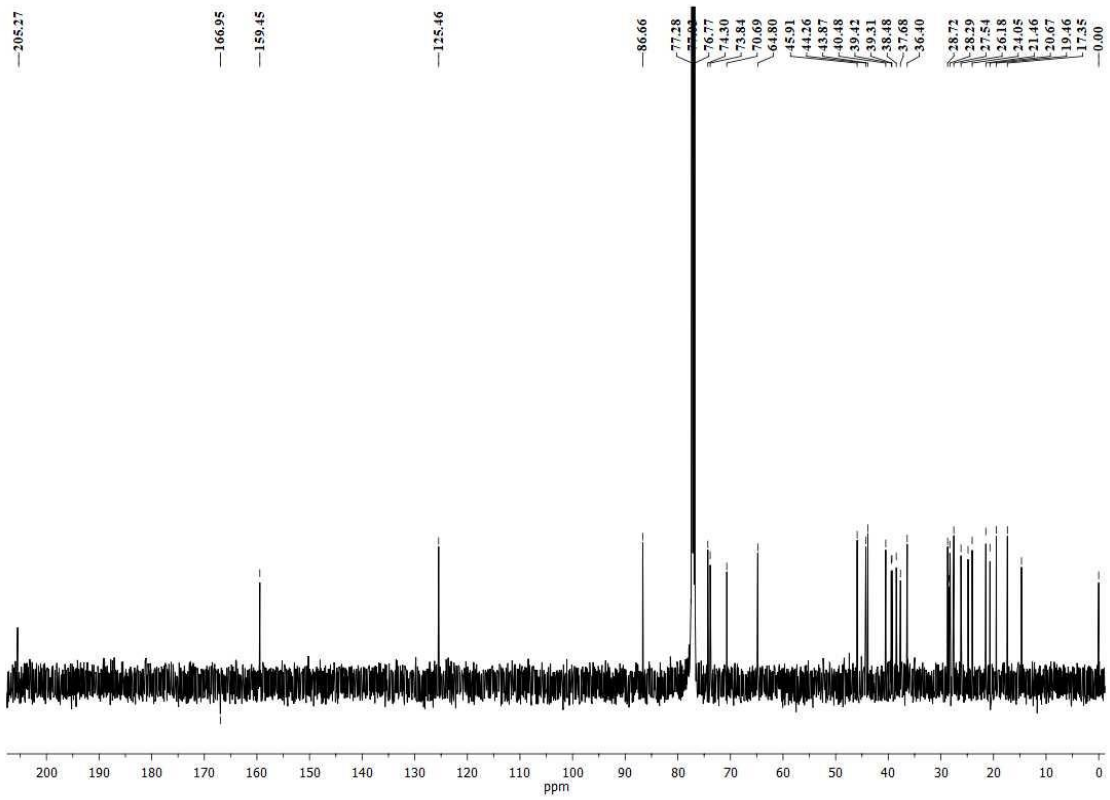

Figure 3.23. ^{13}C NMR spectrum (125 MHz, $CDCl_3$) of novel compound (**24**)

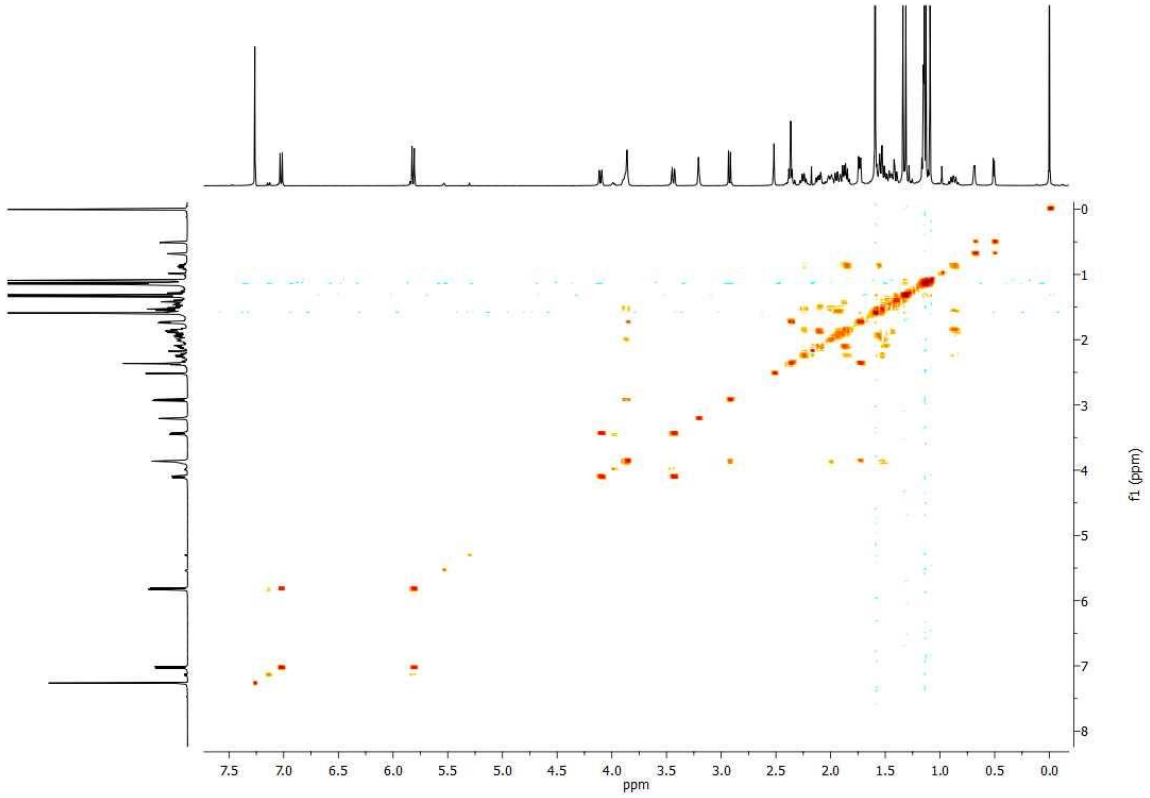

Figure 3.24. ^{1}H-^{1}H COSY NMR spectrum (500 MHz, $CDCl_3$) of novel compound (**24**)

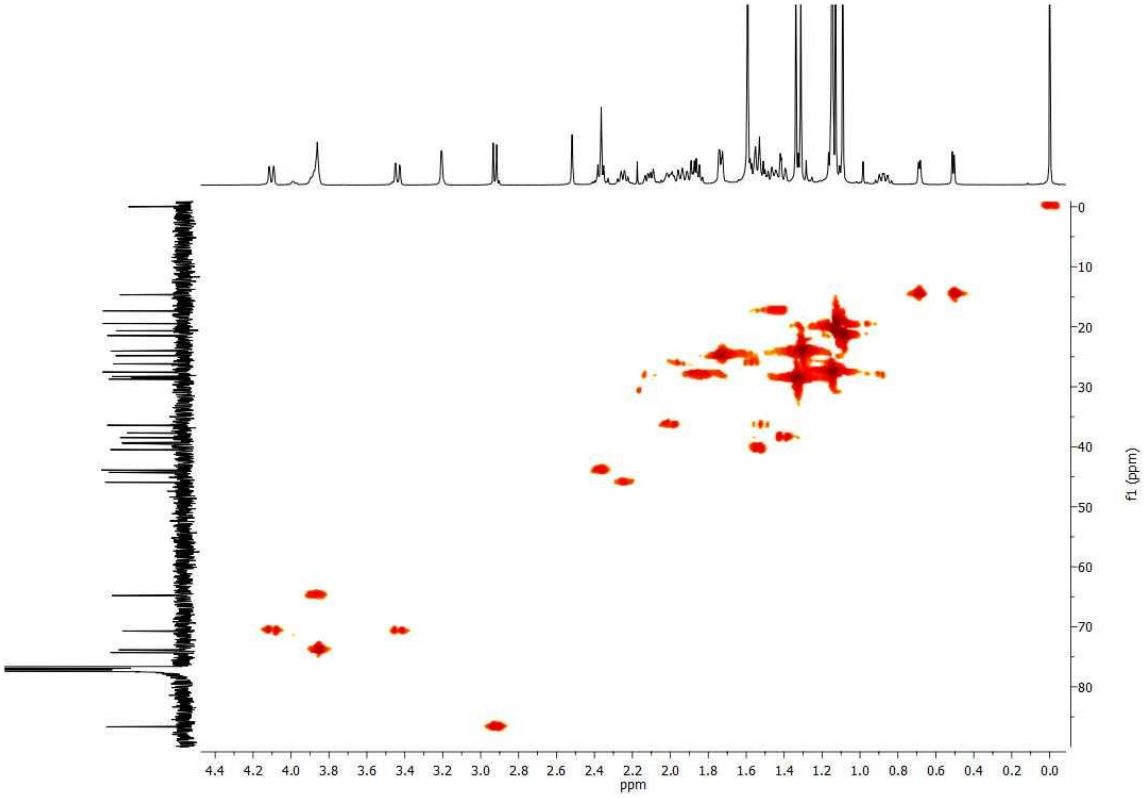

Figure 3.25. HMQC NMR spectrum (125 MHz, $CDCl_3$) of novel compound (**24**)

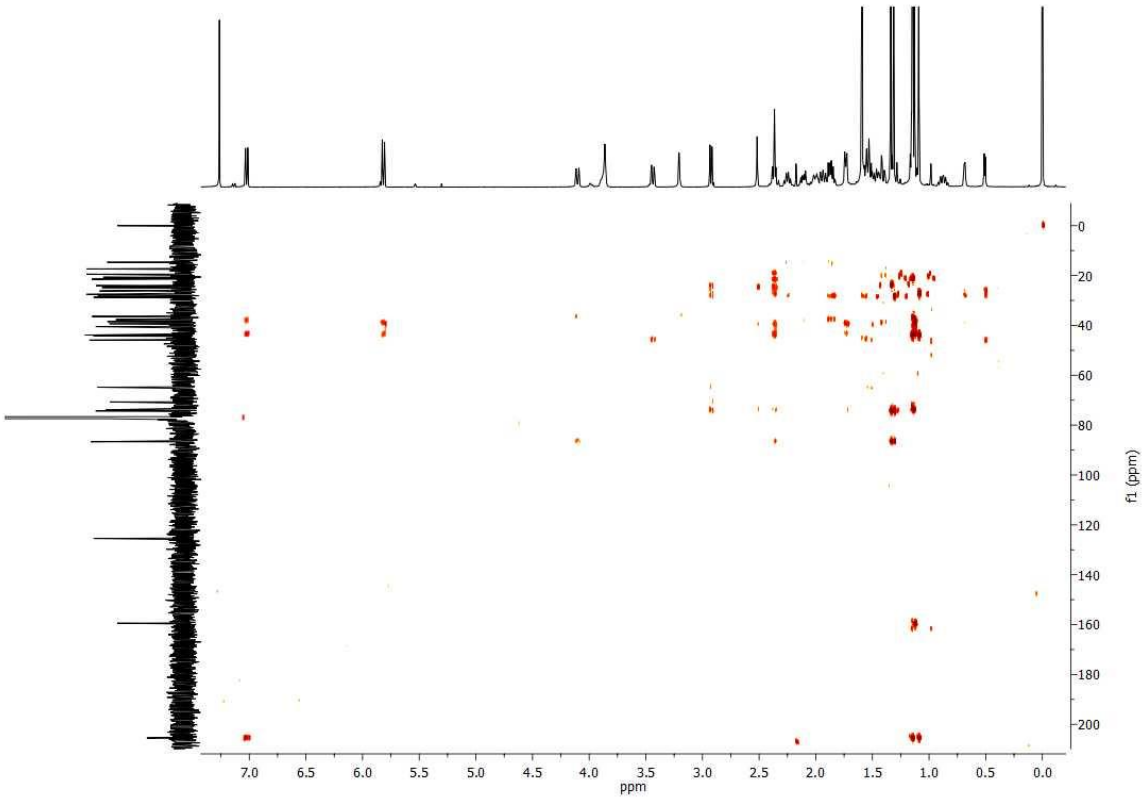

Figure 3.26. HMBC spectrum (125 MHz, $CDCl_3$) of novel compound (**24**)

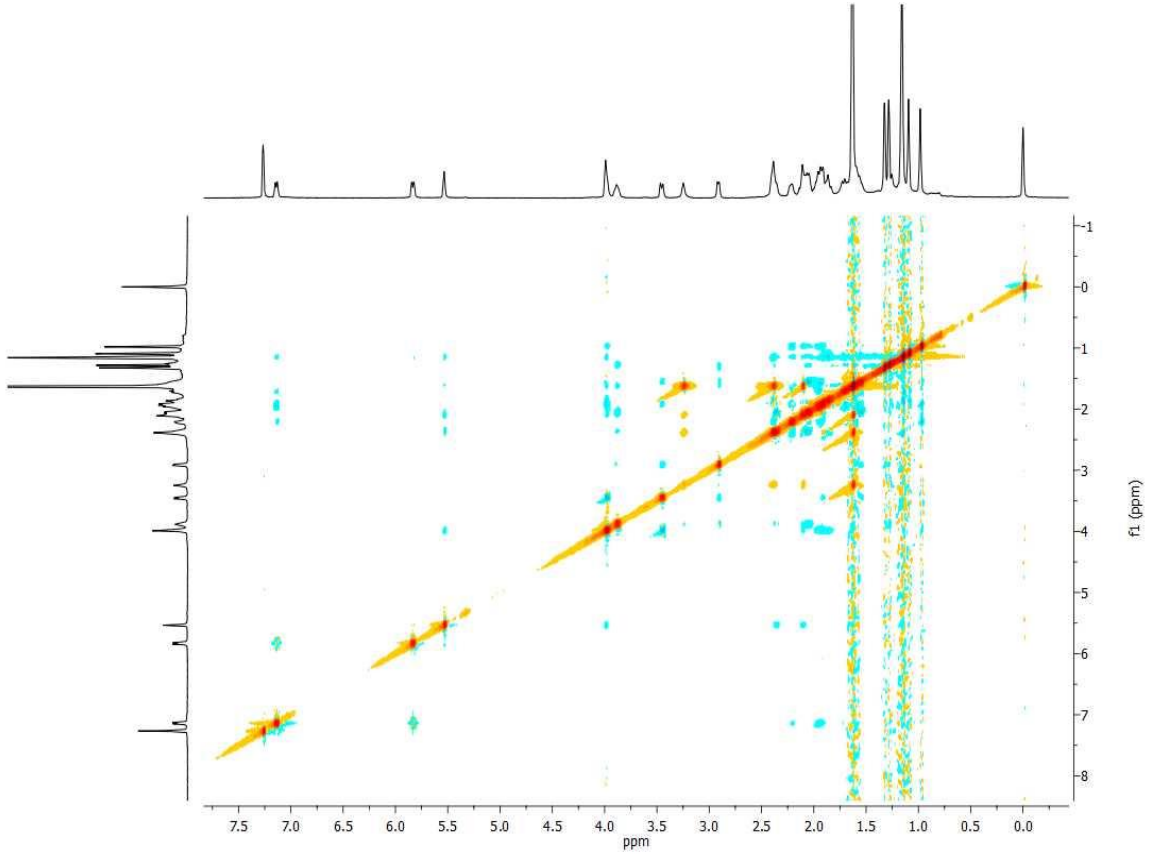

Figure 3.27. NOESY spectrum (500 MHz, $CDCl_3$) of novel compound (**24**)

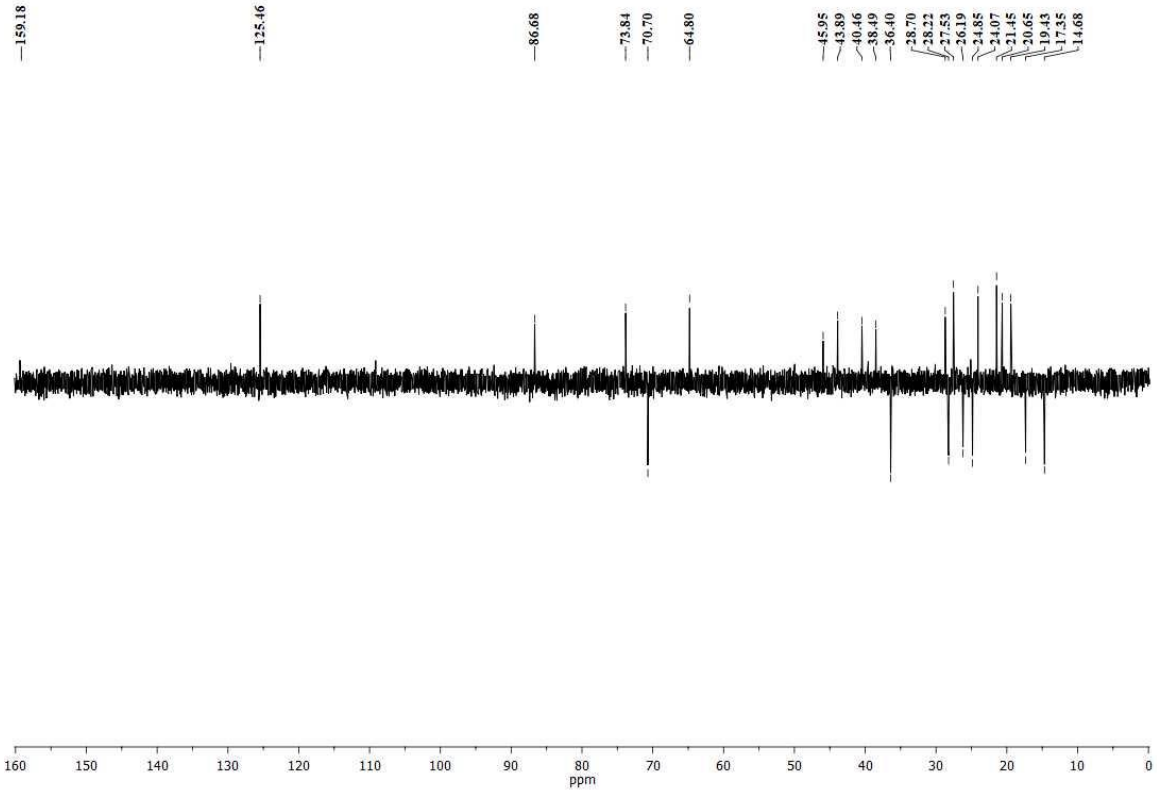

Figure 3.28. DEPT 135 spectrum (125 MHz, $CDCl_3$) of novel compound (**24**)

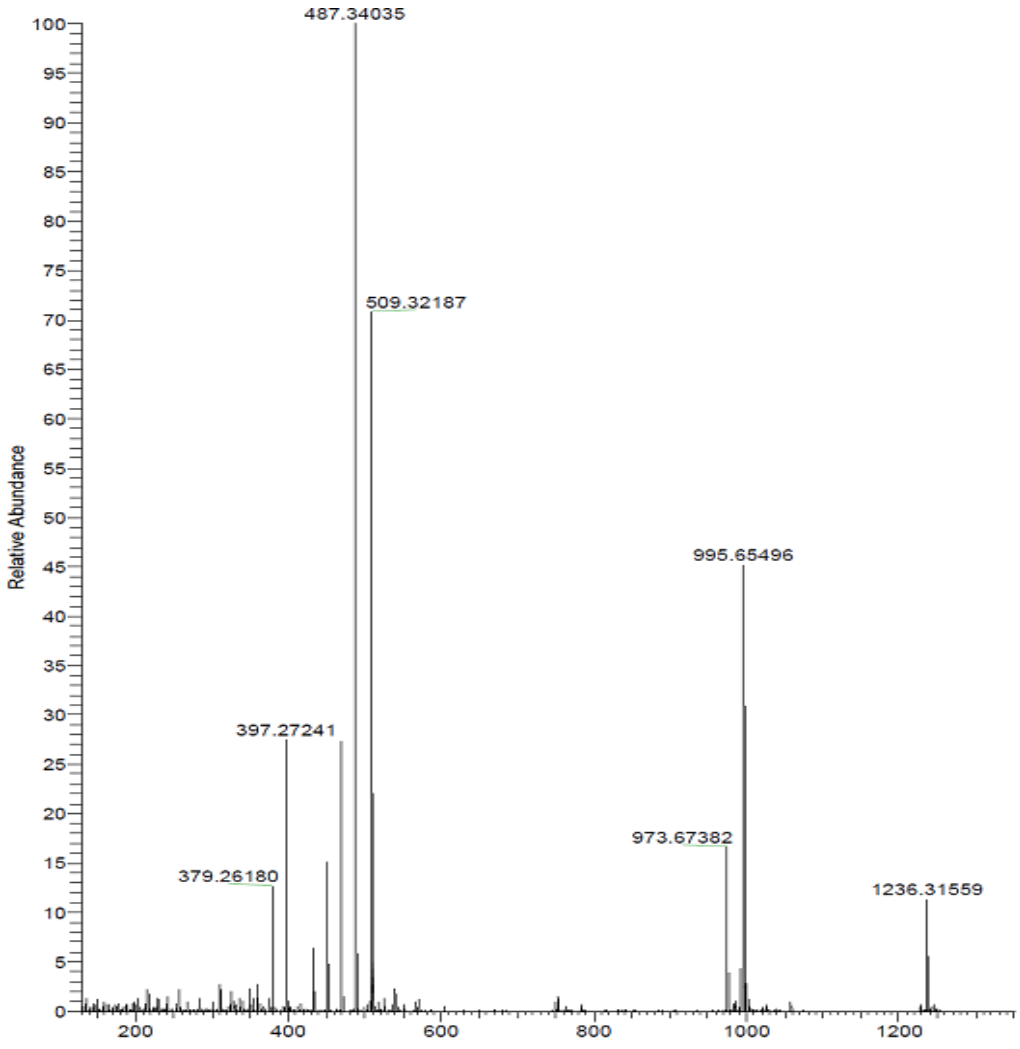

Figure 3.29. HRESIMS spectrum of novel compound (**24**)

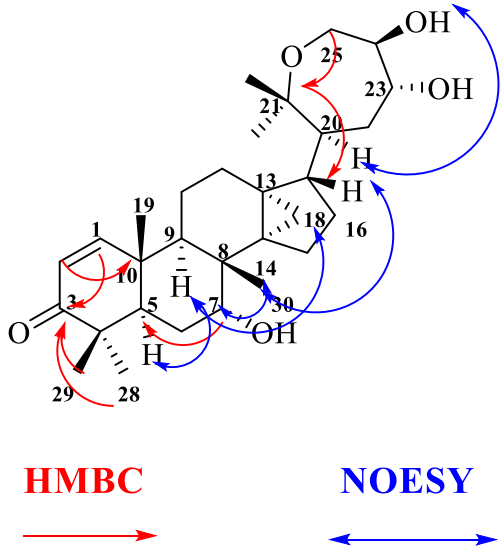

Figure 3.30. Single crystal X-ray analysis of novel compound (**23**)

Table 3.4. ^{1}H (500 MHz) and ^{13}C (125 MHz) NMR data of compound **24** in $CDCl_3$

Position	^{1}H NMR	^{13}C NMR
1	7.02 (d, *J* = 10 Hz, 1H)	159.4
2	5.81 (d, *J* = 10 Hz, 1H)	125.5
3	-	205.3
4	-	44.3
5	2.36 (t, *J* = 9 Hz, 1H)	43.9
6	1.74-1.72 (m, 2H)	24.8
7	3.86 (m, 1H, mergered)	73.8
8	-	39.4
9	1.40 (dd, J_1 = 12.5 Hz, J_2 = 2.5 Hz, 1H)	38.5
10	-	39.4
11	1.57 (m, 2H)	17.3
12	1.94 (m, 2H)	26.2
13	-	28.5
14	-	37.7
15	2.13-2.09 (m, 1H) 0.92-0.83 (m, 1H)	28.2
16	2.13-2.09 (m, 1H) 0.92-0.83 (m, 1H)	28.2
18	0.69 (d, *J* = 5 Hz, 1H) 0.51 (d, *J* = 5 Hz, 1H)	14.7
19	1.13 (s, 3H)	19.5
20	-	74.3
21	2.05-1.98 (m, 1H)	36.4
22	2.97 (d, *J* = 9.5 Hz, 1H)	86.7
23	3.90-3.86 (m, 1H)	64.7
24	2.92 (d, *J* = 9.5 Hz, 1H)	86.7
25	4.10 (d, *J* = 12 Hz, 1H) 3.44 (dd, J_1 = 12 Hz, J_2 = 2 Hz, 1H)	70.7
26	1.34 (s, 3H)	28.7
27	1.31 (s, 3H)	24.0

28	1.15 (s, 3H)	27.5
29	1.09 (s, 3H)	21.5
30	1.14 (s, 3H)	20.7

Compounds **25** and **26** were isolated from fraction pool 11, in 10 and 27 mg, as a colorless solid with a melting point of 314-316 ^{o}C and 258-260 ^{o}C respectively. After the careful analysis of NMR and HRESIMS and in comparison with literature reports, the structures of the molecules were confirmed as *β*-sitosterol-*β*-D-glucoside and stigmasterol-*β*-D-glucoside. The structures of the molecules are shown below.

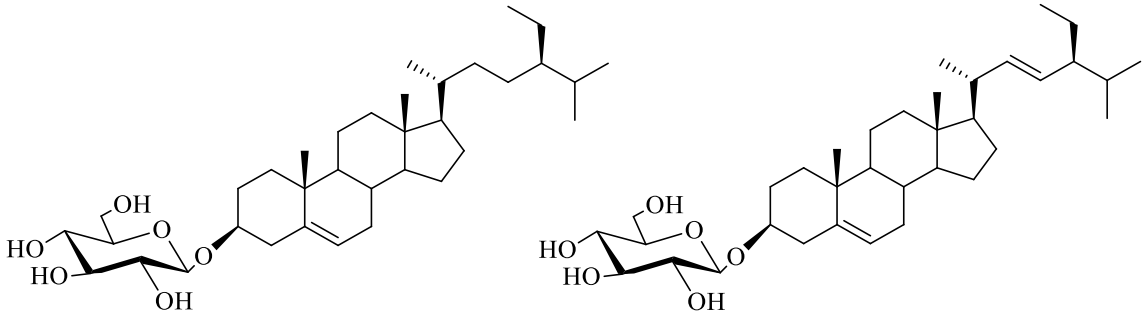

***β* -Sitosterol-*β* -D- glucoside** **Stigmasterol -*β* -D- glucoside**

3.4. Antiinflammatory activity of phytochemicals isolated from *Ailanthus excelsa*

Inflammation is a host response to injury related to chemical or microbiological toxins that leads to the release of a large amount of inflammatory mediators. Macrophages play a key role in the process of inflammation in many different tissues. Lipopolysaccharide (LPS) is a potent initiators of inflammation derived from the outer membrane of gram negative bacteria and it can activates several signaling pathways including inhibitory κB (IκB)/nuclear factor-κB (NF-κB) and mitogen-activated protein kinases (MAPKs) by acting on toll-like receptor (TLR) 4 to induce the expression of inflammatory genes and the release of antiinflammatory mediators such as nitric oxide (NO), tumor necrosis factor-*α* (TNF-*α*), and interleukin-6 (IL-6) [Guha *et al*., **2001**]. NO is a reactive oxygen species and can act as a cytotoxic agent in various pathological processes, particularly in inflammatory disorders [Alderton *et al*., **2001**]. TNF-*α* and IL-6 are crucial pro-inflammatory cytokines which are involved in a variety of immune responses leading to inflammation [Delgado *et al*., **2003**]. In the past few decades, many researchers have reported that natural products are the rich sources of anti-inflammatory drug leads. In the present study, we have examined the effect of phytochemicals isolated

from the stem bark of *Ailanthus excelsa* on inflammatory responses *in vitro*, and determined the underlying mechanism of the action of compound **23** in LPS-stimulated RAW 264.7 macrophages. The compounds chosen for anti-inflammatory study are shown in **Figure 3. 31.**

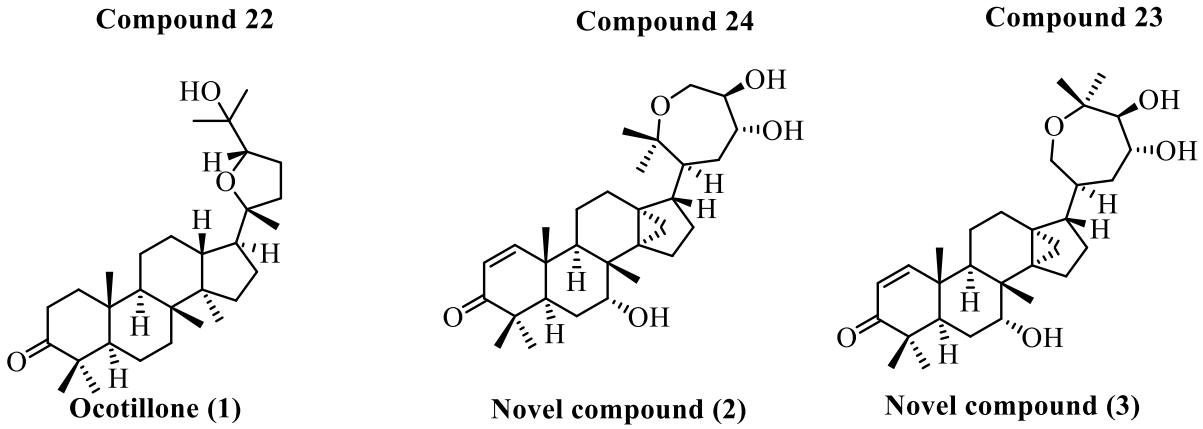

Figure 3. 31. The compounds chosen for anti-inflammatory study

3.4.1. Cytotoxic effects of compounds 1-3 on RAW 264.7 macrophages

Cytotoxic effects of compounds **1-3** in RAW 264.7 macrophages were determined by tetrazolium salt 3-[4, 5-dimethylthiazol-2-yl]-2, 5-bromide (MTT) assay. Cells were treated with different concentrations (1 μM, 5 μM, 10 μM, 25 μM, 50 μM and 100 μM) of compounds **1-3**. From the **Figure 3. 22**., it is clear that compound **3** showed less toxicity in 2.5 μM and 10 μM concentrations. Therefore, 2.5 μM and 10 μM concentrations of compound **3** was taken for further studies.

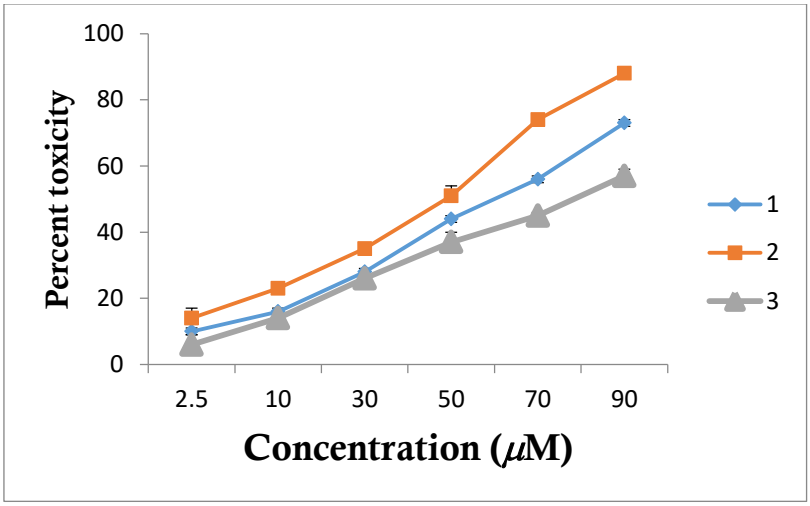

Figure 3.32. Cytotoxic effect of compounds **22-24** in RAW 264.7 macrophages

3.4.2. NO production in LPS-stimulated RAW 264.7 macrophages

Nitric oxide (NO) plays an important role in host defense response against various pathogens. Under normal physiological conditions, NO regulates various pathophysiological processes such as neuronal communication, vasodilatation, and neurotoxicity [Moncada *et al*., **1991**, Nakagawa *et al*., **2002**]. However, overproduction of NO induces tissue damage associated with inflammations [Taira *et al*., **2009**]. Therefore, more attention is now being paid to the development of new drug leads as potent inhibitors of NO production in relation to the treatment of inflammatory diseases [Pacher *et al*., **2007**]. Macrophages are key components of the mammalian immune system, and play a significant role by providing an immediate defense against foreign agents [Moncada *et al*., **1991**]. Lipopolysaccharide (LPS) is a component from the cell walls of gram-negative bacteria and one of the most powerful activators of macrophages. LPS is involved in the production of pro-inflammatory cytokines and widely known as a stimulator of NO production [Nicholas *et al*., 2007]. Hence, inhibition of NO production in lipopolysaccharide (LPS)-stimulated RAW 264.7 macrophages is one of the possible ways to screen various anti-inflammatory drug leads. In the present study, we investigated the effects of compound **5** in LPS-induced RAW 264.7 cells. The level of NO in cell supernatants was determined using Griess reagent. The concentration of NO produced was determined based on a sodium nitrite standard calibration curve. The result showed that NO production remarkably increased in LPS- stimulated RAW 264.7 cells. Cells pre-treated with compound **3** exhibited a significant inhibition in NO production (**Figure 3.33**).

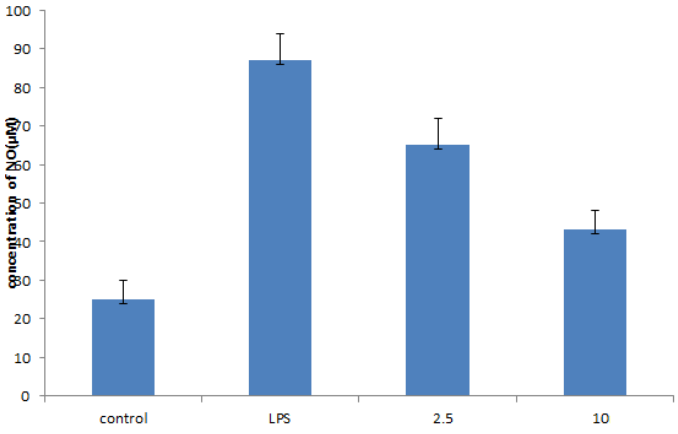

Figure 3.33. Effect of 2.5 μM and 10 μM concentrations of compound **3** on NO production in LPS-stimulated RAW 264.7 cell lines. RAW 264.7 cells were stimulated with 1 μg/mL of LPS. Values are mean of three replicate determinations

(n = 3) ± standard deviation. Bars having different letters are significantly different (P < 0.05).

3.4.3. TNF-α, IL-6, LOX-1, COX-2 and IL10 production in LPS-stimulated RAW 264.7 cell lines

Tumor necrosis factor-α (TNF-α) is a serum factor capable of causing tumor necrosis and is known as a potent immune regulator. TNF-α have multiple regulatory effects; for example, this molecule is believed to mediate the host inflammatory response through its biological effects on various cell types. IL-6 acts as pro-inflammatory mediator and anti-inflammatory cytokine, and can initiate synthesis of prostaglandin E_2. IL-10 produced by Th2 cells, macrophages and CD8+ cell clones and is capable of inhibiting the synthesis of several cytokines from different cells, antigen or mitogen activated. Lectin-like ox-LDL receptor (LOX-1) is one of type II membrane protein, mainly found in endothelial cells and which belongs to the *C*-type lectin family. It consists of a short *N*-terminal cytoplasmic domain, a trans-membrane domain and a *C*-terminal hydrophobic domain. LOX-1 can be induced by lots of pathological stimulus and is expressed in monocytes, platelets, smooth muscle cells, and macrophages. According to the study of Honjo *et al*., LOX-1 inhibition can decrease the inflammatory response, and plays an important role in inflammation [Honjo *et al*., **2003**]. One of the key steps in inflammation is the activation of a cyclooxygenases (COX), which is responsible for production of several inflammatory mediators from arachidonic acid. The two isoforms of cyclooxygenase enzymes are COX-1 and COX-2. The main function of COX-1 is the synthesis of prostaglandins, which is responsible for maintaining normal body function in kidney, gastrointestinal tract and other organs. COX-2 is mainly induced during inflammation. Classical non-steroidal anti-inflammatory drugs (NSAIDs) such as aspirin, diclofenac and indomethacin inhibit both COX isoforms leading to effective antiinflammatory response. But they have some side effects which includes gastric ulceration and kidney damage. Several efforts are on-going in various laboratories for the search of novel COX-2 inhibitors with fewer side effects.

Herein, we investigated the effects of compound **3** on LPS-induced TNF-α, IL-6, LOX-1, COX-2 and IL-10 production in LPS-induced RAW 264.7 cells. Proinflammatory mediators like TNF-α, IL-6, LOX-1 and COX-2 were found to be decreased in RAW 264.7 cells in a dose dependent manner, when compared with LPS control. It is also noted that antiinflammatory cytokine IL-10 was found to be increased

in cell treated with compound **3** when compared with LPS control in a dose dependent manner (**Figure 3.34)**.

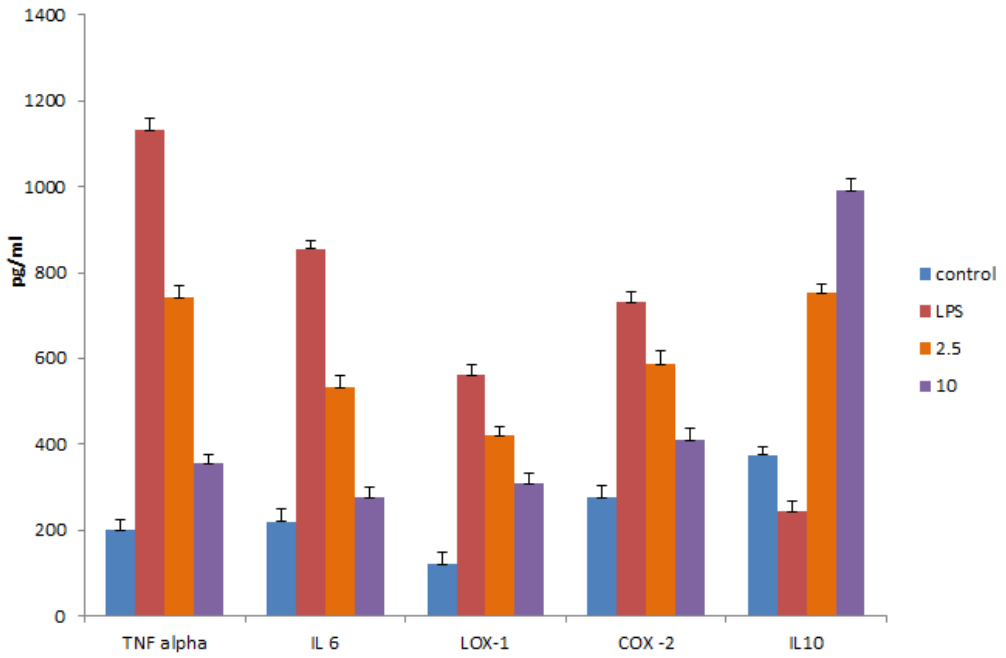

Figure 3.34. Effect of 2.5 μM and 10 μM concentrations of compound **3** on TNF-α, IL-6, LOX-1, COX-2 and IL10 production in LPS-stimulated RAW 264.7 cell lines. RAW 264.7 cells were stimulated with 1 μg/mL of LPS. Values are mean of three replicate determinations (n = 3) ± standard deviation. Bars having different letters are significantly different ($P < 0.05$).

3.4.4. Compound 3 inhibited NF-κB expression in LPS-stimulated RAW 264.7 macrophages

Nuclear factor-κB (NF-κB) is a key transcriptional factor involved in immune and inflammatory responses. Upon activation by external stimuli such as TNF-α and LPS, the IκB protein is phosphorylated and degraded, and translocated into the nucleus. Translocated NF-κB interacts with κB elements in the promoter region of various inflammatory genes, leading to the transcription of pro-inflammatory mediators and cytokines. Thus, NF-κB has been regarded as the key molecular target in development of therapies for inflammatory diseases. We herein demonstrated that compound **3** can inhibited NF-κB production in a dose dependent manner in LPS induced RAW cells (**Figure 3.35**).

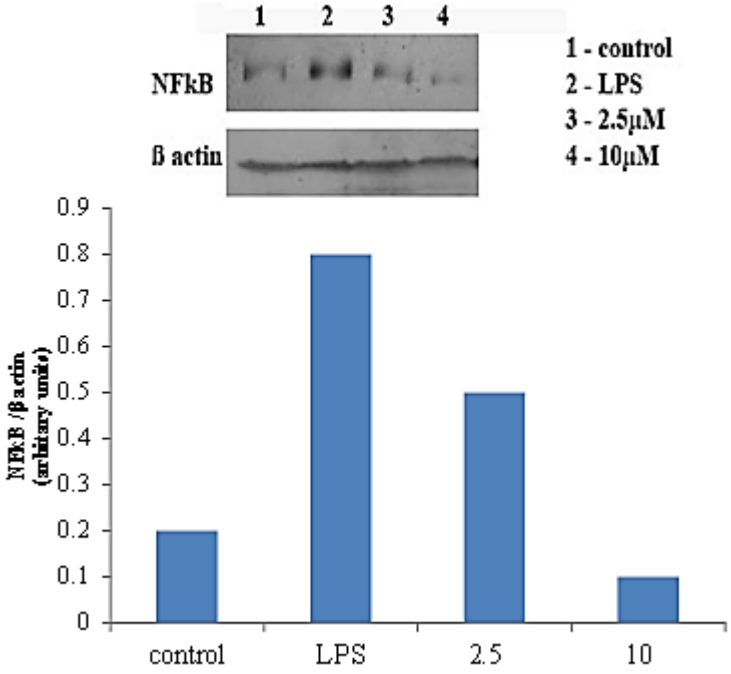

Figure 3.35. Expression level of 2.5 μM and 10 μM concentrations of compound **3** on NF-κB production

3.5. Conclusion

Herein, we have discussed the phytochemical investigation and anti-inflammatory activity of the stem bark of *Ailanthus excelsa*. *Ailanthus excelsa* or "Plant of Heaven" is a deciduous tree that belongs to Simaroubaceae family and is commonly known as Mahanimba and Maharukha. The name '*Ailanthus excelsa*' is derived from two words; *ailanto* which means 'tree of heaven' and *excelsa* which means 'tall'. *Ailanthus excelsa* is a fast growing tree extensively cultivated in many parts of India, towards the vicinity of villages. The ethanol extract was subjected to repeated column chromatographic purifications and resulted in the isolation of **7** compounds. It include two novel molecules (**23**) and (**24**), along with five known compounds. In the present study, we have investigated the anti-inflammatory activity of compounds; ocotillone **(22), 23** and **24.** Among these, compound (**23**) was less toxic in RAW 264.7 macrophages. Compound **23** inhibited the action of pro-inflammatory mediators like NO, TNF-α, IL-6, LOX-1 and COX-2 and promoted the action of anti-inflammatory mediator IL 10 *via* inhibition of NF-κB pathway in LPS-stimulated RAW 264.7 macrophages. These findings provided information on the mechanism of the anti-inflammatory action of compound 2**3** from

Ailanthus excelsa. Further studies on the biological effects of compound 2**3** are warranted in the future.

3.6. Experimental

3.6.1. General experimental procedures and chemicals

The melting points were performed on a Buchi melting point apparatus. The FTIR spectra were achieved using Bruker FT-IR spectrometer, and values are acquired in cm^{-1}. NMR spectra was acquired from Bruker Avance 500 MHz, using $CDCl_3$ as solvents and the chemical shifts are expressed in δ (ppm) relative to the tetramethylsilane peak. The multiplicities of NMR signals were assigned as singlet (s), doublet (d), triplet (t), multiplet (m), and broad singlet (brs). The HRESIMS data was recorded at 60,000 resolution using Thermo Scientific Exactive mass spectrometer. Column chromatography was done using silica gel (100−200 and 230−400 mesh; Merck, Darmstadt, Germany). Merck precoated silica gel F_{254} plates were used for thin-layer chromatography (TLC). Spots were detected on TLC under UV light or by heating after spraying samples with anisaldehyde-sulfuric acid.

3.6.2. Plant material, extraction and isolation procedure

The stem bark of *Ailanthus excelsa* was collected from Eranakulam District, Kerala, India. The stem bark was thoroughly cleaned, cut into small pieces, air dried and then dried in drier maintained at 50 ^{o}C and powereded. The powdered stem bark (5 kg) was subjected to extraction using ethanol (10 L x 3 times x 72 h) at room temperature. After extraction, the solvent was removed under reduced pressure using Büchi rotary evaporator and the temperature of the rotary evaporator was maintained at 50 ^{o}C. The crude extract (11 g) was then subjected to silica gel (100-200 mesh) column chromatography using *n*-hexane, *n*-hexane-EtOAc gradient, EtOAc, EtOAc-methanol gradient and methanol. Thirteen fractions of 200 mL each were collected and concentrated under reduced pressure and the temperature was maintained at 50 ^{o}C. The schematic representation of extraction and isolation procedure was shown in **Figure 3.36.**

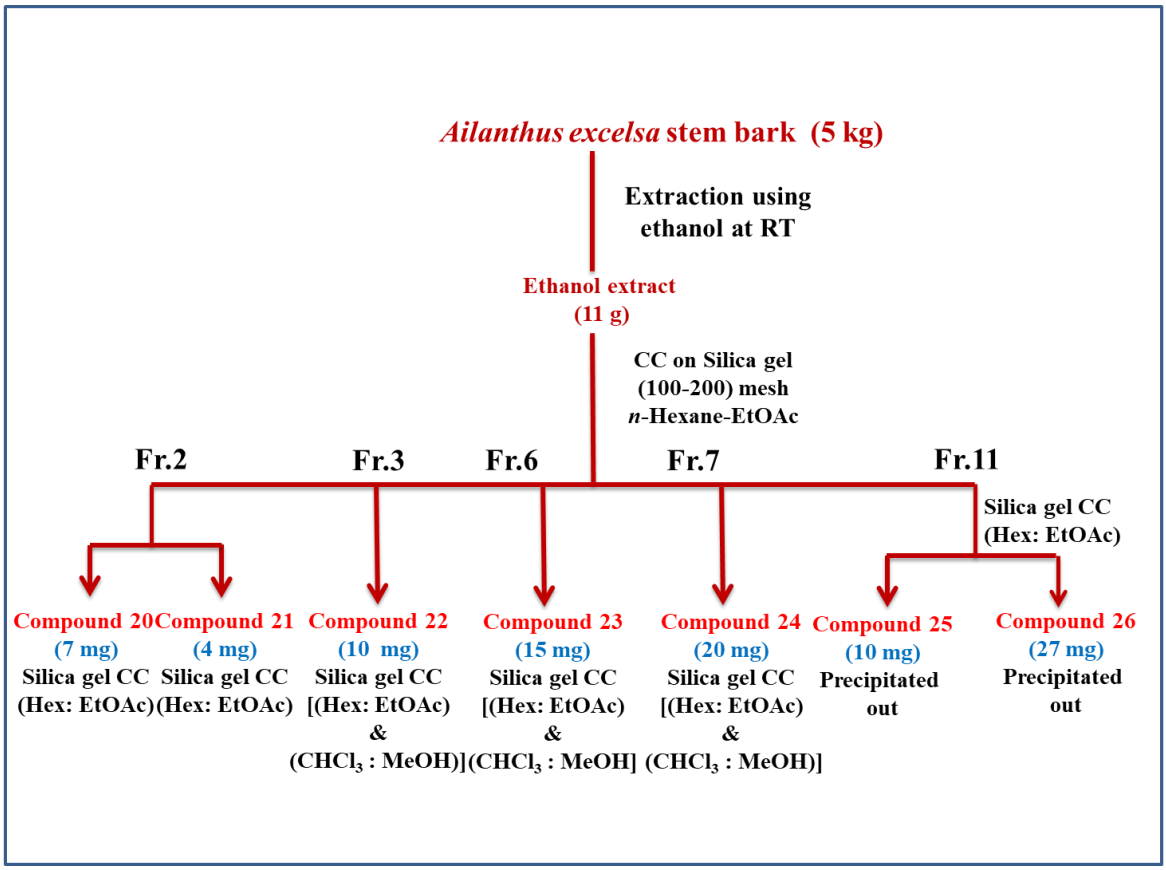

Figure 3.36. The schematic representation of extraction and isolation procedure of stem bark of *Ailanthus excelsa*

3.6.2.1. Isolation of compound 22

Compound **22** (10 mg) was obtained as a colourless solid from the fraction pool 3, on eluting the column (silica gel 100-200 mesh) with 5 % EtOAc in *n*-hexane. The detailed analysis of IR, ^{1}H, ^{13}C, ^{1}H-^{1}H COSY, HMQC, DEPT 135, HMBC NMR spectra and HRESIMS gave compound **22** as ocotillone.

Nature	Colourless amorphous solid
FTIR (KBr, υ_{max})	3430, 2922, 1710, 1464, 1368, 1045 cm^{-1}
^{1}H NMR (500 MHz, $CDCl_3$)	δ 3.73 (t, J = 7.5 Hz, 1H, H24), 2.53-2.47 (m, 1H, H-2), 2.45-2.40 (m, 1H, H-2), 1.94-1.80 (m, 4H), 1.83-1.78 (m, 3H), 1.77-1.69 (m, 2H), 1.66-1.61 (m, 2H), 1.57-1.56 (m, 2H), 1.55-1.50 (m, 2H), 1.48-1.44 (m, 3H), 1.42 (d, J = 3 Hz, 1H), 1.39-1.31 (m, 2H), 1.27-1.23

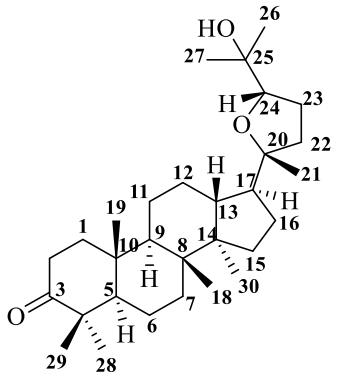

Ocotillone (22)

	(m, 2H), 1.21 (s, 3H, Me), 1.14 (s, 3H, Me), 1.12 (s, 3H, Me), 1.08 (s, 3H, Me), 1.04 (s, 3H, Me), 0.99 (s, 3H, Me), 0.94 (s, 3H, Me), 0.88 (s, 3H, Me) ppm.
^{13}C NMR (125 MHz, $CDCl_3$)	δ 218.3 (C-3), 86.3 (C-24), 83.3 (C-20), 71.4 (C-25), 55.3 (C-5), 50.1 (C-17), 50.0 (C-14), 49.5 (C-9), 47.4 (C-4), 43.1 (C-13), 40.3 (C-8), 39.9 (C-1), 36.8 (C-10), 35.7, 34.6 (C-22), 34.1, 31.4, 27.4 (C-27), 27.3 (C-21), 26.7 (C-28), 26.1 (C-23), 25.7 (C-12), 24.3 (C-26), 23.5, 22.0, 21.0 (C-29), 19.6 (C-6), 16.3, 16.0 (C-18), 15.1 (C-19) ppm.
HRESIMS (m/z)	481.3651

3.6.3. Cell culture and treatment conditions

RAW 264.7 macrophages were procured from NCCS, Pune, India and were maintained in DMEM containing 10 % FBS and 1 % antibiotic–antimycotic mix at 37 °C in humidified air containing 5 % CO_2.

3.6.4. Cytotoxicity assay

Cytotoxicity was assessed by MTT assay. The cells were maintained at 37 ^{o}C in 5 % CO_2 incubator. They were trypsinized and seeded in 24 well plates, treated with different concentrations of the compounds **1-3** (1 μM, 5 μM, 10 μM, 25 μM, 50 μM and 100 μM) for 24 h. After the incubation, cells were treated with MTT reagent (0.5 g/L) for 4 h. Mitochondrial dehydrogenase enzyme is active only in live cells that reduce the yellow dye, MTT, to purple formazan crystals and the crystals were dissolved in 200 μL DMSO. The absorbance was recorded at 570 nm using Synergy 4 Biotek multimode reader. The percentage of cell toxicity was calculated as,

$$\% \text{ of cell toxicity} = \frac{\text{Absorbance of control - Absorbance of sample}}{\text{Absorbance of control}} \text{ x } 100$$

3.6.5. Determination of nitric oxide (NO) production

After pre-incubation of RAW 264.7 cells (2×10^6 cells/mL) with different concentrations of compound **5** and LPS (10 μg/mL) for 24 h, the quantity of nitrite accumulated in the culture medium was measured as an indicator of NO production. Briefly, 100 μL of Griess reagent (1 % sulfanilamide and 0.1 % naphthylethylenediamine dihydrochloride in 2.5 % phosphoric acid), was mixed with an equal volume of cell supernatant, the mixture was incubated at room temperature for 10 min, and the absorbance at 540 nm was measured in a microplate reader. The quantity of nitrite was determined based on a sodium nitrite standard calibration curve. All experiments were done in triplicates.

3.6.6. ELISA of TNF-α, IL-6, LOX-1, COX-2 and IL-10

Concentrations of TNF-α, IL-6, LOX-1, COX-2 and IL-10 in the culture medium were determined using respective ELISA kits according to the manufacturer's protocol and the absorbance was measured at 450 nm using microplate reader (Biotek ELX 800).

3.6.7. Western blot expression study

Expression level of NF-κB was evaluated by Western blotting. Cells were treated with 1 μM and 5 μM of compound 5 for 24 h. After incubation, the cells were lysed in ice-cold lysis buffer (50 mM Tris-HCl, 150 mM sodium chloride, 1.0 % Igepal CA-630, 0.5 % sodium deoxycholate, 0.1 % sodium dodecyl sulfate, 1 % Triton X-100 and protease inhibitor cocktail, pH 8.0) for 30 min on ice and were centrifuged at 12000 *x*g for 10 min. The protein content was then measured using BCA protein assay kit. The lysates (40 μg) were subjected to SDS-PAGE on 10 % gel and transferred on to a polyvinylidene difluoride (PVDF, Immobilon P™, Millipore®, USA) membrane by using Trans-Blot Turbo™ (Bio-Rad). The membranes were blocked by incubating in blocking buffer (5 % skim milk in PBST, PBST-PBS buffer containing 0.1 % Tween 20) for 1 h at room temperature, washed three times with PBST and probed over night at 4 °C with appropriate antibody against NF-κB (1: 1000). Membranes were washed 3 times and incubated for 1 h at room temperature with horse radish peroxidase (HRP) conjugated secondary antibody at 1:1000 dilution and again washed three times in PBST. The bound antibodies were detected using an enhanced chemiluminescence substrate (Biorad, USA) and measured by densitometry by using a Chemi Doc XRS digital imaging system and the Multi Analyst software from Bio-Rad Laboratories (USA).

Isolation and Characterization of Phytochemicals from *Vatica chinensis* L. and their Ameliorative Effect on H_2O_2 Induced Oxidative Stress in H9c2 Cardiomyoblasts

Since prehistoric times, humans have used natural products in medicines to alleviate and treat various life-threatening diseases. Nowadays, the majority of drugs have been developed from plant sources or from synthetically modified plant-based natural products. The search for pharmacologically relevant natural products is an exciting topic to the scientific community. In this aspect, we have focussed on the phytochemical and pharmacological investigation of the stem bark of *Vatica chinensis* L., belonging to the Dipterocarpaceae family.

4A.1. Dipterocarpaceae

Dipterocarpaceae is one of the largest family comprising 17 genera, (**Table 4A.1**) and approximately 695 known species and distributed in South Asian and African timber trees. The name 'Dipterocarpaceae' is a combination of three Greek words (*di* means two, *pteron* means wing and *karpos* means fruit) and refers to the "two-winged fruit". The largest genera of this family are *Shorea, Hopea, Dipterocarpus*, and *Vatica*. The genera *Pakaraimaea* and *Pseudomonotes* are restricted to Amazon (South America). Most of the species of this family consist of lofty trees with aromatic resins. Their clustered, fragrant flowers have five twisted petals and some of the species provide a variety of products along with useful timber. For example, "gurjun balsam" from *Dipterocarpus glandulosa* and "Borneo camphor" from *Dryobalanops aromatic* used as medicines; "Borneo camphor" is also used in varnishes and in embalming; "Indian copal" is a gum resin isolated from *Vateria indica* which is used as a medicine.

4A.2. *Vatica* genus

Vatica, flagship genus of the Dipterocarpaceae family, consists of more than 60 species. The species belongs to this genus grow in the drier areas of tropical evergreen forests found up to 1600 m in altitude. The plants belonging to this genus produce the phytochemicals like resveratrol oligomers and terpenoids. Resveratrol oligomers are known to exhibit diverse biological properties including antibacterial, antifungal, and

anti-HIV activities. Some of the plants belonging to this genus are shown in **Table 4A.2.** A detailed literature survey of some of the *Vatica* species for example; *Vatica affinis, Vatica bantamensis, Vatica cinerea, Vatica diospyroides, Vatica mangachapoi, Vatica odorata, Vatica pauciflora, Vatica parvifolia, Vatica umbonata and Vatica rassak* are discussed in the following sections.

Table 4A.1. Different genus of Dipterocarpaceae family

• *Anisoptera*	• *Monotes*	• *Upuna*
• *Cotylelobium*	• *Neobalanocarpus*	• *Vateria*
• *Dipterocarpus*	• *Parashorea*	• *Vateriopsis*
• *Dryobalanops*	• *Pseudomonotes*	• ***Vatica***
• *Hopea*	• *Shorea*	
• *Marquesia*	• *Stemonoporus*	

Table 4A.2. *Vatica* species and their distribution

Sl. No	Plant	Distribution
1	*Vatica affinis*	Sri Lanka
2	*Vatica badiifolia*	Borneo
3	*Vatica bantamensis*	Java in Indonesia
4	*Vatica bella*	Peninsular Malaysia
5	*Vatica brevipes*	Peninsular Malaysia
6	*Vatica brunigii*	Sumatra & Borneo
7	*Vatica cauliflora*	Borneo
8	*Vatica chartacea*	Borneo
9	*Vatica chinensis*	South Asia
10	*Vatica cinerea*	Cambodia, Malaysia, Burma, Thailand & Vietnam
11	*Vatica compressa*	Borneo
12	*Vatica congesta*	Borneo
13	*Vatica coriacea*	Borneo
14	*Vatica cuspidata*	Peninsular Malaysia
15	*Vatica diospyroides*	Malaysia, Thailand &Vietnam
16	*Vatica elliptica*	Philippines

17	*Vatica flavida*	Peninsular Malaysia
18	*Vatica flavovirens*	Sulawesi in Indonesia
19	*Vatica globosa*	Borneo
20	*Vatica guangxiensis*	China
21	*Vatica havilandii*	Peninsular Malaysia & Borneo
22	*Vatica heteroptera*	Peninsular Malaysia
23	*Vatica hullettii*	Peninsular Malaysia
24	*Vatica latiffii*	Sarawak on Borneo
25	*Vatica lanceaefolia*	Bangladesh, India & Myanmar-Burma
26	*Vatica lobata*	Peninsular Malaysia
27	*Vatica lowii*	Sumatra & Malaysia.
28	*Vatica maingayi*	Sumatra, Malaysia, Singapore & Borneo
29	*Vatica mangachapoi*	Brunei, eastern China (Hainan Island), Malaysia, Philippines, Thailand &Vietnam
30	*Vatica maritima*	Borneo & Philippines
31	*Vatica nitens*	Malaysia & Borneo
32	*Vatica obovata*	Sumatra
33	*Vatica obscura*	Sri Lanka
34	*Vatica odorata*	China to Indochina to Malaysia
35	*Vatica pachyphylla*	Eastern Luzon island & Philippines
36	*Vatica pallida*	Peninsular Malaysia
37	*Vatica parvifolia*	Borneo
38	*Vatica pauciflora*	Sumatra, Peninsular Malaysia, Singapore, & Thailand
39	*Vatica pedicellata*	Borneo
40	*Vatica pentandra*	Borneo
41	*Vatica perakensis*	Sumatra and Peninsular Malaysia & Borneo
42	*Vatica philastraena*	Thailand & Vietnam
43	*Vatica rassak*	Indonesia, Buru, Papua New Guinea & Philippines
44	*Vatica ridleyana*	Sumatra & Singapore
45	*Vatica rotata*	Borneo

46	*Vatica rynchocarpa*	Borneo
47	*Vatica sarawakensis*	Borneo
48	*Vatica scortechinii*	Peninsular Malaysia
49	*Vatica soepadmoi*	Sumatra
50	*Vatica stapfiana*	Sumatra, Peninsular Malaysia &Thailand
51	*Vatica teysmanniana*	Sumatra
52	*Vatica umbonata*	Peninsular Malaysia, Borneo, Philippines & Thailand
53	*Vatica venulosa*	Sumatra, Peninsular Malaysia & Borneo
54	*Vatica xishuangbannaensis*	China

4A.2.1. *Vatica affinis*

Vatica affinis is a critically endangered species and endemic to Sri Lanka. In 1981, Sultanbawa *et al*., reported the isolation of *ε*-viniferin, vaticaffinol and hopeaphenol from the bark of *Vatica affinis* [Sultanbawa *et al*., **1981**] (**Figure 4A.1)**. After that, Subramaniam *et al*., isolated *β* -amyrin acetate, *β*-amyrin, *β*-sitosterol, hexamethoxy coeruleoellagic acid, tetramethoxy- ellagic acid, ursolic acetate, scopoletin, and betulinic acid along with *ε*-viniferin and vaticaffinol from the stem and timber of *Vatica affinis* [Subramaniam *et al*., **1985**].

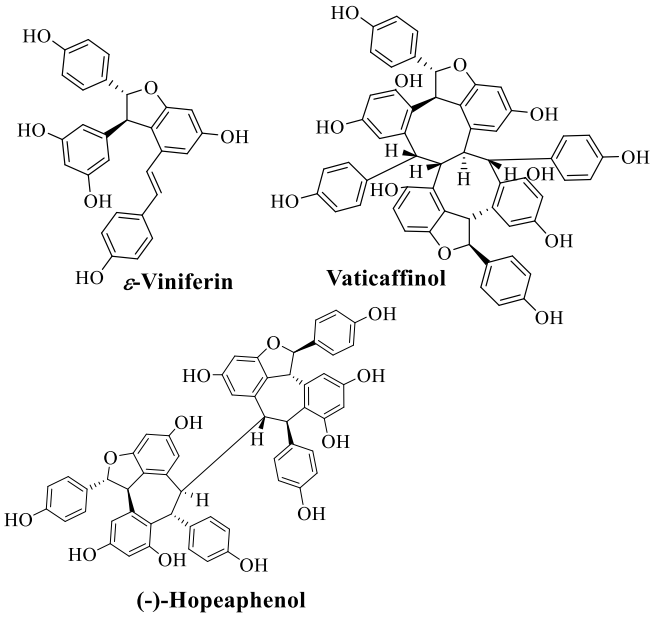

Figure 4A.1. The structures of some of the compounds isolated from *Vatica affinis*

4A.2.2. *Vatica bantamensis*

Vatica bantamensis is an endangered species and endemic to Java in Indonesia. In 2012, Ito *et al*., reported the isolation of 11-*O*-(*E*)-sinapate, 11-*O*-(*E*)-ferulate, 11-*O*-(*Z*)-ferulate, 11-*O*-(*E*)-coumalate, 11-*O*-(*Z*)-coumalate, 11-*O*-syringate, 11-*O*-vanillate, 11-*O*-*p*-hydroxybenzoate and bergenin from the leaves of *Vatica bantamensis* [Ito *et al*., **2012**] (**Figure 4A.2)**.

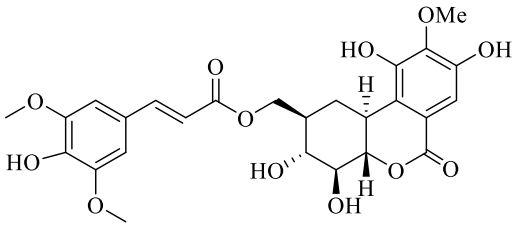

Bergenin 11-*O*-(*E*)-sinapate

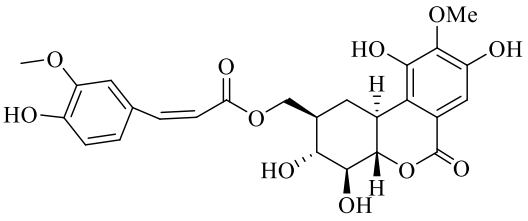

Bergenin 11-*O*-(*E*)-ferulate

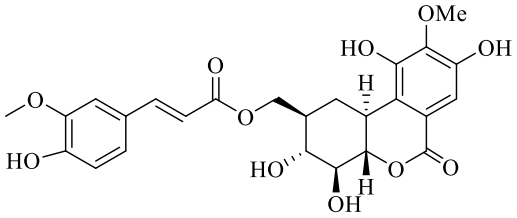

Bergenin 11-*O*-(*Z*)-ferulate

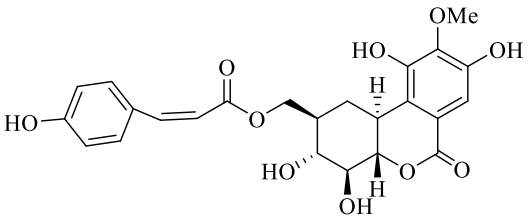

Bergenin 11-*O*-(*Z*)-coumalate

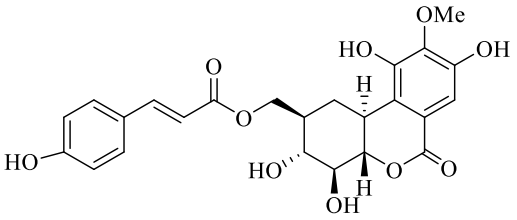

Bergenin 11-*O*-(*E*)-coumalate

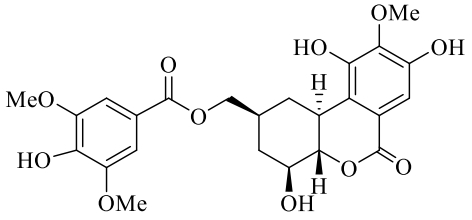

Bergenin 11-*O*-syringate

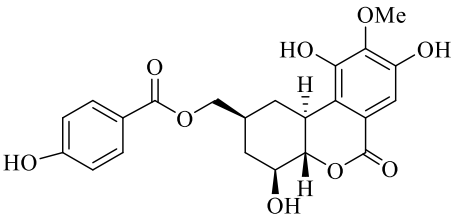

Bergenin 11-*O*-vanillate

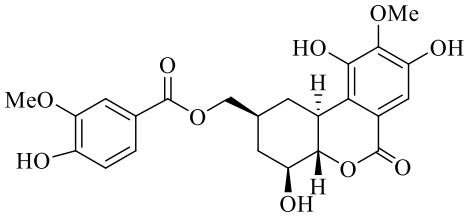

Bergenin 11-*O*-*p*-hydroxybenzoate

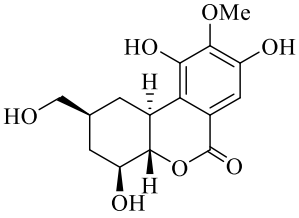

Bergenin

Figure 4A.2. The structures of the compounds isolated from *Vatica bantamensis*

4A.2.3. *Vatica cinerea*

Vatica cinerea is an endangered species and found in Cambodia, Malaysia, Burma, Thailand, and Vietnam. In **2003**, Zhang *et al*., reported the isolation and anti-HIV activity of (23*E*)-27-nor-3*β*-hydroxycycloart-23-en-25-one, vaticinone, mangiferonic acid, dihydroschizandronic acid, (24*E*)-3-oxo-lanosta-8,24-dien-26-oic acid, dammara-20,25-dien-3*β*, 24-diol, (23*E*)-dammara-20,23-dien-3*β*, 25-diol, betulonic acid, betulinic acid, betulin, ursolic acid, erythrodiol and 1-hydroxycyclocolorenone from the dried leaves and twigs of *Vatica cinerea* [Zhang *et al*., **2003**] (**Figure 4A.3**).

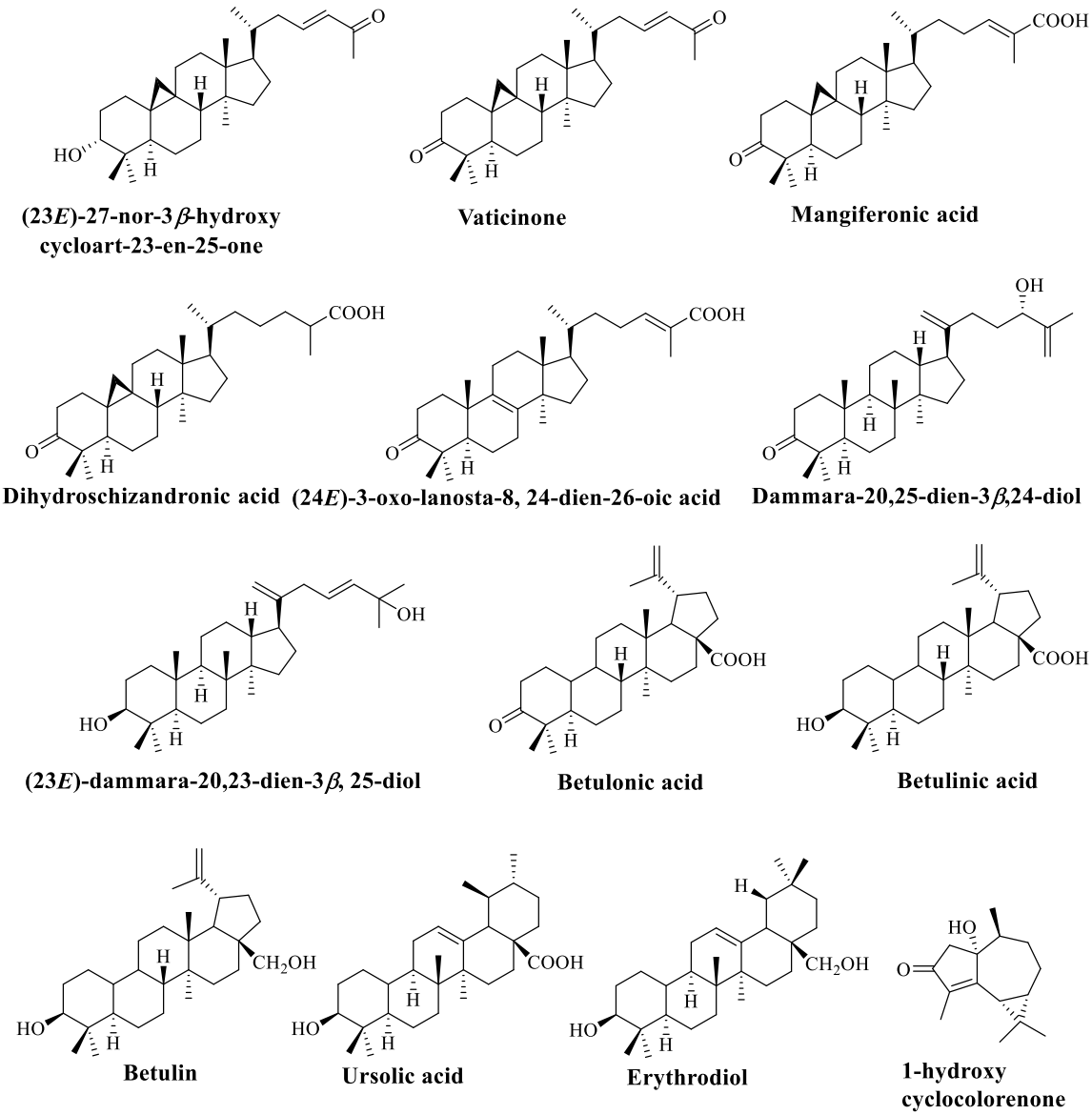

Figure 4A.3. The structures of the compounds isolated from *Vatica cinerea*

4A.2.4. *Vatica diospyroides*

Vatica diospyroides, a critically endangered species and found in Malaysia, Thailand, and Vietnam. In 1999, Seo *et al*., reported the isolation and cytotoxic activity of vatdiospyroidol and vaticaphenol A from the stems of *Vatica diospyroides* [Seo *et al*., **1999**] (**Figure 4A.4**).

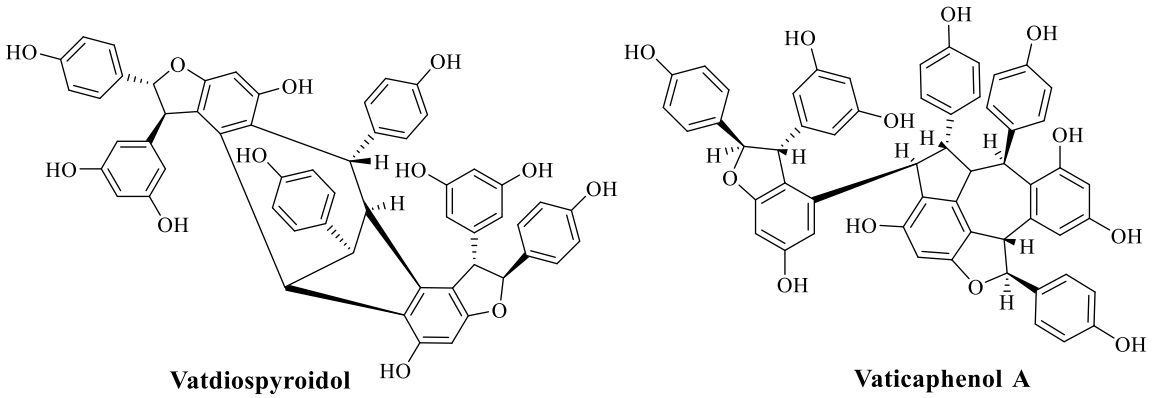

Figure 4A.4. The structures of the compounds isolated from *Vatica diospyroides*

4A.2.5. *Vatica mangachapoi*

Vatica mangachapoi belongs to the family Dipterocarpaceae and found in the Malaysia and China. Phytochemical investigation of the branches and twigs of *Vatica mangachapoi* resulted in the isolation of 20 compounds. They include vaticahainols A–C, vaticanol A, vaticanol E, pauciflorol B, vatdiospyroidol, diptoindonesin D, (+)-parviflorol, (+)-*ε*-viniferin, (+)-ampelopsin F, isoampelopsin F, hopeafuran, (+)-ampelopsin A, hopeahainol D, pauciflorol C, hemsleyanol D, hopeaphenol A, vaticaffinol, and davidol A [Yan *et al*., **2011**]. In 2018, Hui *et al*., reported the isolation of parviflorol, diptoindonesin D, vaticahainol, vitisinol G, malibatol A, vaticahainol C, ampelopsin A, balanocarpol, ampelopsin F, isoampelopsin, vaticaffinol, isohopeaphenol A, *O*-glucosides cordifoloside B, vatalbinoside D and *O*-glucoside paucifloroside B from the stem barks of *Vatica mangachapoi* [Hui *et al*., **2018**]. Recently, Wu *et al*., reported the isolation of vaticahainone, A diptoindonesin D, (-)-ampelopsin A, acuminatol, malibatols A, (-)-shoreaphenol, (+)-shoreaphenol, (+)-ampelopsins B, vaticahainol A, hopeahainol A, hopeahainol D, heimiol A, hopeahainanphenol, (-)-*ε*-viniferin, (+)-cis-*ε*-viniferin, (+)-ampelopsin F, (-)-ampelopsin F, stenophyllol B, paucifloroside B, *α*-viniferin, hopeaphenol A, isohopeaphenol A, stenophyllol C, ampelopsin H, vaticanol B, vaticaphenol A and vaticaside B from the stem of *Vatica mangachapoi* [Wu *et al*.,

2018]. The structures of the compounds isolated from *Vatica mangachapoi* are shown in **Figure 4A.5.**

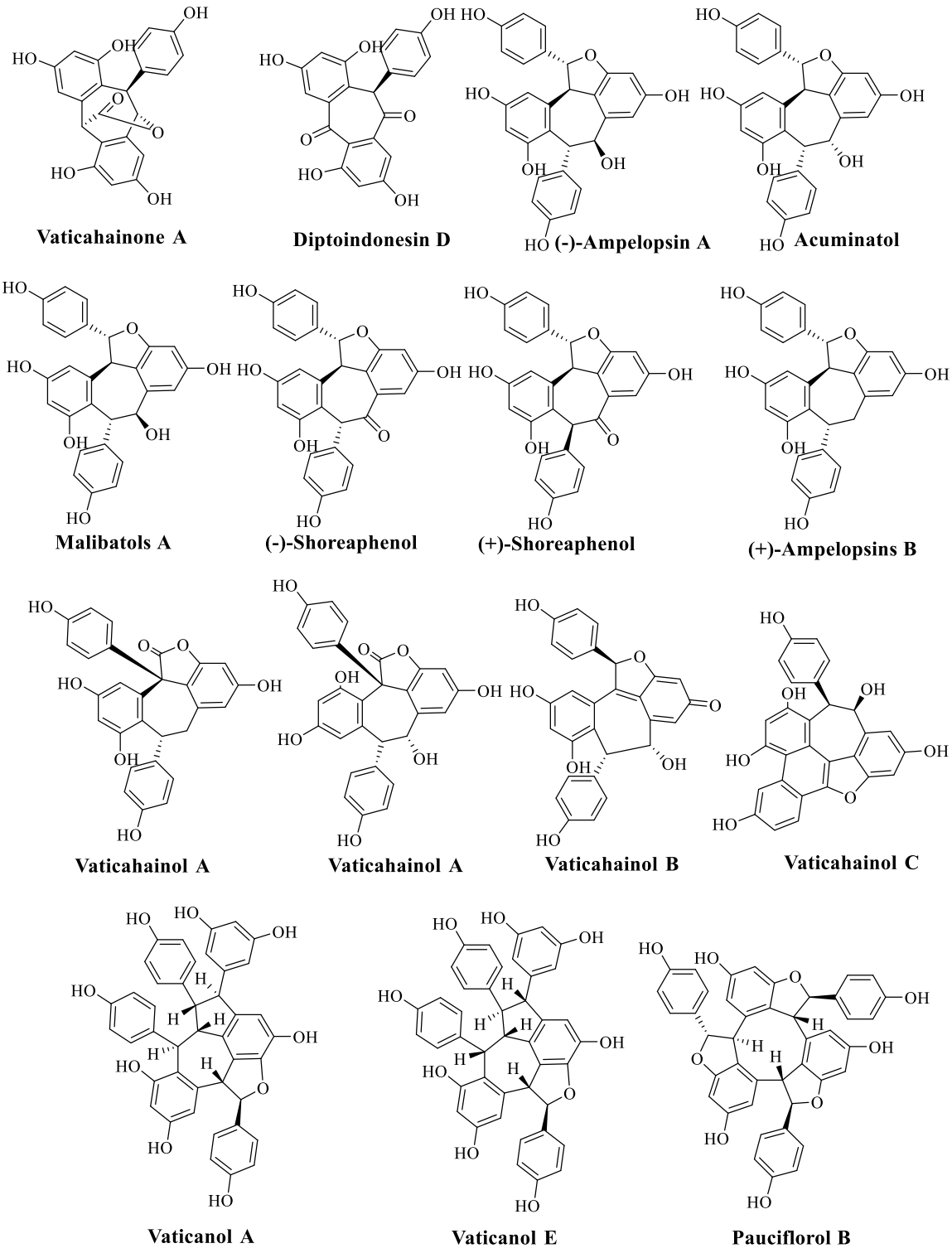

Continued…

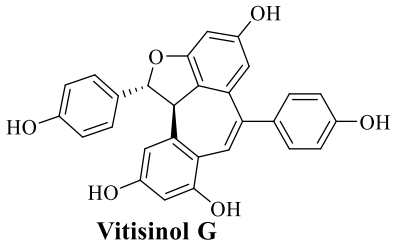
Vitisinol G

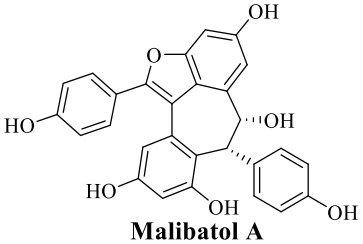
Malibatol A

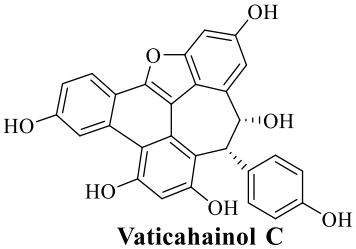
Vaticahainol C

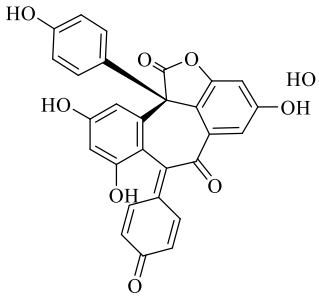
Hopeahainol A

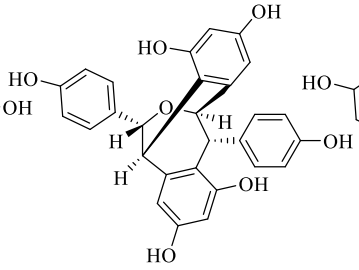
Hopeahainol D

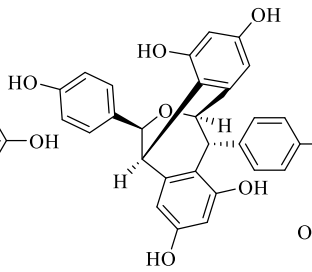
Heimiol A

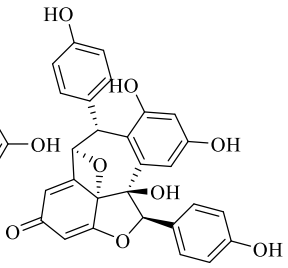
Hopeahainanphenol

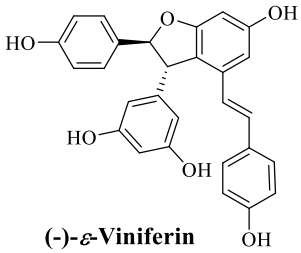
(-)-ε-Viniferin

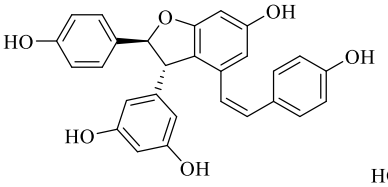
(+)-cis-ε-Viniferin

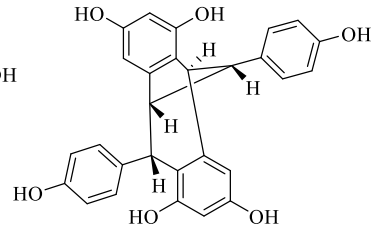
(+) - Ampelopsin F

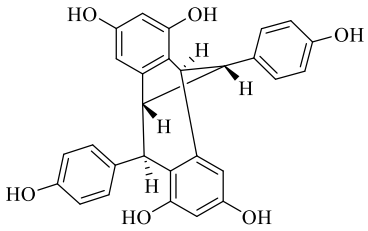
(-)- Ampelopsin F

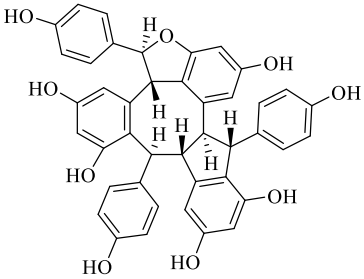
Stenophyllol B

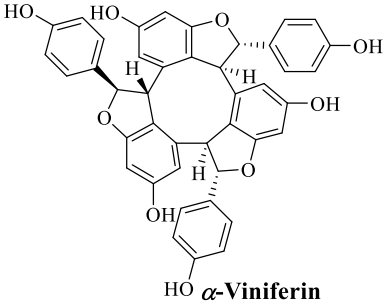
α-Viniferin

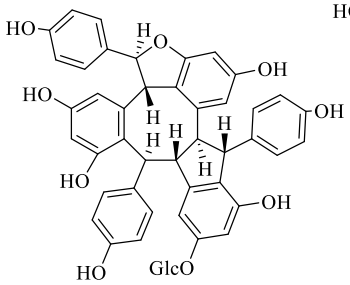
Paucifloroside B

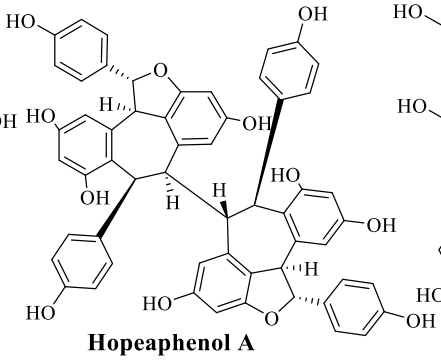
Hopeaphenol A

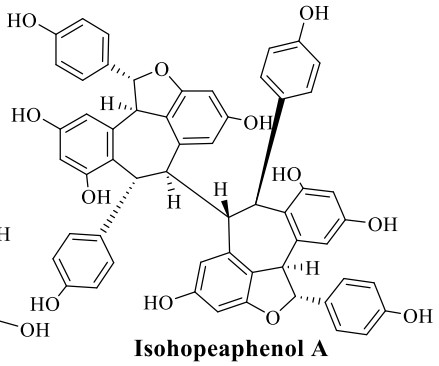
Isohopeaphenol A

Continued…

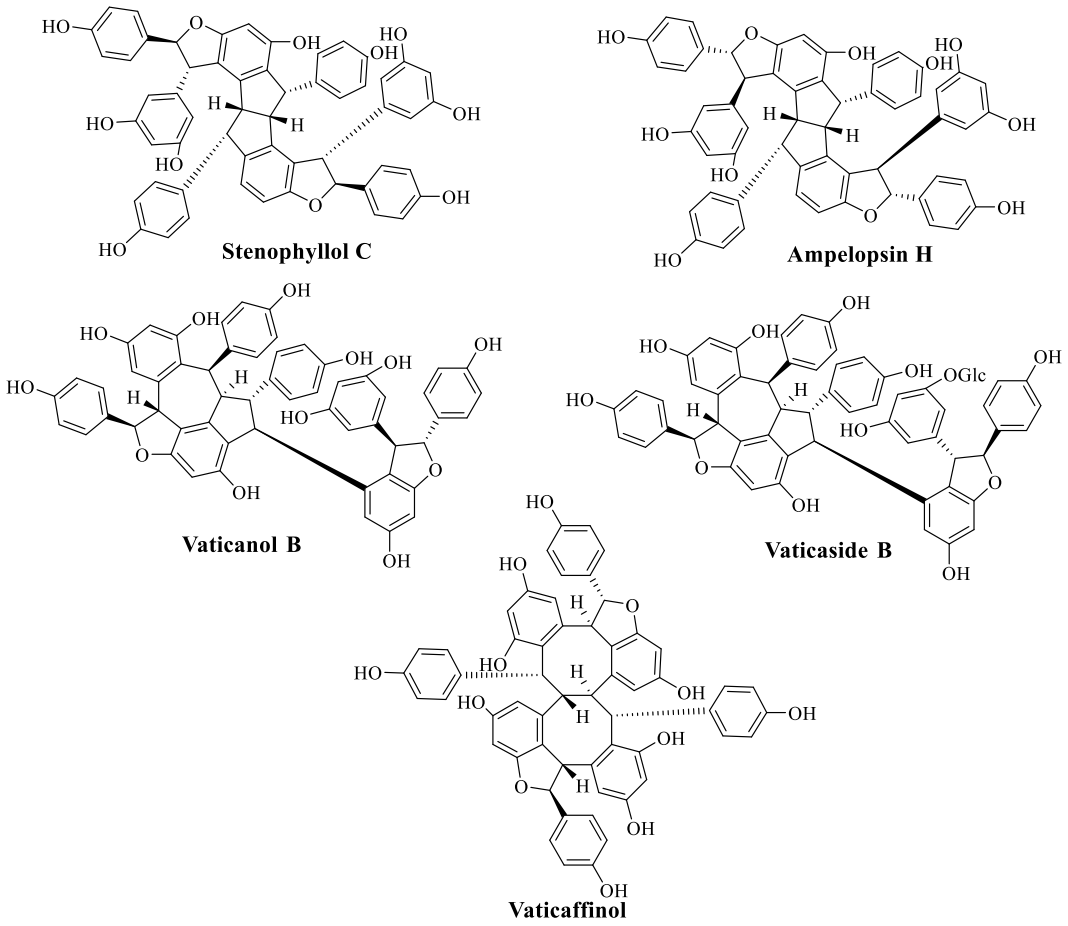

Figure 4A.5. The structures of the compounds isolated from *Vatica mangachapoi*

4A.2.6. *Vatica odorata*

Vatica odorata is found in China and Malaysia. In 2010, Wan *et al*., reported the isolation of laevifonol from the stem bark of *Vatica odorata* [Wan *et al*., **2010**]. In 2011, Jalifah *et al*., reported the isolation and cytotoxic activity of (-)-*trans*-resveratrol-13-*O*-*β*-D-glucopyranoside, (-)-*ε*-viniferin, (-)-laevifonol, (-)-hopeaphenol, (-)-vaticanol B and bergenin from the bark of *Vatica odorata* [Jalifah *et al*., **2011**]. The structures of some of the compounds isolated from *Vatica odorata* are shown in **Figure 4A.6.**

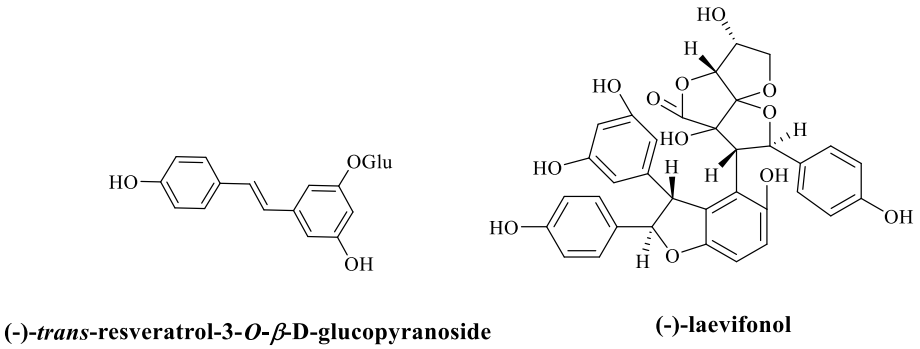

Figure 4A.6. The structures of the compounds isolated from *Vatica odorata*

4A.2.7. *Vatica pauciflora*

Vatica pauciflora is native to Sumatra, Peninsular Malaysia, Singapore, and Thailand. It is commonly seen in freshwater swamps and on riparian river banks. In 2003, Ito *et al*., reported the isolation of pauciflorols A-C, isovaticanols B and C, pauciflorosides A-C, bergenin, (-)-ampelopsin F, (+)-ampelopsin D, davidiol B, hemsleyanols A and D, isoampelopsin F, piceid, stenophyllol B, vateriaphenol B, vaticanols A-C, E and G, vaticaside D, (-)-ε-viniferin and bergenin from the stem bark of *Vatica pauciflora* [Ito *et al*., **2003**]. Next year, Ito *et al*., also reported the isolation of pauciflorol D-F from the stem bark of *Vatica pauciflora* [Ito *et al*., **2004]**. Aisyah *et al*., (2013) reported the isolation and the oxidative effect on Chang cells from the woods and twigs of *Vatica pauciflora* [Aisyah *et al*., **2013]**. In 2014, Ida *et al*., reported the isolation and *α*-glucosidase inhibitory activity of bergenin from the stem bark of raru (*Vatica pauciflora* Blume) [Ida *et al*., **2014**]. Recently, Ida *et al*., reported antidiabetic activity of methoxybergenin isolated from the stem bark of *Vatica pauciflora* [Ida *et al*., **2017**]. The structures of some of the compounds isolated from *Vatica pauciflora* are shown in **Figure 4A.7.**

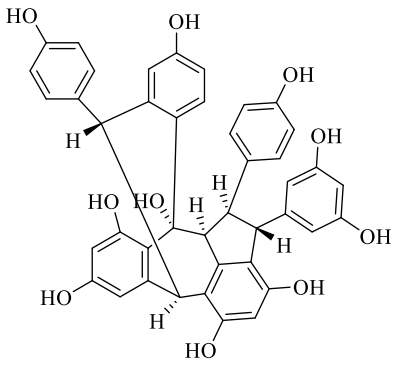

Vaticanol G

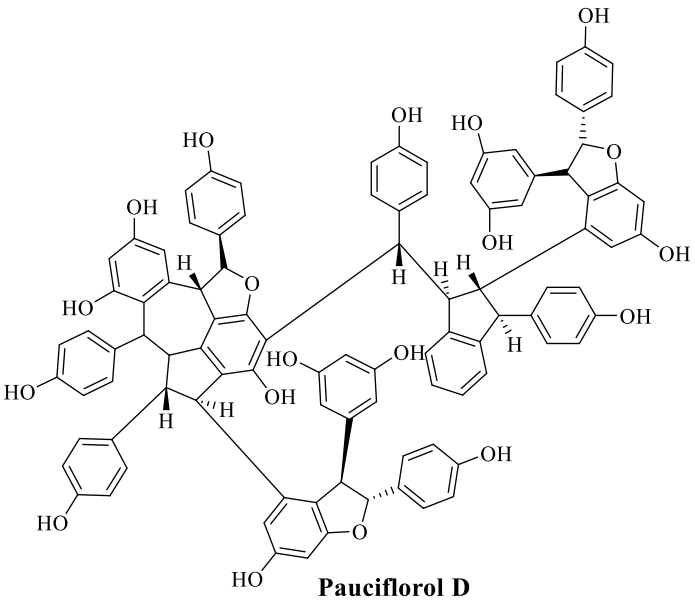

Pauciflorol D

Continued…

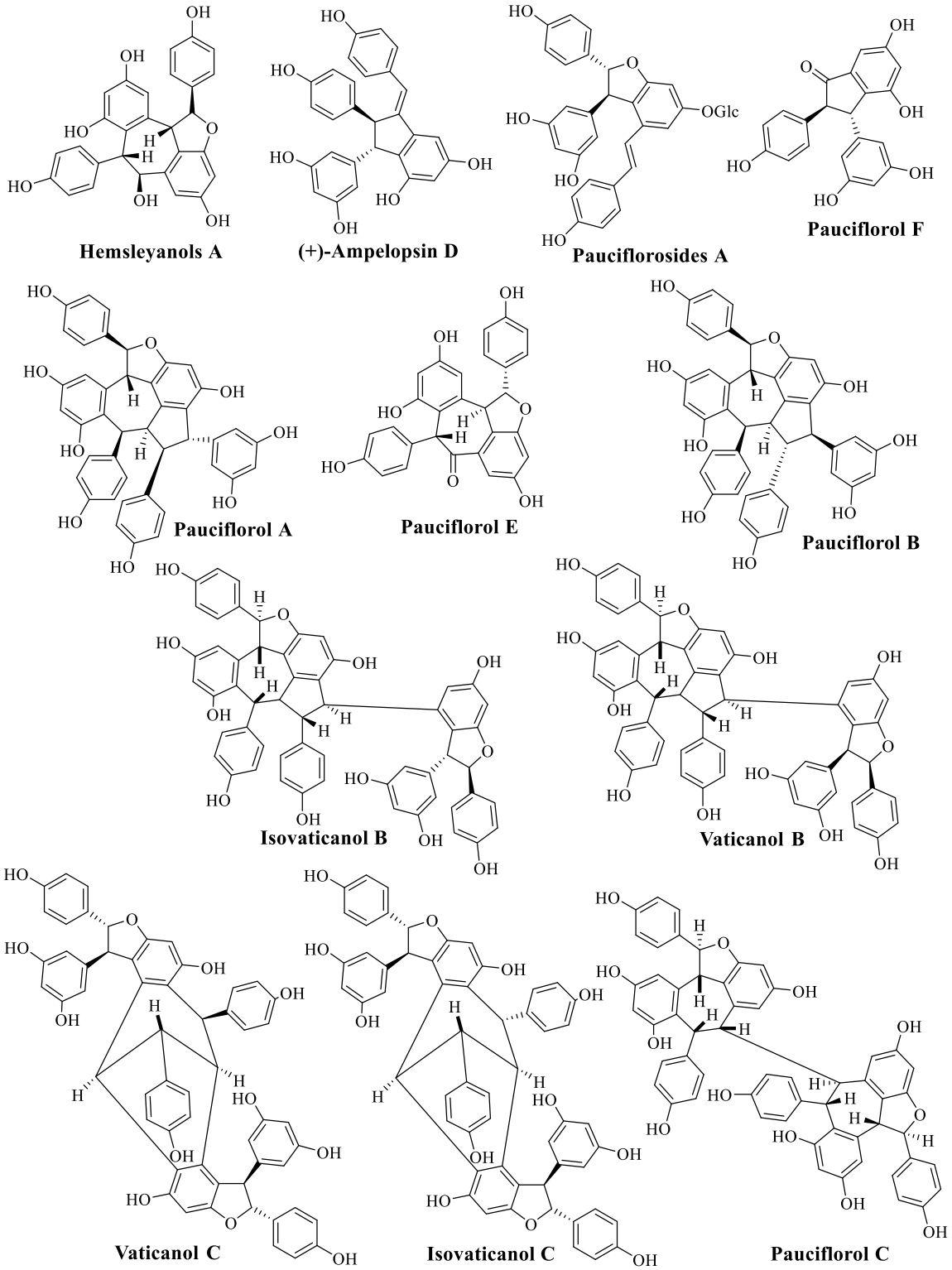

Figure 4A.7. The structures of the compounds isolated from *Vatica pauciflora*

4A.2.8. *Vatica parvifolia*

Vatica parvifolia is a critically endangered species and endemic to Borneo. In 2012, Hui *et al*., reported the isolation and anti-inflammatory activity of vatiparol from the *Vatica parvifolia* [Hui *et al*., **2012**] (**Figure 4A.8**).

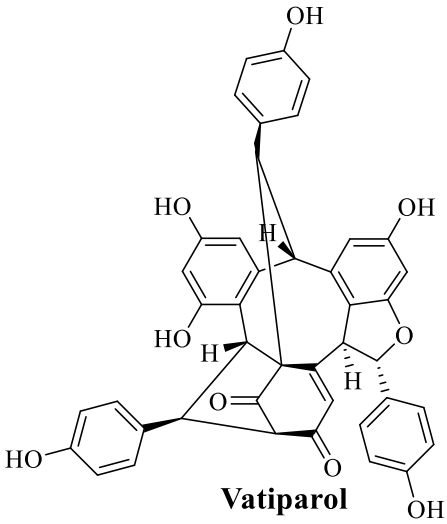

Figure 4A.8. The structure of vatiparol isolated from *Vatica parvifolia*

4A.2.9. *Vatica rassak*

Vatica rassak also belongs to the family Dipterocarpaceae and found in Indonesia, Buru, Papua New Guinea, and the Philippines. In 2000, Toshiyuki *et al.*, reported the isolation of resveratrol hexamer, Vaticanol D from the stem bark of *Vatica rassak* [Toshiyuki *et al.*, **2000**] (**Figure 4A.9**). After that, Ito *et al*., reported the isolation and antitumor effect of resveratrol oligomers, vaticanol C against human cancer cell lines. [Ito *et al*., **2003**]. It is reported that, vaticanol C activates PPARα and PPARβ/δ in cell-based reporter assays [Tomoko *et al*., **2010**].

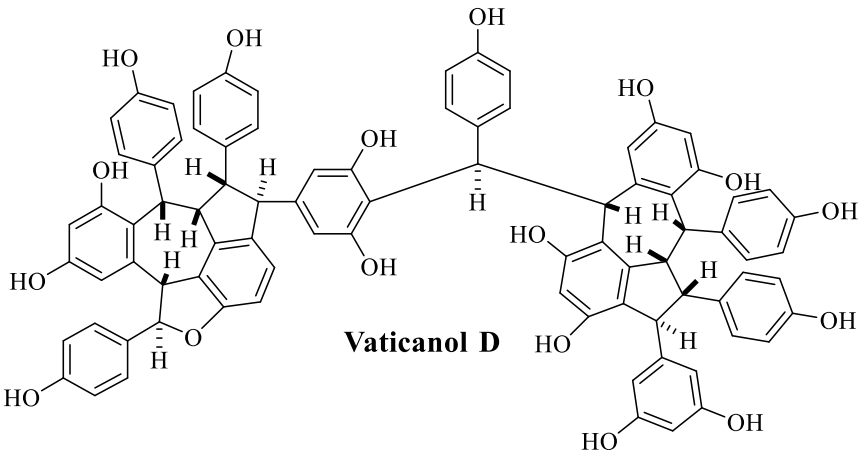

Figure 4A.9. The structure of vaticanol D isolated from *Vatica rassak*

4A.2.10. *Vatica umbonata*

Vatica umbonata belongs to the Dipterocarpaceae family found in Peninsular Malaysia, Borneo, Philippines, and Thailand. In 2004, Atun *et al*., reported the isolation of seven oligostilbenes, namely (-)-ε-viniferin, (-)- ampelopsin F, laevifonol, stenophyllol B, vaticanol B, vaticanol G, (-)-hopeaphenol from the tree bark of *Vatica umbonata* [Atun *et al*., **2004**].

4A.3. Aim and scope of the present investigation

Vatica chinensis L. (**Figure 4A.10***)* is a critically endangered species endemic to South India and Sri Lanka and belongs to the genus *Vatica*. It is locally recognized as "Adakkapine", "Cherupiney" or "Payinipasa". The taxonomic classification of *Vatica chinensis* L. is shown in **Table 4A.3**. In 2015, Ito *et al*. isolated (-)-ε-viniferin, (-)-ampelopsin F, upunaphenol F, vaticanol K, vaticanol L and vaticanol M from *Vatica chinensis* (**Figure 4A.11**) [Ito *et al*., **2015**]. Apart from these, there are no reports on the isolation, characterization and pharmacological activity of *Vatica chinensis* L. Hence, it is suitable and appropriate to carry out the phytochemical and pharmacological investigation of *Vatica chinensis* L. Therefore, as part of my Ph.D. program, a detailed phytochemical and pharmacological evaluations of the stem bark of *Vatica chinensis* L. have been undertaken. In the first part of this chapter, activity oriented extraction and isolation were carried out. The phytochemical investigation of the stem bark of *Vatica chinensis* L. resulted in the isolation of seven major compounds. The compounds were identified as resveratrol dimers; (-) - ε - viniferin (**27**) and (-) - ampelopsin F (**28**), resveratrol tetramers; vaticanol R (**29**) and vaticaphenol A (**30**), resveratrol hexamer; vaticanol M (**31**), bergenin (**32**), and methoxy bergenin (**33**). Vaticanol R, a non-heterocyclic resveratrol tetramer and is being reported for the first time from natural resources. All the compounds (**27-33**) were checked for their antioxidant and cytoprotective properties against H_2O_2 induced oxidative stress in H9c2 cell line.

Figure 4A.10. *Vatica chinensis* L.

Table 4A.3. Scientific classification of *Vatica chinensis*

Kingdom	*Plantae*
Order	*Malvales*
Family	*Dipterocarpaceae*
Genus	*Vatica*
Species	*V. chinensis*
Binomial name	*Vatica chinensis* Linn.

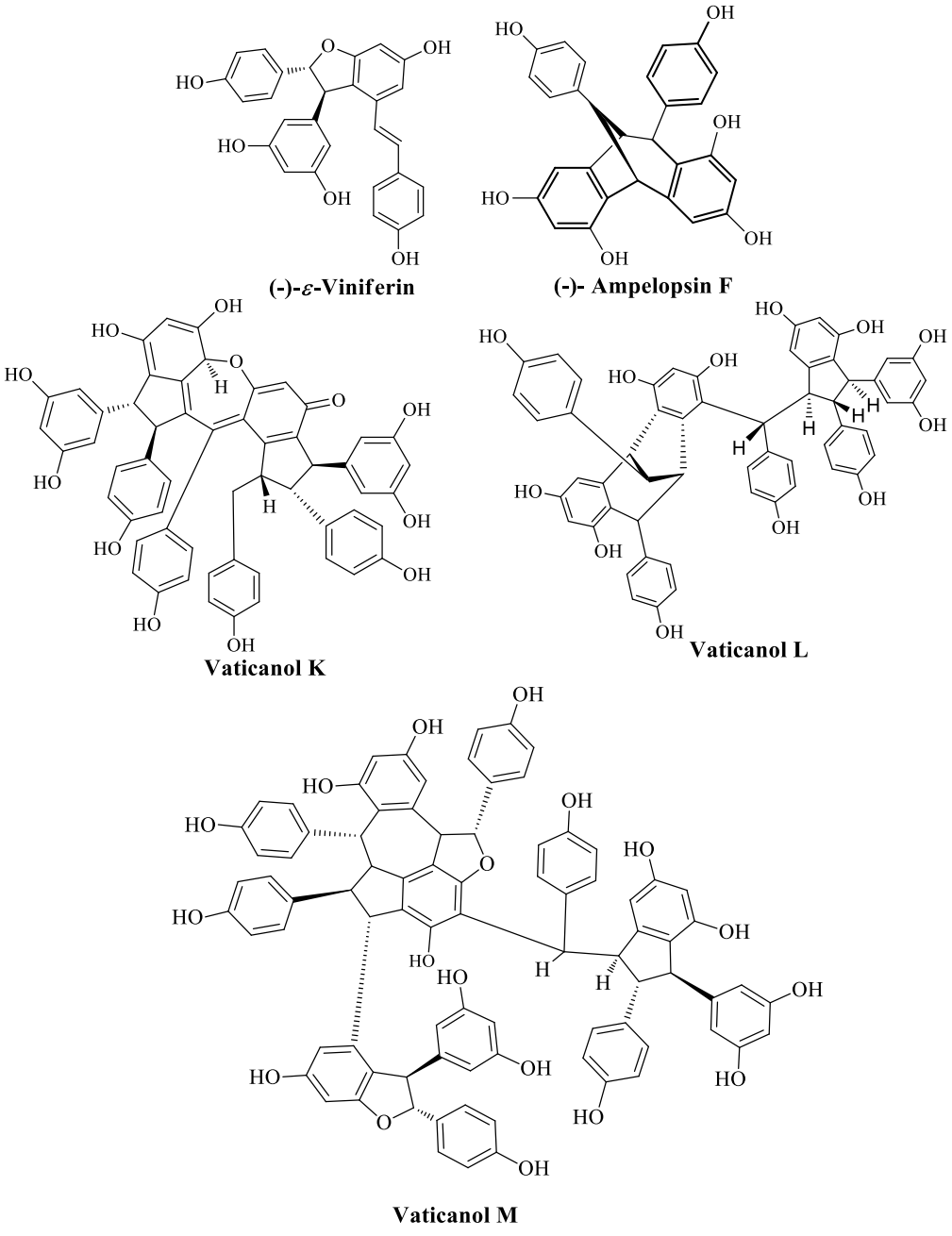

Figure 4A.11. Compounds isolated previously from *Vatica chinensis*

4A.4. Extraction, activity-oriented isolation and characterization of compounds

4A.4.1. Plant material

The stem bark of *Vatica chinensis* L. was collected from Calicut University campus, Calicut, Kerala, India in April 2015. The plant material was authenticated by the plant taxonomist of Calicut University campus, Calicut, Kerala, India and a voucher specimen (Voucher Specimen No. **6389**) was deposited in the Herbarium repository of Calicut University, Kerala, India.

4A.4.2. Extraction and extract level antioxidant activity

The dried and grounded stem bark of *Vatica chinensis* (750 g) was extracted (3L x 48 h x 3 times) successively with *n*-hexane, acetone, ethanol and water at room temperature and filtered. The filtrate was concentrated at 50 °C under reduced pressure to yield hexane extract (VCH, 2 g), acetone extract (VCA, 60 g), ethanol extract (VCE, 38 g), and aqueous extract (VCW, 12 g) respectively. After that, we carried out the extract level total phenolic content (TPC) and DPPH radical scavenging activity. The results demonstrated that acetone extract has the highest content of TPC with the value of 46.41 ± 0.34 mmol equiv. GAE/100 g (gallic acid equivalent/100 gram). To identify the extract with the greatest antioxidant activity, *in vitro* DPPH antioxidant activity was carried out with each extract and the most bioactive extract was then selected for further isolation and purification. For the DPPH radical scavenging assay, the acetone extract demonstrated the highest DPPH scavenging activity with an IC_{50} value of 994.50 ± 4.21 μg/mL. In short, the acetone extract was determined to be the extract with the greatest TPC and DPPH antioxidant activity; therefore, further isolation and purification efforts were focussed on the acetone extract. The results are depicted in **Table 4A.4**.

Table 4A.4. TPC and DPPH radical scavenging activity of different extracts

Extracts	TPC (mg GAE/g dried weight)	DPPH (IC_{50} μg/mL)
VCH	2.22 ± 0.17	NIL
VCA	**101 ± 0.85**	**12.48 ± 0.28**
VCE	97 ± 0.11	58.00 ± 0.57
VCW	69 ± 0.57	38.91 ± 0.30
Gallic acid	-	2.53 ± 0.42

VCH - Hexane extract, VCA – Acetone extract, VCE - Ethanol extract, VCW - Water extract, Note: mean ± SD, N=3.

4A.4.3. Activity-oriented isolation and characterization of compounds

An aliquot of acetone extract (35 g) was subjected to silica gel column (100–200 mesh, 1000 x 60 mm) chromatography and eluted with *n*-hexane, *n*-hexane-EtOAc gradient and EtOAc. Fifteen fractions (Fr.1 - Fr.15) of 200 mL each were collected and concentrated at 50 ^{o}C under reduced pressure.

The Fr.5 was eluted with *n*-hexane/ethyl acetate to afford compound **27** (26 mg) and compound **28** (2.5 g). Compound **27** was obtained as a brown amorphous solid and displayed a molecular ion peak at m/z: 455.1599 for $[M+H]^+$ in the HRESIMS (Calculated for $C_{28}H_{23}O_6$: 455.1595); this result together with the ^{13}C NMR data, allowed the assignment of the molecular formula $C_{28}H_{22}O_6$ to compound **27**. The ^{1}H NMR (**Figure 4A.12**) spectrum exhibited the presence of two sets of *ortho*-coupled aromatic protons signals at δ_H 7.21, (d, *J* = 8 Hz, H-2a and 6a) and 6.84 (d, *J* = 8.5 Hz, H-3a and 5a) ppm; δ_H 7.18 (d, *J* = 8 Hz, H-2b and 6b) and 6.74 (d, *J* = 8.5 Hz, H-3b and 5b) ppm] and *meta*-coupled aromatic hydrogen signals at δ_H 5.94, 6.03, 6.32 and 6.39 (d, *J* = 2.5 Hz, 1H each) ppm. The stereocentre protons 7a and 8a resonated at δ_H 5.43 (d, *J* = 8 Hz, 2H) and 4.47 (d, *J* = 8 Hz, 2H) ppm. The signals at δ_H 6.91 and 6.70 ppm each integrating one proton with *J* value 16.5 Hz could be attributed to *trans* olefinic protons. The phenolic hydroxyl groups resonated at δ_H 8.58 and 8.35 ppm. In the ^{13}C NMR spectrum (**Figure 4A.13**), stereocentre carbons 7a and 8a resonated at δ_C 93.0 and 56.2 ppm. The signals resonated at δ_C 161.5, 159.0, 158.8, 157.4, 157.4 ppm are the diagnostic peaks for aromatic carbons attached to hydroxyl group. The compound displayed specific rotation at $[\alpha]^{25}_D$ -31.5^o (*c* 0.1, MeOH). Further, by comparison of the spectroscopic data [Subramaniam*et al*., **1985**] with the values reported earlier the compound **27** confirmed as (-)-*ε*-viniferin. The structure of the compound **27** is shown below.

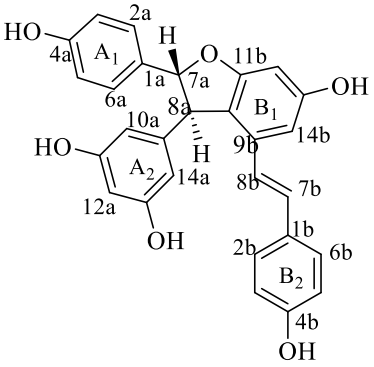

(-)-*ε*-Viniferin (27)

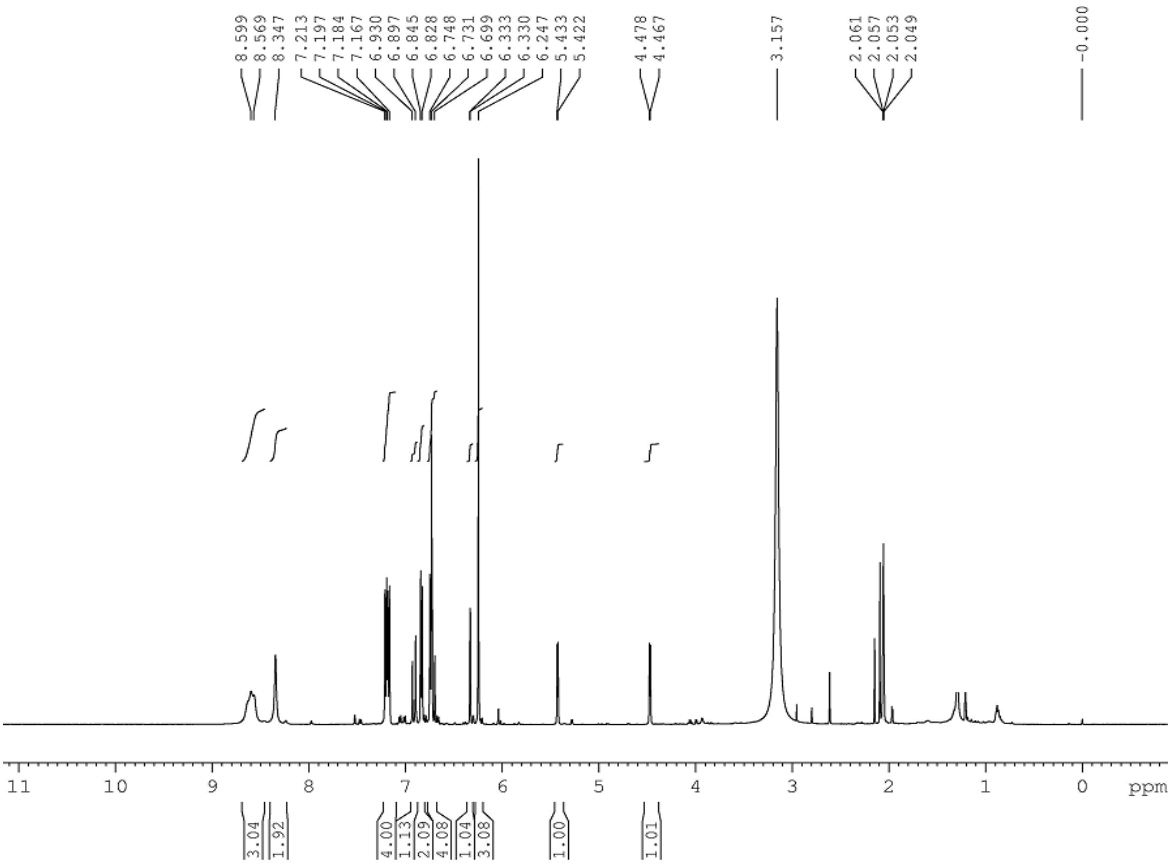

Figure 4A.12. ^{1}H NMR spectrum (500 MHz, Acetone-d_6) of (-) - ε- viniferin (**27**)

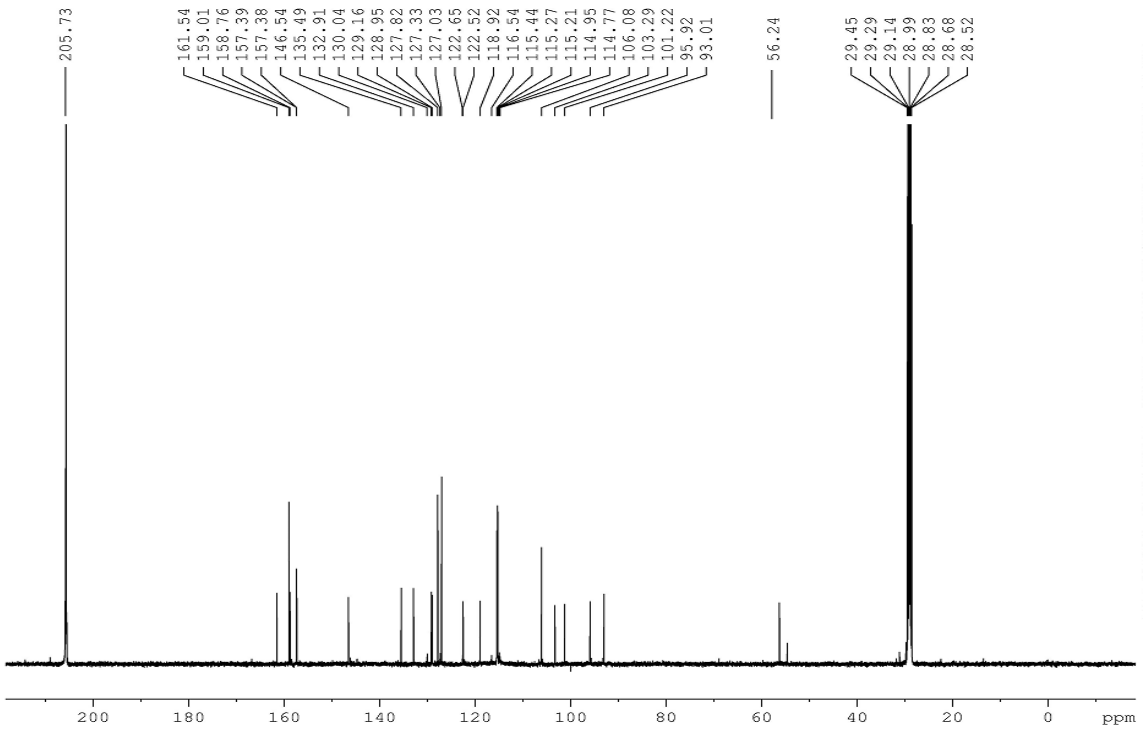

Figure 4A.13. ^{13}C NMR spectrum (125 MHz, Acetone-d_6) of (-) - ε- viniferin (**27**)

The molecular formula was established as $C_{28}H_{22}O_6$ from HRESIMS data [m/z 455.1496 $[M+H]^+$; 455.1495 calculated for $C_{28}H_{23}O_6$] together with NMR spectral data, indicating 18 degrees of unsaturation. The UV and IR spectra indicated the presence of aromatic rings [280 nm; υ_{max}1605 cm^{-1}]. The compound **28** exhibited specific rotation at $[\alpha]^{25}_D$ -13^o (*c* 0.1, MeOH). Assignments of the ^{1}H and ^{13}C NMR spectra of compound **28** in acetone-d_6 were developed using DEPT, HOMOCOSY and HMQC as well as HMBC experiments (Figure **4A.14 - 15**). The ^{13}C NMR spectrum of compound **28** showed 24 signals for 28 carbons, including four sp^3 methine carbons, 12 sp^2 methine carbons, and 12 sp^2 quaternary carbons. The ^{1}H NMR spectrum of compound **28** displayed *ortho*-coupled aromatic hydrogen signals at δ_H 6.96 (d, *J* = 8.5 Hz, 2H, H-2 and H-6), 6.65 (d, *J* = 8.5 Hz, 2H, H-2' and H-6'), 6.63 (d, *J* = 8.5 Hz, 2H, H-3 and H-5) and 6.44 (d, J_1 = 2 & J_2 = 8.5 Hz, 2H, H-3' and H-5') ppm, *meta*-coupled aromatic hydrogen signals at δ_H 6.39 (d, *J* = 2 Hz, 1H, H-14), 6.32 (d, *J* = 2.5 Hz, 1H, H-14'), 6.02 (d, *J* = 2.5 Hz, 1H, H-12') and 5.94 (d, *J* = 2.5 Hz, 1H, H-12) ppm and four aliphatic methine hydrogen signals at δ_H 4.06 (d, *J* = 2 Hz, 1H, H-7), 4.0 (s, 1H, H-8'), 3.51 (s, 1H, H-7') and 3.23 (s, 1H, H-8) ppm. The phenolic hydroxyl groups resonated at δ_H 8.02, 7.96, 7.94, 7.89. 7.79 and 7.35 ppm. The signals resonated at δ_C 158.6, 157.9, 157.2, 156.2, 156.2, and 153.2 ppm are the diagnostic peaks for aromatic carbons attached to hydroxyl group. The stereocentre carbons resonated at δ_C 58.2 (8), 50.5 (7'), 49.7 (8') & 47.2 (7) ppm. Further, by comparison with previous literature reports [Oshima *et al*., **1993**] the compound **28** was confirmed as (-)- ampelopsin F. It is identified as a marker compound in this species. The structure of the compound **28** is shown below.

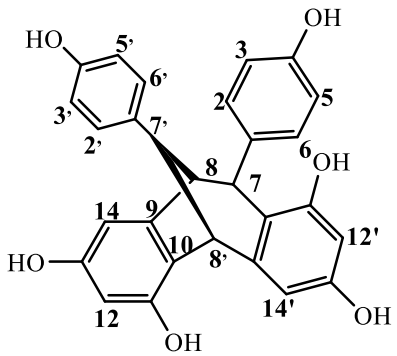

(-)- Ampelopsin F (28)

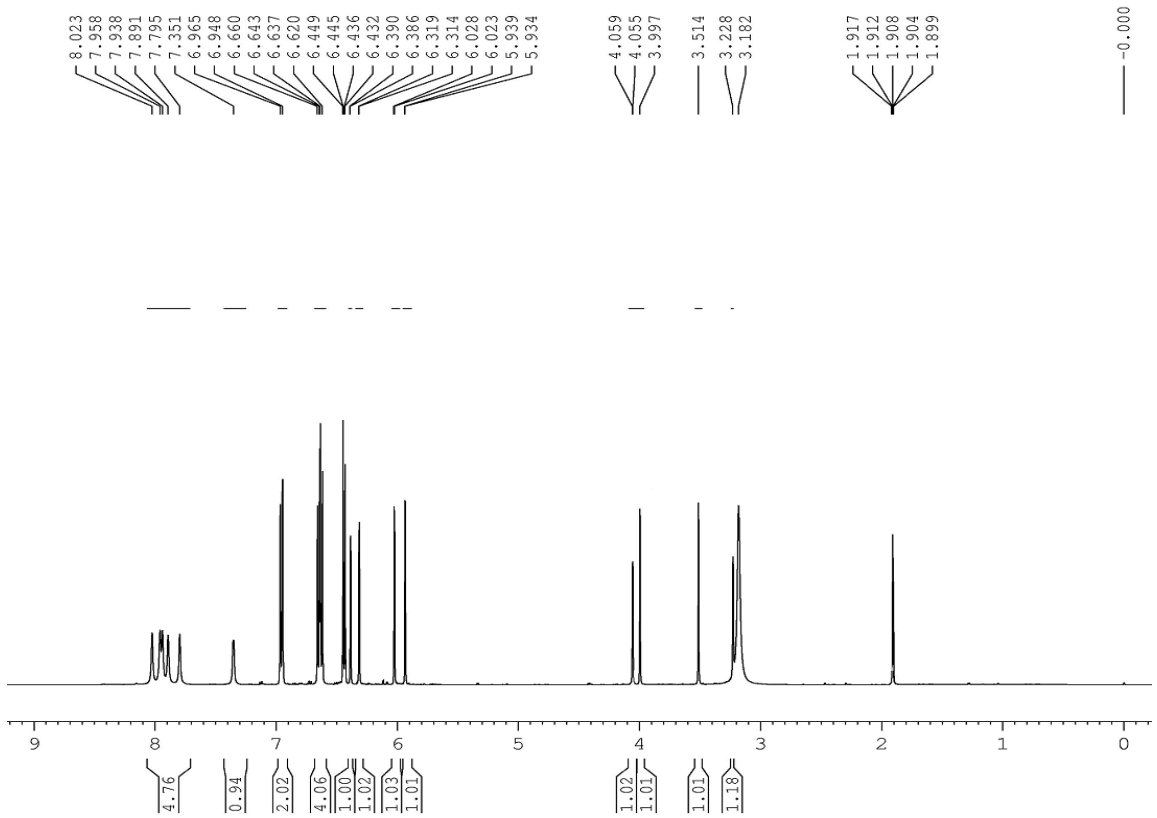

Figure 4A.14. ^{1}H NMR spectrum (500 MHz, Acetone-d_6) of (-) - ampelopsin F (**28**)

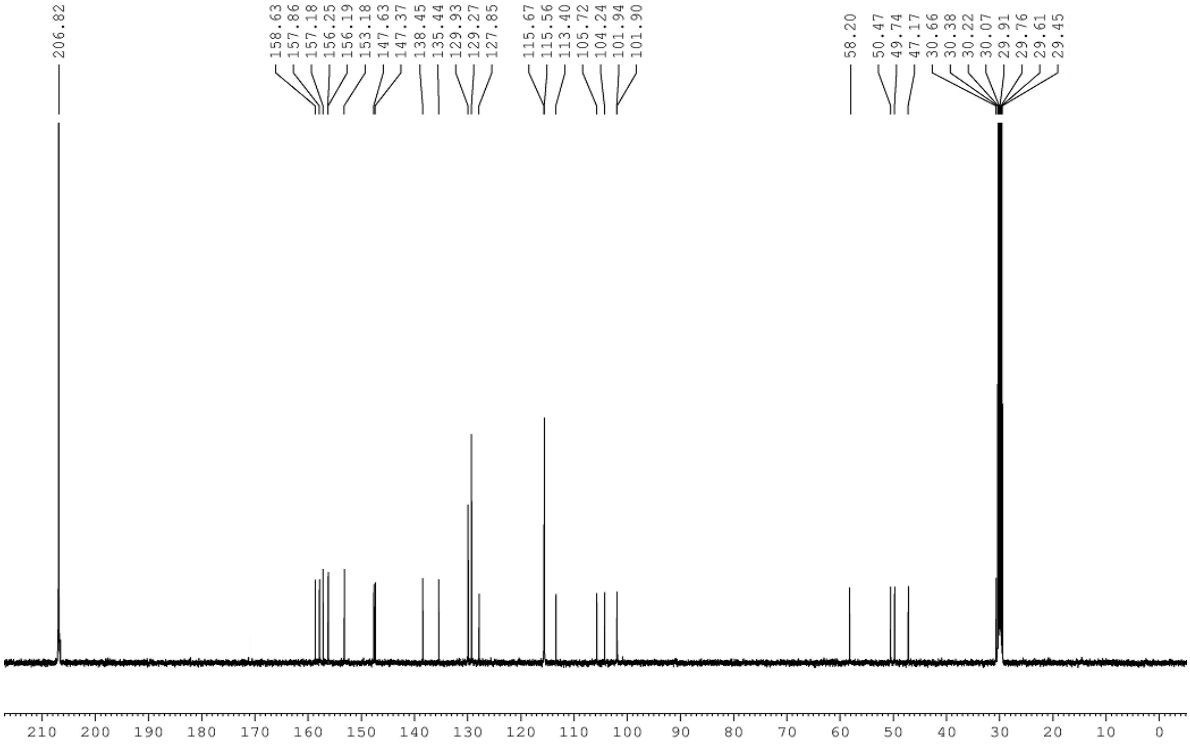

Figure 4A.15. ^{13}C NMR spectrum (125 MHz, Acetone-d_6) of (-) - ampelopsin F (**28**)

Compound **29**, obtained as a pale brown amorphous solid and its molecular formula was established as $C_{56}H_{44}O_{12}$ from HRESIMS (**Figure 4A.24**) together with NMR spectral data, indicating 35^o of unsaturation. The compound **29** exhibited specific rotation at $[\alpha]^{25}_D$: +73.8^o (*c* 0.4, DMSO). The assignments of the ^{1}H and ^{13}C NMR spectra of compound **29** in acetone-d_6 (**Table 4A.5**) were developed using DEPT, DQF COSY, and HMQC as well as HMBC experiments (**Figure 4A.17**- **Figure 4A.22**). The structure is composed of four resveratrol units, which include Res A-B (**1A**) and Res C–D (**1B**). The NMR and CD spectral details of **1A** is similar to (-)-ampelopsin F [Ito *et al.*, **2013**; Oshima *et al.*, **1993**]. The another dimeric unit, Res C-D (**1B**) consists of two 4-hydroxyphenyl groups (C_1 and D_1), a 3, 5-dioxygenated-1, 2-disubstituted benzene ring (C_2), a 3, 5- dihydroxyphenyl group (D_2), and a set of four aliphatic methine protons [CH(7c) – CH(8c)–CH(7d)–CH(8d)]. The stereocentre protons resonated at δ_H 3.93 (7a), 3.63 (8a), 4.27 (7b), 3.58 (8b), 4.35 (7c), 4.99 (8c), 3.40 (7d) & 4.09 (8d) ppm. The stereocentre carbons resonated at δ_C 63.6 (7d), 59.0 (8d), 55.4 (7c), 55.1 (8a), 54.3 (8c), 50.9 (8b), 51.0 (7a) & 45.5 (7b) ppm. In the DQF COSY spectrum, there is a notable correlation observed between the protons 8a/7a/8b/7b and 7c/8c/7d/8d. The connection of the partial structures in **1B** was established by the HMBC correlations observed between H-7c/C-2c(6c), H-8c/C-9c, H-8c/C-10c, H-8c/C-8d, H-8c/C-1d, H-7d/C- 8d, H-7d/C-2d(6d), H-8d/C-10c and H-8d/C-10d/14d, which deduced the 5 C–C bonds C-1c–C-7c, C-8c–C-9c, C-1d–C-7d, C-8d–C-10c, and C-8d–C-9d. The significant correlations observed between H-7c/C-14b, H-7c/C-9b and H-7c/C-13b, which indicates that connection of **1B** and (-)-ampelopsin F (**1A)** [Ito *et al.*, **2016**]. The relative configuration of **1B** was determined by NOESY (**Figure 4A.23**) experiment and analysis of coupling constants. The *J* value for H-7c/H-8c (11 Hz) indicated *trans* orientation for them. In the NOESY spectrum, there is an intense correlation between protons at H-7c/ H-7d/ H-8d. The *cis* stereochemistry of the vicinal methine protons H-7d and H-8d on the indane ring was confirmed on the basis of *J* value (6.5 Hz) and NOEs H-7d and H-8d. Also, there is no notable enhancement in stereocentre protons at H-8c/H-8d and H-8c/H-7d indicates that proton at 8c is in *trans* orientation with respect to protons at H-7d/H-8d . The CD spectrum of compound **29** (**Figure 4A.25**) displayed an enhanced intensity of the negative cotton signal in the region of 218-245 nm, whereas vaticanol L showed a signal at 220-240 nm [Ito *et al*., **2016**] expected due to the difference in the *cis* stereochemistry of protons at 8d with respect to 7d. The structure of the compound and the key HMBC

correlation is shown in **Figure 4A.16**. To the best of our knowledge, this molecule is being reported for the first time or can be considered as a novel molecule and named as vaticanol R.

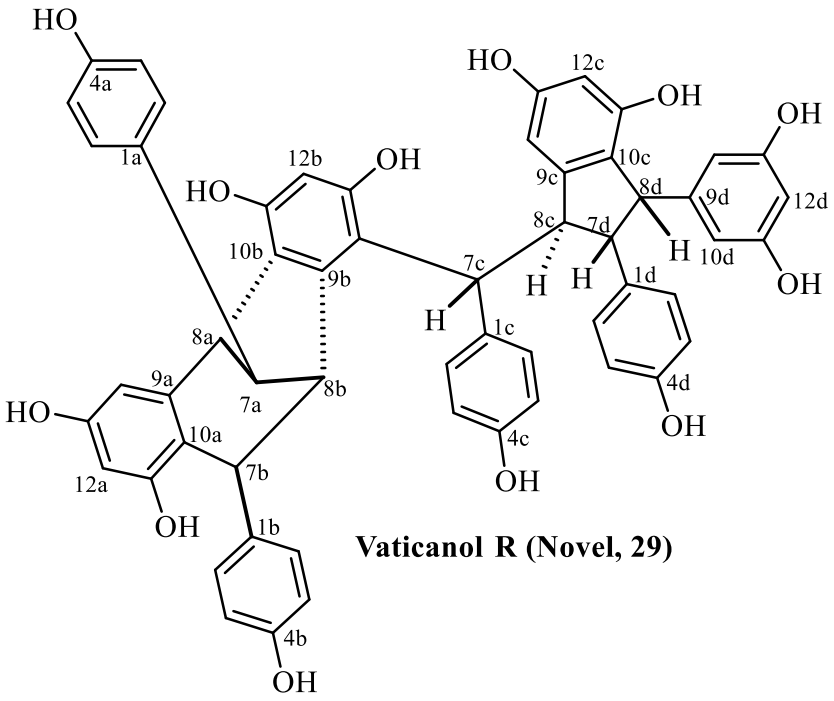

Vaticanol R (Novel, 29)

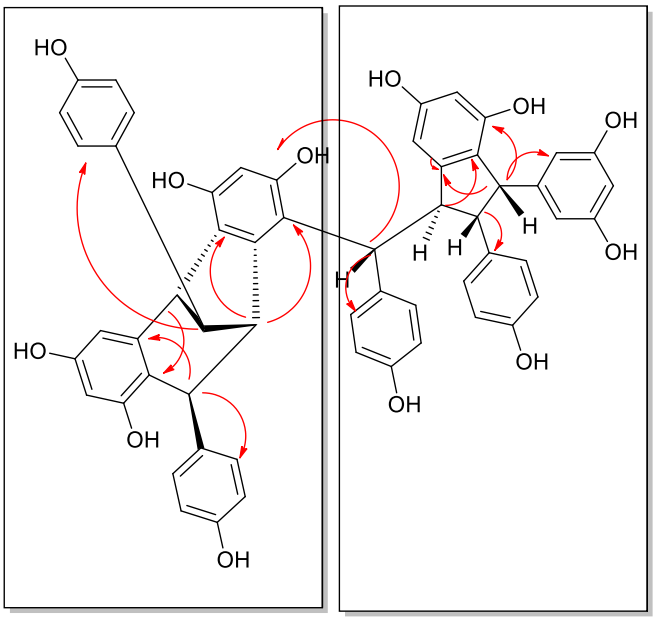

1A **1B**

Figure 4A.16. Structure and key HMBC correlations of vaticanol R (**29**)

Table 4A.5. The 1D and 2D NMR spectra of vaticanol R (Acetone-d_6)

Position	**^{13}C NMR**	**^{1}H NMR**	**HMBC (C → H)**
1a	135.1		
2a (6a)	115.5	6.32 (d, *J* = 8.5 Hz)	135.1, 51.0
3a (5a)	114.9	6.30 (d, *J* = 8.5 Hz)	115.5, 135.1
4a	155.8		
7a	51.0	3.93 (s, 1H)	50.9. 55.1, 106.6, 113.0, 126.8, 135.1, 145.0
8a	55.1	3.63 (s, 1H)	51.0, 113.0, 129.3, 135.1, 145.0, 148.4
9a	148.4		
10a	113.0		
11a	158.4		
12a	105.89	5.52 (s, *J* = 1.5 Hz)	55.1, 158.4
13a	155.4		
14a	105.9	6.44 (d, *J* = 2.5 Hz)	50.9, 113.0
1b	137.4		
2b (6b)	130.1	7.07 (d, *J* = 8.5 Hz)	116.2, 157.2, 45.5
3b (5b)	116.2	6.80 (d, *J* = 8.5 Hz)	137.4
4b	157.2		
7b	45.5	4.27 (s)	113.0, 130.1, 137.4, 145.0, 148.4, 158.4
8b	50.9	3.58 (s)	126.8, 135.1, 145.0, 147.7, 45.5
9b	145.0		
10b	126.8		
11b	151.1		
12b	102.1	5.68 (s)	119.5, 126.8, 151.1, 156.2
13b	156.2		
14b	119.5		

1c	138.1		
2c (6c)	131.4	7.37 (d, J = 8 Hz)	55.45, 156.5
3c (5c)	115.3	6.68 (d, J = 9 Hz)	156.5, 138.1
4c	156.5		
7c	55.45	4.35 (d, J = 11 Hz)	119.5, 131.4, 138.1, 145.0, 156.2, 54.3
8c	54.3	4.99 (dd, J_1 = 11 Hz, J_2 = 6 Hz)	122.2, 135.1, 138.1, 150.9, 55.47
9c	150.9		
10c	122.2		
11c	157.5		
12c	101.8	6.15 (d, J = 2.5 Hz)	157.5, 106.6
13c	154.5		
14c	106.6	6.21 (d, J = 1.5 Hz)	101.8, 122.2, 154.5
1d	135.1		
2d (6d)	129.3	6.59 (d, J = 8.5 Hz)	63.6, 130.1, 115.3 (w), 155.6
3d (5d)	115.3	6.30 (d, J = 8.5 Hz)	135.1
4d	155.6		
7d	63.6	3.40 (t)	129.3, 138.1, 59.0, 55.4, 129.3, 148.4
8d	59.0	4.09 (d, J = 6.5 Hz)	63.6, 107.3, 122.2, 138.1, 148.4
9d	148.4		
10d	107.3	6.20 (d, J = 1.5 Hz)	101.9, 122.2, 159.2, 59.0
11d	159.2		
12d	101.9	6.03 (t, J = 2 Hz)	
13d	159.2		
14d	107.3	6.20 (d, J = 1.5 Hz)	101.9, 122.2, 159.2, 59.0

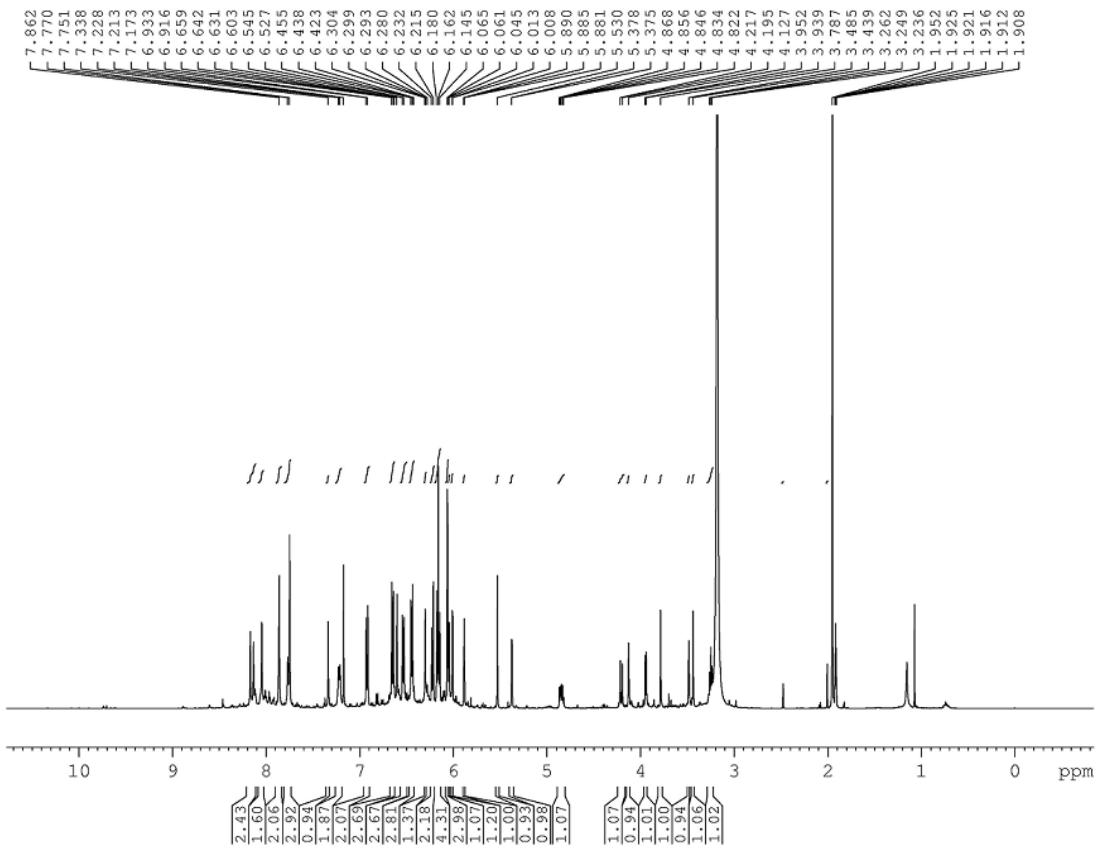

Figure 4A.17. ^{1}H NMR spectrum (500 MHz, Acetone-d_6) of vaticanol R (**29**)

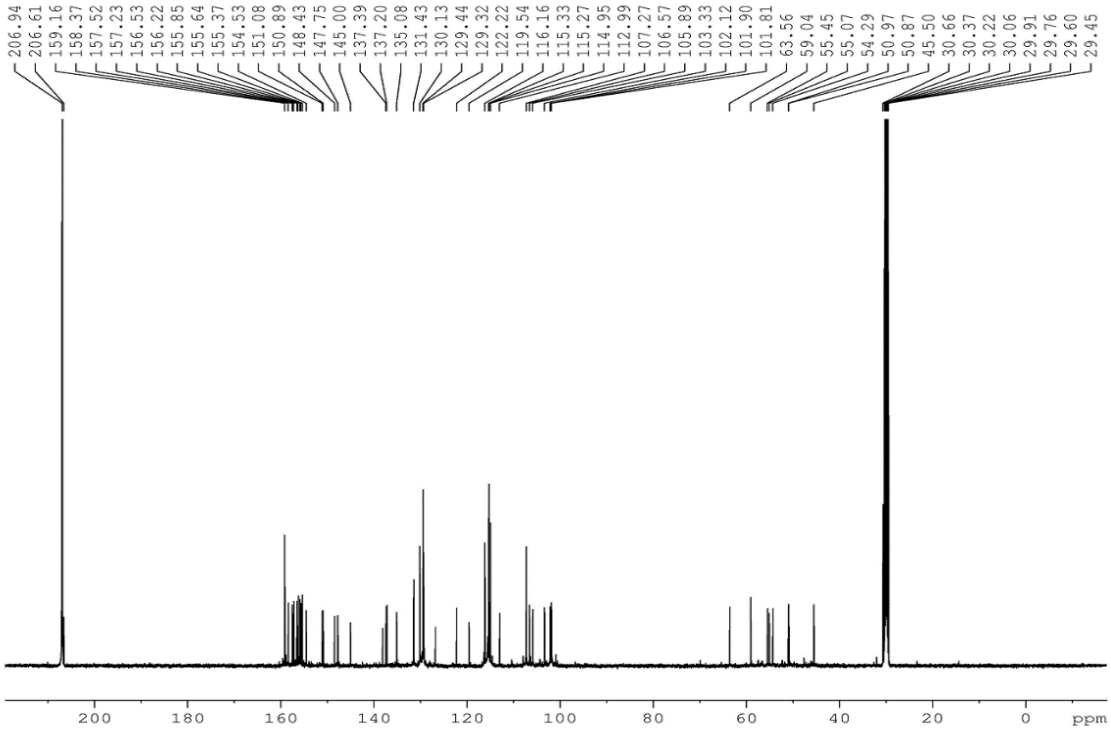

Figure 4A.18. ^{13}C NMR spectrum (125 MHz, Acetone-d_6) of vaticanol R (**29**)

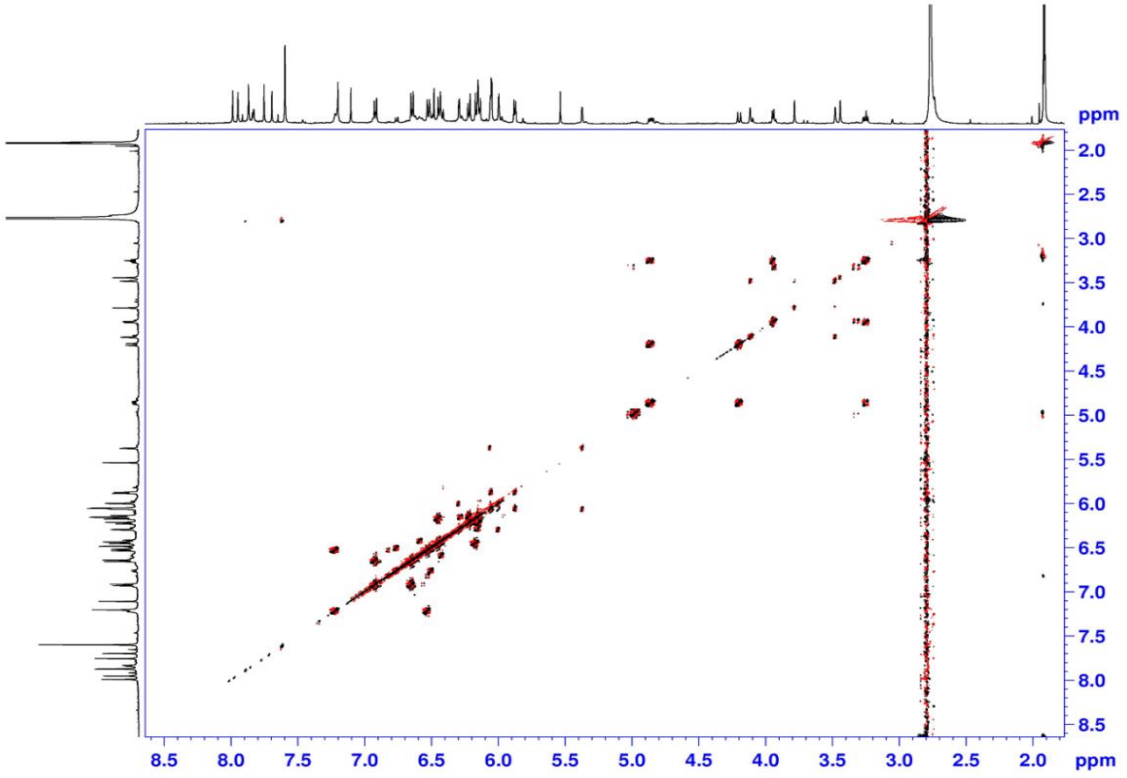

Figure 4A.19. DQF COSY NMR spectrum (500 MHz, Acetone-d_6) of vaticanol R (**29**)

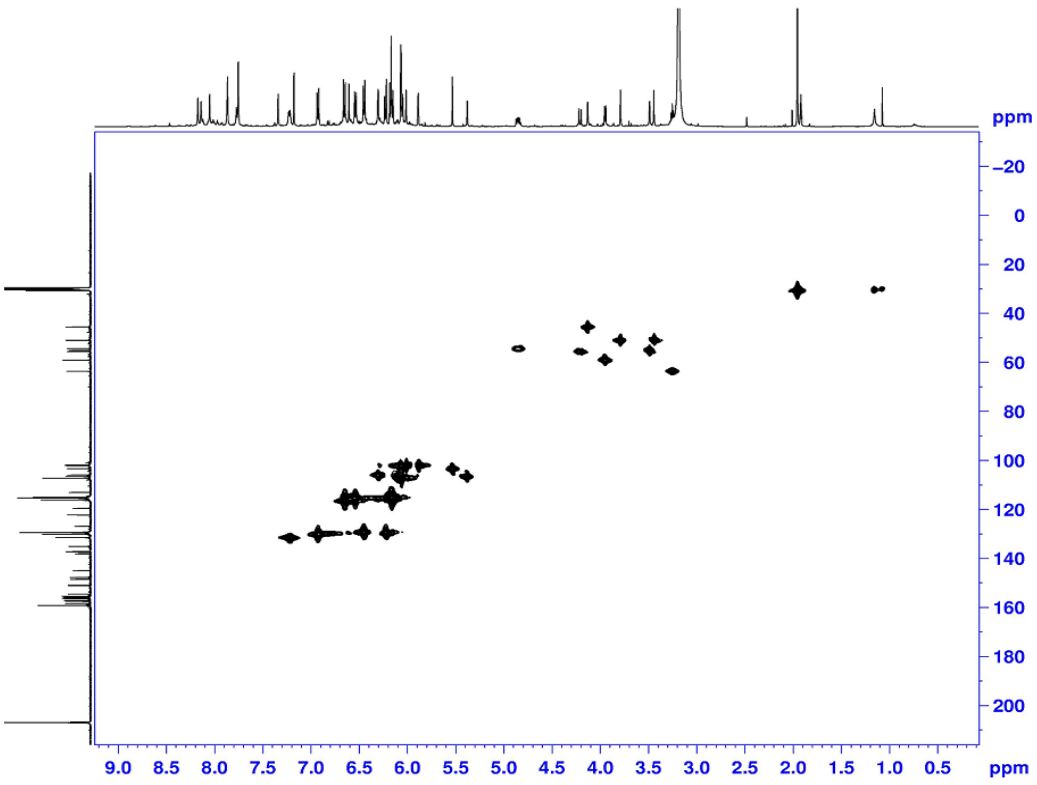

Figure 4A.20. HMQC NMR spectrum (125 MHz, Acetone-d_6) of vaticanol R (**29)**

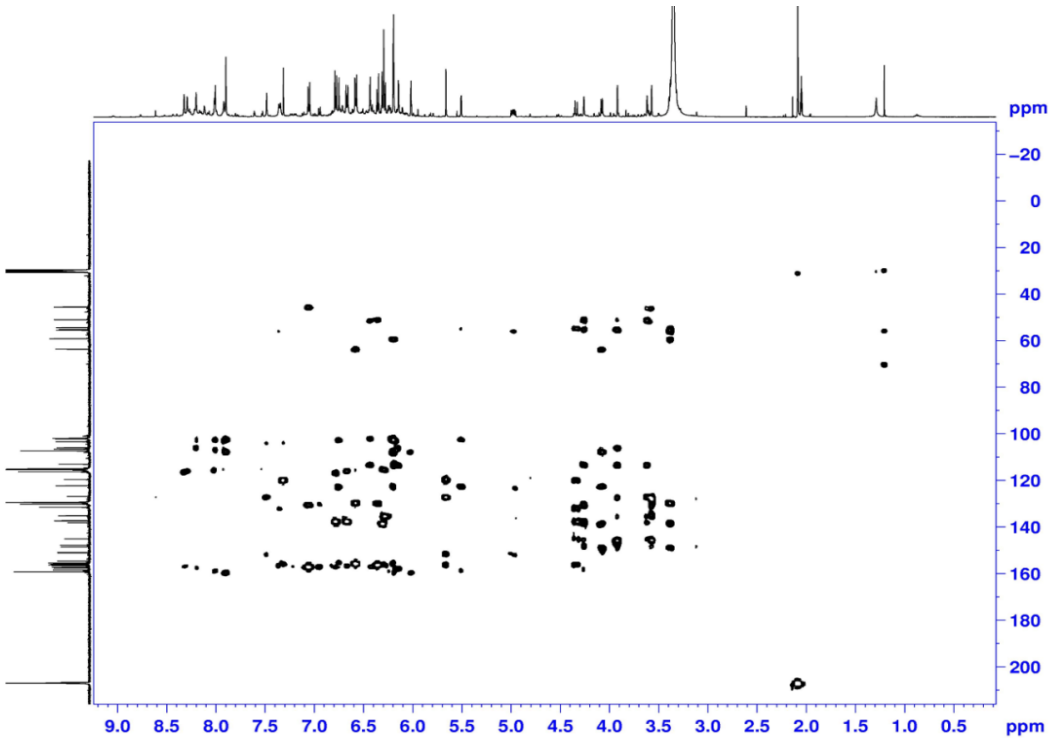

Figure 4A.21. HMBC NMR spectrum (125 MHz, Acetone-d_6) of vaticanol R (**3**)

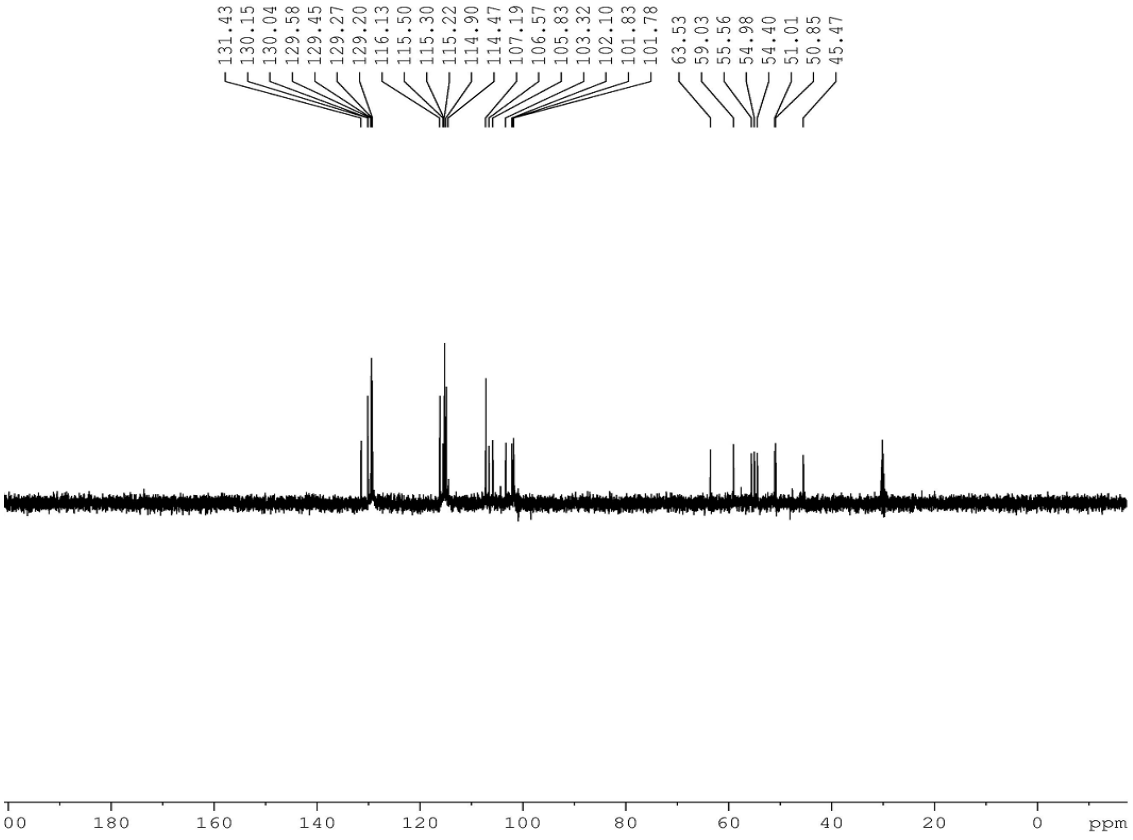

Figure 4A.22. DEPT 135 NMR spectrum (125 MHz, Acetone-d_6) of vaticanol R (**3**)

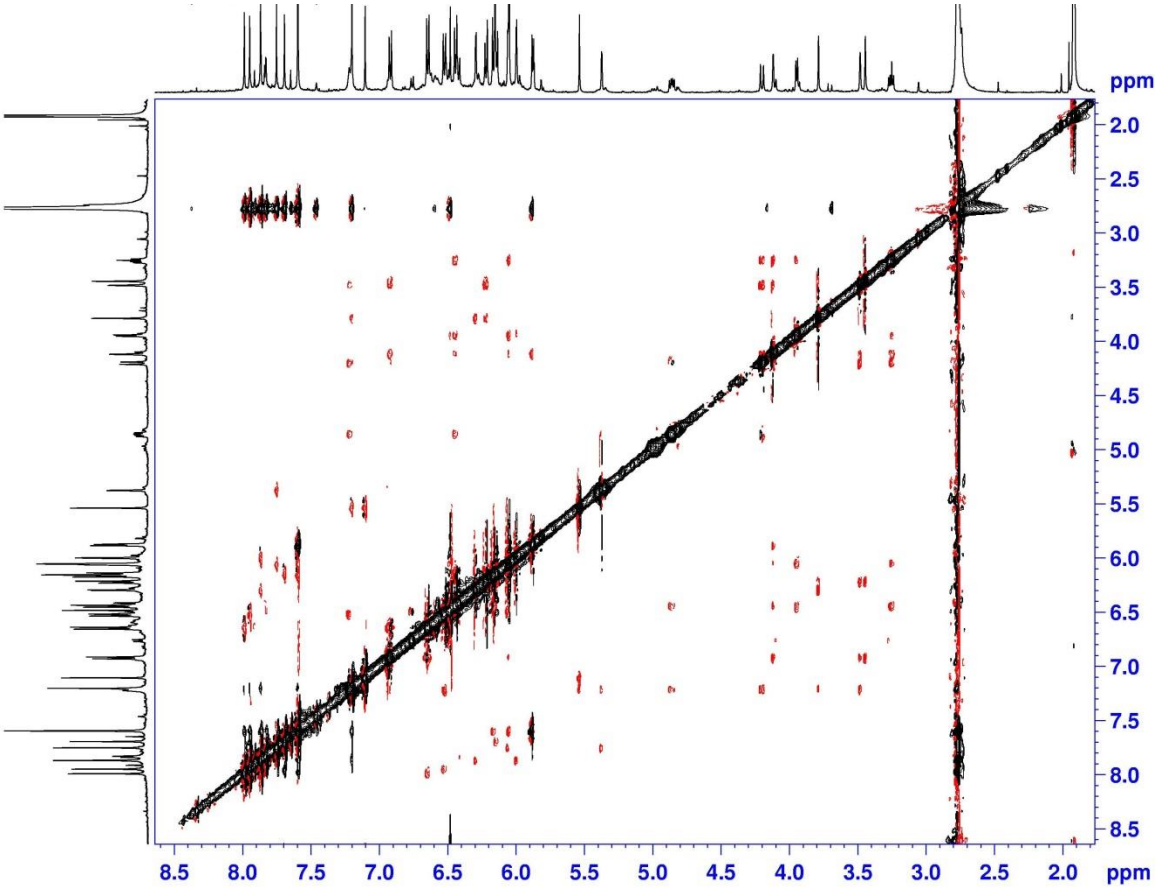

Figure 4A.23. NOESY spectrum (500 MHz, Acetone-d_6) of vaticanol R (**3**)

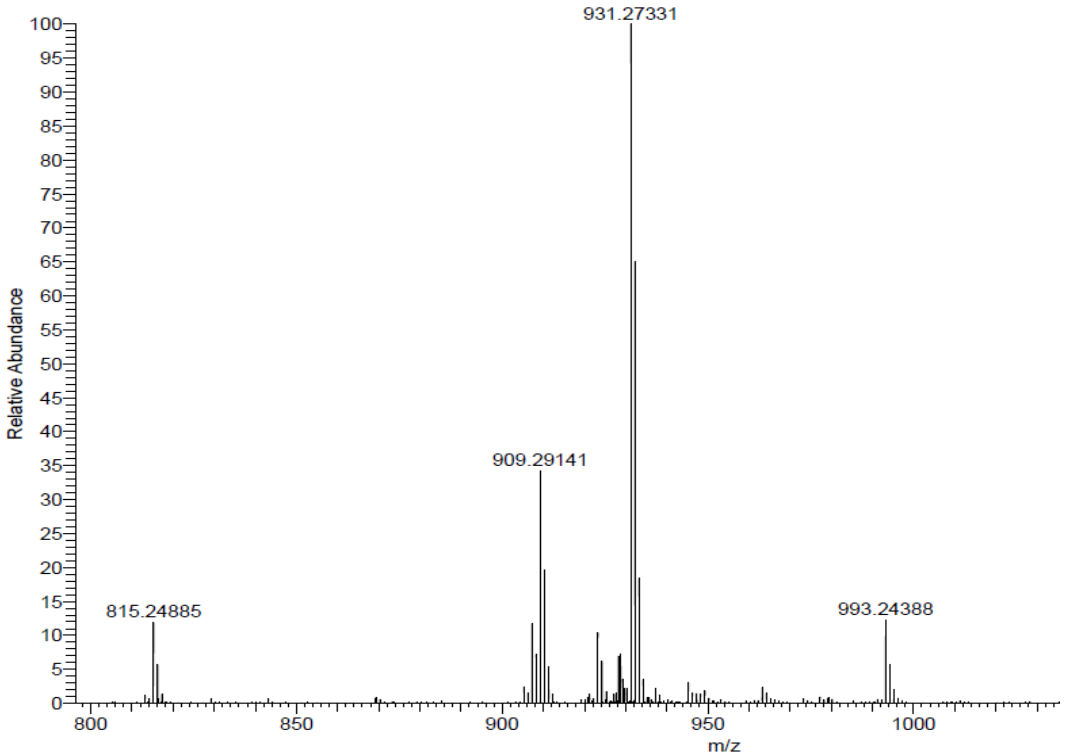

Figure 4A.24. HRESIMS spectrum of vaticanol R (**29**)

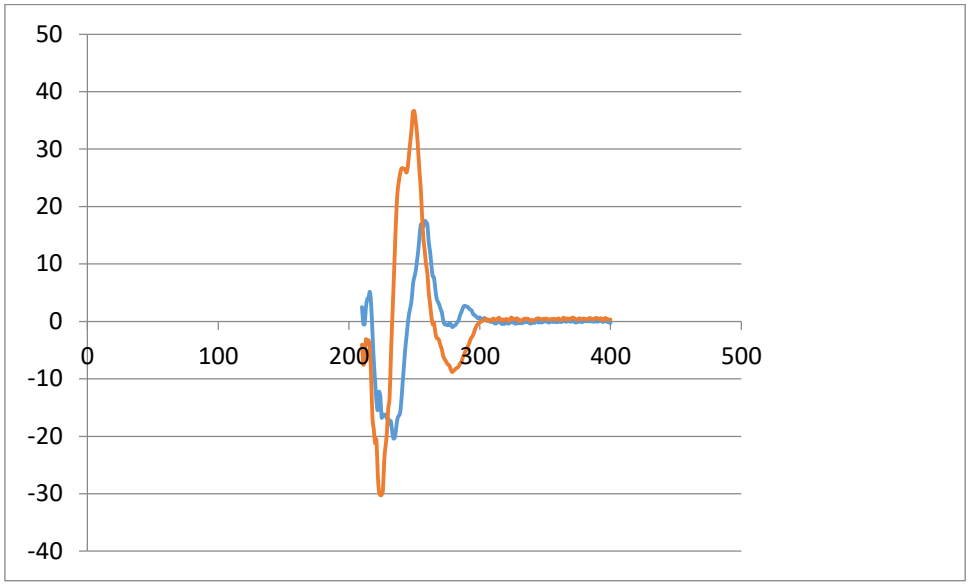

Figure 4A.25. CD spectrum of vaticanol R (**blue**) and (-)- ampelopsin F (**Orange**)

Compound **30** was isolated as brown amorphous solid and showed an $[M+Na]^+$ ion at m/z 931.2712 in positive HRESIMS, which is attributable to the molecular formula $C_{56}H_{42}O_{12}$. In the FTIR spectrum, a strong absorption band at 3366 cm^{-1} indicated the presence of several hydroxyl groups. The UV spectrum of compound **30** showed an absorption maxima at 284 nm, which is consistent with the presence of one or more substituted phenyl rings. The compound **30** showed specific rotation at $[\alpha]^{25}_D$ -28^o (*c* 01, MeOH). The assignments were made on the basis of ^1H, ^{13}C, ^1H-^1H COSY, HMQC, HMBC, NOE difference and NOESY experiments (**Figure 4A.26- 4A.32)**, **(Table 4A.6)**. The ^1H NMR spectrum of compound **30** exhibited eight *ortho*-coupled aromatic signals from four *p*-hydroxyphenyl groups at δ_H 6.52/6.41, 6.71/7.17, 6.79/7.24, and 6.79/7.20 ppm. They were correlated to the ^{13}C NMR signals at δ_C 129.3/115.9, 115.7/130.7, 116.1/128.3, and 116.0/130.3 ppm, respectively. The six signals for *meta*-coupled aromatic protons resonated at δ_H 6.31 (H-12a), 6.30 (H-12d), 6.10 (H-14a), 6.20 (H-12c), 6.48 (H-14c), and 6.13 (H-10d and H-14d) ppm respectively. In the ^{13}C NMR spectrum the *meta*-coupled aromatic protons resonated at δ_C 101.7, 102.2, 105.8, 96.5, 95.7, 106.1, and 107.6 ppm, respectively. The four aliphatic methine groups resonated at δ_H 4.45/5.78 and 4.69/5.38 ppm were correlated to the ^{13}C NMR resonated at δ_C 48.9/90.5 and 57.6/94.7 ppm and were credited to two diaryldihydrobenzofuran moieties. Another four aliphatic methine groups at δ_H 5.21/3.13 and 4.10/4.56 ppm were connected to the ^{13}C NMR resonances at δ_C 37.9/53.2 and 53.2/49.3 ppm and were attributed to two diaryldihydrobenzofuran moieties. The relative stereochemistry of compound **30** was

proposed on the basis of the NOESY NMR spectrum. The H-7b signal at δ_H 5.21 ppm displayed a cross-peak with H-8b at δ_H 3.13 ppm, indicating a *cis* orientation for these two protons. The small coupling constant of 3.5 Hz also supported the *cis* configuration of 7b and 8b. The signals for H-8b and H-7c at δ_H 3.13 (brd, J = 11 Hz, 1H) and 4.11 (t, J = 11.5 and 11 Hz, 1H) ppm respectively, supporting their *trans* configuration. The protons 7c and 8c (J = 11.5 Hz) were also assigned as *trans* configuration. Further evidence was supported by the NOESY (**Figure 4A.32**) correlation between H-7c and H-14c, indicating β orientation of the ring C2. Ring D2 having an α orientation by the NOESY correlation observed between H-8c and H-10d(14d). The vicinal coupled aliphatic protons [H-7a (δ_H 5.76, d, J = 11.0 Hz, 1H)/H-8a (δ_H 4.43, d, J =11.0 Hz, 1H) and H-7d (δ_H 5.37, d, J = 5.5 Hz, 1H)/H-8d (δ_H 4.68, d, J = 5.5 Hz, 1H)] from the two diaryldihydrobenzofuran rings were assigned as *trans* since the NOESY spectrum showed correlations of H-8a/H-2a(6a), H-7d/H-10d(14d), and H-8d/H-2d (6d). The large coupling constant of 11.0 Hz for H-7a/H-8a results from adjacent to a seven-membered ring. The coupling constant of 5.5 Hz for H-7d and H-8d (5.5 Hz) was typical for the *trans* protons in a diaryl-dihydrobenzofuran ring not connected to another ring. The key HMBC and NOESY correlations are shown in **Figure 4A.33**. Based on the complete analysis of 1D and 2D NMR spectrum and previous literature reports [Eun-Kyoun, *et al*., **1999**], the structure of the compound **30** is shown below and the key ^{1}H-^{1}H COSY, HMBC and NOESY correlations are shown in **Figure 4A.25**.

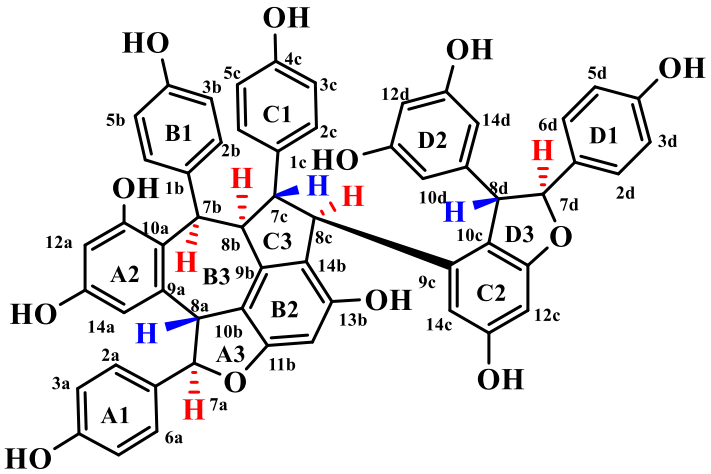

Vaticaphenol A (30)

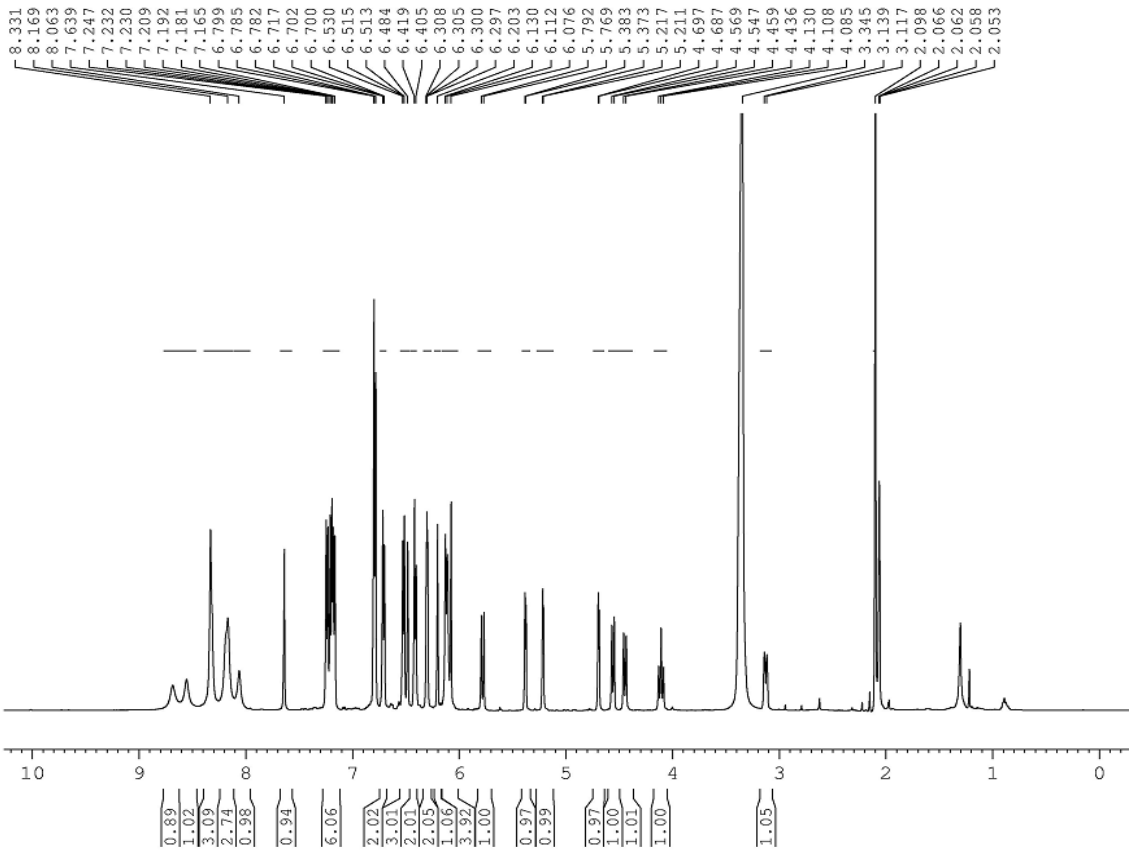

Figure 4A.26. ^{1}H NMR spectrum (500 MHz, Acetone-d_6) of vaticaphenol A (**30**)

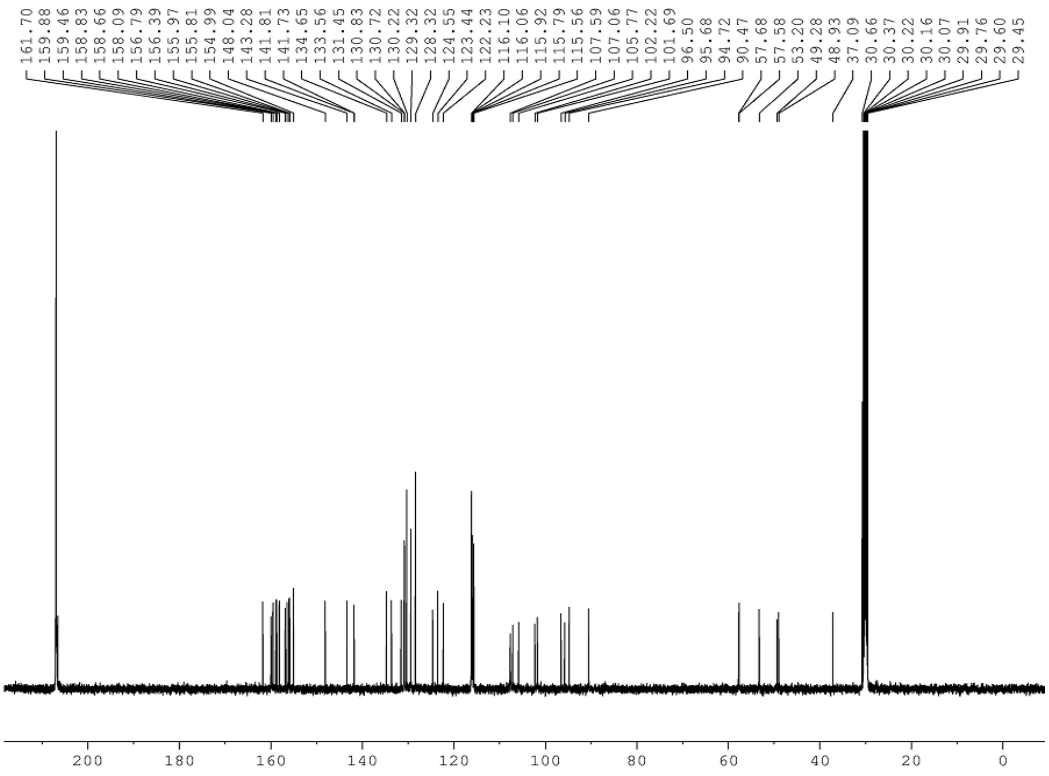

Figure 4A.27. ^{13}C NMR spectrum (125 MHz, Acetone-d_6) of vaticaphenol A (**30**)

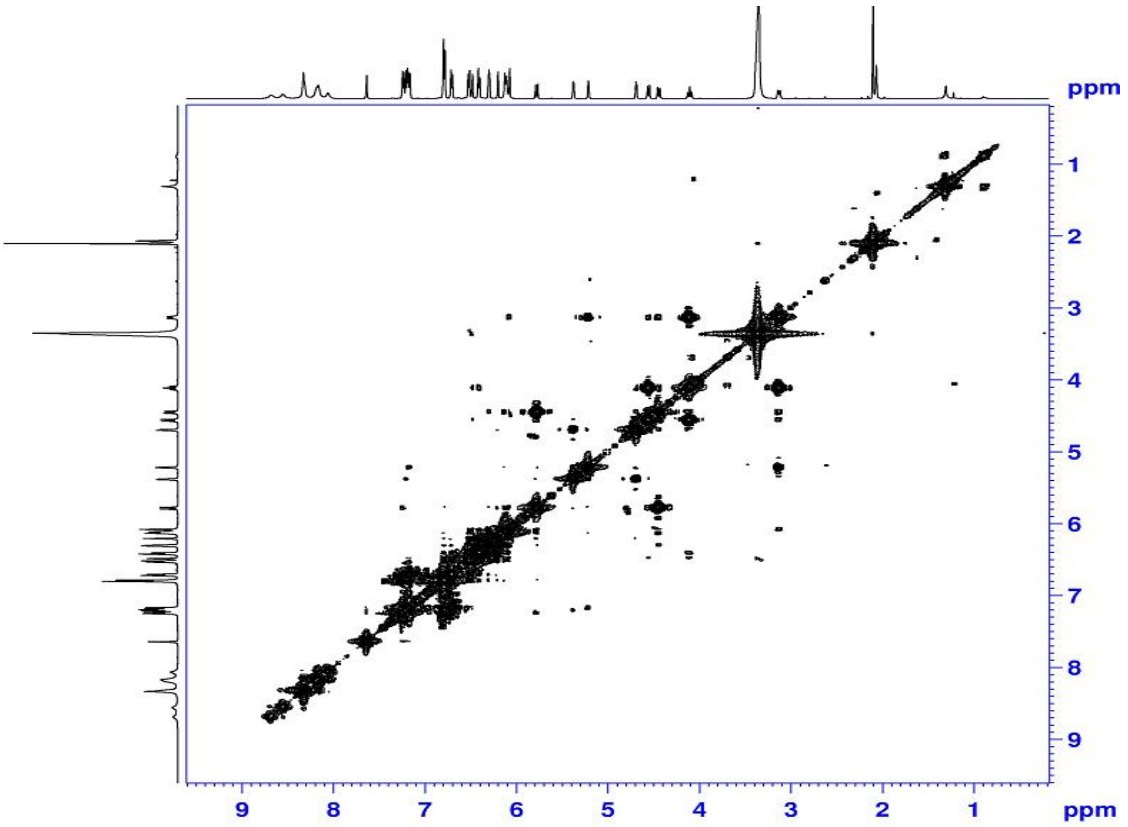

Figure 4A.28. ^{1}H-^{1}H COSY NMR spectrum (500 MHz, Acetone-d_6) of vaticaphenol A (**30**)

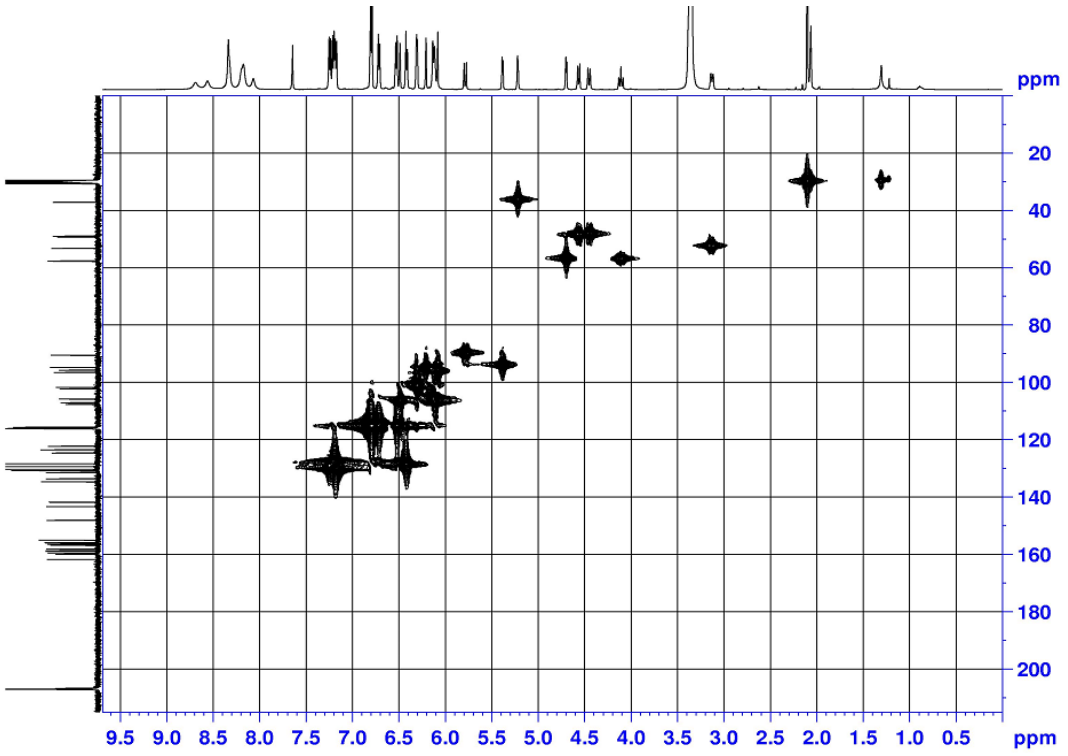

Figure 4A.29. HMQC NMR spectrum (125 MHz, Acetone-d_6) of vaticaphenol A (**30**)

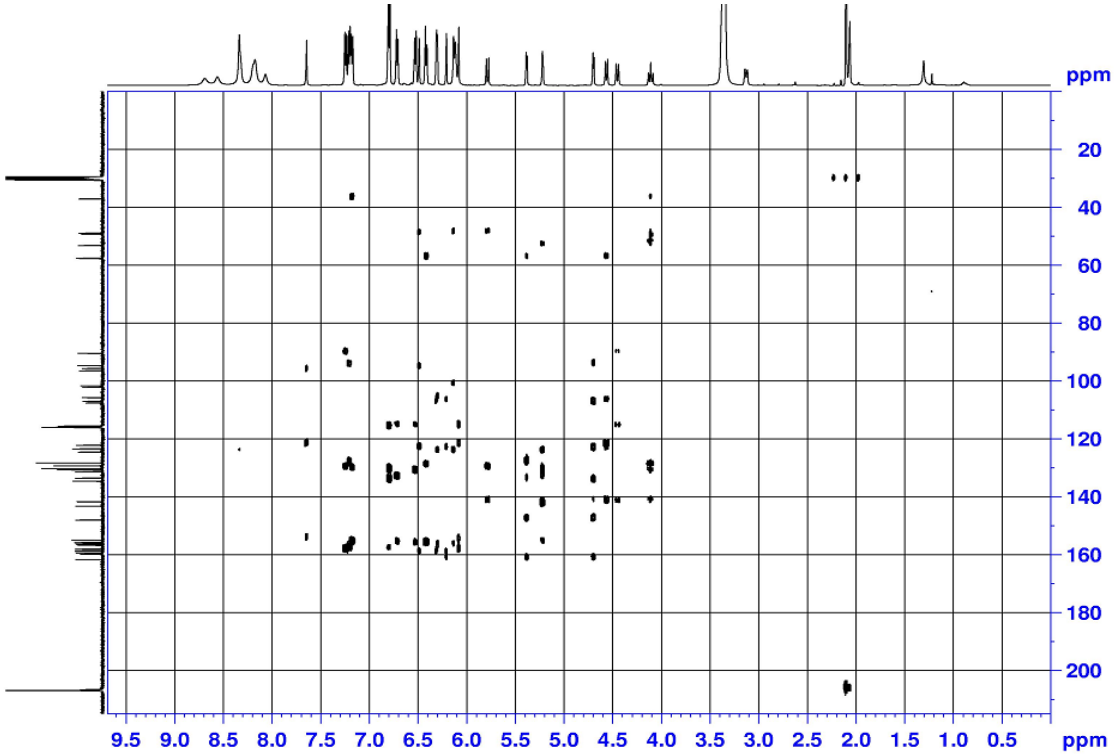

Figure 4A.30. HMBC NMR spectrum (125 MHz, Acetone-d_6) of vaticaphenol A (**30**)

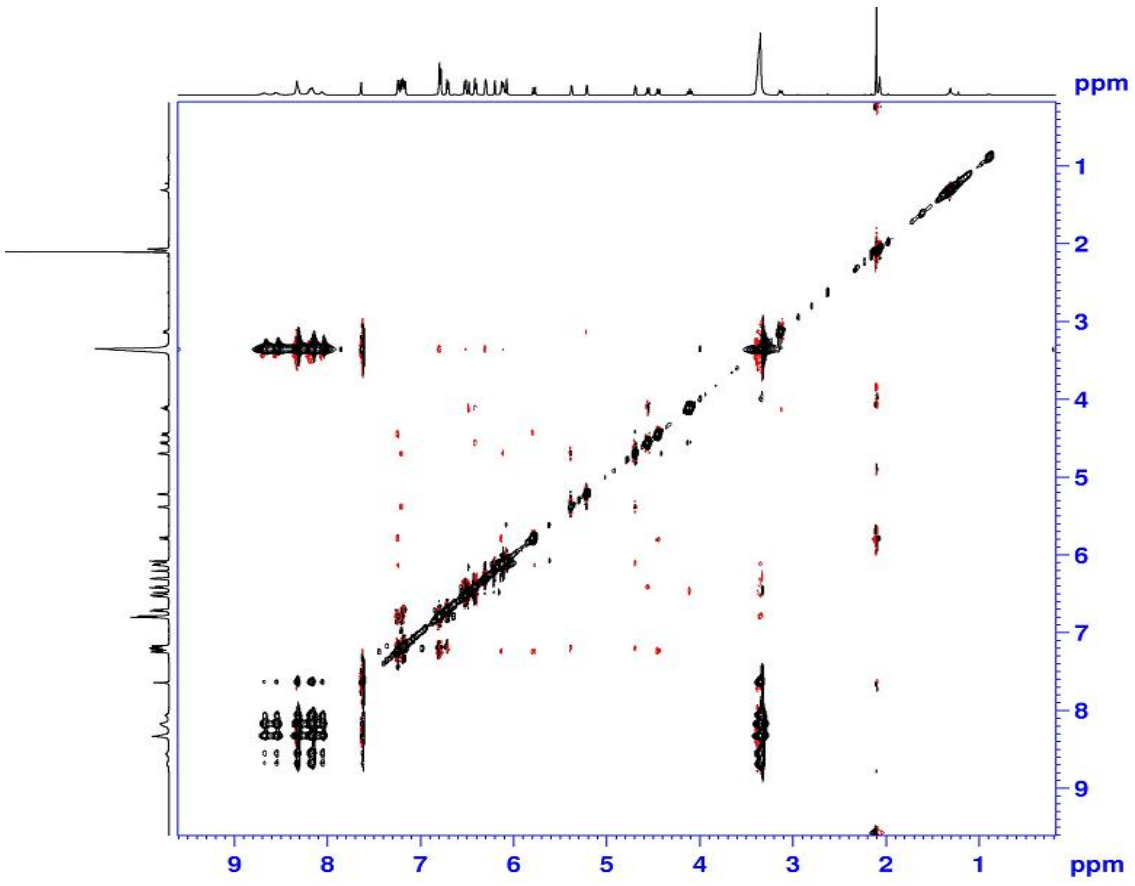

Figure 4A.31. NOESY NMR spectrum (500 MHz, Acetone-d_6) of vaticaphenol A (**30**)

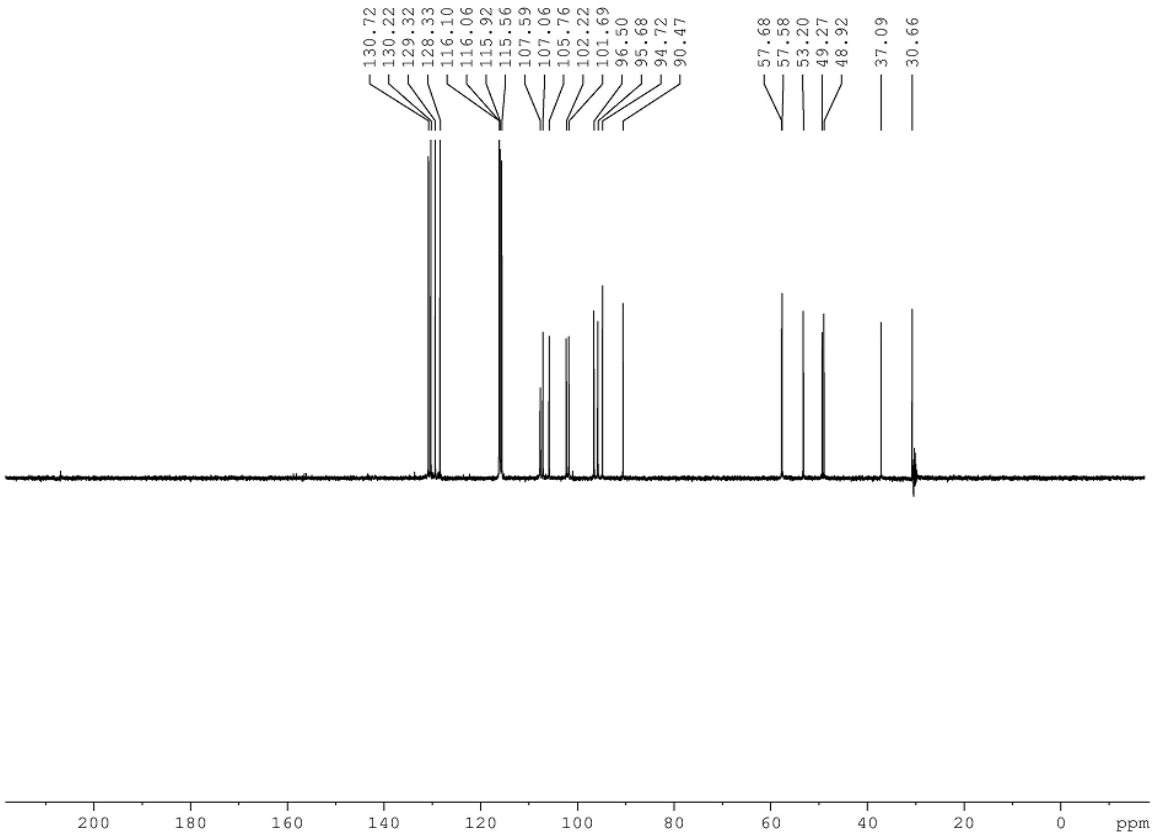

Figure 4A.32. DEPT 135 NMR spectrum (125 MHz, Acetone-d_6) of vaticaphenol A (**30**)

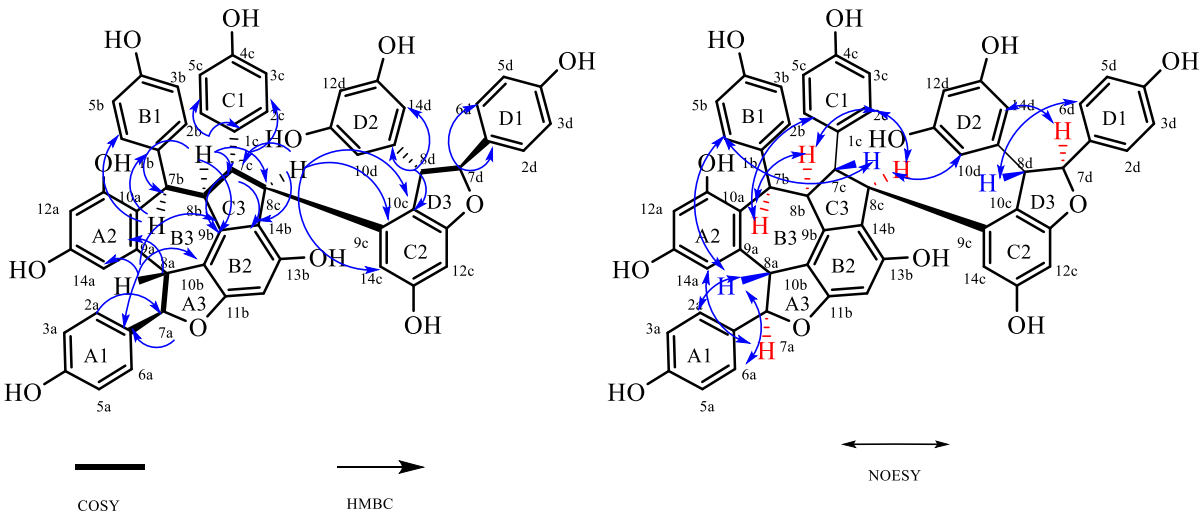

Figure 4A.33. Key ^{1}H-^{1}H COSY, HMBC and NOESY correlations of vaticaphenol A (**30**)

Table 4A.6. The ^{1}H and ^{13}C NMR data of vaticaphenol A (Acetone-d_6)

No.	^{13}C NMR	^{1}H NMR
1a	130.7	-
2a (6a)	130.1	7.22 (d, J = 8.5 Hz)
3a (5a)	115.9	6.78 (d, J = 8.5 Hz)
4a	158.6	-
7a	90.5	5.76 (d, J = 11.0 Hz)
8a	48.9	4.43 (d, J = 11.0 Hz)
9a	141.7	-
10a	124.4	-
11a	155.6	-
12a	101.7	6.27 (d, J = 2.0 Hz)
13a	156.6	
14a	105.7	6.44 (d, J = 2.5 Hz)
1b	133.4	
2b (6b)	130.6	7.16 (d, J = 8.5 Hz)
3b (5b)	115.9	6.96 (d, J = 8.5 Hz)
4b	155.8	
7b	37.1	5.20 (t. 3.2 Hz)
8b	53.2	3.13 (d, J = 11 Hz)
9b	143.1	-
10b	115.6	-
11b	158.8	-
12b	96.4	6.04 (s)
13b	154.8	-
14b	122.1	-
1c	131.3	-
2c (6c)	129.2	6.40 (d, J = 8.5 Hz)
3c (5c)	115.8	6.50 (d, J = 8.5 Hz)
4c	156.5	-

7c	57.7	4.09 (t, J = 11 Hz)
8c	49.3	4.55 (d, J = 11 Hz)
9c	141.6	-
10c	123.3	-
11c	161.7	-
12c	95.7	6.19 (d, J = 2.5 Hz)
13c	159.9	-
14c	107.1	6.47 (d, J = 1.5 Hz)
1d	134.5	-
2d (6d)	128.2	7.19 (d, J = 8.5 Hz)
3d (5d)	116.0	6.67 (d, J = 8.5 Hz)
4d	158.1	-
7d	94.7	5.37 (d, J = 5.5 Hz)
8d	57.6	4.68 (d, J = 5.5 Hz)
9d	147.9	-
10d (14d)	107.6	6.10 (brs)
11d	159.5	-
12d	102.2	6.28 (t, J = 2.5 Hz)

Compound **31** was obtained as a pale yellow amorphous solid. The molecular formula was established from the HRESIMS data [$C_{84}H_{64}O_{18}$, m/z 1361.4183 calcd for $[M+H]^+$ 1361.4165]. The compound **31** exhibited specific rotation at $[\alpha]^{25}_D$ +19^o (*c* 0.1, MeOH). The ^{1}H NMR spectra of compound **31** exhibited broad signals in the whole region due to unstable conformation at ambient temperatures. The doublet at δ_H 3.04 (d, J = 8 Hz) ppm is due to the presence of proton at the position 8b. The singlet at the position 7f resonated at δ_H 3.17 ppm. Other stereocentre protons resonated at the range δ_H 4.02 - 5.59 ppm. The stereocentre carbons resonated at the range δ_C 36.8- 97.7 ppm. The 1D and 2D NMR spectra are shown in **Figure 4A.34-4A.40.** Based on the complete analysis of all spectral data and in comparison with literature reports [Ito *et al*., **2016]** the structure of the compound is shown below.

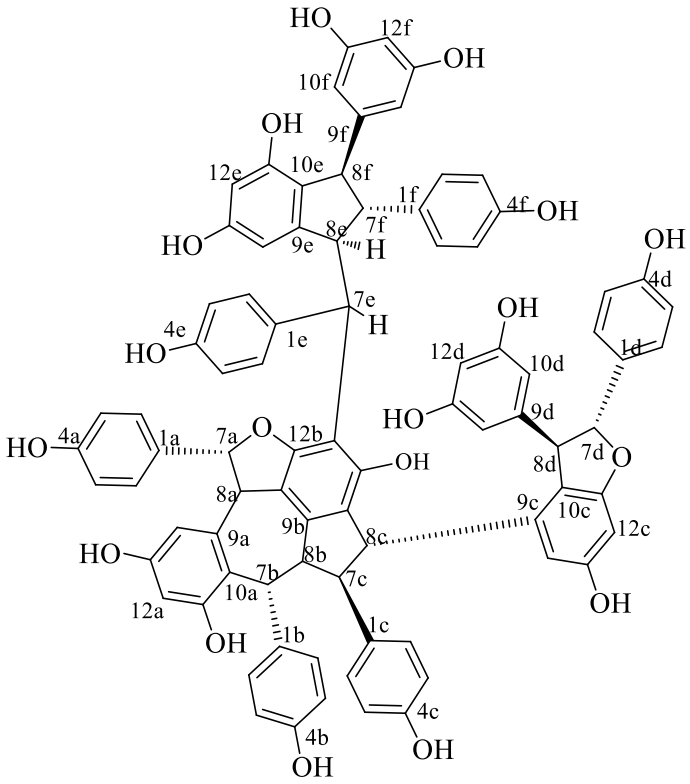

Vaticanol M (31)

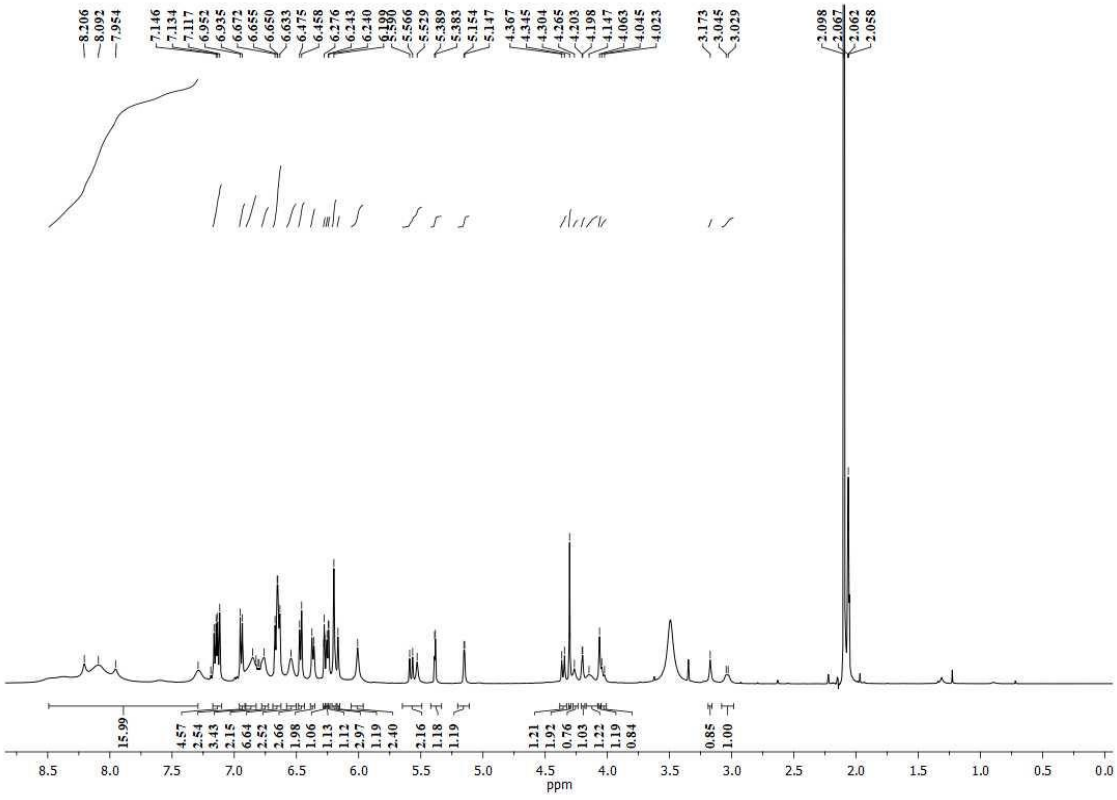

Figure 4A.34. ^{1}H NMR spectrum (500 MHz, Acetone-d_6) of vaticanol M (**31**)

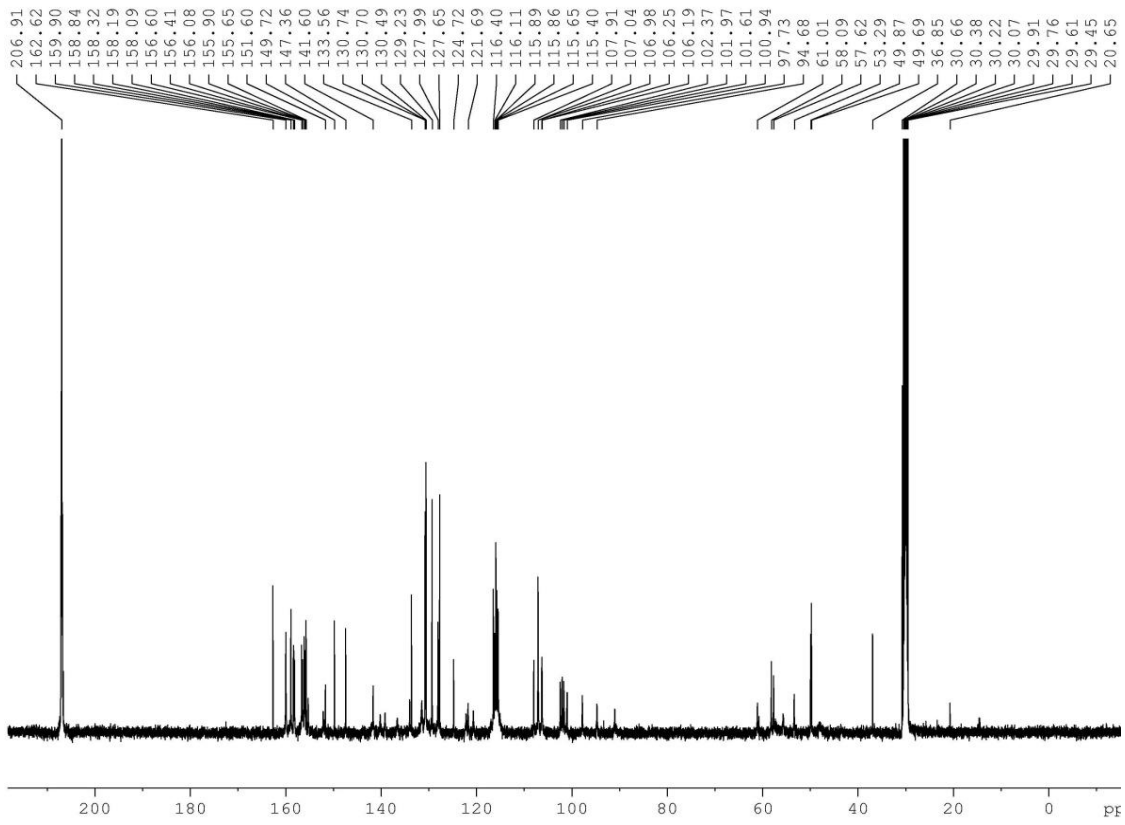

Figure 4A.35. ^{13}C NMR spectrum (125 MHz, Acetone-d_6) of vaticanol M (**31**)

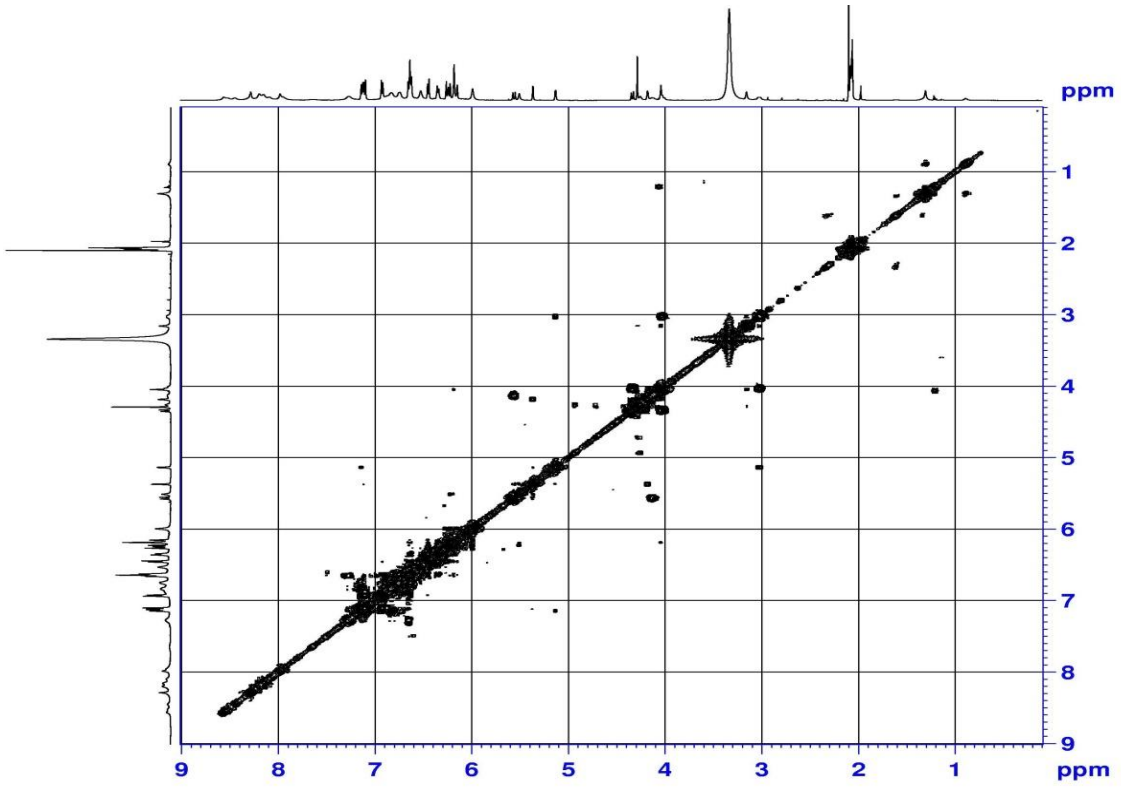

Figure 4A.36. ^{1}H-^{1}H COSY NMR spectrum (500 MHz, Acetone-d_6) of vaticanol M (**31**)

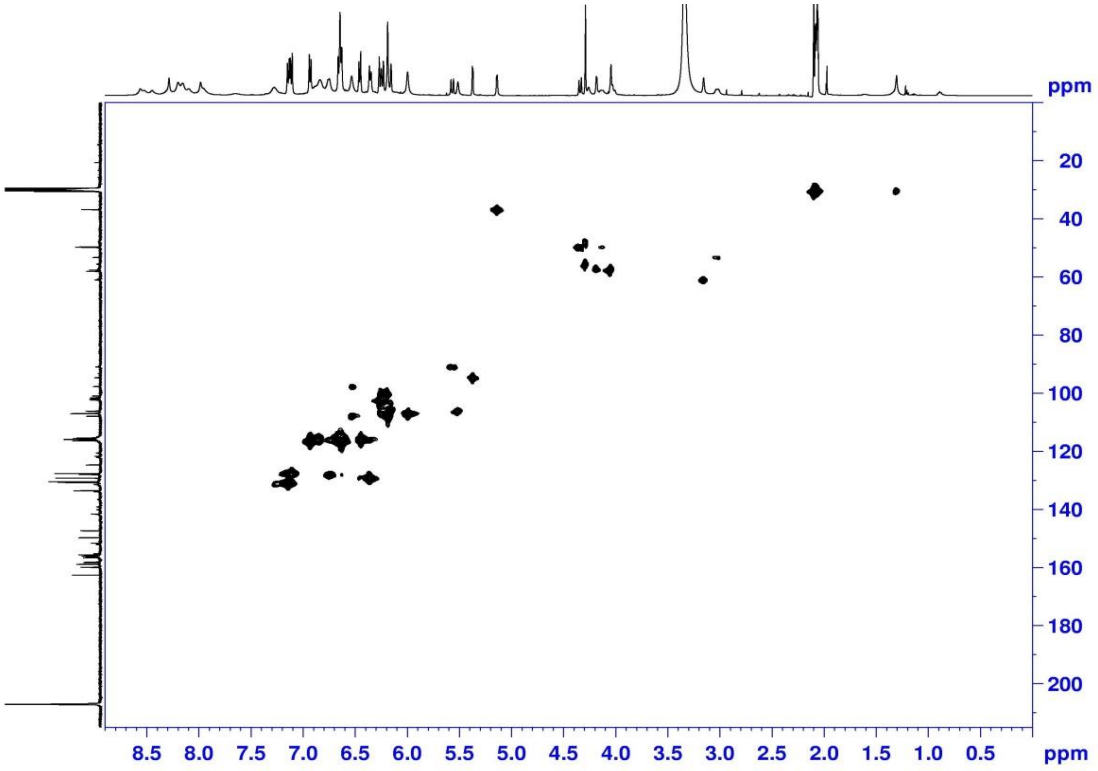

Figure 4A.37. HMQC NMR spectrum (125 MHz, Acetone-d_6) of vaticanol M (**31**)

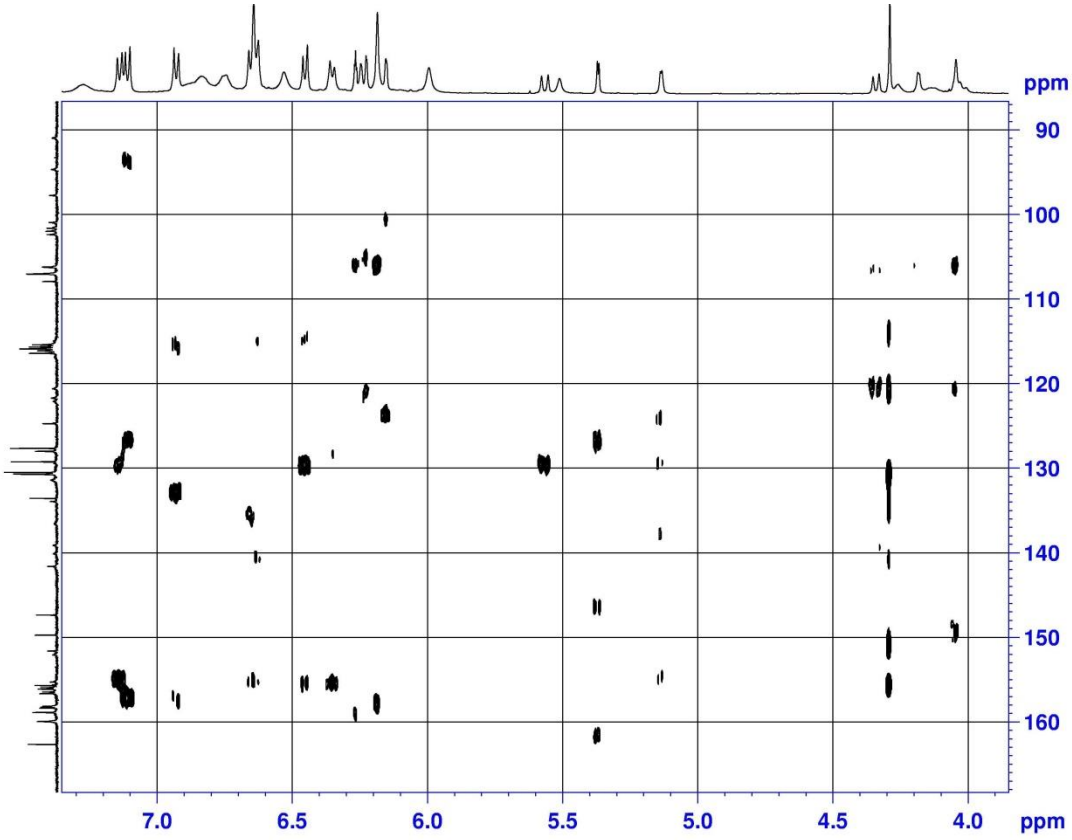

Figure 4A.38. HMBC NMR spectrum (125 MHz, Acetone-d_6) of vaticanol M (**31**)

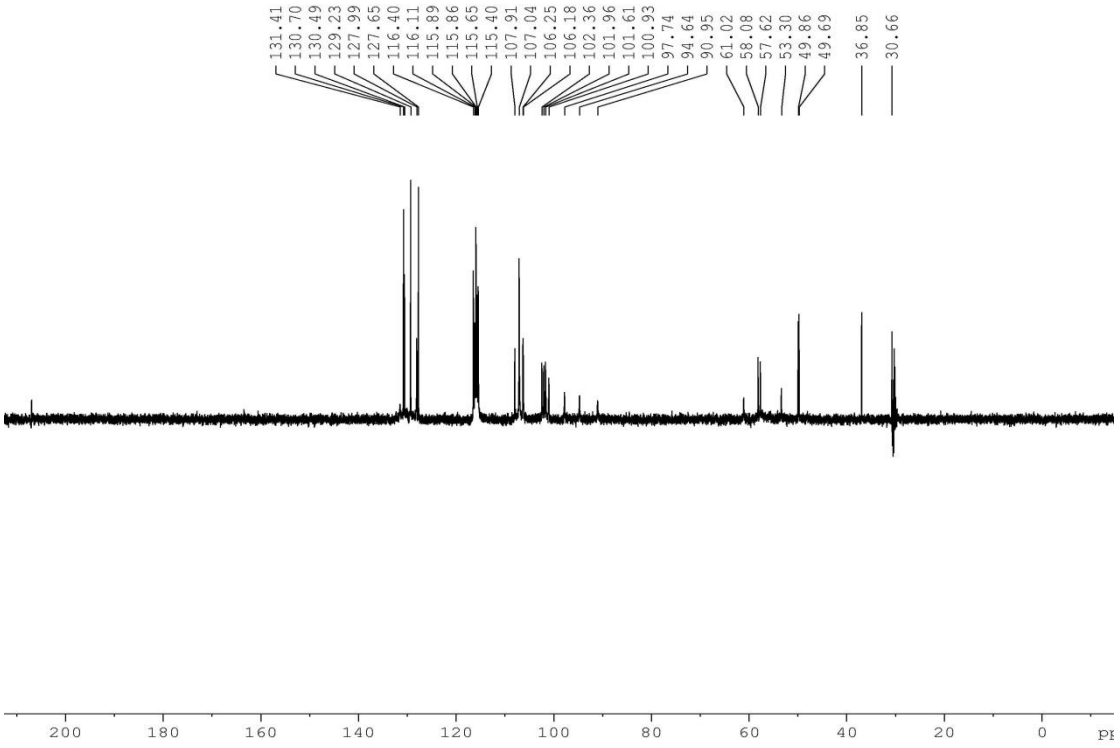

Figure 4A.39. DEPT 135 spectrum (125 MHz, Acetone-d_6) of vaticanol M (**31**)

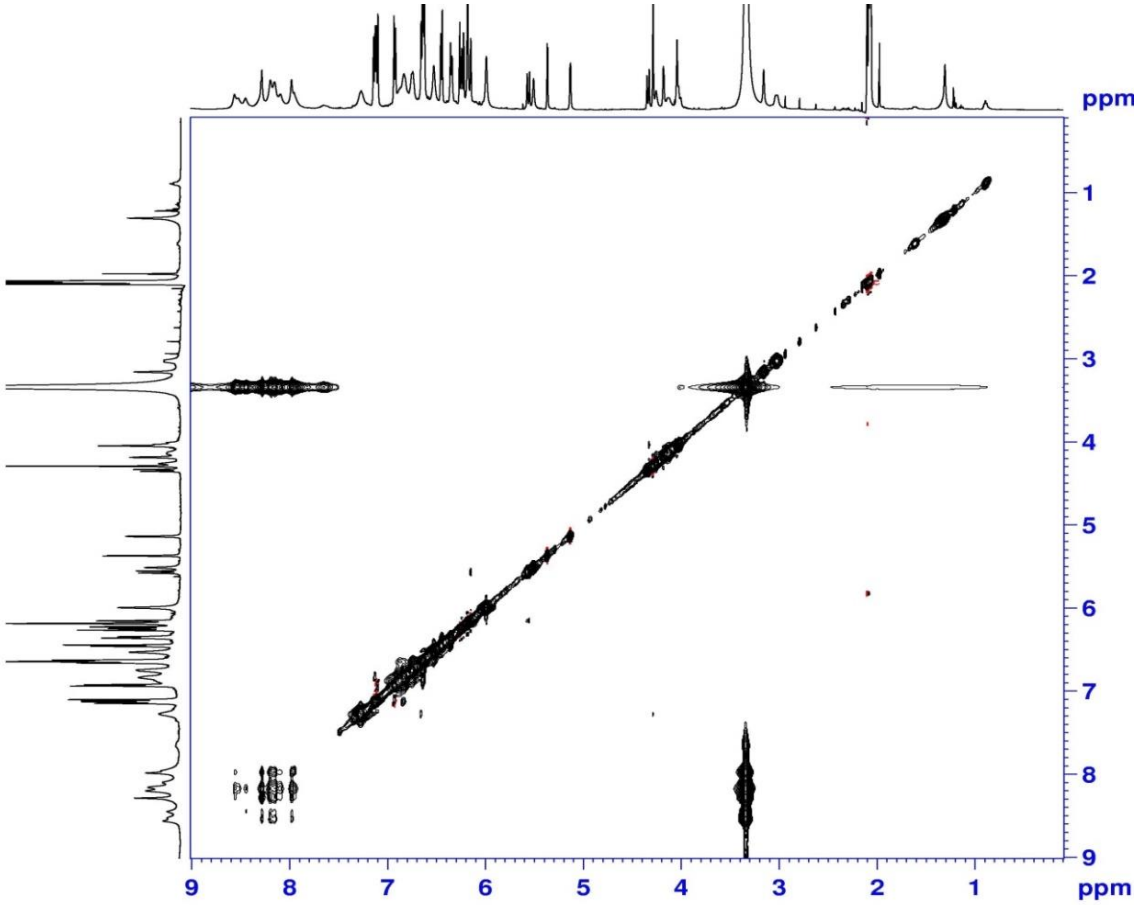

Figure 4A.40. NOESY NMR spectrum (500 MHz, Acetone-d_6) of vaticanol M (**31**)

Compound **32** was isolated as colourless amorphous solid. Its FTIR absorption band showed the presence of hydroxyl (3429 cm^{-1}), methyl group (2926 cm^{-1}), carbonyl (1728 cm^{-1}), benzene ring (1673 and 1471 cm^{-1}) and substituted phenolic groups (1093 and 790 cm^{-1}). The ^{1}H NMR spectrum exhibited a signal for one aromatic proton at δ_H 6.98 (s) ppm and a signal for methoxy protons at δ_H 3.90 (s) ppm. In addition, signals observed between δ_H 3.35 and 4.09 ppm is characteristic of hydroxyl hydrogen and a doublet was seen at δ_H 4.94 (J = 10 Hz, 1H) ppm, suggesting the existence of a sugar moiety of the compound. The ^{13}C NMR spectrum exhibited fourteen carbon signals including the ester carbonyl carbon at δ_C 163.4 ppm, one methoxy carbon at δ_C 59.8 ppm, aromatic carbon at δ_C 109.4, 118.07, 150.36, 140.59, 148.08 and 115.95 ppm. The glycosidic units are observed in the range δ_C 83.0 - 62.6 ppm. Based on the literature survey [Eun-Kyoung *et al*., **1999**] and complete analysis of 1D and 2D NMR spectra (**Figure 4A.42- 4A.47**), the compound **32** was confirmed as bergenin and the structure is shown below.

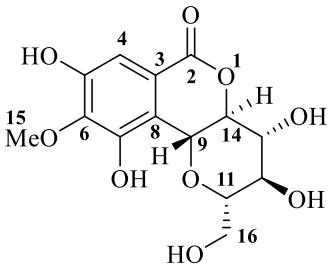

Bergenin (32)

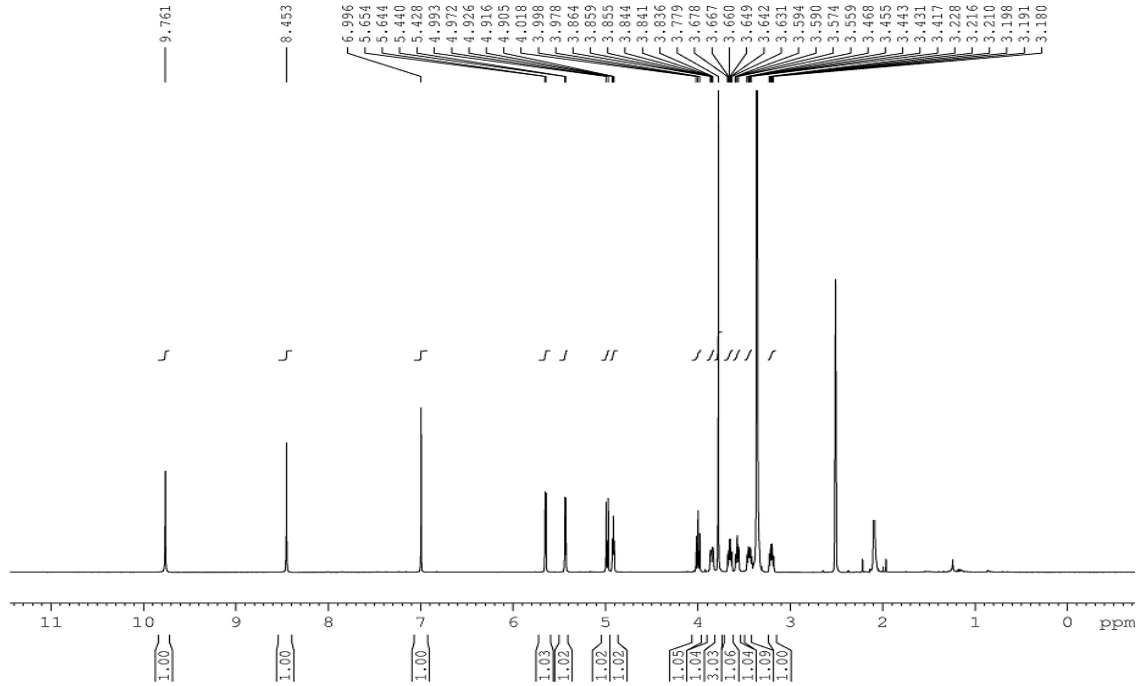

Figure 4A.41. ^{1}H NMR spectrum (500 MHz, DMSO-d_6) of bergenin (**32**)

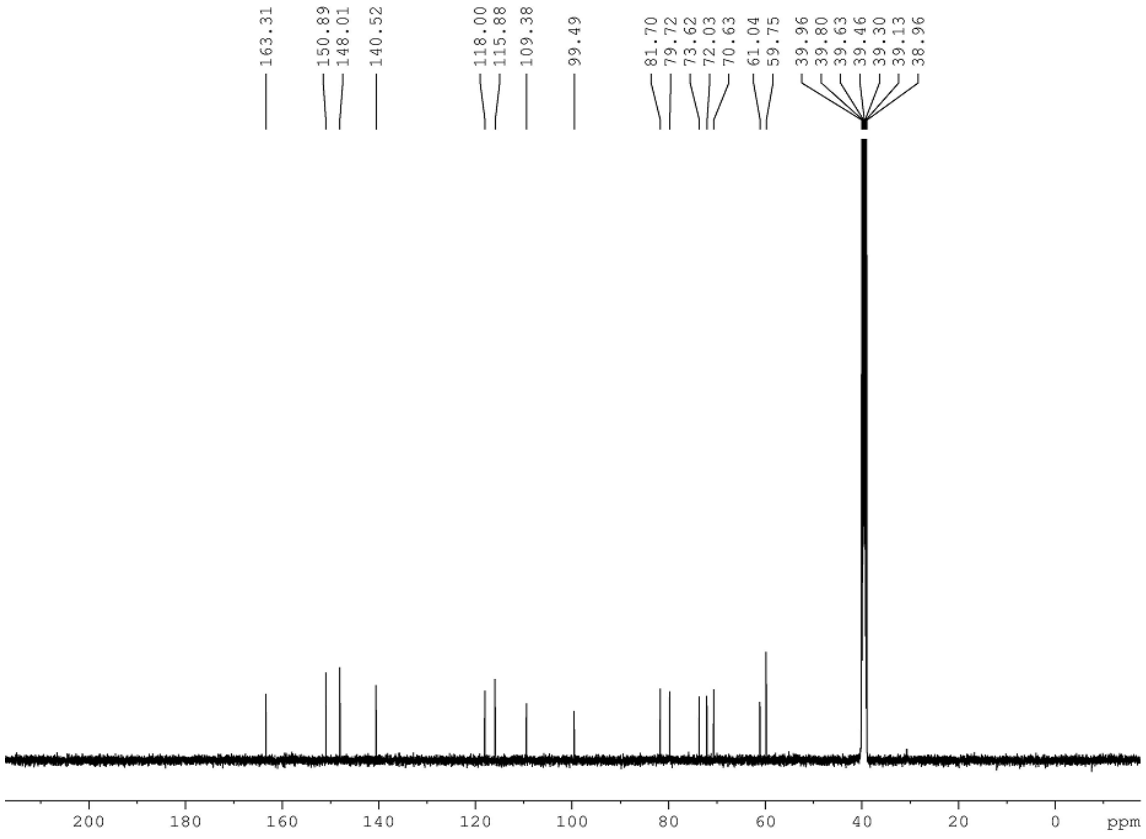

Figure 4A.42. ^{13}C NMR spectrum (125 MHz, DMSO-d_6) of bergenin (**32**)

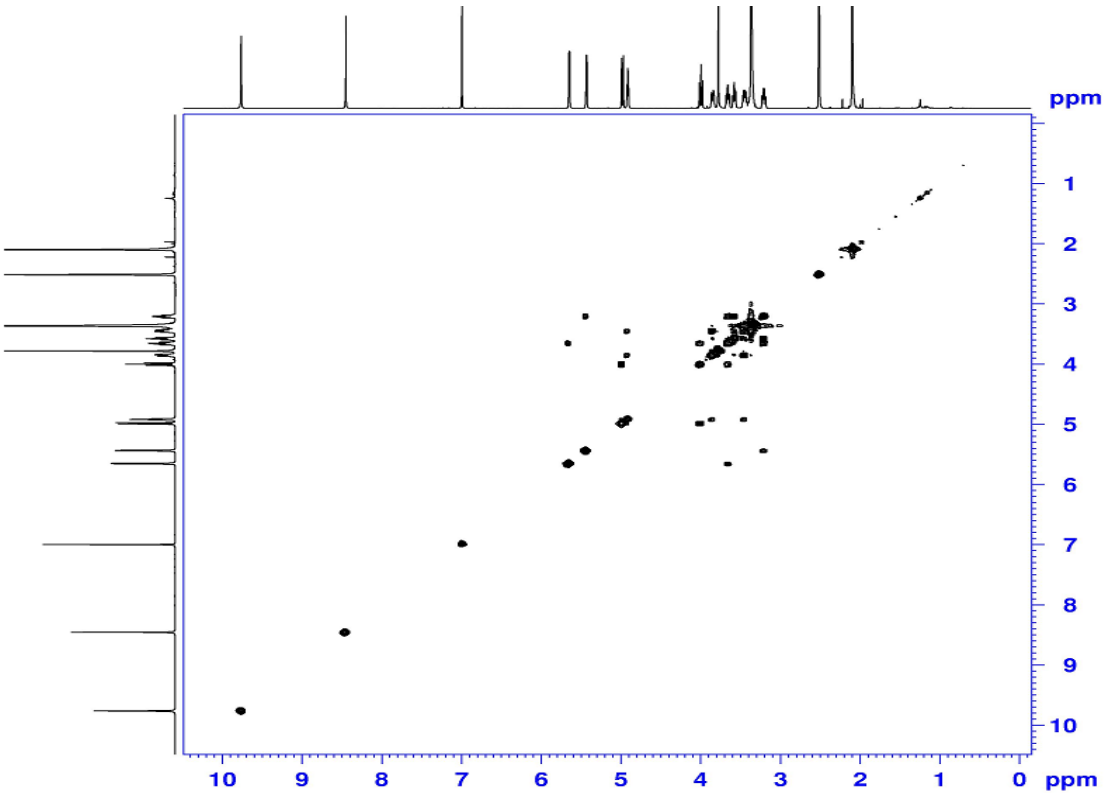

Figure 4A.43. ^{1}H-^{1}H COSY NMR spectrum (500 MHz, DMSO-d_6) of bergenin (**32**)

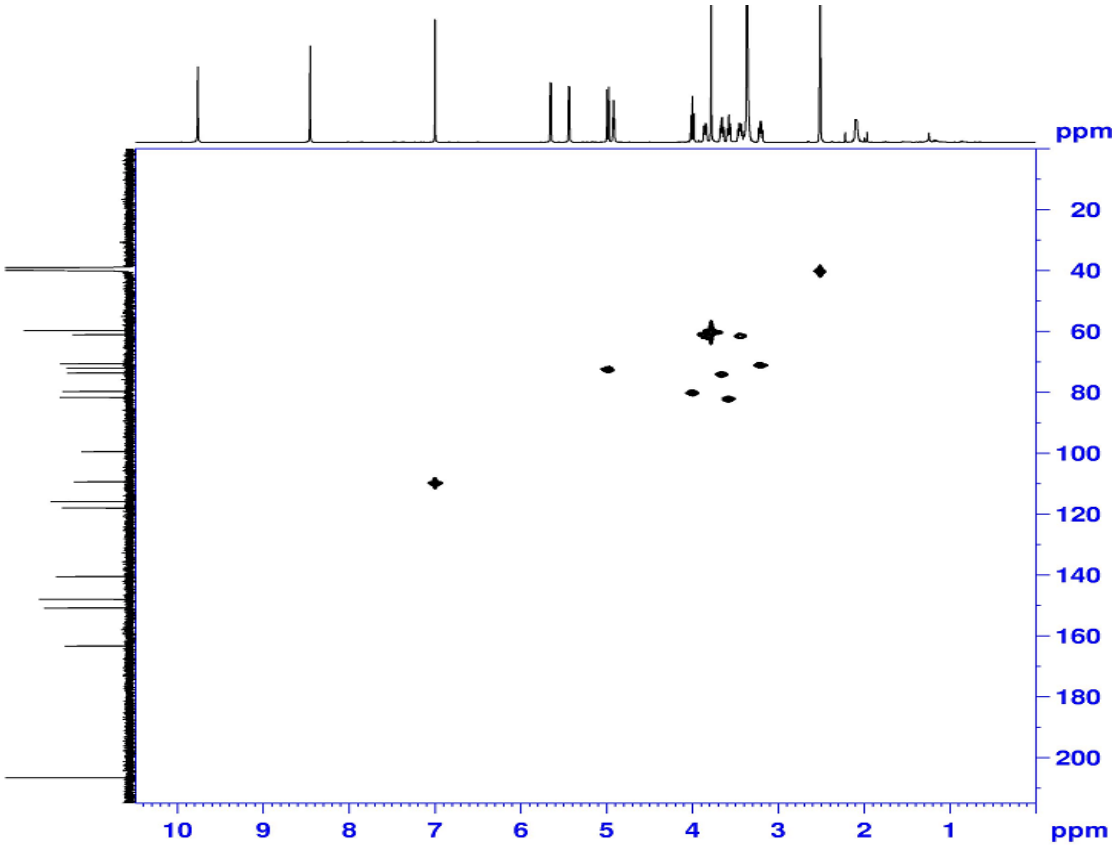

Figure 4A.44. HMQC NMR spectrum (125 MHz, DMSO-d_6) of bergenin (**32**)

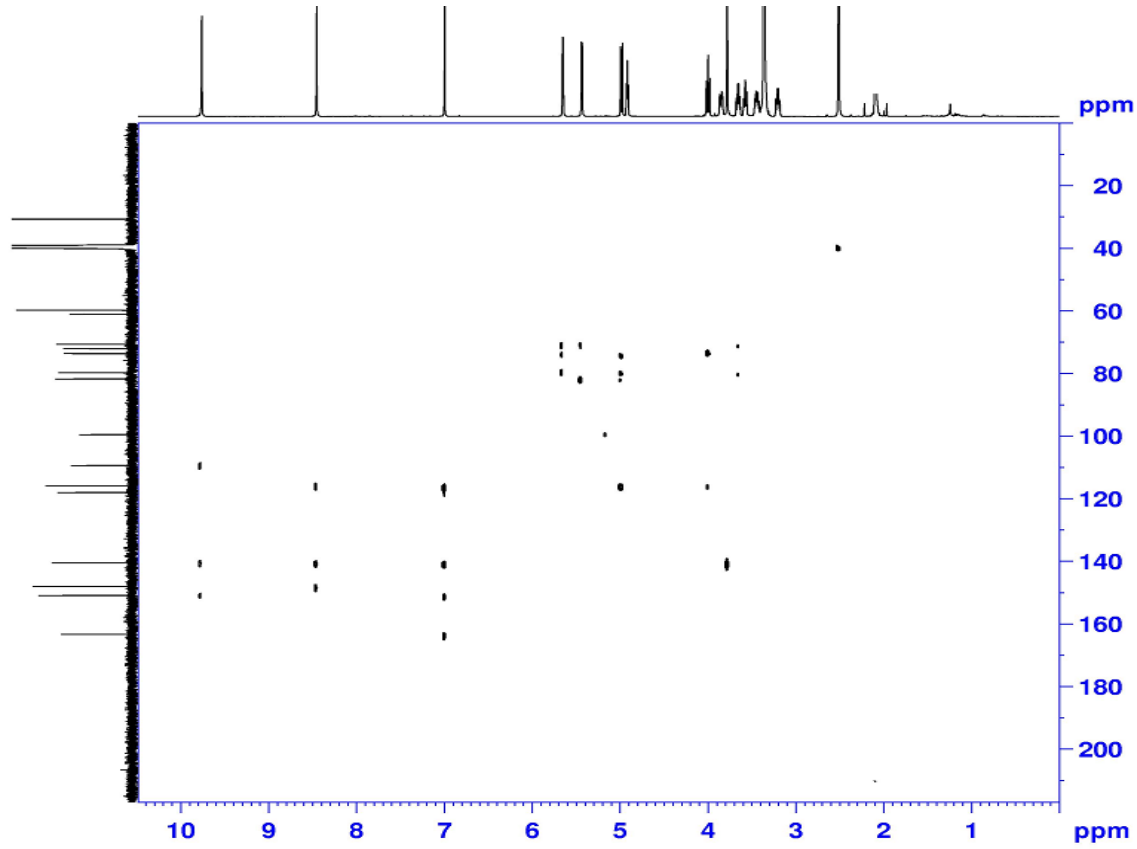

Figure 4A.45. HMBC NMR spectrum (125 MHz, DMSO-d_6) of bergenin (**32**)

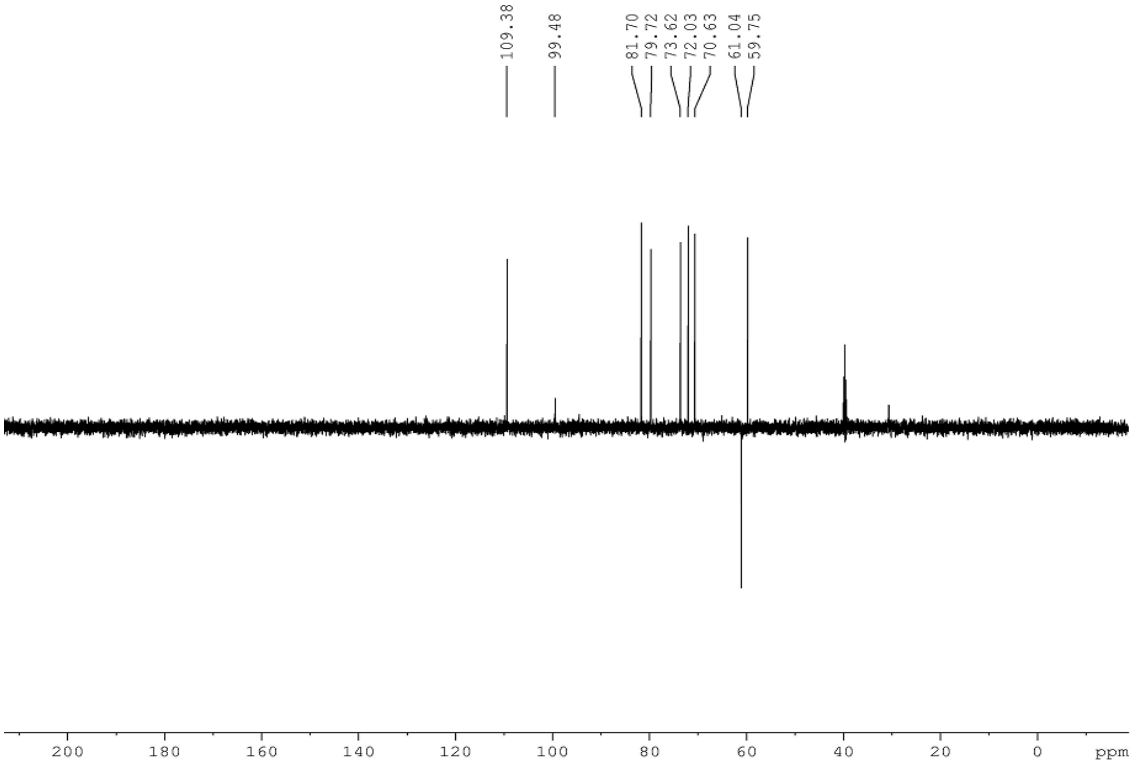

Figure 4A.46. DEPT 135 NMR spectrum (125 MHz, DMSO-d_6) of bergenin (**32**)

Compound **33** was isolated as colourless amorphous solid. Its IR absorption band showed the presence of hydroxyl (3429 cm^{-1}), methyl group (2926 cm^{-1}), carbonyl (1728 cm^{-1}), benzene ring (1673, 1471 cm^{-1}) and substituted phenolic groups (1093 and 790 cm^{-1}). The ^{1}H NMR spectrum exhibited a signal for phenolic hydroxyl group (9.93 brs, 1H), one aromatic proton (7.23, s, 1H) and a signal for methoxy protons δ_H 3.67 and 3.66 (s, 3H each) ppm. The ^{13}C NMR spectrum exhibited fourteen carbon signals including the ester carbonyl carbon at δ_C 163.4 ppm, methoxyl carbon at δ_C (61.0 and 60.9 ppm), aromatic carbon at δ_C 109.4, 118.1, 150.4, 140.6, 148.1 and 115.9 ppm respectively. Based on the literature survey and complete analysis of NMR spectra (**Figure 4A.47-4A.53)**, the compound **33** was confirmed as methoxybergenin and the structure is shown below.

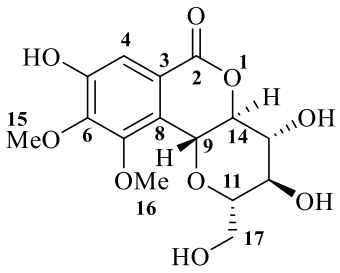

Methoxybergenin (33)

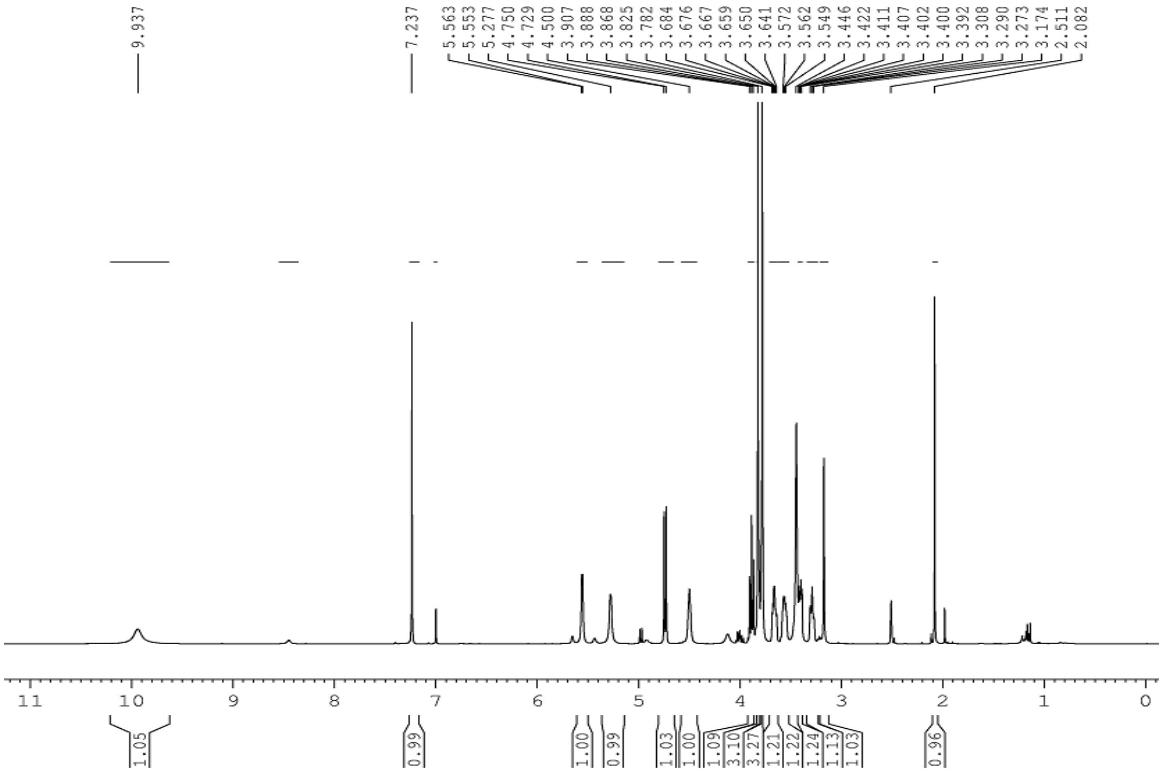

Figure 4A.47. ^{1}H NMR spectrum (500 MHz, DMSO-d_6) of methoxybergenin (**33**)

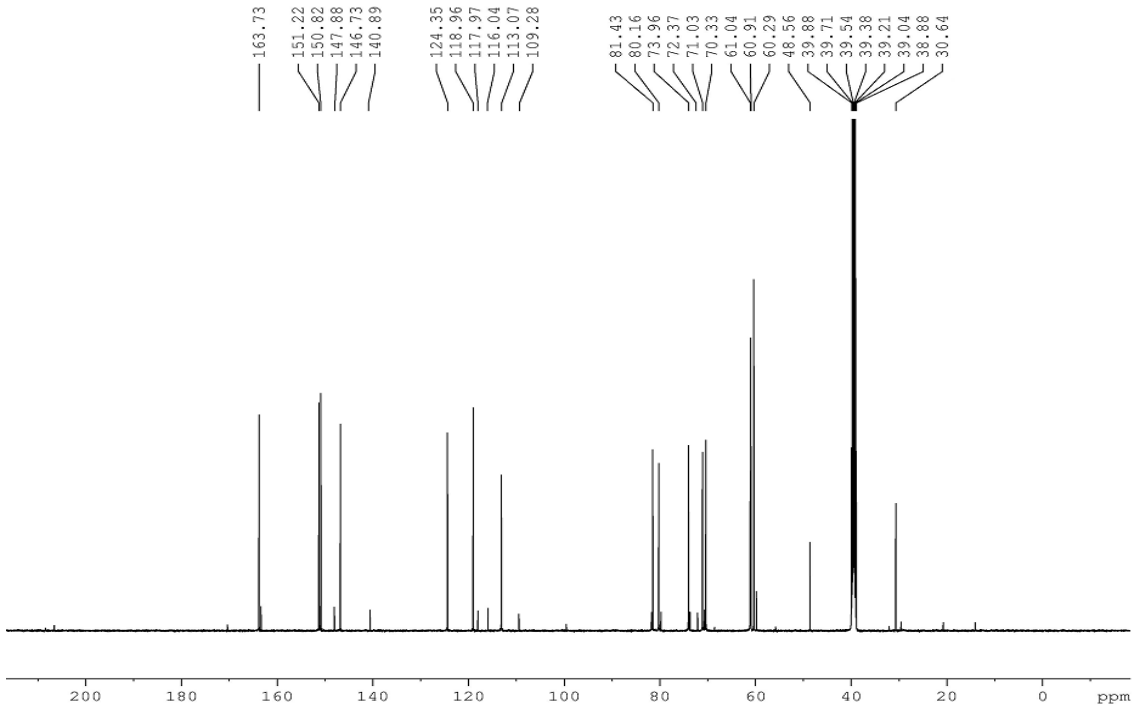

Figure 4A.48. ^{13}C NMR spectrum (125 MHz, DMSO-d_6) of methoxybergenin(**33**)

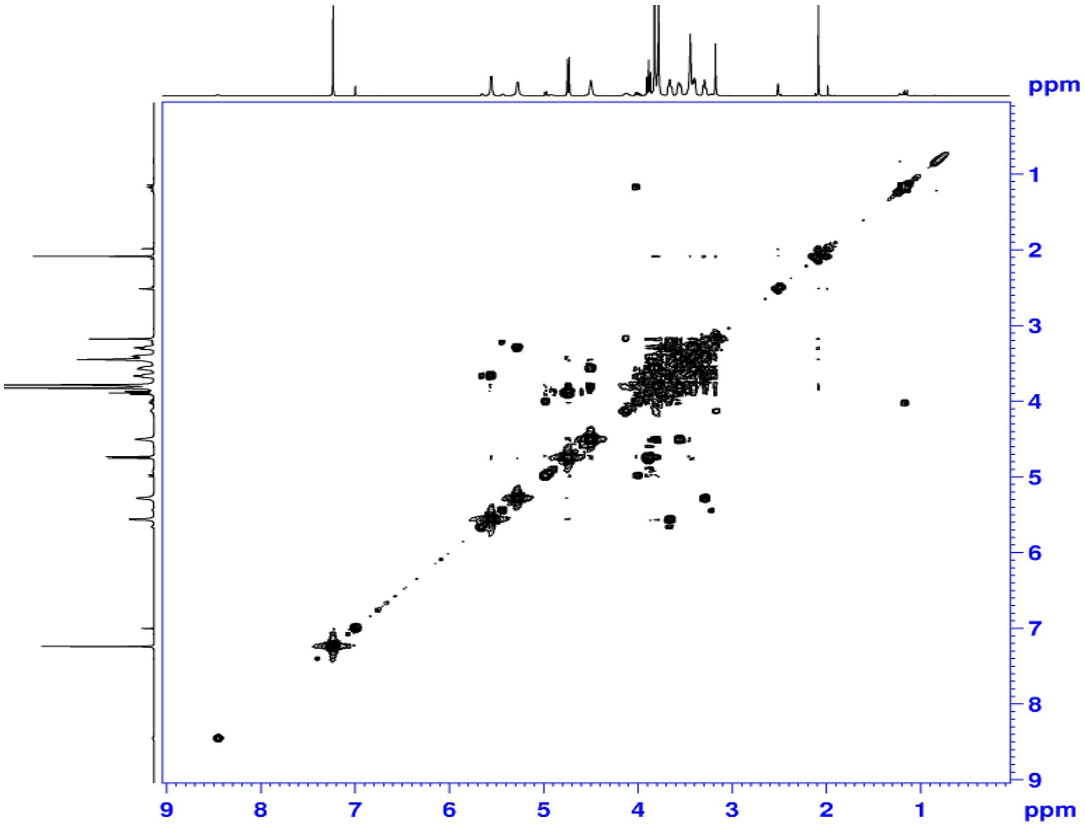

Figure 4A.49. ^{1}H-^{1}H COSY NMR spectrum (500 MHz, DMSO-d_6) of methoxybergenin (**33**)

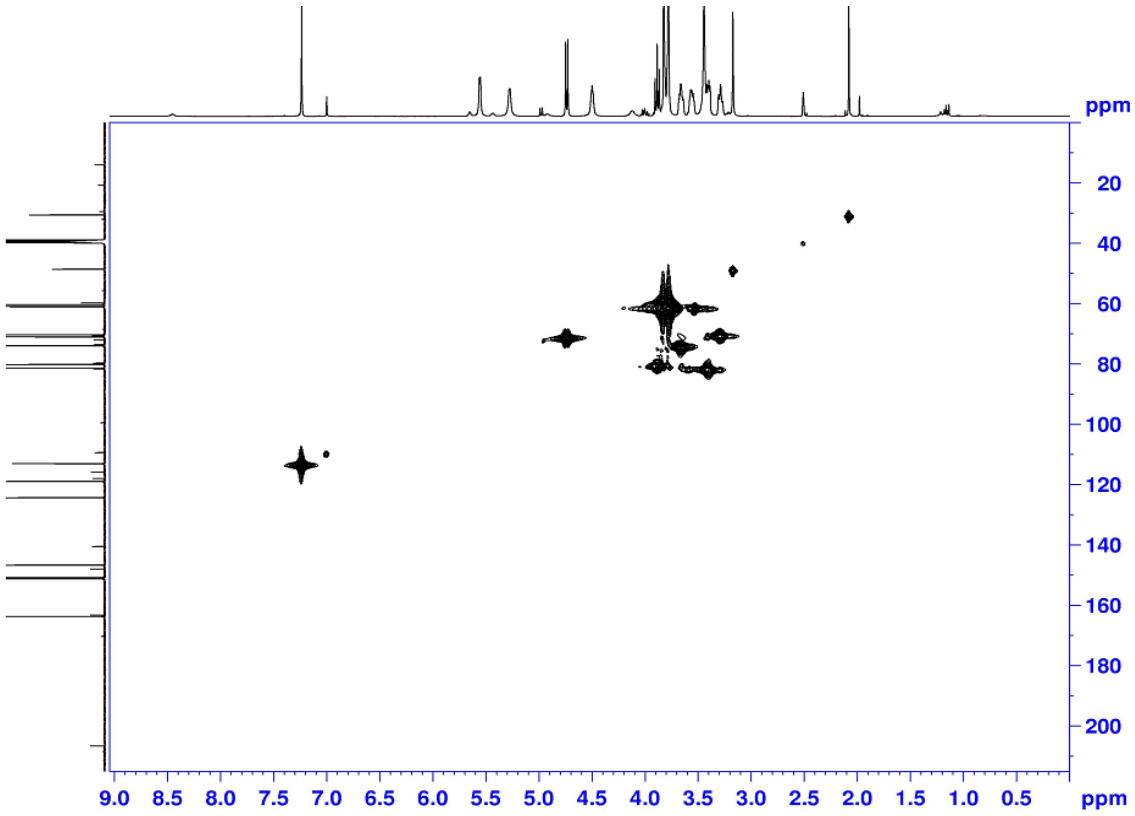

Figure 4A.50. HMQC NMR spectrum (125 MHz, DMSO-d_6) of methoxybergenin (**33**)

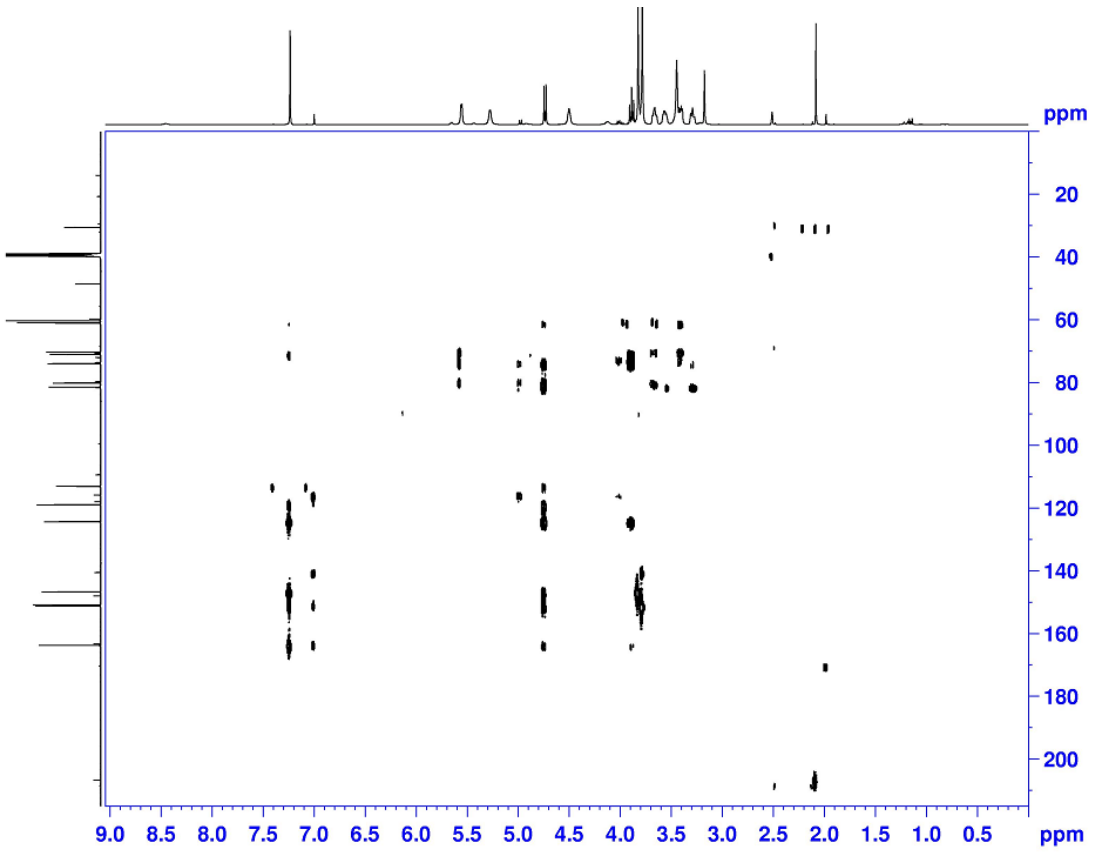

Figure 4A.51. HMBC NMR spectrum (125 MHz, DMSO-d_6) of methoxybergenin (**33**)

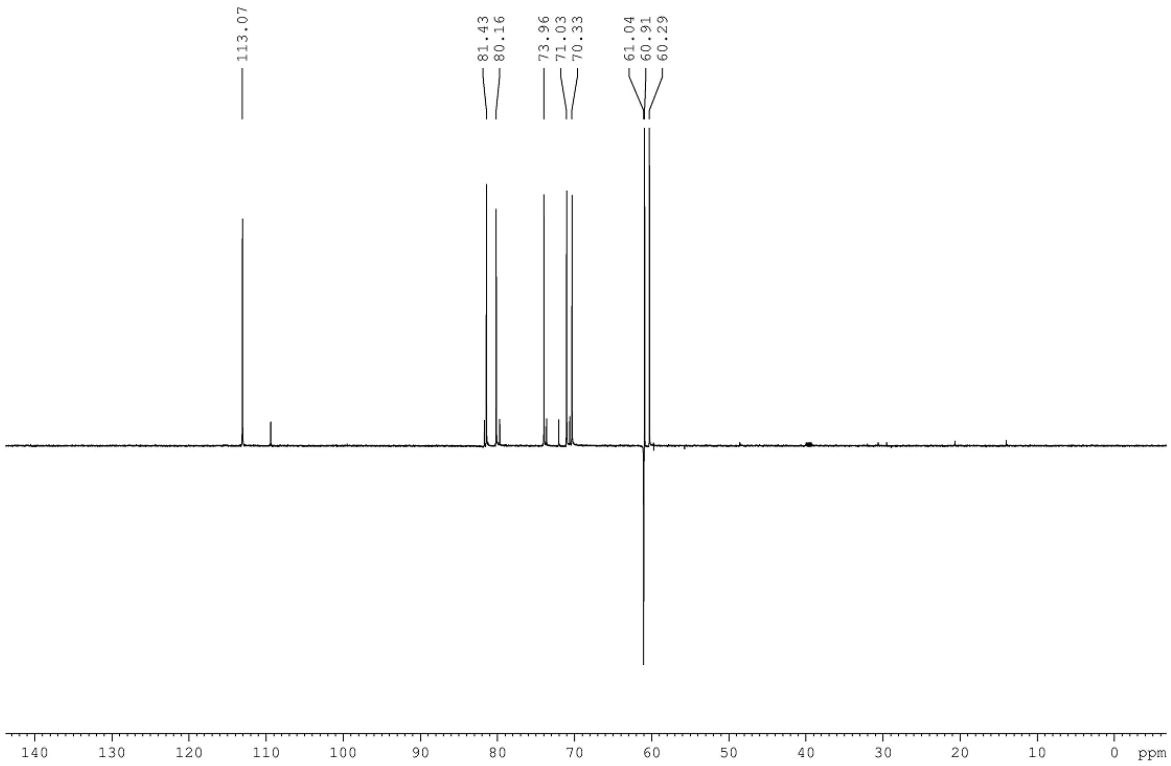

Figure 4A.52. DEPT 135 NMR spectrum (125 MHz, DMSO-d_6) of methoxybergenin (**33**)

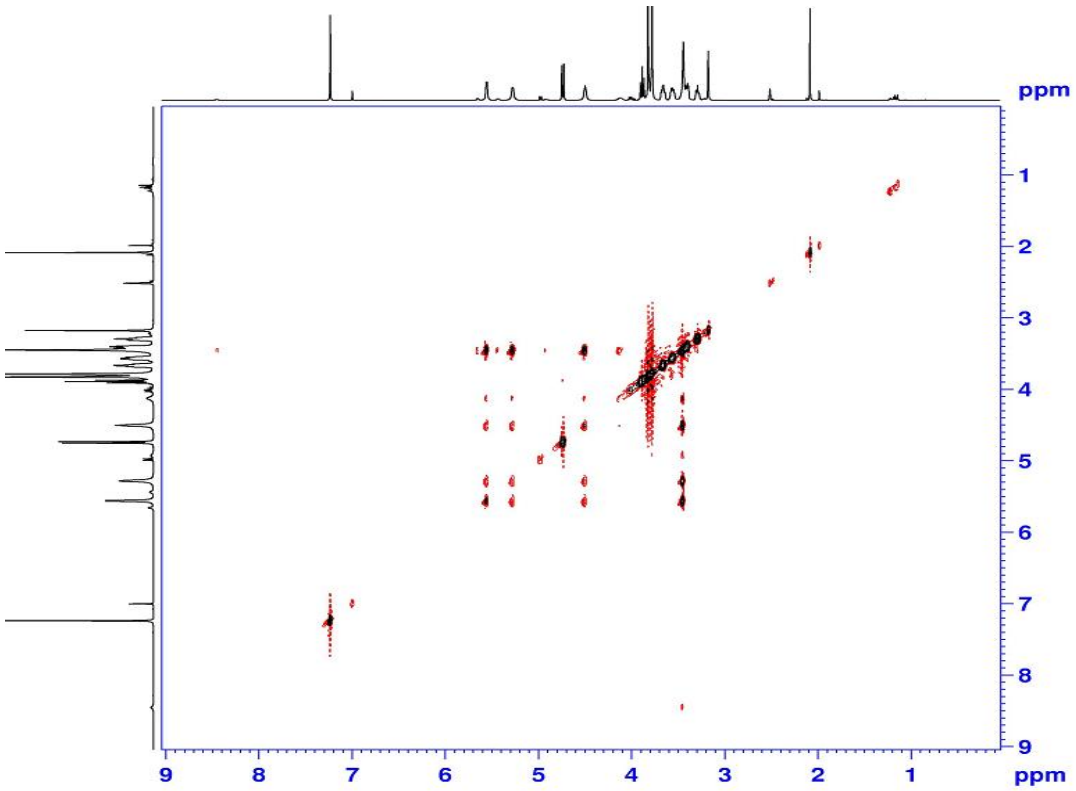

Figure 4A.53. NOESY NMR spectrum (500 MHz, DMSO-d_6) of methoxybergenin (**33**)

4A.5. Biosynthetic pathway of (-)-ε-viniferin, (-)-ampelopsin F and vaticaphenol A

The primary step involves the coupling of phenoxy radical to the dimer of resveratrol in the presence of a putative dirigent protein, which can undergo stereoselective couplings to afford an 8–10 bisquinone methide intermediate. Subsequent 8–10 coupling at the re–re face with concomitant intermolecular cyclization leads to (–)-antipodes of (-) – ε - viniferin (b) and ampelopsin F [Ito *et al*., **2016**] (**Figure 4A.54**). The (-) – ε -viniferin undergoes oxidation followed by radical dimerization yielded vaticaphenol A [Mitchell *et al*., **2015**] (**Figure 4A.55**).

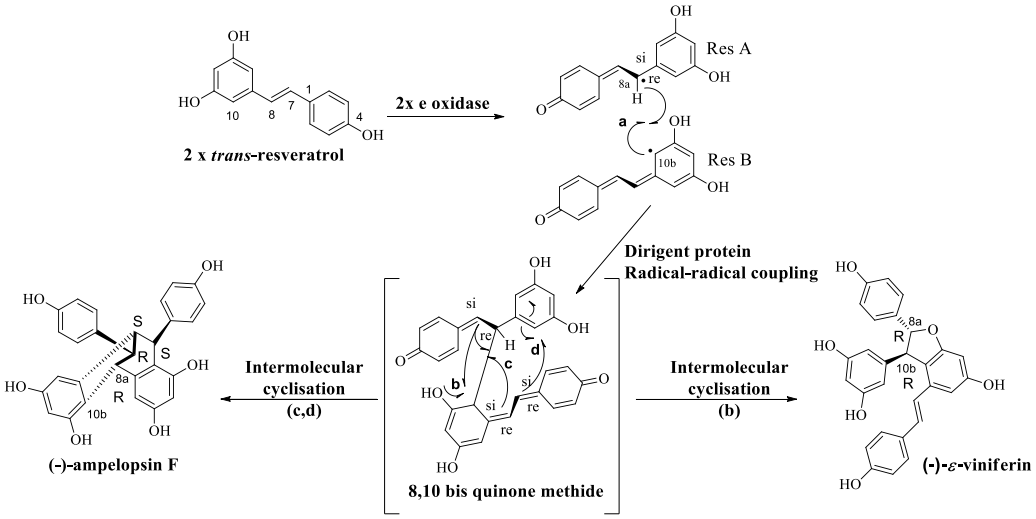

Figure 4A.54. Biosynthetic pathway of (-)-ε-viniferin and (-)-ampelopsin F

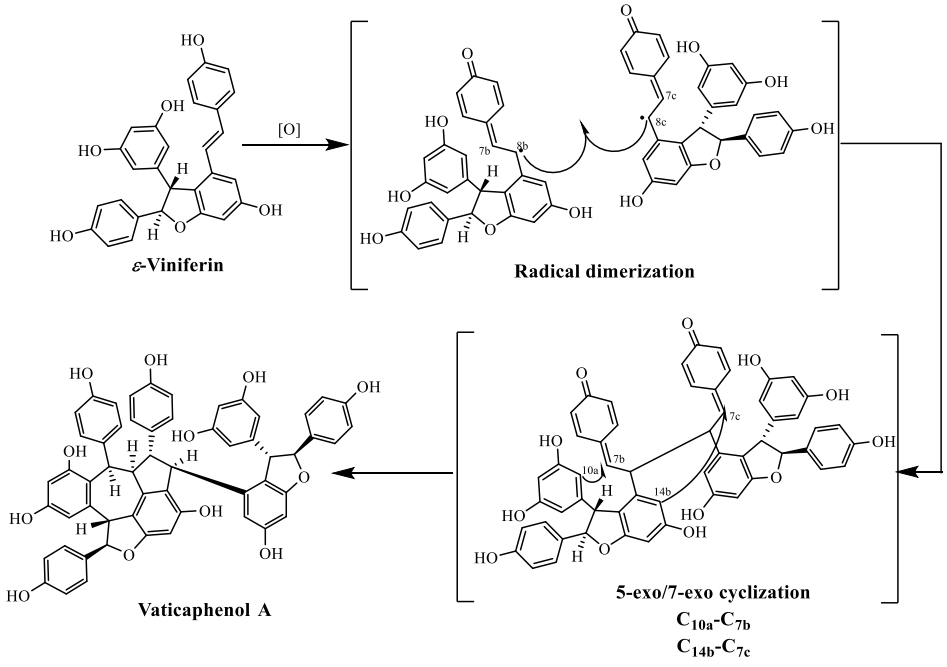

Figure 4A.55. Biosynthetic pathway of vaticaphenol A

4A.6. Antioxidant activity of isolated phytochemicals

Resveratrol and its oligomers possess biologically beneficial activities and are frequently utilized as antioxidant, anticancer, antidiabetic, cardioprotective, anti-HIV and anti-aging agents [Sasikumar *et al*., **2016**; Keylor *et al*., **2016**; Zghonda *et al*., **2012**; Ota **2013**; Dai *et al*., **1998**; Lim *et al*., **2012**; Jang *et al*., **1997**]. In our study, the compounds **27-33** were tested for their antioxidant activity using DPPH and ABTS radical scavenging assay (**Table 4A.7)**. The results obtained from DPPH radical scavenging assay showed significant antioxidant activity for all the compounds (**27-33**) compared to the standard, gallic acid, except for compounds **32** and **33**. In particular, compound **29** exhibited a significant antioxidant activity with IC_{50} value of 9.09 ± 0.589 μM. The results of ABTS assay demonstrated that all the compounds, except compound **33**, displayed significant ABTS radical-scavenging ability than the standard, trolox. Based on the analysis of the results of DPPH and ABTS radical scavenging assays, it is clear that vaticanol R (**29**) and vaticanol M (**31**) display significant antioxidant activity, whereas bergenin (**32**) and methoxy bergenin (**33**) exhibited comparatively low antioxidant potential. The above data suggested that presence of more hydroxyl groups and less steric hindrance in compounds may enhance the antioxidant efficacy [Mikulski *et al*., **2010**; Dar *et al*., **2005**; Amorati *et al*., **2004**; Xu *et al*., **2005**]. This prompted us to check whether these compounds can attenuate ROS under redox imbalance situations.

Table 4A.7. Antioxidant activities of isolated compounds (**27-33**)

Compounds	**DPPH (IC_{50} in μM)**	**ABTS (IC_{50} in μM)**
27	16.53 ± 0.432	13.9 ± 0.390
28	47.27 ± 0.765	9.69 ± 0.718
29	9.09 ± 0.589	6.00 ± 0.590
30	54.67± 0.965	6.01 ± 0.328
31	9.61 ± 0.235	4.29 ± 0.457
32	336.42 ± 0.490	84.31 ± 0.531
33	1216.44 ± 0.541	546.75 ± 0.387
Gallic acid	14.87 ± 0.546	-
Trolox	-	129.04 ± 0.893

Each value represents mean ± SD (standard deviation) from triplicate measurements

4A.7. Cell viability

H9c2 is myogenic cell line derived from the embryonic rat and has same electrical and hormonal signaling pathways that of in adult cardiac cells. Therefore, it can be used as an experimental model to investigate the molecular mechanism of cardiomyocyte pathophysiology [Branco *et al*., **2015**; Witek *et al*., **2016**]. H_2O_2 was used as an oxidant inductor in H9c2 cell lines and cytoprotective effect of the compounds under investigation against H_2O_2 induced oxidative stress was studied.

The viability of cells with different concentration (5 to 200 μM) of compounds (**27**-**33**) for 24 h was determined initially by measuring mitochondrial activity (**Figure 56**). It can be seen that (**Figure 56a**) the viability of cells decreased significantly in a dose dependent manner. The concentration of all compounds above 50 μM was toxic to cells, therefore the concentration between 5 to 25 μM was chosen for further study. Here, H_2O_2 is used as an oxidant inductor because at physiological concentration, it is involved in cell signaling processes and at higher concentrations; it induces oxidative stress [Halliwell *et al*., **1992**]. In order to determine the sub toxic concentrations of hydrogen peroxide, H9c2 cells were exposed to H_2O_2 (from 10 to 500 μM) for 20 min and was assayed by MTT. As shown in the **Figure 56b**, it was found that different concentrations of H_2O_2 significantly reduced cell viability after treatment ($p \leq 0.05$) and 100 μM concentration of H_2O_2 decreases cell viability up to 25 %. Therefore, the cells were exposed to a concentration of 100 μM H_2O_2 for inducing oxidative stress model. In order to find out cytoprotective effect of compounds against H_2O_2 induced toxicity, the cells were pretreated with the subtoxic concentrations of compounds **27**-**33** (5 to 25 μM) for 24 h followed by H_2O_2 of 100 μM for 20 min. From the **Figure 56c**, the results showed that 5 μM & 15 μM concentrations of each compound protected the cells from H_2O_2 induced oxidative stress in dose dependent manner. The data suggested that all the compounds effectively protect H9c2 cells from H_2O_2 induced cytotoxicity.

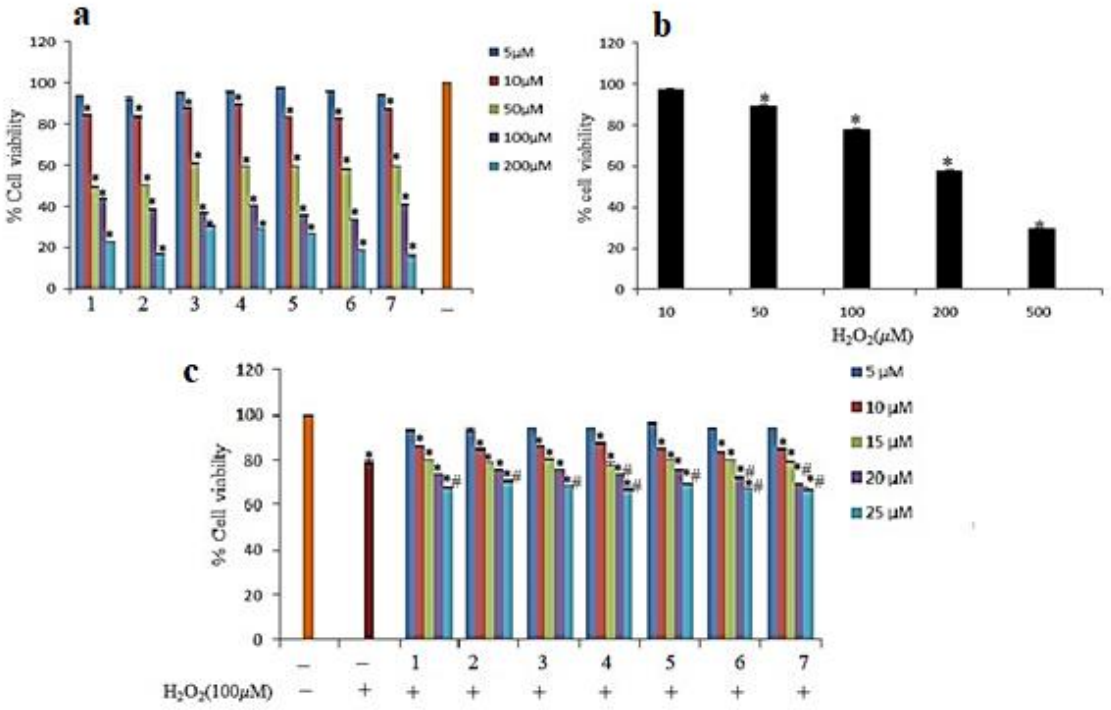

Figure 4A.56. The effect of compounds **(27-33)**), H_2O_2 and 100 μM H_2O_2 pretreatment of cells with compounds (**27-33**), on H9c2 cell viability by MTT assay. (**a**) Cytotoxicity of different concentrations of compounds (**27-33**) on H9c2 cells (**b**) Cytotoxicity of H9c2 cells by different concentrations of H_2O_2 exposure (**c**) The effect of compounds (**1-7**) on H9c2 cell viability in presence of 100 μM H_2O_2.The results are expressed as percentage of control, and each value represents the mean ± SD. The annotation * indicates a *p* value ≤ 0.05 versus control group. The annotation # indicates a *p* value ≤ 0.05 versus H_2O_2 group

4A.8. Intracellular ROS production

The heart is an aerobic organ susceptible to oxidative stress and the unusual accumulation of ROS leads to the progression of myocardial injury. In the present study, hydrogen peroxide promotes the endogenous generation of ROS in cardiomyoblast. To further observe the effect of compounds (**27-33**) on intracellular ROS production, DCFH-DA assay was performed using flow cytometry (BD FACS Aria II, BD Bioscience USA). As shown in **Figure 58**, the exposure of H9c2 cells to 100 μM H_2O_2 induced an increased formation of intracellular ROS (35.7 ± 0.721 %) as compared to the control (2.1 ± 0.875 %). As can be seen the exposure of H9c2 cells to H_2O_2 increased the ROS levels by 16 times with respect to the control cells. The ROS production was decreased significantly on pre-treatment with the compounds (**27-33**) prior to H_2O_2 exposure, as shown in **Figure**

57. All compounds demonstrated decreased ROS production in dose-dependent manner. Of these, compounds **27**, **28**, **30** and **33** with 15 μM exhibited potential reduction in ROS production i.e., 8.6 ± 0.864 %, 6.2 ± 1.011 %, 8.1 ± 0.298 %, and 9.5 ± 0.691 % respectively which demonstrated that all the compounds have the ability to suppress the free radical upregulation under stress condition in cardiac cells. Several studies have proved that resveratrol is the main constituent in Dipterocarpaceae, Vitaceae and Leguminaceae family and exhibits significant antioxidant activity due to the presence of hydroxyl groups. Likewise, the presence of hydroxyl groups in resveratrol oligomers quenches singlet oxygen species, traps peroxyl radicals, inhibits oxidative DNA damage, inhibits peroxidation and stimulates gap junction communication. Results from the present study indicate that resveratrol oligomers can prevent oxidation of DNA by scavenging free radicals in a dose-dependent manner.

4A.9. Effect on antioxidant enzyme system

The superoxide dismutase (SOD) and catalase (CAT) are the most efficient enzymatic antioxidants in the body and their direct action balances the abnormal production of ROS in the cells. The SOD catalyzes the dismutation of $O_2^{\bullet-}$ to O_2 and H_2O_2 [Stone *et al*., **2006**] and, CAT has highest turnover number and it promotes the conversion of H_2O_2 to H_2O and molecular oxygen [Marklund *et al*., **1974**; Aebi *et al*., **1984**]. After evaluating the free radical scavenging activity, cytotoxicity and significant metabolites isolated from *Vatica chinensis* upregulated the SOD and CAT activity under oxidative stress condition. Thus, the present study confirms that resveratrol oligomers containing hydroxyl group at –para/-ortho position and less steric hindrance may promote the SOD and catalyze activity. decrease in ROS levels, it was then investigated as whether the compounds induce or activate the antioxidant enzymes in the body. Here, the enzymatic activities of CAT and SOD were determined by spectrophotometric assay. In our study, the 100 μM H_2O_2 treated H9c2 cells (20 min) considerably reduces SOD and catalyse activity as compared to the control cells. From the **Figure 58**, it is clear that (-)-ampelopsin F (**28**) significantly enhanced the SOD and CAT activity, however, vaticanol R (**29**) promoted the enzymatic activity slightly only.

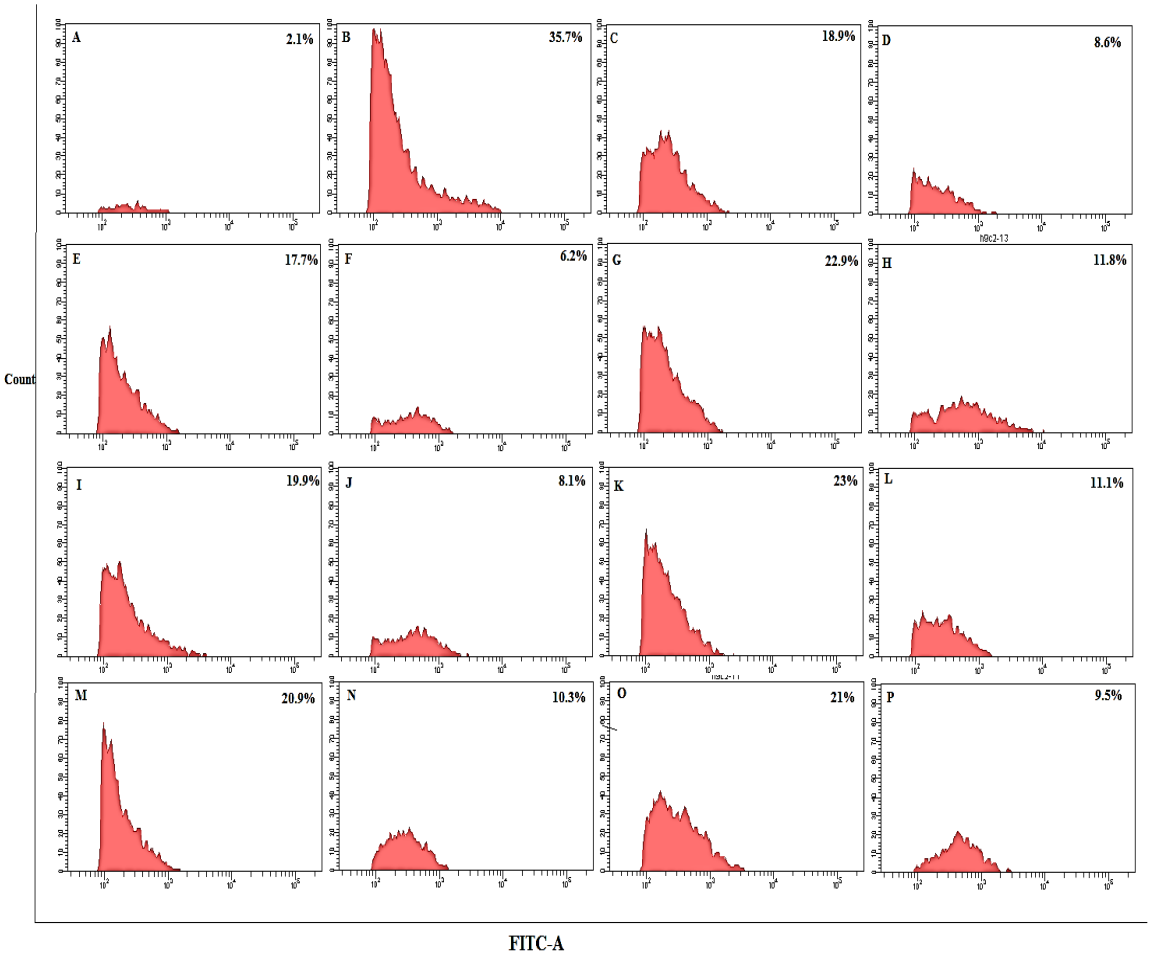

Figure 4A.57. Measurement of ROS production in H9c2 cells were analysed by DCFH-DA dye. The figure represent flow cytometric analysis of ROS production in H9c2 cells by plotting cell count against FITC Fluorescent imaging using fluorescent microscope The figure depicted as, A- Control, B-100 μM H_2O_2, C- 5 μM compound **27**+100 μM H_2O_2, D-15 μM compound **27** +100 μM H_2O_2, E-5 μM compound **28**+100 μM H_2O_2, F-15 μM compound **28**+100 μM H_2O_2, G- 5 μM compound **29**+100 μM H_2O_2, H-15 μM compound **29** +100 μM H_2O_2, I- 5 μM compound **30** +100 μM H_2O_2, J-15 μM compound **30** +100 μM H_2O_2, K- 5 μM compound **31**+100 μM H_2O_2, L-15 μM compound **31**+100 μM H_2O_2, M- 5 μM compound **32**+100 μM H_2O_2, N-15 μM compound **32**+100 μM H_2O_2, O- 5 μM compound **33**+100 μM H_2O_2, P-15 μM compound **33**+100 μM H_2O_2

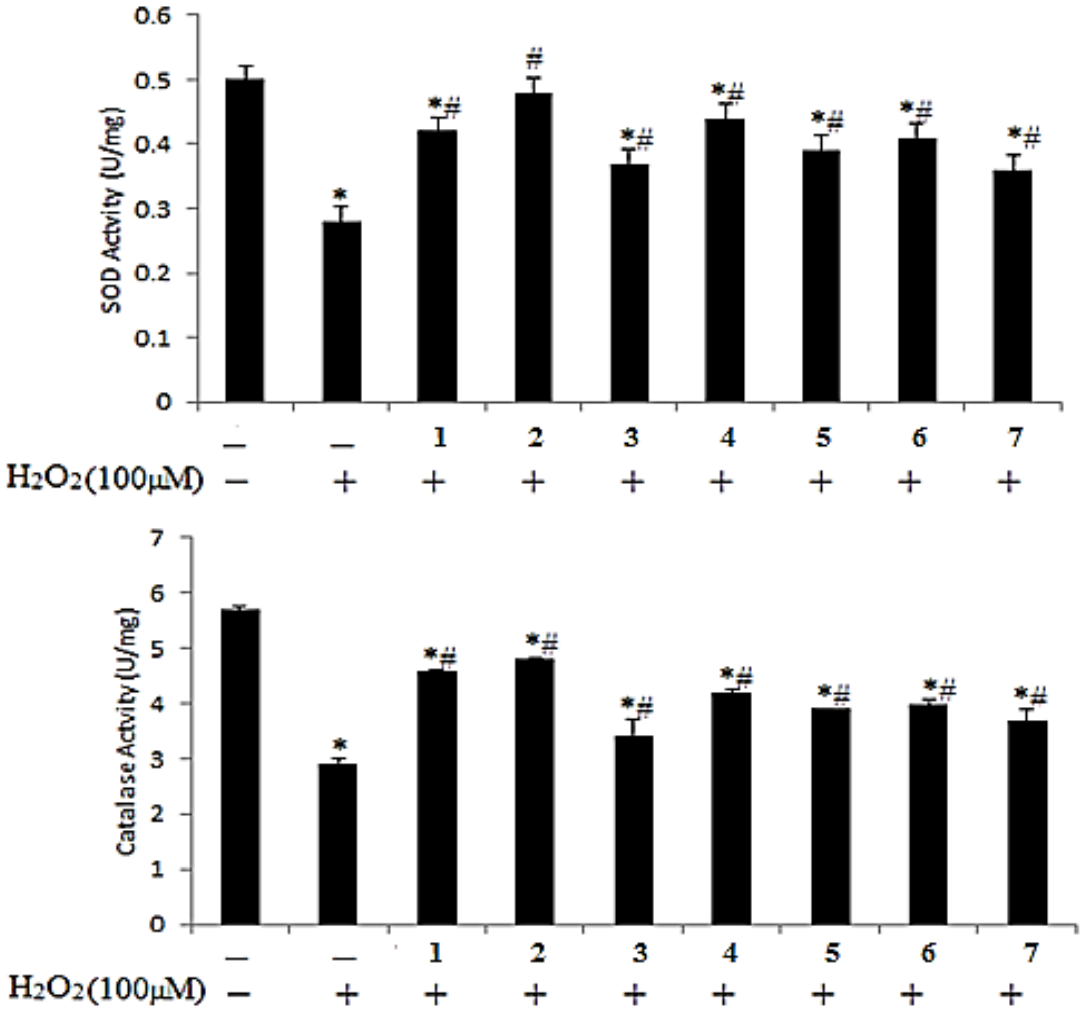

Figure 4A.58. Effect of compound, **27-33** on SOD and CAT activity in H9c2 cells treated with 100 μM H_2O_2. Each value represents mean ± SD from triplicate measurements of three different experiments. Significance levels between different groups were determined by using one way ANOVA, *p ≤ 0.05 versus Control; #p ≤ 0.05 versus H_2O_2

4A.10. Mitochondrial membrane potential ($\Delta\Psi m$) reduction

$\Delta\Psi m$, the charge difference across a membrane that is permeable to ions, is critical for cellular bioenergetics and homeostasis. The collapse of $\Delta\Psi m$ is an important event associated with mitochondrial dysfunction, or even cell death [41]. Rhodamine 123 staining was used in $\Delta\Psi m$ assay, a more specific test for early mitochondrial injury. Rhodamine 123 is a cationic fluorescent dye, which could enter the mitochondrial matrix and cause photoluminescent quenching dependent on $\Delta\Psi m$. The results showed that a rapid reduction in $\Delta\Psi m$ was found when the cells were exposed to 100 μM H_2O_2 as compared to control. As shown in **Figure 59** the fluorescence intensity of H_2O_2 increased

significantly when compared to the untreated group (23 ± 0.962 % and 0.8 ± 0.781 % respectively). The pretreatment of compounds (**1**-**7**) preserve $\Delta\Psi m$, in which 15 μM concentration of compounds **27**, **28** and **30** showed better reduction, 1.7 ± 0.932 %, 2.1 ± 0.648 %, and 4.3 ± 0.865 % respectively. These provide an evidence that all the compounds wielded a protective effect on mitochondria by retaining the mitochondrial membrane potential against oxidative stress.

4A.11. ATP level by HPLC analysis

Mitochondrial ATP production is the main energy source for various metabolic pathways and mitochondrial ATPase is the key enzyme for the cellular energy conversion. In normal mitochondria, $\Delta\Psi m$ is high favoring for ATP synthesis by ATP synthase. The decrease in mitochondrial functioning leads to reduction in $\Delta\Psi$m which in turn effect the production of ATP. In order to study the effect of the compounds in the production of ATP when subjected to oxidative stress, the same was estimated using HPLC method. As can be noted from the **figure 59c**, the ATP production by H9c2 cells under oxidative stress condition was significantly reduced when compared to the untreated cells, indicating that stress induced by H_2O_2 exposure produced a significant cellular energy dysfunction. The results may be an indicative of the inhibition of cellular mitochondrial ATP synthesis, which in turn might have declined the ATP production. As the compounds **1** and **2** demonstrated a significant improvement in mitochondrial membrane potential, we further evaluated these compounds for its potential in enhancing ATP production. As expected, ATP level was found to be increased in a dose dependent manner on pretreatment with the compounds **27** and **28**. These results suggested that the production of ATP by mitochondria under oxidative stress conditions is low and it is reversed in the presence of the compounds under study.

4A.12. Conclusion

In summary, phytochemical investigation of the stem bark of *Vatica chinensis* L. led to the isolation of the seven compounds, which includes a novel compound, vaticanol R (**29**) along with six known compounds. Vaticaphenol A (**30**), bergenin (**32**) and methoxy bergenin (**33**) were isolated for the first time from this species. The biological results indicated the protective effect of all the compounds on cardiomyocytes against H_2O_2-induced oxidative stress. The pretreatment of H9c2 cells with the compounds prior to the oxidative stress induction by H_2O_2 protects the cells from oxidative stress induced damage by decrease in ROS production, increase in SOD/CAT activity, restoration of

mitochondrial membrane potential and ATP levels. The results suggested that the compounds under study may be promising candidates for the prevention and management of oxidative stress and associated cardiovascular diseases. Further *in vivo* studies are mandatory to have better understanding on the potential therapeutic role of these oligostilbenoids in cardiovascular diseases.

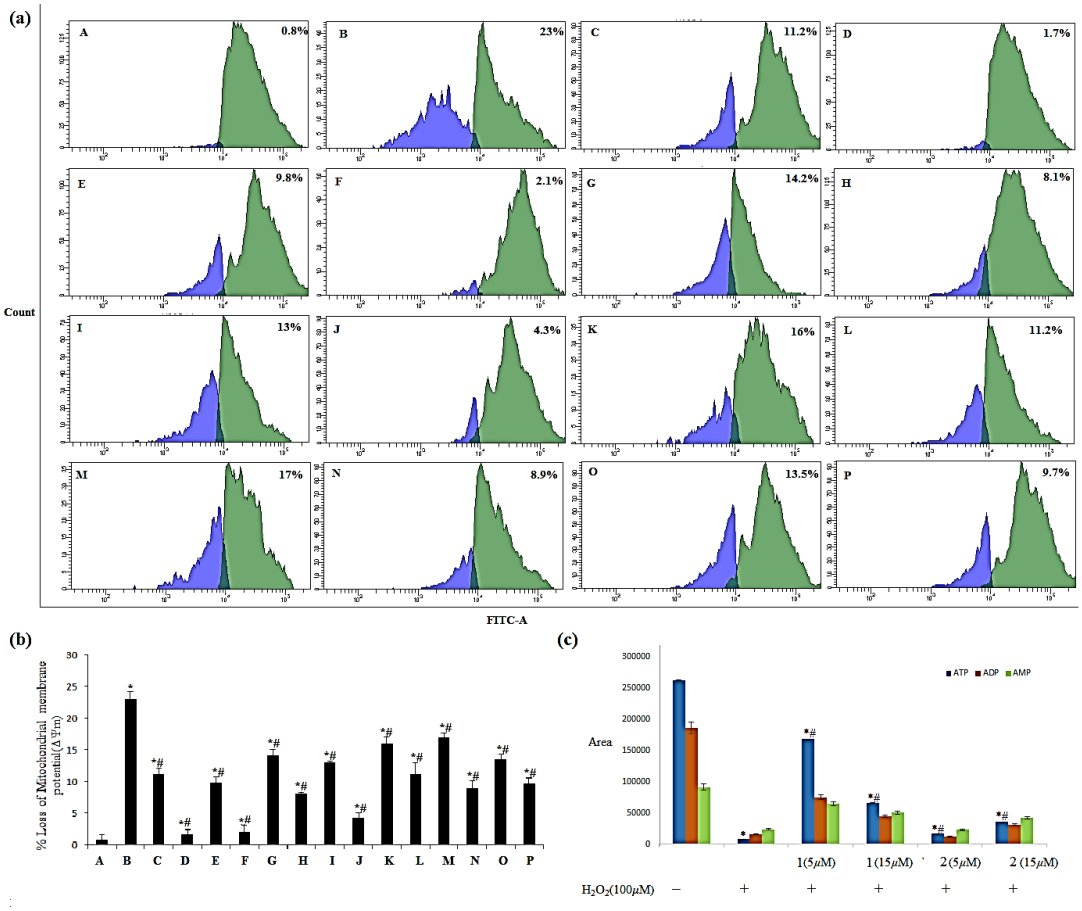

Figure 4A.59. Quantification of Mitochondrial membrane potential by Rhodamine 123 staining and ATP level by staining method. In (**a**) and (**b**) the restoration of mitochondrial membrane potential by compounds **27-33**, were analysed using flow cytometry:-A-Control, B-100 μM H_2O_2, C-5 μM compound **27** +100 μM H_2O_2, D-15 μM compound **27** +100 μM H_2O_2, E-5 μM compound **28** +100 μM H_2O_2, F-15 μM compound **28** + 100 μM H_2O_2, G- 5 μM compound **29** +100μM H_2O_2, H-15 μM compound **29** +100 μM H_2O_2, I-5 μM compound **30** +100 μM H_2O_2, J-15 μM compound **30** +100 μM H_2O_2, K- 5 μM compound **31** +100 μM H_2O_2, L-15 μM compound **31** +100 μM H_2O_2, M- 5 μM compound **32** +100 μM H_2O_2, N-15 μM compound **32** +100 μM H_2O_2, O- 5 μM compound **33** + 100 μM H_2O_2, P-15 μM compound **33** +100 μM H_2O_2. In (**c**) represents

the increased mitochondrial capacity to produce ATP in compounds, **27** & **28** treated cells. The results are expressed as the mean ± SD. Significant level of different groups were analysed by using one way ANNOVA.The annotation * indicates a p value ≤ 0.05 versus control group and # indicates a p value ≤ 0.05 versus H_2O_2 group

4A.13. Experimental section

4A.13.1. General experimental procedure

Optical rotations were determined on a Jasco P-2000 Polarimeter. CD spectrum was recorded on JASCO 810 Spectropolarimeter. The UV data were recorded on Shimadzu UV-1800 Spectrophotometer. The IR spectra were acquired on Bruker FTIR spectrometer. 1 D- and 2 D-NMR experiments were recorded on a Bruker Avance AMX 500 spectrometer; NMR solvents were Acetone-d_6/DMSO-d_6 with 0.03 % TMS used as internal standard. The multiplicities of NMR signals were assigned as singlet (s), doublet (d), triplet (t), multiplet (m), broad (br), and doublet of doublet (dd). Mass spectra were recorded under ESI/HRMS at 60,000 resolution using Thermo Scientific Exactive mass spectrometer. Silica gel (230−400 mesh and 100-200 mesh) and Sephadex LH-20 were used for gravity column chromatography (CC). Analytical thin-layer chromatography (TLC) was carried out on silica gel 60 F254 aluminum-backed TLC plates (Merck). All the solvents used were highest grade available.

4A.13.2. Plant material

The stem bark of *Vatica chinensis* L. were collected in April 2015 from Calicut University Campus, Calicut, Kerala, India and a voucher specimen (Voucher Specimen No. **6389**) is available for inspection at the Herbarium of University of Calicut, Calicut, Kerala, India.

4A.13.3. Extraction and isolation

The dried and milled stem barks of *Vatica chinensis* (750 g) were extracted (3L x 3 times) with *n*-hexane, acetone, ethanol and water for 48 h at room temperature and filtered. The filtered was concentrated at 50 °C under reduced pressure to yield hexane extract (VCH, 2 g), acetone extract (VCA, 60 g), ethanol extract (VCE, 38 g), and aqueous extract (VCW, 12 g) respectively. An aliquot of acetone extract (35 g) was subjected to silica gel column (100–200 mesh, 1000 x 60 mm) chromatography and eluted with *n*-hexane/ethyl acetate gradient to afford 15 fractions (Fr. 01 - Fr. 15). The schematic representation of the isolation procedure is shown in **Figure 4A.60.**

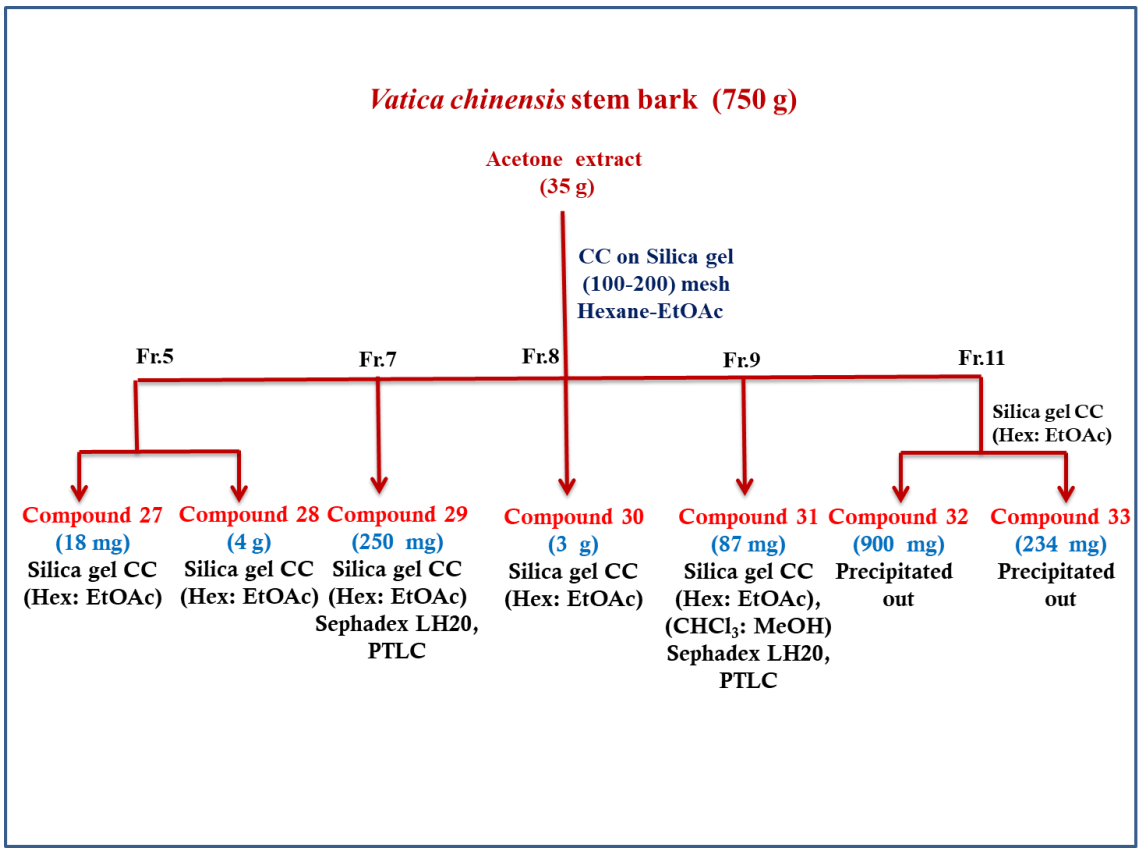

Figure 4A.60. Schematic representation of the isolation procedure of the acetone extract of the stem bark of *Vatica chinensis*

4A.13.3.1. Isolation of compound 27 and 28

Fraction pool 5 was subjected to column chromatographic separation (100-200 mesh) using n-hexane /ethyl acetate polarities resulted in the isolation of compound **27** (18 mg) and **28** (4 g) as brown amorphous solid.

Nature	Brown amorphous solid
FTIR (KBr, υ_{max})	3233, 1703, 1605, 1513, 1447, 1366, 1267, 1167, 998 and 834 cm^{-1}.
^1H NMR (500 MHz, Acetone – d_6)	δ 8.58 (brs, 3H, -OH), 8.35 (brs, 2H, -OH), 7.21 (d, J = 8 Hz, 2H, H-2a, 6a), 7.18 (d, J = 8.5 Hz, 2H, H-2b, 6b), 6.91 (d, J = 16.5 Hz, 1H, H-8b), 6.84 (d, J = 8.5 Hz, 2H), 6.74

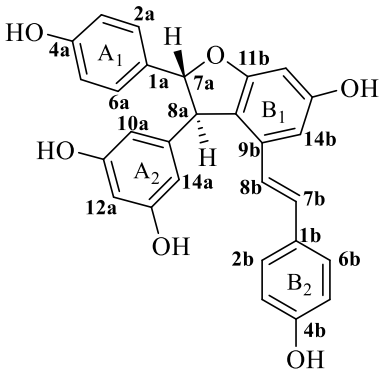

(-)-ε-Viniferin (27)

	(d, *J* = 8.5 Hz, 2H), 6.73 (m, 1H), 6.70 (d, 1H merged), 6.33 (d, *J* = 1.5 Hz, 1H), 6.25 (s, 3H), 5.43 (d, *J* = 5.5 Hz, 1H, H-7a), 4.47 (d, *J* = 5.5 Hz, 1H, H-8a) ppm.
^{13}C NMR (125 MHz, Acetone -d_6)	δ 161.5 (C-OH), 159.0 (C-OH), 158.8 (C-OH), 157.4 (C-OH), 157.4 (C-OH), 146.5, 135.5, 132.9, 130.0, 129.2, 128.9, 127.8, 127.3, 127.0, 122.7, 118.9, 116.5, 115.4, 115.3, 115.2 114.9, 114.8, 106.1, 103.3, 101.2, 95.9, 93.0 (C-7a), 56.2 (C-8a) ppm.
HRESIMS (m/z)	455.1497 $(M+H)^+$

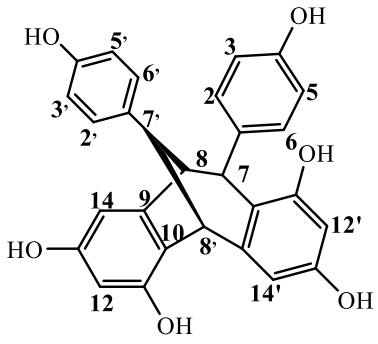

(-)- Ampelopsin F (28)

Nature	Brown amorphous solid
FTIR (KBr, υ_{max})	3704, 2854, 1510 cm^{-1}
^{1}H NMR (500 MHz, Acetone-d_6)	δ 8.02 (s, 1H, -OH), 7.96 (s, 1H, -OH), 7.94 (s, 1H, -OH), 7.89 (s, 1H, -OH), 7.79 (s, 1H, -OH), 7.35 (s, 1H, -OH), 6.96 (d, *J* = 8.5 Hz, 2H, H-2 and H-6), 6.65 (d, *J* = 8.5 Hz, 2H, H-2' and H-6'), 6.63 (d, *J* = 8.5 Hz, 2H, H-3 and H-5), 6.44 (d, J_1 = 8.5 & J_2= 2 Hz, 2H, H-3' and H-5'), 6.39 (d, *J* = 2

	Hz, 1H, H-14), 6.32 (d, *J* = 2.5 Hz, 1H, H-14'), 6.02 (d, *J* = 2.5 Hz, 1H, H-12'), 5.94 (d, *J* = 2.5 Hz, 1H, H-12), 4.06 (d, *J* = 2 Hz, 1H, H-7), 4.0 (s, 1H, H-8'), 3.51 (s, 1H, H-7'), 3.23 (s, 1H, H-8) ppm.
^{13}C NMR (125 MHz, Acetone – d_6)	δ 158.6 (C-14), 157.9 (C-11'), 157.2 (C-13'), 156.3 (C-4'), 156.2 (C-4), 153.2 (C-11), 147.6 (C-10), 147.4 (C-10'), 138.4 (C-1), 135.4 (C-1'), 129.9 (C-2 and 6), 129.3 (C-2' and 6'), 127.8 (C-10), 115.7 (C-3' and 5'), 115.6 (C-3 and 5), 113.4 (C-), 105.7 (C-14'), 104.2 (C-14), 101.9 (C-12), 101.9 (C-12'), 58.2 (C-8), 50.5 (C-7'), 49.7 (C-8'), 47.2 (C-7) ppm.
HRESIMS (m/z)	455.1497 $(M+H)^+$

4A.13.3.2. Isolation of compound 29

Fraction pool 7 was subjected to repeated column chromatographic separation using *n*-hexane/ethyl acetate polarities (100-200 mesh) and gel permeation using Sephadex LH20, followed by PTLC (preparative thin layer chromatography) resulted in the isolation of compound **29** (250 mg) as brown amorphous solid.

4A.13.3.3. Isolation of compound 30

Fraction pool 8 was subjected to column chromatographic separation using *n*-hexane/ethyl acetate polarities (100-200 mesh) resulted in the isolation of compound **30** (3 g) as a brown amorphous solid.

4A.13.3.4. Isolation of compound 31

Fraction pool 8 was subjected to repeated column chromatographic separation using *n*-hexane/ethyl acetate polarities, chloroform-methanol polarities, gel permeation using Sephadex LH20, followed by PTLC resulted in the isolation of compound **31** (87 mg) as a brown amorphous solid.

4A.13.3.5. Isolation of compound 32 and 33

The Fr.11 was subjected to silica gel (100-200 mesh, *n*-hexane/ethyl acetate polarities) followed by precipitation using 55 % *n*-hexane/ethyl acetate resulted in the isolation of bergenin (**32**, 900 mg) and methoxy bergenin (**33**, 234 mg) as colourless amorphous solids.

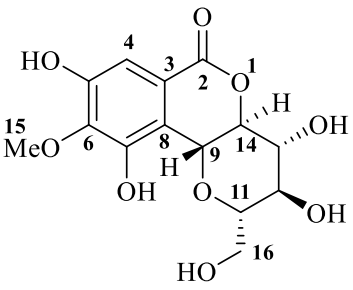

Nature	Colourless crystalline solid
FTIR (KBr, υ_{max})	3429, 2926, 1728, 1673, 1471 1093 and 790 cm^{-1}.
^{1}H NMR (500 MHz, DMSO – d_6)	δ 9.76 (s, 1H, OH-4), 8.45 (s, 1H, OH-6), 7.0 (s, 1H, H-4), 5.65 (d, J = 5 Hz, 1H, OH-13), 5.43 (d, J = 6 Hz, 1H, OH-12), 4.98 (d, J = 10.5 Hz, 1H, H-9), 4.92 (t, J = 5 Hz, 1H, OH-16), 4.00 (t, J = 10 Hz, 2H, H-14), 3.86 – 3.84 (m, 1H, H-16b), 3.78 (s, 3H, -OCH_3), 3.68 -3.63 (m, 1H, H-13), 3.59 – 3.56 (m, 1H, H-11), 3.45 – 3.42 (m, 1H, H-16a), 3.23 -3.21 (m, 1H, H-12), 3.20 – 3.18 (m, 1H, H-12) ppm.
^{13}C NMR (125 MHz, DMSO – d_6)	δ 163.3 (C-2), 150.9 (C-4), 148.0 (C-6), 140.5 (C-5), 118.0 (C-8), 115.9 (C-7),

	109.4 (C-3), 81.7 (C-11), 79.7 (C-14), 73.6 (C-13), 72.0 (C-9), 70.6 (C-12), 61.0 (C-16), 59.7 (C-15) ppm.
HRESIMS (m/z)	351.06979 $(M+Na)^+$

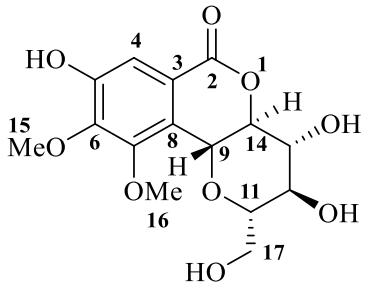

Nature	Colourless amorphous solid
FTIR (KBr, υ_{max})	3429, 2926, 1728, 1673, 1471, 1093, 790 cm^{-1}.
^1H NMR (500 MHz, DMSO– d_6)	δ 9.94 (s, 1H, OH-5), 7.24 (s, 1H, H-4), 5.56 (d, J = 5 Hz, 1H, -OH-13), 5.28 (s, 1H), 4.74 (d, J = 10.5 Hz, 1H), 4.50 (s, 1H), 3.89 (t, J = 10 Hz, 1H, H-14), 3.82 (s, 3H, -OCH_3), 3.78 (s, 3H, -OCH_3), 3.68 - 3.64 (m, 1H), 3.57 – 3.55 (m, 1H), 3.42 -3.39 (m, 1H), 3.29 (t, J = 8.5 Hz, H-16a), 3.17 (s, 1H, H-12) ppm.
^{13}C NMR (125 MHz, DMSO – d_6)	δ 163.7 (C-2), 151.2 (C-4), 150.8 (C-4), 147.9 (C-6), 146.7, 140.9 (C-5), 124.3, 119.0, 118.0 (C-8), 116.0 (C-7), 113.1 (C-7), 109.3 (C-3), 81.4 (C-11), 80.2 (C-14), 74.0 72.4, 71.0 (C-9), 70.3 (C-12), 61.0 (C-16), 60.9 (-OCH_3), 60.3 (-OCH_3) ppm.
HRESIMS (m/z)	365.08549 $(M+Na)^+$

4A.13.4. Chemicals and reagents

The following chemicals and reagents were used: 1,1-diphenyl-2-picrylhydrazyl (DPPH), 2,2-azino-bis(3-ethyl-benzothiazoline-6-sulphonicacid)diammonium salt (ABTS), 6-hydroxy-2,5,7,8-tetramethylchroman-2-carboxylic acid (Trolox), Adenosine triphosphate (ATP) (Sigma-Aldrich Co., St. Louis, USA); thiobarbituric acid (TBA) (Guangdong Guanghua Chemical Factory Co., Ltd. PR China); sodium borohydride ($NaBH_4$), vanillin, aluminium chloride, acetic acid, hydrochloric acid, sodium dihydrogen phosphate, disodium hydrogen phosphate, sodium chloride, potassium chloride, potassium dihydrogen phosphate, sodium carbonate, sodium acetate, ferric trichloride hexahydrate ($FeCl_3 \cdot 6H_2O$), potassium persulfate (Tianjin Bodi Chemical Co., Ltd, PR China).

4A.13.5. Evaluation of total phenolic content

The total phenolic content (TPC) was evaluated by Folin-Ciocalteau colorimetric assay as described previously [Singleton *et al*., **1965**]. The samples were mixed with Folin–Ciocalteu reagent and sodium carbonate allowed to stand for 90 min at room temperature and absorbance was measured against the blank at 750 nm by multimode reader and was expressed as milligrams of gallic acid equivalent per gram of dry weight (mg GAE/ g). The data are reported as the mean ± SD for three replicates.

4A.13.6. DPPH radical scavenging activity

DPPH radical scavenging activity was assessed according to the method of Brand-Williams, Cuvelier and Berset [Yen *et al*., **1994**]. Various concentrations of the extracts and isolated compounds were added to 1 mL of methanolic DPPH solution (0.2 mM) and kept for incubation at room temperature in dark for about 30 minutes. The scavenging activity was determined by measuring the absorbance at 517 nm using multimode reader. The percentage of DPPH radical scavenging activity (% RSA) was calculated as,

$$\% \text{ RSA} = [(A_0 - A_S)/A_0] \times 100$$

Where A_0 is the absorbance of control and A_S is the absorbance of tested samples. A graph was plotted with concentration along X-axis and absorbance along Y-axis. IC_{50} value was calculated and expressed in μg/mL for extracts and μM for phytochemicals. IC_{50} value signifies the concentration of tested samples to scavenge 50 % of the DPPH radical.

4A.13.7. ABTS radical cation scavenging assay

The spectrophotometric analysis of ABTS radical scavenging activity was carried out in a 96 well microplate according to the method of Xie *et al.* with modifications [Xie *et al.*, **2014**]. Briefly, 7 mM ABTS aqueous solution was reacted with 2.45 mM potassium persulfate, and the mixture was stored in the dark at room temperature for 14 h to generate ABTS free radicals. Then, the ABTS was diluted with methanol to a concentration such that the absorbance at 734 nm was 0.7 ± 0.02 to provide a working solution before usage. The absorbance of a mixture of 200 μL of ABTS working solution and the different concentration of each sample was monitored at 734 nm. The ABTS scavenging capacity of the compounds were compared with that of the ascorbic acid, and the percentage inhibition was calculated as,

$$\% \text{ RSA} = [(A_0 - A_S)/A_0] \times 100$$

Where A_0 is the absorbance of control and A_S is the absorbance of tested samples. A graph was plotted with concentration along X-axis and absorbance along Y-axis. IC_{50} value was calculated and expressed in μM for phytochemicals. IC_{50} value signifies the concentration of tested samples to scavenge 50 % of the ABTS radical.

4A.13.8. Cell line and culture conditions

H9c2 cells from rat cardiomyocytes were obtained from NCCS, Pune and were cultured in Dulbbeco's modified Eagle's medium (DMEM) supplemented with 10 % fetal bovine serum (GibcoBRL) and 1 % Antibiotic-antimycotic (GibcoBRL) at 37 °C in a humidified atmosphere containing 5 % CO_2. Cells were subcultured at appropriate density for each analysis and above 80 % confluence were used for all the experiments.

4A.13.9. Cell viability assay

Cell viability of compounds (**27-33**), treated with 100 μM H_2O_2 were determined by MTT assay [Mosmann *et al.*, **1983**]. H9c2 Cells were seeded on 96 well plates and after incubation the cells were subjected for various tratements. After 80 % confluency, different concentrations (5 μM, 10 μM, 15 μM, 20 μM & 25 μM) of compounds (**27-33**) were treated and incubated at 37 °C for 24 h, after incubation 100 μM H_2O_2 was added and kept for 15 min. Sample free media used for negative control and 100 μM H_2O_2 used as positive control. After 24 h incubation, 100 μL MTT reagent (50 μg/well) was added and incubated for 4 h in dark. Then, removed the reagent and 200 μL DMSO was added to all wells, covered with aluminium foil and shake the plate on shaker for 45 min. After

that, absorbance was read at 570 nm using multimode reader. Each assay was carried out three times, and the results were expressed as the mean.

Percentage viability = (OD of test /OD of control) x 100

4A.13.10. Intracellular reactive oxygen species (ROS) levels

The production of ROS was imaged by employing 2', 7'-dichlorodihydrofluoresceindiacetate (DCFH-DA). The cells were seeded and treated with 5 μM and 15 μM concentrations compounds (**27-33**) for 24 h at 37 ºC. After incubation, cells were induced with 100 μM hydrogen peroxide for 15 min. Here, 100 μM H_2O_2 alone was used as a positive control and sample free cells were taken as negative control. Then cells were incubated with DCFH-DA for 20 min and resulting fluorescence was read by fluorescence multimode reader using an excitation wavelength of 488 nm and an emission wavelength of 530 nm [Cathcart *et al*., **1983**]. The values were normalized to the negative control (without treatment) and respective fold change was calculated. Quantification of ROS production by cells were also analyzed by measuring the intracellular DCF fluorescent intensity by flow cytometer (BD FACS Aria II, BD Bioscience, USA).

4A.13.11. Activities of antioxidant enzymes

Superoxide dismutase (SOD) activity was estimated by method of Kakkar *et al.* The assay of SOD is based on the inhibition of the formation of NADH-phenazine methosulphate-nitroblue tetrazolium formazan [Kakkar *et al*., **1984**]. In brief, the assay mixture contained 1.2 mL of sodium pyrophosphate buffer, 0.1 mL of PMS, 0.3 mL of NBT, 0.2 mL of the cell extract and water in a total volume of 2.8 mL. The reaction was initiated by the addition of 0.2 mL of NADH. The mixture was at 30 °C for 90 s and arrested by the addition of 1.0 mL of glacial acetic acid. The reaction mixture was then shaken with 4.0 mL of *n*-butanol, allowed to stand for 10 min and centrifuged. The intensity of the chromogen in the butanol layer was measured at 560 nm in a multimode reader. Catalase (CAT) activity was determined by the method of Cohen *et al.* with slight modifications. Briefly, CAT activity was spectrophotometrically assayed by measuring the disappearance of H_2O_2 at 240 nm. One unit of enzyme activity was defined as 1 μM of H_2O_2 decomposed per minute at 25 °C. The protein concentration was measured using Bradford's method using bovine serum albumin as the standard.

4A.13.12. Rhodamine 123 staining

Loss of mitochondrial membrane potential (ΔΨm) is the major response of oxidative stress. It was determined using Rhodamine 123 staining. Rhodamine 123 is a cationic fluorescent indicator that selectively accumulates within mitochondria in a membrane potential depending manner. After treatment, the cells were directly incubated with 2 μM rhodamine 123 for 25 min at room temperature in the dark, followed by rinsing with several changes of PBS (5 minutes per rinse), then fluorescence was detected by FACS Aria II (BD Bioscience, USA). A reduction in green rhodamine 123 fluorescence indicates reduced ΔΨm [Hengartner *et al*., **2000**].

4A.13.13. Adenosine triphosphate (ATP) production by HPLC analysis

The rate of ATP level in H9c2 cells was measured by using HPLC analysis (E). Adenosine triphosphate (ATP) is an indicator of the energy state in all living cells, and is dependent mainly on mitochondrial function. In cells, mitochondrial protection activity of compounds against oxidative stress was determined by measuring ATP levels. After treatment, the cells were trypsinized and centrifuged at 800×*g* for 3 min. After centrifugation, the pellets were suspended in 4 % perchloric acid on ice for 30 min. The pH of the lysates was adjusted between 6 and 8 with 2 M KOH solution. Precipitated salt was separated by centrifugation at 13,000 *xg* for 10 min at 4 °C. ATP was quantified by using Prominence HPLC system (Shimadzu, Japan) containing LC-20 AD system controller, Phenomenex Gemini C18 column (250 × 4.6 mm, 5 μM), a column oven (CTO-20A), a Rheodyne injector (USA) with a loop of 20 μL volume and a diode array detector (SPD-M20A). A buffer 20 mM KH_2PO_4 and 3.5 mM $K_2HPO_4.3H_2O$ (pH 6.1) was used as the mobile phase. The column was at room temperature, flow rate was 1.0 mL/min and the injection volume was 20 μL. The fractions were monitored at 259 nm. Sample peaks were identified by comparing with retention times of standard peaks and area were quantified. LC Lab Solutions software was used for data acquisition and analysis [Zhang *et al*., **2008**].

4A.13.14. Statistical analysis

All the tests were repeated three times and results were expressed as means ± standard deviations of the control and treated cells. The obtained data were subjected to one-way ANOVA and the significance was calculated by Duncan's multiple range test, using SPSS 16.0 and significance was accepted at $p \leq 0.05$.

Antidiabetic Effects of Resveratrol Oligomers from the Stem Bark of *Vatica chinensis*

4B.1. Introduction

As mentioned in the second chapter, type II diabetes mellitus (T2DM) is a chronic metabolic syndrome due to insulin-resistance in body tissue. The insulin resistance leads to increased blood glucose level, which can damage many of organs. Therapeutic approaches for alleviating T2DM is to suppress the glucose absorption from the intestine through the inhibition of carbohydrate digestive enzymes such as α-amylase and α-glucosidase, advanced glycated end products formation (AGEs formation) and glucose uptake in myocytes and adipose tissues. From this point of view, many studies are ongoing all over the world for safe and effective inhibitors of α-amylase enzyme, α-glucosidase enzyme and protein glycation along with enhanced glucose uptake in adipose tissue and myocytes from medicinal plants to treat T2DM. Here, we evaluated the antidiabetic effect of resveratrol oligomers from the stem bark of *Vatica chinensis*.

4B.2. Aim and scope of the present work

Resveratrol oligomers are major class of stilbenoids which can be biosynthesized by regioselective oxidative coupling of two to eight units of resveratrol monomer and it is mainly found in Vitaceae, Dipterocarpaceae, Leguminosae and Cyperaceae families. Due to their unique structures and pleiotropic pharmacological activities, natural product chemists are increasingly focusing on resveratrol oligomers in the last few years. The current focus of our research aims at identifying resveratrol oligomers from *Vatica chinensis* to facilitate the application of these compounds as a drug candidate for the treatment of T2DM. In 2016, our group reported the antidiabetic potential of resveratrol tetramer; (+)- and (-)- hopeaphenol [Sasikumar *et al*., **2016**]. Here, we evaluated the *in vitro* α-amylase enzyme, α-glucosidase enzyme and protein glycation inhibitory activities various extract of *Vatica chinensis* and the compounds isolated from *Vatica chinensis* [**Figure 4B.1**]. We have also evaluated the glucose uptake in L6 myotubes. To the best of our knowledge, this is the first investigation of the antidiabetic activity of the stem bark of *Vatica chinensis*.

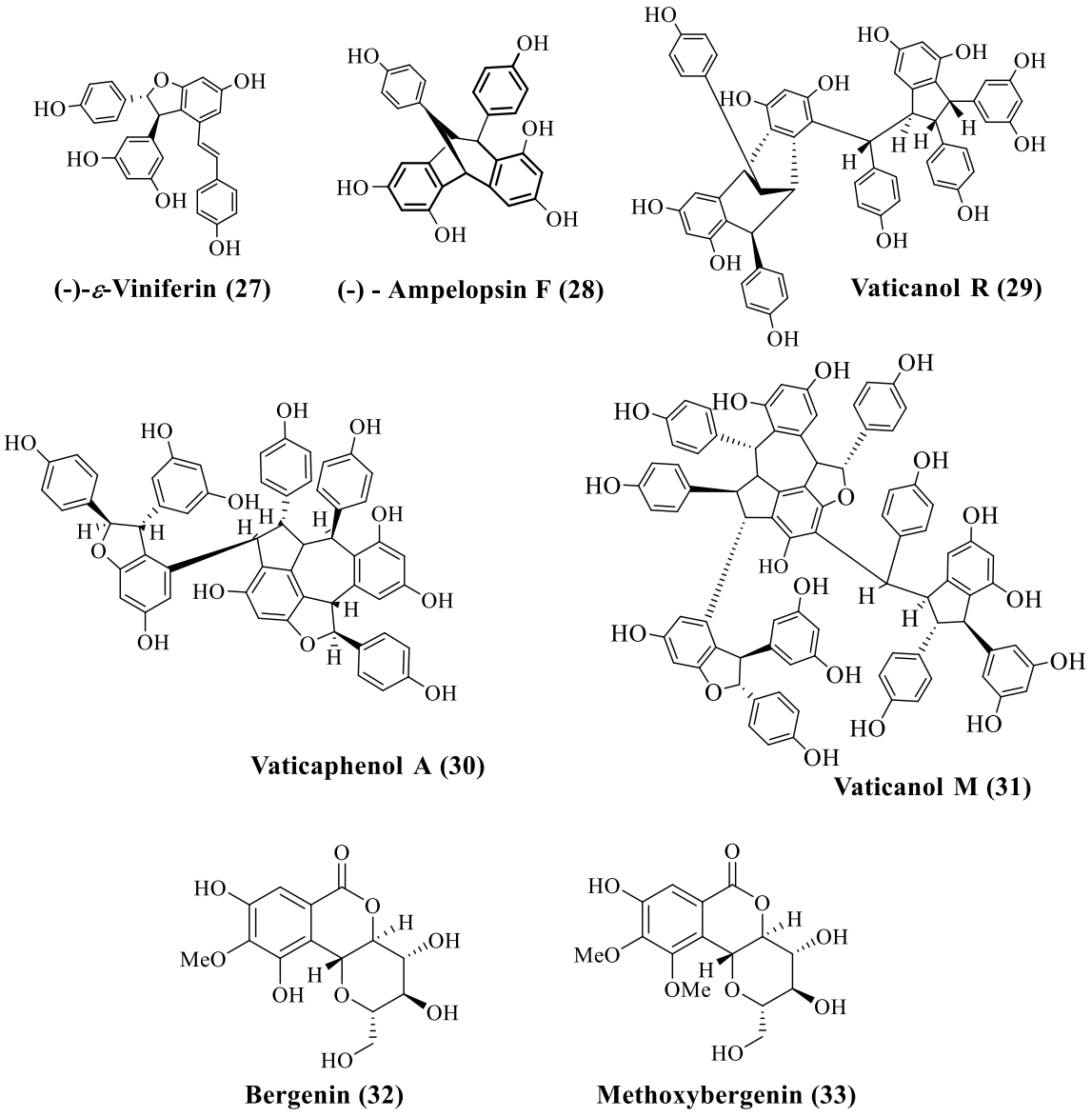

Figure 4B.1. Structures of the compounds for antidiabetic studies

4B.3. Extract level *in vitro* antidiabetic activity

Air and oven dried stem barks of *Vatica chinensis* were subjected to extraction with various solvents such as *n*-hexane, acetone, ethanol and water. These extracts were analysed for its inhibition on digestive enzymes and protein glycation. The results demonstrated that the acetone effectively inhibits α-amylase enzyme (IC_{50} 21.53 ± 0.629 μg/mL), which is less active compared to the standard acarbose used (IC_{50} 5.71 ± 0.282 µg/mL) in this assay. All the extract inhibit α-glucosidase, but acetone extract having highest inhibitory activity with IC_{50} 51.60 ± 0.261 μg/mL, which is better than the standard acarbose used (IC_{50} 50.03 ± 0.233 μg/mL). The result from our study showed

that the acetone extract of *Vatica chinensis* possesses significant antiglycation activity with IC_{50} 114.53 ± 0.629 μg/mL.

Table 4B.1. Extract level antidiabetic activity of the stem bark of *Vatica chinensis*

Extracts	**α- amylase (μg/mL)**	**α-glucosidase (μg/mL)**	**Antiglycation (μg/mL)**
Hexane	NIL	NIL	143.67 ± 0.205
Acetone	**21.53 ± 0.629**	**51.60 ± 0.261**	**114.53 ± 0.629**
Ethanol	49.54 ± 0.664	69.55 ± 0.558	149.54 ± 0.664
Water	366.41 ± 0.523	197.27 ± 1.004	266.41 ± 0.523
Acarbose	5.71 ± 0.282	50.03 ± 0.233	-
Ascorbic acid	-	-	48 ± 0.876

Each value represents mean ± SD (standard deviation) from triplicate measurements

4B.4. α-Amylase inhibitory activity

As described in the previous chapter, α -amylase is a commonly as the known key digestive enzyme that is found in pancreatic juice and saliva and recognized as promising target for the control of postprandial hyperglycaemia, the earliest metabolic condition occurring in diabetes patients. α-Glucosidase enzyme can catalyses the last stage of starch and disaccharides hydrolysis but, α-amylase helps to hydrolyse large starch molecules into small absorbable molecules. It is therefore effective to inhibit the activity of α -amylase as a treatment option for diabetes patients. In this regard, inhibitors can delay the absorption of carbohydrates, slow down postprandial hyperglycaemia, and could be useful in helping patients with diabetes. The mechanism of inhibition for α -amylase involves delaying the breakdown of carbohydrates and prevents absorption of simple sugar in the small intestine. Miglitol, acarbose, and voglibose, are commonly used α-amylase inhibitors that are extremely well-known to reduce postprandial hyperglycaemia by delaying the carbohydrate digesting activity and thus preventing glucose absorption. Resveratrol moiety is often encountered in medicinal chemistry and can be considered as a privileged scaffold. Here, we tested the α-amylase inhibitory activity of phytochemicals isolated from *Vatica chinensis*. All compounds exhibited moderate α-amylase enzyme inhibition.

4B.5. α-Glucosidase inhibitory activity

α-Glucosidase inhibitors are also a key enzyme and commonly used as oral agents for improving postprandial hyperglycemia due to the lack of a hypoglycemic threat and, more importantly, the prospect of blood glucose control without hyperinsulinemia and body weight gain. Inhibition of α-glucosidase enzyme should result in delayed carbohydrate digestion and glucose absorption with attenuation of postprandial hyperglycemic excursions. It has been reported that α-glucosidase inhibitors usually do not alter the total amount of carbohydrate absorbed and, therefore, do not cause any net nutritional caloric loss, although they slow down carbohydrate digestion. Here, we examined the α-glucosidase inhibitory activity of phytochemicals isolated from *Vatica chinensis*. From the **Table 4B.2**, we can clearly see that all the compounds significantly inhibit the activity of α-glucosidase enzyme with IC_{50} value of 1.29 ± 0.344 (**27**), 9.56 ± 0.498 (**28**), 0.56 ± 0.598 (**29**), 0.16 ± 0.987 (**30**), 0.32 ± 0.547 (**31**), 7.92 ± 0.765 (**32**), 7.0 ± 0.784 (**33**) μM. The standard α-glucosidase inhibitor showed IC_{50} value of 52.87 ± 0.224 μM.

Table 4B.2. Molecular level antidiabetic activity of compound **27-33**

Compounds	α-Amylase (*m*M)	α-Glucosidase (μM)	Antiglycation (μM)
(-)-ε-Viniferin (27)	8 ± 0.479	1.29 ± 0.344	125 ± 0.089
(-)-Ampelopsin F (28)	3.0 ± 0.231	9.56 ± 0.498	67.93 ± 0.288
Vaticanol R (29)	1.0 ± 0.589	0.56 ± 0.598	22.13 ± 0.798
Vaticaphenol A (30)	1.42 ± 0.348	0.16 ± 0.987	35.72 ± 0.297
Vaticanol M (31)	0.32 ± 0.176	0.32 ± 0.547	21.17 ± 0.677
Bergenin (32)	5.7 ± 0.439	7.92 ± 0.765	1280.77 ± 0.115
Methoxy bergenin (33)	4.9 ± 0.940	7.0 ± 0.784	1277.04 ± 0.434
Acarbose	8.99 ± 0.48 (μM)	52.87 ± 0.224	
Ascorbic acid	-	-	155.38 ± 0.547

Each value represents mean ± SD (standard deviation) from triplicate measurements

4B.6. Antiglycation property

The increased protein glycation followed by the build-up of glycated end products results in the formation of reactive oxygen species, and the auto-oxidation of these glycated end products contribute towards many diabetic associated complications.

Therefore, searching the plant based natural compounds having potent antiglycation property always offer an economical remedy for the management of many diabetic associated complications. With this background, we have studied the inhibitory effects of protein glycation of resveratrol oligomers from *Vatica chinensis*. Compounds **27-31** significantly inhibit the protein glycation with IC_{50} value of 125 ± 0.089 μM (**27**), 67.93 ± 0.288 μM (**28**), 22.13 ± 0.798 μM (**29**), 35.72 ± 0.297 μM (**30**) and 21.17 ± 0.677 μM (**31**) respectively. Bergenin (**32**) and methoxybergenin (**33**) showed moderate antiglycation property.

4B.7. Molecular simulation studies

The crystal structures of human pancreatic α-amylase (PDB ID: **4GQQ**), the *N*-terminal and *C*-terminal of human maltase glucoamylase (PDB ID: **2QMJ** and **3TOP**) were retrieved from RCSB Protien Data Bank. They contain 496, 870 and 908 amino acids respectively. The structures were cleaned, refined using protein preparation wizard of Schrodinger suite. The grid was generated around the centroid of the workspace ligand and further used for docking using Glide programme Schrodinger suite. The ligands were tested for its conformational stability using LigPrep and the ADME/T properties were checked by the parameters in QikProp. (**Table 4B.3**). All the compounds except **29**, **30** and **31** having M.W in the acceptable region and act as more drug like with few #stars. They have acceptable values of #rotor, CNS, SASA, FISA, HBA and HBD. QPlog Khsa value indicates their excellent binding to human serum albumin with good range octanol-water partition coefficient. Human oral absorption and aqueous solubility promote them as drug like with minimum deviation from Ro5.

The binding affinity was compared based on D-score and G-score analysis. Among the **7** compounds, compound **32** shows best binding with **4GQQ** having G-score -6.01 and D-score -5.99 kcal/mol. The H-bonding with ASP 236, SER 245, GLY 285 and GLU 282 favours the binding (**Figure 4B.1).** The compound **27** has the better affinity (G-score: -6.70 and D-score: -6.70 kcal/mol) to **2QMJ**, followed by compound **32** (G-score: -4.98 and and D-score: -4.95 kcal/mol). The strong H-bonding with ASP 327, GLN 603 and the Π-stacking interaction with TRP 406 stabilises compound **27-2QMJ** complex, while the H-bonding with TYR 605, THR 205, ASP 203 and Π-stacking with PHE 575 favours the complex formation of compound **32** with **2QMJ**. Again with *C*-terminal of glucoamylase compound **31** followed by compound **32** shows better affinities with (-8.17, -5.89 and -6.54, -3.67 respectively. Here, the H-bonded interaction with ASP 1157, ASP

1526 and Π-stacking interaction with PHE 1560 stabilises the compound **32-3TOP** complex. Generally, H-bonding and Π-stackimng are the favourable factors in better affinity. compound **32** is the best among the **7** by comparing the simulation analysis.

Table 4B.3. ADME/T properties of compound **27-33**

Sl. No	**27**	**28**	**29**	**30**	**32**	**33**
M.W	454.478	454.478	908.956	906.941	328.275	342.302
#stars	0	1	11	14	0	0
#rotor	8	6	15	10	7	7
CNS	-2	-2	-2	-2	-2	-2
SASA	714.01	656.875	994.455	1089.364	517.704	529.608
FISA	264.047	289.853	507.192	455.003	258.669	224.608
HBA	4.5	4.5	9	9	12.05	12.05
HBD	5	6	12	10	5	4
QPlogKhsa	0.649	0.433	1.284	1.764	-0.94	-0.913
HOA	2	1	1	1	2	2
% HOA	74.859	51.774	0	2.556	45.284	54.128
QPlogPo/w	3.623	2.641	4.493	5.662	-1.584	-1.061
QPlogS	-5.49	-4.6	-6.222	-9.116	-1.773	-1.747
R Of Five	0	1	3	4	0	0

M.W. (Molecular Weight):130.0 to 725.0; #stars (few stars-more drug-like): 0 to 5; #rotor (Number of non-trivial and non-hindered rotatable bonds):0 to 15; CNS (Central Nervous System activity): -2 to +2; SASA (Total solvent accessible surface area in square angstroms): 300.0 to 1000.0 FISA (Hydrophilic component of total solvent accessable area): 7.0 to 333.0; HBA (Hydrogen bond acceptor): 2.0 to 20.0; HBD (hydrogen bond donor): 0.0 to 6.0; QPlogKhsa (binding to human serum albumin): -1.5 to 1.5; HOA (Human Oral Absorption): 1, 2, or 3 for low medium, and high; % HOA (Percent Human Oral Absorption): >80 % is high, <25 % is poor; QPlogPo/w (octanol/water partition coefficient): -2.0 to 6.5; QPlogS (Aqueous solubility): -6.5 to 0.5; Ro5 (Number of violations of Lipinski's rule of five): maximum is 4.

Table 4B.4. G-score/D-score of isolated compounds with human pancreatic *α*-amylase (**4GQQ**) and human maltase glucoamylase (*N*- terminal, **2QMJ**; *C*- terminal, **3TOP**)

Compounds	4GQQ kcal/mol		2QMJ kcal/mol		3TOP kcal/mol	
	G-Score	D-Score	G-Score	D-Score	G-Score	D-Score
(-)-ε-Viniferin (27)	-3.75	-3.75	-6.7	-6.7	-	-
(-)-Ampelopsin F (28)	-	-	-	-	-	
Vaticanol R (29)	-3.6	-2.33	-4.42	-2.33	-3.56	-1.81
Vaticaphenol A (30)	-3.12	-2.95	-	-	-	-
Vaticanol M (31)	-	-	-	-	-8.17	-6.54
Bergenin (32)	-6.01	-5.99	-4.98	-4.95	-5.89	-3.67
Methoxy bergenin (33)	-3.88	-3.88	-4.71	-4.7	-	-

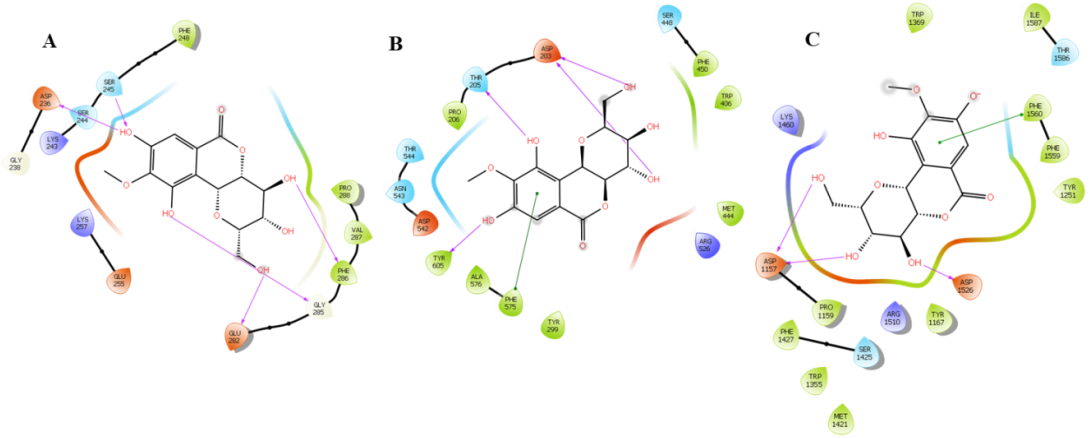

Figure 4B.2. 2D interaction diagram of bergenin **(32)** with **4GQQ (A)**, **2QMJ (B)** and **3TOP (B)**

4B.8. 2-NBDG uptake in L6 myoblasts

The skeletal muscle is the primary tissue for insulin stimulated glucose uptake and disposal and has a paramount role in energy homeostasis. Therefore, skeletal muscle is considered to be a therapeutic target tissue for insulin dependent and non-insulin dependent diabetes mellitus and associated cardiovascular disease. Hence, L6 myotubes

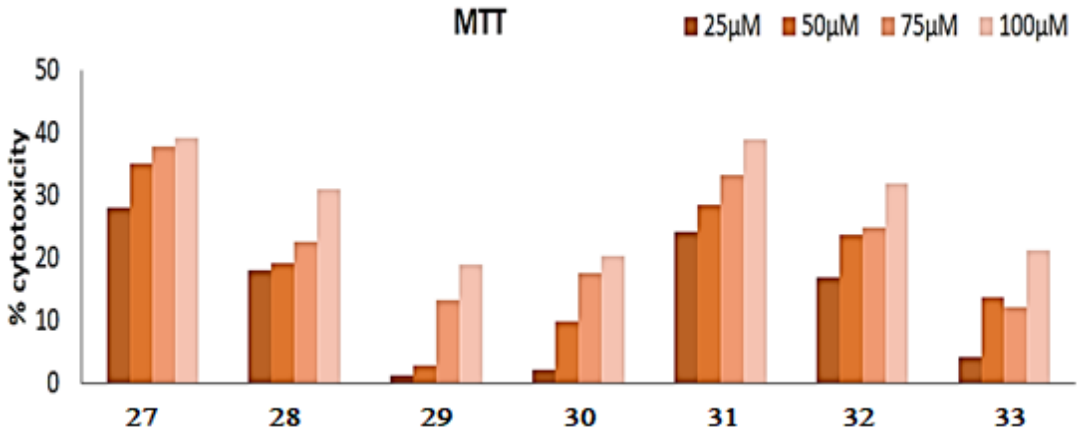

Figure 4B.3. % of cytotoxicity in L6 cell line (**27-33**)

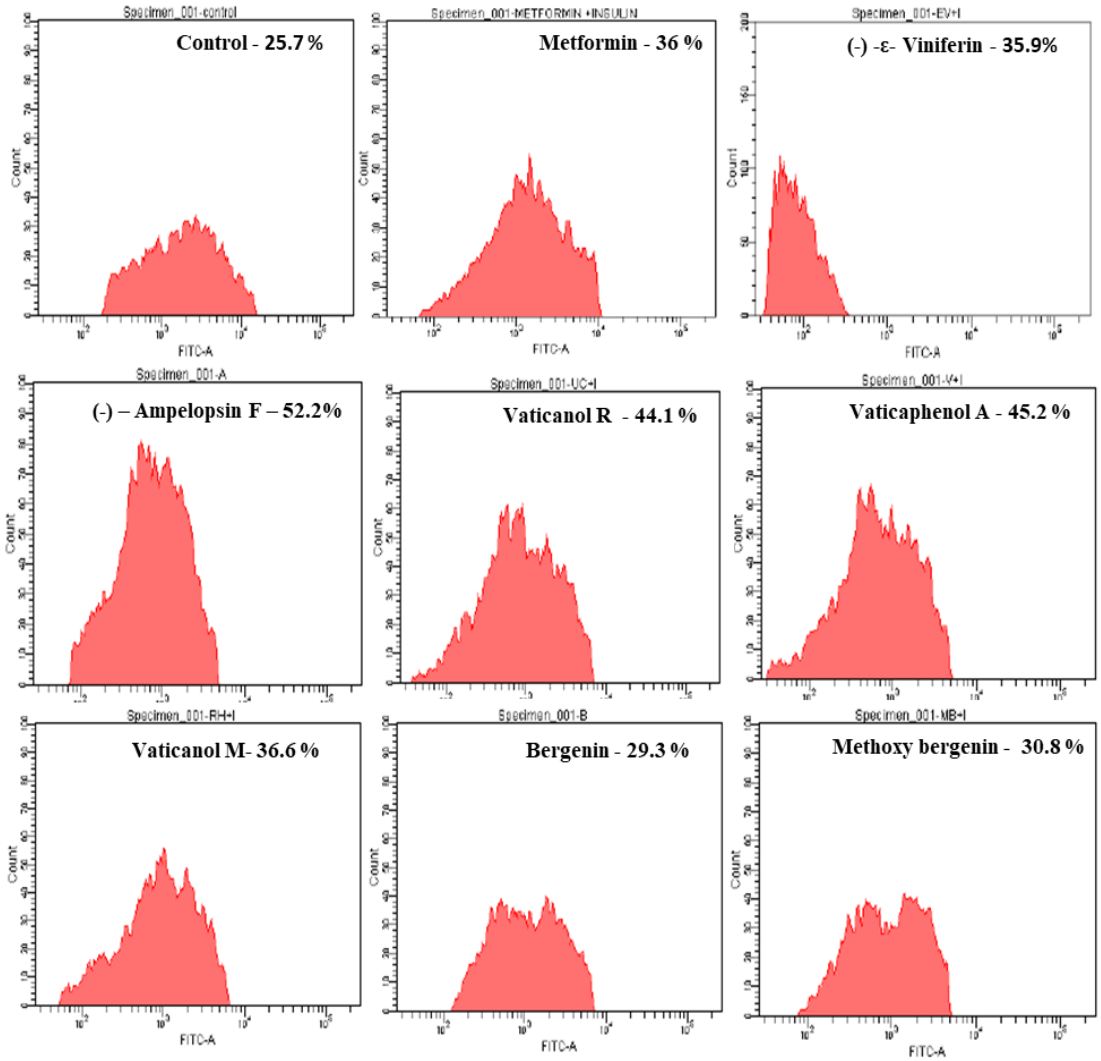

Figure 4B.4. Fluorescence analysis of 2-NBDG uptake by flow cytometry. FACS analysis in differentiated L6 cells using 2-NBDG in control cells, metformin (100 μM) and compounds (**27-33**) pretreated cells.

have been widely used to investigate the mechanism of insulin and exercise stimulated glucose absorption and transport. Several studies suggested that, natural products have been shown to exhibit enhanced uptake of glucose in L6 cell lines. The phytochemicals isolated from *Vatica chinensis* exhibited significant *in vitro* inhibitory activites against α-amylase, α-glucosidase and protein glycation. Therefore, it is encouraged us to carry out the stimulated glucose uptake in L6 myotubes. Hence, the phytochemicals isolated from *Vatica chinensis* were investigated for its effect on glucose uptake using L6 myotubes.

In order to find out the working concentration of phytochemicals, the cytotoxicity of 25, 50, 75 and 100 μM concentrations of compounds **27-33** was examined in L6 cell line by MTT assay. From **figure 4B.2**, it is clear that cell cytotoxicity increased or viability decreased significantly in a dose-dependent manner. Therefore, 25 μM concentration of compounds **27** and **31**, 50 μM concentration of compounds **28** and **32** and 100 μM concentration of compounds **29**, **30** and **33** were selected for cellular 2-NBDG uptake experiment.

The glucose uptake in differentiated L6 cell lines was monitored using the glucose fluorescent analogue, 2-NBDG (50 μM) after the pre-treatment of the L6 myotubes with isolated compounds. Compounds **27-33** displayed a significant stimulation of glucose uptake by 35.9, 52.2, 44.1, 45.2, 36.6, 29.3 and 30.8 % respectively. Metformin was used as a positive control, showed 36 % glucose uptake at 100 μM under identical experimental conditions.

4B.9. Conclusion

In conclusion, this study presented the antidiabetic activity of resveratrol oligomers from *Vatica chinensis*. All compounds showed significant inhibitory activity on α-glucosidase enzyme and protein glycation and moderate inhibition on α-amylase enzyme. The molecular simulation studies also supported the observed antidiabetic property. Resveratrol oligomers [(-)-ε- viniferin (**27**), (-)-ampelopsin F (**28**), vaticanol R (**29**), vaticaphenol A (**30**) and vaticanol M (**31**)] exhibited significant stimulation of glucose uptake in L6 myotubes. Taken together, these results indicated that resveratrol oligomers exhibit promising antidiabetic activity in *in vitro* studies. Further studies are ongoing studies in our laboratory to establish the therapeutic efficacy.

4B.10. Experimental

General experimental procedures and chemicals used were described in section **2A.7** of Chapter **2** Part **A**.

Isolation, Characterization and Antidiabetic Potential of Phytochemicals from the Stem Bark of *Hopea parviflora*

Natural products have served as a source and inspiration for novel drug leads. Along with these, natural world delivers many indispensable services including clean air, water, aesthetic and recreational benefits to human beings. Western Ghats is enriched with variety of flora and fauna and most of them are endemic to that region. In this regard, we selected medicinally and economically important plant species *Hopea parviflora* from Western Ghats for the present study.

5A.1. *Hopea* Genus

Hopea belongs to the family dipterocarpaceae and genus was named after John Hope, the first Regius Keeper of the Royal Botanic Garden, Edinburgh. The genus contains about 104 species and widely distributed in Asia. They are mainly sub canopy trees of lowland rainforest, but some species are emergent trees for example, *Hopea nutans*. Some of the known *Hopea* species and their distribution are listed in **Table 5A.1**.

Table 5A.1. *Hopea* species and their distribution

Sl. No	*Hopea* genus	Distribution
1	*Hopea acuminata*	Philippines
2	*Hopea aequalis*	Borneo, Malaysia & Brunei
3	*Hopea altocollina*	Borneo
4	*Hopea apiculata*	Malaysia, Myanmar & Thailand
5	*Hopea aptera*	Papua New Guinea
6	*Hopea auriculata*	Peninsular Malaysia
7	*Hopea bancana*	Sumatra
8	*Hopea basilanica*	Philippines
9	*Hopea beccariana*	Peninsular Malaysia, Sumatra, Borneo & Thailand

10	*Hopea bilitonensis*	Indonesia & Malaysia
11	*Hopea brachyptera*	Philippines
12	*Hopea brevipetiolaris*	Sri Lanka
13	*Hopea cagayanensis*	Philippines
14	*Hopea canarensis*	India
16	*Hopea celebica*	Indonesia
17	*Hopea centipeda*	Borneo
18	*Hopea chinensis*	China & northern Vietnam
19	*Hopea cordata*	Vietnam
20	*Hopea cordifolia*	Sri Lanka
21	*Hopea coriacea*	Peninsular Malaysia & Borneo
22	*Hopea dasyrrhachia*	Brunei, Indonesia & Malaysia
23	*Hopea depressinerva*	Malaysia
24	*Hopea discolor*	Sri Lanka
25	*Hopea enicosanthoides*	Borneo & Malaysia
26	*Hopea erosa*	India
27	*Hopea exalata*	Southern China
28	*Hopea ferrea*	Cambodia, Malaysia, Myanmar, Thailand & Vietnam
29	*Hopea ferruginea*	Sumatra, Peninsular Malaysia & Borneo
30	*Hopea fluvialis*	Borneo
31	*Hopea foxworthyi*	Philippines
32	*Hopea glabra*	India
33	*Hopea glabrifolia*	Papua New Guinea
34	*Hopea glaucescens*	Peninsular Malaysia

35	*Hopea gregaria*	Indonesia
36	*Hopea griffithii*	Malaysia, Myanmar, Singapore & Thailand
37	*Hopea hainanensis*	China & Vietnam
38	*Hopea helferi*	Cambodia, India, Malaysia, Myanmar & Thailand
39	*Hopea inexpectata*	Papua New Guinea
40	*Hopea jacobi*	India
41	*Hopea johorensis*	Peninsular Malaysia
42	*Hopea jucunda*	Sri Lanka
43	*Hopea kerangasensis*	Sumatra, Peninsular Malaysia & Borneo
44	*Hopea latifolia*	Brunei, Cambodia, Malaysia& Thailand
45	*Hopea longirostrata*	Borneo & Malaysia
46	*Hopea malibato*	Philippines
47	*Hopea megacarpa*	Borneo
48	*Hopea mengerawan*	Indonesia, Malaysia & Singapore
49	*Hopea mesuoides*	Borneo
50	*Hopea micrantha*	Borneo
51	*Hopea mindanensis*	Philippines
52	*Hopea montana*	Sumatra, Peninsular Malaysia & Borneo
53	*Hopea nervosa*	Sumatra, Peninsular Malaysia & Borneo
54	*Hopea nigra*	Sumatra
55	*Hopea nutans*	Peninsular Malaysia & Borneo
56	*Hopea oblongifolia*	Myanmar & Thailand.
57	*Hopea odorata*	Bangladesh, Cambodia, India, Laos, Malaysia, My anmar, Thailand & Vietnam
58	*Hopea ovoidea*	Borneo

59	*Hopea pachycarpa*	Sumatra, Peninsular Malaysia & Borneo
60	*Hopea parviflora*	India
61	*Hopea paucinervis*	Sumatra
62	*Hopea pedicellata*	Cambodia, Indonesia, Malaysia & Thailand
63	*Hopea pentanervia*	Borneo
64	*Hopea philippinensis*	Philippines
65	*Hopea pierrei*	Cambodia, Indonesia, Laos, Malaysia, Thailand & Vietnam
66	*Hopea plagata*	Borneo & Philippines
67	*Hopea polyalthioides*	Peninsular Malaysia
68	*Hopea ponga*	India
69	*Hopea pterygota*	Northern Borneo
70	*Hopea pubescens*	Peninsular Malaysia
71	*Hopea quisumbingiana*	Philippines
72	*Hopea racophloea*	India
73	*Hopea recopei*	Cambodia, Laos, Thailand & Vietnam
74	*Hopea reticulata*	Thailand, Vietnam & China
75	*Hopea samarensis*	Philippines
76	*Hopea sangal*	Indonesia, Malaysia, Myanmar, Singapore & Thailand
77	*Hopea scabra*	Papua New Guinea
78	*Hopea semicuneata*	Indonesia & Malaysia
79	*Hopea shingkeng*	India
80	*Hopea siamensis*	Cambodia, Thailand & Vietnam
81	*Hopea sphaerocarpa*	Borneo

82	*Hopea subalata*	Peninsular Malaysia
83	*Hopea sublanceolata*	Peninsular Malaysia
84	*Hopea sulcata*	Peninsular Malaysia
85	*Hopea tenuivervula*	Borneo
86	*Hopea thorelii*	Laos & Thailand
87	*Hopea ultima*	Papua New Guinea
88	*Hopea utilis*	India
89	*Hopea vaccinifolia*	Borneo, Brunei & Malaysia
90	*Hopea wightiana*	India
91	*Hopea wyatt-smithii*	Borneo

5A.1.1. *Hopea exalata*

Hopea exalata, a vulnerable species endemic to Hainan Island in southern China and now enjoys second-class national protection. In 2006, Hui *et al*., reported the isolation of resveratrol oligomers; hopeanolin, shoreaphenol, vaticanol, *α*-viniferin, pauciflorol A, vaticanol A, *trans*-3,5,4′-trihydroxystilbene-2-*C*-glucoside and hopeanolin from the bark of *Hopea exalata.* All compounds were tested for their antifungal activity and inhibitory effects against jack bean urease. Among them, hopeanolin demonstrated significant antifungal activity in the MIC value range 0.1-22.5 μg/mL [Hui *et al*., **2006**]. Hopeanol is a rearranged resveratrol dimer ester with an unprecedent carbon skeleton was isolated from the bark of *Hopea exalata*. Hopeanol exhibited potent cytotoxicity against six human cancer cell lines [human nasopharynyeal epidermoid tumor (KB), human gastric ademocarcinoma (AGS), human cervical carcinoma (HeLa), human liver cancer (BEL-7402), human colon cancer (SW1116) and human gastric cancer (BGC-803)] with an IC_{50} = 0.52 -19.36 μM [Hui *et al*., **2006**]. Some of the compounds isolated from *Hopea exalata* are shown in Figure **5A.1.**

5A.1.2. *Hopea chinensis*

Hopea chinensis, a critically endangered species and found in China and northern Vietnam. In 2012, Tong *et al*., reported the isolation of hopeachinols C, hopeachinols D, hopeafuran, malibatol A, balanocarpol, heimiol A, caraphenol A, *α*-

viniferin, neoisohopeaphenol, hemsleyanol C, *trans*-piceid, and *trans*-3-*O*-methyl-resveratrol-2-*C*-*β*-glucoside from *Hopea chinensis*. All phytochemicals were tested for their acetylcholinesterase inhibitory activity, and five resveratrol derived compounds (Hopeachinols C, caraphenol A, *α*-viniferin, neoisohopeaphenol and hemsleyanol C) exhibited significant acetylcholinesterase inhibitory activity with IC_{50} values ranging from 4.81 to 11.71 μM [Tong *et al*., **2012**].

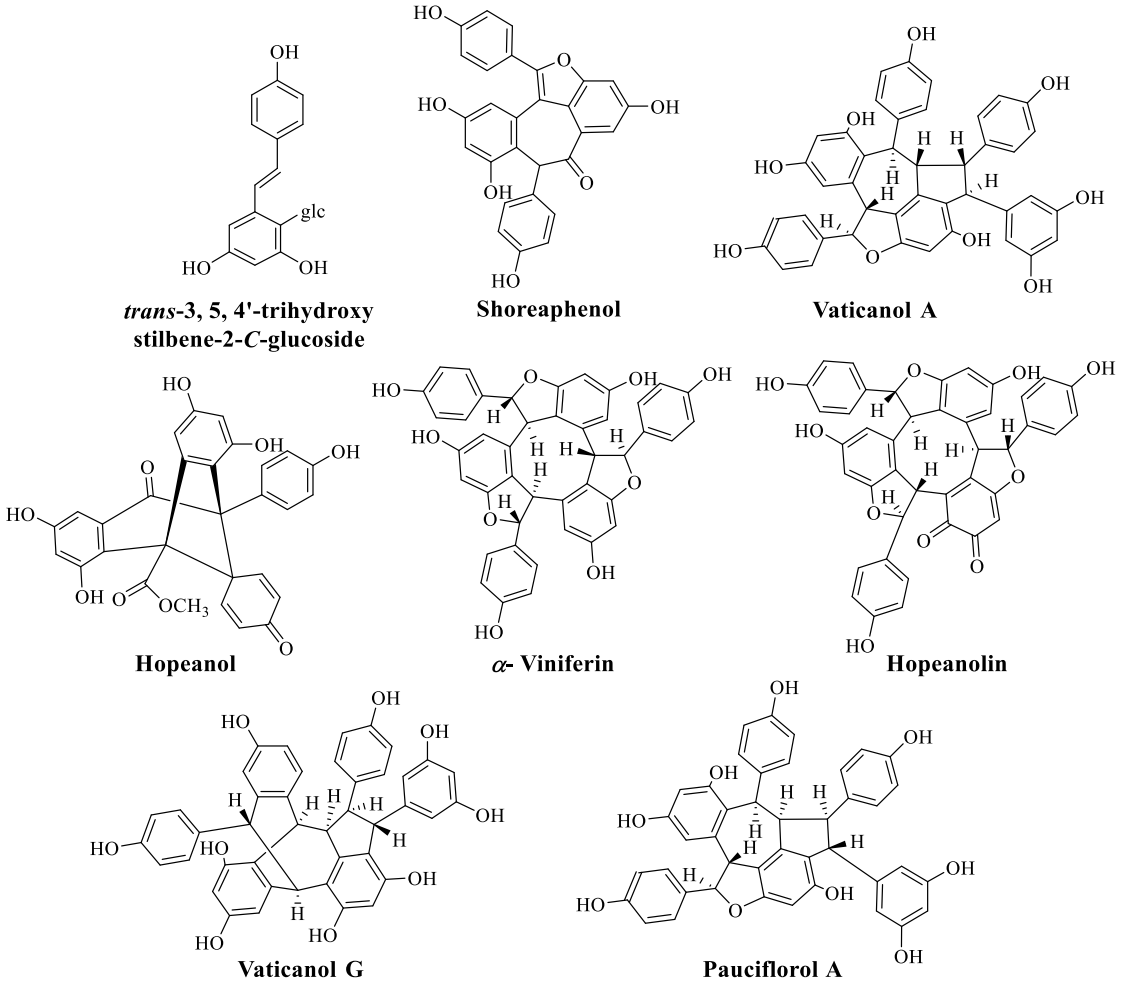

Figure 5A.1. Phytochemicals isolated from *Hopea exalata*

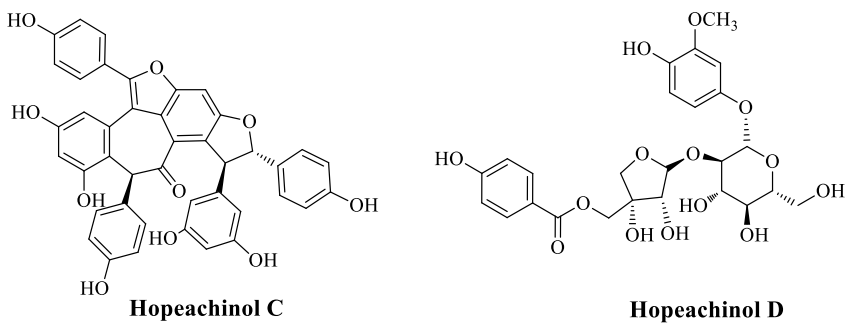

Figure 5A.2. Phytochemicals isolated from *Hopea chinensis*

5A.1.3. *Hopea hainanensis*

Hopea hainanensis, a critically endangered species and found in Hainan Island of China and northern Vietnam. Jun *et al*., reported the isolation, *in vitro* acetylcholinesterase (AChE) inhibitory and antitumor activity of three new resveratrol oligomers, hopeahainanphenol, neohopeaphenol A, and neoisohopeaphenol A from the stem bark of *Hopea hainanensis.* Neohopeaphenol A was active against AChE, with IC_{50} value of 7.66 ± 0.13 Mm [Jun *et al*., **2005**]. In 2008, Hui *et al*., reported the isolation of hopeanol, hopeahainols A, hopeahainols B and hopeanol B from *Hopea hainanensis*. Hopeahainol A was a potent acetylcholinesterase inhibitor with IC_{50} value of 4.33 μM [Hui *et al*., **2008**]. Phytochemical investigation of the stem wood of *Hopea hainanensis* led to the isolation of hopeahainols C, hopeahainols D, hopeahainols F, piceid, hopeahainanphenol, balanocarpol, malibatol A, heimiol A, vaticanol A, vaticanol E and neoisohopeaphenol. All compounds were tested for their radical scavenging activity and total reducing capacities [Jun *et al*., **2009**]. In 2009, Da *et al*., reported the isolation of hopeahainol A and it protects PC12 cells from H_2O_2 injury by modulating endogenous antioxidant enzymes, scavenging ROS and prevention of apoptosis. Therefore, hopeahainol A can be used to treat Alzheimer's disease [Da *et al*., **2009**]. Malibatol A is a resveratrol oligomer from *H. hainanensis* and it prevents ischemic stroke by inhibiting inflammation through activation of PPARγ [Jie *et al*., **2015**] (**Figure 5A.3**).

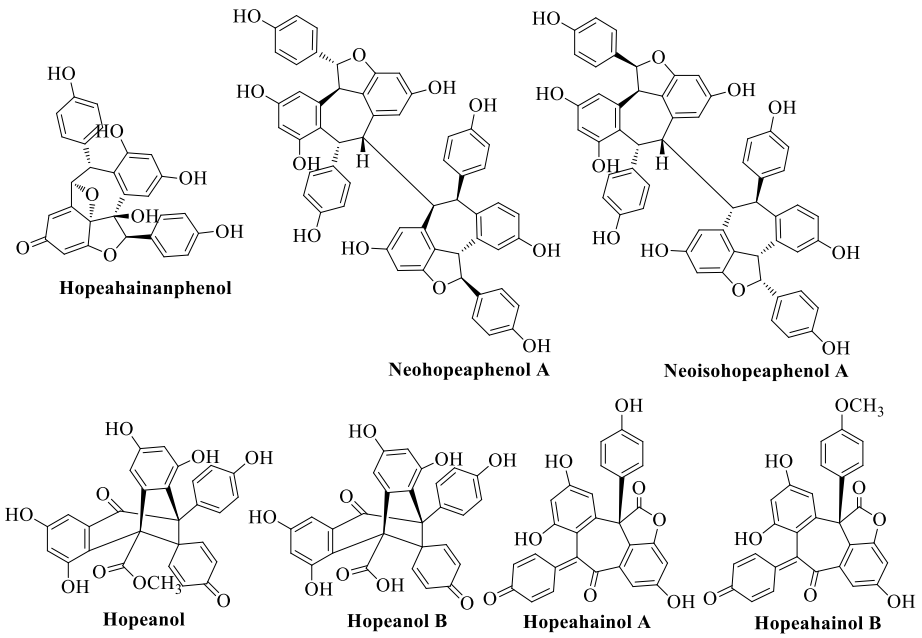

Figure 5A.3. Phytochemicals isolated from *Hopea hainanensis*

5A.1.4. *Hopea malibato*

Hopea malibato is a critically endangered species, endemic to the Philippines. Jin *et al*., reported the isolation of malibatol A, malibatol B, dibalanocarpol and balanocarpol from the leaves of *Hopea malibato*. Dibalanocarpol and balanocarpol exhibited modest HIV-inhibitory activity, while malibatol A and B were cytotoxic to the host cells (CEM SS) in the antiviral assay [Jin *et al*., **1998**] (**Figure 5A.4**).

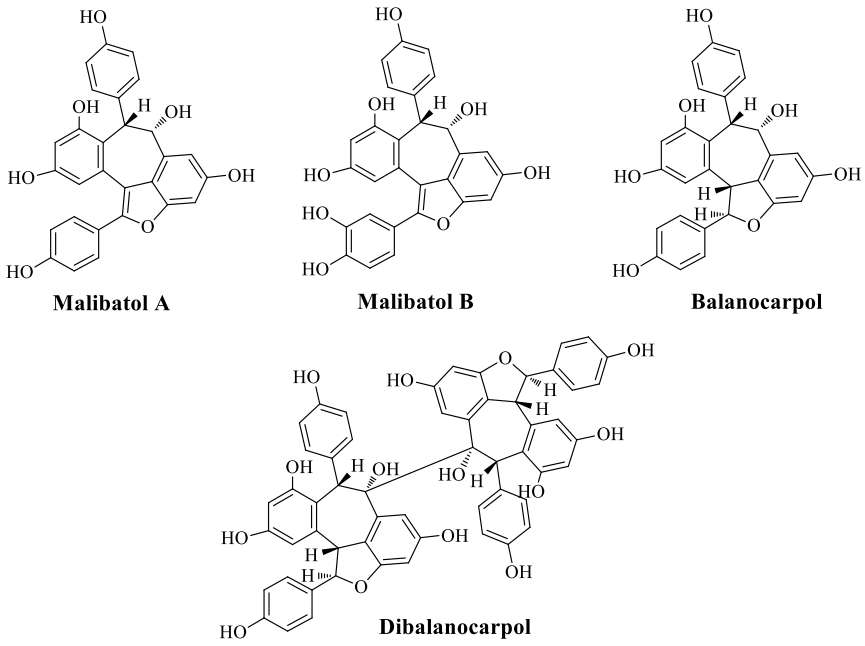

Figure 5A.4. Phytochemicals isolated from *Hopea malibato*

5A.2. Aim and scope of the present investigation

Hopea parviflora Bedd., (**Figure 5A.5**) an endangered species and commonly recognized as "Iron wood of Malabar", "White Kongu", "Thambakam" or "Kampakam". The taxonomic classification *Hopea parviflora* is shown in Table **5A.2**. In 2000, Tanaka *et al*. reported the isolation (+)-parviforol, (-)-ampelopsin A, three known compounds: (+)-balanocarpol, (-)-ε-viniferin and (-)-hopeaphenol from the stem bark of *Hopea parviflora* [Tanaka *et al*., **2000**]. After that, Naohito *et al*. reported hopeasides A, B (resveratrol pentamers), C (resveratrol trimer), and D (resveratrol dimer) together with nine known resveratrol oligomers malibatol, (-)-ampelopsin A, balanocarpol, piceid, vateriaphenol B, (-)-hopeaphenol, pauciflorol C, grandiphenol A and vatalbinoside A from the stems of *Hopea parviflora* [Naohito *et al*., **2011**]. Compounds previously isolated from *Hopea parviflora* are shown in **Figure 5A.6.** Apart from this, there is no report on the phytochemical and pharmacological evaluation of *Hopea parviflora* Bedd.

Therefore, we carried out the phytochemical and pharmacological investigation of *Hopea parviflora*. So as part of this Ph.D. program, a detailed phytochemical and pharmacological evaluation of the stem bark of *Hopea parviflora* has been unertaken. In the first part of this chapter, activity oriented extraction and isolation of the stem barks of *Hopea parviflora* resulted in the isolation of **9** compounds. It included two triterpenes, two resveratrol dimers, two tetramers, 2, 4, 8-trihydroxyphenanthrene-2-*O*-glucoside and ellagic acid 3, 3', 4-trimethoxy-4'-*O*-α-L-rhamnopyranoside along with glycoside of β-sitosterol. Among them, friedelin and friedelin-3β-ol (triterpenes), vaticaphenol A (tetramers), 2, 4, 8-trihydroxyphenanthrene-2-*O*-glucoside and ellagic acid 3,3',4-trimethoxy-4'-O-α-L-rhamnopyranoside, glycoside of β-sitosterol are isolated for the first time from the stem bark of *Hopea parviflora*. All the compounds were tested for their *in vitro* and *in silico* inhibitory activities on carbohydrate digestive enzymes (α-amylase and α-glucosidase), delaying of AGEs formation. Based on these results, we have also evaluated whether these compounds enhance the 2-NBDG uptake in L6 myotubes.

Figure 5A.5. *Hopea parviflora* Bedd.

Table 5A.2. Scientific classification of *Hopea parviflora*

Kingdom	Plantae
Order	Magnoliopsida
Family	Dipterocarpaceae
Genus	*Hopea*
Species	*H. parviflora*
Binomial name	*Hopea parviflora* Bedd.

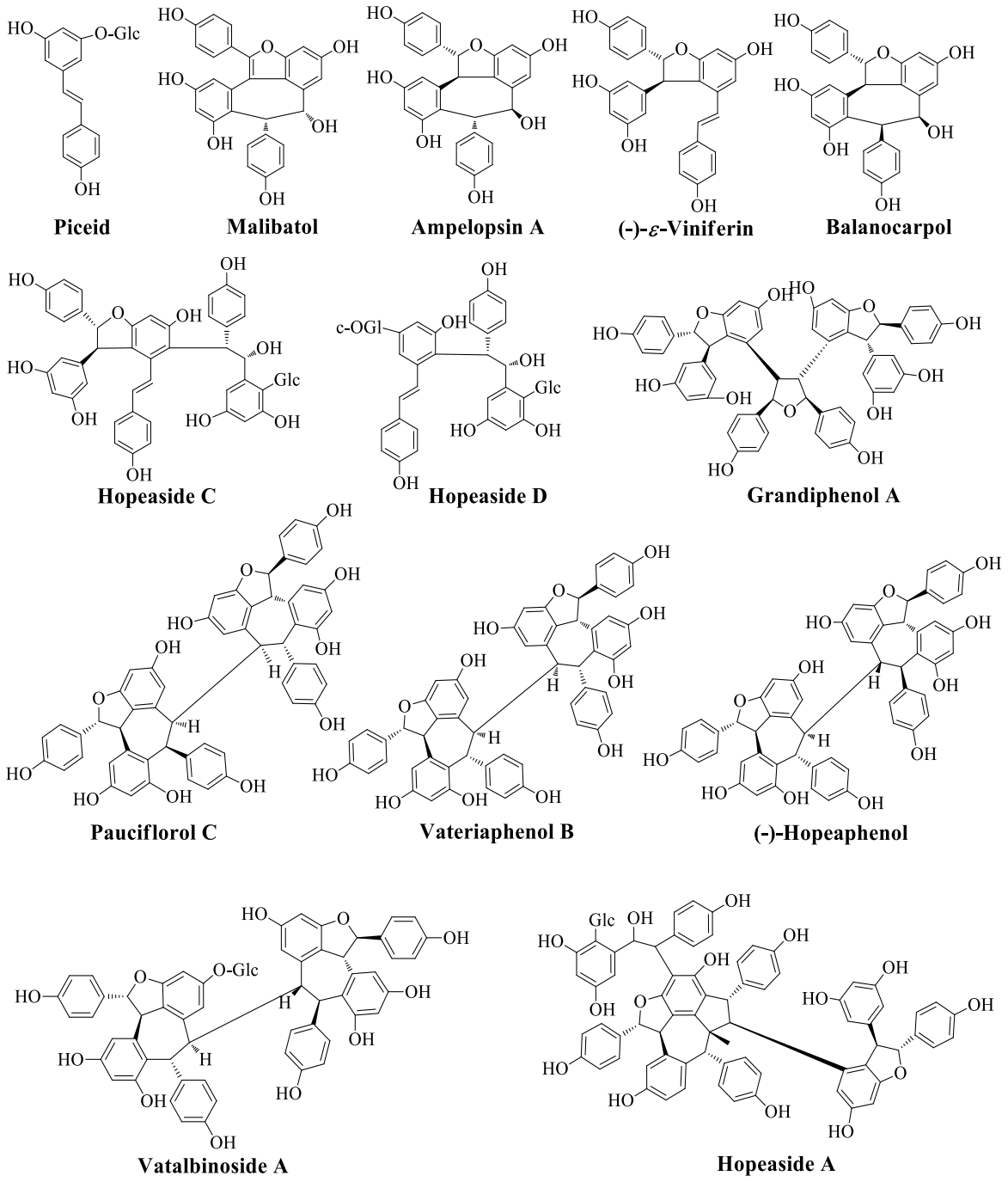

Figure 5A.6. Compounds previously isolated from *Hopea parviflora*

5A.3. Plant material collection, extraction, bio guided isolation and characterization of compounds from the stem bark of *Hopea parviflora* Bedd.

5A.3.1. Plant material

The stem barks of *Hopea parviflora* (700 g) were collected from Western Ghats region of Wayanad district, Kerala, India, during the period Apirl 2015 and identified by

plant taxonomist of M.S. Swaminathan Research Foundation, Wayanad, Kerala, India and a voucher specimen was deposited in the Herbarium of repository of the same institute.

5A.3.2. Extraction, bio-guided isolation and characterization of secondary metabolites

Air and oven-dried stem barks of *Hopea parviflora* (700 g) were crushed and extracted successively with *n*-hexane (2.5 L x 72 h x 3 times; 750 mg), acetone (2.5 L x 72 h x 3 times; 90 g), EtOH (2.5 L x 72 h x 3 times; 24 g) and water (2.5 L x 72 h x 3 times; 10 g). All extracts were checked for their *in vitro* antidiabetic activities on digestive enzymes as well as for their antiglycation properties. The results are shown in **Table 5A.3**. The acetone extract exhibited promising activity on carbohydrate hydrolyzing enzyme and antiglycation property. Therefore, further isolation and purification was focused on acetone extract.

Table 5A.3. Extract level *in vitro* antidiabetic activity of *Hopea parviflora*

Extracts	***α*-Amylase (*μ*g/mL)**	***α*-Glucosidase (*μ*g/mL)**	**Antiglycation (*μ*g/mL)**
***n*-Hexane**	26.11 ± 0.007	43.67 ± 0.205	143.67 ± 0.205
Acetone	**17.60 ± 0.261**	**14.53 ± 0.629**	**114.53 ± 0.629**
Ethanol	20.55 ± 0.558	49.54 ± 0.664	149.54 ± 0.664
Water	218.27 ± 1.004	366.41±0.523	266.41 ± 0.523
Acarbose	50.035 ± 0.233	45.37 ± 0.681	-
Ascorbic acid	-	-	115.51 ± 0.876

Each value represents mean ± SD (standard deviation) from triplicate measurements

An aliquot of acetone extract (60 g) was subjected to column chromatographic separation on 100-200 mesh sized silica gel and eluted with *n*-hexane, *n*-hexane- ethyl acetate, ethyl acetate and ethyl acetate-methanol polarity mixtures which resulted in 180 fractions and these fractions were pooled together to get 20 fraction pools after analyzing the TLC.

Fraction pool 2 was subjected to column chromatography on silica gel (100-200 mesh) using 5 % ethyl acetate in *n*-hexane, followed by crystallization in ethyl acetate and *n*-hexane mixture, affording compound **34** (15 mg) and compound **35** (8 mg) as

colourless crystals. The FTIR spectrum of compound **34** showed an intense band at 1716 cm^{-1}, which is consistent with a six membered ring ketone. In the ^{1}H NMR spectrum (**Figure 5A.7**), quartet signal resonated at δ_H 2.25 ppm assigned to C-4 position. The eight methyl peaks resonated at δ_H 0.72 (s, C-24), 0.87 (s, C -25), 0.88 (s, C -23), 0.95 (s, C -30), 1.00 (s, C-29), 1.01 (s, C-27), 1.05 (s, C-26) and 1.18 (s, C-28) ppm. The signal at δ_H 1.95 and 2.40 ppm is due to unequivalent methylene protons at C-2 position. The ^{13}C NMR spectrum displayed the presence of thirty carbon resonances (**Figure 5A.8**). The peak at δ_H 213.3 ppm in ^{13}C NMR spectrum confirmed the presence of ketone. The mass spectrum showed a molecular ion peak at 427.1497, which is the $(M+H)^+$ peak. Further, by comparison of the spectroscopic data with the values reported earlier [Carmen *et al*., **2000**], it was confirmed that the compound **34** was friedelin and the structure of which is shown below.

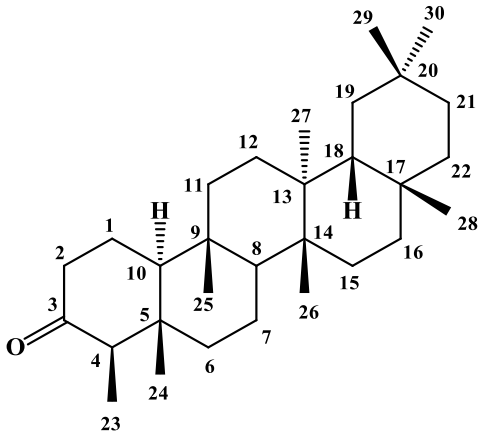

Friedelin (34)

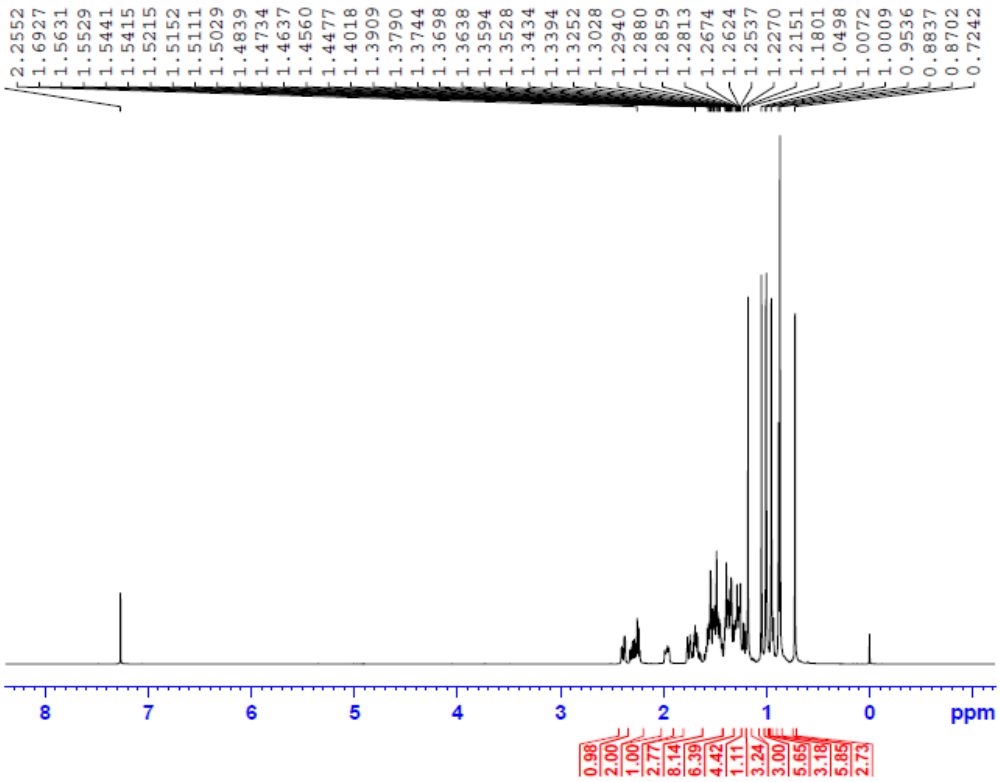

Figure 5A.7. ^{1}H NMR spectrum (500 MHz, $CDCl_3$) of friedelin (**34**)

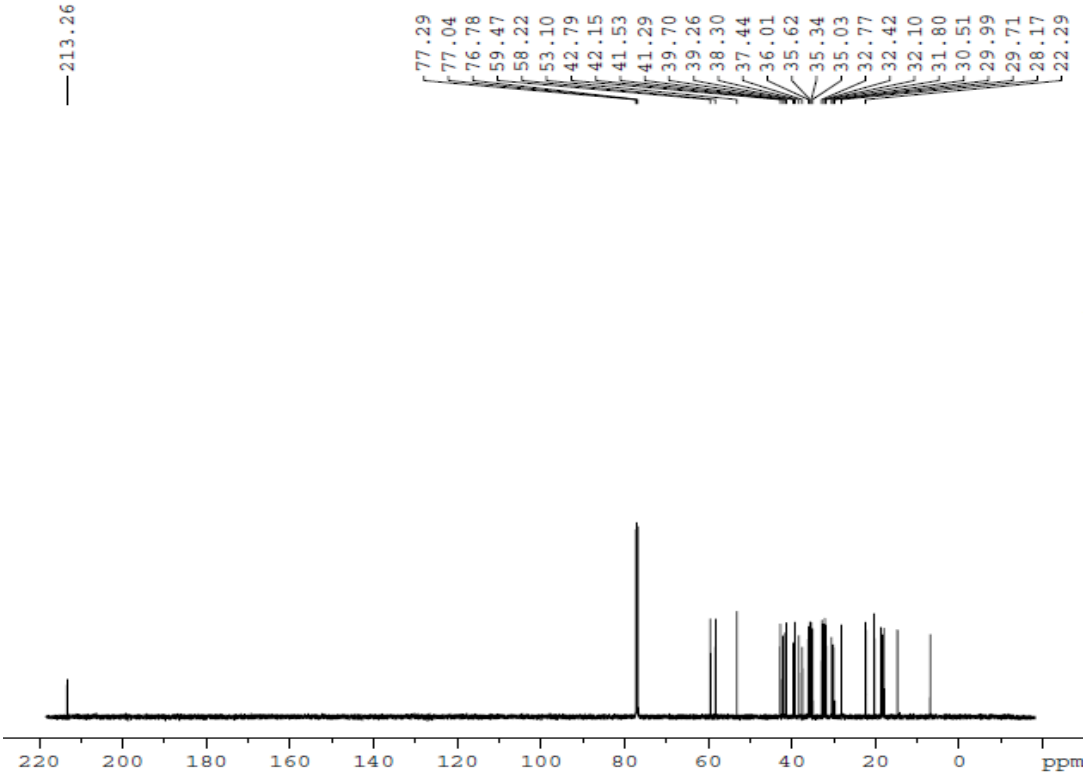

Figure 5A.8. ^{13}C NMR spectrum (125 MHz, $CDCl_3$) of friedelin (**34**)

Fraction pool 2 was subjected to column chromatography (silica 100-200 mesh) using *n*-hexane-ethyl acetate mixtures to yield the compound **35** (8 mg) along with compound **34** as colorless crystalline solid. FTIR spectrum showed an intense broad band at 3480 cm^{-1} due to the presence of hydroxyl group. In the ^{1}H NMR spectrum (**Figure 5A. 9**) the peak resonated at δ_H 3.73 ppm assigned to the proton at C-3 position. The signal at δ_H 1.95 and 2.40 ppm is due to the presence of unequivalent methylene protons at C-2 position. The ^{13}C NMR spectrum (**Figure 5A.10**) showed the presence of thirty carbon resonances. The peak at δ_C 72.8 (C-3) ppm indicated the presence of hydroxyl group attached carbon atom. The mass spectrum showed the molecular ion peak at 429.1042, which is the $(M+H)^+$ peak. Further, by comparison of the spectroscopic data with the values reported earlier [Carmen *et al*., **2000**], the compound was confirmed as friedelan-3*β*-ol and the structure of the compound **35** is shown below.

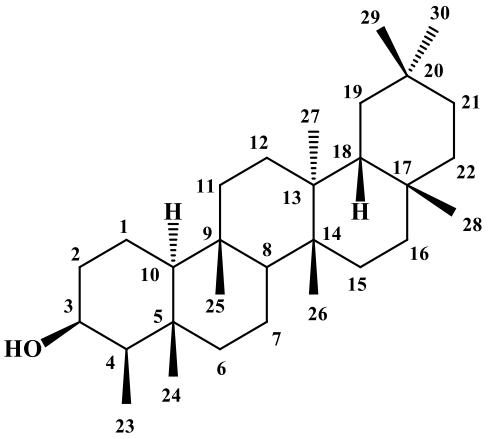

Friedelan-3*β*-ol (35)

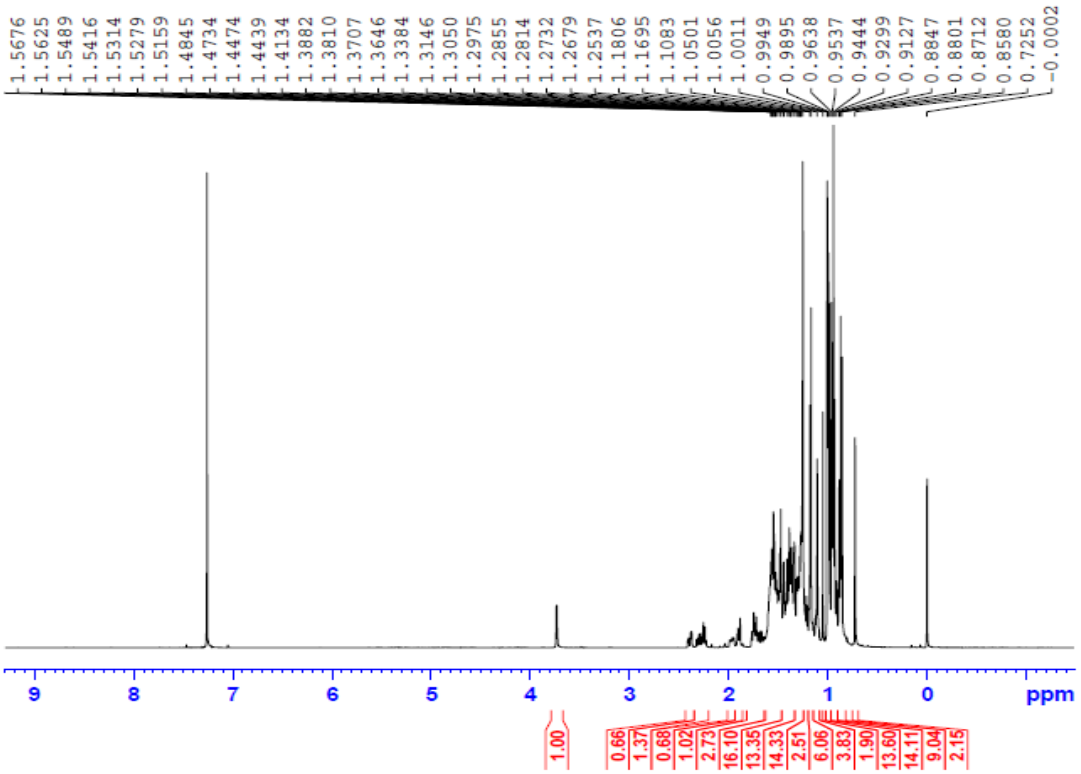

Figure 5A.9. ^{1}H NMR spectrum (500 MHz, $CDCl_3$) of friedelan-3β-ol (**35**)

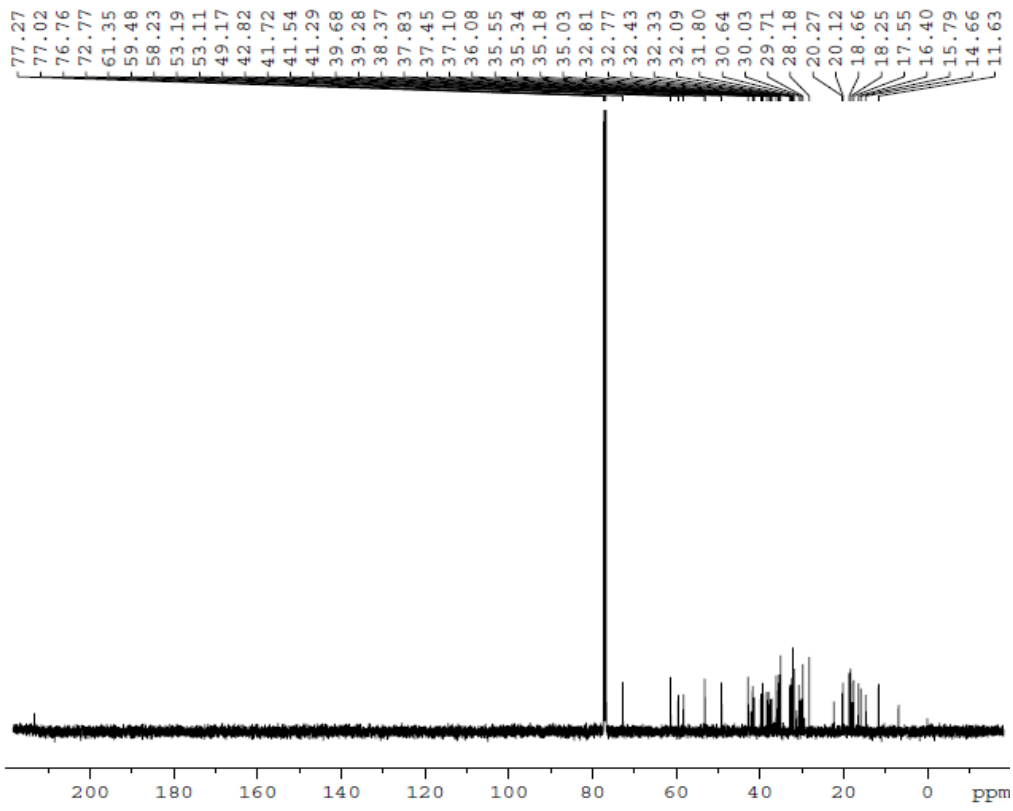

Figure 5A.10. ^{13}C NMR spectrum (125 MHz, $CDCl_3$) of friedelan-3β-ol (**35**)

The fraction pool 5 on column chromatographic separation using silica gel 100-200 mesh resulted in the isolation of compound **36**, which is obtained as a brown amorphous solid and gave an $[M+H]^+$ ion at m/z 455.14998 in HRESIMS corresponding to molecular formula $C_{28}H_{22}O_7$. From NMR analysis and the literature reports [Reniero *et al*., **1996**], the compound was (-)-*ε*-viniferin and structure has shown below.

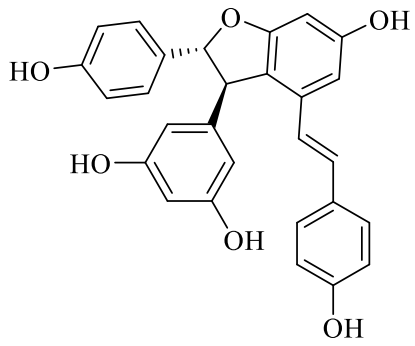

(-)-*ε*-Viniferin (36)

Compound **37** was obtained from fraction pool 6 as a brown amorphous solid and gave $[M+Na]^+$ ion peak at m/z 493.12674 in the HRESIMS corresponding to molecular formula $C_{28}H_{22}O_7$. The 1D and 2D NMR spectra are shown in **Figure 5A.11-15**. The ^1H NMR spectrum displayed the presence of two sets of *ortho*-coupled protons assignable to two 4-hydroxyphenyl groups [δ_H 6.88 (d, J = 8.5 Hz, 2H, H-2a and 6a), 6.62 (d, J = 9 Hz, 2H, H-3a, 5a); δ_H 7.10 (d, J = 8.5 Hz, 2H, H-2b and 6b), 6.76 (d, J = 8.5 Hz, 2H, H-3b and 5b) ppm], two sets of *meta*-coupled aromatic protons on a 1,2,3,5-tetrasubstituted benzene ring [δ_H 6.59 (d, J = 2 Hz, 1H, H-14a), 6.14 (d, J = 2 Hz, 1H, H-12a); δ_H 6.22 (s, H-14b, 1H), 6.42 (d, J = 2 Hz, 1H, H-12b) ppm], an aliphatic hydroxyl group at δ_H 3.47 (d, J = 7.5 Hz, 1H) ppm and phenolic hydroxyl groups resonated at δ_H 8.61, 8.44, 8.40, 8.23 and 8.20 ppm. Two sets of mutually coupled benzylic methine protons were also observed δ_H 4.14 (d, J = 11.5 Hz, 1H, H-8b), 5.39 (t, J = 7 Hz or 5 Hz, 1H, H-7b); δ_H 5.43 (brd, J = 4.5 Hz, 1H, H-8a), 5.75 (d, J = 11.5 Hz, 1H, H-7a) ppm. In the ^{13}C NMR spectrum, stereocentres carbons resonated at δ_C 88.7, 71.2, 49.6 and 43.6 ppm respectively; two 4-hydroxyphenyl carbons resonated at δ_C 129.9, 128.7, 116.0 and 115.5 ppm, respectively, two sets of *meta*-coupled aromatic protons on a 1,2,3,5-tetrasubstituted benzene ring resonated at δ_C 110.5, 108.2, 105.2 and 101.6 ppm, respectively. In the HMBC spectrum, long-range correlations were observed between the methine protons and aromatic protons as follows; H-7a/H-2(6)a, H-7b/ H-2(6)b and H-

8a/H-14a, respectively. The absolute configuration of compound 37 was established on the basis of optical activity with the value of $[\alpha]^{25}_{D}$ -39.5^{o} (c, 0.1 MeOH). Further, by comparison of the spectroscopic data with the values reported earlier [Reniero *et al*., **1996**], the compound was confirmed as (-)-ampelopsin A and the structure of the compound **37** is shown below

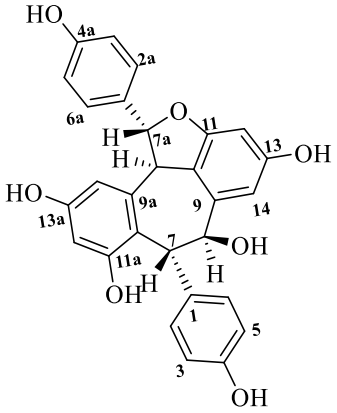

(-)-Ampelopsin A (37)

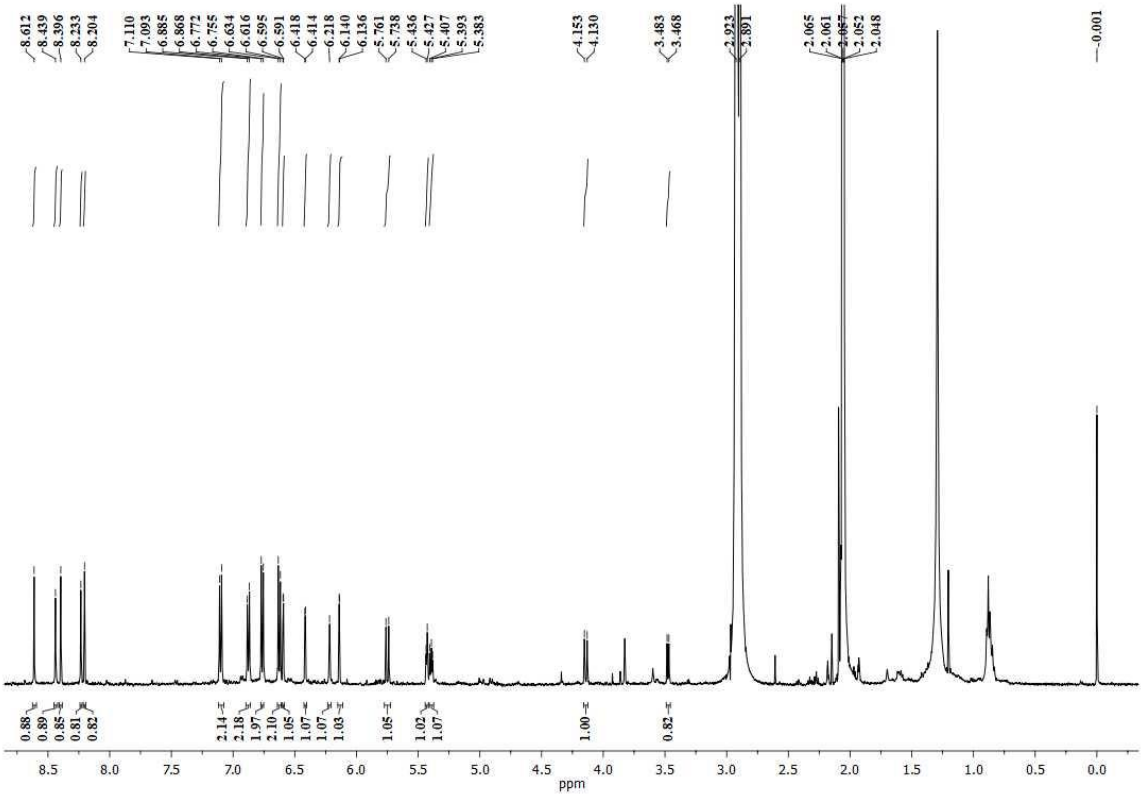

Figure 5A.11. ^{1}H NMR spectrum (500 MHz, Acetone-d_6) of **(-)-**ampelopsin A (**37**)

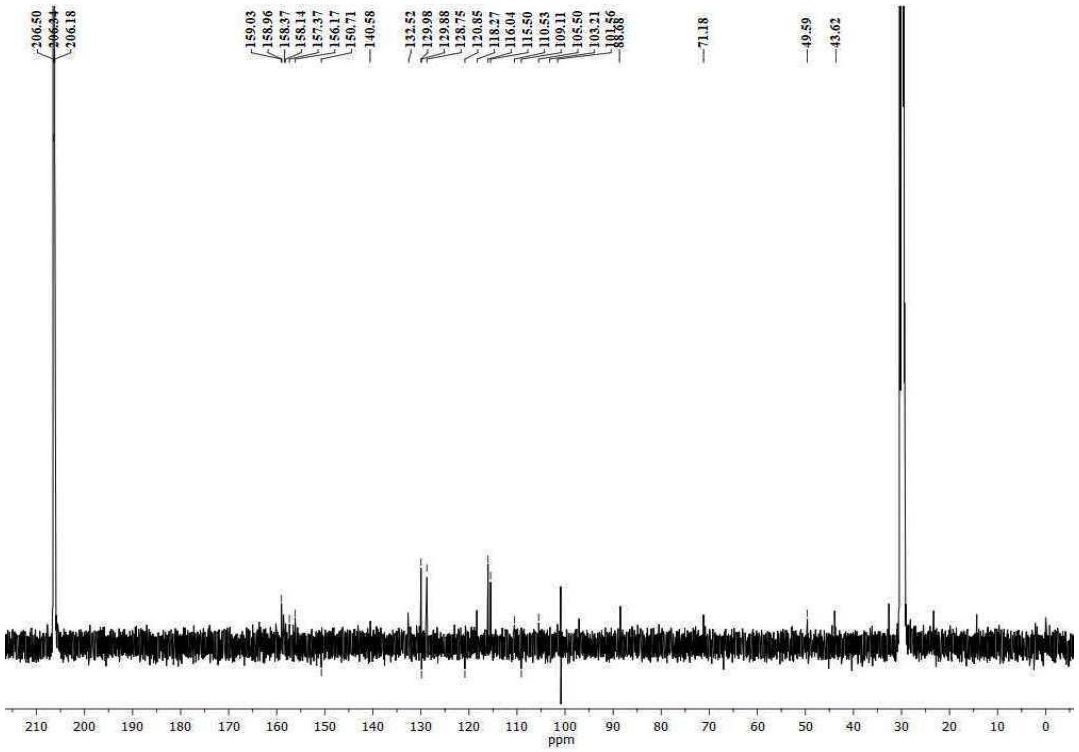

Figure 5A.12. ^{13}C NMR spectrum (125 MHz, Acetone-d_6) of **(-)**-ampelopsin A (**37**)

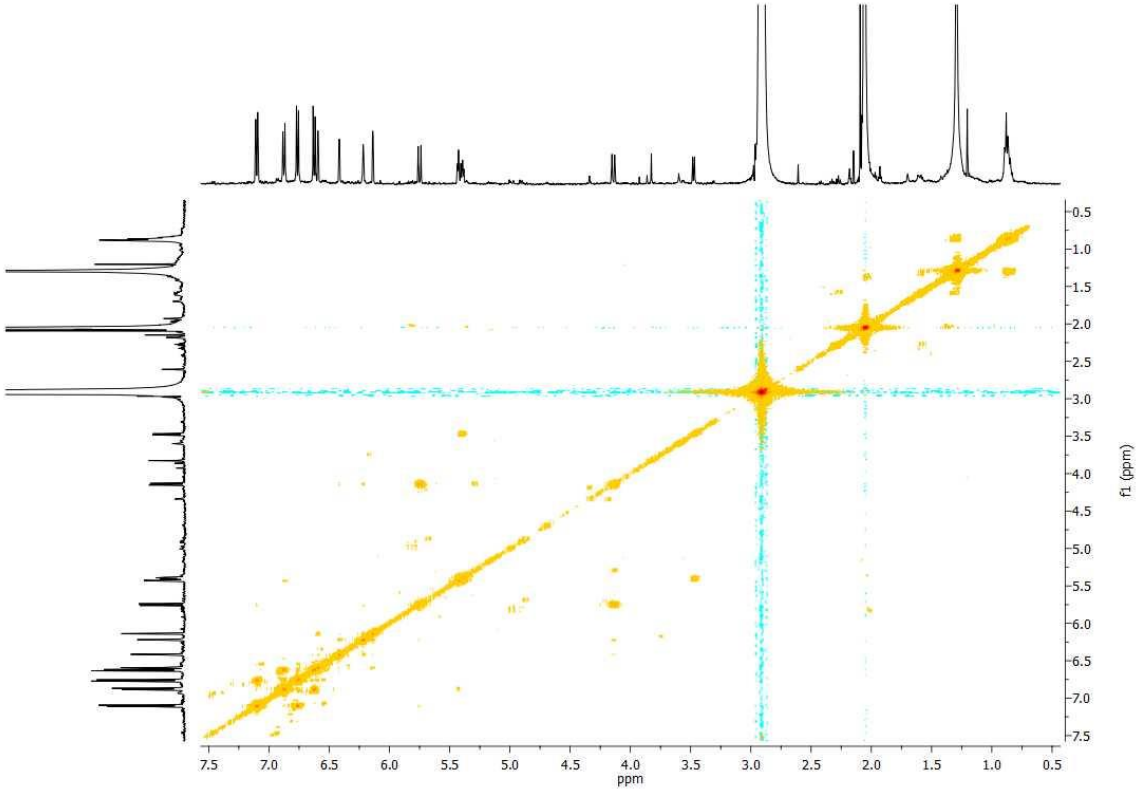

Figure 5A.13. ^{1}H-^{1}H COSY NMR spectrum (500 MHz, Acetone-d_6) of **(-)**-ampelopsin A (**37**)

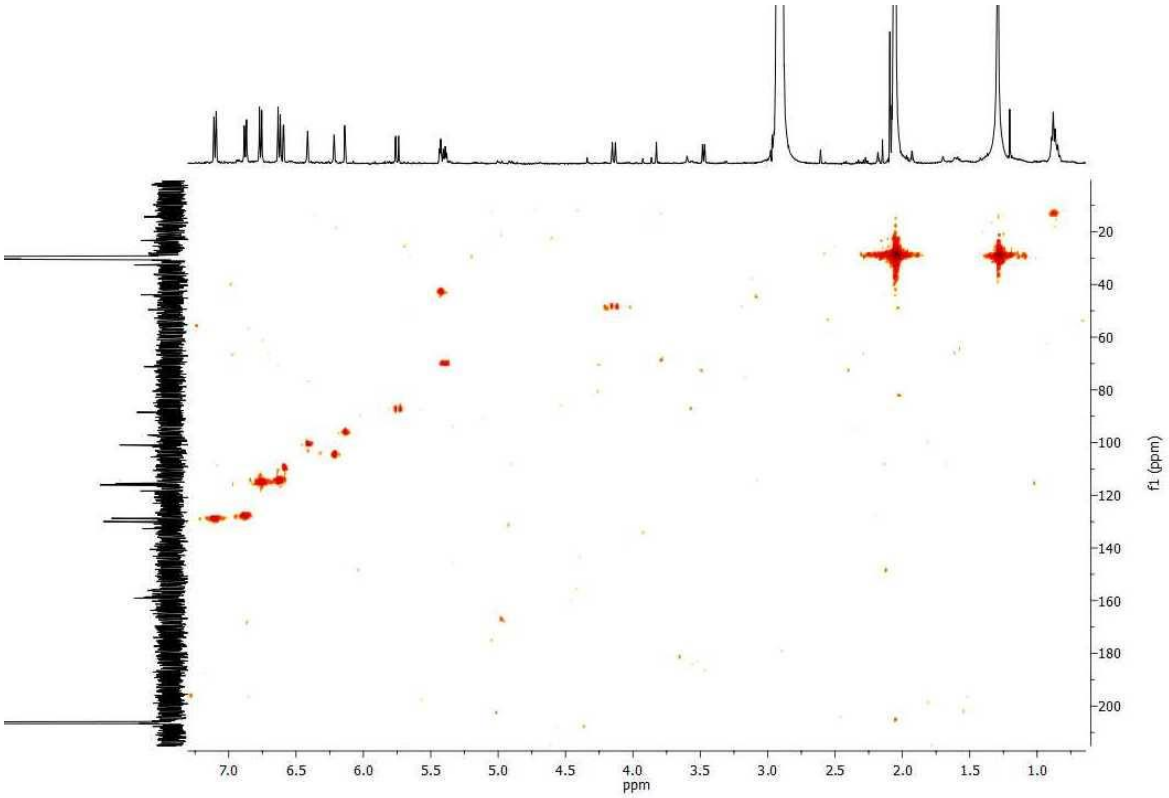

Figure 5A.14. HMQC NMR spectrum (125 MHz, Acetone-d_6) of **(-)**-ampelopsin A (**37**)

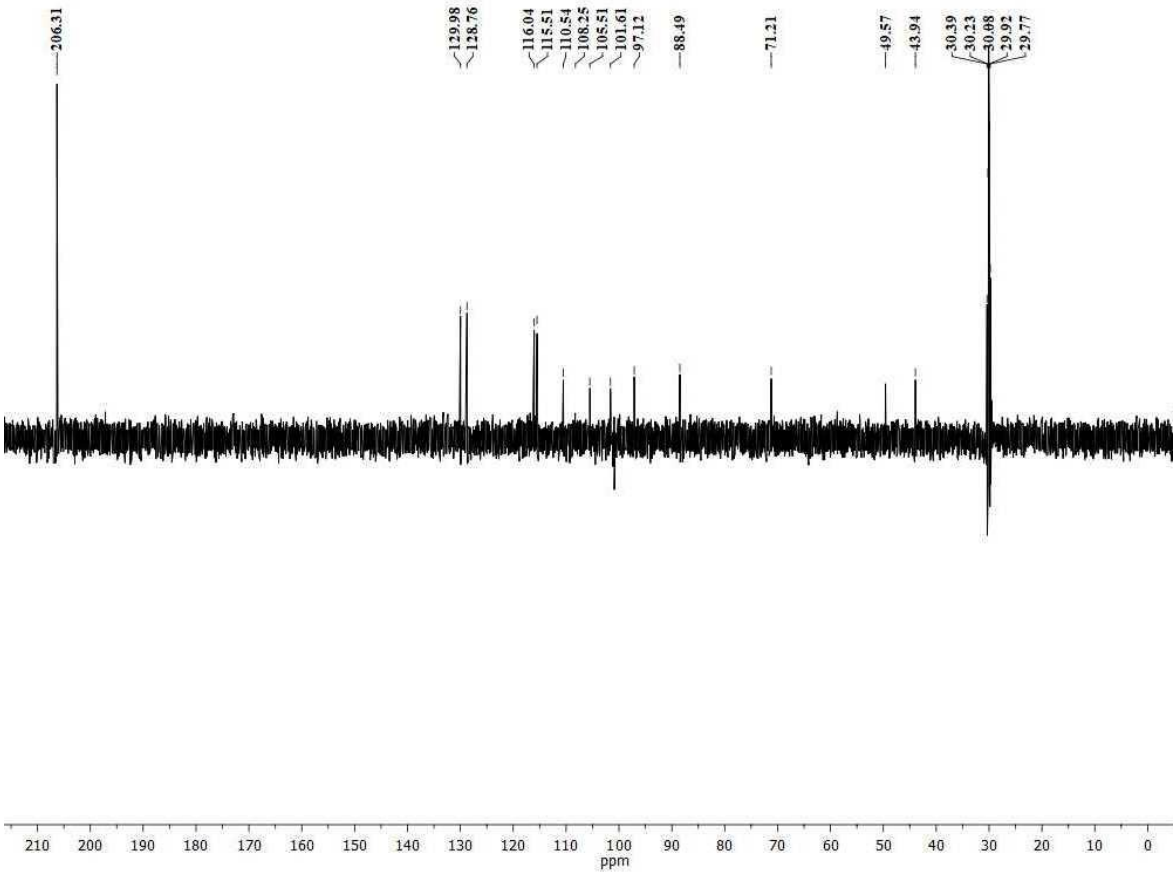

Figure 5A.15. DEPT 135 spectrum (125 MHz, Acetone-d_6) of **(-)**-ampelopsin A (**37**)

The fraction pool 8 obtained from the main column of acetone extract was purified by precipitation method using chloroform to yield compound **38** as pale yellow amorphous solid. In the ^{1}H NMR spectrum (**Table 5A.4**), stereocentre protons 7a, 7b, 8a and 8b resonated at δ_H 5.77 (d, J = 12.5 Hz), 5.82 (d, J = 5.5 Hz), 4.25 (d, J = 12 Hz), and 3.95 (s) ppm, respectively. Aromatic protons 12b, 14b, (2a, 6a), (3a, 5a), 14a, 12a, (2b, 6b) and (3b, 5b) resonated at δ_H 5.74 (s), 5.18 (s), 7.15 (d, J = 8.5 Hz), 6.80 (d, J = 5.5 Hz), 6.31 (d, J = 1 Hz), 6.57 (dd, J_1 = 13.5 Hz, J_2 = 8.5 Hz) and 6.92 (d, J = 8.5 Hz) ppm, respectively. The hydroxyl protons resonated in the range δ_H 7.45-8.56 ppm. In the ^{13}C NMR spectrum, the stereocentre carbons 7a, 7b, 8a and 8b resonated at δ_C 89.3, 42.3, 50.9 and 49.3 ppm respectively. From the detailed analysis of 1D and 2D NMR spectra (**Figure 5A. 16-21**), the compound is having two identical units. The mass spectra of the compound **38** gave molecular ion peak 907.2758 $(M+H)^+$. In the NOESY spectrum, there is a noticeable correlation observed between the proton at positions 8a/8b, 8a/2b(6b), 7a/14a. This confirms that 8a and 8b; 8a and 2b(6b) are β-orientation and 7a and 14a are α-orientation. The selected HMBC and NOESY correlations are shown in **Figure 5A.16.** The absolute configuration of compound **38** was established on the basis of optical activity with the value of $[\alpha]^{25}_{D}$ -369^{o} (c 0.1, MeOH). Based on the detailed literature survey [Reniero *et al*., **1996]** and various spectroscopic methods, compound **38** was confirmed as (-)-hopeaphenol. The structure of compound **38** is shown below.

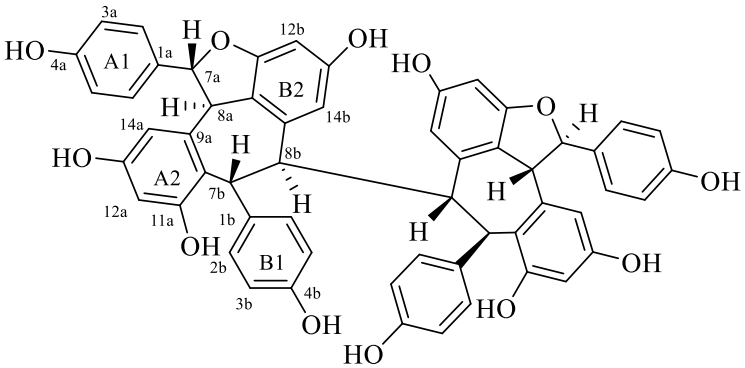

(-)-Hopeaphenol (38)

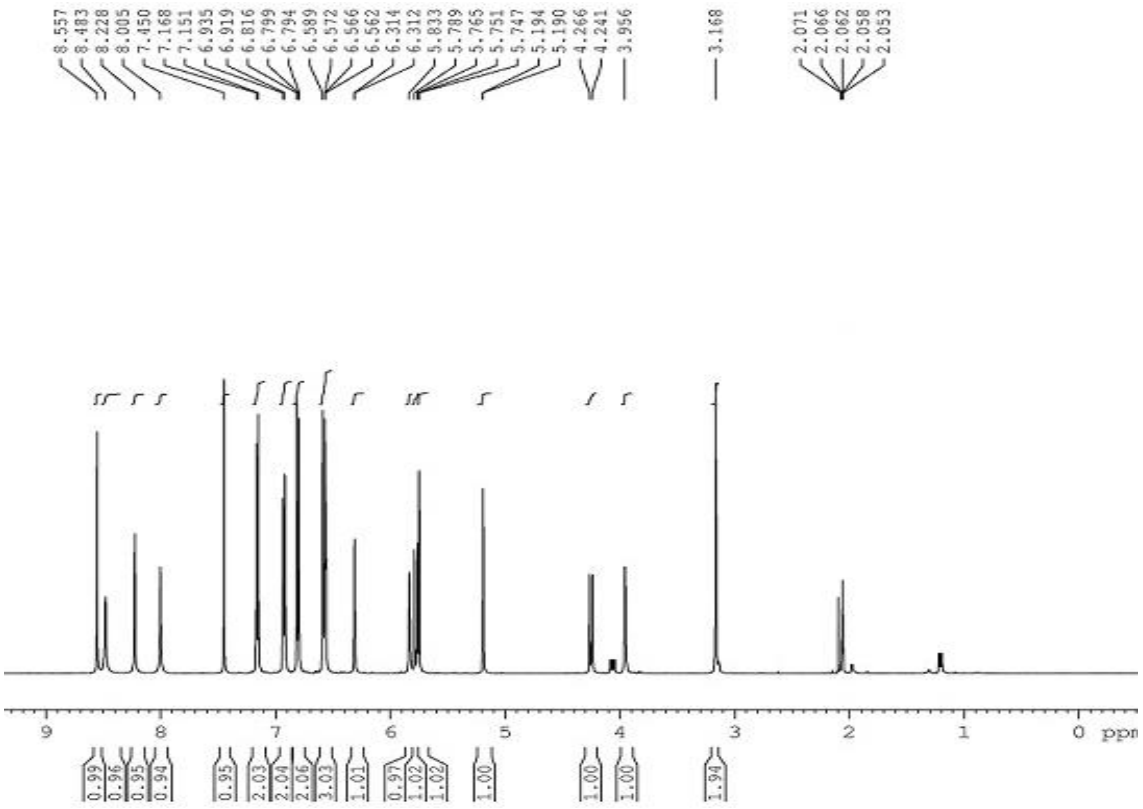

Figure 5A.16. ^{1}H NMR spectrum (500 MHz, Acetone-d_6) of (-)-hopeaphenol (**38**)

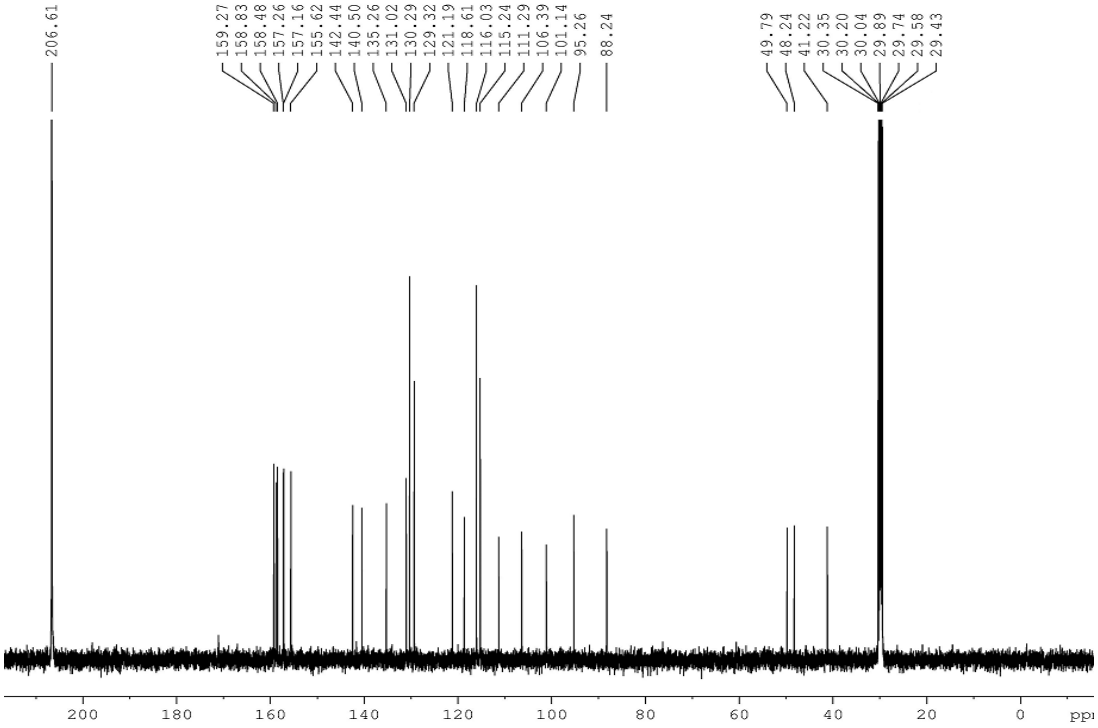

Figure 5A.17. ^{13}C NMR spectrum (125 MHz, Acetone-d_6) of (-)-hopeaphenol (**38**)

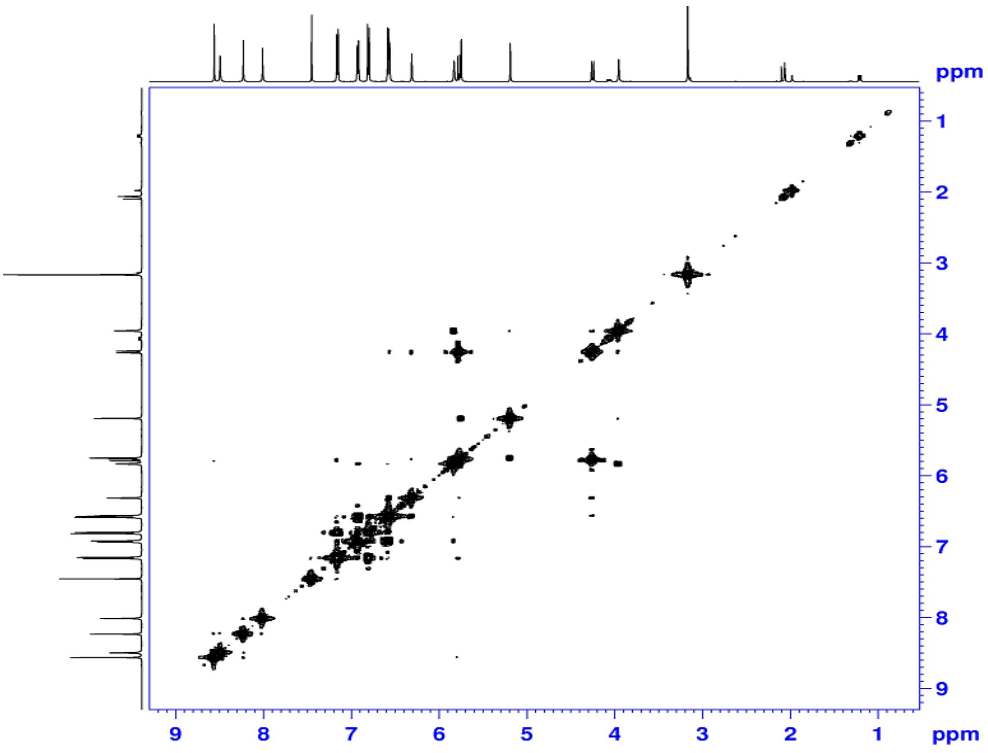

Figure 5A.18. ^{1}H-^{1}H COSY NMR spectrum (500 MHz, Acetone-d_6) of (-)-hopeaphenol (**38**)

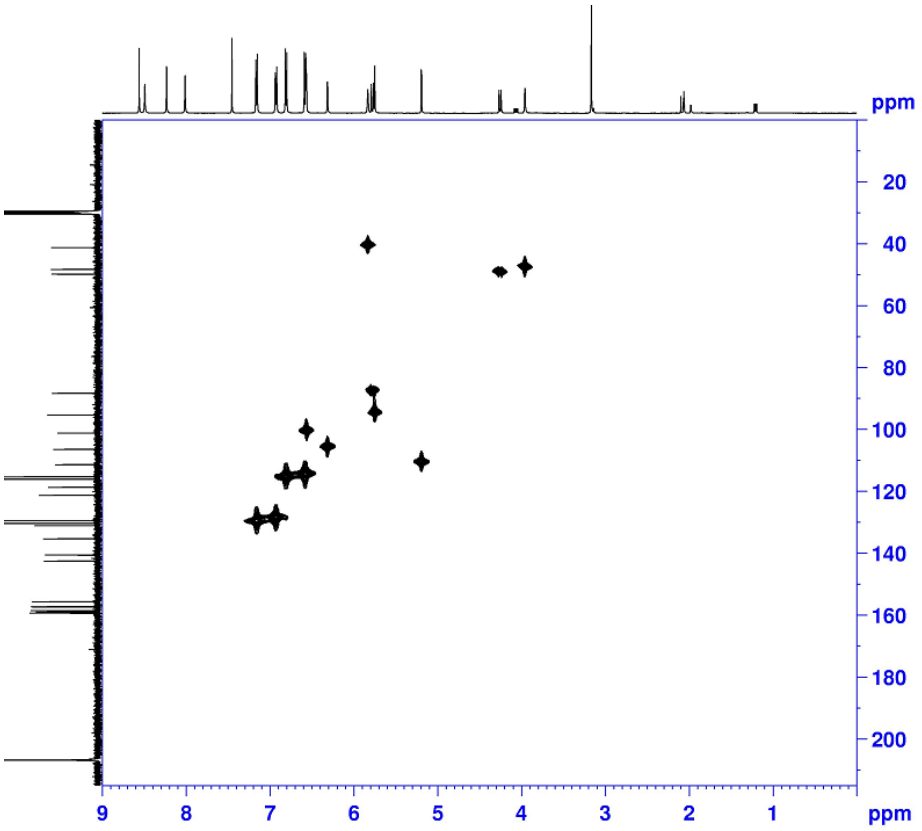

Figure 5A.19. HMQC NMR spectrum (125 MHz, Acetone-d_6) of (-)-hopeaphenol (**38**)

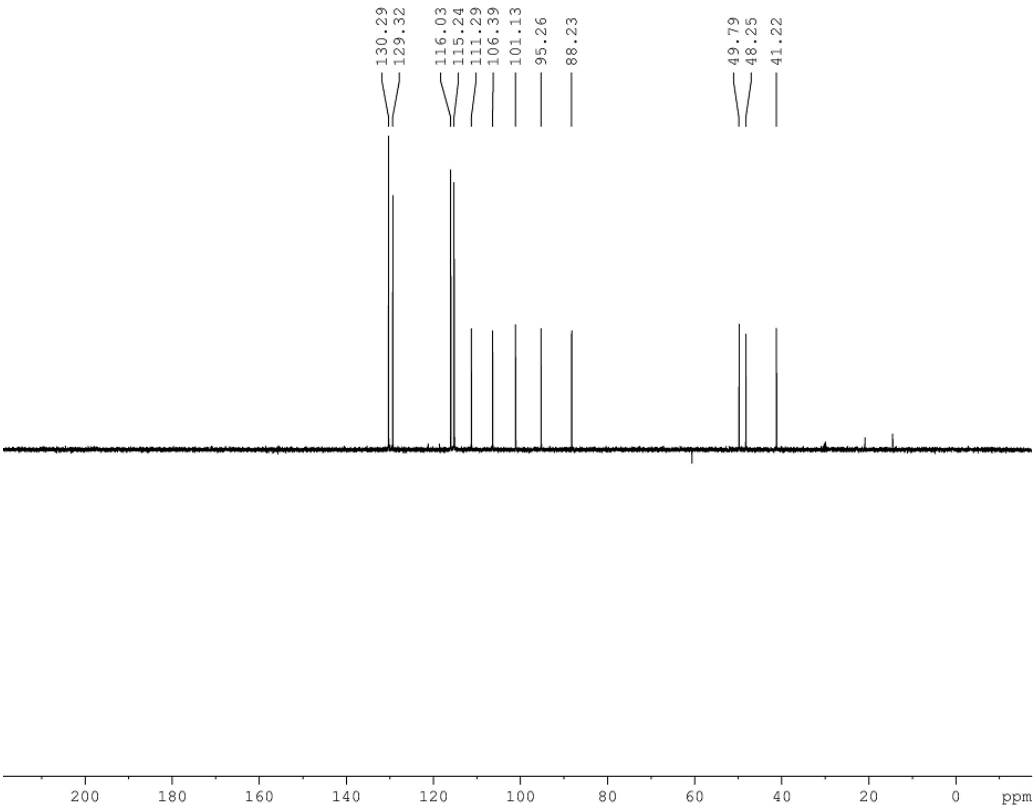

Figure 5A.20. DEPT 135 spectrum (125 MHz, Acetone-d_6) of (-)-hopeaphenol (**38**)

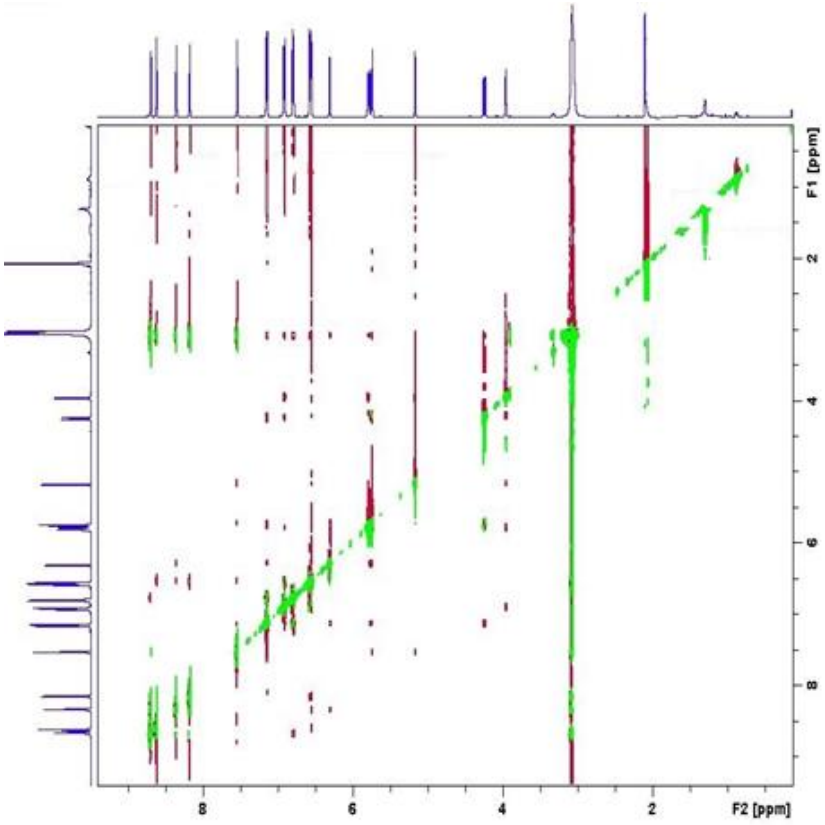

Figure 5A.21. NOESY NMR spectrum (500 MHz, Acetone-d_6) of (-)-hopeaphenol (**38**)

Table 5A.4. ^{1}H and ^{13}C NMR spectra of (-)-hopeaphenol in Acetone –d_6

Position	^{1}H NMR (500 MHz)	^{13}C NMR (125 MHz)	COSY
1a		132.1	
2a	7.15 (d, *J* = 8.5 Hz)	131.3	3a
3a	6.80 (d, *J* = 8.5 Hz)	116.3	2a
4a	OH	C-OH	
5a	6.80 (d, *J* = 8 Hz)	116.3	6a
6a	7.15 (d, *J* = 8.5 Hz)	131.3	5a
7a	5.77 (d, *J* = 12.5 Hz)	89.3	8a
8a	4.25 (d, *J* = 12 Hz)	50.8	7a
9a		143.5	
10a		122.2	
11a	OH	C-OH	
12a	6.57 (d, *J* = 5.5 Hz)	102.2	
13a	OH	C-OH	
14a	6.31 (s)	107.4	
1b	-	136.3	
2b	6.92 (d, *J* = 8 Hz)	130.4	3b
3b	6.58 (d, *J* = 5.5 Hz)	117.1	2b
4b	OH	C-OH	
5b	6.58 (d, *J* = 5.5 Hz)	117.1	6b
6b	6.92 (d, *J* = 8 Hz)	130.4	5b
7b	5.82 (d, *J* = 5.5 Hz)	42.3	8b
8b	3.95 (s)	49.3	7b
9b		141.5	
10b		119.6	
11b		overlapped	
12b	5.74 (s)	96.3	14b
13b	OH	C-OH	
14b	5.18 (s)	112.3	

Fraction pool 9 on column chromatographic separation using ethyl acetate in *n*-hexane, followed by gel permeation chromatographic separation using Sephadex LH 20 and eluting with methanol resulted in the isolation of compound **39** (8 mg) as brown amorphous solid. The HRESIMS measured with positive ion mode gave a parent ion peak at m/z 931.2712 ($[M+Na]^+$ calc. for $C_{56}H_{42}O_{12}Na$ 931.2724). This result together with NMR analysis, the structure of the compound was a resveratrol tetramer, vaticaphenol A. Vaticaphenol A (**39**) is isolated for the first time from *Hopea parviflora* and the structure is shown below.

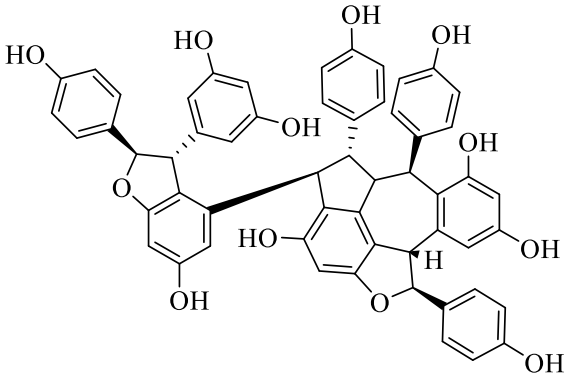

Vaticaphenol A (39)

Compound **40** was obtained as brown amorphous solid. The HRESIMS gave a peak at m/z 389.1246 ($[M+H]^+$ calc. for $C_{20}H_{21}O_8$ requires 389.1232). These results together with ^{13}C NMR spectroscopic analysis proposed the molecular formula $C_{20}H_{20}O_8$ for **40**. The FTIR spectrum exhibited characteristic absorptions for hydroxyl groups (3320 cm^{-1}) and aromatic rings (1606 cm^{-1}). The 1D and 2D NMR spectra are shown in **Figure 5A.22-25**. In its ^1H NMR spectrum, 20 proton signals including six hydroxyl groups, seven aromatic signals, seven oxygenated protons. The anomeric proton signal appeared as a doublet at δ_H 4.83 (J = 9.5 Hz) ppm, and attributed to an β-configurated anomeric proton. The ^{13}C NMR spectrum of **40** exhibited 18 signals including three oxygenated aromatic carbons [δ_C 157.6, 157.2 and 143.3 ppm], four aromatic quaternary carbons, five aromatic methine carbons, three oxygenated methine carbons, one oxygenated methylene carbon and the anomeric carbon [δ_C 80.8 ppm]. Based on the complete analysis of various spectroscopic data and literature reports [Baderschneider *et al*., **2000**], compound **40** was identified as 2, 4, 8 - trihydroxyphenanthrene-2-*O*-glucoside and the structure is given below. 2, 4, 8 - trihydroxyphenanthrene-2-*O*-glucoside is formed from *cis*-piceid by photochemical reactions as well as enzymatic reaction. To the best of our knowledge, 2,

4, 8 - trihydroxyphenanthrene-2-*O*-glucoside (**40**) is reported here for the first time from *Hopea parviflora*.

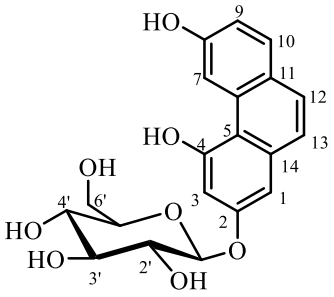

2, 4, 8 - trihydroxyphenanthrene-2-*O*-glucoside (40)

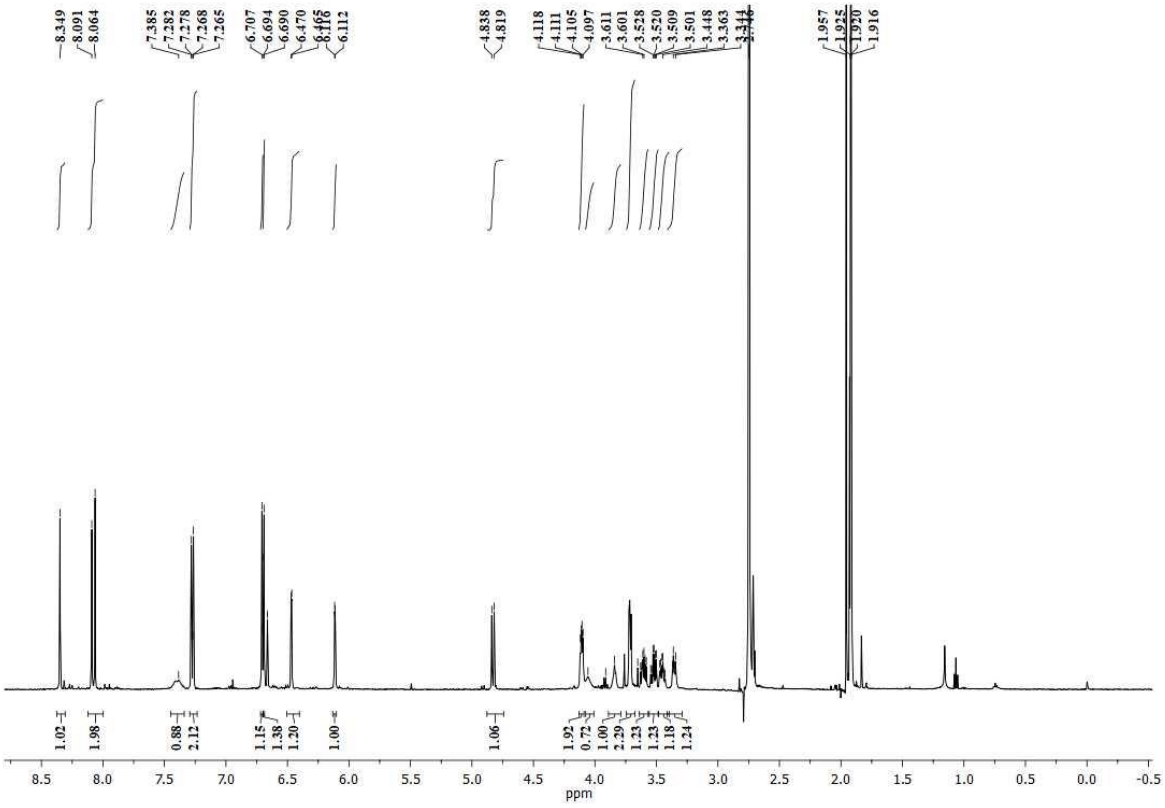

Figure 5A.22. ^{1}H NMR spectrum (500 MHz, Acetone-d_6) of 2, 4, 8-trihydroxyphenanthrene-2-*O*-glucoside (**40**)

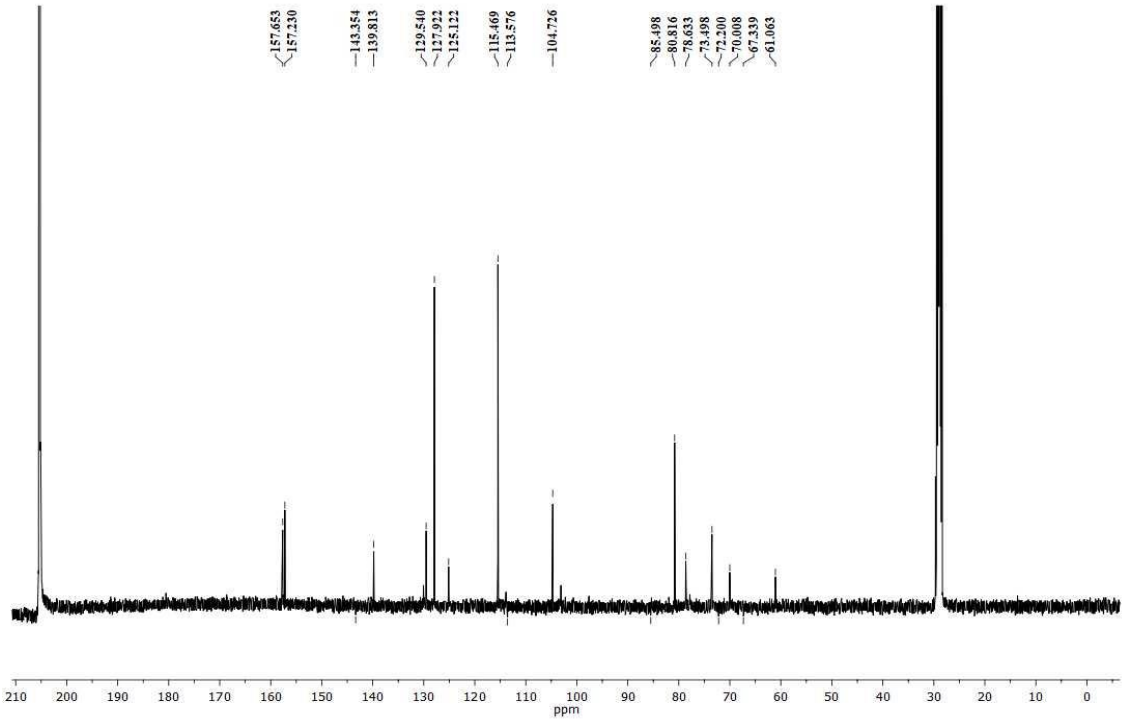

Figure 5A.23. ^{13}C NMR spectrum (125 MHz, Acetone-d_6) of 2, 4, 8-trihydroxyphenanthrene-2-*O*-glucoside (**40**)

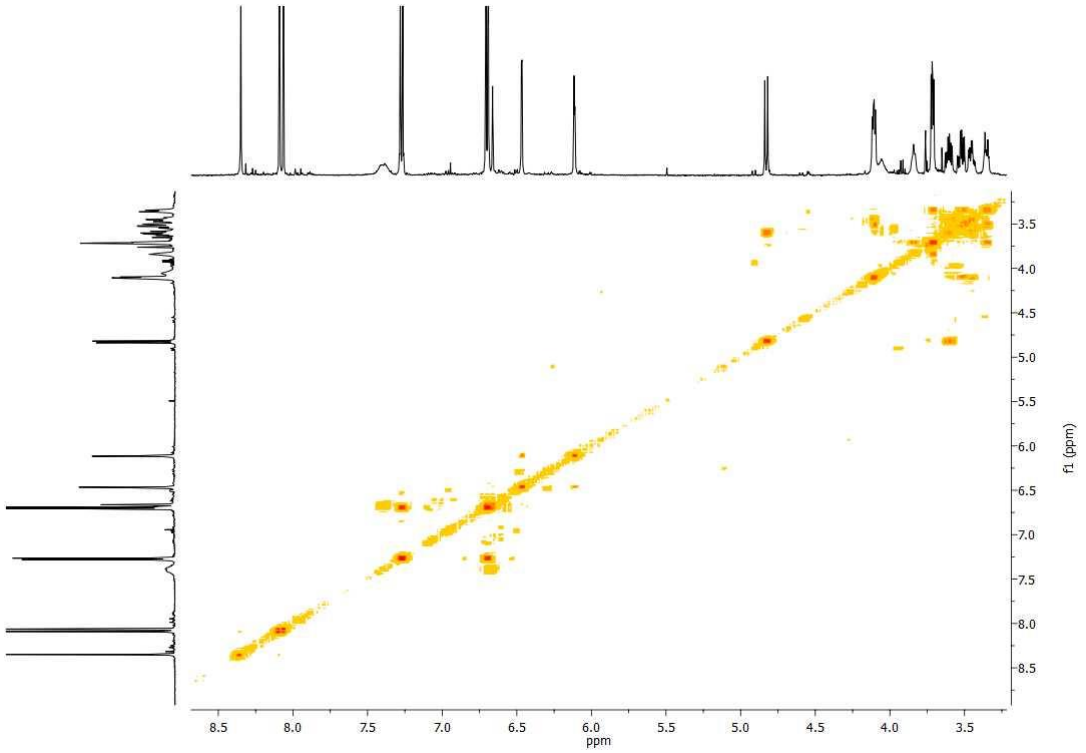

Figure 5A.24. ^{1}H-^{1}H COSY NMR spectrum (500 MHz, Acetone-d_6) of 2, 4, 8-trihydroxyphenanthrene-2-*O*-glucoside (**40**)

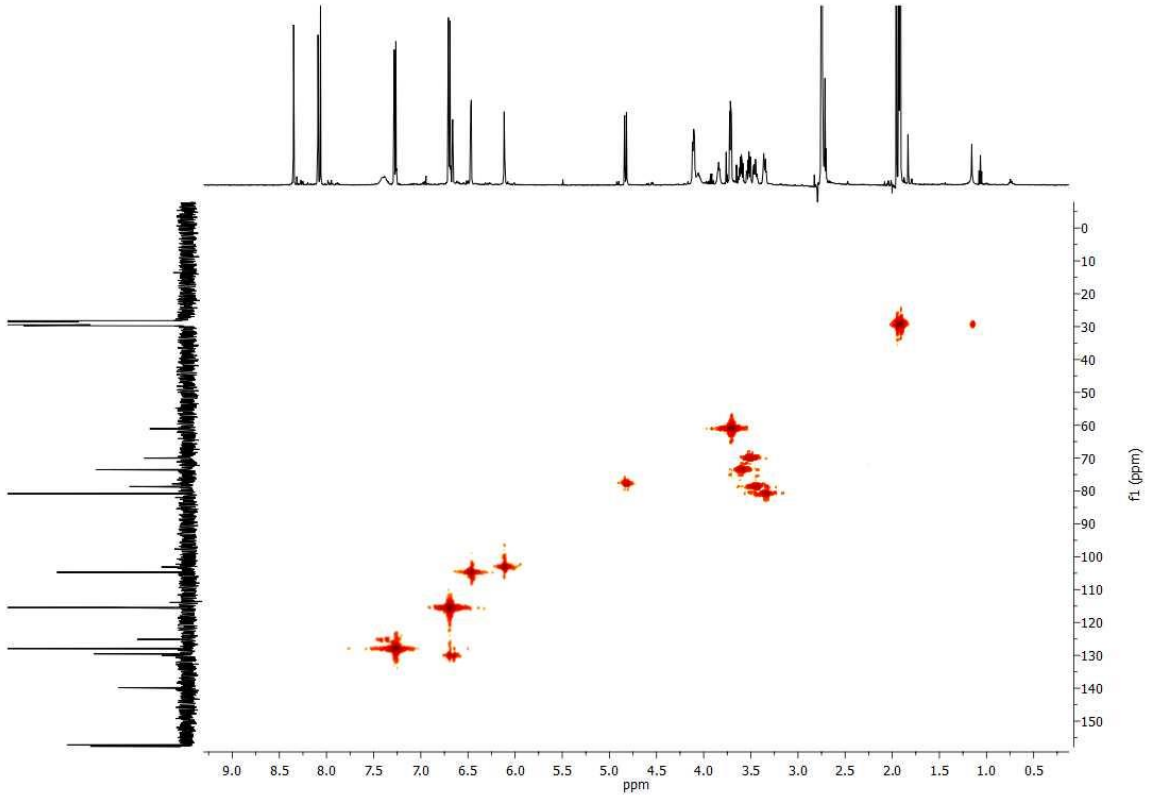

Figure 5A.25. HMQC NMR spectrum (125 MHz, Acetone-d_6) of 2, 4, 8-trihydroxyphenanthrene-2-*O*-glucoside (**40**)

Compound **41** was obtained as colourless amorphous solid. The HRESIMS measured with positive ion mode gave a parent ion peak at m/z 491.1215 $(M+H)^+$ ($[M+H]^+$ calc. for $C_{23}H_{23}O_{12}$ requires 491.1229). These results together with ^{13}C NMR spectroscopic analysis proposed the molecular formula $C_{23}H_{22}O_{12}$ for **41**. The FTIR spectrum exhibited characteristic absorptions for hydroxyl groups (3411 cm^{-1}), α, β-unsaturated lactone functions (1727 cm^{-1}) and aromatic rings (1606 cm^{-1}). The 1D and 2D NMR spectra are shown in **Figure 5A.26-31**. In its ^1H NMR spectrum, 14 proton signals including two aromatic singlets [δ_H 7.78 (s) and 7.60 (s) ppm], three singlet methoxyl signal [δ_H 4.09 (s), 4.06 (s), 4.01 (s) ppm], five oxygenated methine protons [δ_H 5.58 (s), 3.98 (s), 3.72 (s), 3.53(s) ppm and one proton is merged with water peak of DMSO] and hydroxyl protons [δ_H 5.25 (d, J = 3.5 Hz), 5.01 (d, J = 5.5 Hz), and 4.88 (d, J = 5.5 Hz) ppm] were observed, along with a doublet methyl signal [δ_H 1.15, J = 6 Hz) ppm] indicating the existence of one 6-deoxysugar. The anomeric proton signal appeared as singlet at δ_H 5.58 ppm, attributed to an α-configurated anomeric proton. The ^{13}C NMR spectrum of compound **41** exhibited 22 signals including two overlapped ester carbons (–COOR) at δ_C 158.16 ppm due to α, β-unsaturated lactones, six oxygenated aromatic

carbons (δ_C 154.2, 150.6, 141.7, 141.2, 141.0 and 140.9 ppm), four aromatic quaternary carbons (δ_C 113.5, 112.6, 112.4 and 112.3 ppm), two isolated aromatic methine carbons at δ_C 111.7 and 107.5 ppm, three methoxyl carbon at δ_C 61.6, 61.3 and 56.7 ppm and a methyl carbon at δ_C17.9 ppm and five oxygenated methine carbons were resonated at δ_C 71.5, 70.4, 70.3, 70.0 ppm. The peak at δ_C 99.7 ppm is due to the presence of anomeric carbon in the rhamnose moiety. The HRESIMS spectrum of **41** was dominated by two fragment ion peaks at m/z 315 and 145 due to the aglycone and the rhamnose moiety, respectively. Based on the literature reports [Hoang *et al*., **2012**] and NMR analysis, the compound **41** was ellagic acid- 3,3',4-trimethoxy-4'-*O*-*α*-L-rhamnopyranoside and the structure is shown below.

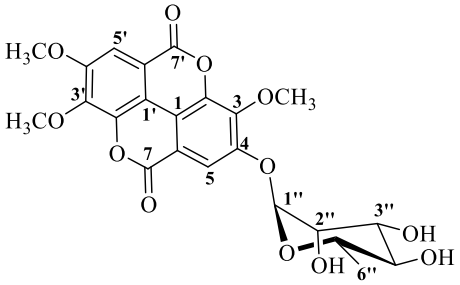

Ellagic acid-3, 3', 4-trimethoxy-4'-*O*-*α*-L-rhamnopyranoside (41)

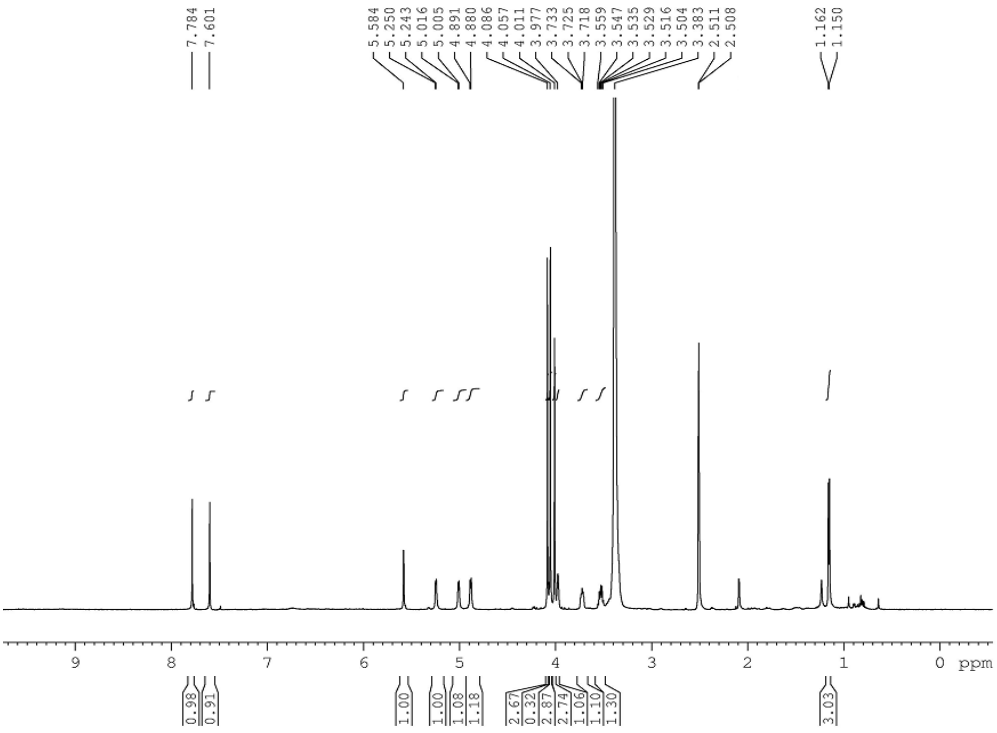

Figure 5A.26. ^{1}H NMR spectrum (500 MHz, DMSO-d_6) of ellagic acid-3,3', 4-trimethoxy-4'-*O*-*α*-L-rhamnopyranoside (**41**)

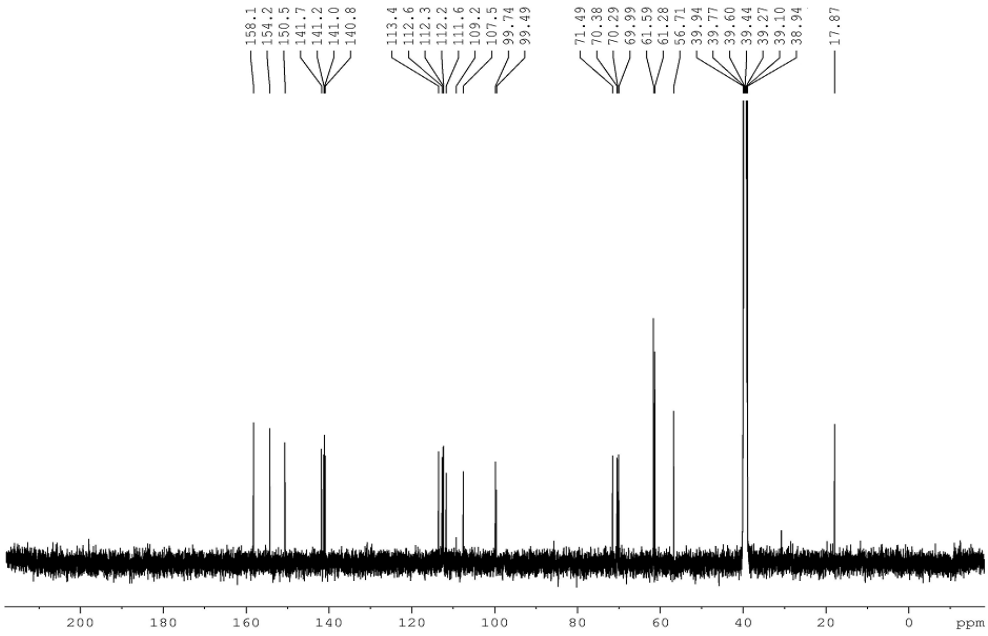

Figure 5A.27. ^{13}C NMR spectrum (125 MHz, DMSO-d_6) of ellagic acid-3,3', 4-trimethoxy-4'-*O*-α-L-rhamnopyranoside (**41**)

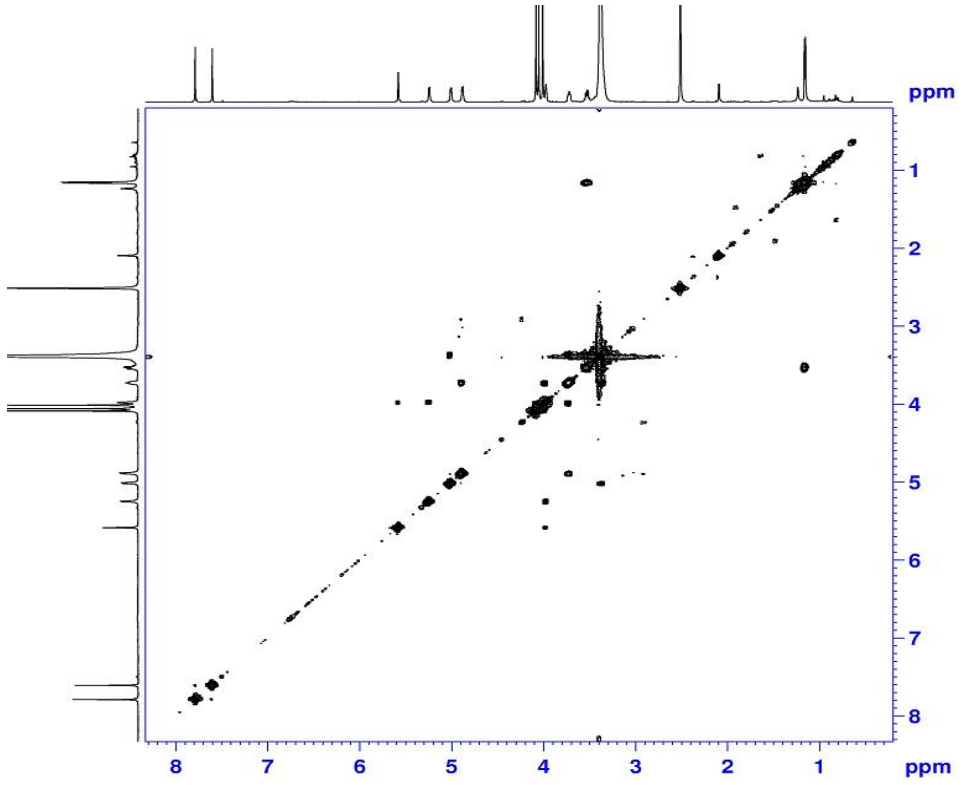

Figure 5A.28. ^{1}H-^{1}H COSY NMR spectrum (500 MHz, DMSO-d_6) of ellagic acid-3,3', 4-trimethoxy-4'-*O*-α-L-rhamnopyranoside (**41**)

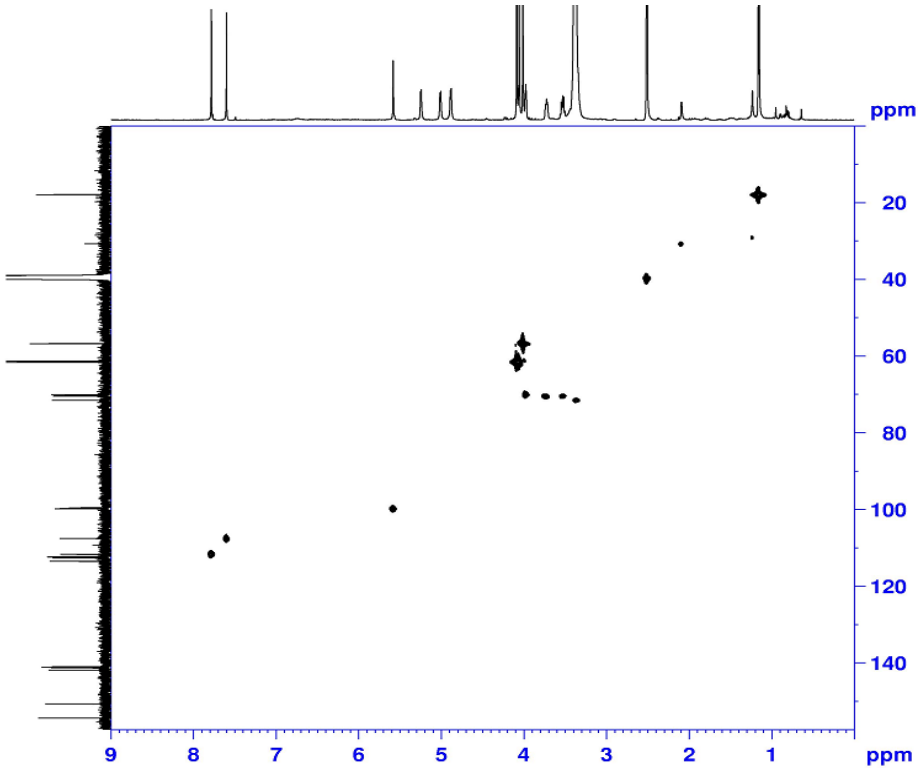

Figure 5A.29. HMQC NMR spectrum (125 MHz, DMSO-d_6) of ellagic acid-3,3', 4-trimethoxy-4'-*O*-α-L-rhamnopyranoside (**41**)

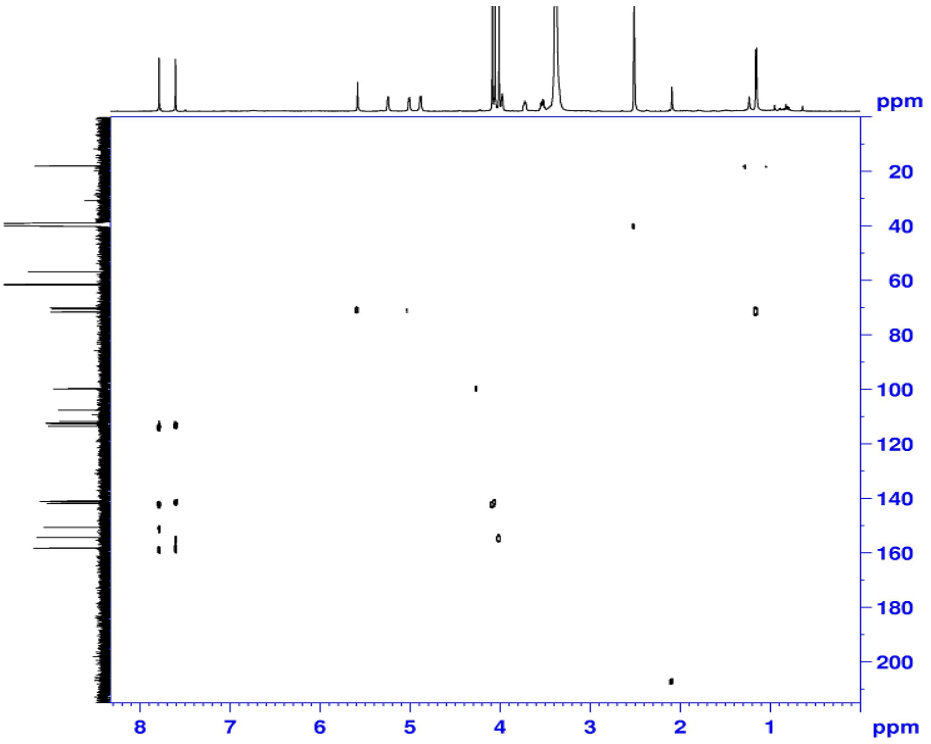

Figure 5A.30. HMBC spectrum (125 MHz, DMSO-d_6) of ellagic acid-3,3', 4-trimethoxy-4'-*O*-α-L-rhamnopyranoside (**41**)

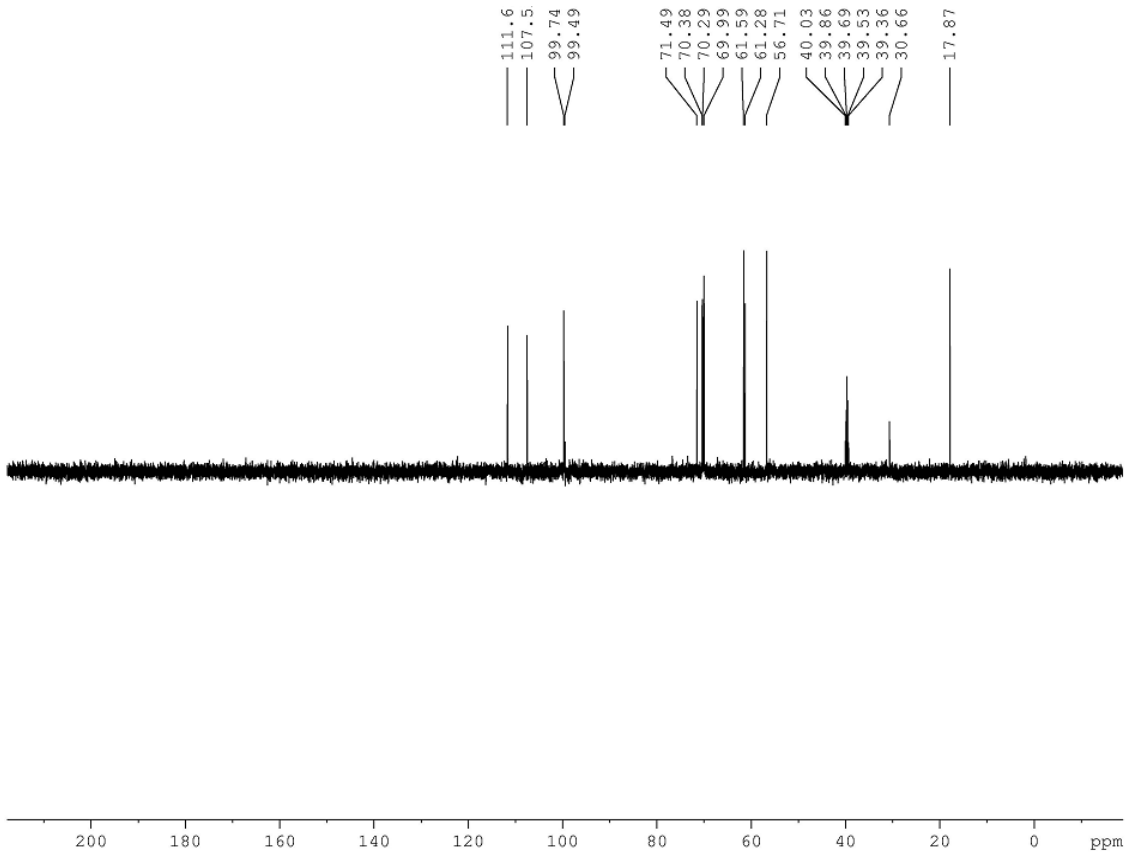

Figure 5A.31. DEPT 135 spectrum (125 MHz, DMSO-d_6) of ellagic acid-3,3', 4-trimethoxy-4'-*O*-α-L-rhamnopyranoside (**41**)

From the fraction pool 15, a white amorphous solid was precipitated out. Based on physical nature and spectroscopic analysis, compound was glucoside of β-sitosterol (**42**). The structure is shown below.

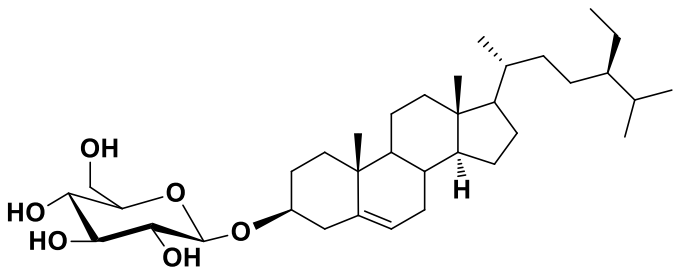

β-Sitosterol-β-D-glucoside (42)

5A.4. Biosynthetic pathway of (-)-hopeaphenol

The resveratrol oligomers are a highly diverse class of natural products that are produced by the coupling of phenoxyl radicals. The dimerization usually occurs through three regioisomeric modes: the 8-10', 8-8' and 8-12' coupling. ε-Viniferin forms *via* 8-10' stereospecific radical dimerization of two resveratrol. The 8-8' oxidative dimerization

of two molecules of ε-viniferin leads to the formation of series of resveratrol tetramers. This *bis*-paraquinone methide can undergo symmetric cyclization leads to hopeaphenol [Keylor *et al*., **2015**] (**Figure 5A.32**).

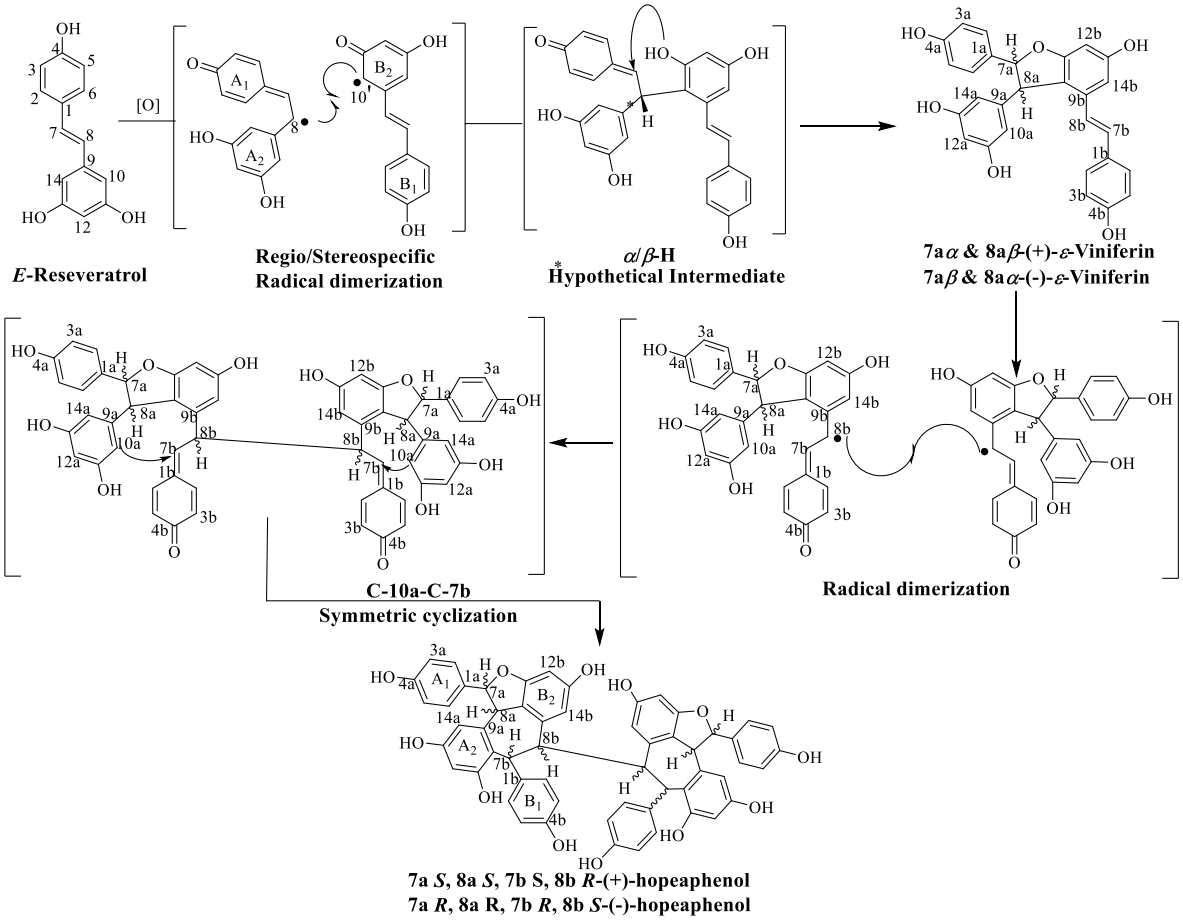

Figure 5A.32. Biosynthetic pathway of (-)-hopeaphenol

5A.5. Antidiabetic property of phytochemicals isolated from *Hopea parviflora*

Diabetes mellitus mostly characterized by increased blood glucose level and their complications such as neuropathy, nephropathy and retinopathy increase the morbidity and mortality risks for diabetic patients. Now days, nearly 90 % of the world's diabetic population have type 2 diabetes mellitus. Currently approved anti-diabetic drugs have some restricted safety alarms, and temporally improve blood glucose levels, improves diabetes complications, as well as in the treatment of obesity but accompanied with gastrointestinal side-effects. The consumption of natural products is known to have anti-diabetic effects, offering numerous exciting potentials for the future progress and development of successful therapies. The acetone extract of *Hopea parviflora* showed significant antidiabetic potential. Thus, as part of our continuing interest in this area, we

have analyzed the antidiabetic property of phytochemicals isolated from *hopea parviflora*.

5A.5.1. *α*-Amylase inhibitory activity

We herein reported the *α*-amylase inhibitory activity of isolated compounds [friedelin (**34**), friedelin-3*β*-ol (**35**), (-)-ampelopsin A (**37**), (-)-hopeaphenol (**38**), 2,4,8-trihydroxyphenanthrene-2-*O*-glucoside (**40**) and ellagic acid 3,3',4-trimethoxy 4'-*O*-*α*-L-rhamnopyranoside (**41**)]. The results obtained are summarised in **Table 5A.5**. All the tested compounds showed moderate to weak inhibition of *α*-amylase enzyme compared to the standard, acarbose.

5A.5.2. *α*-Glucosidase inhibitory activity

As mentioned in the previous chapters, *α*-glucosidase enzyme catalyzes the cleavage of polysaccharides to glucose in the small intestine. The inhibition of *α*-glucosidase enzyme can contribute to the control over the post-prandial hyperglycemia and thereby prevents diabetics and its associated complications. Commonly used *α*-glucosidase inhibitors are acarbose, voglibose and miglitol, they compete with the oligosaccharides for the binding of the enzyme and successfully decrease the post-prandial blood glucose levels in diabetic patients. But, these inhibitors are known to cause flatulence, diarrhea and abdominal discomfort and having low efficacy with high IC_{50} values against *α*-glucosidase enzyme. Herein, we screened the *α*-glucosidase inhibition of friedelin (**34**), friedelin-3*β*-ol (**35**), (-)-ampelopsin A (**37**), (-)-hopeaphenol (**38**), 2,4,8-trihydroxyphenanthrene-2-*O*-glucoside (**40**) and ellagic acid-3,3',4-trimethoxy 4'-*O*-*α*-L-rhamnopyranoside (**41**). Most of the compounds (**37**, **38**, **40** and **41**) demonstrated significant *in vitro* *α*-glucosidase inhibitory properties with IC_{50} values in the range of 44.23 ± 0.215 - 57.49 ± 0.231 *μ*M, while friedelin (**34**) and friedelin-3*β*-ol (**35**) showed weak inhibition having IC_{50} value of > 200 *μ*M (**Table 5A.5**).

5A.5.3. Antiglycation property

The increased blood glucose level promotes protein glycation, which resulted in the formation of advanced glycated end products (AGEs). These AGEs play a key role in the pathogenesis of several diabetic complications like retinopathy, nephropathy, neuropathy, cardiomyopathy *etc*. From our study, it is evident that the compounds **37**, **38**, **40** and **41** possesses significant antiglycation activity with IC_{50} 104.45 ± 0.412, 122.09 ± 0.516, 145.82 ± 0.976 and 127.51 ± 0.781 *μ*M, respectively (**Table 5A.5**).

Table 5A.5. *α*-Amylase, *α*-glucosidase and protein glycation inhibitory activities of compounds isolated from *Hopea parviflora*

Compounds	*α*-Amylase (*μ*M)	*α*-Glucosidase (*μ*M)	Antiglycation (*μ*M)
34	46.47 ± 0.245	> 200	> 300
35	97.80 ± 0.712	> 200	> 300
37	> 100	57.49 ± 0.231	104.45 ± 0.412
38	> 100	52.07 ± 0.490	122.09 ± 0.516
40	56.23 ± 0.345	47.31 ± 0.217	145.82 ± 0.976
41	75.23 ± 0.692	44.23 ± 0.215	127.51 ± 0.781
Acarbose	8.76 ± 312	53.95 ± 0.432	-
Ascorbic acid	-	-	152.43 ± 0.427

Each value represents mean ± SD (standard deviation) from triplicate measurements

5A.6. Molecular simulation studies

Molecular simulation studies were carried out to understand the binding modes of isolated compounds [friedelin (**34**), friedelin-3*β*-ol (**35**), (-)-ampelopsin A (**37**), (-)-hopeaphenol (**38**), 2,4,8-trihydroxyphenanthrene-2-*O*-glucoside (**40**) and ellagic acid 3, 3', 4-trimethoxy 4'-*O*-*α*-L-rhamnopyranoside (**41**)] on the active sites of human pancreatic *α*-amylase (**4GQQ**) enzyme and human maltase glucoamylase (*N*- terminal, **2QMJ**; *C*-terminal, **3TOP**) enzyme using the glide program of Schrodinger suite 2017-2. The G-/D-score of all compounds are displayed in **Table 5A.7**. The pharmacophore parameters were analyzed by qikprop and the results (**Table 5A.6**) revealed that all phytochemicals isolated from *Hopea parviflora* satisfy the adsorption, distribution, metabolism and excretion/toxicity (ADME/T) properties and Lipinski Rule of Five.

In human pancreatic *α*-amylase (**4GQQ**) enzyme, compound **40** [2,4,8-trihydroxyphenanthrene-2-*O*-glucoside] observed prominent interaction with G-/D-score of -4.33/-4.32 kcal/mol, respectively. The resveratrol dimer, (-)-ampelopsin A (**37**) observed G/D-score of -3.52/-3.33 kcal/mol, respectively. (-)-Ampelopsin A also displayed significant interaction with *N*- and *C*- terminal human maltase glucoamylase enzyme with G-/D-score of -6.77/-6.58 and -5.24/-5.05 kcal/mol, respectively. In the case of **4GQQ** protein, (-) ampelopsin A forms strong hydrogen bond donor interaction with ASP 236, GLY 285 and PHE 286. The *N*-terminal human maltase glucoamylase enzyme

formed hydrogen bond donor and pi-pi stacking interaction with (-) ampelopsin A. The *C*-terminal human maltase glucoamylase enzyme (**3TOP**) only forms pi-pi stacking interaction (TRP 1369, TRP 1355 and PHE 1560) with (-) ampelopsin A (**Figure 5A.33**). Ellagic acid 3,3',4-trimethoxy 4'-*O*-*α*-L-rhamnopyranoside (**41**) interact with **4GQQ** (hydrogen bond donor) and **2QMJ** (Π-Π staking interaction, hydrogen bond donor and acceptor interactions) enzyme with G/D-score of -2.1/-2.1 and -6.4/-6.4 kcal/mol, respectively (**Figure 5A.34)**.

Table 5A.6. ADME/T properties of compounds

Sl. No	**34**	**35**	**37**	**38**	**40**	**41**
M.W	426.724	428.74	470.478	906.941	388.373	490.42
#stars	4	6	6	14	0	0
#rotor	0	1	6	10	9	8
CNS	1	1	-2	-2	-2	-2
SASA	679.955	693.998	670.313	1039.036	613.92	678.29
FISA	40.412	40.527	270.028	476.869	251.067	223.643
HBA	2	40.527	6.2	9	10.75	14.8
HBD	0	1	6	10	6	3
QPlogKhsa	2.05	2.063	0.281	1.692	-0.69	-0.865
HOA	1	1	1	1	2	2
% HOA	100	100	53.431	0	42.273	46.228
QPlogPo/w	6.957	7.032	2.349	5.186	-0.106	-0.225
QPlogS	-8.055	-8.159	-4.552	-8.289	-2.635	-2.592
R Of Five	1	1	1	4	1	1

M.W. (Molecular Weight):130.0 to 725.0; #stars (few stars-more drug-like): 0 to 5; #rotor (Number of non-trivial and non-hindered rotatable bonds):0 to 15; CNS (Central Nervous System activity): -2 to +2; SASA (Total solvent accessible surface area in square angstroms): 300.0 to 1000.0 FISA (Hydrophilic component of total solvent accessable area): 7.0 to 333.0; HBA (Hydrogen bond acceptor): 2.0 to 20.0; HBD

(hydrogen bond donor): 0.0 to 6.0; QPlogKhsa (binding to human serum albumin): -1.5 to 1.5; HOA (Human Oral Absorption): 1, 2, or 3 for low medium, and high; % HOA (Percent Human Oral Absorption): >80 % is high, <25 % is poor; QPlogPo/w (octanol/water partition coefficient): -2.0 to 6.5; QPlogS (Aqueous solubility): -6.5 to 0.5; Ro5 (Number of violations of Lipinski's rule of five): maximum is 4.

Table 5A.7. G-Score/D-Score of isolated compounds with human pancreatic *α*-amylase (**4GQQ**) and human maltase glucoamylase (*N*- terminal, **2QMJ**; *C*- terminal, **3TOP**)

Compounds	**4GQQ (kcal/mol)**		**2QMJ (kcal/mol)**		**3TOP (kcal/mol)**	
	G-Score	D-Score	G-Score	D-Score	G-Score	D-Score
34	-0.53	-0.53	-	-	-	-
35	-	-	-	-	-3.65	-3.65
37	-3.52	-3.33	-6.77	-6.58	-5.24	-5.05
38	-	-	-3.52	-3.02	-4.41	-3.12
40	-4.33	-4.32	-	-	-	-
41	-2.1	-2.1	-6.4	-6.4	-	-

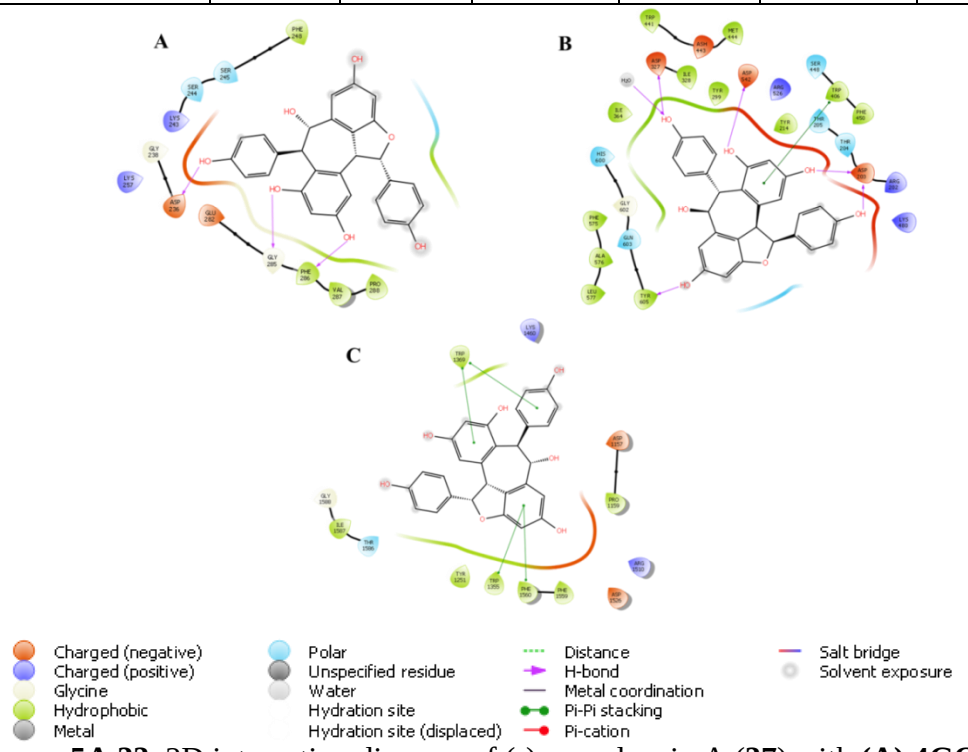

Figure 5A.33. 2D interaction diagram of (-)-ampelopsin A (**37**) with **(A) 4GQQ, (B) 2QMJ** and **(C) 3TOP**

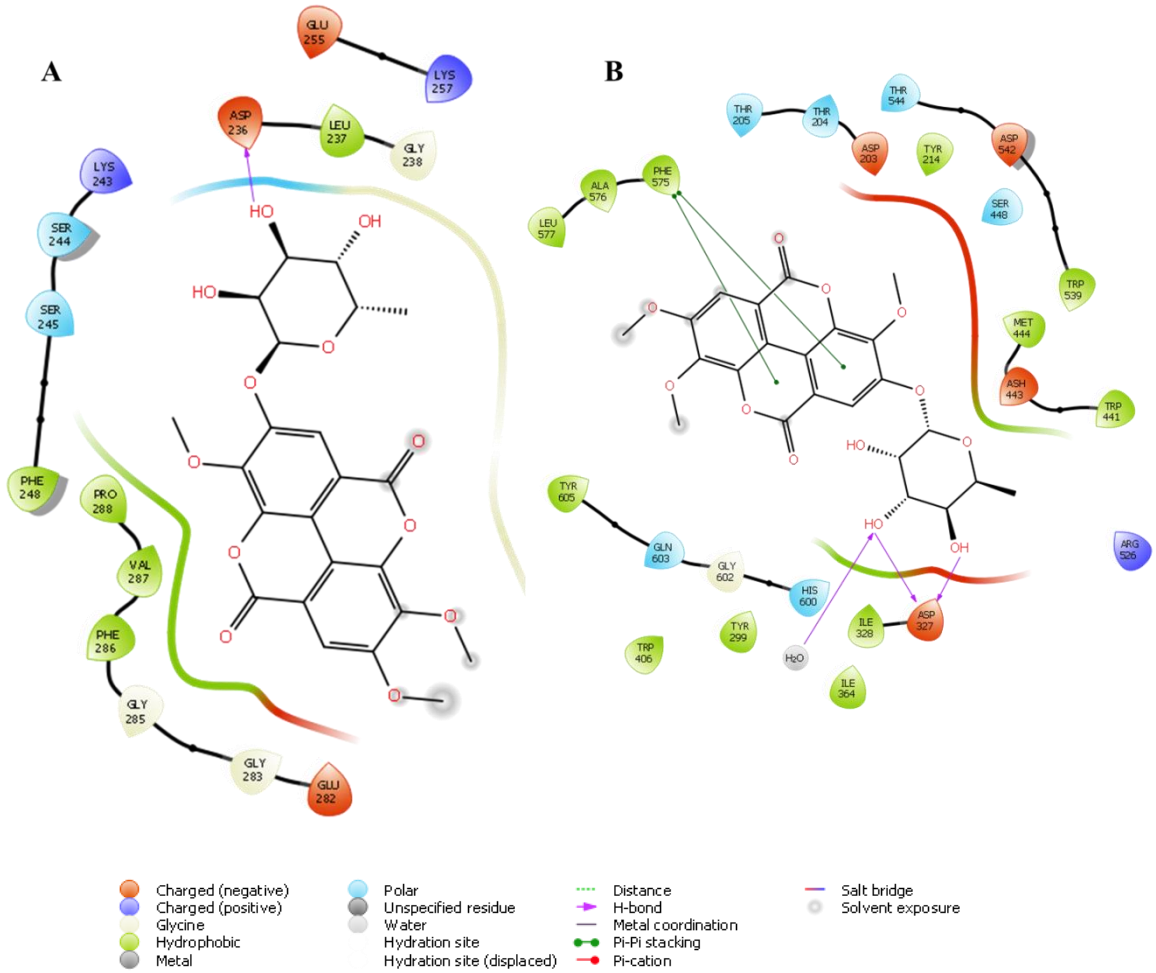

Figure 5A.34. 2D interaction diagram of ellagic acid 3, 3', 4-trimethoxy-4'-*O*-*α*-L-rhamnopyranoside (**41**) with **(A) 4GQQ** and **(B) 2QMJ**

5A.7. Glucose uptake in L6 myotubes

As metioned in the previous chapters, glucose uptake mainly takes place in myocytes. We herein checked the glucose uptake of friedelin (**34**), friedelin-3*β*-ol (**35**), (-)-ampelopsin A (**37**) and ellagic acid 3,3',4-trimethoxy-4'-*O*-*α*-L-rhamnopyranoside (**41**). In order to find out the suitable working concentrations of the compounds, first we carried out the cytotoxicity in L6 cell line using MTT assay (**Figure 5A.35**). All the compounds showed a dose-dependent increase in toxicity. A concentration of 10 μM caused cell viability to decrease by about 30 %. Therefore, 5 μM and 10 μM concentrations of compounds were selected for cellular 2-NBDG uptake experiments. It was monitored using the fluorescently labeled glucose analogue, 2-NBDG (10 μM) after the pre-treatment of the differentiated L6 myotubes with 10 and 20 μM concentrations of compounds. From **Figure 5A.36**, it is clear that ellagic acid 3,3',4-trimethoxy 4'-*O*-*α*-L-

rhamnopyranoside (**41**) exhibited significant glucose uptake by 47.2 % and 17.4 % respectively, which is comparable than that of rosiglitazone standard (100 nM), showing 38 % of 2-NBDG uptake.

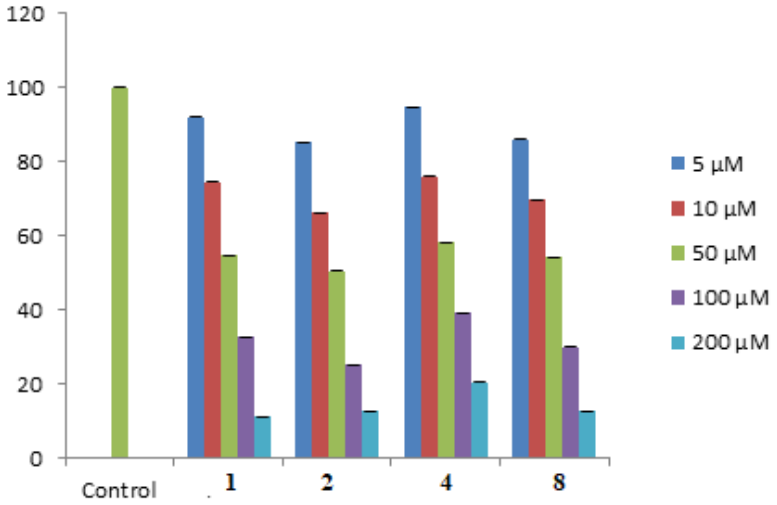

Figure 5A.35. Cytotoxicity of compounds

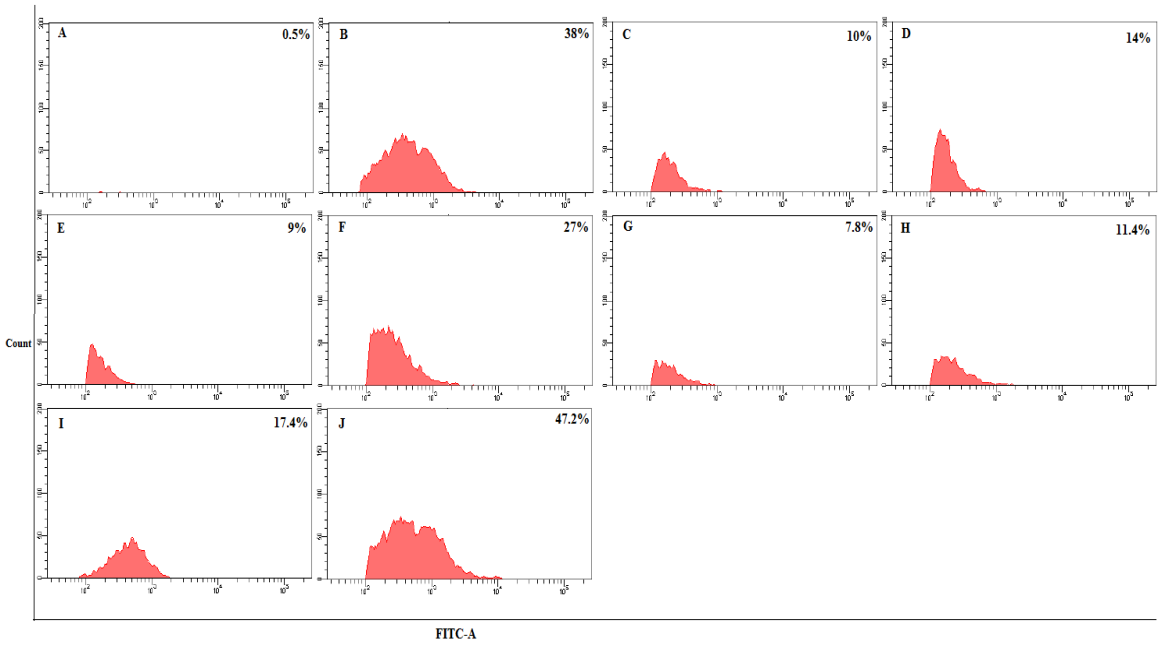

Figure 5A.36. 2-NBDG assay by flow cytometry in L6 myotubes. (A)-Blank (B)-Positive control, (C and D)- 10 and 20 % friedelin (**34**), (E and F)- 10 and 20 % friedelin-3*β*-ol (**35**), (G and H)- 10 and 20 % (-)-ampelopsin A (**37**) and (I and J)- 10 and 20 % ellagic acid 3, 3', 4-trimethoxy 4'-*O*-*α*-L-rhamnopyranoside (**41**)

5A.8. Conclusion

Phytochemical investigation of the stem bark of *Hopea parviflora* afforded **9** compounds including two triterpenoids (friedelin and friedelin-3*β*-ol), two resveratrol

dimers ((-)-ε-viniferin and (-)-ampelopsin A), two resveratrol tetramers (vaticaphenol A and (-)-hopeaphenol), 2,4,8-trihydroxyphenanthrene-2-*O*-glucoside, ellagic acid 3,3',4-trimethoxy-4'-*O*-α-L-rhamnopyranoside and glycoside of β-sitosterol. Herein, friedelin, friedelin-3β-ol, vaticaphenol A, 2, 4, 8-trihydroxyphenanthrene-2-*O*-glucoside, ellagic acid 3, 3', 4-trimethoxy 4'-*O*-α-L-rhamnopyranoside and glycoside of β-sitosterol are reported for the first time from *Hopea parviflora*. The structure elucidation was done by spectroscopic 1D and 2D NMR techniques *viz*., ^{1}H, ^{13}C, DEPT 135, HMQC, HMBC, and ^{1}H-^{1}H COSY, and NOESY, HRESIMS and compared with the reported literature. All compounds were evaluated for their α-amylase and α-glucosidase inhibitory activity and antiglycation potential. The molecular docking studies showed that all the active compounds well accommodate in the active site of the **4GQQ**, **2QMJ** and **3TOP** enzyme. Moreover, pharmacokinetic properties of the compounds were predicted *in silico*, suggesting that the compounds possess drug like properties and excellent ADME/T profile. *In vitro* antidiabetic activity in L6 myotubes revealed that ellagic acid 3,3',4-trimethoxy-4'-*O*-α-L-rhamnopyranoside (**41**) significantly enhances the glucose uptake in a dose dependant manner. Further studies are ongoing in our lab to establish the therapeutic efficacy and safety of compounds as a promising antidiabetic agent from *Hopea parviflora.*

5A.9. Experimental

5A.9.1. General experimental procedures and chemicals

As mentioned in the first part of Chapter 2.

5A.9.2. Plant material and extraction

The stem bark of *Hopea parviflora* was collected from Western Ghats region of Wayanad District, Kerala, India. The stem bark was cleaned, cut into small pieces, air dried and then dried in drier maintained at 50 ^{o}C and powdered. The powdered stem bark (700 g) was subjected to extraction using *n*-hexane (2.5 L x 72 h x 3 times; 750 mg), acetone (2.5 L x 72 h x 3 times; 90 g), EtOH (2.5 L x 72 h x 3 times; 24 g) and water (2.5 L x 72 h x 3 times; 10 g). After extraction, the solvent was removed under reduced pressure using Büchi rotary evaporator. All the extracts were checked for their preliminary antidiabetic activity. Among the extract, acetone extract showed siginifant antidiabetic activity. The crude acetone extract (60 g) was subjected to silica gel (100-200 mesh) column chromatography using *n*-hexane, *n*-hexane-EtOAc gradient, EtOAc and EtOAc-MeOH gradient polarities. Eighteen fractions of 200 mL each were collected and concentrated under reduced

pressure and temperature was maintained at 50 ^{o}C. The schematic representation of isolation procedure is shown in **Figure 5A.37.**

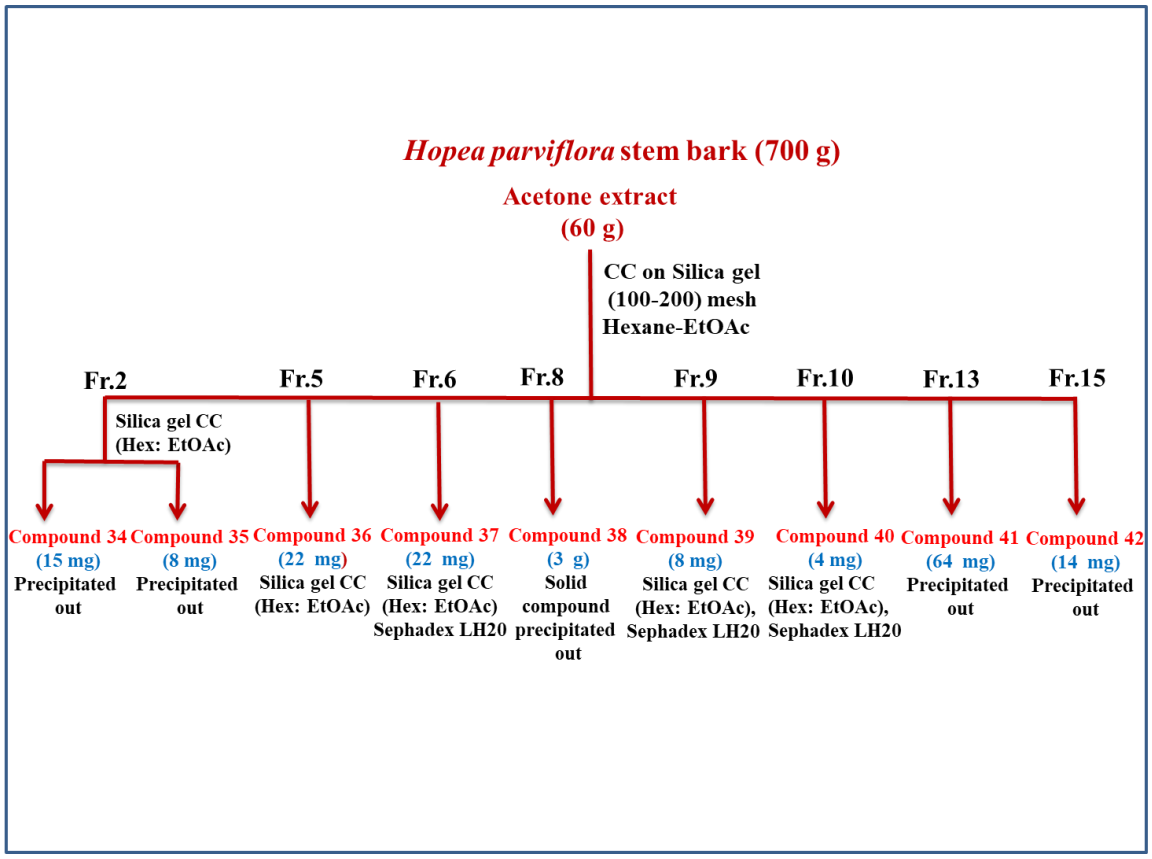

Figure 5A.37. Schematic representation of isolation procedure of the acetone extract of the stem bark of *Hopea parviflora*

5A.9.2.1. Isolation of compound 34

The isolation procedure of compound **34** is represented in **Figure 5A.37**. Compound **34** (15 mg) was obtained as colorless crystalline solid, on eluting the column (silica gel 100-200 mesh) with 5 % EtOAc in *n*-hexane. The detailed analysis of FTIR, ^{1}H NMR, ^{13}C NMR spectrum and HRESIMS gave compound **34** as Fredelin.

Nature	colorless crystalline solid
Melting Point	262-264 °C
FTIR (KBr, υ_{max})	3432, 2930, 2870, 1716, 1460, 1388, 1188, 1110, 1074 cm^{-1}.
^{1}H NMR (500 MHz, $CDCl_3$)	δ 2.4 (m, 1H, H-2b), 2.29 (m, 1H, H-2a), 2.25 (q, 1H, H-4), 1.95 (m,

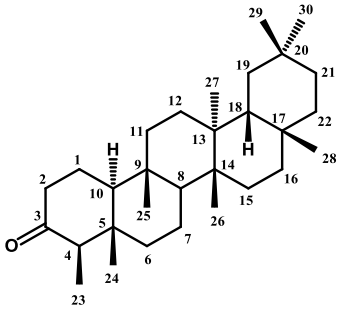

,

	1H, H-1a), 1.69 (m, 3H), 1.25 (m, 2H), 1.56-1.44 (m, 8H), 1.40-1.33 (m, 6H), 1.32-1.28 (m, 4H), 1.24 (m, 1H), 1.18 (s, 3H, -Me), 1.08 (s, 3H, -Me), 1.00 (6H,s, -Me), 0.95 (s, 3H, -Me), 0.87 (s, 3H, -Me), 0.88 (s, 3H, -Me), 0.72 (s, 3H, -Me) ppm.
^{13}C NMR (125 MHz, $CDCl_3$)	δ 213.3 (C-3), 59.5 (C-10), 58.2 (C-4), 53.1 (C-8), 42.8 (C-18), 42.1 (C-5), 41.5 (C-2), 41.3 (C-6), 39.7 (C-22), 39.3 (C-14), 38.3, 37.4, 36.0, 35.6, 35.3, 35.0, 32.8, 32.4, 32.1, 31.8, 30.5, 30.0, 28.2 (C-20), 22.3 (C-1), 20.3 (C-26), 18.7 (C-27), 18.2 (C-7), 18.0 (C-25), 14.7 (C-24), 6.7 (C-23) ppm.
HRESIMS (m/z)	427.1497 $(M+H)^+$.

5A.9.2.2. Isolation of compound 35

Fraction pool 2 on silica gel column chromatographic separation by 5 % EtOAc in *n*-hexane, we got compound **35** (8 mg) as colourless amorphous solid.

Nature	colourless crystalline solid
Melting Point	280-282 °C
FTIR (KBr, υ_{max})	3417, 2900, 1475, 1356, 1192, 1115, 1090 cm^{-1}
^{1}H NMR (500 MHz, $CDCl_3$)	δ 3.7 (brs, 1H), 2.4 (m, 1H), 2.25 (m, 2H), 1.95 (m, 1H), 1.9 (m, 1H), 1.73 (m, 3H), 1.23 (m, 3H, Me), 1.14 (s, 6H, Me), 1.08 (d, 4H), 1.05

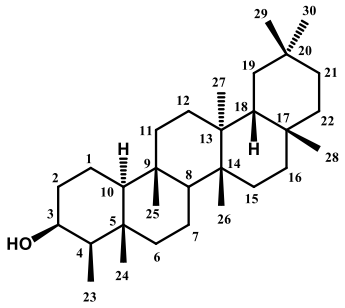

	(s, 2H), 0.86 (s, 9H, Me), 0.72 (s, 3H, Me) ppm.
^{13}C NMR (125 MHz, $CDCl_3$)	δ 72.8 (C-3), 61.3, 53.2, 42.8, 41.7, 41.5, 41.3, 39.7, 39.3, 38.4, 37.8, 37.4, 37.1, 36.1, 35.5, 35.2, 35.0, 32.4, 32.3, 32.1, 31.8, 30.6, 29.7, 28.2, 20.3, 20.1, 18.7, 18.2, 15.8, 7.0 (C-23) ppm.
HRESIMS (m/z)	429.1042 $(M+H)^+$.

5A.9.2.3. Isolation of compound 36

Compound **36** (22 mg) was obtained as brown amorphous solid, on eluting the column (silica gel 100-200 mesh) with 55 % EtOAc in *n*-hexane. The detailed analysis of 1D and 2D NMR spectra and HRESIMS gave compound **36** as (-)- ε-viniferin.

5A.9.2.4. Isolation of compound 37

Compound **37** (22 mg) was obtained as brown amorphous solid, on eluting the column (silica gel 100-200 mesh) with 55 % EtOAc in *n*-hexane, followed by gel permeation in Sephadex LH20 using MeOH as eluent. The detailed analysis of FTIR, ^{1}H, ^{13}C, ^{1}H-^{1}H COSY, HMQC, DEPT 135 and HMBC spectra and HRESIMS gave compound **37** as (-)- ampelopsin A.

Nature	Brown amorphous solid
^{1}H NMR (500 MHz, Acetone-d_6)	δ 8.61 (s, 1H, -OH), 8.44 (s, 1H, -OH), 8.40 (s, 1H, -OH), 8.23 (s, 1H, -OH), 8.20 (s, 1H, -OH), 7.10 (d, J = 8.5 Hz, 2H, H-2a and 6a), 6.88 (d, J = 8.5 Hz, 2H, H-2 and 6), 6.76 (d, J = 8.5 Hz, 2H, H-3a and 5a), 6.62 (d, J = 9 Hz, 2H, H-3 and

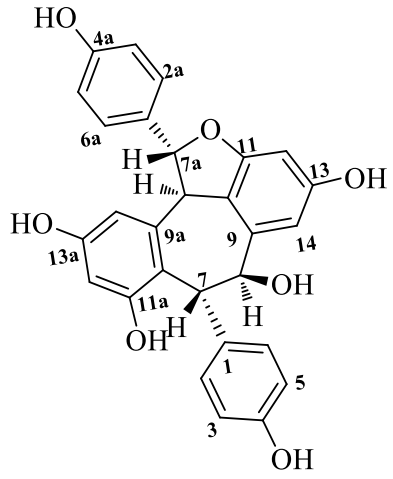

5), 6.59 (d, *J* = 2 Hz, 1H, H-14), 6.42 (d, *J* = 2 Hz, 1H, H-12'), 6.22 (s, 1H, H-14'), 6.14 (d, *J* = 2 Hz, 1H, H-12), 5.75 (d, *J* = 11.5 Hz, 1H, H-7'), 5.43 (d, *J* = 4.5 Hz, 2H, H-7), 5.39 (t, *J* = 7 Hz or 5 Hz, 1H, H-8), 4.14 (d, *J* = 7.5 Hz, 1H, H-8') ppm.

^{13}C NMR (125 MHz, Acetone-d_6)	δ 159.0 (C-OH), 159.0 (C-OH), 158.4 (C-OH), 158.1 (C-OH), 157.4 (C-OH), 156.2 (C-OH), 150.7, 140.6, 132.5, 130.0, 129.9, 128.7, 123.0, 120.8, 118.3, 116.0, 115.5, 115.3, 110.5 (C-14), 108.2, 105.2 (C-14'), 103.2 (C-12'), 101.6 (C-12), 88.7 (C-7'), 71.2 (C-8), 49.6 (C-8'), 43.6 (C-7) ppm.
HRESIMS (m/z)	493.12674 $(M+Na)^+$.

5A.9.2.5. Isolation of compound 38

The isolation procedure of compound **38** is represented in **Figure 5A.37**. Compound **38** (3 g) was obtained as a pale yellow amorphous solid, on precipitation using chloroform. The detailed analysis of 1D and 2D NMR spectra and HRESIMS gave compound **38** as (-)-hopeaphenol.

5A.9.2.6. Isolation of compound 39

Compound **39** (8 mg) was obtained as brown amorphous solid, on eluting the column (silica gel 100-200 mesh) with 70 % EtOAc in *n*-hexane, followed by gel

permeation in Sephadex LH20 using MeOH as eluent. The detailed analysis of FTIR, 1D and 2D NMR spectra and HRESIMS gave compound **39** as vaticaphenol A.

5A.9.2.7. Isolation of compound 40

The silica gel and sephadex LH 20 column chromatographic separation resulted in the isolation of compound **40** (4 mg) as pale yellow amorphous solid. The detailed analysis of FTIR, ^{1}H NMR, ^{13}C, ^{1}H-^{1}H COSY, HMQC, DEPT 135 and HMBC spectra and HRESIMS gave compound **40** as 2, 4, 8-trihydroxyphenanthrene-2-*O*-glucoside.

Nature	colorless crystalline solid
Melting Point	258-260 °C
FTIR (KBr, υ_{max})	3360, 2925, 1695, 1600, 1512, 1450, 1370, 1245, 1148, 1061, 901 cm^{-1}
^{1}H NMR (500MHz, Acetone-d_6)	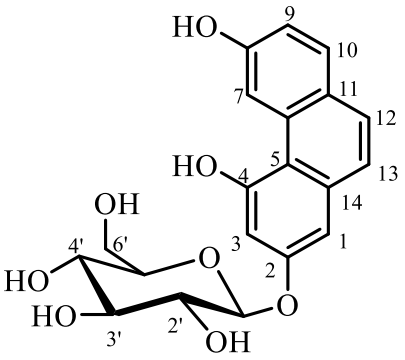 δ 8.35 (s, 1H, H-OH), 8.32 (s, 1H, H-OH), 8.09 (s, 1H, H-OH), 8.06 (s, 1H, H-OH), 7.38 (s, 1H, H-OH), 7.27 (dd, J_1 = 7 Hz, J_2 = 2 Hz), 6.71 (t, J_1 = 3 Hz, J_2 = 2 Hz, 1H), 6.69 (t, J_1 = 3 Hz, J_2 = 2 Hz, 2H), 6.47 (d, J = 2.5 Hz, 1H), 6.11 (J = 2 Hz, 1H), 4.83 (d, J = 9.5 Hz, 1 Hz, H-1'), 4.12-4.10 (m, 2H), 4.06 (brs, 1H), 3.84 (brs, 1H), 3.72- 3.71 (m, 1H), 3.62-3.58 (m, 1H), 3.55-3.50 (m, 1H), 3.47- 3.43 (m, 1H), 3.37-3.34 (m, 1H) glucose moiety] ppm.
^{13}C NMR (125 MHz, Acetone-d_6)	δ 157.6 (C-OH), 157.2 (C-OH), 143.3 (C-OH), 139.8 (C-5 and 6), 132.6 (C-7), [129.5

	127.9, 126.7 (C-), 125.1 (C-), 124.1, 115.5, 113.6 (other aromatic protons)], 104.7 (C-3), 85.5 (C-1'), [80.8, 78.6, 76.2, 73.5, 72.2, 70.0, 67.3 61.1, 53.5 (glucose moiety)] ppm.
HRESIMS (m/z)	389.1246 $(M+H)^+$.

5A.9.2.8. Isolation of compound 41

From the fraction pool 13, colourless amorphous solid (64 mg) was precipitated out. The detailed analysis of IR, ^1H, ^{13}C, ^1H-^1H COSY, HMQC, DEPT 135 and HMBC NMR spectra and HRESIMS gave ellagic acid-3,3',4-trimethoxy-4'-*O*-*α*-L-rhamnopyranoside.

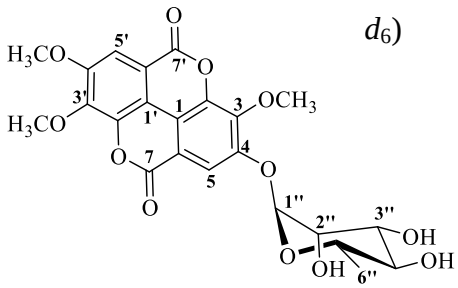

Nature	Colorless crystalline solid
Melting Point	220-222 °C
FTIR (KBr, υ_{max})	3440, 2956, 2870, 1716, 1480, 1400, 1110, 1031, 978 cm^{-1}.
^1H NMR (500 MHz, DMSO-d_6)	δ 7.78 (s, 1H, H-5), 7.60 (s, 1H, H-5'), 5.58 (s, 1H, H-1''), 5.25 (d, J = 3.5 Hz, 1H), 5.01 (d, J = 5.5 Hz, 1H), 4.88 (d, J = 5.5 Hz, 1H), 4.09 (s, 3H, -OCH_3) , 4.06 (s, 3H, -OCH_3), 4.01 (s, 3H, -OCH_3), 3.73-3.72 (m, 1H, H-3''), 3.55-3.52 (m, 1H, H-4''), 1.15 (d, J = 6 Hz, 3H, H-6'') ppm.
^{13}C NMR (125 MHz, DMSO-d_6)	δ 158.2 (C-7. 7'), 154.2 (4'), 150.6 (C-4), 141.7 (C-2'), 141.2 (C-3), 141.0 (C-2), 140.9 (C-3'), 113.5 (C-1), 112.6 (C-6), 112.4

	(C-6'), 112.3, 111.7 (C-5. 5'), 107.5 (C-1'), 99.5 (C-1''), 71.5 (C-4''), 70.4 (C-3''), 70.3 (C-5''), 70.0 (C-2''), 61.6 ($-OCH_3$), 61.3 ($-OCH_3$), 56.7 ($-OCH_3$), 17.9 (C-6'') ppm.
HRESIMS (m/z)	491.1200 $(M+H)^+$.

5A.9.2.9. Isolation of compound 42

From the fraction pool 15, colourless amorphous solid (14 mg) was precipitated out. The detailed analysis of FTIR, ^1H and ^{13}C NMR spectra and HRESIMS gave compound **41** as glucoside of β-sitoterol.

Anti-inflammatory Effects and Mechanisms of Action of Ellagic acid-3, 3', 4-trimethoxy-4'-*O*-*α*-L-rhamnopyranoside Isolated from *Hopea parviflora* Bedd. in Lipopolysaccharide-Stimulated RAW 264.7 Macrophages

5B.1. Introduction

As described in the chapter 3, inflammation is a complex biological process that occurs when tissues are infected or injured by harmful stimuli such as pathogens, damage or irritants. Immune cells, blood vessels, and molecular mediators are involved in this process. But, uncontrolled inflammation can lead to the development of various diseases, such as diabetes, asthma, inflammatory bowel disease, atherosclerosis, rheumatoid arthritis, neurodegenerative disorders, and sepsis. Lipopolysaccharide (LPS) is also known as lipoglycans and endotoxins; an exogenous bacterial endotoxin, activates macrophages such that they produce various pro-inflammatory cytokines [interleukin-beta (IL-*β*), IL-12, IL-18, tumor necrosis factor-*α* (TNF--*α*), interferon-γ (IFN-*γ*), and granulocyte-macrophage colony stimulating factor] and mediators [nitric oxide (NO), and prostaglandin E2 (PGE2)]. Nuclear factor-κB (NF-κB) is present in the cytoplasm as an inactive complex associated with an inhibitory protein (IκB) and a key transcriptional factor involved in immune and inflammatory responses.

Plants continue to be a vital source of new drug leads including anti-inflammatory agents. As mentioned in the first part of chapter 5, *Hopea parviflora* Bedd. is an endangered plant species and is native to India. Previous reports showed that resveratrol oligomers are the major phytochemical constituents present in this plant. species. Resveratrol and its oligomers possess various biological activities such as antioxidant, antiHIV, antidiabetic and so on. We herein report the anti-inflammatory effects and mechanisms of action of compounds isolated from *Hopea parviflora* in lipopolysaccharide-stimulated RAW 264.7 macrophages. The compounds chosen for anti-inflammatory study are shown in **Figure 5B.1.**

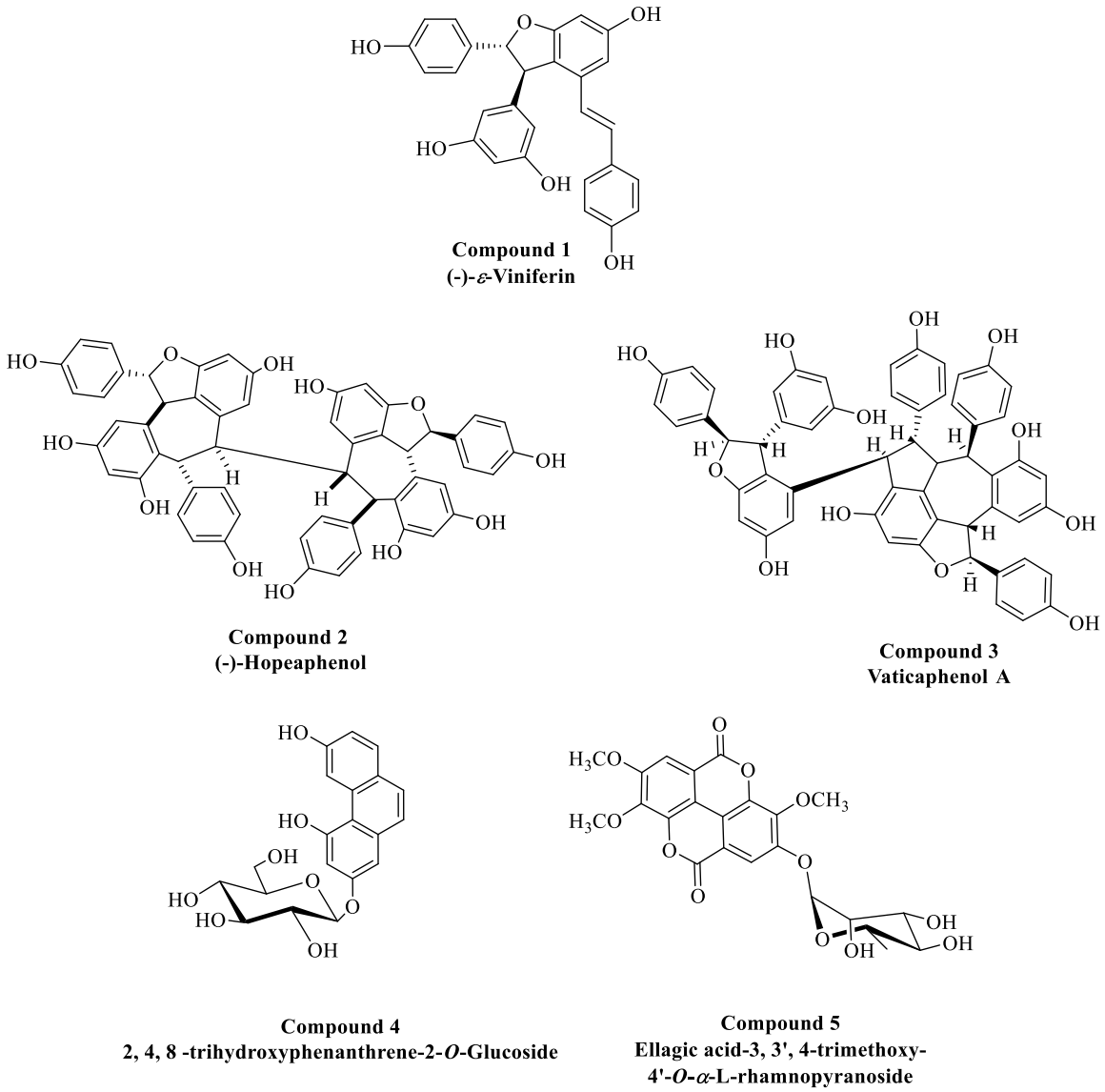

Figure 5B.1. Isolated compounds for anti-inflammatory study

5B.2. Cytotoxic effect of compounds 1-5 in RAW 264.7 macrophages

Cytotoxic effects of compounds **1-5** in RAW 264.7 macrophages were determined by tetrazolium salt 3-[4, 5-dimethylthiazol-2-yl]-2, 5-bromide (MTT) assay. Cells were treated with different concentrations (1 μM, 5 μM, 10 μM, 25 μM, 50 μM and 100 μM) of compounds **1-5**. From the **Figure 5B.2**., it is clear that compound **5** showed less toxicity in 1 μM and 5 μM concentrations. Therefore, 1 μM and 5 μM concentrations of compound **5** was taken for further studies.

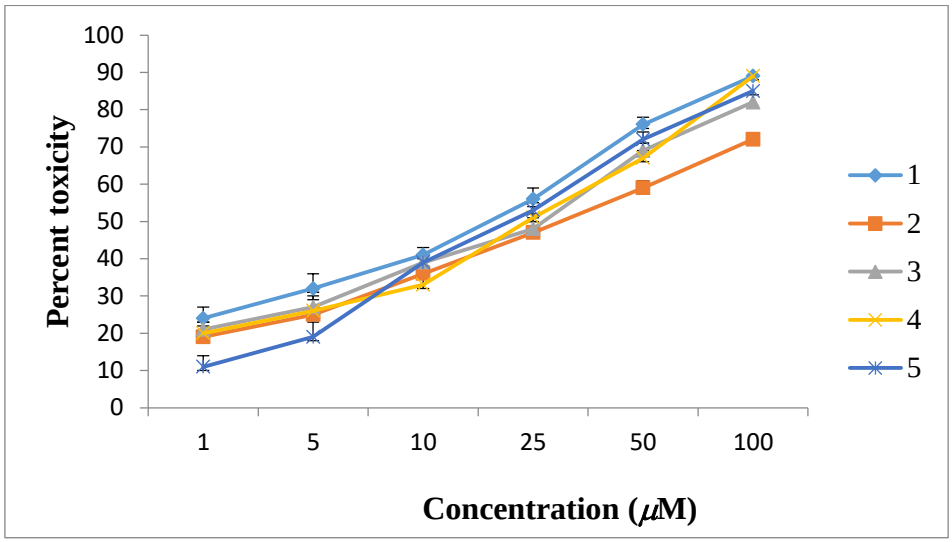

Figure 5B.2. Cytotoxic effect of compounds **1-5** in RAW 264.7 macrophages

5B.3. NO production in LPS-stimulated RAW 264.7 cell lines

Nitric oxide (NO) plays a vital role in host defence response against various pathogens. Under normal physiological conditions, NO regulates various pathophysiological processes such as neuronal communication, vasodilatation, and neurotoxicity [Moncada *et al*., **1991**; Nakagawa *et al*., **2002**]. However, over-production of NO induces tissue damage associated with inflammations [Taira *et al*., **2009**]. Therefore, more attention is now being paid to the development of new drug leads as potent inhibitors of NO production in relation to the treatment of inflammatory diseases [Pacher *et al*., **2007**]. Macrophages are key components of the mammalian immune system, and play a significant role by providing an immediate defense against foreign agents [Moncada *et al*., **1991**]. Lipopolysaccharide (LPS) is a component from the cell wall of gram-negative bacteria and one of the most powerful activators of macrophages. LPS induce the production of pro-inflammatory cytokines and thereby NO production [Nicholas *et al*., **2007**]. Hence, inhibition of NO production in lipopolysaccharide (LPS)-stimulated RAW 264.7 macrophages is one of the possible ways to screen new chemical entities for anti-inflammatory activity. Herein, we investigated the effects of compound **5** in LPS-induced RAW 264.7 cells. The level of NO in cell supernatants was determined using Griess reagent. The concentration of NO produced was determined based on a sodium nitrite standard calibration curve. The result showed that NO production remarkably increased in LPS- stimulated RAW 264.7 cells. Cells pre-treated with compound **5** showed a significant inhibition in NO production (**Figure 5B.3**).

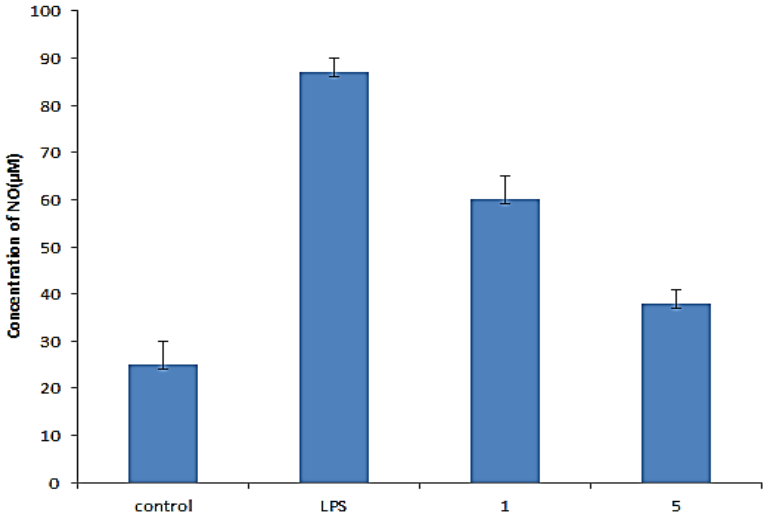

Figure 5B.3. Effect of 1 μM and 5 μM concentrations of compound **5** on NO production in LPS-stimulated RAW 264.7 cell lines. RAW 264.7 cells were stimulated with 1 μg/mL of LPS. Values are mean of three replicate determinations (n = 3) ± SD. Bars having different letters are significantly different ($P < 0.05$).

5B.4. TNF-α, IL-6, LOX-1, COX-2 and IL-10 production in LPS-stimulated RAW 264.7 macrophages

Tumor necrosis factor-α (TNF-α), originally described as a serum factor capable of causing tumor necrosis and is recognized as a potent immune regulator. The main sources of TNF-α are macrophages and monocytes. TNF-α is produced by macrophages and monocytes in response to a variety of stimuli, including the cytokine interferon-γ (IFN-γ) and bacterial lipopolysaccharide (LPS). TNF-α have multiple regulatory effects; for example, this molecule is believed to mediate the host inflammatory response through its biological effects on various cell types. IL-6 acts as pro-inflammatory and anti-inflammatory cytokine, and can initiate synthesis of prostaglandin E_2. IL-10 produced by Th2 cells, macrophages and CD8+ cell clones and is capable of inhibiting the synthesis of several cytokines from different cells, antigen or mitogen activated. Lectin-like ox-LDL receptor (LOX-1) is one of type II membrane protein, mainly found in endothelial cells and which belongs to the *C*-type lectin family. It consists of a short *N*-terminal cytoplasmic domain, a trans-membrane domain and a *C*-terminal hydrophobic domain. LOX-1 can be induced by lots of pathological stimulus and is expressed in monocytes, platelets, smooth muscle cells, and macrophages. According to the study of Honjo *et al*., LOX-1 inhibition can decrease the inflammatory response, and plays an important role in

inflammation. One of the key steps in inflammation is the activation of a cyclooxygenases (COX), which is responsible for production of several inflammatory mediators from arachidonic acid. The two isoforms of cyclooxygenase enzymes are COX-1 and COX-2. The main function of COX-1 is the synthesis of prostaglandins, which is responsible for maintaining normal body function in kidney, gastrointestinal tract and other organs. COX-2 is mainly induced during inflammation. Classical non-steroidal anti-inflammatory drugs (NSAIDs) such as aspirin, diclofenac and indomethacin inhibit both COX isoforms leading to effective antiinflammatory response. But they have some side effects which includes gastric ulceration and kidney damage. Several efforts are on-going in various laboratories for the search of novel COX-2 inhibitors with fewer side effects.

Herein, we investigated the effects of compound **5** on LPS-induced TNF-α, IL-6, LOX-1, COX-2 and IL-10 production in LPS-induced RAW 264.7 cells. Proinflammatory mediators like TNF-α, IL-6, LOX-1 and COX-2 were found to be decreased in RAW 264.7 cells in a dose dependent manner, when compared with LPS control. It is also noted that antiinflammatory cytokine IL-10 was found to be increased in cell treated with compound **5** when compared with LPS control in a dose dependent manner (**Figure 5B.4)**.

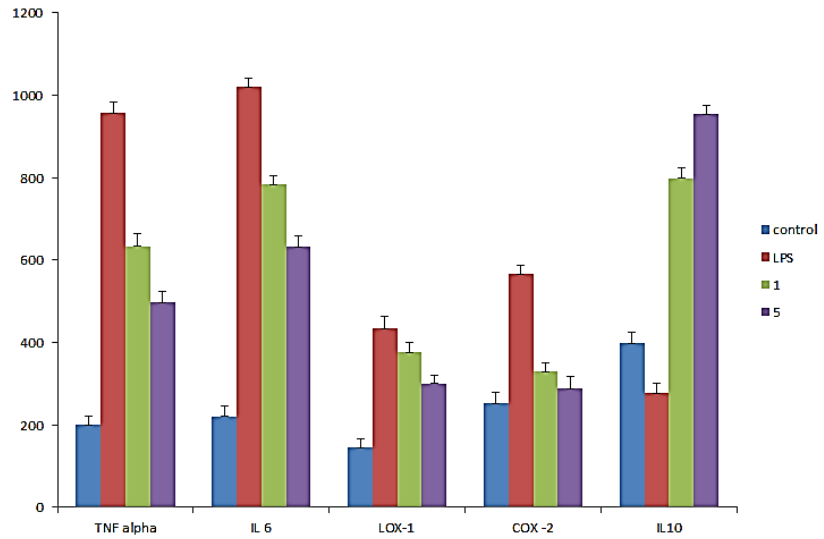

Figure 5B.4. Effect of 1 μM and 5 μM concentrations of compound 5 on TNF-α, IL-6 and IL10 production in LPS-stimulated RAW 264.7 cell lines. RAW 264.7 cells were stimulated with 1 μg/mL of LPS. Values are mean of three replicate determinations (n = 3) ± standard deviation. Bars having different letters are significantly different (P < 0.05).

5B.5. Compound 5 inhibited NF-κB expression in LPS-stimulated RAW 264.7 macrophages

Nuclear factor-κB (NF-κB); transcriptional factor mainly involved in immune and inflammatory responses. Upon activation by external stimuli such as TNF-α and LPS, the IκB protein is phosphorylated and degraded, and translocated into the nucleus. Translocated NF-κB interacts with κB elements in the promoter region of several inflammatory genes, leading to the transcription of pro-inflammatory mediators and cytokines. Thus, NF-κB has been regarded as the main molecular target in development of therapies for inflammatory diseases. We herein found out that compound **5** inhibited NF-κB productions in a dose dependent manner in LPS induced RAW 264.7 macrophages (**Figure 5B.5**).

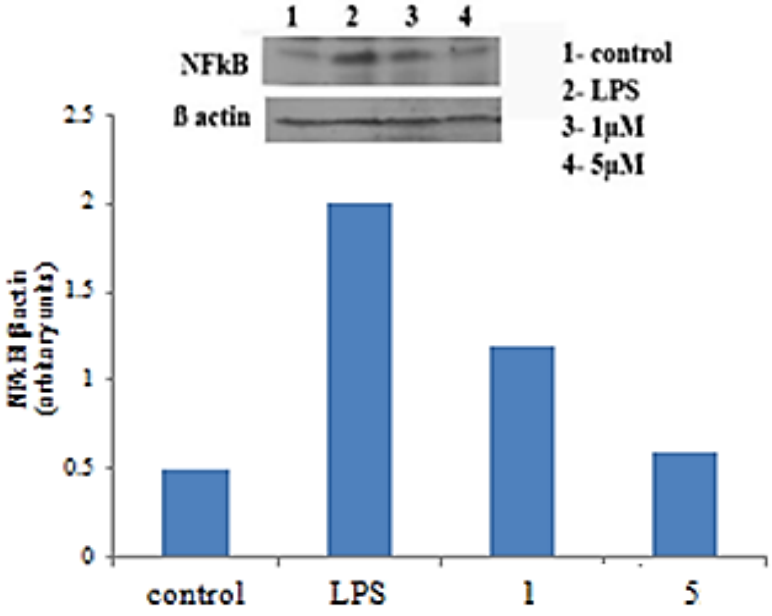

Figure 5B.5. Expression level of 1 and 5 μM concentrations of compound **5** on NF-κB production

5B.6. Conclusion

In summary, we have investigated the anti-inflammatory activity of compounds isolated from the stem bark of *Hopea parviflora*. Among the isolated compounds, ellagic acid- 3, 3', 4-trimethoxy 4'-*O*-α-L-rhamnopyranoside (**5**) is less toxic in RAW 264.7 macrophages. Compound **5** inhibited the action of pro-inflammatory mediators like NO, TNF-α, IL-6, LOX-1 and COX-2 and promote the action of anti-inflammatory mediator

IL 10 *via* inhibition of NF-κB pathway in LPS-stimulated RAW264.7 macrophages. These findings provided information on the mechanism of action of ellagic acid-3, 3', 4-trimethoxy-4'-*O*-*α*-L-rhamnopyranoside (**5**). Further studies on the biological effects of ellagic acid-3, 3', 4-trimethoxy-4'-*O*-*α*-L-rhamnopyranoside (**5**) are warranted in future.

5B.7. Experimental

5B.7.1. Cell culture and treatment conditions

RAW 264.7 macrophages were procured from NCCS, Pune, India and were maintained in DMEM containing 10 % FBS and 1 % antibiotic–antimycotic mix at 37 °C in humidified air containing 5 % CO_2.

5B.7.2. Cytotoxicity assay

Cytotoxicity was assessed by MTT assay. The cells were maintained at 37 ^{o}C in 5 % CO_2 incubator. They were trypsinized and seeded in 24 well plates, treated with different concentrations of the compounds **1-5** (1 μM, 5 μM, 10 μM, 25 μM, 50 μM and 100 μM) for 24 h. After the incubation, cells were treated with MTT reagent (0.5 g/L) for 4 h. Mitochondrial dehydrogenase enzyme is active only in live cells that reduce the yellow dye, MTT, to purple formazan crystals and the crystals were dissolved in 200 μL DMSO. The absorbance was recorded at 570 nm using Synergy 4 Biotek multimode reader. The percentage of cell toxicity was calculated as,

$$\% \text{ of cell toxicity} = \frac{\text{Absorbance of control - Absorbance of sample}}{\text{Absorbance of control}} \text{ x } 100$$

5B.7.3. Determination of nitric oxide (NO) production

After pre-incubation of RAW 264.7 cells (2×10^6 cells/mL) with different concentrations of compound **5** and LPS (10 μg/mL) for 24 h, the quantity of nitrite accumulated in the culture medium was measured as an indicator of NO production. Briefly, 100 μL of Griess reagent (1 % sulfanilamide and 0.1 % naphthylethylenediamine dihydrochloride in 2.5 % phosphoric acid), was mixed with an equal volume of cell supernatant, the mixture was incubated at room temperature for 10 min, and the absorbance at 540 nm was measured in a microplate reader. The quantity of nitrite was determined based on a sodium nitrite standard calibration curve. All experiments were done in triplicates.

5B.7.4. ELISA of TNF-α, IL-6, LOX-1, COX-2 and IL-10

Concentrations of TNF-α, IL-6, LOX-1, COX-2 and IL-10 in the culture medium were determined using respective ELISA kits according to the manufacturer's protocol and the absorbance was measured at 450 nm using microplate reader (Biotek ELX 800).

5B.7.5. Western blot expression study

Expression level of NF-κB was evaluated by Western blotting. Cells were treated with 1 μM and 5 μM of compound 5 for 24 h. After incubation, the cells were lysed in ice-cold lysis buffer (50 mM Tris-HCl, 150 mM sodium chloride, 1.0 % Igepal CA-630, 0.5 % sodium deoxycholate, 0.1 % sodium dodecyl sulfate, 1 % Triton X-100 and protease inhibitor cocktail, pH 8.0) for 30 min on ice and were centrifuged at 12000 *x*g for 10 min. The protein content was then measured using BCA protein assay kit. The lysates (40 μg) were subjected to SDS-PAGE on 10 % gel and transferred on to a polyvinylidene difluoride (PVDF, Immobilon P™, Millipore®, USA) membrane by using Trans-Blot Turbo^{TM} (Bio-Rad). The membranes were blocked by incubating in blocking buffer (5 % skim milk in PBST, PBST-PBS buffer containing 0.1 % Tween 20) for 1 h at room temperature, washed three times with PBST and probed over night at 4 °C with appropriate antibody against NF-κB (1: 1000). Membranes were washed 3 times and incubated for 1 h at room temperature with horse radish peroxidase (HRP) conjugated secondary antibody at 1:1000 dilution and again washed three times in PBST. The bound antibodies were detected using an enhanced chemiluminescence substrate (Biorad, **USA**) and measured by densitometry by using a Chemi Doc XRS digital imaging system and the Multi Analyst software from Bio-Rad Laboratories (**USA**).

Isolation, Characterization and Antidiabetic Potential of Phytochemicals from the Stem Bark of *Myristica fatua* Houtt.

Plants, since the time immemorial, have been used fundamentally in all civilizations as a source of medicine. Nowadays, medicinal plants have increasing application in the field of food, cosmetics and pharmaceutical products. *Myristica fragrans*, a renowned species of Myristicaceae family is consumed as a spice and has numerous pharmacological activities. Several phytochemicals showing great medicinal value have been reported from this plant and researches are on the periphery in the case of other Myristicaceae species. In the first part of the final chapter, we have focussed on the isolation, characterization and antidiabetic activity of phytochemicals present in the stem bark of *Myristica fatua* Houtt. var. *magnifica* (Bedd.) Sinclair.

6A.1. Myristicaceae

Myristicaceae (Nutmeg family) is a family of flowering plants native to Asia, America, Pacific islands and Africa. This family consists of more than 440 species comprised of 19 different genera [**Table 6A.1**]. The two important genera of this family are *Virola* and *Myristica*. Majority of the Myristicaceae members are large trees, some of which are sources of valuable timber. Plants belonging to this family (for example; *Myristica fragrans* and *Myristica malabarica*) are widely used as a spice and also in the traditional system of medicine.

Table 6A.1. Different genus of Myristicaeceae family

- *Bicuiba*
- *Brochoneura*
- *Cephalosphaera*
- *Coelocaryon*
- *Compsoneura*
- *Endocomia*
- *Gymnacranthera*
- *Haematodendron*
- *Horsfieldia*
- *Iryanthera*
- *Knema*
- *Mauloutchia*
- ***Myristica***
- *Osteophloeum*
- *Otoba*
- *Pycnanthus*
- *Scyphocephalium*
- *Staudtia*
- *Virola*

6A.2. *Myristica* Genus

Myristica, a flagship genus belonging to the family Myristicaceae found in different parts of the world. A few numbers of the species are found in India and their habitat varies from the sea level to an altitude as high as 2000 m in the Western Ghats and the Himalayas. The word '*Myristica*' is derived from the Greek word 'Myron', a sweet liquid distilled from plant. Some of the known *Myristica* species are listed in **Table 6A.2.**

Table 6A.2. *Myristica* species and their distribution

Sl. No	*Myristica* species	Distribution
1	*Myristica alba*	Maluku Islands of Indonesia
2	*Myristica ampliata*	Queensland &Australia
3	*Myristica andamanica*	India
4	*Myristica arfakensis*	West Papua (Indonesia)
5	*Myristica argentea*	New Guinea
6	*Myristica atrescens*	Papua New Guinea
7	*Myristica basilanica*	Philippines
8	*Myristica brachypoda*	Papua New Guinea
9	*Myristica brevistipes*	Papua New Guinea
10	*Myristica buchneriana*	New Guinea
11	*Myristica byssacea*	Papua New Guinea
12	*Myristica ceylanica*	Sri Lanka.
13	*Myristica cinnamomea*	Sumatra, Peninsular Malaysia, Singapore & Borneo
14	*Myristica coacta*	Papua New Guinea
15	*Myristica colinridsdalei*	Philippines
16	*Myristica conspersa*	West Papua (Indonesia)
17	*Myristica corticata*	Borneo
18	*Myristica crassa*	Peninsular Malaysia, Singapore & Borneo

19	*Myristica dactyloides*	Sri Lanka
20	*Myristica dasycarpa*	Papua New Guinea
21	*Myristica depressa*	Sumatra, Peninsular Malaysia & Borneo
22	*Myristica devogelii*	Sulawesi in Indonesia
23	*Myristica elliptica*	Sumatra, Peninsular Malaysia, Singapore & Borneo
24	*Myristica extensa*	Borneo
25	*Myristica fasciculate*	Papua New Guinea
26	*Myristica fatua*	India
27	*Myristica filipes*	Papua New Guinea
28	*Myristica fissurata*	Maluku, Indonesia
29	*Myristica flavovirens*	West Papua (Indonesia)
30	*Myristica fragrans*	China, Taiwan, Indonesia, Malaysia, Caribbean, India, Sri Lanka & America
31	*Myristica frugifera*	Philippines
32	*Myristica gigantea*	Sumatra, Peninsular Malaysia & Borneo
33	*Myristica gillespieana*	Fiji
34	*Myristica globosa*	Papua New Guinea, Solomon Islands & Australia
35	*Myristica grandifolia*	Fiji
36	*Myristica guadalcanalensis*	Solomon Islands
37	*Myristica guatteriifolia*	Indonesia, Malaysia, Myanmar, Philippines & Vietnam
38	*Myristica guillauminiana*	Fiji & Solomon Islands
39	*Myristica hollrungii*	Papua New Guinea

40	*Myristica inaequalis*	West Papua (Indonesia)
41	*Myristica incredibilis*	Papua New Guinea
42	*Myristica iners*	Singapore & Borneo
43	*Myristica inundata*	Papua New Guinea
44	*Myristica irya*	Burma, India, Malaysia, Papua New Guinea, Singapore, Solomon Islands, Sri Lanka, Thailand, & Vietnam
45	*Myristica kalkmanii*	New Guinea
46	*Myristica kjellbergii*	Sulawesi in Indonesia
47	*Myristica lasiocarpa*	Papua New Guinea
48	*Myristica leptophylla*	Papua New Guinea
49	*Myristica longipetiolata*	Philippines
50	*Myristica lowiana*	Sumatra, Singapore, Peninsular Malaysia & Borneo
51	*Myristica macrantha*	Fiji
52	*Myristica magnifica*	India
53	*Myristica maingayi*	Sumatra, Peninsular Malaysia & Singapore
54	*Myristica maxima*	Peninsular Malaysia, Singapore & Borneo
55	*Myristica mediterranea*	New Guinea
56	*Myristica millepunctata*	West Papua (Indonesia)
57	*Myristica nana*	Papua New Guinea
58	*Myristica olivacea*	Papua New Guinea
59	*Myristica ornata*	Papua New Guinea
60	*Myristica ovicarpa*	Papua New Guinea
61	*Myristica pachycarpidia*	Papua New Guinea
62	*Myristica papillatifolia*	New Guinea

63	*Myristica petiolata*	Solomon Islands
64	*Myristica perlaevis*	Maluku in Indonesia
65	*Myristica philippensis*	Philippines
66	*Myristica pilosella*	Papua New Guinea
67	*Myristica pilosigemma*	Philippines
68	*Myristica polyantha*	Papua New Guinea
69	*Myristica psilocarpa*	Manus Island & Papua New Guinea
70	*Myristica pubicarpa*	Maluku Islands in Indonesia
71	*Myristica pygmaea*	Papua New Guinea
72	*Myristica robusta*	Maluku Islands in Indonesia
73	*Myristica sangowoensis*	Maluku in Indonesia
74	*Myristica sarcantha*	West Papua (Indonesia)
75	*Myristica schlechteri*	Papua New Guinea
76	*Myristica simulans*	Papua New Guinea
77	*Myristica sinclairii*	Papua New Guinea
78	*Myristica sogeriensis*	Papua New Guinea
79	*Myristica succadanea*	Maluku Islands in Indonesia
80	*Myristica tamrauensis*	West Papua (Indonesia)
81	*Myristica teijsmannii*	Java in Indonesia
82	*Myristica trianthera*	Java in Indonesia
83	*M. ultrabasica*	Sulawesi in Indonesia
84	*M. verruculosa*	West Papua (Indonesia)
85	*M. xylocarpa*	Solomon Islands
86	*Myristica yunnanensis*	Southern Yunnan, China, Thailand & Vietnam

6A.3. *Myristica* species found in Kerala

Myristica fragrans Houtt., *Myristica malabarica* Lam., *Myristica beddomei* King ssp. *ustulata* and *Myristica fatua* Houtt. var. *magnifica* (Bedd.) Sinclair are the common plant species found in Kerala. *Myristica fragrans* and *Myristica malabarica* are commonly used as spices. Remaining are the wild relatives of nutmeg. *Myristica beddomei* is an endangered species distributed across Kerala.

6A.3.1. *Myristica fragrans* Houtt.

Myristica fragrans Houtt. is commonly known as "nutmeg", "Jathiphala", or "Jathikka". It is native to India, Indonesia, Sri Lanka, South Africa and Southeast Asia and produces two spices: mace and nutmeg. Numerous phytochemicals have been isolated from *Myristica fragrans* Houtt., which includes lignans, neolignans, diphenylalkanes, phenylpropanediols, steroids and cyclobutanones. Hattori *et al.* reported the isolation of fragransins A_2, B_1, B_2, B_3, C_1, C_2, C_{3a}, C_{3b}, nectandrin B, verrucosin, fragransol C, fragransol D, myristicanol A and myristicanol B from *Myristica fragrans* [Hattori *et al*, **1987**; Hattori *et al*., **1988**]. The neolignans; licarin A and B, myrifralignans A-E and myrislignan were isolated from *Myristica fragrans* [Aiba *et al.* **1977**; Giang *et al.* **2006**]. Recently from our institute, *erythro*-surinamensin, virolane, grandisin, and (7*S*,8*S*,7′*R*,8′*R*)-3,3′,4,4′,5,5′-hexamethoxy-7,7′,8,8′-lignan were reported from *Myristica fragrans* [Sajin *et al.* **2014**; Sajin *et al.* **2018**]. Nutmeg also exhibited various pharmacological activities such as analgesic, antifungal, and antimicrobial, anti-inflammatory, anticancer as well as hepatoprotective activities in various *in vitro* and *in vivo* studies [Kuete, **2017**]. Some of the phytochemicals present in *Myristica fragrans* are shown in **Figure 6A.1**.

6A.3.2. *Myristica malabarica* Lam.

Myristica malabarica Lam. is commonly recognized as "Malabar nutmeg", "Rampatri", Ponnampu' and "Kattujathi", a vulnerable species; native to India mainly found in Western Ghats of South India. The seed and its aril are used as a spice in Indian foods because they enhance the taste and aromatic flavour of the food. Major pharmacological activities credited with *Myristica malabarica* are anti-carcinogenic [Patro *et al*., **2010**], antipromastigote activity [Sen *et al*., **2007**], antiulcer [Maity *et al*., **2008**], anti-inflammatory [Maity *et al*., **2012**] activities and it is found as a constituent in many ayurvedic preparations such as Pasupasi. Previous phytochemical investigations of the fruit rind of *Myristica malabarica* Lam. revealed the presence of four diaryl

nonanoids named as malabaricones A-D [Purushothaman *et al*., **1977**] and an aryl tetradecanoid [Bauri *et al*., **2016**]. In addition, a lignan malabaricanol A and an isoflavone, biochanin have been isolated from *Myristica malabarica* [Purushothaman *et al*., **1974**; Talukdar *et al*., **2000**]. The phytochemicals isolated from *Myristica malabarica* are shown in **Figure 6A.2**.

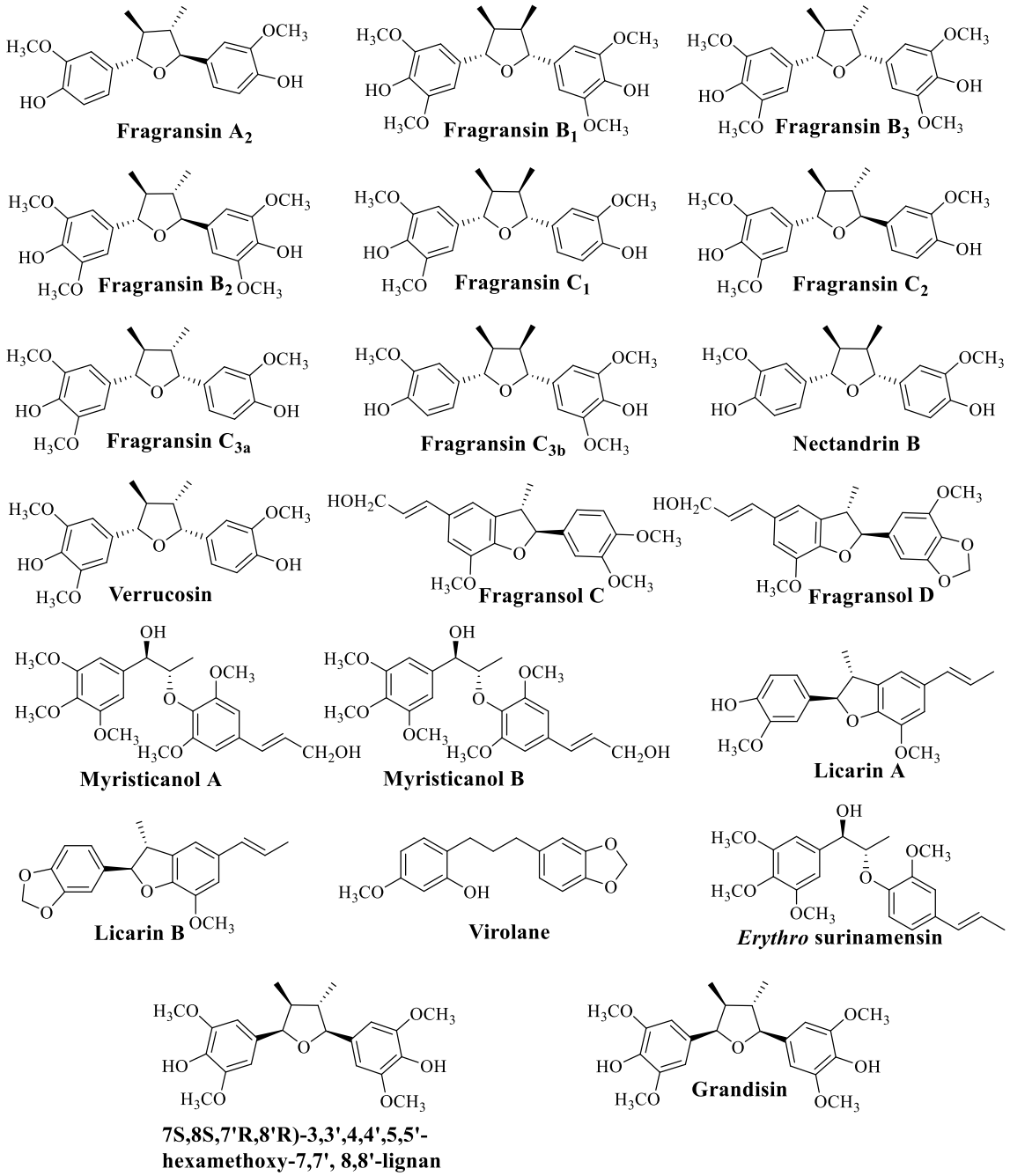

Figure 6A.1. Phytochemicals isolated from *Myristica fragrans*

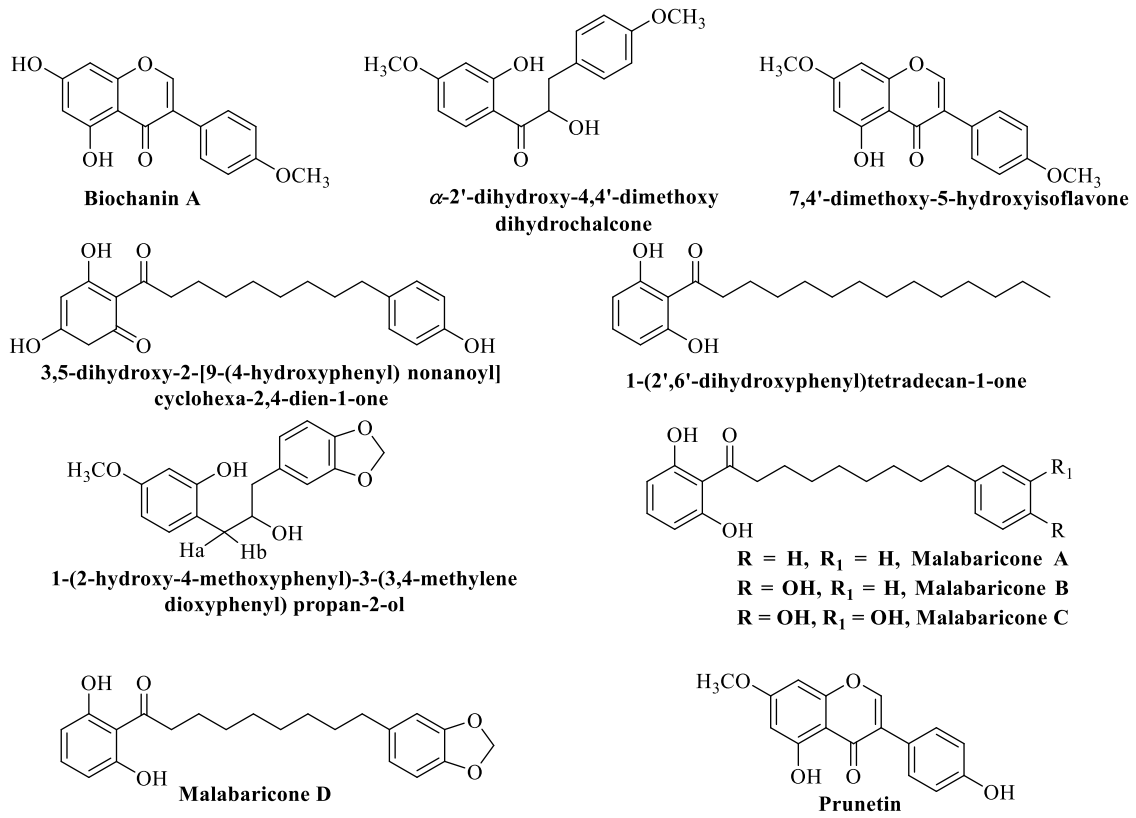

Figure 6A.2. Phytochemicals isolated from *Myristica malabarica*

6A.4. Aim and scope of the present investigation

Myristica fatua Houtt. var. *magnifica* (Bedd.) Sinclair (**Figure 6A.3**) is a wild relative of nutmeg (*Myristica fragrans*), mainly found in evergreen forests of Western Ghats of Kerala. It belongs to Myristicaceae family and the flagship genus *Myristica*. The taxonomic classification of *Myristica fatua* is shown in **Table 6A.3**. It is commonly recognized as "Long Nutmeg", "Wild Nutmeg" or "Mountain Nutmeg" and locally known as "Kottapannu", "Churapayin", "Kotthapanu" and "Kothapayin". It exhibits anti-mycobacterial [Billoa *et al*., **2005]**, anti-bacterial [Viveka *et al*., **2016**], anti-parasitic [Desrivot *et al*., **2007**], cytotoxic [Pandey *et al*., **2016**; Fajriah *et al*., **2017**] and antioxidant activities [Viveka *et al*., **2016**]. In 2016, Kumar *et al*. reported the antiproliferative activity of *Myristica fatua* extract and identified 16 compounds from the different fruit parts of *Myristica fatua* using efficient and sensitive LC–MS/MS methods [Pandey *et al*., **2016**]. Fajriah *et al.* isolated novel cytotoxic lignan and diaryl nonanoid derivatives from the leaves of *Myristica fatua* [Fajriah *et al*., **2017**]. Recently, the same group also reported malabaricone B and malabaricone C from the stem bark of *Myristica fatua* [Megawati *et al*., **2017**]. The previously isolated compounds from *Myristica fatua* are shown in **Figure 6A.4**. Apart from these, there are no reports on the phytochemical

and pharmacological evaluation of *Myristica fatua*. Therefore, it performed suitable and relevant to carry out the phytochemical and pharmacological investigation of *Myristica fatua*. So as part of this Ph.D. program, a detailed investigation of *Myristica fatua* stem bark and seed has been undertaken. In the first part of final chapter, the dichloromethane (DCM) extract of *Myristica fatua* was subjected to column chromatographic purification, which led to the isolation of seven compounds. It included a novel compound [3-tridecanoylbenzoic acid (**43**)] with no previous reports from any natural sources and six known acyl phenols [(1-(2-hydroxy-6-methoxyphenyl)tetradecan-1-one (**44**), 1-(2,6-dihydroxyphenyl) tetradecan-1-one (**45**), malabaricone A (**46**), 1-(2-hydroxy-6-methoxyphenyl)-9-(4-hydroxyphenyl)nonan-1-one (**47**), malabaricone B (**48**) and malabaricone C (**49**)], of which four of them (compound **44**, **45**, **46**, and **47**) are isolated for the first time from the stem bark of *Myristica fatua*. All the compounds were tested for their *in vitro* and *in silico* inhibitory activities on carbohydrate hydrolysing enzymes and delaying of AGEs formation. Based on these results, we have also evaluated whether these compounds enhance the 2-NBDG uptake in L6 myotubes.

Figure 6A.3. *Myristica fatua* Houtt. var. *magnifica* (Bedd.) Sinclair

Table 6A.3. Scientific classification of *Myristica fatua*

Kingdom	Plantae
Order	Magnoliales
Family	Myristicaceae
Genus	*Myristica*
Species	*M. fatua*
Binomial name	*Myristica fatua* Houtt. var. *magnifica* (Bedd.) Sinclair

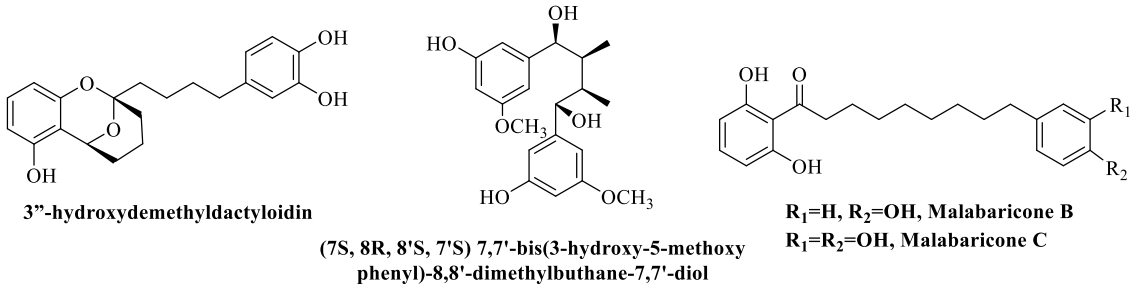

Figure 6A.4. Compounds previously isolated from *Myristica fatua* Houtt.

6A.5. Isolation and characterization of compounds from *Myristica fatua* stem bark

6A.5.1. Plant material

Stem bark of *Myristica fatua* Houtt. var. *magnifica* (Bedd.) Sinclair was collected from Agasthyamalai biosphere reserve of south Western Ghats region of Kollam District, Kerala, India in December 2016. The plant material was authenticated by plant taxonomist of Jawaharlal Nehru Tropical Botanic Garden and Research Institute, Palode, Kerala, India and a voucher specimen (**TBGT 83441**) is deposited in the Herbarium of repository of Jawaharlal Nehru Tropical Botanic Garden and Research Institute, Palode, Kerala, India.

6A.5.2. Isolation and characterization of secondary metabolites

850 g of the dried and grounded stem bark of *Myristica fatua* was extracted with dichloromethane; yielded 25 g of dichloromethane extract; this was subjected to silica gel (100-200 mesh) column chromatography using *n*-hexane, *n*-hexane-EtOAc gradient and EtOAc. Twelve fractions of 200 mL each were collected and concentrated at 50 ^{o}C under reduced pressure.

Fraction pool 3 was subjected to column chromatographic purification using EtOAc/*n*-hexane as eluent which gave compound **43** (80 mg) as a pale yellow amorphous solid. Compound **1** displayed a molecular ion peak at m/z 317.21184 for $[M-H]^+$ in the HRESIMS (Calculated for $C_{20}H_{29}O_3$: 317.2117); this result together with the ^{13}C NMR data, allowed the assignment of the molecular formula $C_{20}H_{30}O_3$ to compound **43**. The IR spectrum showed absorptions for carbonyls at 1744, 1658 and 1621 cm^{-1}, aromatic at 1598 and 1461 cm^{-1}, methylenes at 2925 and 2854 cm^{-1}. The ^{1}H NMR spectrum showed a broad singlet [δ_H 12.57 ppm] for carboxylic acid proton, a 1, 3-disubstituted aromatic moiety [δ_H 7.48 (t, J = 8 Hz, 1H), 6.85 (d, J = 8.5 Hz, 1H), 6.76 (d, J = 8 Hz, 1H) and,

6.10 (s, 1H) ppm], a methylene group neighbouring the carbonyl group [δ_H 2.60 (t, J = 7.5 Hz, 2H) ppm], a $C_{11}H_{23}$ alkyl residue [δ_H 1.74-1.69 (m, 2H), 1.41-1.26 (m, 18H) and 0.88 (t, J = 7 Hz, 3H) ppm]. Its ^{13}C NMR (125 MHz, $CDCl_3$) spectrum showed resonances for a carbonyl carbon [δ_C 183.6 ppm], a carboxylic acid carbon [δ_C 171.3 ppm], aromatic carbons [δ_C 160.8-106.8 ppm], a methylene carbons [δ_C 34.3-22.7 ppm] and methyl group [δ_C 14.1 ppm]. Based on ^1H, ^{13}C, HOMOCOSY, HMQC, DEPT 135 and HRESIMS data (**Figure 6A.5-11)** the structure of the compound **43** was confirmed to be 3-tridecanoylbenzoic acid and the structure is shown below. Compound **43** was a novel compound with no previous report from any natural resources.

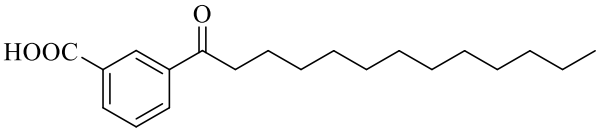

3-tridecanoylbenzoic acid (43)

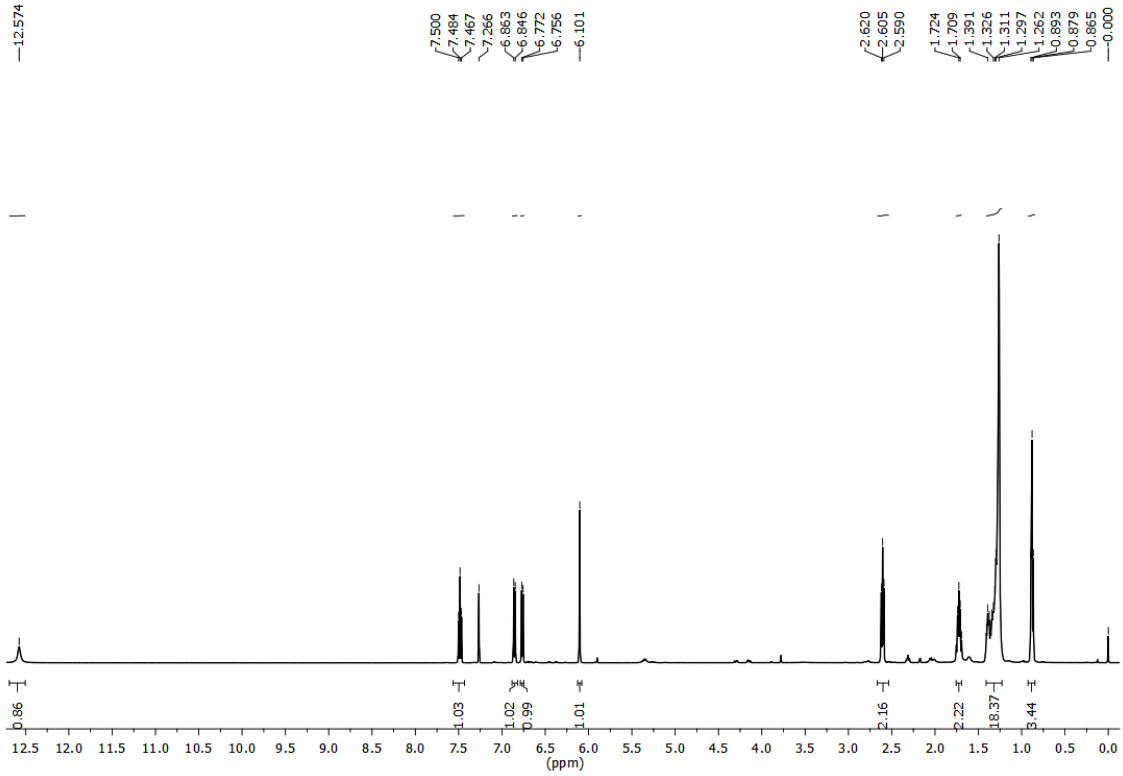

Figure 6A.5. ^1H NMR spectrum (500 MHz, $CDCl_3$) of 3-tridecanoylbenzoic acid (**43**)

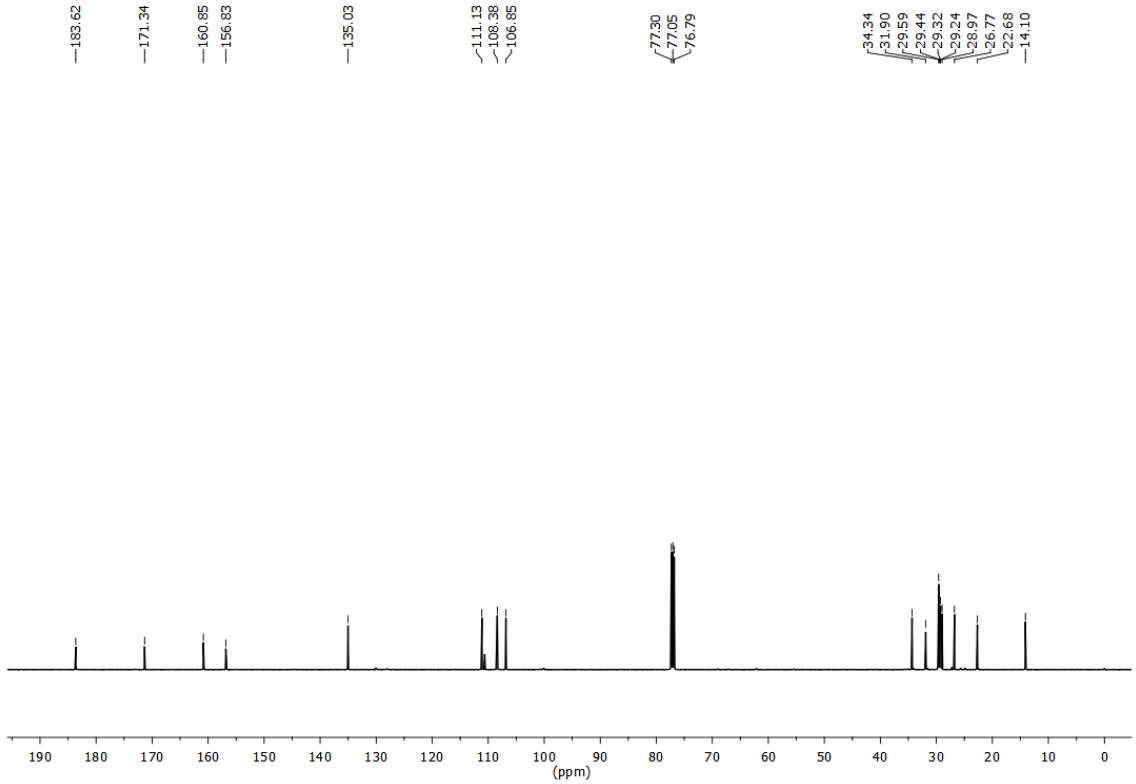

Figure 6A.6. ^{13}C NMR spectrum (125 MHz, $CDCl_3$) of 3-tridecanoylbenzoic acid (**43**)

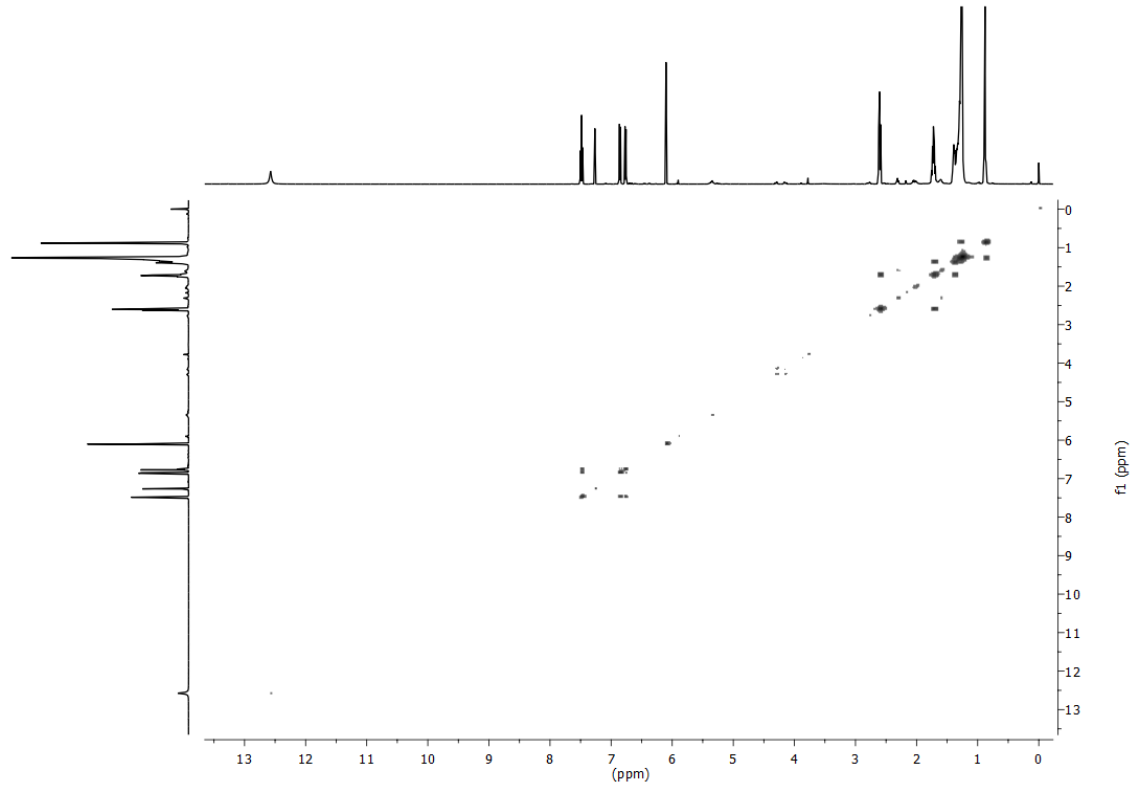

Figure 6A.7. ^{1}H- ^{1}H COSY spectrum (500 MHz, $CDCl_3$) of 3-tridecanoylbenzoic acid (**43**)

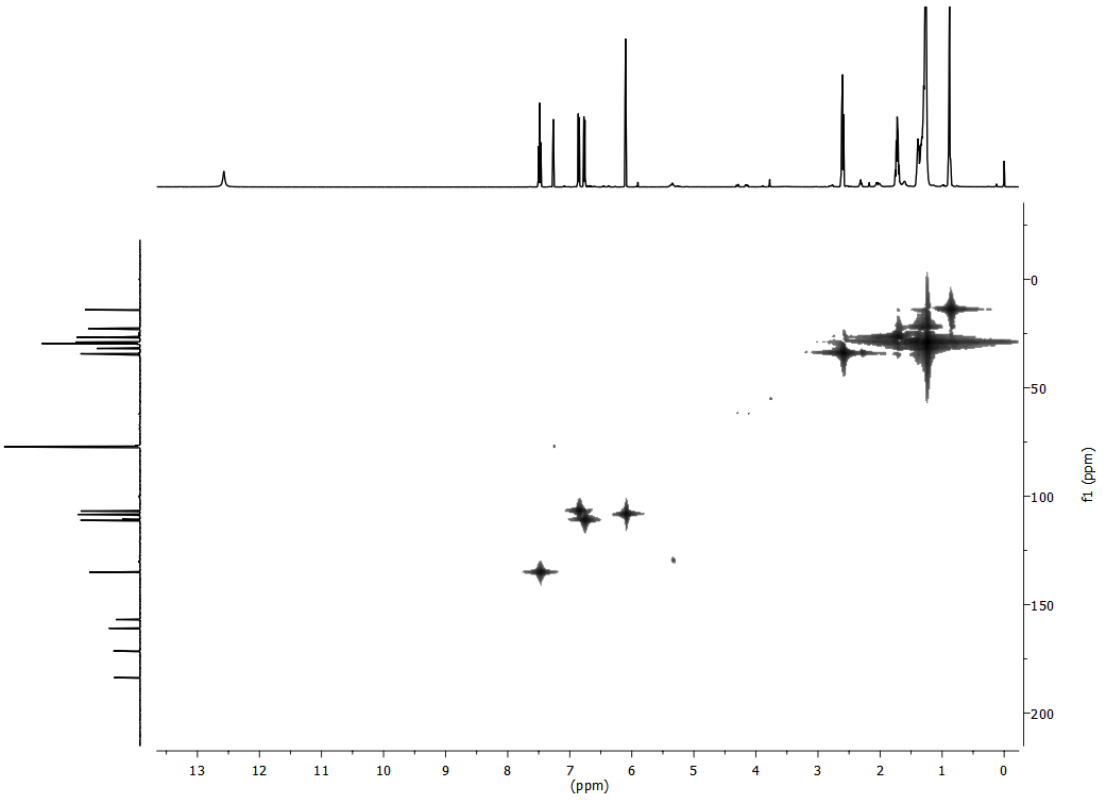

Figure 6A.8. HMQC spectrum (125 MHz, $CDCl_3$) of 3-tridecanoylbenzoic acid (**43**)

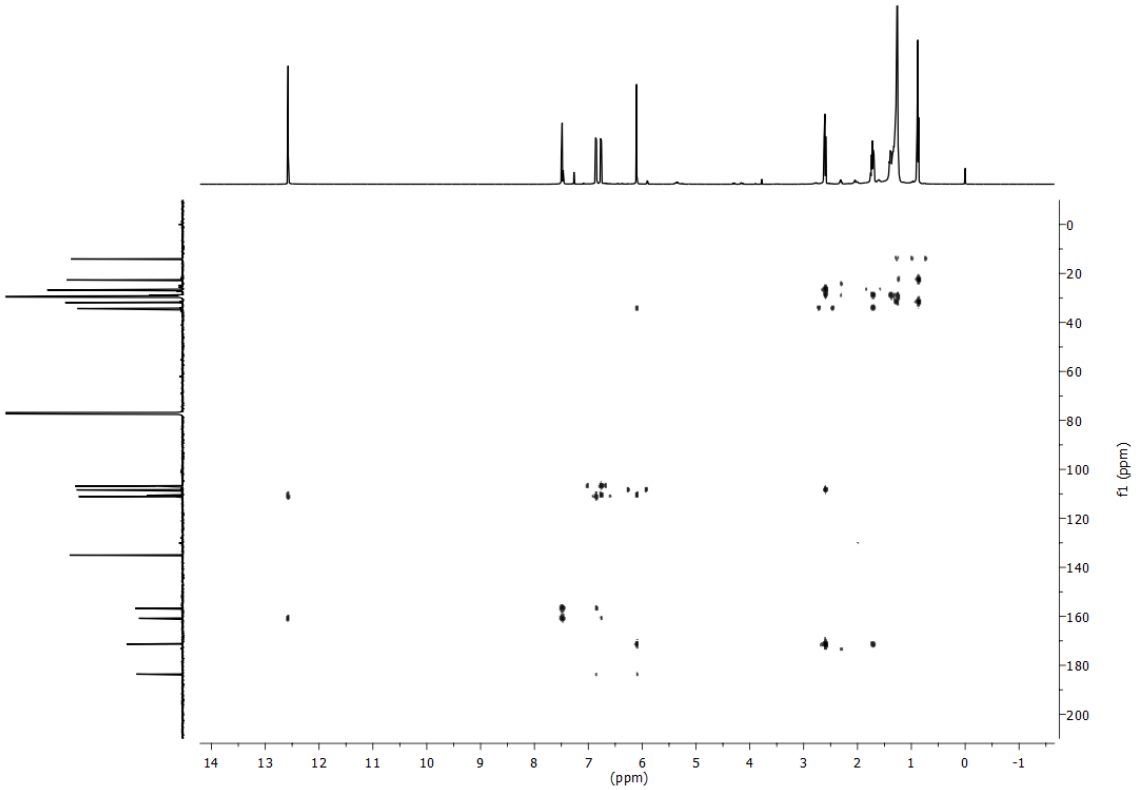

Figure 6A.9. HMBC spectrum (125 MHz, $CDCl_3$) of 3-tridecanoylbenzoic acid (**43**)

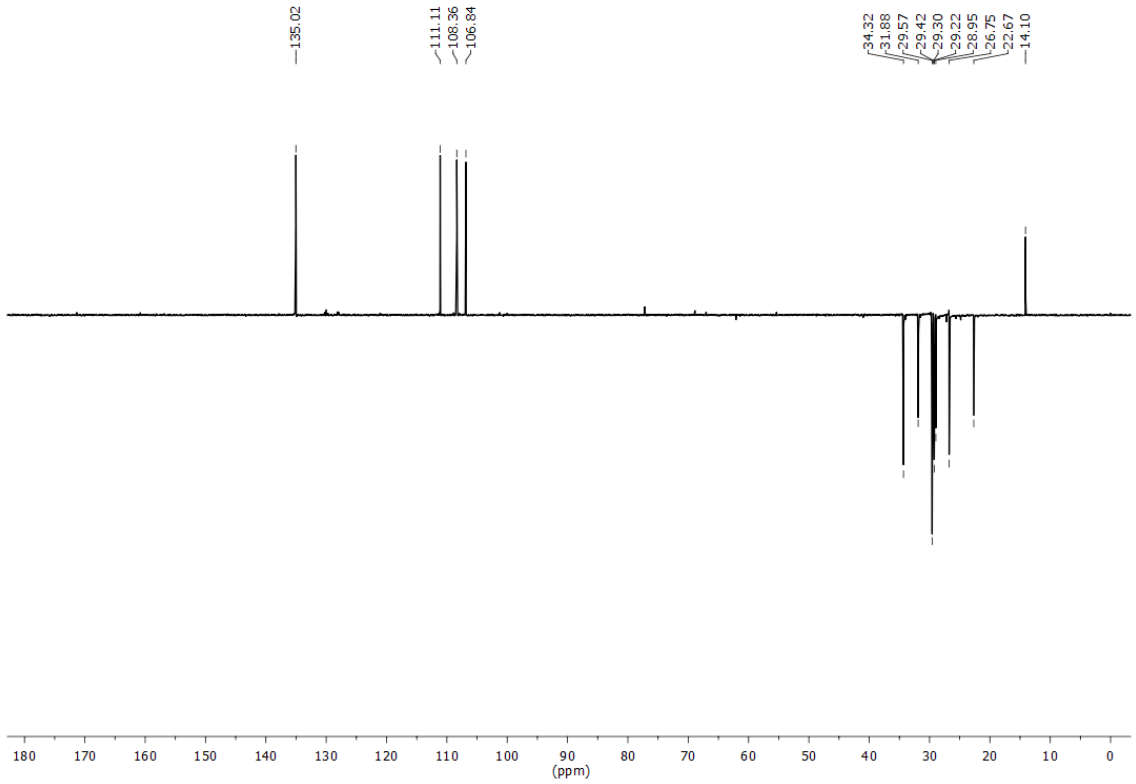

Figure 6A.10. DEPT 135 spectrum (125 MHz, $CDCl_3$) of 3-tridecanoylbenzoic acid (**43**)

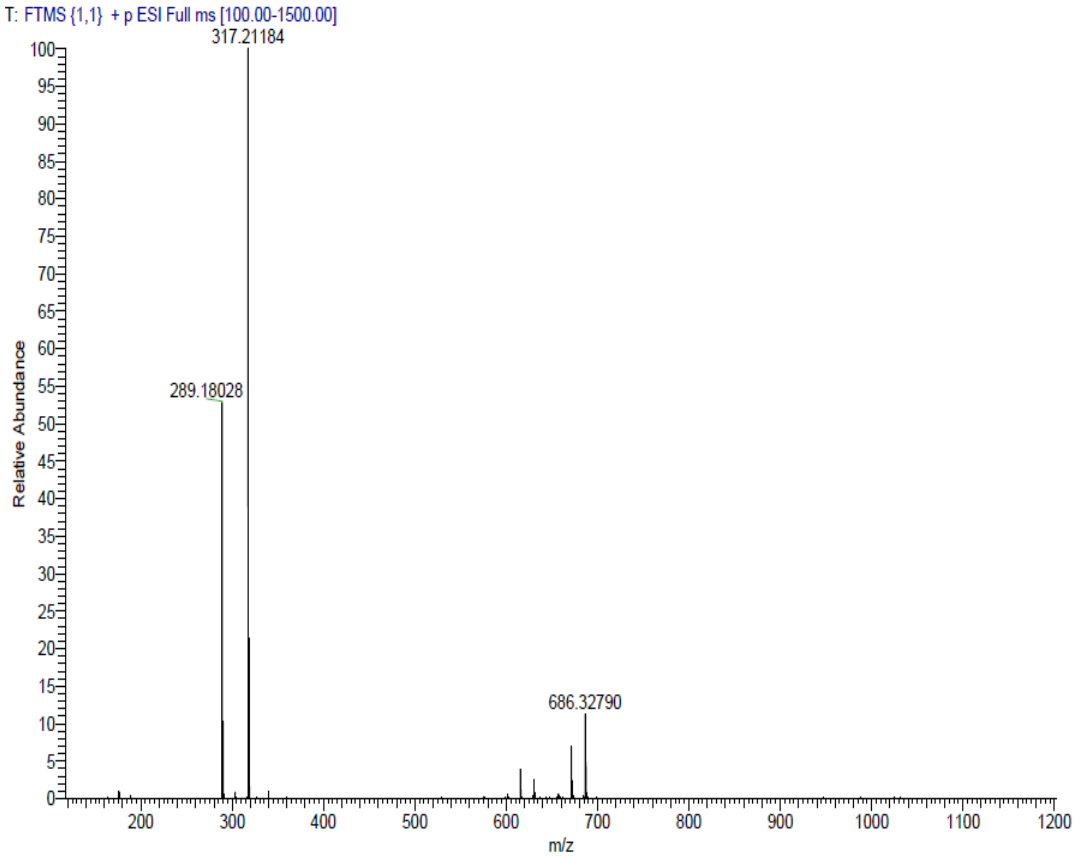

Figure 6A.11. HRESIMS spectrum of 3-tridecanoylbenzoic acid (**43**)

Fraction pool 2 on column chromatographic separation using 2 % EtOAc/*n*-hexane as eluent to give two compounds. The compounds **44** (108 mg) and **45** (300 mg) were obtained as pale yellow amorphous solids. The FTIR and NMR spectra (**Figure 6A. 12-13)** of compound **44** displayed the presence of a conjugated carbonyl group [υ_{max} 1620 cm^{-1} and δ_C 208.0 ppm], a single hydrogen bonded phenolic hydroxyl group [δ_H 13.28 (s, 1H) ppm] , a 1,2,3- trisubstituted benzene ring [δ_H 7.32 (t, J = 8.5 Hz, 1H) ppm, 6.57 (dd, J_1 = 8 Hz, J_2 = 1 Hz, 1H), 6.39 (dd, J_1 = 8.5 Hz , J_2 = 1 Hz) ppm], a methoxy group [δ_H 3.89 (s, 3H) and δ_C 55.6 ppm], an extended polymethylene side chain with one methylene group flanking the carbonyl group [δ_H 3.04 (t, J = 7.5 Hz, 2H) ppm and δ_C 45.20 ppm] and a $C_{12}H_{28}$ alkyl residue [δ_H 1.67 (m, 2H), 1.20 (m, 20H) ppm] and the methyl group [δ_H 0.88 (t, J = 6.5 Hz, 3H) and δ_C 14.1 ppm]. Hence it was assumed that compound **44** had the structure 1-(2-methoxy-6-hydroxyphenyl)tetradecan-l-one and the structure is shown below. Additional support for this structure was obtained from the HRESIMS [$(M+H)^+$:335.2593; calculated for $C_{21}H_{35}O_3$:335.2586] and in comparison with literature reports [Pham *et al*., **2000**].

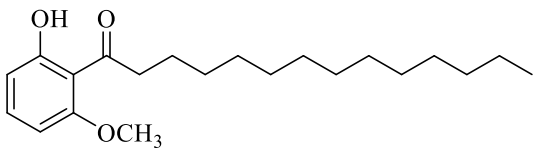

1-(2-methoxy-6-hydroxyphenyl)tetradecan-l-one (44)

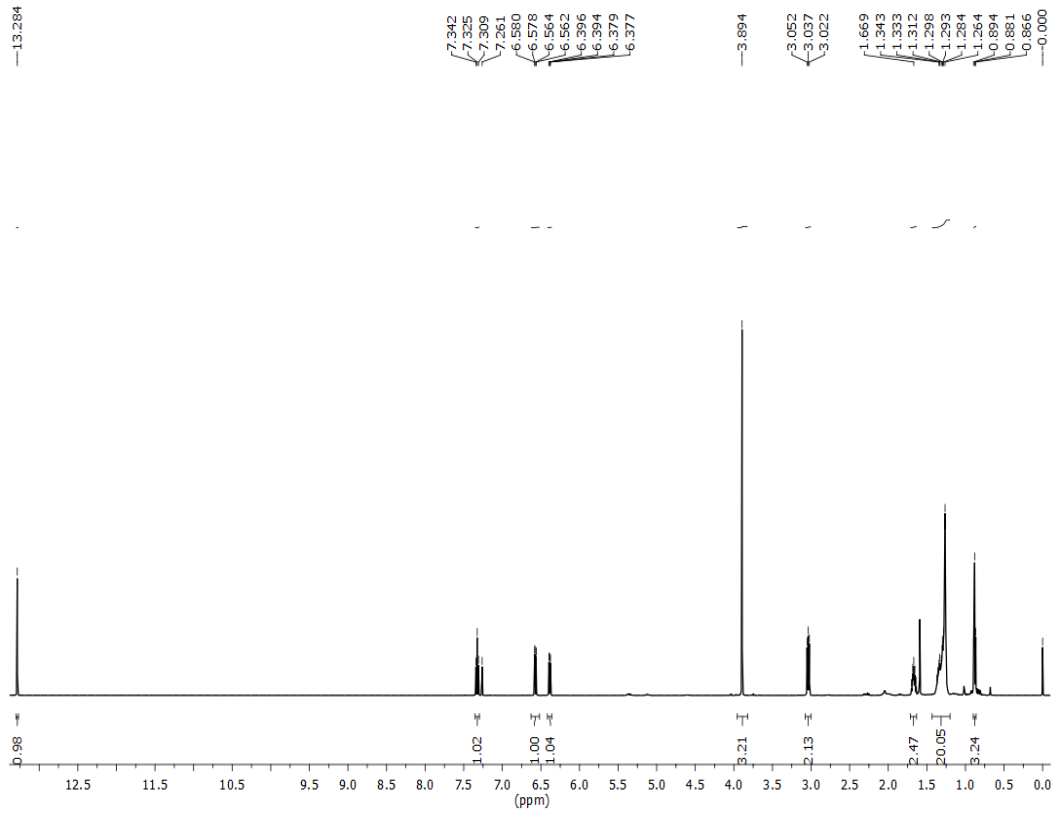

Figure 6A.12. ^{1}H NMR spectrum (500 MHz, $CDCl_3$) of 1-(2-methoxy-6-hydroxyphenyl)tetradecan-l-one (**44**)

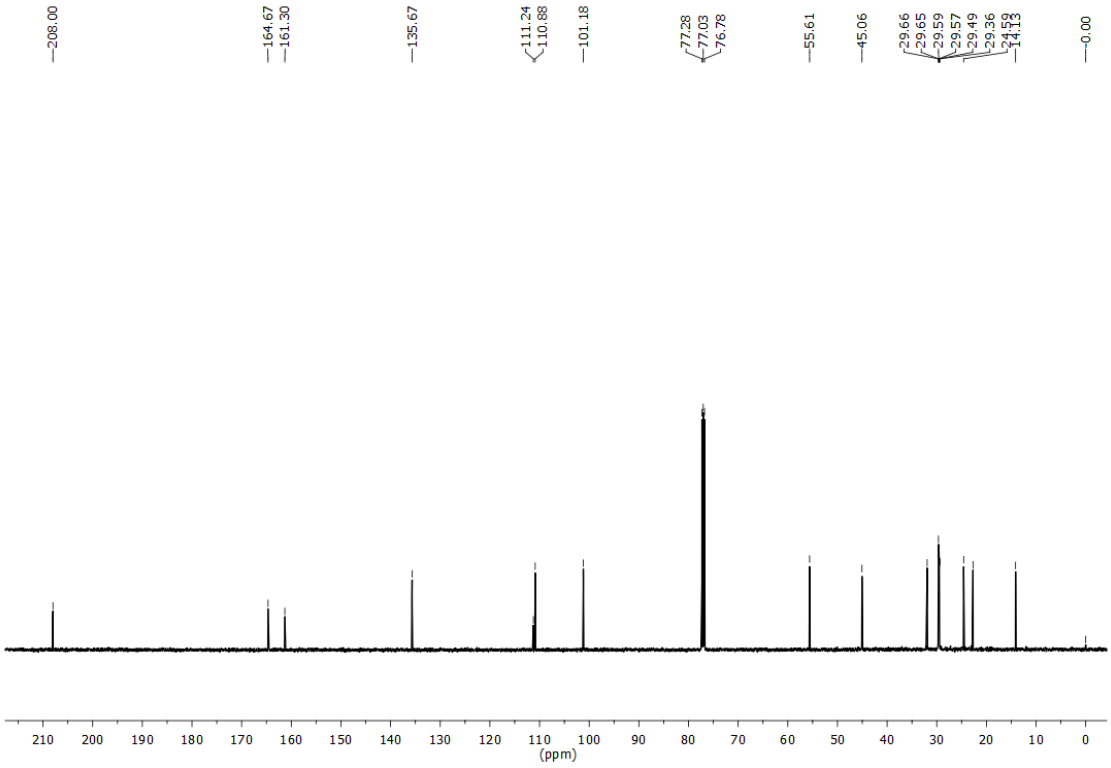

Figure 6A.13. ^{13}C NMR spectrum (125 MHz, $CDCl_3$) of 1-(2-methoxy-6-hydroxyphenyl)tetradecan-l-one (**44**)

The FTIR and NMR spectra (**Figure 6A.14-15)** of compound **45** displayed the presence of a conjugated carbonyl group [υ_{mix} 1620 cm^{-1} and δ_C 208.5 ppm], a single hydrogen bonded phenolic hydroxyl group [δ_H 9.98 (brs, 2H) ppm] , a 1, 2, 3-trisubstituted benzene ring [δ_H 7.22 (t, J = 8 Hz, 1H) ppm, 6.41 (d, J = 8.5 Hz, 1H) ppm], an extended polymethylene side chain with one methylene group flanking to the carbonyl group [δ_H 3.14 (t, J = 7.5 Hz, 2H) ppm and δ_C 44.9 ppm] and a $C_{12}H_{28}$ alkyl residue [δ_H 1.74-1.68 (m, 2H) ppm, 1.37 - 1.29 (m, 20H) ppm] and the methyl group [δ_H 0.88 (t, J = 7 Hz, 3H) ppm and δ_C 14.1 ppm]. From detailed NMR, HRESIMS [$(M+H)^+$: 321.2430; Calculated for $C_{20}H_{33}O_3$: 321.2430] and in comparison with literature reports [Pham *et al.*, **2000**] compound **45** had the structure 1-(2,6-dihydroxyphenyl) tetradecan-1-one and the structure is shown below.

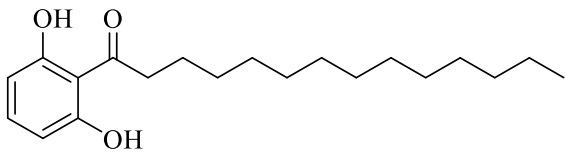

1-(2, 6-dihydroxyphenyl) tetradecan-1-one (45)

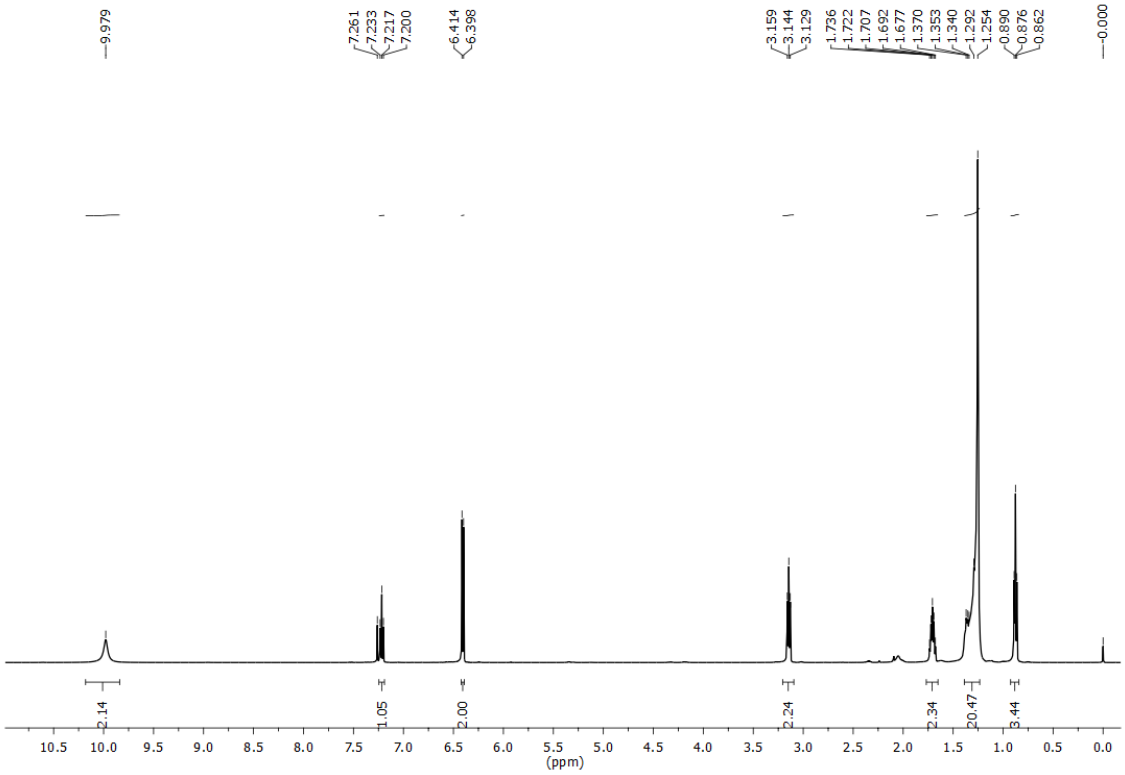

Figure 6A.14. ^1H NMR spectrum (500 MHz, $CDCl_3$) of 1-(2, 6-dihydroxyphenyl) tetradecan-1-one (**45**)

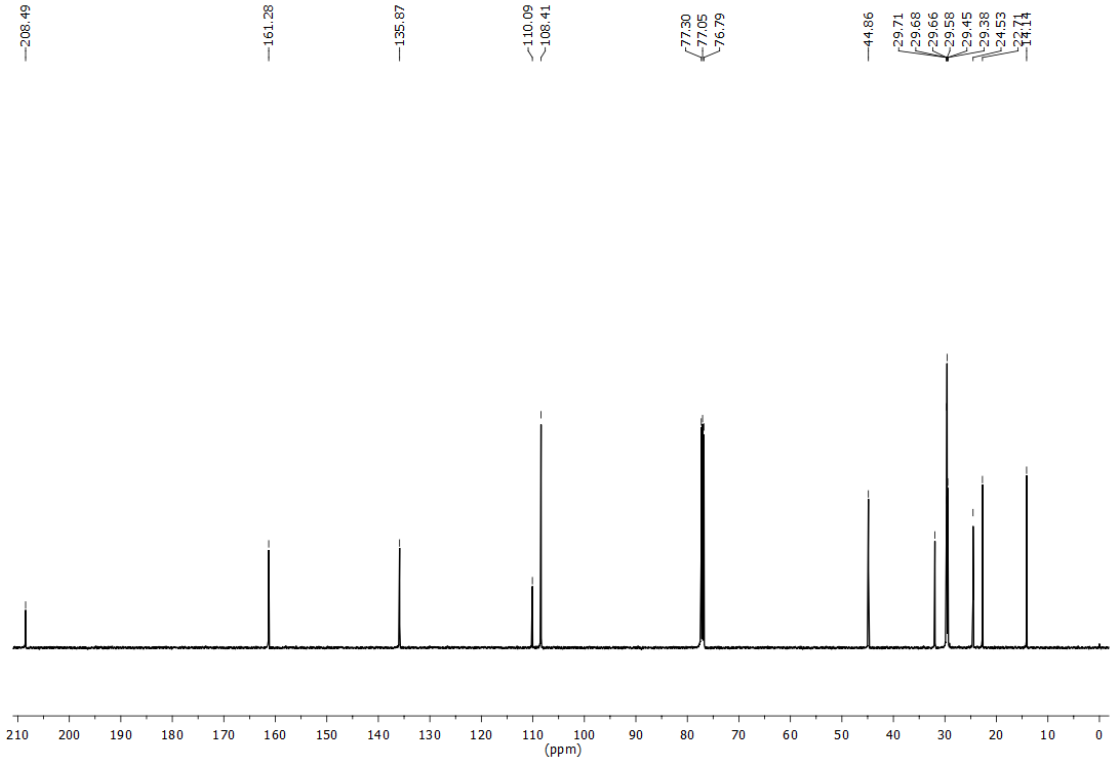

Figure 6A.15. ^{13}C NMR spectrum (125 MHz, $CDCl_3$) of 1-(2, 6-dihydroxyphenyl) tetradecan-1-one (**45**)

Similarly, silica gel column chromatographic separation of fraction pool 4 yielded compound **46** (40 mg) as a pale yellow solid. The FTIR and NMR spectra (**Figure 6A.16-17)** of compound **46** displayed the presence of a conjugated carbonyl group [υ_{max} 1620 cm^{-1} and δ_C 208.7 ppm], hydrogen bonded phenolic hydroxyl groups [δ_H 9.67 (brs, 2H) ppm], eight methylene groups with one flanking the carbonyl group [δ_H 3.11 (t, J = 7.5 Hz, 2H) ppm, δ_C 44.8 ppm], and one benzylic methylene group [δ_H 2.59 (t, J = 7.5 Hz, 2H) ppm, δ_C 36.0 ppm]. The presence of two benzene rings, one of which was a 1, 2, 3-trisubstituted benzene ring [δ_H 7.21 (t, J = 8 Hz, 1H) ppm, 6.38 (d, J = 8 Hz, 2H) ppm] and the second benzene ring was deduced to be 1-alkyl substituted [δ_H 7.28 (t, J = 8 Hz, 1H) ppm, 7.18 (d, J = 8 Hz, 2H) ppm, 7.16 (t, J = 8 Hz, 1H) ppm]. From detailed NMR and HRESIMS analysis [$(M+H)^+$:327.19595; Calculated for $C_{21}H_{27}O_3$: 327.1960] and in comparison with literature reports [Pham *et al.*, **2000**] compound **46** had the structure malabaricone A and the structure is shown below.

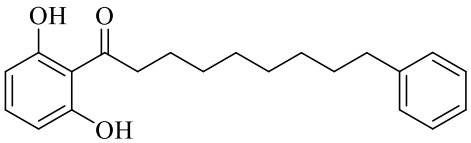

Malabaricone A (46)

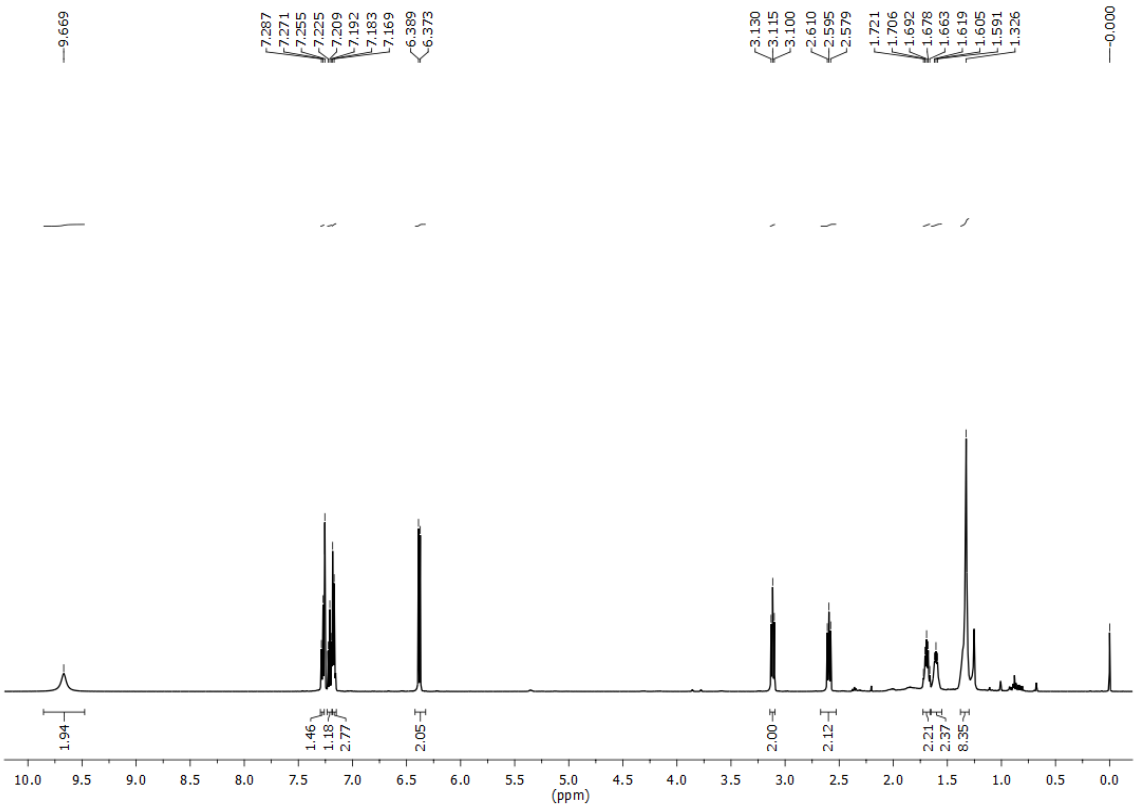

Figure 6A.16. ^{1}H NMR spectrum (500 MHz, $CDCl_3$) of malabaricone A (**46)**

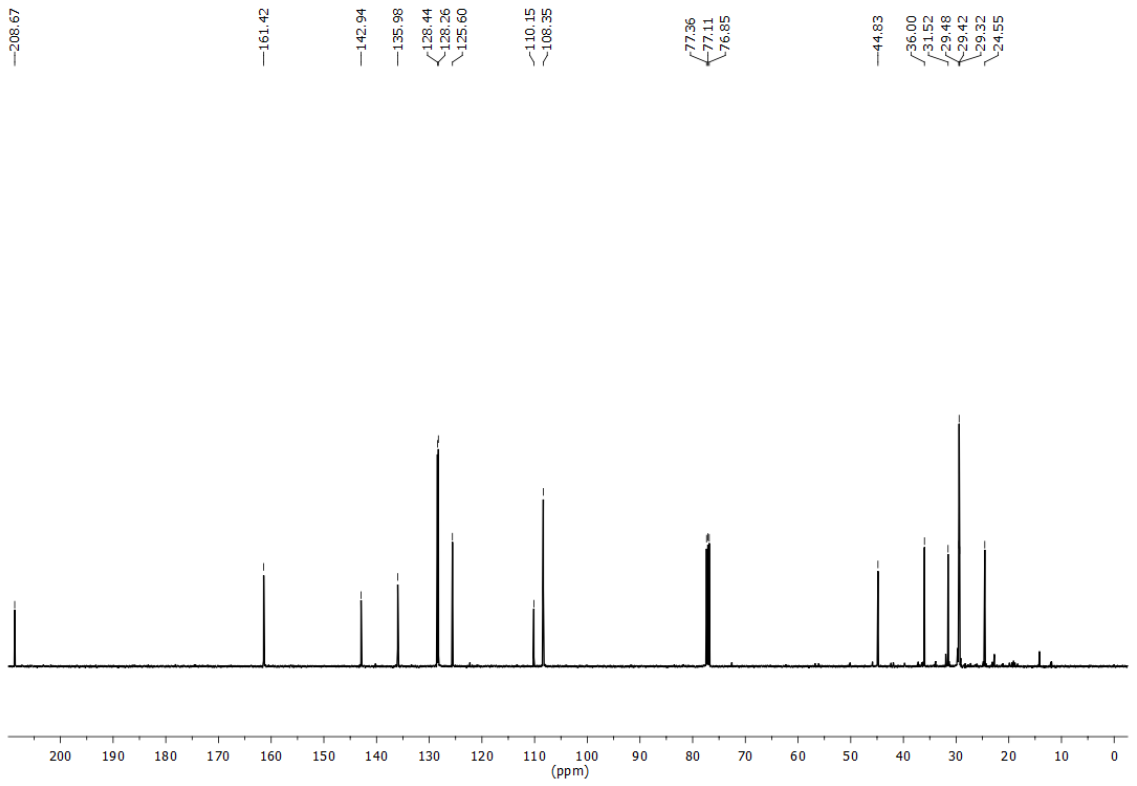

Figure 6A.17. ^{13}C NMR spectrum (125 MHz, $CDCl_3$) of malabaricone A (**46)**

Silica gel column chromatographic separation (100-200 mesh) of fraction pool 10 yielded compound **47** (25 mg) as a pale yellow amorphous solid. The FTIR and NMR spectra (**Figure 6A. 18-19)** of compound **5** showed the presence of a conjugated carbonyl group [υ_{maix} 1620 cm^{-1} and δ_C 208.1 ppm], a single hydrogen bonded phenolic hydroxyl group [δ_H 13.33 (brs, 1H) ppm], methoxy group [δ_H 3.69 (s, 3H) ppm], eight methylene groups with one flanking the carbonyl group [δ_H 3.03 (t, J = 7 Hz) ppm, δ_C 45.0 ppm], and one benzylic methylene group [δ_H 2.52 (t, J = 7.5 Hz) ppm, δ_C 35.0 ppm]. The presence of two benzene rings, one of which was a 1, 2, 3- trisubstituted benzene ring [δ_H 7.32 (t, J = 8 Hz, 1H), 6.57 (d, J = 8.5 Hz, 1H) and 6.38 (d, J = 8.5 Hz, 2H) ppm] and the second benzene ring [δ_H 7.02 (d, J = 8 Hz, 2H) and 6.74 (d, J = 7 Hz, 2H ppm)]. From detailed NMR and HRESIMS analysis [$(M+Na)^+$: 379.18603; calculated for $C_{22}H_{28}O_4Na$: 379.1885] and in comparison with literature reports [Pham *et al*., **2000**] compound **47** had the structure 1-(2-hydroxy-6-methoxyphenyl)-9-(4-hydroxy phenyl)nonan-one (**47**) and the structure is shown below.

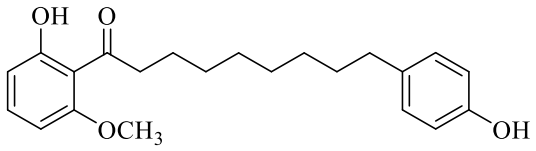

1-(2-hydroxy-6-methoxyphenyl)-9-(4-hydroxy phenyl)nonan-one (47)

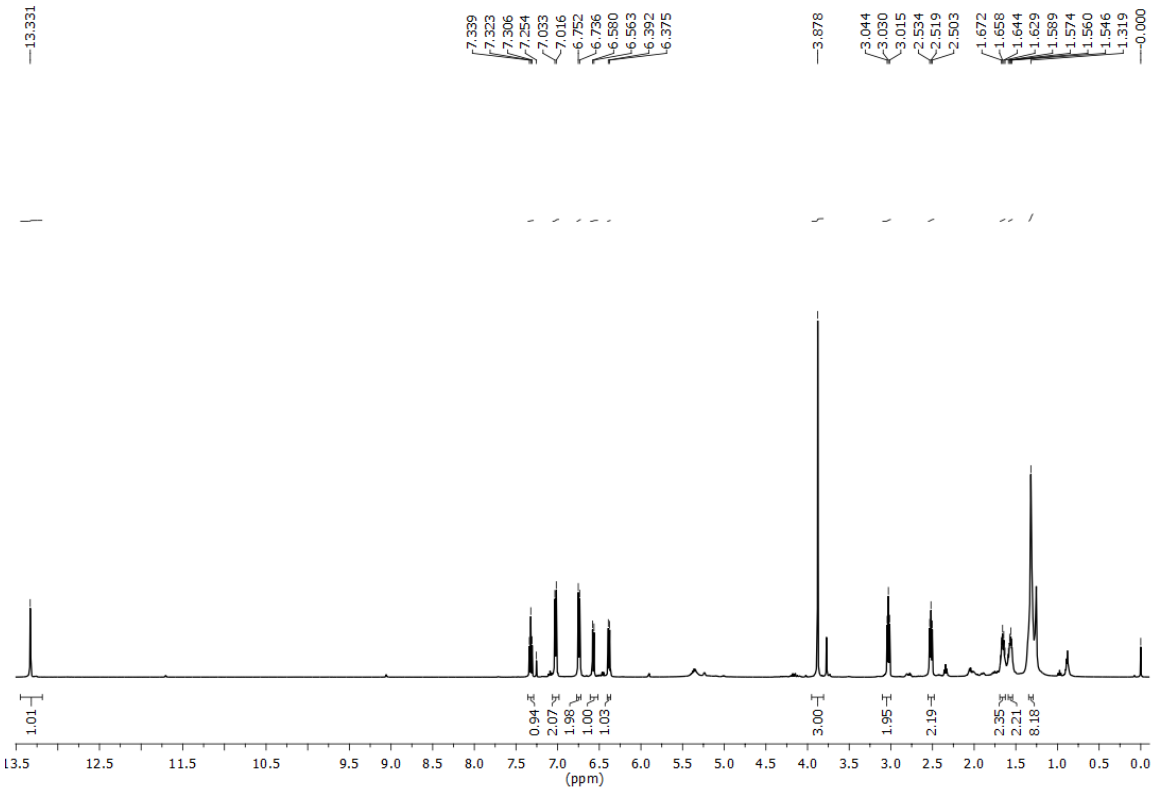

Figure 6A.18. ^{1}H NMR spectrum (500 MHz, $CDCl_3$) of 1-(2-hydroxy-6-methoxyphenyl)-9-(4-hydroxy phenyl)nonan-one (**47**)

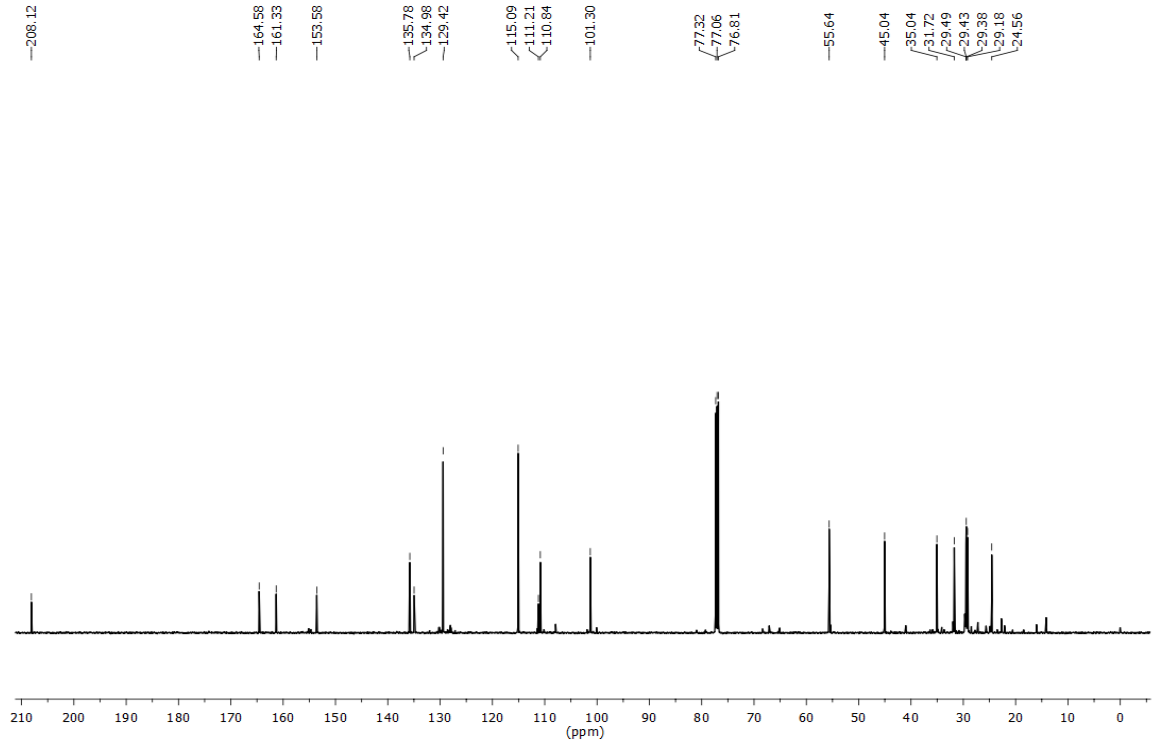

Figure 6A.19. ^{13}C NMR spectrum (125 MHz, $CDCl_3$) of 1-(2-hydroxy-6-methoxyphenyl)-9-(4-hydroxy phenyl)nonan-1-one (**47**)

Similarly, silica gel column chromatographic purification of fraction pool 13 yielded compound **48** (8 mg) as a pale yellow amorphous solid. The FTIR and NMR spectra (**Figure 6A.20-21)** of compound **6** displayed the presence of a conjugated carbonyl group [υ_{mix} 1620 cm^{-1} and δ_C 207.9 ppm], hydrogen bonded phenolic hydroxyl groups [δ_H 9.55(brs, 2H) ppm], eight methylene groups with one flanking the carbonyl group [δ_H 3.10 (t, J = 7.5, 2H) ppm, δ_C 44.8 ppm], and one benzylic methylene group [δ_H 2.52 (t, J = 7.5 Hz, 2H) ppm, δ_C 35.0 ppm]. The presence of two benzene rings, one of which was a 1,2,3- trisubstituted benzene ring [δ_H 7.21(t, J = 8 Hz, 1H) ppm, 6.38 (d, J = 8 Hz, 2H) ppm] and the second benzene ring was [δ_H 7.04 (d, J = 8 Hz, 2H) ppm, 6.75 (d, J = 8.5 Hz, 2H) ppm] From detailed NMR and HRESIMS analysis [$(M+H)^+$: 343.1909; calculated for $C_{21}H_{27}O_4$: 343.19141] and by comparing with literature reports [Pham *et al*., **2000**] the structure of compound **48** was assigned as malabaricone B and the structure is shown below.

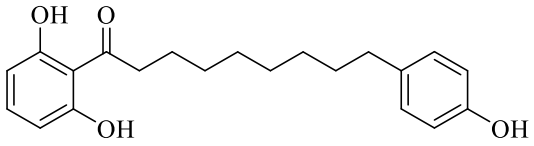

Malabaricone B (48)

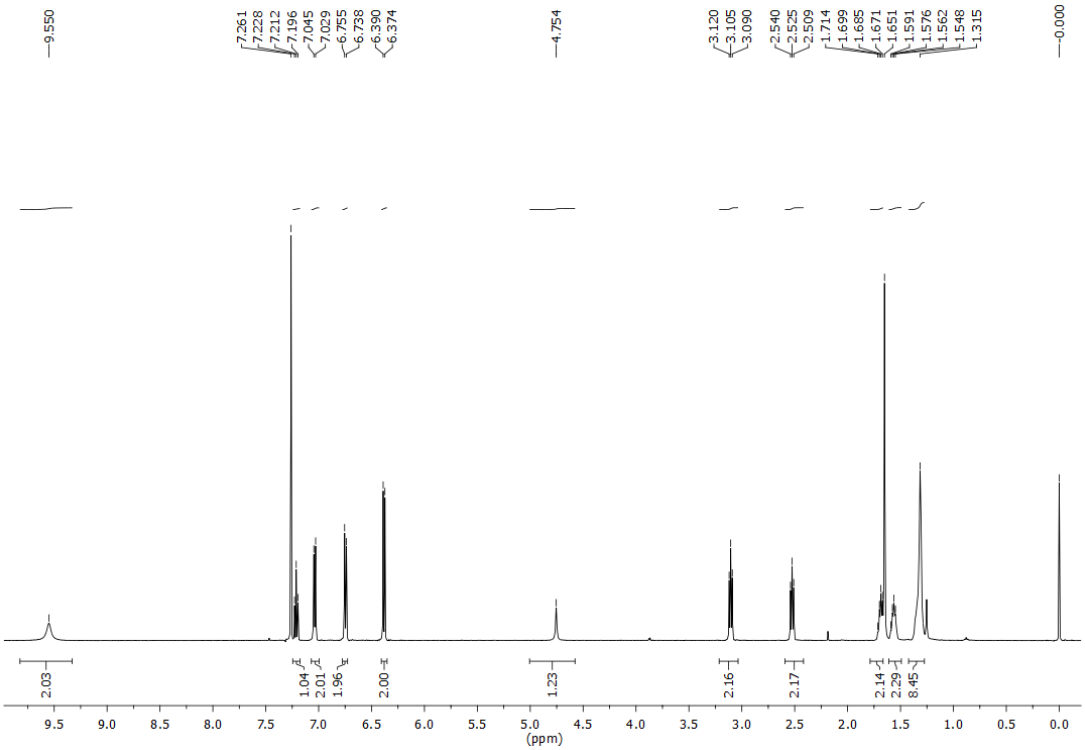

Figure 6A.20. ^1H NMR spectrum (500 MHz, $CDCl_3$) of malabaricone B (**48)**

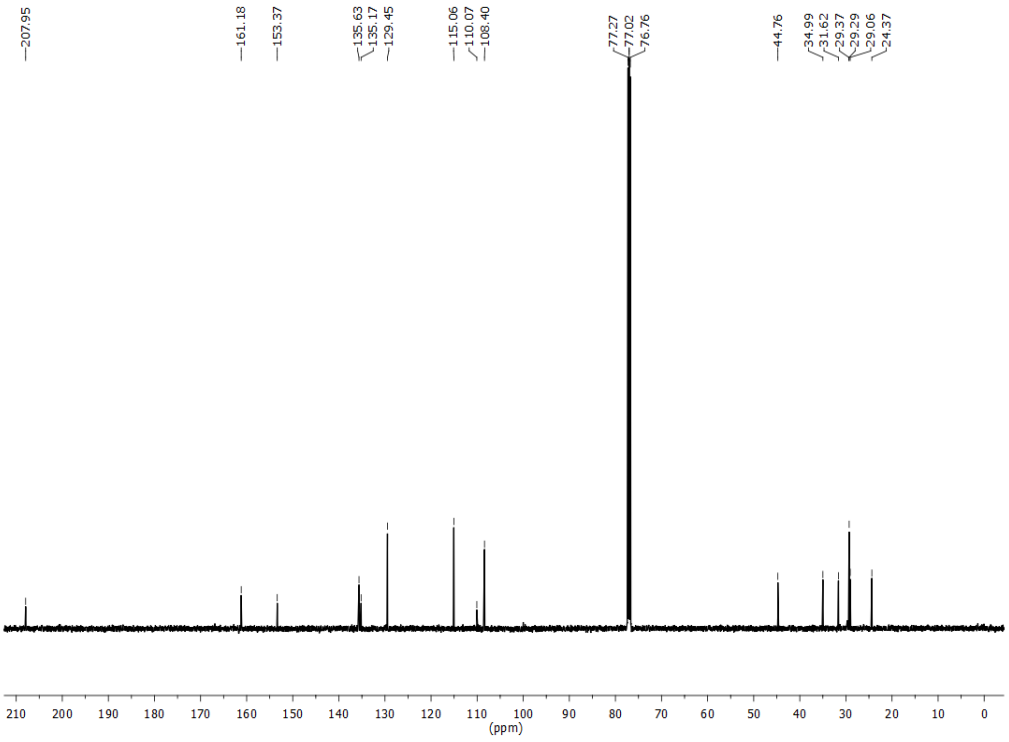

Figure 6A.21. ^{13}C NMR spectrum (125 MHz, $CDCl_3$) of malabaricone B (**48)**

Finally, fraction pool 18 on column chromatographic purification using 25 % EtOAc/*n*-hexane as eluent, afforded compound **49** as colourless crystal (310 mg). The FTIR and NMR spectra (**Figure 6A.22-23**) of compound **49** displayed the presence of a conjugated carbonyl group [υ_{max} 1625 cm^{-1} and δ_C 208.9 ppm], hydrogen bonded phenolic hydroxyl groups [δ_H 11.26 (s, 2H) ppm], eight methylene groups with one neighbouring the carbonyl group [δ_H 3.03 (t, J = 7.5 Hz, 2H) ppm, δ_C 44.8 ppm], and one benzylic methylene group [δ_H 2.32 (t, J = 7.5 Hz, 2H) ppm, δ_C 35.0 ppm]. The presence of two benzene rings, one of which was a 1,2,3- trisubstituted benzene ring [δ_H 7.12 (t, J = 8.5 Hz, 1H) ppm, 6.29 (d, J = 8.5 Hz, 2H) ppm] and the second benzene ring was [δ_H 6.56 (d, J = 8 Hz, 1H) ppm, 6.38 (d, J = 2 Hz, 1H) ppm, 6.37 (d, J = 2 Hz, 1H) ppm]. From detailed NMR and HRESIMS analysis [(M+H)$^+$: 359.18567; Calculated for $C_{21}H_{27}O_5$: 359.1858] and in comparison with literature reports [Pham *et al*., **2000**] compound **49** had the structure malabaricone C and the structure is shown below.

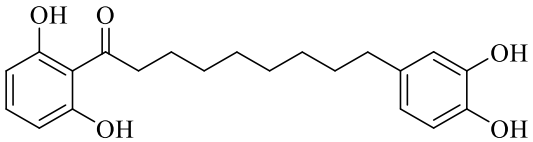

Malabaricone C (49)

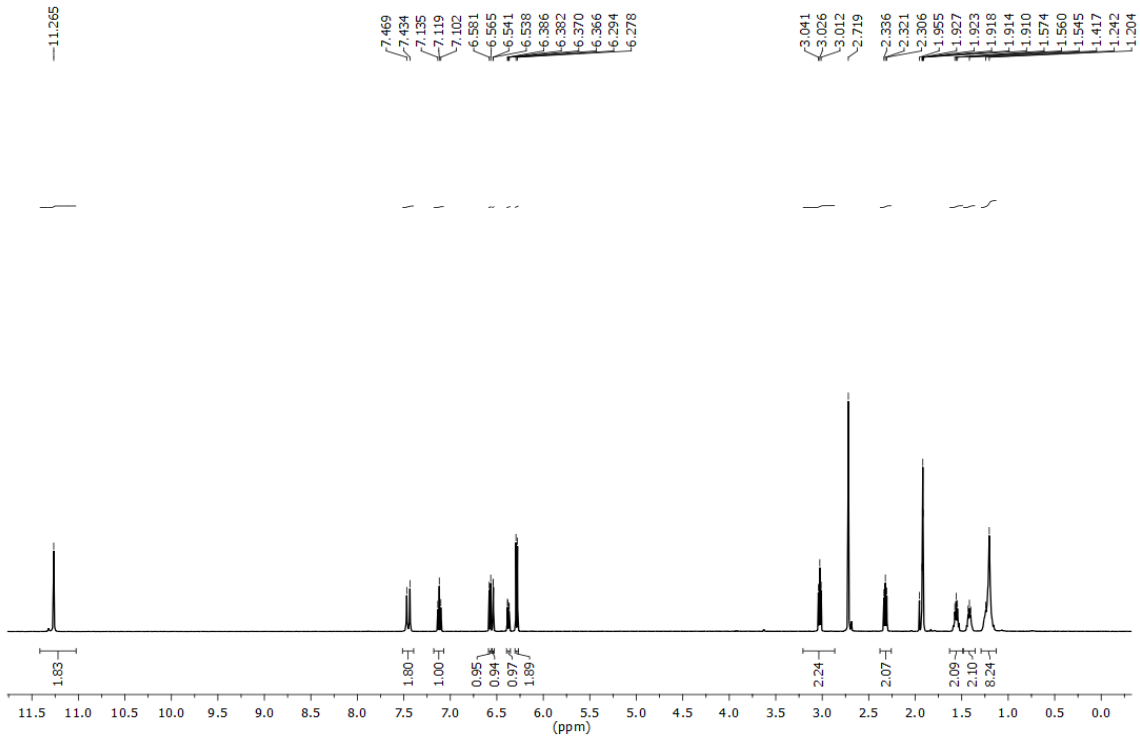

Figure 6A.22. ^{1}H NMR spectrum (500 MHz, Acetone-d_6) of malabaricone C (**49**)

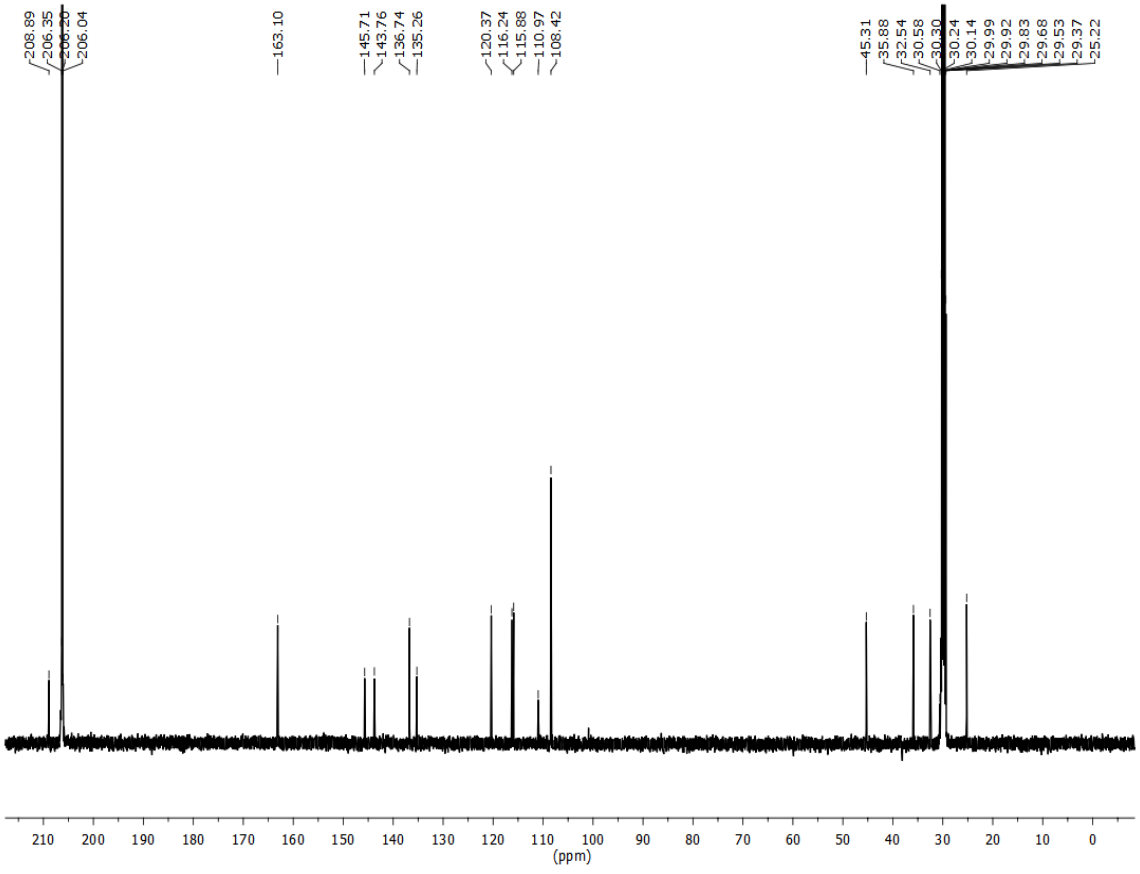

Figure 6A.23. ^{13}C NMR spectrum (125 MHz, Acetone-d_6) of malabaricone C (**49**)

6A.6. Biosynthetic pathway of malabaricones

The biosynthesis of malabaricones starts from phenyl alanine. The elongation of a cinnamoyl type precursor and its hydroxyderivatives (tyrosine or DOPA) by six acetate (malonate) units, followed by reduction of the first three acetate units and cyclisation of the last three acetate units into a triketonic cyclohexane ring according to the phloroglucinol type cyclisation. After that, the reduction of the para-carbonyl group into an alcohol yields promalabaricones and further dehydration and enolisation gives to malabaricones (**Figure 6A.24**) [Van *et al*., **2000**].

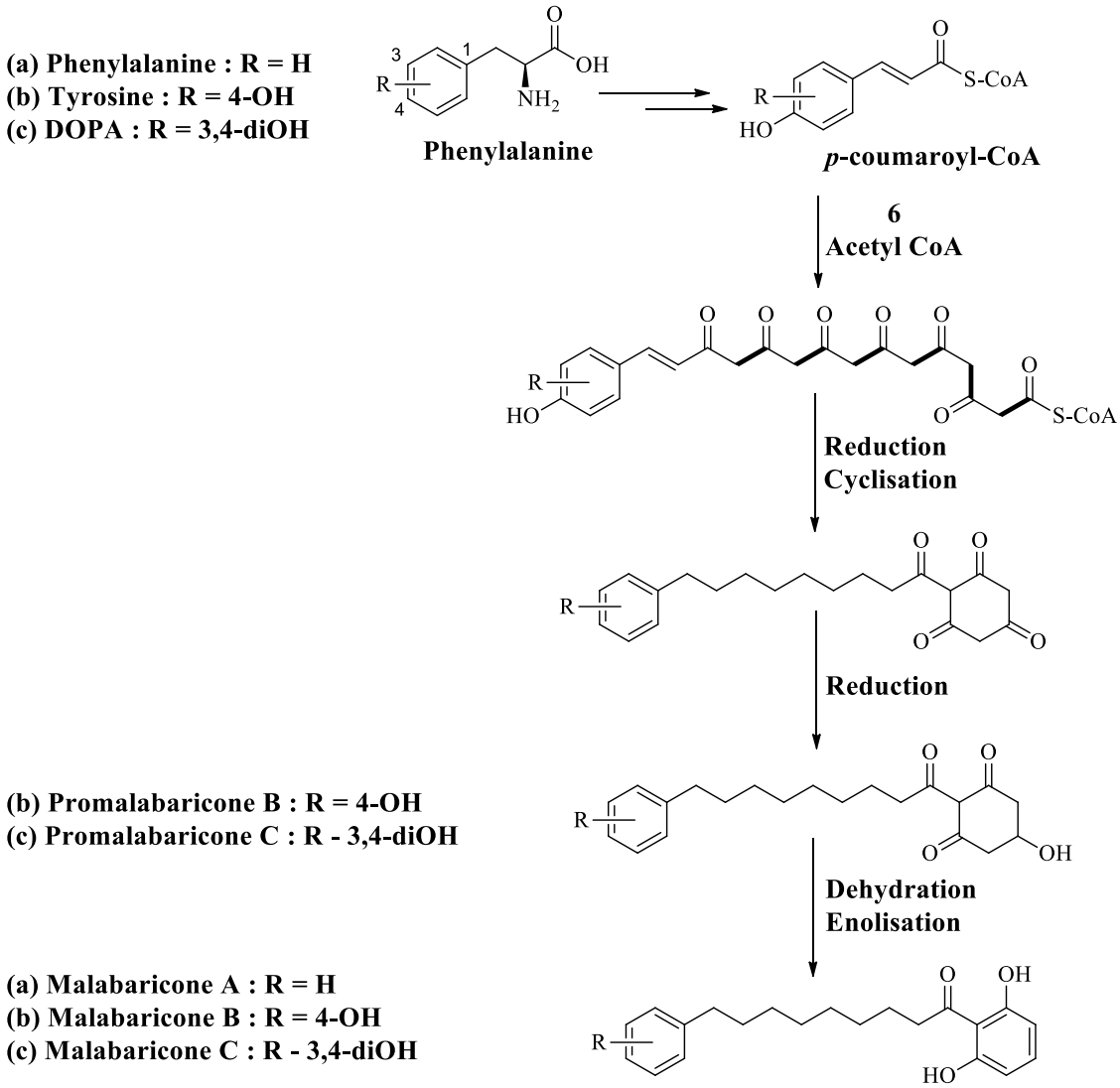

Figure 6A.24. Hypothetical pathway for malabaricones biosynthesis

6A.7. Antidiabetic property of phytochemicals isolated from *Myristica fatua* Houtt.

Type II diabetes mellitus (T2DM) is a noncommunicable chronic metabolic disease, characterized by hyperglycemia because of the impairment in insulin secretion and resistance to the action of insulin on the targeted tissues [Ross *et al*., **2004**].

Nowadays, more than 422 million people live with diabetes due to environmental and hereditary factors, energy- rich diet and sedentary lifestyle [WHO Reports **2016**]. Inhibition of carbohydrate enzymes, delaying of advanced glycated end products (AGEs) formation and enhancing the glucose uptake in muscle cells are the main strategies for the prevention and control of T2DM [Trapero *et al*., **2012**; Yonemoto *et al*., **2014**; Riya *et al*., **2015**; Patel *et al*., **2016**; Prabhakar *et al*., **2011**]. Even though the currently available drugs are effective to the patients, some have adverse side effects including hepatotoxicity, weight gain and cardiovascular problems [Victor *et al.*, **2006**; Hollander *et al.*, **2007**; Nissen *et al.*, **2007**]. Nature has gifted numerous structurally diverse and biologically active scaffolds that are now enjoying significant recognition by the scientific community because of their low toxicity, bioavailability, and food additive properties. Hence, search for new antidiabetic leads from natural cradles are on-going all over the world. Thus, as part of our continuing interest in this area, we have checked the antidiabetic property of phytochemicals isolated from *Myristica fatua* Houtt. var. *magnifica* (Bedd.) Sinclair.

6A.7.1. α-Amylase inhibitory activity

In human beings α-amylase helps to hydrolyse α-1, 4- starch to glucose and maltose. In the present study, porcine pancreatic α-amylase is used as a model for human pancreatic α -amylase, because it contains 496 amino acid residues and it has 83 % homology with human pancreatic α-amylase [Sui *et al*., **2016**; Sun *et al*., **2016**]. All compounds were evaluated for their porcine pancreatic α-amylase inhibitory activity. Here, the standard α-amylase inhibitor acarbose was used as a positive control. The IC_{50} values of all the compounds are shown in **Table 6A.4**. Malabaricone A (**46**), B (**48**), and C (**49**) displayed significant α-amylase inhibitory activity with IC_{50} values 19.07 ± 0.517, 12.89 ± 0.068, and 10.63 ± 0.171 μM, respectively. Compounds, 3-tridecanoylbenzoic acid (**43**), 1-(2-hydroxy-6-methoxyphenyl) tetradecan-1-one (**44**), 1-(2, 6-dihydroxyphenyl)tetradecan-1-one (**45**), and 1-(2-hydroxy-6-methoxy phenyl)-9-(4-hydroxyphenyl) nonan-1-one (**47**) ($p<0.01$) were comparatively less active than malabaricone A (**46**), B (**48**), and C (**49**). From the studies, we interpret that aromatic moiety and hydroxyl groups are responsible for inhibitory potential, whereas the methoxy group suppress the activity of α- amylase enzyme.

6A.7.2. *α*-Glucosidase inhibitory activity

α-Glucosidase inhibitors are commonly used as oral antidiabetic agents for preventing the early-onset of diabetic problems by supressing postprandial hyperglycemia. They inhibit the action of *α*-glucosidase enzymes found in small intestine and delay the release of glucose from polysaccharides. A considerable body of literature reports that traditional medicinal plants and plant derived constituents have been known to exhibit *α*-glucosidase inhibitory activity. In 2015, Sivasothya and coworkers reported a potent *α*-glucosidase inhibitor, giganteone D from the stem bark of *Myristica cinnamomea* King [Sivasothya *et al*., **2016**]. Apart from this, there is no report on *α*-glucosidase inhibitory activity of acylphenols. As shown in **Table 6A.4**; all isolated compounds exhibited moderate to significant inhibition of rat intestinal *α*-glucosidase compared to the standard *α*-glucosidase inhibitor, acarbose. Among them, malabaricone B (**48**) and C (**49**) exhibited significant *α*-glucosidase inhibitory activity than other compounds with IC_{50} value of 63.70 ± 0.546, and 43.61 ± 0.620 *μ*M ($p < 0.01$) respectively, indicating that more hydroxyl group and aromatic systems are essential for *α*-glucosidase inhibition.

Table 6A.4. Porcine pancreatic *α*-amylase inhibitory activity, rat intestinal *α*-glucosidase inhibitory activity and antiglycation property of compounds isolated from *Myristica fatua*

Compounds	*α*-Amylase (*μ*M)	*α*-Glucosidase (*μ*M)	Antiglycation (*μ*M)
43	36.644 ± 0.336*	372.45 ± 1.392*	410.82 ± 0.967*
44	39.01 ± 1.20*	256.71 ± 0.492*	192.09 ± 0.915*
45	74.12 ± 1.278*	171.90 ± 0.890*	120.84 ± 0.547*
46	19.07 ± 0.517*	91.44 ± 1.245*	19.28 ± 0.0454*
47	32.27 ± 0.500*	94.53 ± 0.875*	104.27 ± 0.933*
48	12.89 ± 0.068*	63.70 ± 0.546*	40.34 ± 0.0948*
49	10.63 ± 0.171*	43.61 ± 0.620*	14.99 ± 0.114*
Acarbose	8.93 ± 0.48	66.57 ± 0.982	-
Ascorbic acid	-	-	155.38 ± 0.547*

Each value represents mean ± SD (standard deviation) from triplicate measurements. Significance test between various groups was determined by using one-way analysis of variance, followed by Dunnett's t test. *$p<0.01$ versus positive control

6A.7.3. Antiglycation property

Advanced glycated end products (AGEs) represent a heterogeneous group of molecules formed by the non-enzymatic reaction of reducing sugars with proteins, lipids and nucleic acids. The formation and accumulation of advanced glycated end products are mainly responsible for the secondary complications, such as retinopathy, nephropathy, or atherosclerosis in diabetic patients [Adrover *et al*., **2014**]. Several studies suggested that natural products and its derivatives exhibited antiglycation property. Encouraged with these observations, we examined the antiglycation property of all the isolated compounds (**Table 6A.4**). Of them, compound **45-49** [1-(2,6-dihydroxyphenyl) tetradecan-1-one (**45**), malabaricone A (**46**), 1-(2-hydroxy-6-methoxyphenyl)-9-(4-hydroxy phenyl) nonan-1-one (**47**), malabaricone B (**48**) and malabaricone C (**49**)] showed significant ability to inhibit advanced glycated end products formation with IC_{50} value of 120.84 ± 0.547, 19.28 ± 0.0454, 104.27 ± 0.933, 40.34 ± 0.0948, and 14.99 ± 0.114 μM respectively ($p < 0.01$).

6A.7.4. Molecular simulation studies

In order to predict the probable binding modes of isolated compounds on digestive enzymes present in our body, we selected human pancreatic α- amylase (**4GQQ**), human maltase-glucoamylase *C*-terminal (**2QMJ**) and *N*-terminal (**3TOP**) for *in silico* studies [Ross *et al*., **2004**]. The pharmacophore parameters were analysed by qikprop and the results (**Table 6A.5**) revealed that the compounds isolated from *Myristica fatua* satisfy the adsorption, distribution, metabolism and excretion/toxicity (ADME/T) properties and Lipinski Rule of Five. In human pancreatic α-amylase enzyme, malabaricone C (**49**) exhibits G-Score/D-Score of -5.48 and -5.4 kcal/mol respectively. These findings are in good agreement with experimental value because porcine pancreatic α-amylase shows 83 % resemblance with human pancreatic α-amylase. The amino catalytic domains of human maltase glucoamylase (**2QMJ**) catalyze the cleavage of short α-(1→4) oligosaccharide units. Malabaricone C (**49**) effectively binds with **2QMJ** followed by malabaricone B (**48**). The hydroxyl groups and carbonyls group of malabaricone C (**49**) formed a strong H-bond donor interaction with the ASP327 and GLN603. The carbonyl terminal catalytic domains of human maltase glucoamylase (**3TOP**) also show better interaction with malabaricone C (**49**) having a G-Score/D-Score of -6.94/-6.86 kcal/mol. These results suggested that malabaricone C (**49**) act as a promising target for the treatment of T2DM. The 2D interaction diagram of malabaricone C (**49**) with **4GQQ**,

2QMJ and **3TOP** are shown in **Figure 6A.25** and the G-Score/D-score of all the isolates are shown in **Table 6A.5**.

Table 6A.5. ADME/T properties of compounds

Sl. No	**43**	**44**	**45**	**46**	**47**	**48**	**49**
M.W	318.455	334.498	320.471	326.435	356.461	342.434	358.433
#stars	0	2	3	3	0	0	0
#rotor	13	15	15	12	13	13	14
CNS	-2	-2	-2	-2	-2	-2	-2
SASA	728.863	764.319	729.068	697.858	735.251	701.324	715.598
FISA	146.316	73.177	115.108	114.984	128.242	169.717	216.82
HBA	4	2.5	1.5	1.5	3.25	2.25	3
HBD	1	0	0	0	1	1	2
QPlogKhsa	0.496	1.13	1.212	1.188	0.908	0.939	0.702
HOA	2	1	1	1	1	3	3
% HOA	79.598	100	100	100	95.14	86.654	87.297
QPlogPo/w	5.055	6.326	6.297	5.989	5.363	5.116	4.378
QPlogS	-5.965	-7.015	-6.806	-6.703	-6.372	-6.132	-5.717
R Of Five	1	1	1	0	1	1	1

M.W. (Molecular Weight):130.0 to 725.0; #stars (few stars-more drug-like): 0 to 5; #rotor (Number of non-trivial and non-hindered rotatable bonds):0 to 15; CNS (Central Nervous System activity): -2 to +2; SASA (Total solvent accessible surface area in square angstroms): 300.0 to 1000.0 FISA (Hydrophilic component of total solvent accessable area): 7.0 to 333.0; HBA (Hydrogen bond acceptor): 2.0 to 20.0; HBD (hydrogen bond donor): 0.0 to 6.0; QPlogKhsa (binding to human serum albumin): -1.5 to 1.5; HOA (Human Oral Absorption): 1, 2, or 3 for low medium, and high; % HOA (Percent Human Oral Absorption): >80 % is high, <25 % is poor; QPlogPo/w (octanol/water partition coefficient): -2.0 to 6.5; QPlogS (Aqueous solubility): -6.5 to 0.5; Ro5 (Number of violations of Lipinski's rule of five): maximum is 4.

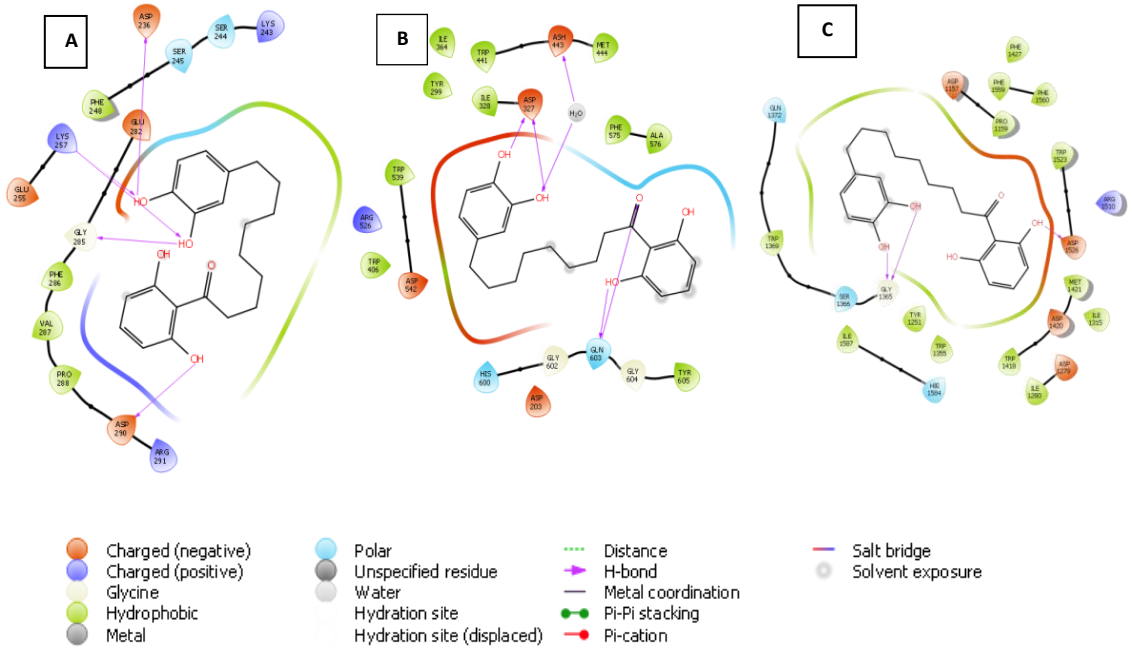

Figure 6A.25. 2D interaction diagram of malabaricone C with **(A) 4GQQ, (B) 2QMJ,** and **(C) 3TOP**

Table 6A.7. G-Score/D-Score of isolated compounds with human pancreatic α-amylase (**4GQQ**) and human maltase glucoamylase (*N*- terminal, **2QMJ**; *C*- terminal, **3TOP**)

Compounds	**4GQQ** (kcal/mol)		**2QMJ** (kcal/mol)		**3TOP** (kcal/mol)	
	G-Score	D-Score	G-Score	D-Score	G-Score	D-Score
43	-1.18	-1.18	-1.15	-1.15	-5.09	-5.09
44	-1.67	-1.63	-4.06	-4.03	-4.74	-4.7
45	-2.06	-1.98	-3.75	-3.67	-4.67	-4.59
46	-3.34	-3.27	-3.94	-3.86	-5.16	-5.08
47	-3.34	-3.3	-4.44	-4.4	-6.03	-4.38
48	-4.07	-3.99	-7.81	-6.57	-6.51	-5.27
49	-5.48	-5.4	-8.88	-8.8	-6.94	-6.86

To gain an insight into the stability and conformational flexibility of **2QMJ**-malabaricone C complex, molecular dynamics (MD) simulation was done at 3 ns using OPLS-2005 force field. Molecular dynamics simulations have evolved into a mature technique that can be used successfully to realize macromolecular structure-to-function relationships. To understand how a ligand binds to its macromolecular counterpart is a key issue in the understanding of function itself, and it is the basis of CADD (Computer Aided Drug Design). Molecules are flexible entities, and the dynamic recognition process itself implies structural rearrangements, and this shape adjustment is part of the binding process not only from the structural point of view, but also from the energetics.

The root mean square deviation (RMSD) for the protein lies below 1.2 Å which accounts for the structural stability of the protein throughout the simulation (**Figure 6A.25**). There is a noticeable deviation in the case of ligand RMSD, means that the ligand has diffused away from its initial binding site. The protein-ligand (P-L) contacts give the exact binding positions and modes of interactions, which is included as **Figure 6A.26**. There are two strong H-bonds formed between the terminal -OH groups of malabaricone C with negatively charged ASP327, which lasts throughout the simulation time of the selected trajectory. There is also a π–stacking interaction from the terminal benzene ring to the hydrophobic TYR299 for about 33 % of the period. In addition to these, there is an extra H- bond with ASP542 and hydrophobic interactions of TYR299, PHE575, ILE364, TRP406, TRP441, ALA576 and TYR605 as depicted in the bar diagram.

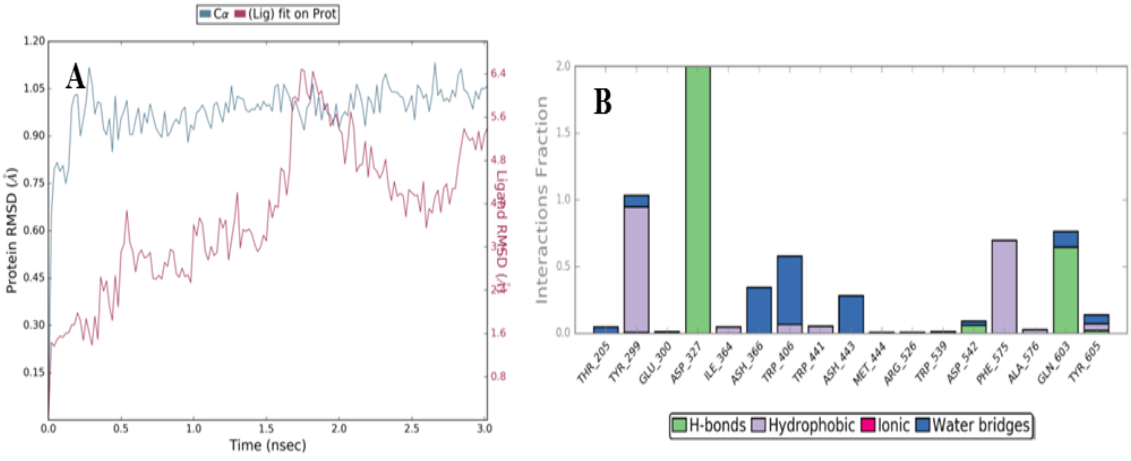

Figure 6A.26. (A) Root mean square deviation of **2QMJ** with malabaricone C and (B) **2QMJ**- Malabaricone C contacts

6A.7.5. Pharmacophore modelling

A ligand-based pharmacophore model was created using seven-point hypothesis based on best alignment and common structures (**Figure 6A.27**). It consists of an aromatic ring (orange circle), a hydrogen bond donor (pink) and two hydrophobic moieties (green sphere). This model helps us to develop a potential α-glucosidase inhibitors from natural products with less toxicity and high efficacy.

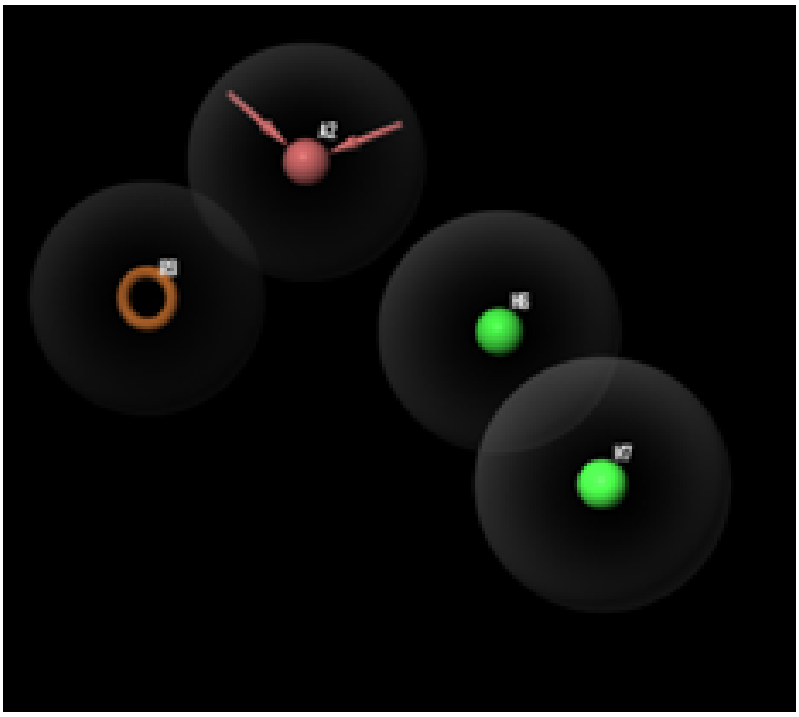

Figure 6A.27. Pharmacophore modelling

6A.7.7. Cytotoxicity in L6 cell line

To study the effect of the compounds **43-49** on the utilization of glucose in skeletal muscles, first we carried out MTT assay to evaluate their cytotoxicity in L6 myocytes. Results confirmed that upto 50 μM concentration of compounds (**43-49**) for 24 h did not induce significant cytotoxicity (**Figure 6A.28**). Therefore, 10, 25 and 50 μM concentrations of compounds (**43-49**) were used for studying glucose uptake in L6 cell line.

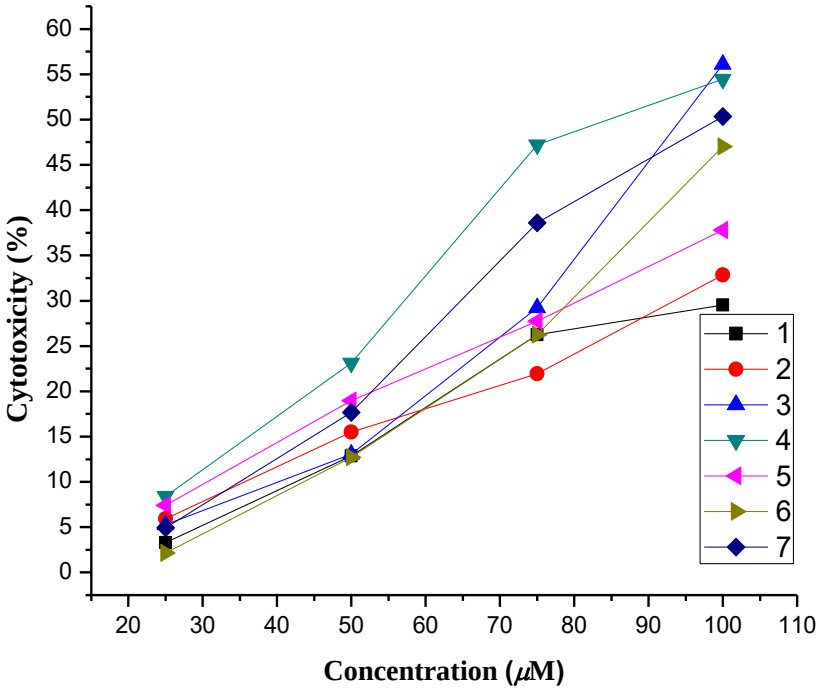

Figure 6A.28. Cytotoxicity of compounds **43-49** in L6 cell line. [3-tridecanoylbenzoic acid (**1**), (1-(2-hydroxy-6-methoxyphenyl)tetradecan-1-one (**2**), 1-(2,6-dihydroxyphenyl) tetradecan-1-one (**3**), malabaricone A (**4**), 1-(2-hydroxy-6-methoxyphenyl) -9-(4-hydroxy phenyl)nonan-1-one (**5**), malabaricone B (**6**) and malabaricone C (**7**)]

6A.7.7. Glucose uptake in L6 myotubes

The skeletal muscle is a key thespian of glucose utilization in the body and more than 70 % insulin stimulated glucose uptake occurs here. Impaired glucose uptake resulted in the imbalance of glucose homeostasis that leads to T2DM [Ross *et al*., **2004].** All the compounds showed moderate to significant glucose uptake in a dose dependent manner. Malabaricone B (**48**) demonstrated a significant stimulation of glucose uptake [37.5 % (10 μM), 45.8 % (25 μM), 52.7 % (50 μM)] as compared to the control (20.0 %). The standard antidiabetic drug, metformin served as a positive control, showed 36.6 % of glucose uptake at 100 μM under identical experimental conditions (**Figure 6A.29**).

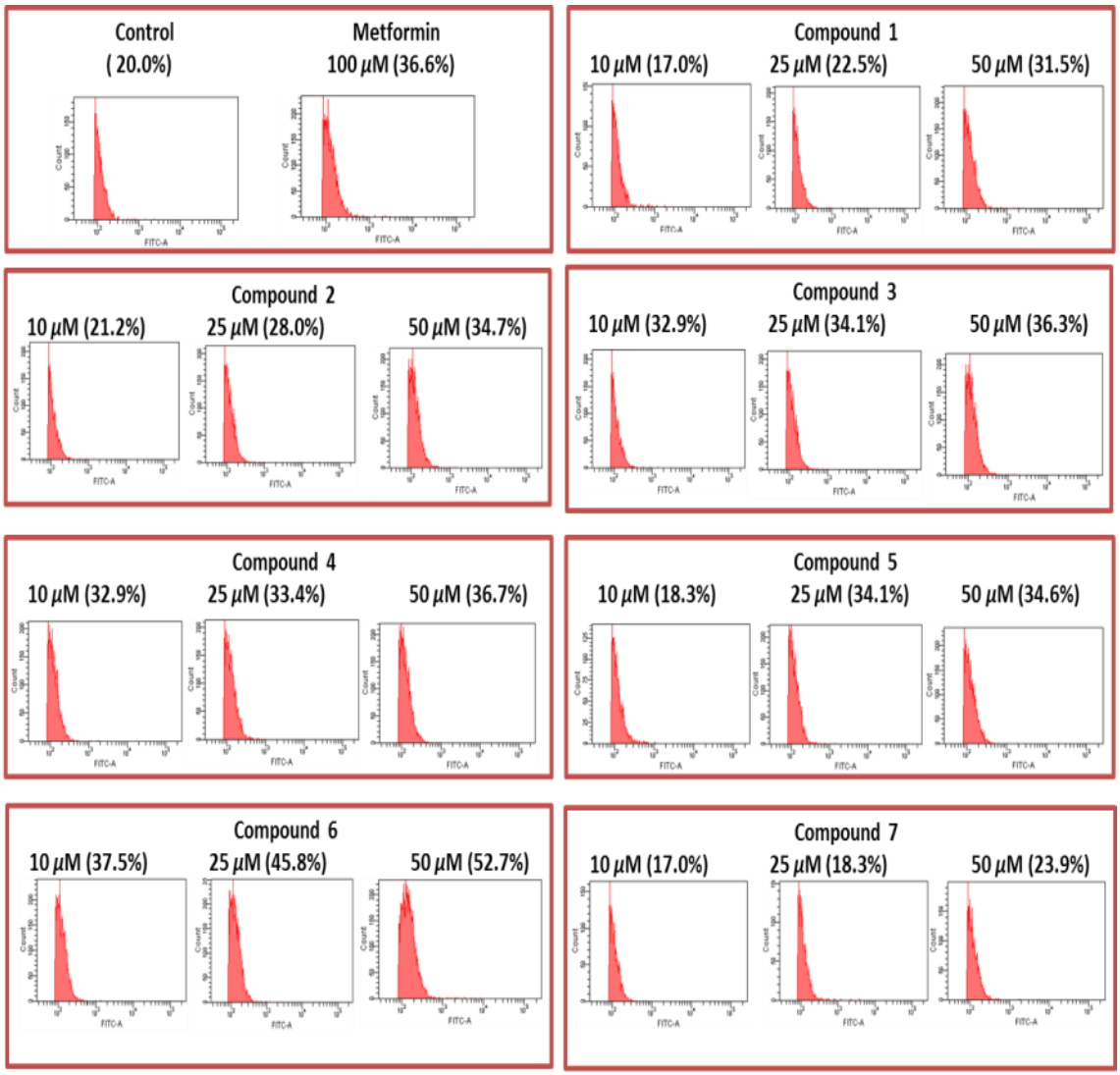

Figure 6A.29. Fluorescence analysis of 2-NBDG uptake by flow cytometry. FACS analysis in differentiated L6 cells using 2-NBDG in control cells, metformin (100 μM) and compounds (**43-49**) pretreated cells. [3-tridecanoylbenzoic acid (**1**)**,** (1-(2-hydroxy-6-methoxyphenyl)tetradecan-1-one (**2**), 1-(2,6-dihydroxyphenyl)tetradecan-1-one (**3**), malabaricone A (**4**), 1-(2-hydroxy-6-methoxyphenyl) -9-(4-hydroxy phenyl)nonan-1-one (**5**), malabaricone B (**6**) and malabaricone C (**7**)]

6A.8. Conclusion

In conclusion, phytochemical investigation of stem bark of *Myristica fatua* led to the isolation of a novel compound, 3-tridecanoylbenzoic acid (**43**) along with six known acyl phenols [(1-(2-hydroxy-6-methoxyphenyl)tetradecan-1-one (**44**), 1-(2,6-dihydroxyphenyl) tetradecan-1-one (**45**), malabaricone A (**46**), 1-(2-hydroxy-6-methoxyphenyl) -9-(4-hydroxy phenyl)nonan-1-one (**47**), malabaricone B (**48**) and malabaricone C (**49**)], of which four of them [(1-(2-hydroxy-6-methoxyphenyl)

tetradecan-1-one (**44**), 1-(2,6-dihydroxyphenyl)tetradecan-1-one (**45**), malabaricone A (**46**) and 1-(2-hydroxy-6-methoxy phenyl)-9-(4-hydroxy phenyl)nonan-1-one (**47**)] are reported for the first time from *Myristica fatua* Houtt. All compounds exhibited moderate α-amylase inhibitory activity and significant α-glucosidase inhibitory activity. Malabaricone B (**48**) and malabaricone C (**49**) exhibited promising α- glucosidase inhibitory activity with IC_{50} value of 63.70 ± 0.546 and 43.61 ± 0.620 μM. The molecular simulation studies indicated that malabaricone C (**49**) effectively binds the pocket of *N*-terminal human maltase glucoamylase (**2QMJ**). Malabaricones A (**46**), B (**48**) and C (**49**) showed potent antiglycation property with IC_{50} value of 19.28 ± 0.045, 40.34 ± 0.094, and 14.99 ± 0.114 μM respectively. *In vitro* antidiabetic activity in L6 myotubes revealed that malabaricone B (**48**) significantly enhances the glucose uptake in a dose dependant manner. Further studies are in progress to establish the therapeutic efficacy and safety of compounds as a promising antidiabetic agent from *Myristica fatua* Houtt.

6A.9. Experimental

6A.9.1. General experimental procedures and chemicals

The melting points were performed on a Buchi melting point apparatus. The IR spectra were achieved using Bruker FTIR spectrometer, and values are acquired in cm^{-1}. NMR spectra was acquired from Bruker Avance 500 MHz, using $CDCl_3$ and acetone-d_6 as solvents and the chemical shifts are expressed in δ (ppm) relative to the tetramethylsilane peak. The multiplicities of NMR signals were assigned as singlet (s), doublet (d), triplet (t), multiplet (m), and broad singlet (brs). The HRESIMS data was recorded at 60,000 resolution using Thermo Scientific Exactive mass spectrometer. Column chromatography was done using silica gel (100−200 and 230−400 mesh; Merck, Darmstadt, Germany). Merck precoated silica gel F_{254} plates were used for thin-layer chromatography (TLC). Spots were detected on TLC under UV light or by heating after spraying samples with anisaldehyde-sulfuric acid.

Porcine pancreatic α-amylase, rat intestinal α-glucosidase, acarbose, bovine serum albumin (BSA), α-D-glucose, ascorbic acid, metformin, 4-nitrophenyl-α-D-glucopyranoside (*p*-NPG), Dulbecco's modified Eagle's media (DMEM), fetal bovine serum (FBS), antibiotic-antimycotic solution (Pencillin–streptomycin–amphotericin B mix) and 3-(4,5-dimethylthiazol -2-yl)-2, 5-diphenyltetrazolium bromide (MTT) were procured from M/s Sigma–Aldrich Chemicals (St. Louis, MO, **USA**). 2-(*N*-(7-nitrobenz-

2-oxa-1, 3-diazol-4-yl)amino)-2-deoxy glucose (2-NBDG) was obtained from molecular probe (Invitrogen Life Technologies, Carlsbad, CA, USA).

6A.9.2. Plant material and isolation procedure

The stem bark of *Myristica fatua* was collected Agasthyamalai biosphere reserve of south Western Ghats region of Kollam District, Kerala, India. The stem bark was cleaned, cut into small pieces, air dried and then dried in drier maintained at 50 ^{o}C and powdered. The powdered stem bark (850 g) was subjected to extraction using dichloromethane (2 L x 3 times) at room temperature. After extraction, the solvent was removed under reduced pressure using Büchi rotary evaporator. The crude extract (25 g) was subjected to silica gel (100-200 mesh) column chromatography using *n*-hexane, *n*-hexane-EtOAc gradient and EtOAc. Twelve fractions of 200 mL each were collected and concentrated under reduced pressure. The schematic representation of extraction and isolation procedure was shown in **Figure 6A.30.**

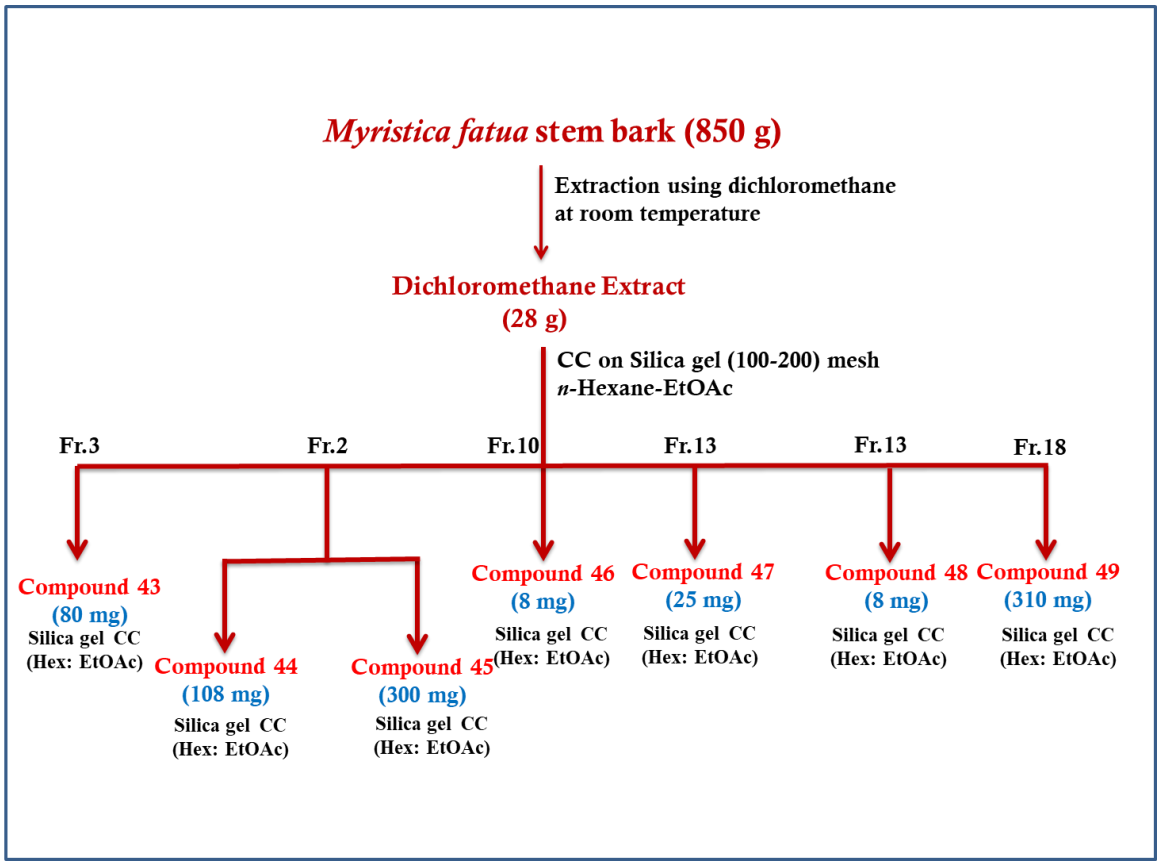

Figure 6A.30. Schematic representation of the extraction and isolation of phytochemicals from the stem bark of *Myristica fatua* Houtt.

6A.9.2.1. Isolation of compound 43

The isolation procedure of compound **43** is represented in **Figure 6A.30.** Compound **43** (80 mg) was obtained as a pale yellow amorpous solid, on eluting the column (silica gel 100-200 mesh) with 4 % EtOAc in *n*-hexane. The detailed analysis of FTIR, ^{1}H, ^{13}C, ^{1}H-^{1}H HOMOCOSY, HMQC, DEPT 135 and HMBC NMR spectra and HRESIMS gave compound **43** as a novel compound.

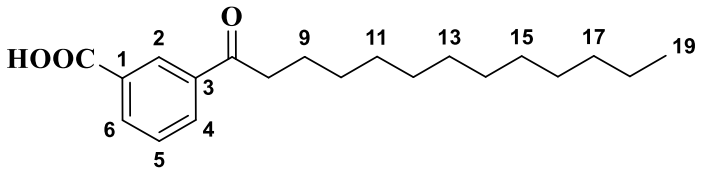

Nature	Pale yellow amorphous solid
Melting Point	44- 46 ^{o}C
FTIR (KBr, υ_{max})	2925, 2854, 1744, 1658, 1621, 1598, 1542, 1476, 1461, 1411, 1366, 1255, 1231, 1155, 1057, 1037, 956 cm^{-1}.
^{1}H NMR (500 MHz, $CDCl_3$)	δ 12.57 (s, -COOH), 7.48 (t, *J* = 8 Hz, H-5), 6.85 (d, 8.5 Hz, H-6), 6.76 (d, 8.5 Hz, H-4), 6.10 (s, H-2), 2.60 (t, *J* = 7.5 Hz, H-8), 1.74-1.69 (m, H-9), 1.41-1.26 (m, 18H, H-10 to H-18), 0.88 (t, *J* = 7 Hz, H-19) ppm.
^{13}C NMR (125 MHz, $CDCl_3$)	δ 183.6 (C-7), 171.3 (COOH), 160.8 (C-3), 156.8 (C-1), 135.03 (C-5), 111.1 (C-4), 108.4 (C-2), 106.8 (C-6), 34.3 (C-8), 31.9 (C-9), 29.6 (C-10-C-12), 29.4 (C-13-C-14), 29.3 (C-15), 29.2 (C-16), 29.0 (C-17-C-18), 14.1 (C-19) ppm.
HRESIMS (m/z)	317.21184 $[M-H]^{+}$

6A.9.2.2. Isolation of compound 44

Fraction pool 2 on column chromatographic purification (silica gel 100-200 mesh) using 2 % EtOAc/*n*-hexane as eluent afforded compound **44** as pale yellow amorphous solid.

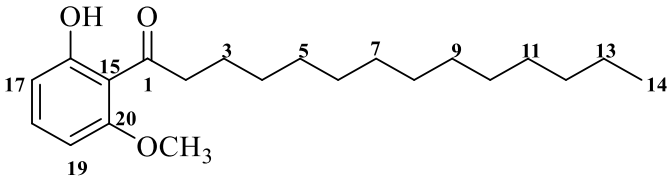

Nature	Pale yellow amorphous solid
Melting Point	50-52 °C
FTIR (KBr, υ_{max})	2912, 2853, 1621, 1588, 1452, 1372, 1231, 1183, 1092, 819, 778 and 715 cm^{-1}
^1H NMR (500 MHz, $CDCl_3$)	δ 13.28 (brs, 1H, -OH), 7.32 (t, J = 8.5 Hz, 1H, H-18), 6.57 (dd, J_1= 1 Hz, J_2 = 8 Hz, 1H, H-17), 6.39 (dd, J_1 = 1 Hz, J_2 = 8.5 Hz, 1H, H-16), 3.89 (s, 3H, -OCH_3), 3.04 (t, J = 7.5 Hz, 2H, H-2), 1.67 (m, 2H, H-3), 1.30 (m, 20H, H-4 to H-13), 0.88 (t, J = 6.5 Hz, 3H, H-14) ppm.
^{13}C NMR (125 MHz, $CDCl_3$)	δ 208.0 (C-1), 164.7 (C-16), 161.3 (C-20), 135.7 (C-15), 111.2 (C-18), 110.9 (C-17), 101.2 (C-19), 55.6 (-OCH_3), 45.1 (C-2), 29.7 (C-3), 29.6 (C4-C9), 29.5 (C-10), 29.4 (C-11), 24.6 (C-12), 22.7 (C-13), 14.1 (C-14) ppm.
HRESIMS (m/z)	335.2593 $(M+H)^+$

NMR spectral assignments were made on the basis of ^1H-^1H HOMOCOSY, HMQC, DEPT 135 and HMBC analysis and in comparison with the literature reports.

6A.9.2.3. Isolation of compound 45

Fraction pool **2** on column chromatographic separation (silica gel 100-200 mesh) using 2 % EtOAc/*n*-hexane as eluent afforded compound **45** (300 mg) as pale yellow solid.

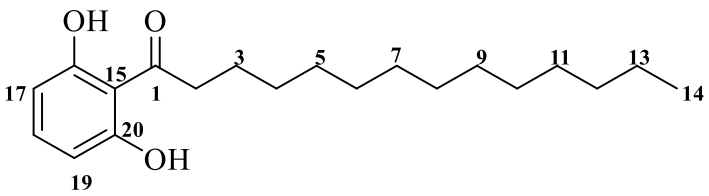

Nature	Pale yellow amorphous solid
Melting Point	91-92 °C
FT-IR (KBr, υ_{max})	3450, 2927, 2852, 1624, 1601, 1448, 1243, 1028, 963, 782 and 720 cm^{-1}
^1H NMR (500 MHz, $CDCl_3$)	δ 9.98 (brs, 2H, -OH), 7.22 (t, *J* = 8 Hz, 1H, H-18), 6.41 (d, *J* = 8 Hz, 2H, H-17-H-19), 3.14 (t, *J* = 7 Hz, 2H, H-2), 1.71 (m, 2H, H-3), 1.37- 1.25 (m, 20H, H-4-H-13), 0.88 (t, *J* = 6.5 Hz, 3H, H-14) ppm.
^{13}C NMR (125 MHz, $CDCl_3$)	δ 208.5 (C-1), 161.3 (C-16, C-19), 135.9 (C-15), 110.1 (C-), 108.3 (C-), 44.9 (C-), 31.9 (C-), 29.7 (C-), 29.6 (C-), 29.4 (C-), 24.5 (C-), 22.7 (C-), 14.1 (C-) ppm.
HRESIMS (m/z)	321.24246 $[M+H]^+$

6A.9.2.4. Isolation of compound 46

Fraction pool **4** on column chromatographic separation (silica gel 100-200 mesh) using 8 % EtOAc/*n*-hexane as eluent gave compound **46** (8 mg) as pale yellow amorphous solid.

Nature	Pale yellow amorphous solid
Melting Point	80-82 ^oC
FTIR	3254 (OH), 2925, 2850, 1635 (C=O), 1600, 1471, 1246, 1038,

(KBr, υ_{max})	966, 876 cm^{-1}.
^{1}H NMR (500 MHz, $CDCl_3$)	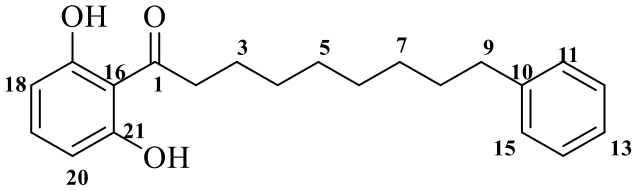 δ 9.67 (brs, 2H, -OH), 7.28 (brd, J = 8 Hz, 1H), 7.25 (brs, 1H), 7.21 (t, J = 8 Hz, 1H, H-19), 7.18 (d, J = 7 Hz, 2H, H-18 and 20), 7.15 (brd, 1H, H-13), 6.38 (d, J = 8 Hz, 2H), 3.11 (t, J = 7.5, 2H, H-2), 2.59 (t, J = 7.5 Hz, 2H, H-9), 1.69 (t, J = 7 Hz, 2H, H-3), 1.60 (t, J = 7 Hz, 2H, H-8), 1.33 (brs, 8H, H-4 to H-7) ppm.
^{13}C NMR (125 MHz, $CDCl_3$)	δ 207.9 (C-1), 161.2 (C-OH), 153.4 (C-21), [135.6 135.2, 129.4, 115.1, 110.1, 108.4 (other aliphatic protons)], 44.8 (C-2), 35.0 (C-9), 31.6 (C-3), 29.4 (C-8), [29.3, 29.1, 24.4 (other aliphatic protons)] ppm.
HRESIMS (m/z)	327.19595 $(M+H)^+$

6A.9.2.5. Isolation of compound 47

Fraction pool 10 on column chromatographic purification (silica gel 100-200 mesh) using 12 % EtOAc/*n*-hexane as eluent afforded compound **47** as pale yellow amorphous solid.

Nature	Pale yellow amorphous solid
Melting Point	65-67 °C
FTIR (KBr, υ_{max})	3500, 2895, 2850, 1620, 1590, 1510, 1460, 1240, 1090, 830,780 and 720 cm^{-1}.
^{1}H NMR (500 MHz, $CDCl_3$)	δ 13.33 (brs, 1H, -OH), 7.32 (t, J = 8 Hz, 1H, H-19), 7.02 (d, J = 8 Hz, 2H), 6.74 (d, J = 7 Hz, 2H),

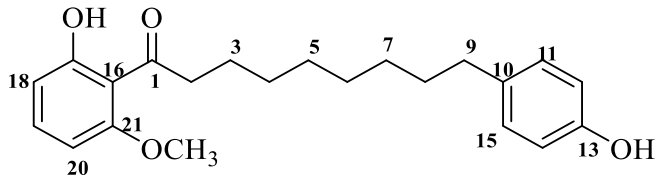

	6.57 (d, *J* = 8.5 Hz, 1H), 6.38 (d, *J* = 8.5 Hz, 2H) 4.75 (brs, 1H, -OH), 3.88 (s, 3H, -OCH_3), 3.03 (t, *J* = 7 Hz, 2H, H-2), 2.52 (t, *J* = 7.5 Hz, 2H, H-9), 1.67-1.64 (m, 2H, H-3), 1.63-1.55 (m, 2H, H-4), 1.32 (brs, 8H, H-4 to H-8) ppm.
^{13}C NMR (125 MHz, $CDCl_3$)	δ 208.1 (C-1), 164.6 (C-OH), 161.3 (C-OCH_3) 153.6 (C13-OH), [135.8, 135.0, 129.4 115.1, 111.2, 110.8, 101.3 (other aromatic protons)] 55.6 (-OCH_3), 45.0 (C-2), 35.0 (C-9), 31.7 (C-3), 29.5 (C-8), [29.4, 29.4, 29.2, 24.6 (other aliphatic protons)] ppm.
HRESIMS (m/z)	379.18603 $(M+Na)^+$

6A.9.2.6. Isolation of compound 48

Fraction pool 13 on column chromatographic purification (silica gel 100-200 mesh) afforded compound **48** as pale yellow amorphous solid.

Nature	Pale yellow amorphous solid
Melting Point	112 – 110 ^oC
FTIR (KBr, υ_{max})	3260 (OH), 2920, 2850, 1635 (C=O), 1600, 1471, 1246, 1038, 966, 876.
^{1}H NMR (500 MHz, $CDCl_3$)	δ 9.55 (brs, 2H, -OH), 7.21 (t, *J* = 8 Hz, 1H, H-19), 7.04 (d, *J* = 8 Hz, 2H), 6.75 (d, *J* = 8.5 Hz, 1H), 6.38 (d, *J* = 8 Hz, 2H), 4.75 (brs, 1H, -OH), 3.10 (t, *J* = 7.5, 2H, H-2), 2.52 (t, *J* = 7.5 Hz, 2H, H-9),

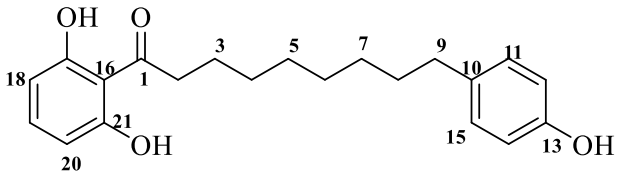

	1.71-1.65 (m, 2H, H-3), 1.60-1.55 (m, 2H, H-8), 1.31 (brs, 8H, H-4 to H-7) ppm.
^{13}C NMR (125 MHz, $CDCl_3$)	δ 207.9 (C-1), 161.2 (C17, 21-OH), 153.4 (C13-OH), [135.6, 135.2, 129.4 115.1, 110.1, 108.4 (other aromatic protons)], 44.8 (C-2), 35.0 (C-9), 31.6 (C-3), 29.4 (C-8), [29.3, 29.1, 24.4 (other aliphatic protons)] ppm.
HRESIMS (m/z)	343.19141 $(M+H)^+$

6A.9.2.7. Isolation of compound 49

Finally, fraction pool 18 on column chromatographic purification using EtOAc/*n*-hexane as eluent, gave compound **49** as colourless crystal (310 mg).

Nature	Colorless crystal
Melting Point	122-124 ^oC
FTIR (KBr, υ_{max})	3347, 2962, 2849, 2349, 1865, 1623, 1592, 1517, 1432, 1340, 1246, 1120 cm^{-1}
^{1}H NMR (500 MHz, Acetone-d_6)	δ 11.23 (s, 2H, -OH), 7.46 (s, 1H), 7.43 (s, 1H), 7.12 (t, J = 8.5 Hz, 1H, H-19), 6.57 (d, J = 8 Hz, 1H), 6.54 (d, J = 2 Hz, 1H), 6.38 (dd, J_1 = 2 Hz, J_2 = 8 Hz, 1H), 6.29 (d, J = 8.5 Hz, 2H), 3.03 (t, J = 7.5 Hz, 2H, H-2), 2.32 (t, J = 7.5 Hz, 2H, H-9), 1.59-1.53 (m, 2H, H-3), 1.45-1.39 (m, 2H, H-8), 1.20 (brs, 8H, H-4 to H-7) ppm

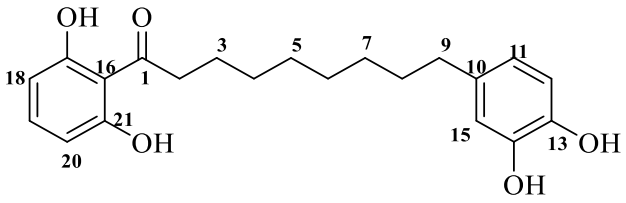

^{13}C NMR (125 MHz, Acetone-d_6)	208.0 (C-1), 162.3 (C17 and 21-OH), 144.9 (C14-OH), 142.9 (C13-OH), [135.9, 134.1, 119.3 115.5, 110.2, 107.7 (other aromatic protons)], 44.8 (C-2), 35.0 (C-9), 31.7 (C-3), 29.4 (C-8), [29.3, 29.1, 29.0, 24.3 (other aliphatic protons)] ppm.
HRESIMS (m/z)	359.18567 $(M+H)^+$

6A.9.3. α-Amylase inhibitory activity

α-Amylase inhibitory activity was analyzed based on the starch-iodine test [Xio *et al*., **2006**]. Starch containing α-amylase solution, (1U mL^{-1}) along with different concentrations of compounds (**43-49**) were incubated at 50 ^oC for 30 min. After incubation, the reaction was terminated with 1 M HCl. Then, 100 μL of iodine reagent was added to the reaction mixture. Enzymatic activity was quantified by measuring absorbance at 580 nm using Synergy 4 Biotek multimode reader (USA). The results were expressed in terms of IC_{50}, which is defined as the concentration of α-amylase inhibitor that inhibited 50 % of enzyme activity. Acarbose was used as a positive control and the percentage of inhibition was calculated using following equation,

$$\% \text{ of inhibition} = \frac{\text{Absorbance of control - Absorbance of sample}}{\text{Absorbance of control}} \times 100$$

6A.9.4. α-Glucosidase inhibitiory activity

α-Glucosidase inhibitory activity was determined using a previous method with slight modification [Apostolidis *et al*., **2007**]. Different concentrations of compounds **43-49** and 100 μL of rat intestinal α-glucosidase solution (1.0 U/mL) in 0.1M phosphate buffer (pH 6.9) were incubated at 25 °C for 10 min. After that, 50 μL of 5 mM *p*-nitrophenyl-α-D-glucopyranoside solution in 0.1 M phosphate buffer (pH 6.9) was added and the mixture was again incubated at 25 ^oC for 5 min. Enzymatic activity was quantified by measuring absorbance at 405 nm using Synergy 4 Biotek multimode reader (**USA**) and the percentage of inhibition (IC_{50}) was calculated using the above equation. The standard drug, acarbose was used as a positive control.

$$\% \text{ of inhibition} = \frac{\text{Absorbance of control - Absorbance of sample}}{\text{Absorbance of control}} \times 100$$

6A.9.5. Antiglycation property

Antiglycation property was measured as previously reported with slight modifications [Jedsadayanmata *et al*., **2005**]. Briefly, 1 mg/mL of BSA was incubated with 400 μL of α-D-glucose (500 mM) and different concentrations of compounds (**43-49**) in 0.2 M potassium phosphate buffered saline at 60 ^{o}C for 24 h. The reaction was terminated by adding 100 % trichloroacetic acid (TCA) and kept at 4 ^{o}C for 10 min. Further, the compounds were subjected to centrifugation (10,000 *x*g) and the precipitate was again dissolved in alkaline PBS. The fluorescence of the glycated end products was measured by excitation at 370 nm and emission at 440 nm using Synergy 4 Biotek multimode reader (USA). Ascorbic acid serves as a positive control. The AGEs formation was calculated using the following equation,

$$\text{AGEs formation} = \frac{\text{Fluorescence of control - Fluorescence of sample}}{\text{Fluorescence of control}} \times 100$$

6A.9.6. *In silico* studies

The molecular docking simulation studies were carried out by glide program of Schrodinger suite 2017-2. The crystal structures of human pancreatic α-amylase (PDB Code: **4GQQ**) [Williams *et al*., **2012**], human maltase glucoamylase *C*-terminal (PDB Code: **2QMJ**) [Ren *et al*., **2011**] and human maltase glucoamylase *N*-terminal protein (PDB Code: **3TOP**) [Sim *et al*., **2008**] were retrieved from the Protein Data Bank and the cleaned PDB files were further used for grid generation and simulation studies. The conformers of the ligands were prepared by ligprep and the pharmacokinetic parameters were analyzed using qikprop data. The molecular dynamics simulation studies were done by Schrodinger-Desmond programme for 3 ns using OPLS-2005 force field. The pharmacophore modeling was generated by pharmacophore hypothesis generation using seven point hypothesis.

6A.9.7.Cell culture and treatment conditions

L6 myocytes were bought from National Centre for Cell Sciences (NCCS), Pune, India and were cultured in DMEM supplemented with 10 % FBS and 0.5 % antibiotic-antimycotic (pencillin-streptomycin-amphotericin B mix) solution at 37 ^{o}C in a humidified atmosphere containing 5 % CO_2. When the myocytes were confluent, they are

treated with differentiation inducers (DMEM containing 2 % HS) for 5 days. The medium was replaced for every 2 days.

6A.9.8. Cytotoxicity assay

Cytotoxicity was evaluated using MTT assay [Mosmann *et al*., **1983**]. Cultures were maintained at 37 ^{o}C in 5 % CO_2 incubator. The cells were trypsinized and seeded in 24 well plates ($1x10^4$ cells per well). Cells after attaining the confluency, were treated with 25 μM, 50 μM, 75 μM, and 100 μM concentrations of the compounds (**43-49**) for 24 h. After incubation, cells were treated with MTT reagent (0.5 g/L) for 4 hours. Mitochondrial dehydrogenase enzyme is active only in live cells that reduce the yellow dye, MTT to purple formazan crystals. The formazan crystals were dissolved in 200 μL DMSO and the absorbance was read at 570 nm using Synergy 4 Biotek multimode reader (**USA**). The untreated cells were used as a control and the percentage of cell toxicity was calculated as,

$$\% \text{ of Cell toxicity} = \frac{\text{Absorbance of control - Absorbance of sample}}{\text{Absorbance of control}} \times 100$$

6A.9.9. Glucose uptake assay

Differentiated myotubes were pre-treated with 10, 25 and 50 μM concentration of compounds (**43-49**) for 24 h. After removal of the culture medium, the cells were washed two times with pre-cooled PBS. The cells were then treated with the fluorescent analog of glucose, 2- NBDG and incubated for 30 min. The uptake of 2-NBDG by the cells, was stopped by removing the incubation medium, and the cells were washed twice with PBS. Following incubation, the cells were washed twice with PBS, trypsinized and subsequently resuspended in 1 mL PBS. For each measurement, data from 10,000 single cell events were collected using Fluorescence Activated Cell Sorting (BD FACS Aria II, BD Bioscience, **USA**) and BD FACS Diva software. Metformin (100 μM) served as positive control [Somwar *et al*., **1998**; Tamrakar, *et al*., **2011**].

6A.9.10. Statistical analysis

The experimental results were expressed as means ± SD of triplicate measurements. The statistical analyses were performed by one-way analysis of variance, followed by Dunnett's t test. The difference was considered to be statistically significant when the *p* value was less than 0.01.

Dactyloidin and Promalabaricone B from *Myristica fatua* Houtt. Seeds Exhibit Antidiabetic Effects *via* AMPK Pathway in L6 Myotubes

As described in the first part of the final chapter, type 2 diabetes mellitus (T2DM) is a metabolic disorder, characterized by hyperglycemia. The current therapeutic antidiabetic drugs are blessings to the patients, but have some side effects. Therefore, search for new antidiabetic agents from natural sources are on-going all over the world. In this regard, we have focussed on the isolation and characterization of phytochemicals from the seeds of *Myristica fatua* Houtt var. *magnifica* (Bedd.) Sinclair and antidiabetic activity of dactyloidin and promalabaricone B *via* AMPK pathway in L6 myotubes will be discussed.

6B.1. Aim and scope of the present work

Type 2 diabetes mellitus (T2DM) is a group of heterogeneous metabolic disorder, characterized by hyperglycemia because of defects in impaired insulin secretion or insulin resistance on target tissues [DeFronzo *et al*., **2015**]. The incidence of T2DM has increased over the last few decades, and it is predicted to rise to 629 million by 2045 [IDF Report, **2017**]. The current therapeutic approaches for preventing T2DM is the inhibition of carbohydrate-hydrolyzing enzymes, delaying of advanced glycated end products formation (AGEs) and increasing of glucose uptake in myocytes or adipocytes [Trapero *et al*., **2012**; Prabhakar *et al*., **2011**]. Glucose uptake in myocytes is mediated by two major signals, i.e., insulin and exercise. The insulin-dependent pathway involves an insulin-receptor substrate (IRS)/phosphoinositide 3-kinase (PI3K)/protein kinase B (AKT) signal and insulin-independent glucose uptake or exercise stimulated mechanism involving the 5′-adenosine-monophosphate- activated protein kinase (AMPK) signal [Lizcano *et al*., **2002**; Sweeney *et al*., **1999**]. The schematic representation of AMPK pathway is shown in **Figure 6B.1.**

Activation of AMPK could enhance insulin sensitivity, enhance glucose uptake in myocytes and adipocytes, and inhibit glucose production in the liver hepatocytes [Xiong *et al*., **2018**]. Moreover, AMPK pathway is one of the major biological pathways involved

in maintaining energy homeostasis and there is a growing interest to target it for pharmacological manipulation to combat the insulin resistance. Interestingly, several drugs that are being used in the treatment of diabetes exert their beneficial effects through the indirect activation of AMPK. However, to date, no direct AMPK activators have reached clinical use for the treatment of metabolic disease. In this regard further research on AMPK's regulation will lead to new activation strategies or to the development of clinically efficacious AMPK activator, to make it as an attractive target for T2DM. In this context, several research efforts have screened for effective antidiabetic agents from natural resources and their molecular mechanism for regulating blood glucose levels are ongoing all over the world [Han *et al*., **2015**; Zhu *et al*., **2017**; Yuan *et al*., **2014**].

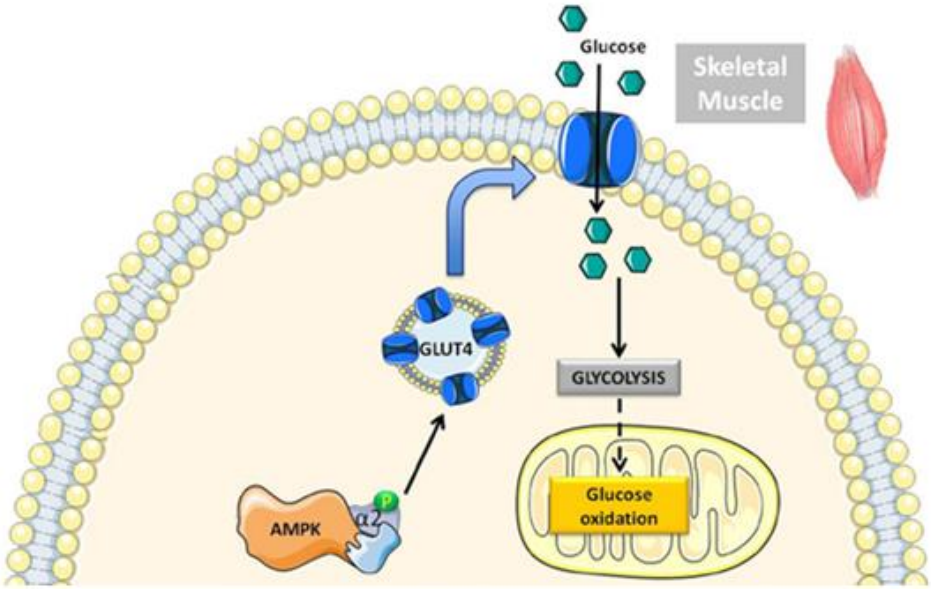

Figure 6B.1. Schematic representation of AMPK pathway

The detailed literature survey of *Myristica fatua* Houtt. and antidiabetic effect of compounds isolated from the stem bark of *Myristica fatua* Houtt. was described in the first part of the final chapter. In the second part of this chapter, phytochemical investigation of the seeds of *M. fatua* Houtt. resulted in the isolation of seven major compounds; trimyrisitin (**50**), 1-(2,6-dihydroxyphenyl)tetradecan-1-one (**51**), malabaricone A (**52**), malabaricone B (**53**), malabaricone C (**54**), dactyloidin (**55**) and promalabaricone B (**56**). Herein, we also evaluated the antidiabetic effect of dactyloidin (**55**) and promalabaricone B (**56**) and to elucidate the molecular mechanism leading to improved glucose uptake in L6 skeletal muscle cells.

6B.2. Plant material collection, isolation and characterization of compounds from *Myristica fatua* Houtt. seeds

6B.2.1. Plant material

Seeds of *Myristica fatua* Houtt. var. *magnifica* (Bedd.) Sinclair was collected from Agasthyamalai biosphere reserve of south Western Ghats region of Kollam District, Kerala, India in December 2016. The plant material was authenticated by plant taxonomist of Jawaharlal Nehru Tropical Botanic Garden and Research Institute, Palode, Kerala, India and a voucher specimen (**TBGT 83441**) is deposited in the herbarium of repository of the same institute.

6B.2.2. Isolation and characterization of secondary metabolites

850 g of the dried and milled stem bark of *Myristica fatua* was extracted with dichloromethane yielded 60 g of dichloromethane extract; this was subjected to silica gel (100-200 mesh) column chromatography using *n*-hexane, *n*-hexane-EtOAc gradient and EtOAc. Eighteen fractions of 200 mL each were collected and concentrated at 50 ^{o}C under reduced pressure. From the fraction pools 1 and 2, afforded compound **50** (7 g) as white amorphous solid. The fraction pool 3 and 4 was subjected to column chromatographic separation using 3 % EtOAc in *n*-hexane as eluent which afforded compound **51** as pale yellow solid (3 g). Similarly, silica gel column chromatographic separation (100-200 mesh) of fraction pool 6 yielded compound **52** (25 mg) as a pale yellow solid. Fraction pool 7 on column chromatographic separation using 12 % EtOAc/*n*-hexane as eluent gave compound **53** (15 mg) as white amorphous solid. The compound **54** (8 g) was obtained as major component in the fraction pools 8 to 10, as pale amorphous solid. From the fraction pool 11 afforded compound **55** (45 mg) as white crystalline solid. Finally, fraction pool 13 and 14 on column chromatographic separation using 25 % EtOAc/*n*-hexane as eluent, afforded compound **56** as colourless solid (150 mg). The structures of the compounds isolated from the seeds of *Myristica fatua* are shown in **Figure 6B.2.**

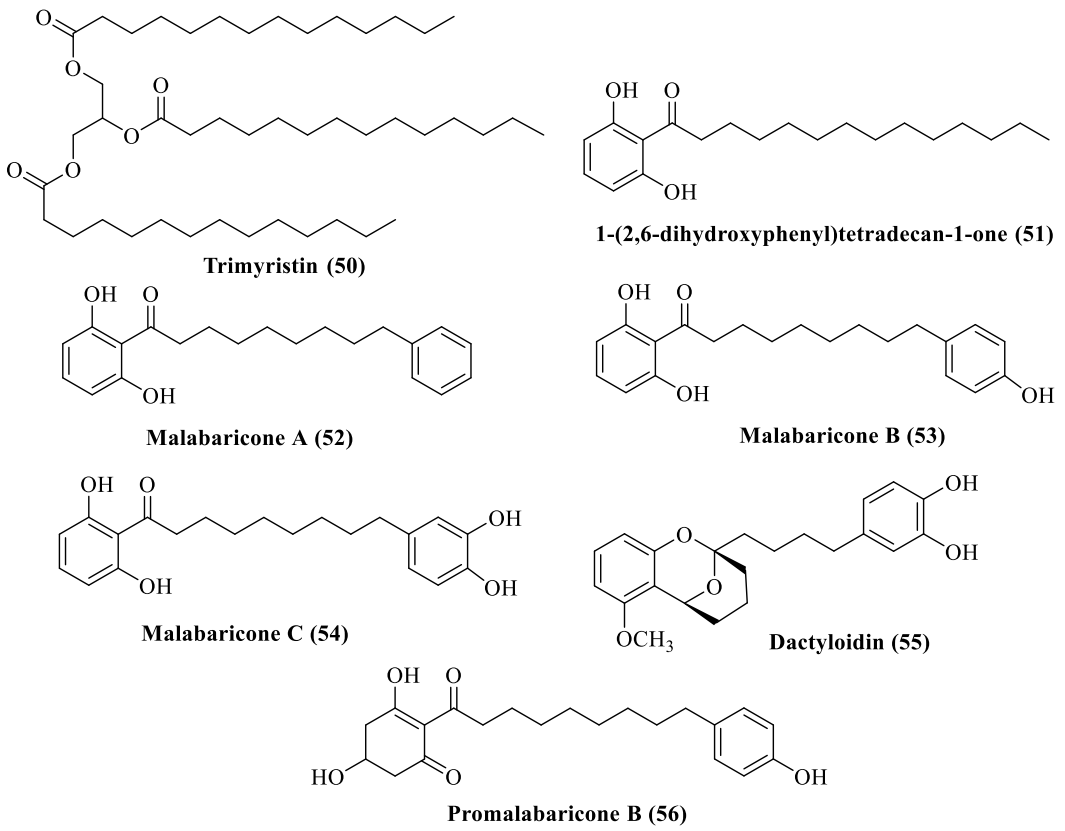

Figure 6B.2. Structures of the compounds isolated from the seeds of *Myristica fatua*

The ^{1}H NMR spectrum of compound **55** displayed the presence of two aromatic rings; one benzene ring with three substituents adjacent to each other was shown by the two doublets at δ_H 6.47 (J = 8 Hz, 1H) ppm and 6.41 (J = 8 Hz, 1H) ppm, a double doublet at δ_H 7.10 (J_1 = 8.5, J_2 = 8 Hz, 1H) ppm; a 1, 4-disubstituted aromatic moiety at δ_H 7.03 (d, J = 8.5 Hz, 2H) ppm and 6.75 (d, J = 8.5 Hz, 2H) ppm. A sharp singlet at δ_H 3.81 ppm in the 'H NMR spectrum and a methyl signal at δ_C 55.4 in the ^{13}C NMR spectrum indicated the presence of methoxyl group attached to a benzene ring. The broad doublet appeared at δ_H 5.15 ppm in the 'H NMR spectrum was assigned to the proton attached to C-1 position. Based on the complete analysis of NMR spectra (**Figure 6B.3-8**), single crystal X-ray analysis (**Figure 6B.9**) and the literature reports [Herath *et al*., **1998**] the compound was dactyloidin and the structure of the compound is shown below.

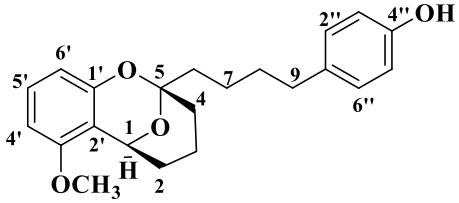

Dactyloidin (55)

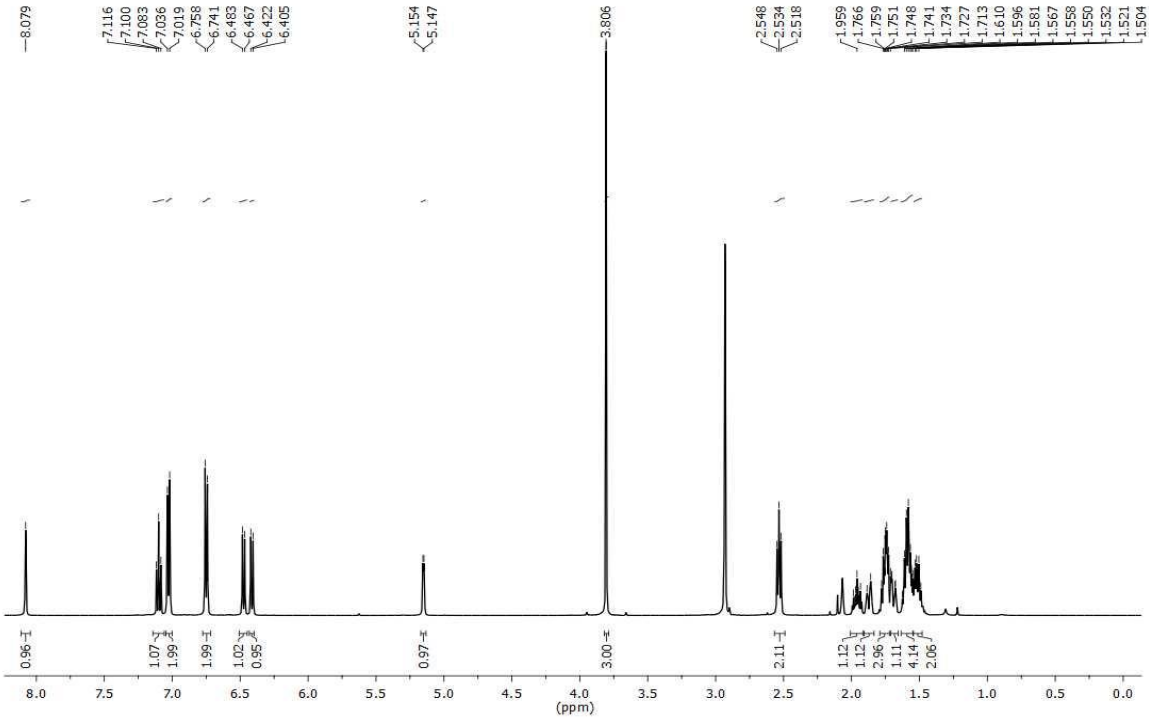

Figure 6B.3. ^{1}H NMR spectrum (500 MHz, Acetone-d_6) of dactyloidin (**55**)

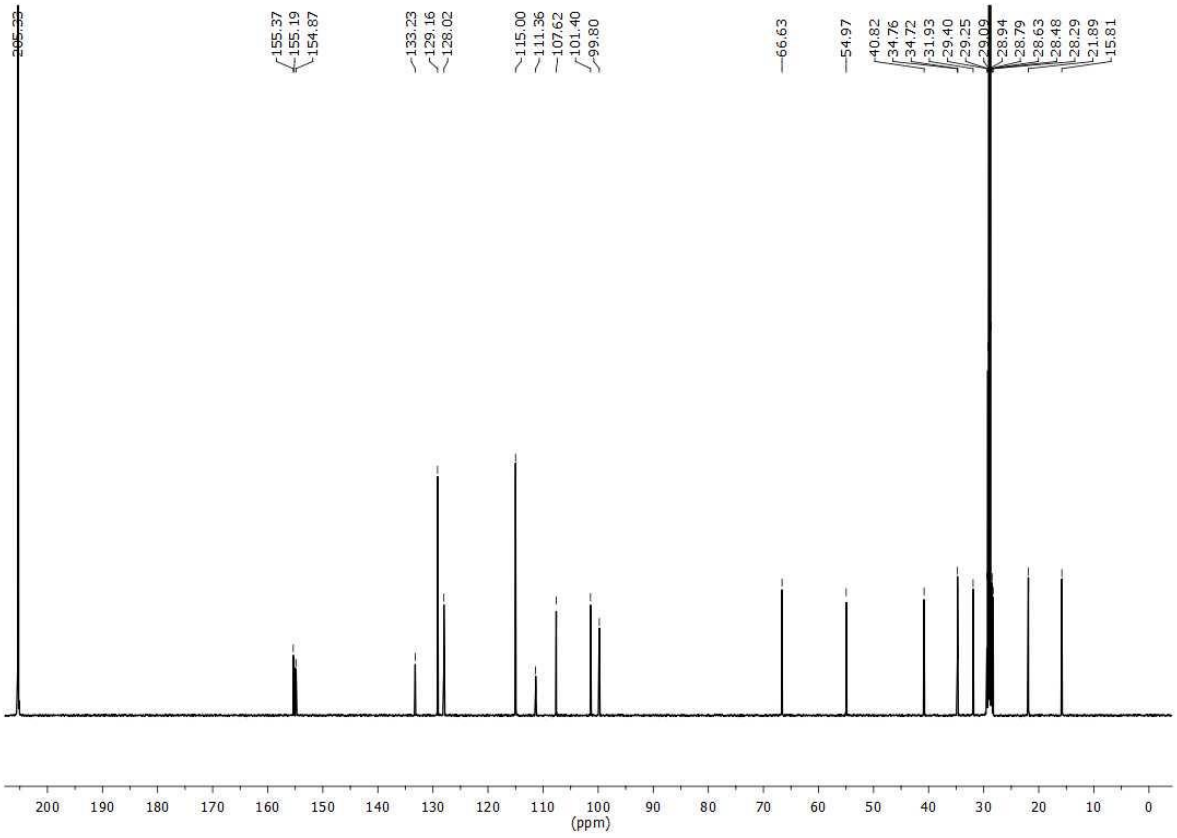

Figure 6B.4. ^{13}C NMR spectrum (125 MHz, Acetone-d_6) of dactyloidin (**55**)

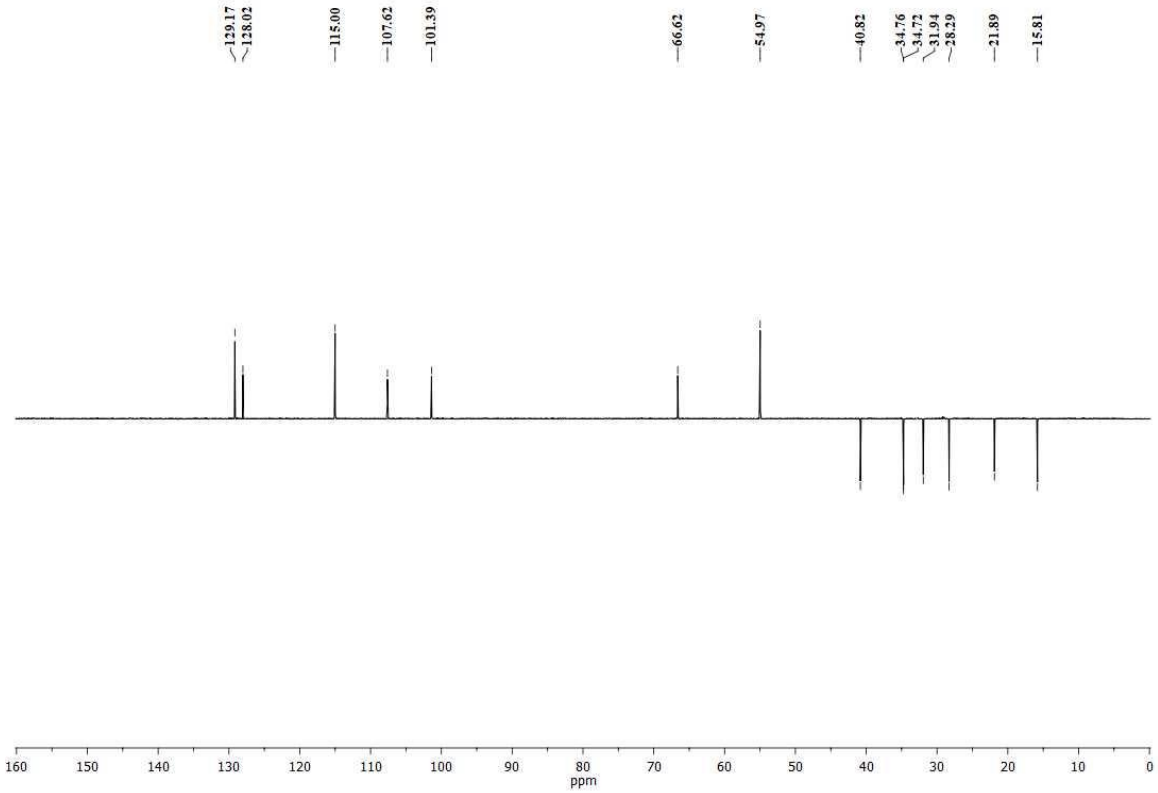

Figure 6B.5. DEPT 135 NMR spectrum (125 MHz, Acetone-d_6) of dactyloidin (**55**)

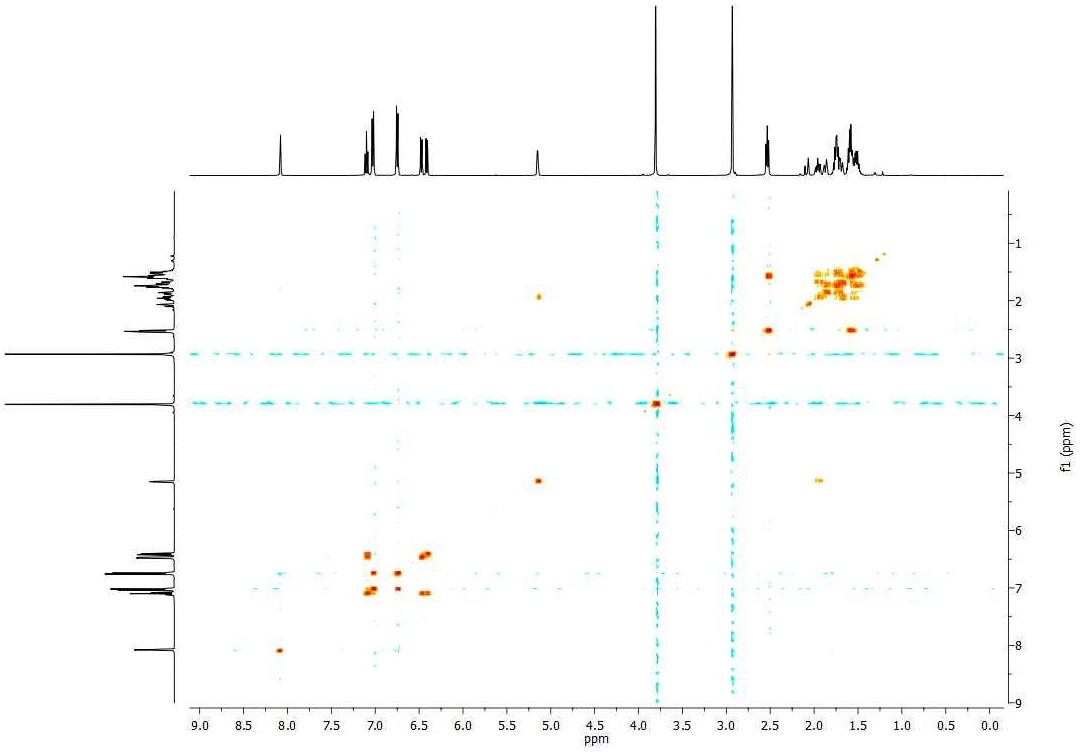

Figure 6B.6. ^{1}H-^{1}H COSY NMR spectrum (500 MHz, Acetone-d_6) of dactyloidin (**55**)

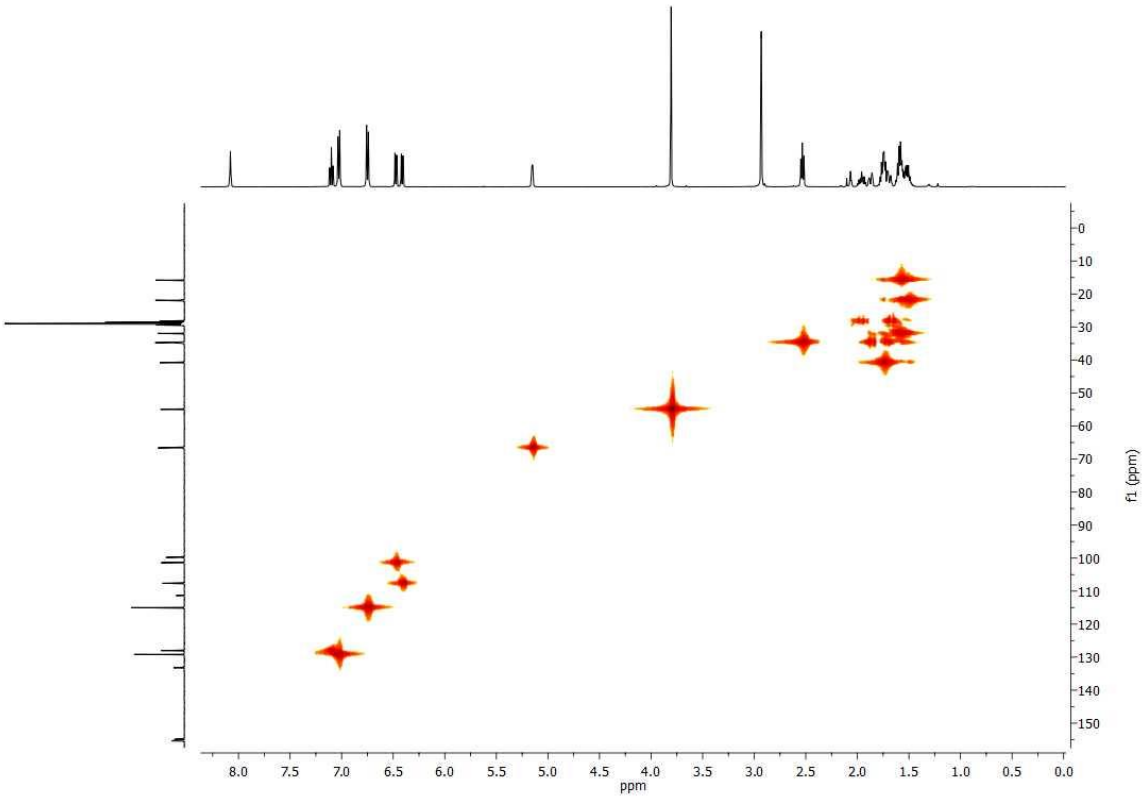

Figure 6B.7. HMQC NMR spectrum (125 MHz, Acetone-d_6) of dactyloidin (**55**)

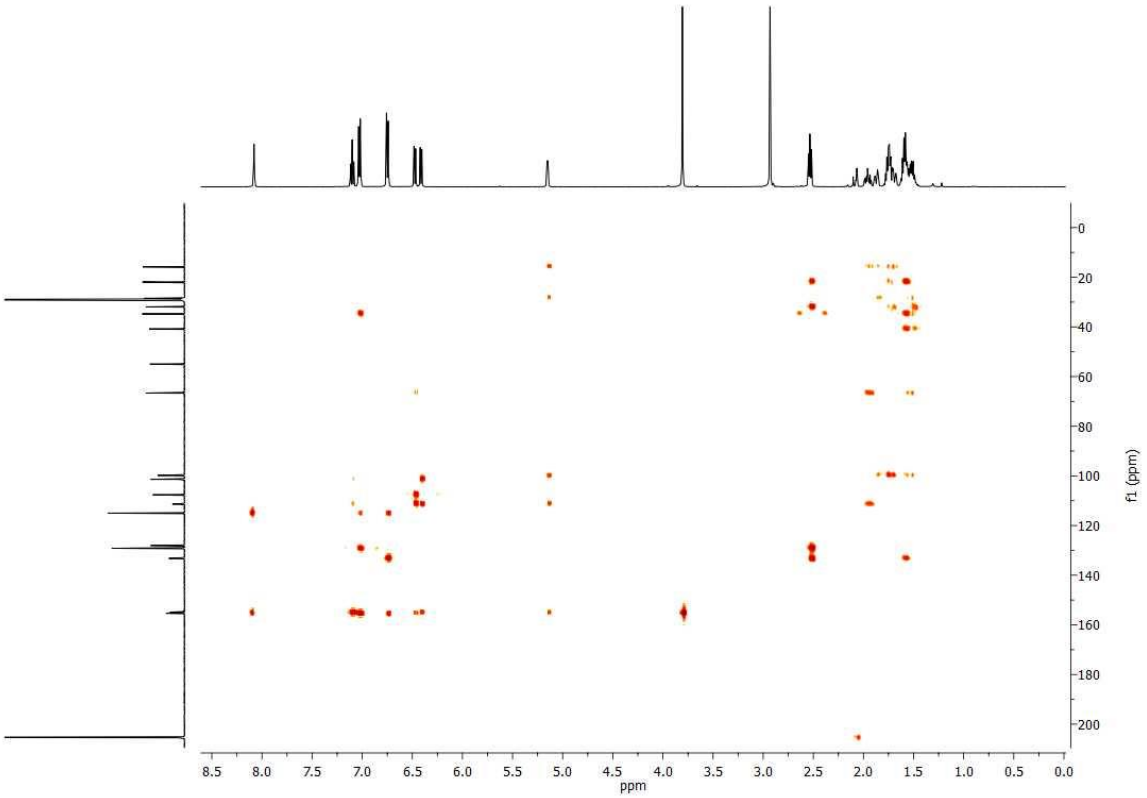

Figure 6B.8. HMBC NMR spectrum (125 MHz, Acetone-d_6) of dactyloidin (**55**)

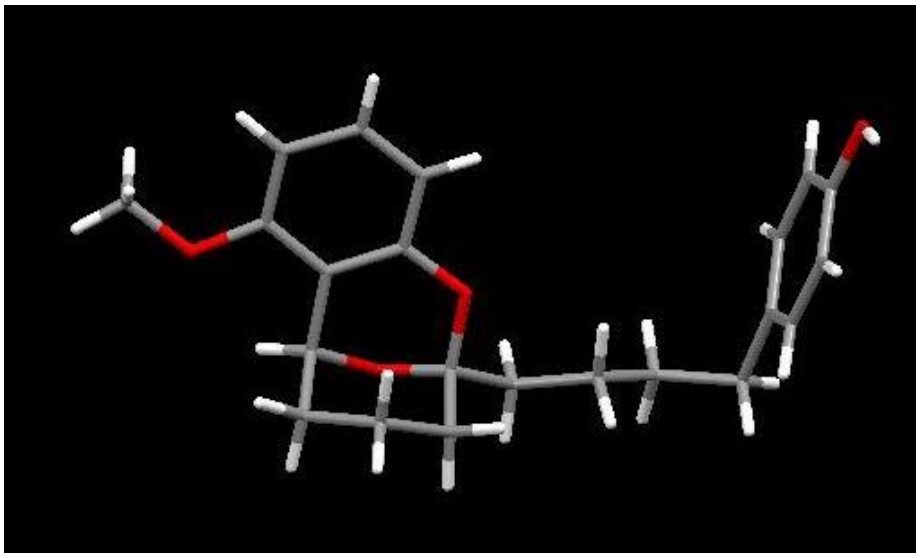

Figure 6B.9. Single crystal X-ray analysis of dactyloidin (**55**)

Compound **56 (**Promalabaricone B**)** was obtained as a pale yellow amorphous solid and displayed a molecular ion peak at m/z 383.1856 for $[M+Na]^+$ in the HRESIMS (calculated for $C_{21}H_{28}NaO_5$: 383.1834); this result together with the ^{13}C NMR data, allowed the assignment of the molecular formula $C_{21}H_{28}O_5$ to compound **56**. The IR spectrum showed absorptions for hydroxyls at 3425, methylenes at 2920 and 2854 and carbonyls at 1720 and 1640 $cm^{-1.}$ The ^1H NMR spectrum showed a broad singlet (δ_H 7.95 ppm) for aromatic hydroxyl group, a 1, 4-disubstituted [δ_H 6.87 (d, J = 8.5 Hz, 2H) and 6.60 (d, J = 8.5 Hz, 2H)] aromatic moiety. The enclosable hydroxyl group displayed a broad doublet at δ_H 4.31 ppm. The hydroxyl group attached to the methine proton showed a multiplet in the range δ_H 4.25-4.21 ppm. The $-CH_2-$ group flanking the aromatic moiety displayed a triplet at δ_H 2.85 ppm. The $-CH_2-$ group neighbouring to the carbonyl group displayed a triplet at δ_H 2.37 ppm. Another four methylene groups showed a broad singlet at δ_H 1.20 ppm. From detailed 1D and 2D NMR spectra (**Figure 6B.10-15**) and HRESIMS analysis and in comparison with literature reports [Van *et al.*, **2000**] compound **56** had the structure promalabaricone B and the structure is shown below.

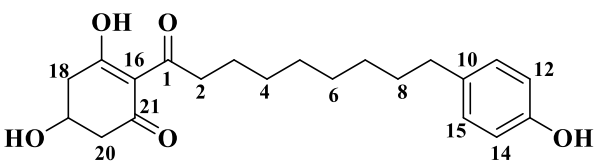

Promalabaricone B (56)

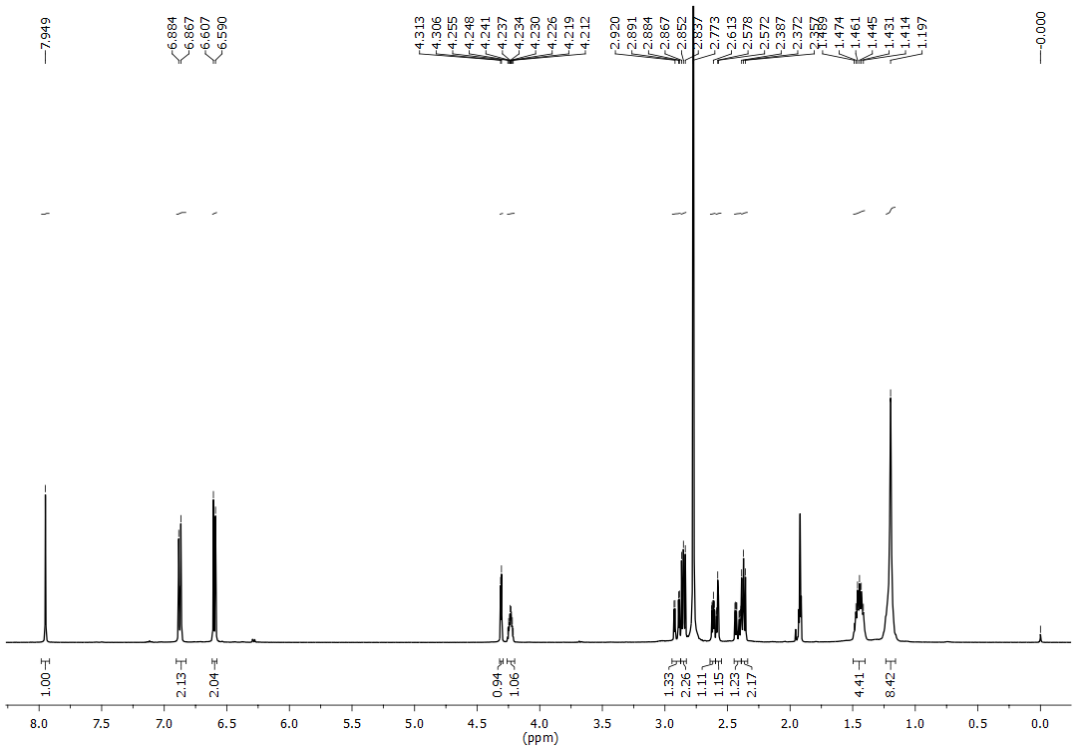

Figure 6B.10. ^{1}H NMR spectrum (500 MHz, Acetone-d_6) of promalabaricone B (**56**)

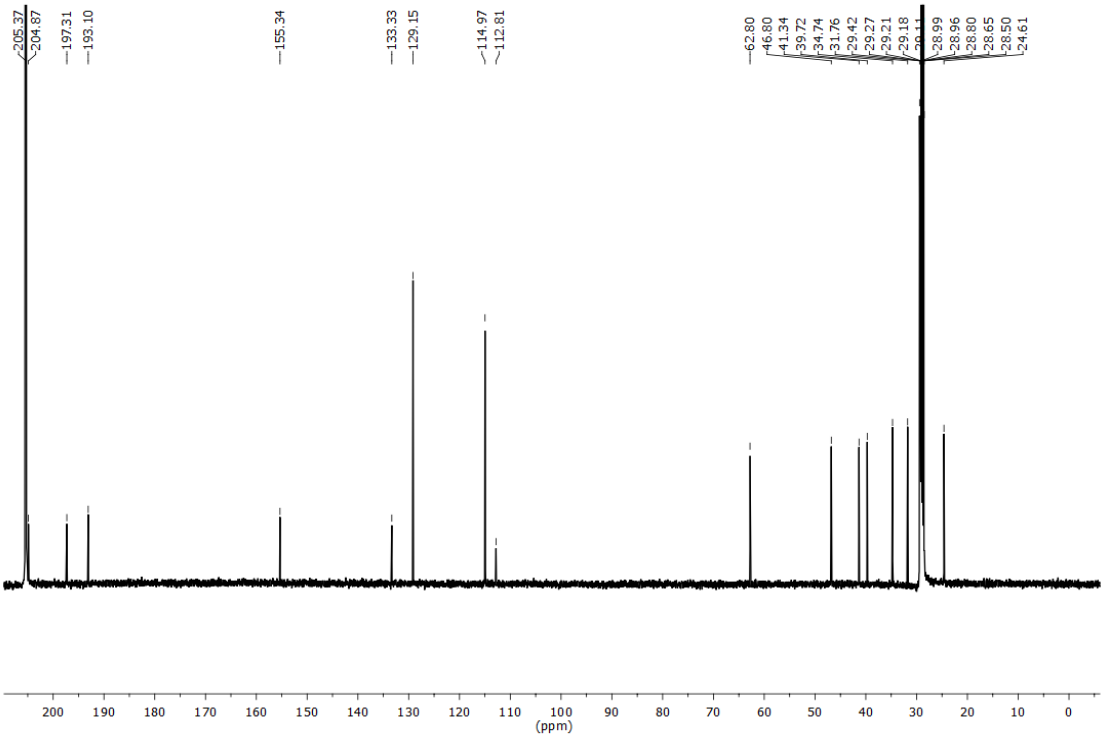

Figure 6B.11. ^{13}C NMR spectrum (125 MHz, Acetone-d_6) of promalabaricone B (**56**)

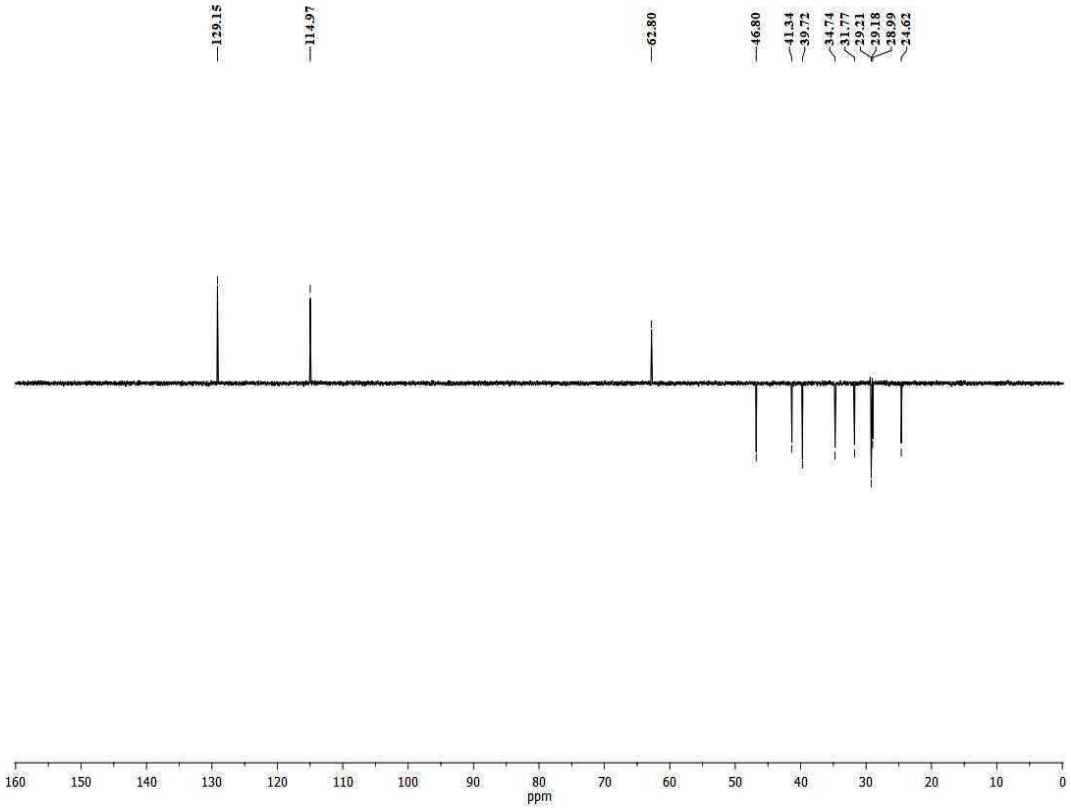

Figure 6B.12. DEPT 135 NMR spectrum (125 MHz, Acetone-d_6) of promalabaricone B (**56**)

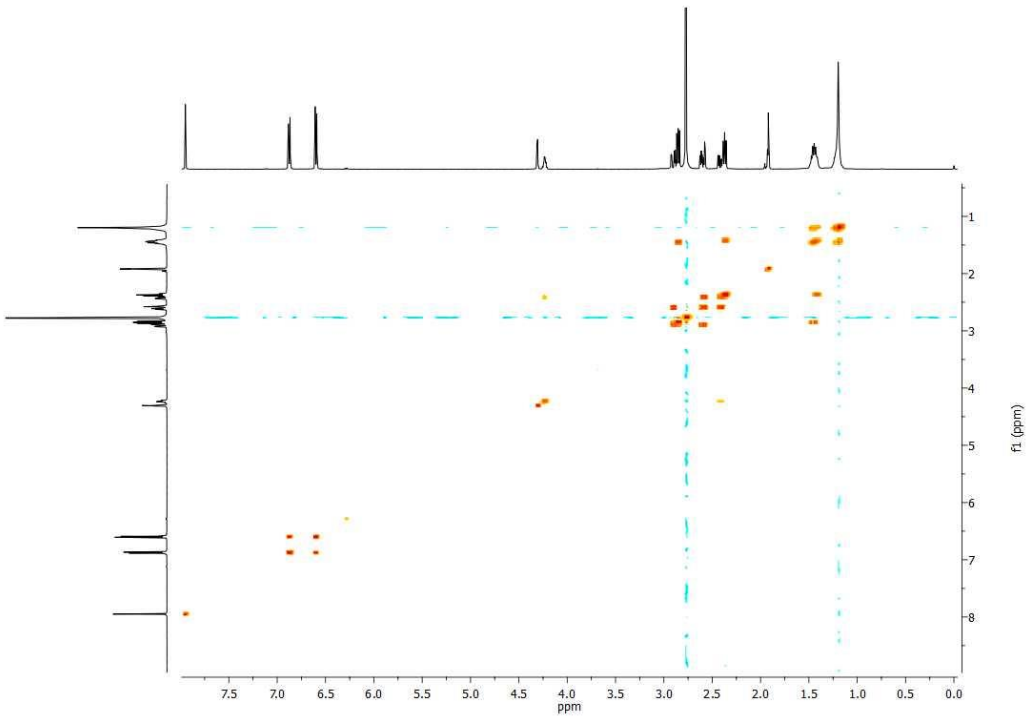

Figure 6B.13. ^{1}H-^{1}H COSY NMR spectrum (500 MHz, Acetone-d_6) of promalabaricone B (**56**)

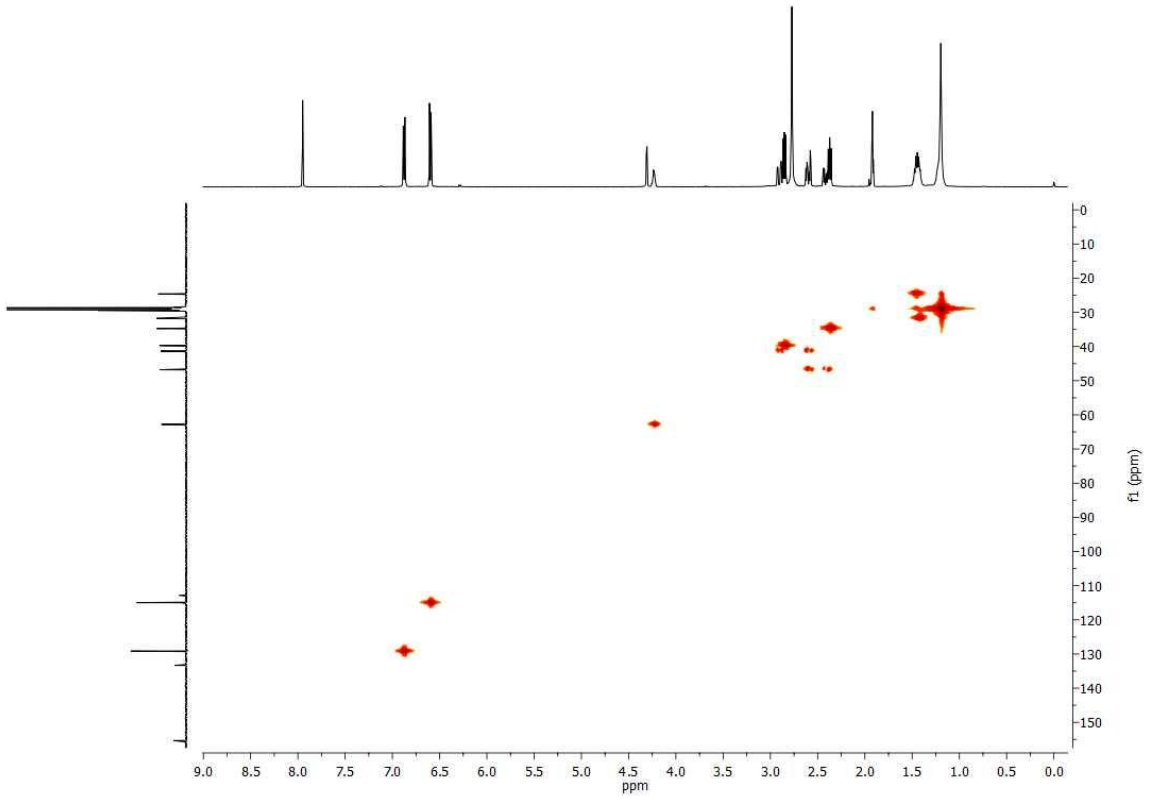

Figure 6B.14. HMQC NMR spectrum (125 MHz, Acetone-d_6) of promalabaricone B (**56**)

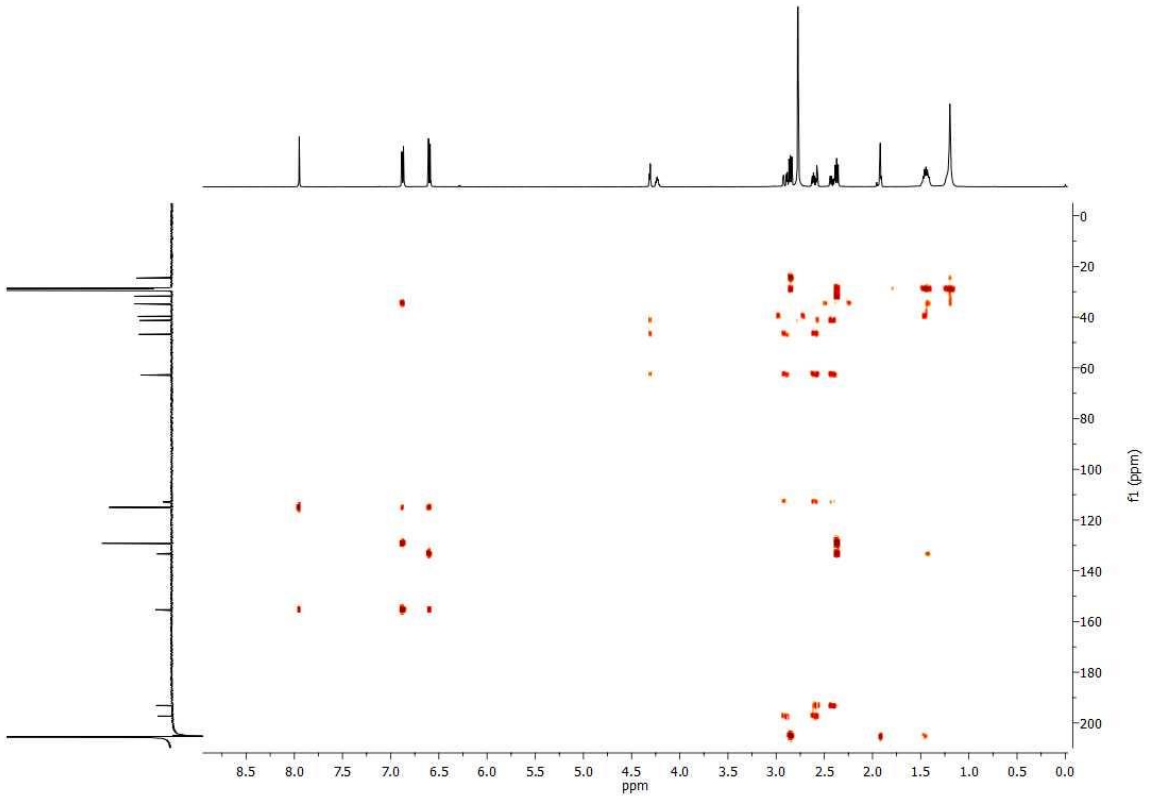

Figure 6B.15. HMBC NMR spectrum (125 MHz, Acetone-d_6) of promalabaricone B (**56**)

6B.3. Antidiabetic property of dactyloidin (55) and promalabaricone B (56)

6B.3.1. Effect on digestive enzymes

One of the therapeutic methods for alleviating T2DM is to reduce the glucose absorption from the intestine through the inhibition of digestive enzymes such as α-amylase and α-glucosidase. α-Amylase present in the saliva and pancreatic juice breaks down large insoluble carbohydrate molecules into oligosaccharides. α-Glucosidase is mainly found in the brush border in the small intestine, which breakdown disaccharides to glucose. Inhibitors of α-amylase and α-glucosidase can delay the digestion of carbohydrates in the small intestine and reduce the level of postprandial blood glucose. From this point of view, many studies have examined for safe and effective inhibitors of α-amylase and α-glucosidase from medicinal plants to treat T2DM. Herein, first we evaluate the inhibitory effect of porcine pancreatic α-amylase and rat intestinal α-glucosidase on dactyloidin (**55**) and promalabaricone B (**56).** Dactyloidin (**55**) and promalabaricone B (**56)** exhibited moderate inhibitory activity on α-amylase with IC_{50} value of 32.55 ± 0.833 μM and 81.97 ± 1.233 μM respectively, the positive control acarbose displayed IC_{50} value of 8.197 ± 1.233 μM. The dactyloidin (**55**) and promalabaricone B (**56**) exhibited significant α-glucosidase inhibitory activity with IC_{50} value of 55.08 ± 0.857 μM and 32.67 ± 0.469 μM. The standard α-glucosidase inhibitor showed IC_{50} value of 52.04 ± 872 μM. Taken together, these results recommend that dactyloidin (**55**) and promalabaricone B (**56)** has dual inhibitory activity against α-glucosidase and α-amylase and alleviates hyperglycemia, making it as a potential drug candidate for the management of T2DM.

6B.3.2. Antiglycation property

It is well recognized that AGE's and their derivatives are involved in the pathogenesis of several diabetic complications such as retinopathy, nephropathy, atherosclerosis and neurodegenerative diseases. A plethora of natural products and their synthetically modified motifs showed promising antiglycation property. Exhilarated with these observations, we tested the protein glycation property of dactyloidin (**55**) and promalabaricone B (**56**). The dactyloidin (**55**) and promalabaricone B (**56**) exhibited moderate protein glycation property with IC_{50} value of 262.73 ± 0.577 μM and 227.26 ± 0.773 μM. Here, we used ascorbic acid as a positive control that shows IC_{50} value of 155.38 ± 0.547 μM.

6B.3.3.Molecular simulation studies

In order to predict the probable binding modes of dactyloidin (**55**) and promalabaricone B (**56)** on digestive enzymes present in our body, we have selected human pancreatic *α*-amylase (**4GQQ**), human maltase-glucoamylase *C*-terminal (**2QMJ**) and *N*-terminal (**3TOP**) for *in silico* studies. In detailed pharmacokinetic studies, dactyloidin (**55**) and promalabaricone B (**56)** displayed significant ADME/T properties (**Table 6A.1**). The dactyloidin (**55**) and promalabaricone B (**56)** are nontoxic to central nervous system with a CNS value of 0 and -2. The hydrogen bond donor (HBD), hydrogen bond acceptor (HBA), octanol-water partition coefficient (QPlogPo/w) and percentage of human oral adsorption of dactyloidin (**55**) and promalabaricone B (**7)** were (1 and 2), (3 and 6.2), (5.338 and 3.169), and (100 and 81.22) respectively and it also satisfy Lipinski Rule of Five; which demonstrates that dactyloidin (**55**) and promalabaricone B (**7)** could act as a promising drug candidate.

Table 6B.1. ADME/T properties of compound **55** and **56**

Sl. No	**Dactyloidin (55)**	**Promalabaricone B (56)**
M.W	354.445	360.449
#stars	0	0
#rotor	7	13
CNS	0	-2
SASA	665.093	725.605
FISA	54.673	209.734
HBA	3	6.2
HBD	1	2
QPlogKhsa	0.947	0.219
HOA	3	2
% HOA	100	81.422
QPlogPo/w	5.338	3.169
QPlogS	-6.16	-5.009
R Of Five	1	0

M.W. (Molecular Weight):130.0 to 725.0; #stars (few stars-more drug-like): 0 to 5; #rotor (Number of non-trivial and non-hindered rotatable bonds):0 to 15; CNS (Central Nervous System activity): -2 to +2; SASA (Total solvent accessible surface area in

square angstroms): 300.0 to 1000.0 FISA (Hydrophilic component of total solvent accessable area): 7.0 to 333.0; HBA (Hydrogen bond acceptor): 2.0 to 20.0; HBD (hydrogen bond donor): 0.0 to 6.0; QPlogKhsa (binding to human serum albumin): -1.5 to 1.5; HOA (Human Oral Absorption): 1, 2, or 3 for low medium, and high; % HOA (Percent Human Oral Absorption): >80 % is high, <25 % is poor; QPlogPo/w (octanol/water partition coefficient): -2.0 to 6.5; QPlogS (Aqueous solubility): -6.5 to 0.5; Ro5 (Number of violations of Lipinski's rule of five): maximum is 4.

In human pancreatic α-amylase enzyme (**4GQQ**), dactyloidin (**55**) and promalabaricone B (**56)** exhibits G-Score/D-Score of -2.32 and -2.87 kcal/mol respectively. In the case of *N*-terminal human maltase glucoamylase (**2QMJ**) dactyloidin (**55**) and promalabaricone B (**56)** shows G-Score/D-Score of -3.37 and -4.78 kcal/mol respectively. The hydroxycarbonyl- terminal catalytic domain of human maltase glucoamylase (**3TOP**) displayed G-Score/D-Score of -5.69 and -6.81 kcal/mol respectively. The phenolic -OH of dactyloidin (**55**) form strong H-bond with ASP 236 and –O with SER 245 of **4GQQ**. While in **3TOP** and **2QMJ**, the phenolic -OH forms H-bonds with ASP 203 and ARG 202 and there are π-stacking interactions of the two terminal benzene rings with LYS 480 and PHE 575. The promalabaricone B (**56)** interacted moderately with the **2QMJ** protein via hydrogen bond interactions. The *p*-hydroxy phenolic group and secondary hydroxyl group formed a strong H-donor interaction with the ASP 327 and ASP 474 residues. The acyl group forms a strong hydrogen bond acceptor interaction with THR 205. The promalabaricone B (**56)** ligand and **3TOP** protein interaction sites were mainly composed of hydrogen bonding and arene-arene interactions. The *p*-hydroxy phenolic group and secondary hydroxyl group showed a strong H-donor interaction with the ASP 1279 and GLY 1365 residue. The acyl group formed a strong hydrogen bond acceptor interaction with TYR 1251. The phenyl moiety displayed a strong Π- Π stacking interaction with TYR 1251 residue. In addition to these, the enolisable hydroxyl group formed salt bridge with ARG 1377. The 2D interaction diagram of dactyloidin (**55**) and promalabaricone B (**56)** with **4GQQ, 2QMJ** and **3TOP** is depicted in **Figure 6B.16.**

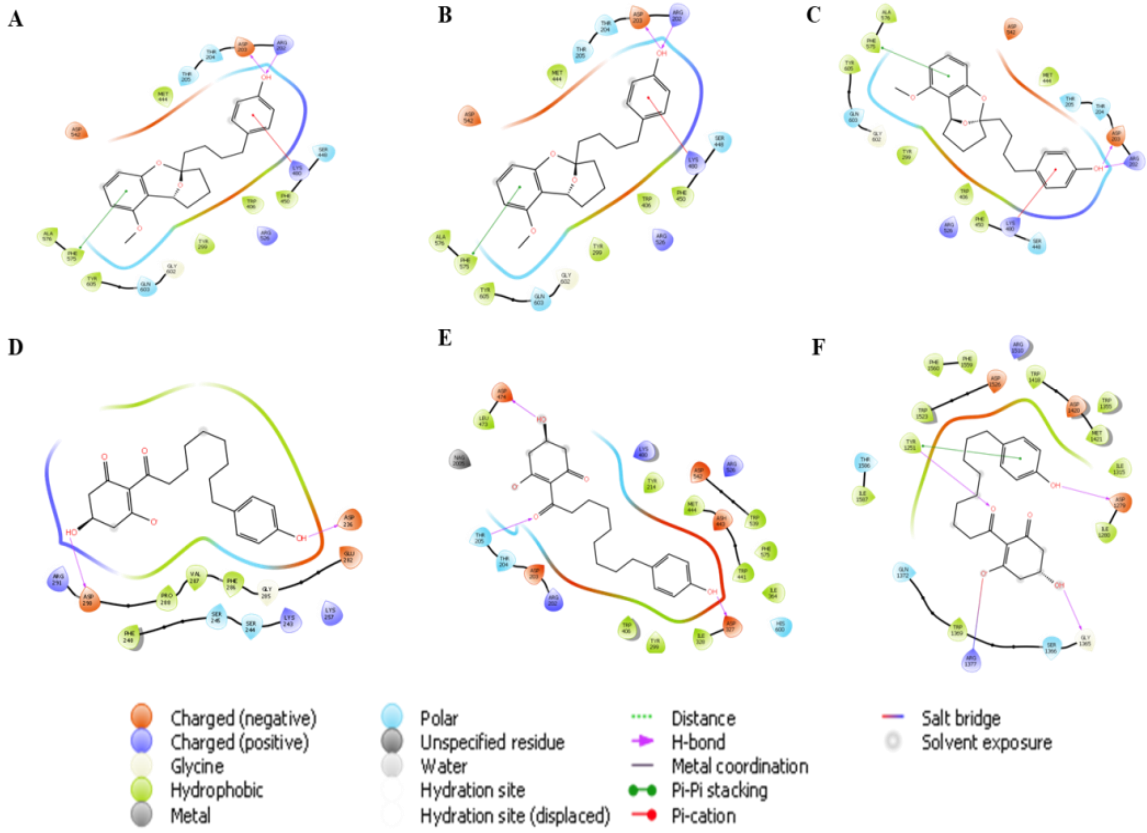

Figure 6B.16. 2D interaction diagram of dactyloidin with **4GQQ** (A)**, 2QMJ** (B) and **3TOP** (C) and promalabaricone B with **4GQQ** (D), **2QMJ** (E) and **3TOP** (F)

Molecular dynamics simulations were carried out for 3 ns using OPLS-2005 forcefield to find out the stability and conformational flexibility of the ligand promalabaricone B (**56**) inside the binding pocket of **3TOP**. The root mean square deviation (RMSD) of the protein (left Y-axis) and the ligand (right Y-axis) shows that the protein and the ligand are fluctuated from the initial binding mode around 4.5 Å and attains a stable conformation at the end of the trajectory (**Figure 6B.17A**). The interactions of the **3TOP** protein and the ligand promalabaricone B (**56**) is well depicted in the histogram (**Figure 6B.17B)** and it shows that there is a strong H-bonded interaction between the *p*-hydroxy phenolic group and ASP 1279 which lasts for 92 % of interaction time whereas the H-bond between enolizable hydroxyl and ARG 1371 lasts for 106 % and the acyl group and TRP 1369 lasts for 62 % of the simulation time. In addition to these interactions, H-bond formed by the residues TRP 1251, GLN 1286, GLN 1372 and GLY 1365 and hydrophobic interactions of TYR 1251, ILE 1280, ILE 1315, TRP 1355, TRP 1369, TRP 1418, PHE 1559, ARG 1582 and HIS 1584 are the major binding forces which hold the ligand PMB inside the binding site during the simulation time.

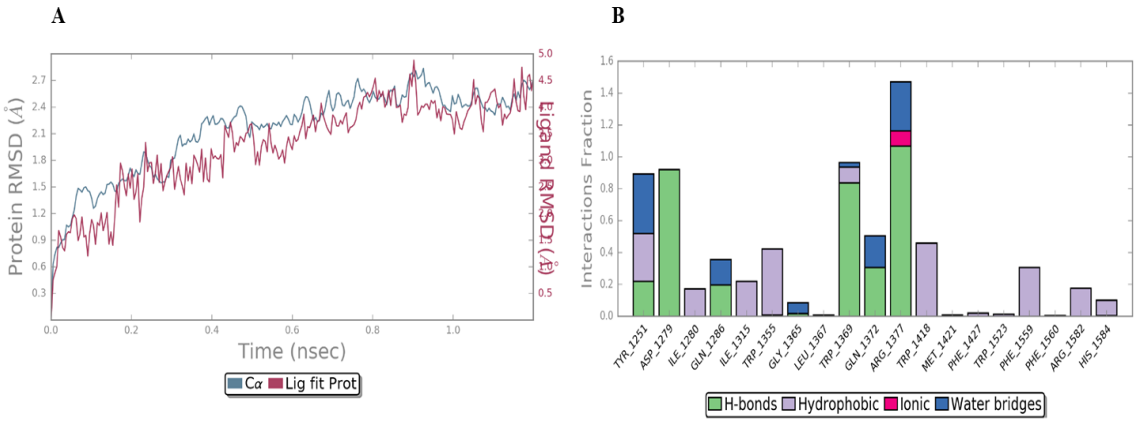

Figure 6B.17. (A) Root mean square deviation of **3TOP** with promalabaricone B and (B) **3TOP** - promalabaricone B contacts

6B.3.4. Cell toxicity

Cell toxicity studies were performed in L6 cell lines by MTT assay. Cells were treated with different concentration of dactyloidin (**55**) and promalabaricone B (**56)** ranging from 2.5 μM to 100 μM and after 24 h treatment it was found that dactyloidin (**55**) and promalabaricone B (**56)** was less than 20 % toxic up to 2.5 μM concentration (**Figure 6B.18**). This concentration was taken for further studies.

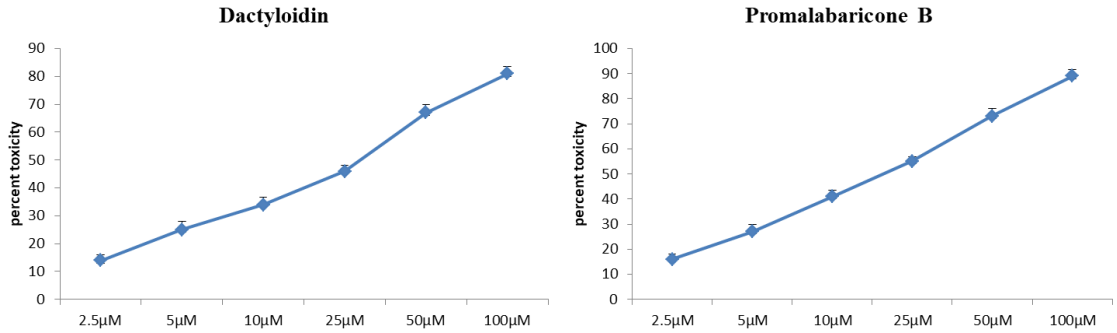

Figure 6B.18. Cytotoxicity of dactyloidin (**55**) and promalabaricone B (**56)** was evaluated in L6 myoblast at varying concentrations. Values are the mean of three independent experiments done in duplicates.

6B.3.5. 2-NBDG uptake

Myocytes are the key player of glucose consumption in our body and majority of insulin stimulated glucose uptake occurs here. The imbalance of glucose homeostasis leads to T2DM. The effect of dactyloidin (**55**) and promalabaricone B (**56**) on glucose uptake was assessed in differentiated skeletal myotubes. From flow cytometry analysis, we found that dactyloidin (**55**) and promalabaricone B (**56)** have a remarkable potential to increase glucose uptake in cells to an extent of 31.5 % and 46.3 % respectively, which

was higher than that of positive control, metformin (35.2 %, P≥0.05) (**Figure 6B.19**). The results suggest the possibility that dactyloidin (**55**) and promalabaricone B (**56**) can activate downstream biological pathways of glucose uptake that's by revealing its therapeutical potential.

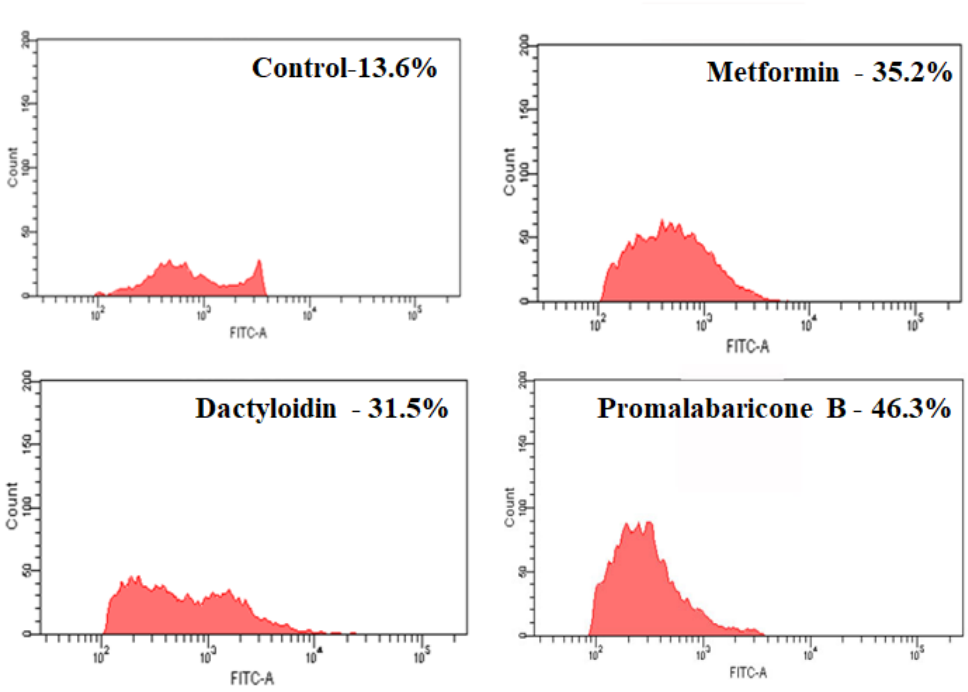

Figure 6B. 19. 2-NBDG uptake in L6 skeletal myotubes. Flow cytometry analysis carried out using 2- NBDG in differentiated L6 myotubes by plotting cell count against FITC revealed that 13.6 % uptake in NBDG control cells, 35.3 % in positive control treated cells, 31.5 % uptake cells treated with dactyloidin (**55**) and 46.3 % uptake cells treated with promalabaricone B (**56**).

6B.3.6. GLUT4 translocation

Glucose uptake in myocytes was achieved *via* glucose transporters, which are membrane proteins that facilitate the transport of glucose across the plasma membrane. Among 13 transporter proteins in our body, GLUT4 is highly expressed in skeletal muscle and translocated to the plasma membrane by insulin and other stimuli. Depletion of GLUT4 in either adipose tissue or skeletal muscle causes insulin resistance. To gain further insight into the mechanisms by which dactyloidin (**55**) and promalabaricone B (**56**) acts as a potential antidiabetic molecule, GLUT4 upregulation in L6 myotubes were examined by immunoblot analysis. Results (**Figure 6B.20**) confirmed that dactyloidin (**55**) and promalabaricone B (**56)** can activate GLUT4 expression in differentiated cells,

showing its efficacy for diabetic management. The changes in GLUT4 protein levels could beneficially translate into the normal physiology thus to combat the insulin resistance. So, therapeutic strategies to enhance GLUT4 expression may facilitate drug discovery. Therefore the mechanisms that regulate GLUT4 expression are much gaining more importance in this field.

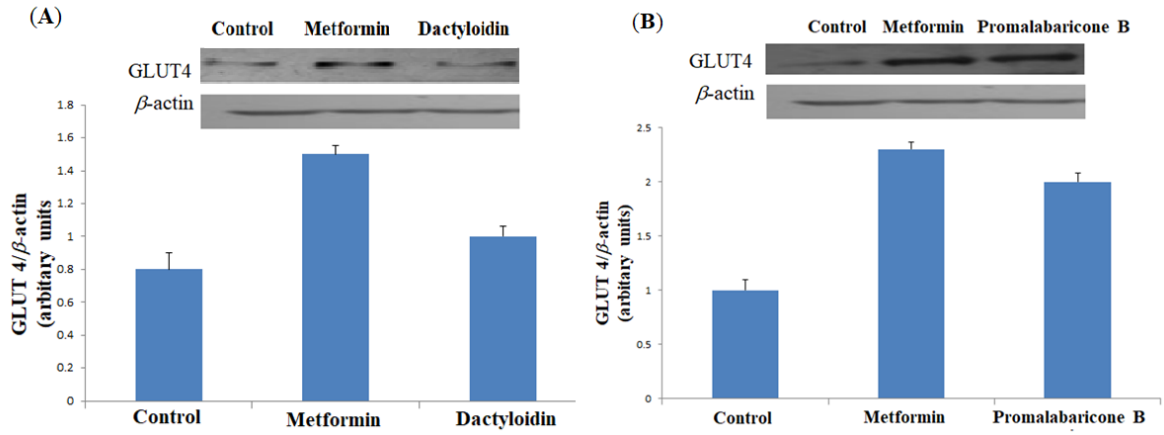

Figure 6B.20. Western blot analysis for the expression of GLUT4 in L6 myotubes. Differentiated L6 cells were treated with (**A**) 2.5 μM dactyloidin and (**B**) 2.5 μM promalabaricone B and was subjected to western blot analysis. A representative western blot using β- actin served as loading control. Band intensities were expressed as mean of three experiments ± SD.

6B.3.7. AMPK signalling

AMPK is believed to be a target for diabetes treatment based on studies demonstrating its modulation by several therapeutic agents. To elucidate the mechanism by which dactyloidin (**55**) and promalabaricone B (**56**) exerts its antidiabetic potential, involvement of AMPK signaling in dactyloidin (**55**) and promalabaricone B (**56**) treated differentiated skeletal myotubes were examined by western blot analysis. Results (**Figure 6B.21**) confirmed that dactyloidin (**55**) and promalabaricone B (**56**) have the potential to activate AMPK pathway, showing its antidiabetic activity. Parallely, our results supports the finding that increased intrinsic activity of GLUT4 could potentially induce the enhancement of glucose uptake after AMPK activation in L6 myocytes. To the best of our knowledge, this is the first study which explored the antidiabetic activity of dactyloidin (**55**) and promalabaricone B (**56**) and the mechanism by which exerts its action in the physiology. This study provides the promising activity of dactyloidin (**55**) and

promalabaricone B (**56**) as an AMPK activator, so as to target the metabolic syndrome through the downstream molecular pathways.

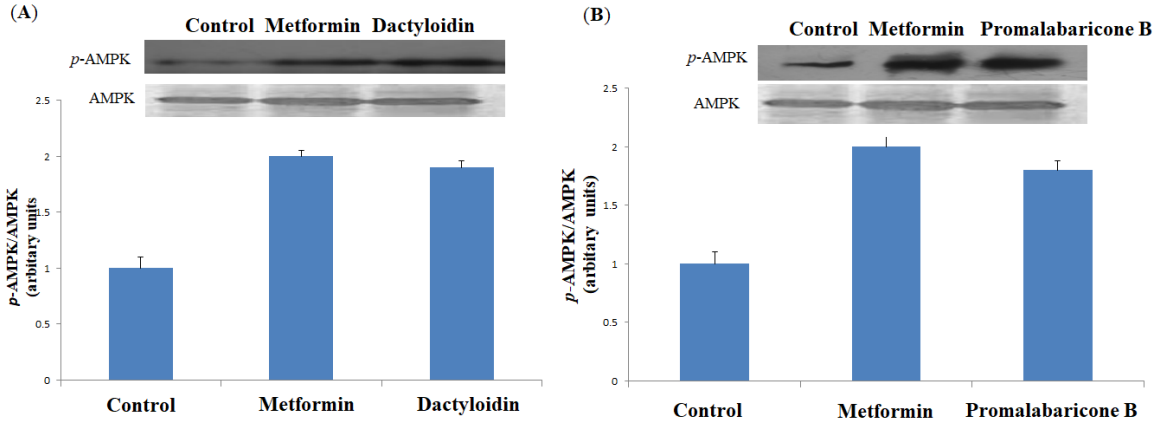

Figure 6B.21. Western blot analysis for the expression of AMPK in L6 myotubes. Differentiated L6 cells were treated with (**A**) 2.5 μM dactyloidin and (**B**) 2.5 μM promalabaricone B and was subjected to western blot analysis. A representative western blot using total AMPK served as loading control. Band intensities were expressed as mean of three experiments ± SD.

All together, the antidiabetic activity of dactyloidin (**55**) and promalabaricone B (**56**) on skeletal muscles through the activation of AMPK pathway and thus enhancing glucose uptake by the upregulation of GLUT4 gives evidence for its novel therapeutic role in diabetes management. Furthermore, the present study explores the unidentified activity of dactyloidin (**55**) and promalabaricone B (**56**) as an AMPK activator. The physiological action of dactyloidin (**55**) and promalabaricone B (**56**) highlights the need to explore its activities in an *in vivo* system.

6B.4. Conclusion

In conclusion, the phytochemical investigation of the seeds of *M. fatua* led to the isolation of seven major compounds. It included trimyrisitin (**50**), 1-(2, 6-dihydroxyphenyl) tetradecan-1-one (**51**), malabaricone A (**52**), malabaricone B (**53**), malabaricone C (**54**), dactyloidin (**55**) and promalabaricone B (**56**). The antidiabetic potential of dactyloidin (**55**) and promalabaricone B (**56**) were analyzed and dactyloidin (**55**) and promalabaricone B (**56**) exhibited moderate inhibitory activity on α-amylase and AGE's formation. Dactyloidin (**55**) and promalabaricone B (**56**) significantly inhibited the activity of α-glucosidase enzyme with IC_{50} value of 55.08 ± 0.857 μM and 32.67 ± 0.469 μM. The molecular docking and dynamics simulation studies revealed that dactyloidin (**55**) and promalabaricone B (**56**) effectively binds the pocket of *C* (**2QMJ**) - and *N*

(**3TOP**)-terminal human maltase glucoamylase. From these studies, we also confirmed the potential of dactyloidin (**55**) and promalabaricone B (**56**) in inducing glucose uptake in L6 cell lines indicating its efficacy in reducing blood glucose levels, which is one of the most important factor in the management of diabetes. Further experiments, revealed that dactyloidin (**55**) and promalabaricone B (**56**) stimulated the glucose uptake in skeletal muscle cells by enhancing the translocation and expression of GLUT4. Our results indicate that dactyloidin (**55**) and promalabaricone B (**56**) acts as a potential therapeutic option for diabetes treatment, and its hypoglycemic effect may be mediated by a main mechanism that includes AMPK activation and induction of GLUT4 translocation.

6B.5. Experimental

6B.5.1. General experimental procedures and chemicals used

General experimental procedures are same as described in the first part of this chapter. Porcein pancreatic α-amylase, *Saccharomyces cerevisiae* α-glucosidase, acarbose, bovine serum albumin (BSA), α-D-glucose, ascorbic acid, metformin, 4-nitrophenyl-α-D-glucopyranoside (*p*-NPG), Dulbecco's modified Eagle's media (DMEM), fetal bovine serum (FBS), antibiotic-antimycotic solution (Pencillin–streptomycin–amphotericin B mix) and 3-(4, 5-dimethylthiazol-2-yl)-2,5-diphenyl tetrazolium bromide (MTT) were procured from M/s Sigma-Aldrich Chemicals (St. Louis, MO, USA). 2-(N-(7-nitrobenz-2-oxa-1, 3-diazol-4-yl) amino)-2-deoxyglucose (2-NBDG) was procured from molecular probe (Invitrogen Life Technologies, Carlsbad, CA, USA). Phospho-specific or pan-specific antibodies against AMPK and GLUT 4 were procured from Santa Cruz Biotechnology, United States. All other chemicals and reagents used were of highest grade available.

6B.5.2. Plant material

The seeds of *M. fatua* were collected in December 2016 from Agasthyamalai Biosphere Reserve of South Western Ghats region of Kollam District, Kerala, India. The plant material was identified by the plant taxonomist of Jawaharlal Nehru Tropical Botanic Garden and Research Institute, India and a voucher specimen (**TBGT 83441**) has been deposited in the herbarium repository of the same institute.

6B.5.3. Extraction, isolation and characterization of secondary metabolites

850 g of the dried and ground seeds of *M. fatua* was extracted three times with dichloromethane. The combined extracts were concentrated to dryness (60 g) under reduced pressure using a rotary evaporator at 50 °C. The extract was separated into 18

fraction pools by silica gel CC (silica 100-200 mesh) using mixtures of solvents (*n*-hexane, *n*-hexane-EtOAc gradient and EtOAc) of increasing polarity. The schematic representation of extraction and isolation procedure was shown in **Figure 6B. 22.**

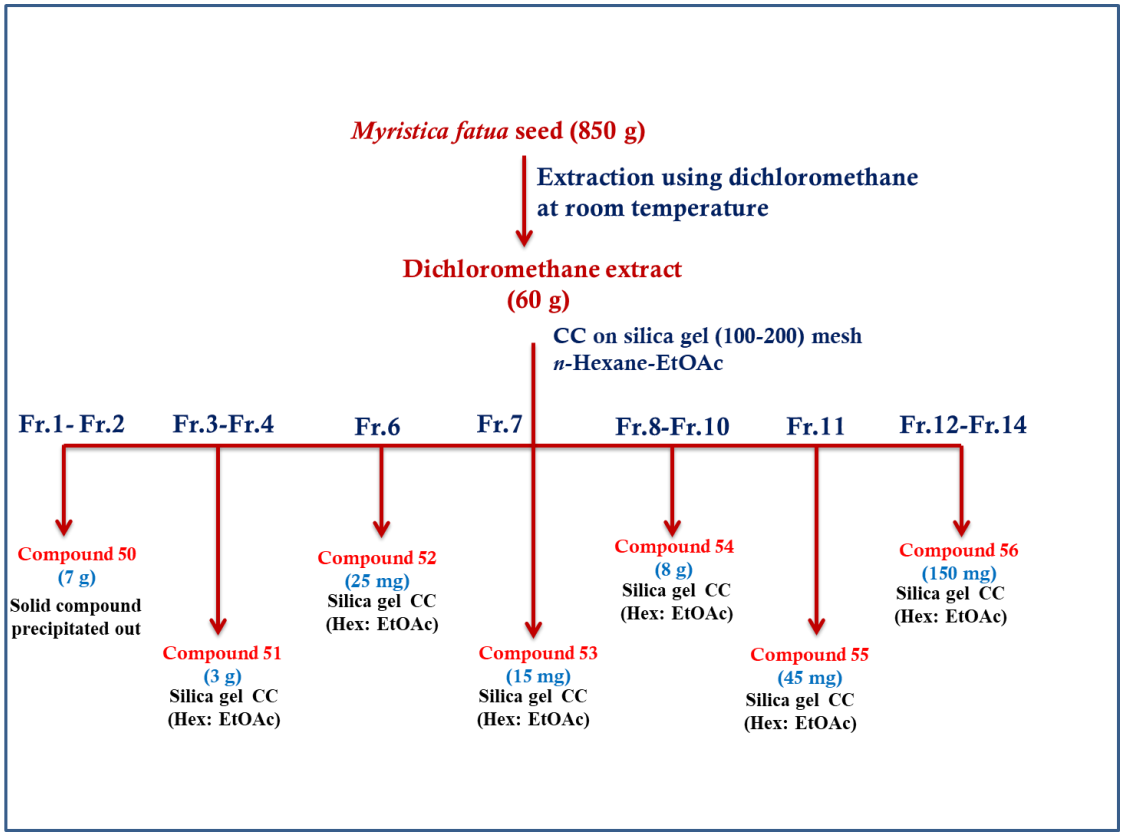

Figure 6B.22. Schematic representation of the extraction and isolation of phytochemicals from the seeds of *Myristica fatua* Houtt.

6B.5.3.1. Isolation of compound 55

The isolation procedure of compound **55** is represented in **Figure 6B.22.** Compound **6** (45 mg) was obtained as a colourless crystalline solid, on eluting the column (silica gel 100-200 mesh) with 15 % EtOAc in *n*-hexane. The detailed analysis of FTIR, ^{1}H, ^{13}C, ^{1}H-^{1}H COSY, HMQC, DEPT 135 and HMBC NMR spectra and HRESIMS gave compound **55** as dactyloidin.

Nature	Colourless crystalline solid
FTIR (KBr, υ_{max})	3300, 2900, 1600, 1510, 1460, 1340, 1240, 1160, 1130, 1070, 1010 cm^{-1}.
^{1}H NMR	δ 8.08 (s, 1H, -OH), 7.10 (t, J_1 = 8 Hz, J_2 = 8.5 Hz,

	(500 MHz, Acetone-d_6)	1H, H-5'), 7.03 (d, *J* = 8.5 Hz, 2H, H-2'' and H-6''), 6.75 (d, *J* = 8.5 Hz, 2H, H-5'' and H-3''), 6.47 (d, *J* = 8 Hz, 1H, H-6'), 6.41 (d, *J* = 8 Hz, 1H, H-4'), 5.15 (d, *J* = 3.5 Hz, 1H, H-1), 3.81 (s, 3H, -OCH_3), 2.53 (t, *J* = 7 and 8 Hz, 2H, H-9), 1.96 (m, 1H), 1.87 (brd, *J* = 13.5 Hz, 1H), 1.74 (m, 3H), 1.70 (m, 1H), 1.62-1.55 (m, 4H, H-7 and H-9), 1.53-1.49 (m, 2H, H-8) ppm.
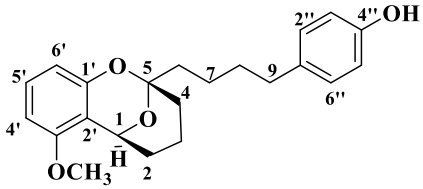	^{13}C NMR (125 MHz, Acetone-d_6)	δ 155.4 (C-3'), 155.2 (C-1'), 154.9 (C-4''), 133.2 (C-1''), 129.2 (C-2'' and C-6''), 128.0 (C-5', 115.0 (C-3'' and C-5''), 111.4 (C-5), 107.6 (C-6'), 101.4 (C-4'), 66.6 (-OCH_3), 55.0 (C-1'), 40.8, 34.8, 34.7, 31.9 (C-8), 29.4 (C-2), 21.9 (C-7), 15.8 (C-3) ppm.
	HRESIMS (m/z)	377.1726 $[M+Na]^+$

6B.5.3.2. Isolation of compound 56

The isolation procedure of compound **56** is represented in **6B. 22.** Compound **56** (80 mg) was obtained as a pale yellow amorphous solid, on eluting the column (silica gel 100-200 mesh) with 25 % EtOAc in *n*-hexane. The detailed analysis of FTIR, ^{1}H NMR,

^{13}C, HOMOCOSY, HMQC, DEPT 135 and HMBC NMR spectrum and HRESIMS gave compound **56** as promalabaricone B [Van *et al*., **2000**].

Nature	Pale yellow amorphous solid
FTIR (KBr, υ_{max})	2925, 2854, 1744, 1658, 1621, 1598, 1542, 1476, 1461, 1411, 1366, 1255, 1231, 1155, 1057, 1037, 956 cm^{-1}.
^{1}H NMR (500 MHz, Acetone-d_6)	δ 7.95 (s, 1H, -OH), 6.87 (d, J = 8.5 Hz, 2H, H-11 and H-15), 6.60 (d, J = 8.5 Hz, 2H, H-12 and H-14), 4.31 (d, J = 3.5 Hz, 1H, -OH), 4.25-4.21 (m, 1H, H-19), 2.91 (dd, J_1= 18 Hz, J_2 = 3.5 Hz, 1H), 2.85 (t, J = 7.5 Hz, 2H, H-2), 2.63-2.60 (m, 1H), 2.59-2.57 (m, 1H), 2.42 (ddd, J_1 = 16.5 Hz, J_2 = 6 Hz, J_3 = 2 Hz, 1H), 2.37 (t, J = 7.5 Hz, 2H, H-9), 1.49-1.41 (m, 4H), 1.20 (brs, 8H) ppm.
^{13}C NMR (125 MHz, Acetone-d_6)	δ 204.9 (C-1), 197.3 (C-21), 193.1 (C-17), 155.3 (C-13), 133.3 (C-10), 129.1 (C-15 and C-11), 115.0 (C-16), 112.8 (C-12 and C-14), 62.8 (C-19), 46.8 (C-18 and C-20), 41.3

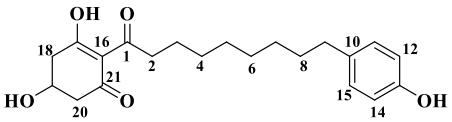

Promalabaricone B (56)

	(C-2), 39.7 (C-9), [34.7, 31.8, 24.6 (other aliphatic protons)] ppm.
HRESIMS (m/z)	383.1856 $[M+Na]^+$

6B.5.4. α-Amylase inhibitory activity, α-glucosidase inhibitiory activity, antiglycation property, *In silico* studies, cell culture and treatment conditions, cytotoxicity assay and fluorescence analysis of 2-NBDG uptake by flow cytometry

As same as described in the first part of this chapter.

6B.5.5. Western blot for the expression of AMPK and GLUT4 in L6 myotubes

Expression level of AMPK and GLUT4 protein was assessed by Western blotting. L6 myotubes were treated with 2.5 μM of dactyloidin (**55**) and promalabaricone B (**56**) for a period of 24 h. After incubation, the cells were lysed in ice-cold lysis buffer (50 mM Tris-HCl, 150 mM sodium chloride, 1.0 % Igepal CA-630, 0.5 % sodium deoxycholate, 0.1 % sodium dodecyl sulfate, 1 % Triton X-100 and protease inhibitor cocktail, pH 8.0) for 30 min on ice and were centrifuged at 12000 xg for 10 min. The protein content was then measured using BCA protein assay kit. The lysates (40 μg) were subjected to SDS-PAGE on 10 % gel and transferred on to a poly vinylidene di fluoride (PVDF, Immobilon P™, Millipore®, USA) membrane by using Trans-Blot Turbo™ (Bio-Rad). The membranes were blocked by incubating in blocking buffer (5 % skim milk in PBST, PBST-PBS buffer containing 0.1 % Tween 20) for 1 h at room temperature, washed three times with PBST and probed over night at 4 ^oC with appropriate antibody against AMPK and GLUT4 (1:1000). Membranes were washed 3 times and incubated for 1 h at room temperature with horse radish peroxidase (HRP) conjugated secondary antibody at 1:1000 dilution and again washed three times in PBS. The bound antibodies were detected using an enhanced chemiluminescence substrate (Biorad, **USA**) and measured by densitometry using a Chemi Doc XRS digital imaging system and the Multi Analyst software from Bio-Rad Laboratories (**USA**).

6B.5.6. Statistical analysis

Statistical analysis was carried out by Graph Pad prism statistical software. Statistical difference between two sets of data was determined using unpaired Student's t test. 'P' value of less than 0.05 was considered as statistically significant.

Summary and Conclusions

Natural products and their derivatives are widely used as drugs and novel drug leads for the treatment of various life threatening ailments. Before the development of high throughput screening (HTS) and molecular modelling, around 80 % of the drugs were either derived from natural products or from their derivatives. Furthermore, the natural product inspired designs and synthesis resulted in the discovery of many modern medicines. India is considered as the “Botanical Garden of World” with nearly 45,000 plant species, which is also a source of the next generation medicines. Ayurveda is one of our nation’s traditional system of medicines and it is derived from two Sanskrit roots: “Ayus” which means life and “Veda” which means knowledge. Thus Ayurveda roughly transforms as "Knowledge for life". Considering the renewed interest in medicinal plants and traditional systems of medicines, we have focused on the phytochemical and pharmacological investigation of five selected plant species of Simaroubaceae, Dipterocarpaceae and Myristicaceae family, found in the Western Ghats of Kerala.

Chapter 1 gives an overview of plant derived natural products with special emphasizes on antidiabetic, anti-inflammatory and cardiovascular drugs.

The isolation, characterization and antidiabetic activity of quassinoids isolated from the seeds of *Quassia indica* Gaertn. is the subject matter of the first part of chapter 2. The plant *Quassia indica* Gaertn. (synonym: *Samadera indica* Gaertn.), commonly recognized as “Niepa bark tree”, “Lokhanadi” or “Karinjotta” belongs to the family Simaroubaceae. In our preliminary studies, the ethanol extract of the seeds of *Quassia indica* exhibited significant antidiabetic potential; this result encouraged us to isolate compounds from ethanol extract. The ethanol extract was subjected to repeated column chromatographic purification, which resulted in the isolation of **8** quassinoids. It include two novel quassinoids (**6**) and (**8**), along with six known quassinoids [samaderin A (**1**), samaderin B (**2**), dihydrosamaderin B (**3**), samaderin C (**4**), cedronin (**5**) and brucein D (**7**)]. All the quassinoids exhibited moderate α-amylase inhibitory activity and moderate to significant α-glucosidase inhibitory activity. Among the isolated quassinoids, cedronin (**5**) exhibited promising α-glucosidase inhibitory activity with IC_{50} value of 28.03 ± 0.231 μM. The molecular simulation studies indicated that novel compound (**8**) effectively

binds the pocket of isomaltase from *Saccharomyces cerevisiae* (**3A4A**), *N*- (**2QMJ**) and *C*- (**3TOP**) terminal human maltase glucoamylase. Also, all the quassinoids showed moderate antiglycation property. The *In vitro* antidiabetic activity study in L6 myotubes revealed that all the compounds moderately stimulates the 2-NBDG uptake in a dose dependant manner (**Figure 1**).

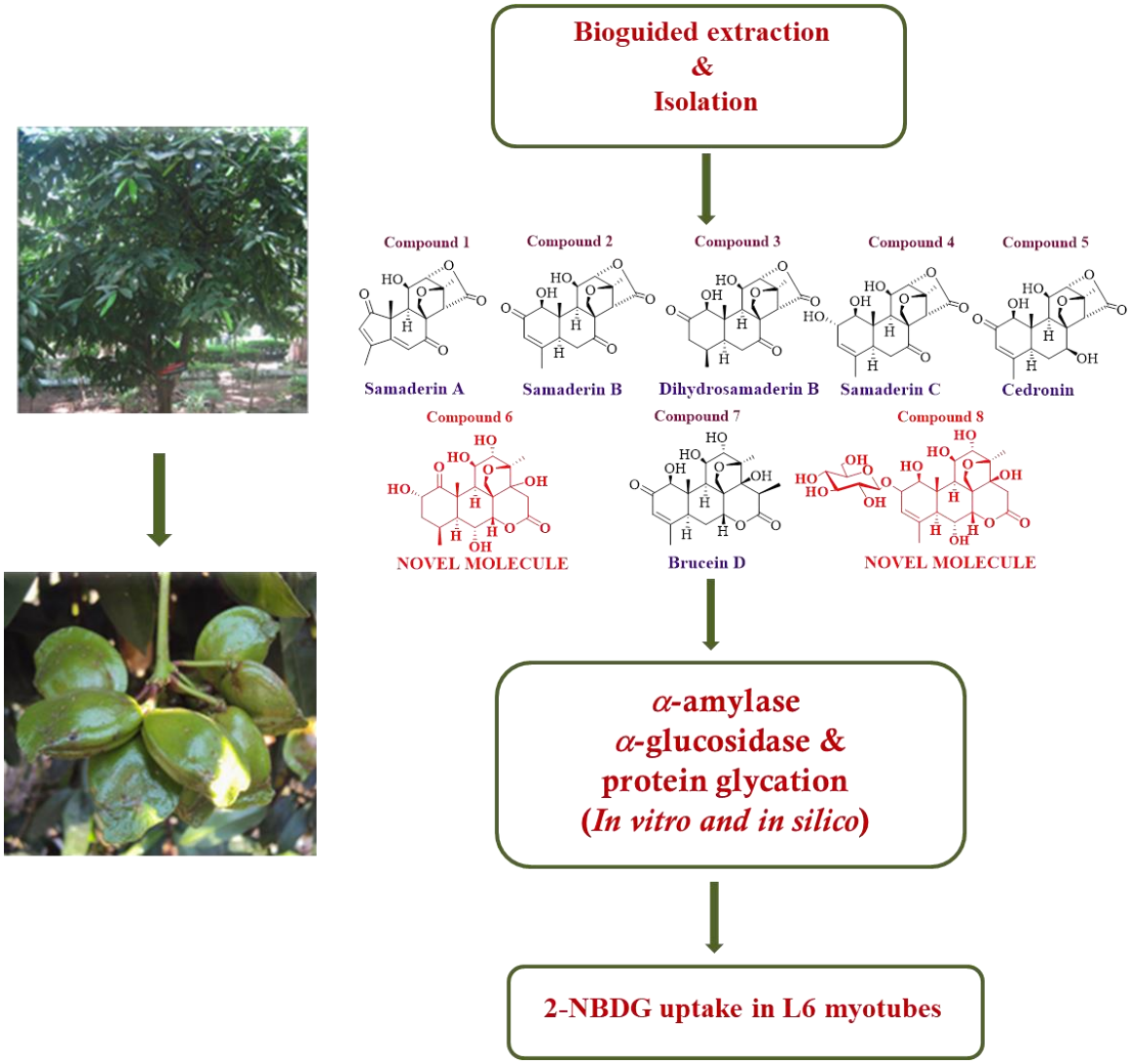

Figure 1. Schematic representation of phytochemical investigation and antidiabetic potential of quassinoids isolated from the seeds of *Quassia indica*

The second part of chapter 2 deals with the isolaton, characterization and antidiabetic potential of phytochemicals from the stem barks of *Quassia indica*. The acetone extract of the stem bark exhibited promising inhibitory activities on carbohydrate hydrolyzing enzyme and protein glycation. Inspired with these results, we isolated phytochemicals from the stem bark of *Quassia indica*, which resulted in the isolation of 11 compounds. It include lupenone (**9**), *β*-sitosterol (**10**), stigmasterol (**11**), 18*α*-olean-19*α*

-ol-3-one (**12**), ferulic acid (**13**), scopoletin (**14**), samaderin A (**15**), samaderin B (**16**), dihydrosamaderin B (**17**), samaderin C (**18**) and *β*-sitosterol- *β*-D-glucoside (**19**). Ferulic acid (**13**) and scopoletin (**14**) were isolated from the stem bark of *Quassia indica* for the first time. We have tested the *in vitro* antidiabetic activity of lupenone (**9**), 18*α*-olean-19*α* -ol-3-one (**12**), ferulic acid (**13**) and scopoletin (**14**). Lupenone (**9**) and 18*α*-olean-19*α* -ol-3-one (**12**) exhibited significant inhibitory activity on *α*-amylase with IC_{50} value of 7.35 ± 0.255 and 14.88 ± 0.42 *μ*M. In the case of *α*-glucosidase enzyme, ferulic acid (**13**) and scopoletin (**14**) displayed promising inhibitory activity with IC_{50} value of 54.87 ± 0.734 and 51.44 ± 1.278 *μ*M. We have also carried out molecular docking studies with porcine pancreatic *α*-amylase (**3AJ7**), isomaltase from *Saccharomyces cerevisiae* (**3A4A**), human pancreatic *α*- amylase (**4GQQ**), human maltase-glucoamylase *C*-terminal (**2QMJ**) and *N*-terminal (**3TOP**) (**Figure 2**).

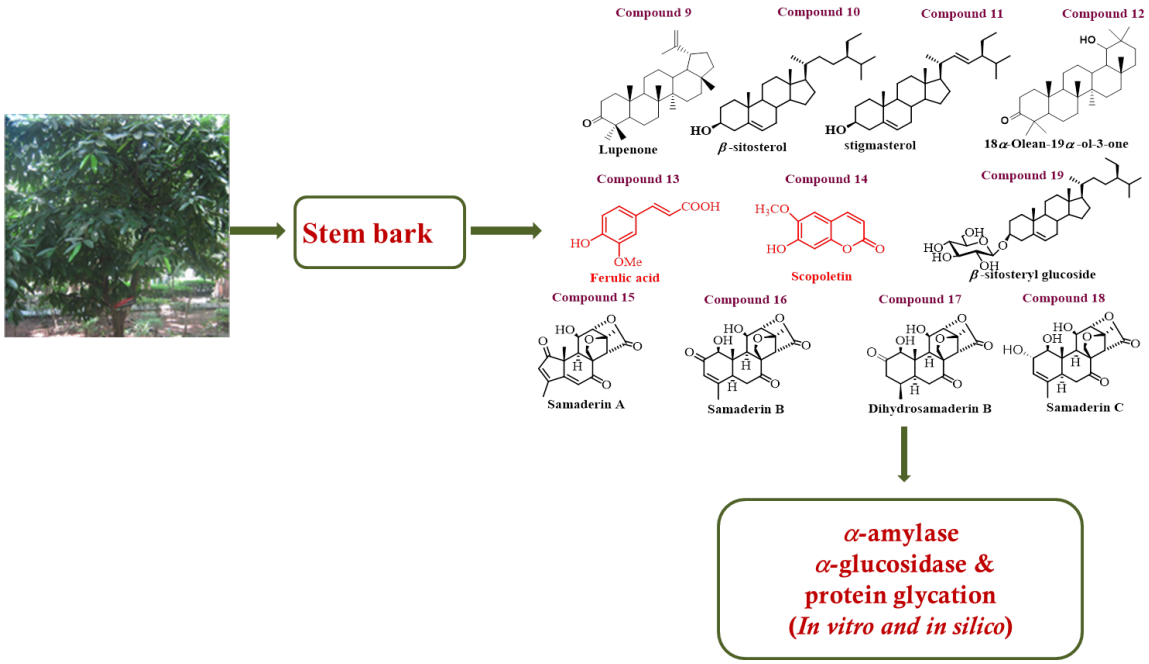

Figure 2. Schematic representation of phytochemical investigation and antidiabetic potential of compounds isolated from the stem bark of *Quassia indica*

In the third chapter, we have discussed the phytochemical investigation and anti-inflammatory activity of the stem bark of *Ailanthus excelsa*. *Ailanthus excelsa* or "Plant of Heaven" is a deciduous tree that belongs to Simaroubaceae family and is commonly known as Mahanimba and Maharukha. The name '*Ailanthus excelsa*' is derived from two words; *ailanto* which means 'tree of heaven' and *excelsa* which means 'tall'. *Ailanthus excelsa* is a fast growing tree extensively cultivated in many parts of India, towards the

vicinity of villages. The ethanol extract was subjected to repeated column chromatographic purifications and resulted in the isolation of **7** compounds. It include two novel molecules (**23**) and (**24**), along with five known compounds. In the present study, we have investigated the anti-inflammatory activity of compounds; ocotillone **(22), 23** and **24.** Among these, compound (**23**) was less toxic in RAW 264.7 macrophages. Compound **23** inhibited the action of pro-inflammatory mediators like NO, TNF-α, IL-6, LOX-1 and COX-2 and promoted the action of anti-inflammatory mediator IL 10 *via* inhibition of NF-κB pathway in LPS-stimulated RAW 264.7 macrophages. These findings provided information on the mechanism of the anti-inflammatory action of compound 2**3** from *Ailanthus excelsa*. Further studies on the biological effects of compound 2**3** are warranted in the future (**Figure 3**).

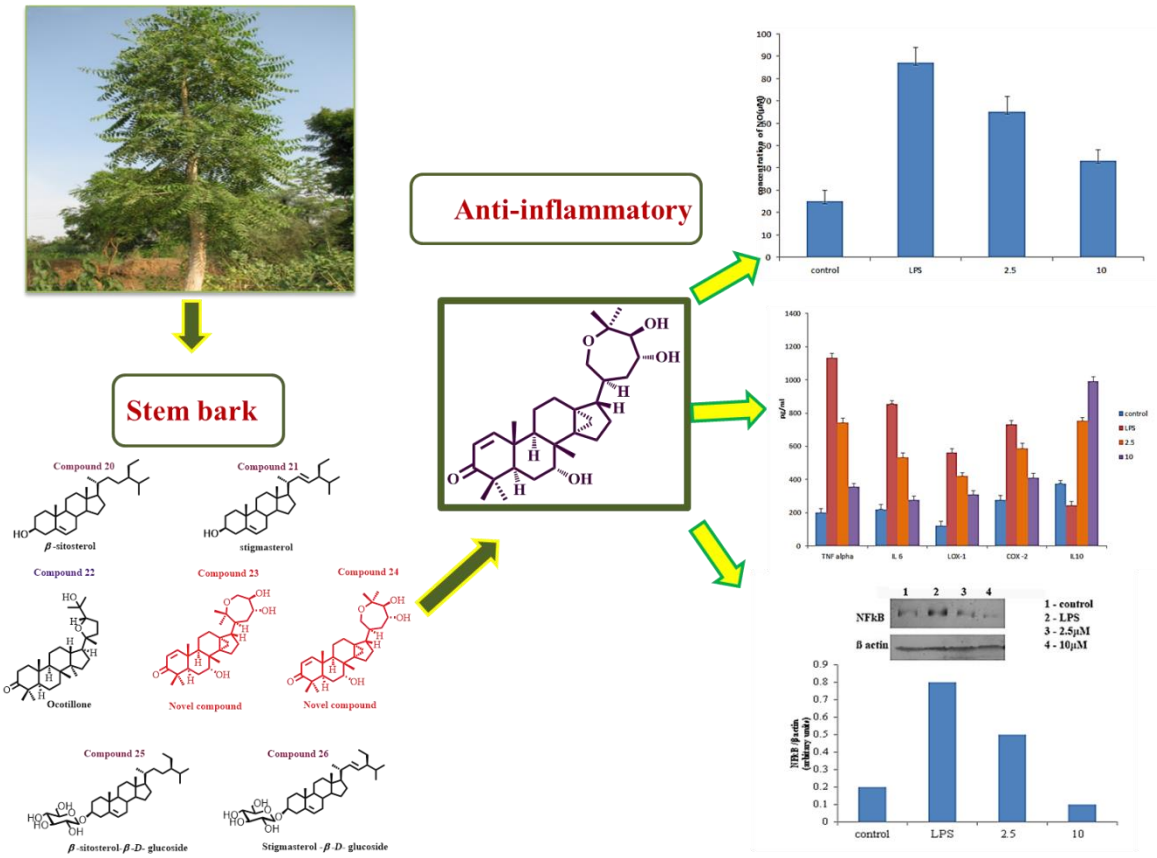

Figure 3. Schematic representation of phytochemical investigation and anti-inflammatory potential of compounds from the stem bark of *Ailanthus excelsa*

Isolation and characterization of phytochemicals from *Vatica chinensis* L. and their ameliorative effect on H_2O_2 induced oxidative stress in H9c2 cardiomyoblasts is the

subject matter of first part of chapter 4. *Vatica chinensis* L. is a critically endangered species endemic to South India and Sri Lanka, and belongs to the family Dipterocarpaceae. It is locally recognized as "Adakkapine", "Cherupiney" or "Payinipasa". Phytochemical investigation of the stem bark of *Vatica chinensis* L. led to the isolation of the seven compounds, which include a novel compound, vaticanol R (**29**) along with six known compounds. Vaticaphenol A (**30**), bergenin (**32**) and methoxy bergenin (**33**) were isolated for the first time from this species. All the compounds were examined for their antioxidant (DPPH and ABTS radical scavenging activity) and cytoprotective properties against H_2O_2 induced oxidative stress in H9c2 cell line. The results indicated a protective effect of all the compounds on cardiomyocytes against H_2O_2-induced oxidative stress. The pre-treatment of H9c2 cells with the compounds prior to the oxidative stress induction by H_2O_2 protects the cells from oxidative stress induced damage by decrease in ROS production, increase in SOD/CAT activity, restoration of mitochondrial membrane potential and ATP levels. The results suggested that the compounds under study may be promising candidates for the prevention and management of oxidative stress and associated cardiovascular diseases. Further *in vivo* studies are mandatory to have better understanding on the potential therapeutic role of these oligostilbenoids in cardiovascular diseases (**Figure 4**).

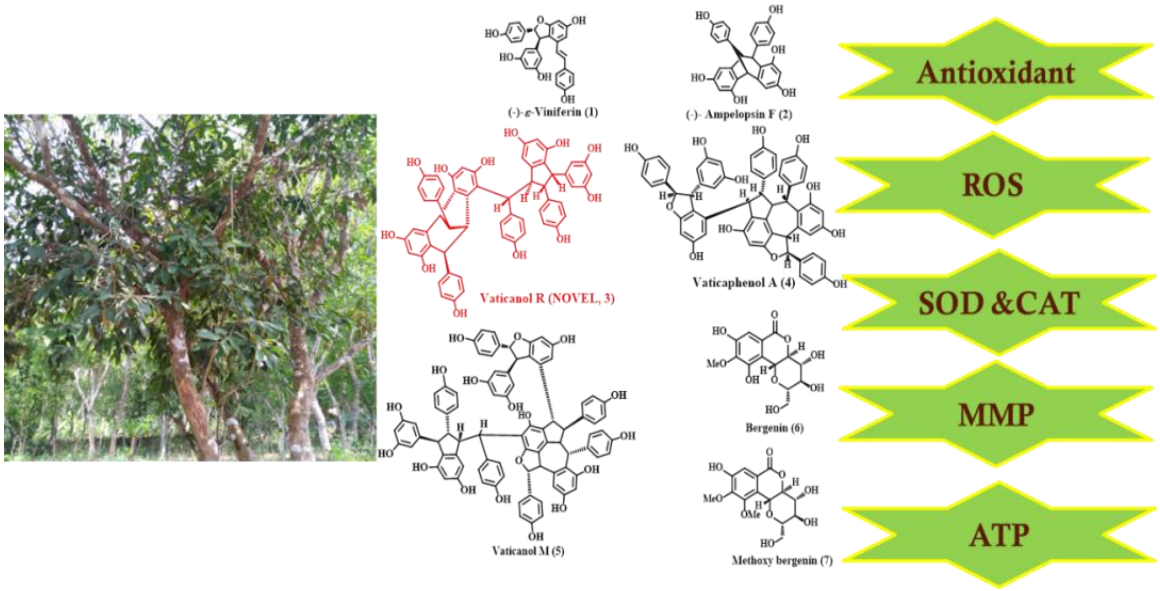

Figure 4. Schematic representation of phytochemical investigation and their ameliorative effect on H_2O_2 induced oxidative stress in H9c2 cardiomyoblasts

In the second part of chapter **4**, we have described the antidiabetic activity of resveratrol oligomers from *Vatica chinensis*. All compounds showed significant inhibitory activity on α-glucosidase enzyme and protein glycation, and moderate inhibition on α-amylase enzyme. The molecular simulation studies well supported the observed inhibitory activities on carbohydrate hydrolyzing enzymes. Resveratrol oligomers [(-)-ε- viniferin (**27**), (-)-ampelopsin F (**28**), vaticanol R (**29**), vaticaphenol A (**30**) and vaticanol M (**31**)] exhibited significant stimulation of glucose uptake in L6 myotubes. Taken together, these results indicated that resveratrol oligomers exhibit promising antidiabetic activity in *in vitro* studies (**Figure 5**).

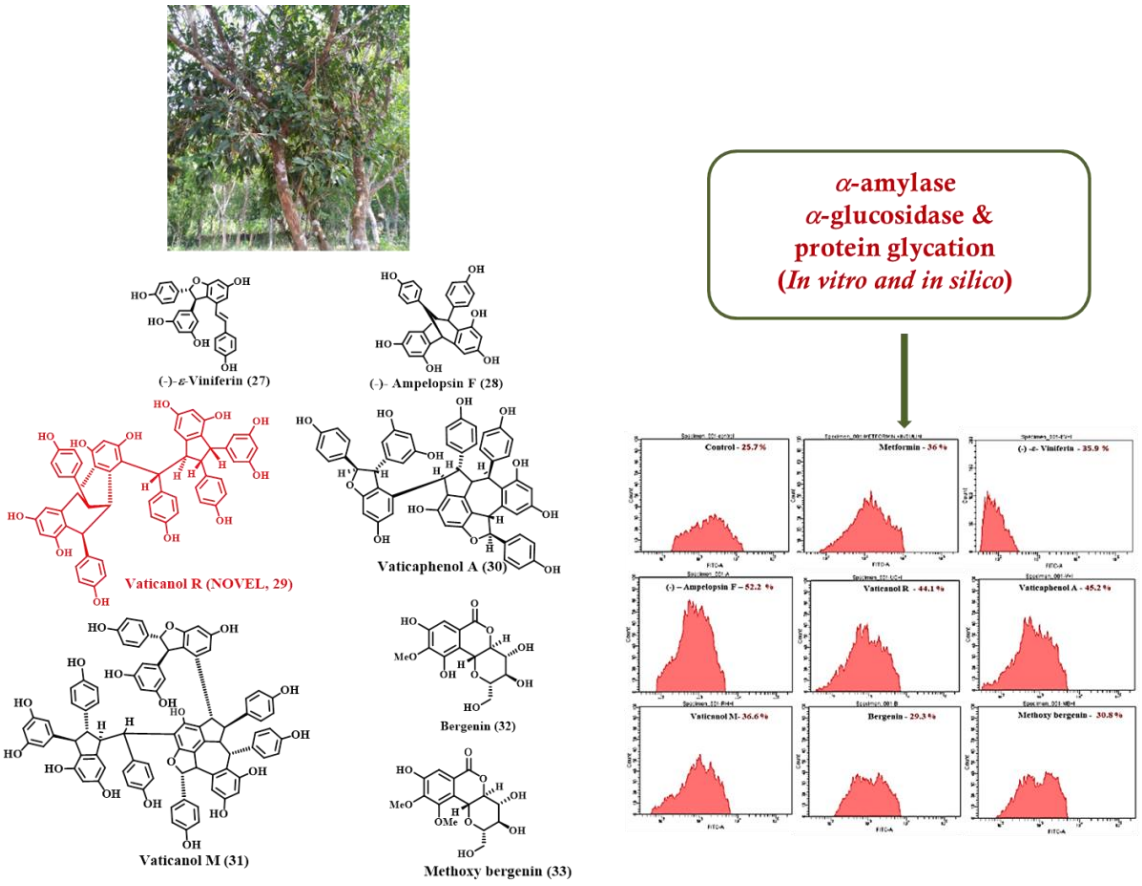

Figure 5. Schematic representation of antidiabetic potential of compounds isolated from the stem bark of *Vatica chinensis*

Isolation, characterization and antidiabetic potential of phytochemicals from *Vatica chinensis* L. is the subject matter of first part of chapter 5. *Hopea parviflora* Bedd., an endangered species and commonly recognized as “Iron wood of Malabar”, “White Kongu”, “Thambakam” or “Kampakam”. In this part, activity oriented extraction and isolation of the stem barks of *Hopea parviflora* resulted in the isolation of **9**

compounds. It included two triterpenes, two resveratrol dimers, two tetramers, 2, 4, 8-trihydroxyphenanthrene-2-*O*-glucoside and ellagic acid 3, 3', 4-trimethoxy-4'-*O*-α-L-rhamnopyranoside along with the glycoside of β-sitosterol. Among them, friedelin and friedelin-3β-ol (triterpenes), vaticaphenol A (tetramers), 2, 4, 8-trihydroxyphenanthrene-2-*O*-glucoside and ellagic acid-3,3',4-trimethoxy-4'-O-α-L-rhamnopyranoside, glycoside of β-sitosterol are isolated for the first time from the stem bark of *Hopea parviflora*. The structure elucidation was done by spectroscopic 1D and 2D NMR techniques (*viz*., ^{1}H, ^{13}C, DEPT 135, HMQC, HMBC, and ^{1}H-^{1}H COSY, and NOESY), HRESIMS and compared with the reported literature. All compounds were evaluated for their α-amylase and α-glucosidase inhibitory activity and antiglycation potential. The molecular docking studies proved that all the active compounds well accommodate in the active site of the **4GQQ**, **2QMJ** and **3TOP** enzyme. Furthermore, pharmacokinetic properties of the compounds were predicted *in silico*, suggesting that the compounds possess drug like properties and excellent ADME/T profile. *In vitro* antidiabetic activity in L6 myotubes revealed that ellagic acid 3,3',4-trimethoxy-4'-*O*-α-L-rhamnopyranoside (**41**) significantly enhances the glucose uptake in a dose dependant manner. Further studies are ongoing in our lab to establish the therapeutic efficacy and safety of compounds from *Hopea parviflora* as a promising antidiabetic agent (**Figure 6**).

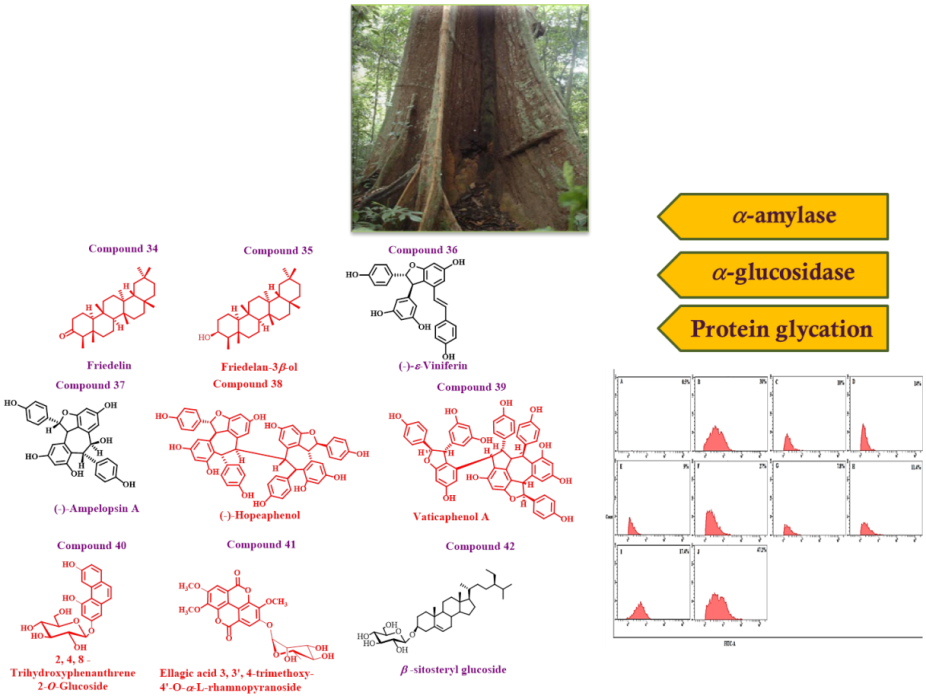

Figure 6. Schematic representation of antidiabetic potential of compounds isolated from the stem bark of *Hopea parviflora*

In the second part of chapter 5, we have investigated the anti-inflammatory activity of compounds isolated from the stem bark of *Hopea parviflora*. Among the isolated compounds, ellagic acid-3, 3', 4-trimethoxy 4'-*O*-*α*-L-rhamnopyranoside (**41**) is less toxic in RAW 264.7 macrophages. Compound **41** also inhibited the action of pro-inflammatory mediators like NO, TNF-*α*, IL-6, LOX-1 and COX-2 and promoted the action of anti-inflammatory mediator IL 10 *via* inhibition of NF-κB pathway in LPS-stimulated RAW264.7 macrophages. These findings provided information on the mechanism of action of ellagic acid-3, 3', 4-trimethoxy-4'-*O*-*α*-L-rhamnopyranoside (**41**). Further studies on the biological effects of ellagic acid 3, 3', 4-trimethoxy-4'-*O*-*α*-L-rhamnopyranoside (**41**) are warranted in the future (**Figure 7**).

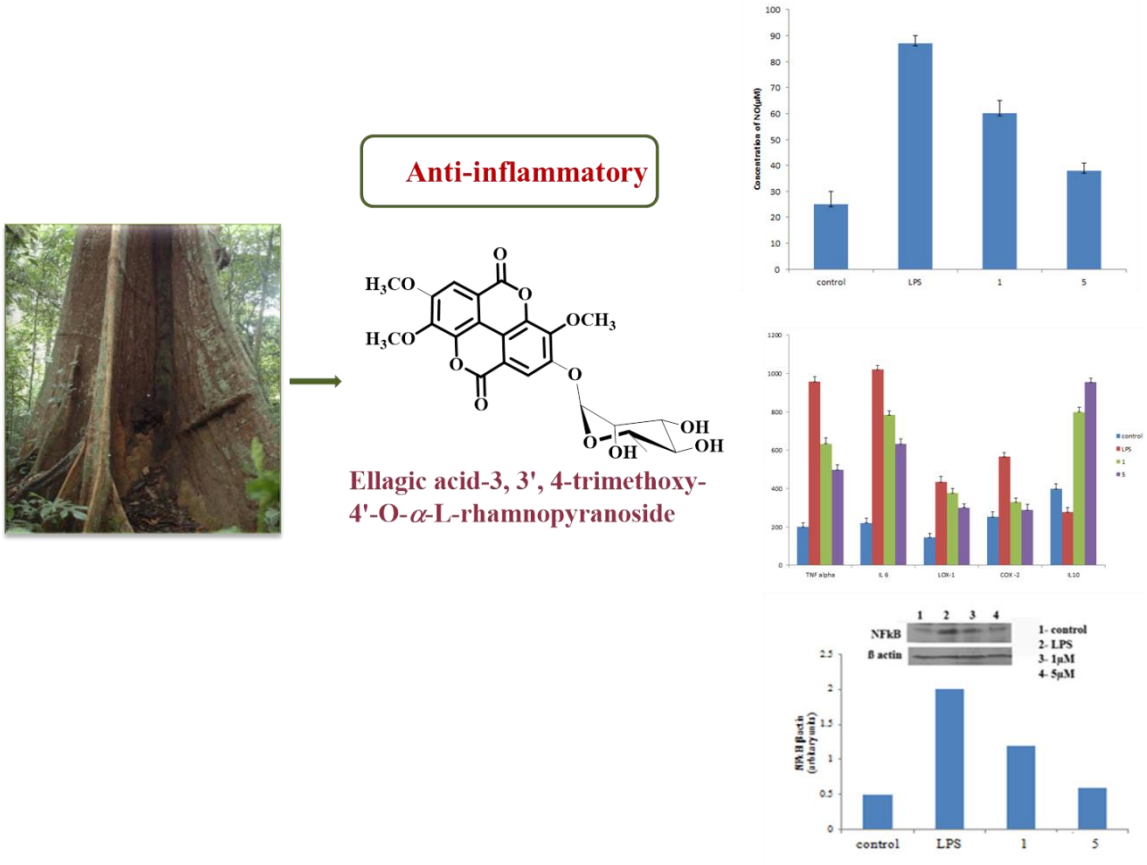

Figure 7. Schematic representation of anti-inflammatory activity of compounds isolated from the stem bark of *Hopea parviflora*

In the first part of chapter 6, the phytochemical investigation of stem bark of *Myristica fatua* led to the isolation of a novel compound, 3-tridecanoylbenzoic acid (**43**) along with six known acyl phenols [(1-(2-hydroxy-6-methoxyphenyl)tetradecan-1-one (**44**), 1-(2,6-dihydroxyphenyl) tetradecan-1-one (**45**), malabaricone A (**46**), 1-(2-

hydroxy-6-methoxyphenyl) -9-(4-hydroxy phenyl)nonan-1-one (**47**), malabaricone B (**48**) and malabaricone C (**49**)], of which four of them [(1-(2-hydroxy-6-methoxyphenyl) tetradecan-1-one (**44**), 1-(2,6-dihydroxyphenyl)tetradecan-1-one (**45**), malabaricone A (**46**) and 1-(2-hydroxy-6-methoxy phenyl)-9-(4-hydroxy phenyl)nonan-1-one (**47**)] are isolated for the first time from *Myristica fatua* Houtt. All compounds exhibited moderate α-amylase and significant α-glucosidase inhibitory activity. Malabaricone B (**48**) and malabaricone C (**49**) exhibited promising α-glucosidase inhibitory activity with IC_{50} values of 63.70 ± 0.546 and 43.61 ± 0.620 μM respectively. The molecular simulation studies indicated that malabaricone C (**49**) effectively binds the pocket of *N*-terminal human maltase glucoamylase (**2QMJ**). Malabaricones A (**46**), B (**48**) and C (**49**) showed potent antiglycation property with IC_{50} value of 19.28 ± 0.045, 40.34 ± 0.094, and 14.99 ± 0.114 μM respectively. *In vitro* antidiabetic activity in L6 myotubes revealed that malabaricone B (**48**) significantly enhances the glucose uptake in a dose dependant manner. Further studies are in progress to establish the therapeutic efficacy and safety of compounds from *Myristica fatua* Houtt. as a promising antidiabetic agent (**Figure 8**).

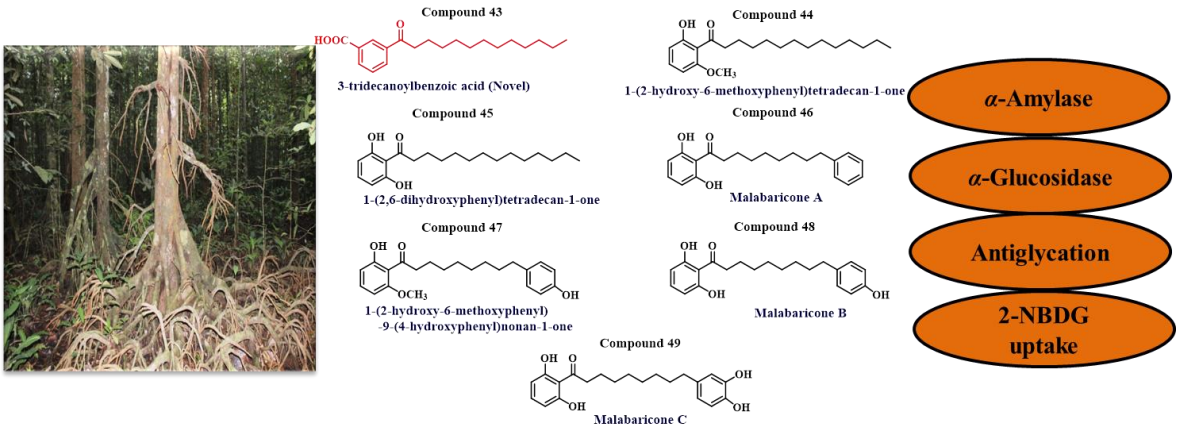

Figure 8. Schematic representation of phytochemical and antidiabetic potential of compounds isolated from the stem bark of *Myristica fatua*

In the last part of final chapter, the phytochemical investigation of the seeds of *Myristic fatua* led to the isolation of seven major compounds. It includes trimyrisitin (**50**), 1-(2, 6-dihydroxyphenyl) tetradecan-1-one (**51**), malabaricone A (**52**), malabaricone B (**53**), malabaricone C (**54**), dactyloidin (**55**) and promalabaricone B (**56**). In the antidiabetic studies of dactyloidin (**55**) and promalabaricone B (**56**), they exhibited moderate inhibitory activity on α-amylase and AGE's formation. Dactyloidin (**55**) and

promalabaricone B (**56**) significantly inhibited the activity of α-glucosidase enzyme with IC_{50} value of 55.08 ± 0.857 μM and 32.67 ± 0.469 μM. The molecular docking and dynamics simulation studies revealed that dactyloidin (**55**) and promalabaricone B (**56**) effectively binds the pocket of *C* (**2QMJ**) - and *N* (**3TOP**)-terminal human maltase glucoamylase. From these studies, we also confirmed the potential of dactyloidin (**55**) and promalabaricone B (**56**) in inducing glucose uptake in L6 cell lines indicating its efficacy in reducing blood glucose levels, which is one of the most important factor in the management of diabetes. Further experiments, revealed that dactyloidin (**55**) and promalabaricone B (**56**) stimulated the glucose uptake in skeletal muscle cells by enhancing the translocation and expression of GLUT4. Our results indicate that dactyloidin (**55**) and promalabaricone B (**56**) acts as a potential therapeutic option for diabetes treatment, and its hypoglycemic effect may be mediated by a main mechanism that includes AMPK activation and induction of GLUT4 translocation (**Figure 9**).

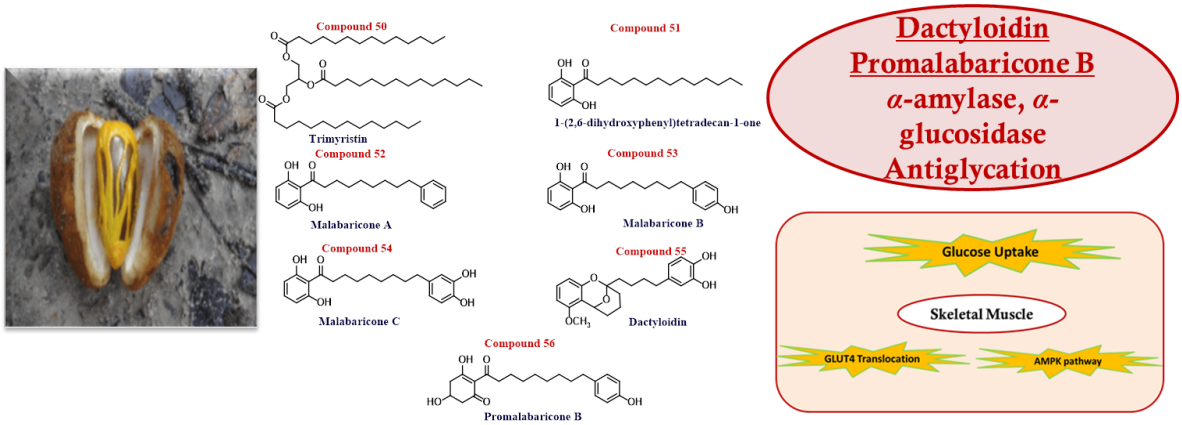

Figure 9. Schematic representation of phytochemical and antidiabetic potential of compounds isolated from the seeds of *Myristica fatua*

Bibliography and References

Abdulfatai, B. O.; Olusegun, A. O.; Lateefat, B. O. "Type 2 diabetes mellitus: A review of current trends", *Oman Med. J.* **2012**, *27(4)*, 269-273.

Abe, N.; Ito, T.; Ohguchi, K.; Nasu, M.; Masuda, Y.; Oyama, M.; Nozawa, Y.; Ito, M.; Iinuma, M. "Resveratrol oligomers from *Vatica albiramis*", *J. Nat. Prod.* **2010**, *73*, 1499-1506.

Adesanwo, J. K.; Aiyelaagbe, O.O.; Moronkola, D.O. "Antimicrobial and cytotoxic activity of the stem and root bark extracts of *Quassia undulata* and isolated constituents", *Toxicol. Environ. Chem.*, **2009**, *91(5)*, 999-1003.

Adewole, L. O.; Rachel, E. B.; Steven, J. C.; Anna, O.; Daniel, E. G.; Walter, H. L. "Antiplasmodial activity of extracts and quassinoids isolated from seedlings of *Ailanthus altissima* (Simaroubaceae)", *Phytother. Res.* **2003**, *17*, 675–677.

Adrover, M.; Laura, M.; Sanchis, P.; Pauwels, K.; Kraan, Y.; Lebrun, P.; Vilanova, B.; Muñoz, F.; Broersen, K.; Donoso, J. "Mechanistic insights in glycation-induced protein aggregation". *Biomacromolecules*, **2014**, *15*, 3449-3462.

Aebi, H. "Catalase *in vitro*", *Methods Enzymol.* **1984**, *105*, 121-125.

Aiba, C. J.; Correa, C. R. G.; Gottlieb, O. R. "Natural occurrence of Erdtman's dehydrodiisoeugenol". *Phytochemistry*, **1973**, *12*, 1163-1164.

Aisyah, S. K.; Jalifah, L.; Yana, M S.; Norfadilah, R.; Anuar, J. "Oligostilbenoids from *Vatica pauciflora* and the oxidative effect on Chang cells", *J. Phy. Conf. Ser.* **2013**, *423*, 1-5.

Akhmad, D.; Soleh K.; Leonardus, B. S. K.; Yana, M. S. "Scopoletin, a coumarin derivative compound isolated from *Macaranga gigantifolia* Merr", *Journal of Applied Pharmaceutical Science*, **2012**, *2 (12)*, 175-177.

Alan, L. H. "Toxins and drug discovery", *Toxicon*, **2014**, *92*, 193-200.

Alderton, W. K.; Cooper, C. E.; Knowles, R. G. "Nitric oxide synthases: structure, function and inhibition". *Biochem. J*. **2001**, *357*, 593-615.

American Diabetics Association, "Diagnosis and classification of diabetes mellitus". *Diabetes Care*, **2012**, *36*, 67-74.

Amorati, R.; Lucarini, M.; Mugnaini, V.; Pedulli, G. F. "Antioxidant activity of hydroxystilbene derivatives in homogeneous solution", *J. Org. Chem.* **2004**, *69*,

7101-7107.

Anuj, P.; Bipin, C. J.; Ram, P. S.; Anakshi, K. " New quassinoids from *Ailanthus excelsa*", *Med. Chem. Res*. **2004**, *13*, 781-789.

Apollinaire, T.; Francis, M. A.; Victor, K. "Lignans and stilbenes from African medicinal plants", *Medicinal Plant Research in Africa: Pharmacology and Chemistry*, **2013**, *12*, 435-478.

Apostolidis, E.; Kwon, Y. I.; Shetty, K. "Inhibitory potential of herb, fruit, and fungal-enriched cheese against key enzymes linked to type 2 diabetes and hypertension", *Innov. Food Sci. Emerg.* **2007**, *8*, 46-54.

Arun K. T.; D. C. Jain, D.C. "Excelsin: an insect feeding-deterrent isolated from *Ailanthus excelsa* (Simarubaceae)", *Phytother. Res*. **1993**, *7*, 323-325.

Arnold, L. D. "Importance of microbial natural products and the need to revitalize their discovery", *J. Ind. Microbiol. Biotechnol*. **2014**, *41(2)*, 185–201.

Ashley M. Z.; Raghunandan Y.; Elizabeth M. U. "A review of the efficacy and safety of sodium-glucose cotransporter 2 inhibitors: A focus on diabetic ketoacidosis", *Diabetes Spectr.* **2017**, *30(2)*, 137-142.

Ataa S.; Rosa, T.; Usama, W. H.; Salah, M. E.; Khaled, R.; Federica, M.; Marco, B.; Antje, H.; Monica R. L.; Francesco, M. "*In vitro* antioxidant and antiproliferative activities of flavonoids from *Ailanthus excelsa* (Roxb.) (Simaroubaceae) leaves", Z. Naturforsch. **2010**, *65c*, 180 -186.

Atun, S.; Sjamsul, A. A.; Emilio, L. G.; Euis, H. H.; Lukman, M.; Yana, M. S. "Oligostilbenoids from *Vatica umbonata* (Dipterocarpaceae)", *Biochem. Syst. Ecol.*, **2004**, *32*, 1051-1053.

Baderschneider, B.; Winterhalter, P. "Isolation and characterization of novel stilbene derivatives from riesling wine", *J. Agric. Food Chem.* **2000**, *48*, 2681-2686.

Bandaranayake, W. M.; Gunasekera, S. P.; Karunanayake, S.; Sotheeswaran, S.; Sultanbawa, M. U. S. "Terpenes of Dipterocapus and doona species", *Phytochemistry*, **1975**, *14*, 2043-2048.

Barbetti, P.; Grandolini, G.; Fardella, G.; Chiappini, I. "Indole Alkaloids from *Quassia amara*", *Planta Med*. **1987**, *53(3)*, 289-290.

Barbetti, P.; Grandolini, G.; Fardella, G.; Chiappini, I.; Mastalia, A. "New canthin-6-one alkaloids from *Quassia amara*", *Planta Med*. **1990**, *56*, 216-217.

Barbetti, P.; Grandolini, G.; Fardella, G.; Chiappini, I. "Quassinoids from *Quassia*

amara", *Phytochemistry*, **1993**, *32(4),* 1007-1013.

Bauri, A. K.; Foro, S.; Do, N. Q. N. "1-(2, 6-Dihydroxyphenyl)tetradecan-1-one: isolated from the fruit rinds of *Myristica malabarica*", *IUCrData* , **2016**, *1*, 1-3.

Belay, B.; Belachew, B.; Habitamu, D. "Review on application and management of medicinal plants for the livelihood of the local Community", *Journal of Resources Development and Management*, **2016**, *22*, 33-39.

Belz, G. G.; Aust, P. E.; Schneider, B. "Time course of the effect of single intravenous doses of digitoxin and dioxin in normal volunteers." *J. Cardiovasc. Pharmacol.* **1981**, *3*, 1116-1125.

Billoa, M.; Cabalionb, P.; Waikedreb, J.; Fourneaua, C.; Bouttierc, S.; Hocquemillera, R.; Fourneta, A. "Screening of some New Caledonian and Vanuatu medicinal plants for antimycobacterial activity". *J. Ethnopharmacol.* **2005**, *96*, 195-200.

Bipin, C. J.; Anuj, P.; Ram, P. S.; Anakshi, K. "Quassinoids from *Ailanthus excelsa",* *Phytochemistry*, **2003**, *62*, 579-584.

Bisset, N. G.; Diaz-Parra, M. A.; Ehret, C.; Ourisson, G.; "Etudes chimitaxonomiques dns la famile des Dipterocarpaceae", *Phytochemistry*, **1967**, *6*, 1395- 1405.

Branco, A. F.; Pereira, S. P.; Gonzalez, S.; Gusev, O.; Rizvanov, A. A.; Oliveira, P. J. "Gene expression profiling of H9c2 myoblast differentiation towards a cardiac-like phenotype", PLoS ONE, **2015**, *10*, 1-18.

Carmen, L.Q.; Guilherme, F. S.; Patricia, C. D.; Ana, P.; Joao, E. D. C. "Evaluation of the antiulcerogenic activity of friedelan-3*β*-ol and friedelin isolated from *Maytenus ilicifolia* (Celastraceae)", *J. Ethnopharmacol.* **2000**, *72*, 465-468.

Cathcart, R.; Schwiers, E.; Ames, B. N. "Detection of picomole levels of hydroperoxides using a fluorescent dichlorofluorescein assay", *Anal. Biochem*. **1983**, *134*, 111-116.

Chaturvedula, V. S. P.; Indra, P. "Isolation and structural characterization of lupine triterpenes from *Polypodium Vulgare*", *Res. J. Pharmaceutical Sci.* **2012**, *1(1),* 23-27.

Cragg, G. M.; Newman, D. J. "Biodiversity: A continuing source of novel drug leads". *Pure Appl. Chem.* **2005**, *77*, 7-24.

Cragg, G. M.; Newman, D. J. "Natural products: A continuing source of novel drug leads", *Biochim. Biophys. Acta*. **2013**, *1830(6)*, 3670-3695.

Cragg, G. M. Newman, D. J. "Plants as a source of anti-cancer agents", *J. Ethnopharmacol.* **2005**, *100*, 72-79.

Da, C. H.; Xiao-Jie, G.; Pei, G. X. "Phytochemical and biological research of Papaver pharmaceutical resources", *Medicinal plants: chemistry, biology and omics*, **2015**, *6*, 217-251.

Da, H. S.; Jun, H. W.; Hui, M. G.; Ren, X. T. "Protective effect of hopeahainol A, a novel acetylcholinesterase inhibitor, on hydrogen peroxide-induced injury in PC12 cells", *Environ. Toxicol. Pharmacol.* **2009**, *28*, 30-36.

Dai, J. -R.; Hallock, Y. F.; Cardellina, J. H. II.; Boyd, M. R. "HIV-inhibitory and cytotoxic oligostilbenes from the leaves of *Hopea malibato*", *J. Nat. Prod.* **1998**, *61*, 351-353.

Daniel, A. D.; Sylvia, U.; Ute, R. "A historical overview of natural products in drug discovery", *Metabolites*, **2012**, *2*, 303-336.

Dar, A.; Faizi, S.; Naqvi, S.; Roome, T.; Zikir-ur-Rehman, S.; Ali, M. F.; Moin, S. S. T. "Analgesic and antioxidant activity of mangiferin and its derivatives: the structure activity relationship", *Biol. Pharm. Bull.* **2005**, *28*, 596-600.

DeFronzo, R. A.; Ferrannini, E.; Groop, L.; Henry, R. R.; Herman, W. H.; Holst, J. J.; Hu, F. B.; Kahn, C. R.; Raz, I.; Shulman, G. I.; Simonson, D. C.; Testa, M. A.; Weiss, R. "Type 2 diabetes mellitus", *Nature Reviews Disease Primers*, **2015**, *1*, 1-22.

Delgado, A. V.; McManus, A. T.; Chambers, J. P. "Production of tumor necrosis factor-α, interleukin1-β, interleukin 2, and interleukin 6 by rat leukocyte subpopulations after exposure to substance P". *Neuropeptides*, **2003**, *37*, 355-361.

Desrivot, J.; Waikedre, J.; Cabalion, P.; Herrenknecht, C.; Bories, C.; Hocquemiller, R.; Fournet, A. "Antiparasitic activity of some new caledonian medicinal plants". *J. Ethnopharmacol.* **2007**, *112*, 7-12.

DeSouza, A. M.; Carvalho, T. L. G.; Sabino, P. M.; Vives, D.; Fontes, C. F. L.; Lopes, A. G.; Caruso-Neves, C. "Characterization and partial isolation of ouabain-insensitive Na^+-ATPase in MDCK I cells", *Biochimie*, **2007**, *89*, 1425-1432.

Dinesh K.; Bhat, Z. A.; Singh, P.; V. Khatanglakar, V.; Bhujbal, S. S. "Antiasthmatic and antiallergic potential of methanolic extract of leaves of *Ailanthus excelsa*", *Revista Brasileira de Farmacognosia Brazilian Journal of Pharmacognosy*, **2011**, *21(1)*, 139-145.

Douglas, L. "Rauwolfia in the treatment of hypertension", *Integr. Med. (Encinitas).* **2015** *14(3)*, 40-46.

Ehrenkranz, J. R.; Lewis, N. G.; Kahn, C. R.; Roth, J. "Phlorizin: a review", *Diabetes Metab. Res.* **2005**, *21*, 31-38.

Emeline, H.; Stéphane, B.; Geneviève, B.; Eric, D.; Valérie, J.; Alexis, V.; Séverine, C.; Didier, S. "Quassinoid constituents of *Quassia amara* L. leaf herbal tea. Impact on its antimalarial activity and cytotoxicity", *J. Ethnopharmacol.*, **2009**, *126*, 114-118.

Eun-Kyoung, S.; Heebyung, C.; Howard, L. C.; Thawatchai, S.; Vichai, R.; Christopher, W. W. B.; Norman, R. F.; Geoffrey, A. C.; John, M. P.; Douglas, A. K. "Resveratrol tetramers from *Vatica diospyroides", J. Org. Chem.* **1999**, *64*, 6976-6983.

Fajriah, S.; Darmawan, A.; Megawati.; Hudiyono, S.; Kosela, S.; Hanafi, M. "New cytotoxic compounds from *Myristica fatua* Houtt. leaves against MCF-7 cell lines". *Phytochem. Lett.* **2017**, *20*, 36-39.

Finkel, T.; Holbrook, N. J. "Oxidants, oxidative stress and the biology of ageing", *Nature*, **2000**, *408*, 239-247.

Friesner, R. A.; Murphy, R. B.; Repasky, M. P.; Frye, L. L.; Greenwood, J. R.; Halgren, T. A.; Sanschagrin, P. C.; Mainz, D. T. "Extra precision glide: Docking and scoring incorporating a model of hydrophobic enclosure for protein-ligand complexes. *J. Med. Chem*. **2006**, *49*, 6177–6196.

Fürst, R.; Zündorf, I. "Plant-derived anti-Inflammatory compounds: Hopes and disappointments regarding the translation of preclinical knowledge into clinical progress", *Mediators Inflamm.* **2014**, *2014*, 1-9.

Ganellin, C. R. "Chapter 15 - Discovery of the cholesterol absorption inhibitor, ezetimibe", *Introduction to Biological and Small Molecule Drug Research and Development*, **2013**, 399-416.

Giang, P. H.; Son, P. T.; Matsunami, K.; Otsuka, H. "New neolignans and lignans from Vietnamese medicinal plant *Machilus odoratissima* Nees". *Chem. Pharm. Bull.* **2006**, *54*, 380-383.

Global report on diabetes, World Health Organisation. April **2016**. http://apps.who.int/iris/bitstream/10665/204871/1/9789241565257_eng.pdf

Graddlini, G.; Camovit, C. G.; Barbetti, P.; Fardella, G. "A new neoquassin derivative

from *Quassia amarda*", *Phytochem.* **1987**, *26(II),* 3085-3087.

Guha, M.; Mackman, N. "LPS induction of gene expression in human monocytes". *Cell Signal,* **2001**, *13*, 85-94.

Gulam M. H.; Paras, N. S.; Rakesh, K. S; Vikas, K. "Antidiabetic activity of standardized extract of *Quassia amara* in Nicotinamide–Streptozotocin-induced diabetic rats", *Phytother. Res.* **2011**, *25*, 1806-1812.

Gunawardana, Y. A. G. P.; Sultanbawa, M. U. S.; Balasubramamiam, S. "Distribution of some triterpenes and phenolic compounds in the extractives of endemic dipterocarpaceae species of Sri Lanka", *Phytochemistry,* **1980**, *19*, 1099-1102.

Guo, Z.; Vangapandu, S.; Sindelar, R.W.; Walker, L.A.; Sindelar, R.D. "Biologically active quassinoids and their chemistry: Potential leads for drug design", *Curr. Med. Chem*. **2005**, *12*, 173-190.

Gutzeit, H. O.; Ludwig-M€uller, J. Plant Natural Products: Synthesis, Biological Functions and Practical Applications, First Edition. **2014**, Wiley-VCH Verlag GmbH & Co. KGaA.

Halgren, T. A.; Murphy, R. B.; Friesner R. A.; Beard, H. S.; Frye L. L.; Pollard, W. T.; Banks, J. L. "Glide: A new approach for rapid, accurate docking and scoring. 2. enrichment factors in database screening. *J. Med. Chem.* **2004**, *47*, 1750–1759.

Halliwell, "Reactive oxygen species and the central nervous system", *J. Neurochem.* **1992**, *59*, 1609-1623.

Han, J. - H.; Zhou, W.; Li, W.; Tuan, P. Q.; Khoi, N. M.; Thuong, P. T.; Na, M.; Myung, C.- S. "Pentacyclic triterpenoids from *Astilbe rivularis* that enhance glucose uptake *via* the activation of Akt and Erk1/2 in C2C12 myotubes", *J. Nat. Prod.* **2005**, *78(5)*, 1005-1014.

Hattori, M.; Hada, S.; Kawata, Y.; Tezuka, Y.; Kikuchi, T.; Namba, T. "New 2, 5-bisaryl-3, 4-dimethyltetrahydrofuran lignans from the aril of *Myristica fragrans*". *Chem. Pharm. Bull*. **1987**, *35*, 3315-3322.

Hattori, M.; Yang, X-W, Y.; Shu, Y-Z.; Kakiuchi, N.; Tezuka, Y.; Kikuchi, T.; Namba, T. "New constituents of the aril of *Myristica fragrans*". *Chem. Pharm. Bull*. **1988**, *36*, 648-653.

Hengartner, M. O. "The biochemistry of apoptosis", *Nature,* **2000**, *407*, 770-776.

Herath, H. M.T.B.; Priyadarshani, A. M.A.; Jamie, J.; "Dactyloidin, a new diaryl nonanoid from *Myristica dactyloides*", *Nat. Prod. Lett.* **1998**, *12(2),* 91-95.

Hoang, T. L.; Do, T. H.; Chau, T. A. M.; Tae, H. K.; Phan, V. K.; Nguyen, D. T.; Minkyun, N. "Constituents from the stem barks of *Canarium bengalense* with cytoprotective activity against hydrogen peroxide-induced hepatotoxicity", *Arch. Pharm. Res.* **2012**, *35 (1)*, 87-92.

Hollander, P. "Anti-diabetes and anti-obesity medications: Effects on weight in people with diabetes", *Diabetes Spectr.* **2007**, *20*, 159-165.

Hong-Jie, Z.; Ghee Teng, T.; Vu, D. H.; Nguyen, V. H.; Nguyen, M. C.; Doel, D. S.; John, M. P.; Harry, H. S. F. "Natural anti-HIV agents. part IV. anti-HIV constituents from *Vatica cinerea", J. Nat. Prod.* **2003**, *66*, 263-268.

Hota, R. K.; Bapuji, M. "Triterpenoids from the resin of *Shorea robusta*", *Phytochemistry*, **1993**, *32*, 466-468.

Hui, M. G.; Bo H.; Shu, H. T.; Da, H. S.; Yong, C. S.; Ren, X. T. "Bioactive oligostilbenoids from the stem bark of *Hopea exalata*", *J. Nat. Prod.* **2006**, *69*, 1800-1802.

Hui, M. G.; Chen, X.; Xiao, T. W.; Bo H.; Ren, X. T. "Hopeanol: A potent cytotoxin with a novel skeleton from *Hopea exalata*", *Eur. J. Org. Chem.* **2006**, 5551-5554.

Hui, M. G.; Chun, H. Z.; Da, H. S.; Li, D. Z.; Dai, Q. X.; Jie, Y.; Seik, W. N.; Ren, X. T. "Hopeahainol A: An acetylcholinesterase inhibitor from *Hopea hainanensis*", *Chem. Eur. J.* **2008**, *14*, 376-381.

Hui, M. G.; Wen, -H. Y.; Jie, Z.; Ren, X. T. "Antioxidant oligostilbenoids from the stem wood of *Hopea hainanensis*", *J. Agric. Food Chem.* **2009**, *57*, 5756-5761.

Hye, M. K.; Jin, S. L.; Jurdas, S.; Jaeyoung, K.; Miran, J.; Dongho, L.; Jung-Hye, C.; Dae, S. J. "A new canthinone-type alkaloid isolated from *Ailanthus altissima* Swingle", *Molecules*, **2016**, *21*, 1-10.

Jung, M.; Park, M.; Lee, H. C.; Kang, Y. H.; Kang, E. S.; Kim, S. K. "Antidiabetic agents from medicinal plants", *Curr. Med. Chem.* **2006**, *13*, 1203-1218.

Hollander, P. "Anti-diabetes and anti-obesity medications: Effects on weight in people with diabetes". *Diabetes Spectr.* **2007**, *20*, 159-165.

Honjo, M.; Nakamura, K.; Yamashiro, K.; Kiryu, J.; Tanihara, H.; McEvoy, L. M.; Honda, Y.; Butcher, E. C.; Masaki, T.; Sawamura, T. "Lectin-like oxidized LDL receptor-1 is a cell-adhesion molecule involved in endotoxin-induced inflammation". *Proc. Natl. Acad. Sci. USA.* **2003**, *100(3)*, 1274-1279.

Iasmine, A. B. S. A.; Henrique M. M.; Luiz, A. L. S.; Karina, P. R. "Simaroubaceae

family: botany, chemical composition and biological activities", *Rev. Bras. Farmacogn.* **2014**, *24*, 481-501.

Ida, D. R.; Tonel, B.; Partomuan, S.; Basuki, W. "Isolation and structure elucidation of bioactive compounds chemical as inhibitors of the enzyme *α*-glucosidase raru bark ethanol extract (*Vatica pauciflora* Blume)", *International Journal of Chemistry*, **2014**, *6(2)*, 15-21.

International Diabetes Federation, **2017**. http://www.diabetesatlas.org

Isao, K.; Taifo, M.; Ko-ichi, Y.; Shinsaku, N.; Tadanori, M.; Motomasa, K.; Hirotaka, S. "Indonesian medicinal plants XVII. Characterization of Quassinoids from the stems of *Quassia indica*", *Chem. Pharm. Bull.* **1996**, *44(11)*, 2009-2014.

Ito, T.; Hara, Y.; Kubota, Y.; Sawa, R.; Iinuma, M. "Absolute structure of resveratrol hexamers in Dipterocarpaceaeous plants", *Tetrahedron*, **2016**, *72*, 891-899.

Ito, T.; Iinuma, M. "Isolation and structure elucidation of a novel resveratrol tetramer, vaticanol K, with a fused 2, 7-dihydrooxepine–quinone methide from *Vatica chinensis*", *Tet. Lett.* **2015**, *56*, 5020-5023.

Ito, T.; Iinuma, M. "Occurrence of non-heterocyclic resveratrol tetramer in *Vatica chinensis*", *Phytochem. Lett.* **2016**, *15*, 37-41.

Ito, T.; Toshiyuki, T.; Munekazu, I.; Ibrahim, I.; Ken-ichi, N.; Zulfiqar, A.; Yoshikazu, T.; Ryuichi, S.; Yoshiaki, S.; Jin, M.; Dedy, D. "New resveratrol oligomers in the stem bark of *Vatica pauciflora*", *Tetrahedron*, **2003**, *59*, 5347–5363.

Ito, T.; Toshiyuki, T.; Munekazu, I.; Ken-ichi, N.; Yoshikazu, T.; Ryuichi, S.; Jin, M.; Dedy, D. "Three new resveratrol oligomers from the stem bark of *Vatica pauciflora"*, *J. Nat. Prod.* **2004**, *67*, 932-937.

Ito, T.; Yasumasa, H.; Masayoshi, O.; Toshiyuki, T.; Jin, M.; Dedy, D.; Munekazu, I. "Occurrence of bergenin phenylpropanoates in *Vatica bantamensis", Phytochem. Lett.* **2012**, *5*, 743-746.

Ito, T.; Toshiyuki, T.; Yoshimi, I.; Ken-ichi, N.; Munekazu, I.; Yoshikazu, T.; Hiroshi, N.; Soedarsono, R. "Five oligostilbenes with one or two dihydrofurans from the stem bark of *Vatica rassak*", *Heterocycles*, **2000**, *55(3)*, 557-567.

Ito, T.; Yukihiro, A.; Hong, Y.; Kenji, O.; Kenji, M.; Toshiyuki, T.; Munekazu, I.; Yoshinori, N. "Antitumor effect of resveratrol oligomers against human cancer cell lines and the molecular mechanism of apoptosis induced by vaticanol C", *Carcinogenesis*, **2003**, *24(9)*, 1489-1497.

Jacek, Z.; Joy, J.; Adam, S.; Micael, H.; Olivier, O.; Jeannette, V. -V.; Gang, C.; Marcos, L.; Balaraman, "Mitochondria-targeted triphenylphosphonium-based compounds: syntheses, mechanisms of action, and therapeutic and diagnostic applications", *Chem. Rev.* **2017**, *117*, 10043-10120.

Jalifah, L.; Wan, Z. W. M. Z.; Norizan, A.; Bohari, M. Y.; Nik, I. N. Y.; Yana, M. S.; Sjamsul, A. A. "Cytotoxic oligostilbenoids from *Vatica odorata*", *Aust. J. Basic Appl. Sci*. **2011**, *5(6)*, 113-118.

Jang, M.; Cai, L.; Udeani, G. O.; Slowing, K. V.; Thomas, C. F.; Beecher, C. W. W.; Fong, H. H. S.; Farnsworth, N. R.; Kinghorn, A. D.; Mehta, R. G.; Moon, R. C.; Pezzuto, J. M. "Cancer chemopreventive activity of resveratrol, a natural product derived from grapes", *Science*, **1997**, *275*, 218-220.

Jedsadayanmata, A. "*In vitro* antiglycation activity of arbutin". *J. Naresun University*, **2005**, *13*, 35-41.

Jian-Cheng, N.; Jian-Ting, S.; Qing-Wei, T.; Qi-Jian, C. "Phenylpropionamides, piperidine, and phenolic derivatives from the fruit of *Ailanthus altissima*, *Molecules*, **2017**, *22*, 1-12.

Jie, P.; Jia, L. J.; Hui, M. G.; Kai, L. Y.; Xiang, C.; Li, J. H.; Yan, C.; Lai, Q.; Xiao, X. L.; Yun, X. "Malibatol A regulates microglia M1/M2 polarization in experimental stroke in a PPARγ-dependent manner", *J. Neuroinflammation*, **2015**, *12(51*), 1-11.

Jin, R. D.; Yali, F. H.; John, H. C.; Michael, R. B. "HIV-inhibitory and cytotoxic oligostilbenes from the leaves of *Hopea malibato*", *J. Nat. Prod*. **1998**, *61*, 351-353.

John, K. V. "Sterols and other triterpenoids: source specificity and evolution of biosynthetic pathways", *Org. Geochem*., **2005**, *36*, 139-159.

John, W. D.; Garraffo, H. M.; Spande, T. F. Decker, M. W. Sullivan, J. P. Michael, W. "Alkaloids from frog skin: the discovery of epibatidine and the potential for developing novel non-opioid analgesics", *Nat. Prod. Rep*. **2000**, *17*, 131-135.

Jones, B.; Kazlauskas, R. J. "Natural product biosynthesis: The road to L.", *Nat. Chem.* **2015**, *7(1)*, 11-12.

Jun, Y. L.; Yong, H. Y.; Lei, W.; Da, H. S.; Ren, X. T. "New resveratrol oligomers from the stem bark of *Hopea hainanensis*", *Helv. Chim. Acta*, **2005**, *88*, 2910-2917.

Kakkar, P.; Das, B.; Viswanathan, P. N. "A modified spectrophotometric assay of superoxide dismutase". *Indian J. Biochem. Biophys.* **1984**, *21*, 130-132.

Kapoor, S. K.; Ahmad, P. I.; Zaman, A. "Chemical constituents of *Ailanthus excelsa*", *Phytochemistry*, **1971**, *10*, 3333.

Kaori, T.; Shinya, T.; Tomoya, H.; Shigeru, M.; Hiroyuki, K.; Akio, K.; Ayumi, O. "Amarastelline A: A fluorescent alkaloid from *Quassia amara* and its properties in living cells", *ChemPlusChem*, **2012**, *77*, 427-431.

Kazuo, K.; Taichi, O. Indaquassin A and B: Quassinoids from *Quassia indica*, *Phytochemistry*, **1993**, *34(2)*, 505-509.

Kazuo, K.; Taichi, O. Quassinoids from *Quassia indica*, *Phytochemistry*, **1994**, *35(2)*, 459- 463.

Kengo, K.; Narihiko, F.; Tomomi, H.; Masayoshi, O.; Kiyoshi, T.; Kuo-Hsiung, L. "Two new quassinoids, Ailantinols C and D from *Ailanthus altissima", Bull. Chem. Soc. Jnp.,* **1996**, *69*, 3613-3617.

Keylor, M. H.; Bryan, S. M.; Corey, R. J. S. "Chemistry and biology of resveratrol-derived natural products", *Chem Rev.* **2015**, *115(17)*, 8976–9027.

Keylor, M. H.; Matsuura, B. S.; Griesser, M.; Chauvin, J. R.; Harding, R. A.; Kirilova, M. S.; Zhu, X.; Fischer, O. J.; Pratt, D. A.; Stephenson, C. R. "Synthesis of resveratrol tetramers *via* a stereoconvergent radical equilibrium", *Science*, **2016**, *354*, 1260-1265.

Kengo, K.; Narihiko, F.; Tomomi, H.; Masayoshi, O.; Kiyoshi, T.; Kuo-Hsiung, L. "Two new quassinoids, Ailantinols A and B, and related compounds from *Ailanthus altissima*", *J. Nat. Prod.* **1996**, *59*, 683-686.

Kuete, V. "*Myristica fragrans*: A Review." Medicinal Spices and Vegetables from Africa, **2017**, *23*, 497–512.

Kupchan, S. M.; Streelman, D. R. "Quassimarin, a new antileukemic quassinoid from *Quassia amara*", *J. Org. Chem*., **1976**, *41(21)*, 3481-3482.

Kurihara, H.; Kawabata, J.; Ichikawa, S.; Mizutani, J. "(-)-ε-Viniferin and related oligostilbenes from *Carex* pum", *Agric. Biol. Chem.* **1990**, *54*, 1097-1099. *13*, 35-41.

Li, C.; Xu, X.; Tao, Z.; Wang, X. J.; Pan, Y. "Resveratrol dimers, nutritional components in grape wine, are selective ROS scavengers and weak Nrf2 activators", *Food Chem.* **2015**, *173*, 218-223.

Lim, K. G.; Gray, A. I.; Pyne, S.; Pyne, N. J. "Resveratrol dimers are novel sphingosine kinase 1 inhibitors and affect sphingosine kinase 1 expression and cancer cell

growth and survival", *J. Pharmacol.* **2012**, *166*, 1605-1616.

Lizcano, J. M.; Alessi, D. R. "The insulin signaling pathway", *Curr. Biol.* 2002, *12(7)*, 236-238.

Lopez, M. V.; Cuadrado, M. P.; Ruiz-Poveda, O. M.; Del Fresno, A. M.; Accame, M. E. "Neuroprotective effect of individual ginsenosides on astrocytes primary culture", *Biochim. Biophys. Acta.* **2007**, *1770*, 1308-1316.

Loretta, F. "Zontivity (Vorapaxar), first-in-class PAR-1 antagonist, receives FDA approval for risk reduction of heart attack, stroke, and cardiovascular death", *Am. Health Drug Benefits*, **2015**, *8*, 148-151.

Luyenhi, L.; Maurice, V. "Indole alkaloids and quassin from *Quassia africana*", *J. Nat. Prod*. **1985**, *49(5)*, 940.

Maity, B.; Banerjee, D.; Bandopadhyay, S. K.; Chattopadhyay, S. "*Myristica malabarica* heals stomach ulceration by increasing prostaglandin synthesis and angiogenesis", *Planta Med.* **2008**, *74*, 1774-1778.

Maity, B.; Sudhir, K. Y.; Birija, S. P.; Mrityunjay, T.; Sandip, K. B.; Subrata, C. "Molecular mechanism of the anti-inflammatory activity of a natural diarylnonanoid, malabaricone C", *Free Radic. Biol. Med.* **2012**, *52*, 1680-1691.

Manish, S. L.; Santosh, K.; Shri, H. M.; Sandhya, L. S. "A novel triterpenoid isolated from the root bark of *Ailanthus excelsa* Roxb (Tree of Heaven), AECHL-1 as a potential anti-cancer agent", *PLoS ONE*, **2009**, *4(4)*, 1-11.

Marklund, S.; Marklund, G. "Involvement of the superoxide anion radical in the autoxidation of pyrogallol and a convenient assay for superoxide dismutase", *Eur. J. Biochem.* **1974**, *47*, 469-474.

Mary, M. S.; Robert, P. B.; Masaru, O.; Geoffrey, A. C.; Norman, R. F. "3S, 24S, 25-Trihydroxytirucall-7-ene from *Ailanthus excelsa*", *Phytochemistry*, **1980**, *19*, 1499-1501.

Megawati; Darmawan, A. "Resorcinol compounds isolated from the bark of *Myrisitica fatua* Houtt". *Indonesian J. Pharm*. **2017**, *28*, 82-90.

Mikulski, D.; Molski, M. "Quantitative structure–antioxidant activity relationship of *trans*-resveratrol oligomers, *trans*-4, 4′-dihydroxystilbene dimer, *trans*-resveratrol- 3-*O*-glucuronide, glucosides: *trans*-piceid, *cis*-piceid, *trans*-astringin and *trans*-resveratrol-4′-*O*-*β*-D-glucopyranoside", *Eur. J. Med. Chem.* **2010**, *45*, 2366-2380.

Miran, J.; Hye, M. K.; Ji-Hye, A.; Kyung-Tae, L.; Dae, S. J.; Jung-Hye, C. "9-Hydroxycanthin-6-one isolated from stem bark of *Ailanthus altissima* induces ovarian cancer cell apoptosis and inhibits the activation of tumor-associated macrophages", *Chem.-Biol. Interact.* **2018**, *280*, 99-108.

Moncada, S.; Palmer, R.M.; Higgs, E.A. "Nitric oxide: physiology, pathophysiology, and pharmacology", *Pharmacol. Rev.* **1991**, *43*, 109-142.

Mosmann, T. Rapid colorimetric assay for cellular growth and survival: application to proliferation and cytotoxicity assays". *J. Immunol. Methods.* **1983**, *65*, 55-63.

Mtunzi, F.; Ledwaba, I.; Klink, M.; Dikio, E.; Ejidike, P.; Pakade, V. "Antibacterial activity of a triterpene isolated from *Combretum Erythrophyllum* ethyl acetate fraction", *Organic & Medicinal Chem*. **2017,** *4(3)*, 1-6.

Nakagawa, T.; Yokozawa, T. "Direct scavenging of nitric oxide by green tea". *Food Chem. Toxicol.* **2002**, *40*, 1745-1750.

Naohito, A.; Tetsuro, I.; Masayoshi, O.; Ryuichi, S.; Yoshikazu, T.; Veliah, C.; Munekazu, I. "Occurrence of *C*-glucoside of resveratrol oligomers in *Hopea parviflora*", *Chem. Pharm. Bull.* **2011**, *59(2)*, 239-248.

Naziroglu, M. "New molecular mechanisms on the activation of TRPM2 channels by oxidative stress and ADP-ribose", *Neurochem. Res.* **2007**, *32*, 1990-2001.

Newman, D. J.; Cragg, G. M. "Natural products as sources of new drugs over the 30 years from 1981 to 2010". *J. Nat. Prod*. **2016**, *79*, 629-661.

Nicholas, C.; Batra, S.; Vargo, M.A.; Voss, O.H.; Gavrilin, M.A.; Wewers, M.D.; Guttridge, D. C.; Grotewold, E.; Doseff, A.I. "Apigenin blocks lipopolysaccharide-induced lethality *in vivo* and proinflammatory cytokines expression by inactivating NF-kappa B through the suppression of p65 phosphorylation", *J. Immunol.* **2007**, *179*, 7121-7127.

Nissen, S. E.; Wolski, K. "Effect of rosiglitazone on the risk of myocardial infarction and death from cardiovascular causes". *N. Eng. J. Med.* **2007**, *356*, 2457-2471.

Nonomura, S.; Kanagawa, H.; Makimoto, A. "Chemical constituents of polygonaceous plants studies on the components of ko-j o-kon. (*Polygonum cuspidatum* sieb. et zucc.) ", *Yakugaku Zassh*i, **1963**, *83*, 988-990.

Oshima, Y. "Ampelopsins from ampelopsis F and G, novel bridged plant oligostilbenes *brevipedunculata* var. hancei Roots (Vitaceae)", **1993**, *Tetrahedron, 49(26),* 5801-5804.

Oshima, Y.; Ueno, Y.; Hisamichi, K.; Takeshita, M. "Ampelopsins-F and ampelopsins-G, novel bridged plant oligostilbenes from *Ampelopsis-brevipedunculata* var hancei roots (Vitaceae)", *Tetrahedron,* **1993**, *49*, 5801-5804.

Ota, H.; Masahiro, A.; Tani, H.; Tatefuji, T.; Ogawa, S.; Iijima, K.; Eto, M.; Shirasawa, T.; Ouchi, Y. "*Trans*-resveratrol in *Gnetum gnemon* protects against oxidative-stress-induced endothelial senescence", *J. Nat. Prod.* **2013,** *76*, 1242-1247.

Pacher, P.; Beckman, J. S.; Liaudet, L. "Nitric oxide and peroxynitrite in health and disease", *Physiol. Rev.* **2007**, *87*, 315–424.

Pandey, R.; Mahar, R.; Hasanain, M.; Shukla, S. K.; Sarkar, J.; Rameshkumar, K. B.; Kumar, B. "Rapid screening and quantitative determination of bioactive compounds from fruit extracts of *Myristica* species and their *in vitro* antiproliferative activity", *Food Chem.* **2016**, *211*, 483-493.

Patel, O. P. S.; Mishra, A.; Maurya, R.; Saini, D.; Pandey, J.; Taneja, I.; Raju, K. S. R.; Kanojiya, S.; Shukla, S. K.; Srivastava, M. N.; Wahajuddin, M.; Tamrakar, A. K.; Srivastava, A. K.; Yadav, P. P. "Naturally occurring carbazole alkaloids from *Murraya koenigii* as potential antidiabetic agents". *J. Nat. Prod.* **2016**, *79*, 1276-1284.

Patro, B. S.; Bauri, A. K.; Shilpa, M.; Subrata, C. "Antioxidant activity of *Myristica malabarica* extracts and their constituents", *J. Agric. Food Chem.* **2005**, *53*, 6912-6918.

Patro, B. S.; Tyagi, M.; Saha, J.; Chattopadhyay, S. "Comparative nuclease and anticancer properties of the naturally occurring malabaricones". *Bioorg. Med. Chem*. **2010**, *18*, 7043-7051.

Philip, H. C.; Naidoo, D.; Mulholland, D. A.; Randrianarivelojosia, M. "Quassinoids from the leaves of the Madagascan Simaroubaceae *Samadera madagascariensis*, *Phytochemistry*, **2005**, *66*, 2734-2739.

Prabhakar, P. K.; Doble, M. "Interaction of cinnamic acid derivatives with commercial hypoglycemic drugs on 2-deoxyglucose uptake in 3T3-L1 adipocytes". *J. Agric. Food Chem.* **2011**, *59*, 9835-9844.

Pullela, V. S.; Ranga, R. R.; J. Madhusudana, R. J. "Two new tetracyclic triterpenes from the heartwood of *Ailanthus excels* Roxb.", *Chem. Biodivers*. **2006**, *3*, 930-934.

Purushothaman, K. K.; Sarada, A.; Connolly, J. D. "Malabaricones A-D, novel diarylnonanoids from *Myristica malabarica* Lam. (Myristicaceae) ". *J. Chem. Soc., Perkin Trans. 1*, **1977**, *0*, 587-588.

Qing-Wei, T.; Ming-An, O.; Zu-Jian, W. "A new seco-neolignan glycoside from the root bark of *Ailanthus altissima*", *Nat. Prod. Res.* **2012**, *26(15)*, 1375-1380.

Reniero, F.; Rudolph, M.; Angioniz, A.; Bernreuther, A.; Cabrasz, P.; Mattivi, F. "Identification of two stilbenoids from *Vitis* roots", *Vitis*, **1996**, *35 (3)*, 125-127.

Renana, S.; Safra, R.; Bareket, D.; Olga, V.; Vered, A.; Michal, R.; Kamesh, R. A.; Alex, P.; Jordan, H. C.; Arie, G.; Shai, R. "Multifunctional cyclic d,l-*α*-peptide architectures stimulate non-insulin dependent glucose uptake in skeletal muscle cells and protect them against oxidative stress", *J. Med. Chem.* **2013**, *56*, 6709-6718.

Ren, L. M.; Qin, X. H.; Cao, X. F.; Wang, L. L.; Bai, F.; Bai, G.; Shen, Y. "Structural insight into substrate specificity of human intestinal maltase-glucoamylase", *Protein Cell*, **2011**, *2*, 827-836.

Riris, I. D. "Identification of chemistry bioactivity structure of *α*-glucosidase inhibitor from ethanol extract of the stem bark raru, (*Vatica Pauciflora* Blume) ", *IOSR J. Appl. Chem.* **2014**, *7*, 35-40.

Riya, M. P.; Antu, K. A.; Pal, S.; Chandrakanth, K. C.; Anilkumar, K. S.; Tamrakar, A. K.; Srivastava, A. K.; Raghu. K. G. "Antidiabetic property of *Aerva lanata* (L.) Juss. ex Schult.is mediated by inhibition of alpha-glucosidase, protein glycation and stimulation of adipogenesis", *J. Diabet.* **2015**, *7*, 548-561.

Ross, S. A.; Gulve, E. A.; Wang, M. "Chemistry and biochemistry of type 2 diabetes". *Chem. Rev.* **2004**, *104*, 1255-1282.

Ruxing, W.; Qian, X.; Lei, L.; Xiujun, L.; Luyang, C.; Manli, Z.; Qingwen, S. "Antitumour activity of 2-dihydroailanthone from the bark of *Ailanthus altissima* against U251", *Pharm. Biol.* **2016**, *54(9)*, 1641-1648.

Ru-Xing, W.; Xiao-Xia, M.; Jian, Z.; Man-li, Z.; Yi-Bing, W.; Chang-Hong, H.; Qing-Wen, S.; Francoise, S.; Yu-Cheng, G. "Antitumor activities of six quassinoids from *Ailanthus altissima", Chem. Nat. Compd.* **2017**, *53(1)*, 28-32.

Sadaaki, T.; Narihiko, F.; Masayoshi, O.; Junko, K.; Kazuo, K.; Harukuni, T.; Wataru, A.; Junko, T.; Masashi, K.; Hoyoku, N. "Three New Quassinoids, Ailantinol E, F, and G, from *Ailanthus altissima*", *Chem. Pharm. Bull*. **2003**, *51(4)*, 385-389.

Sadaaki, T.; Narihiko, F.; Masayoshi, O.; Junko, K.; Kazuo, K. "A new quassinoid, ailantinol H, from *Ailanthus altissima*", *Nat. Prod. Res.*, **2006**, *20(13),* 1211-1215.

Sajin, K. F.; Beena, J.; Sunil V.; Mangalam, S. N. "Phytochemical investigation on *Myristica fragrans* stem bark", *Nat. Prod. Res.* **2018**.

Sajin, K. F.; Suresh, E.; Mangalam S. N. "Chemical constituents from *Myristica fragrans* fruit". *Nat. Prod. Res.* **2014,** *28* (20), 1664–1668.

Sandra, A.; Kanyanga, C.; Dirk, V. B.; Els, V.M.; Albert, O. L.; Andre, F.; Arnold, V.; Luc, P. "Antiviral activity of simalikalactone D, a quassinoid from *Quassia africana*". *Planta Med*. **2002**, *68*, 20-24.

Sanit, T.; Jutatip, B.; Hunsa, P.; Chulabhorn, M.; Somsak, R. "Ailanthusins A-G and nor-lupane triterpenoids from *Ailanthus triphysa*", *Phytochemistry*, **2017,** *134,* 98-105.

Sarfaraj, H. M.; Sheeba, F.; Saba, A.; Mohd, S. K. "Marine natural products: A lead for anti-cancer", *Indian J. Mar, Sci*. **2012**, *41(1)*, 27-39.

Sasikumar, P.; Prabha, B.; Reshmitha, T. R.; Sheeba, V.; Pradeep, A. K.; Rohit, K. R.; Dhanya, B. P.; Sivan, V. V.; Jithin, M. M.; Anil, K. N.; Shibi, I. G.; Nisha, P.; Radhakrishnan, K. V. "Comparison of antidiabetic potential of (+) and (−)-hopeaphenol, a pair of enantiomers isolated from *Ampelocissus indica* (L.) and *Vateria indica* Linn., with respect to inhibition of digestive enzymes and induction of glucose uptake in L6 myotubes", *RSC Adv*. **2016**, *6*, 77075-77082.

Schoner, W. "Endogenous cardiac glycosides, a new class of steroid hormones", *Eur. J. Biochem.* **2002**, *269*, 2440-2448.

Sen, R.; Ajay, K. B.; Subrata, C.; Mitali, C. "Antipromastigote activity of the malabaricones of *Myristica malabarica* (Rampatri)", *Phytother. Res.* **2007**, *21*, 592-595.

Seo, E. -K.; Chai, H.; Constant, H. L.; Santisuk, T.; Reutrakul, V.; Beecher, C. W. W.; Farnsworth, N. R.; Cordell, G. A.; Pezzuto, J. M.; Kinghorn, A. D. "Resveratrol tetramers from *Vatica diospyroides*", *J. Org. Chem*. **1999**, *64*, 6976-6938.

Seon, W. H.; Jun, L.; Ji-Sun, S.; Jae, Y. L.; Kyung-Tae, L.; Dae, S. J. "Inhibitory effects of phenylpropanoids isolated from the bark of *Ailanthus altissima* on COX-2 activity", *Bull. Korean Chem. Soc*. **2012**, *33(8)*, 2759-2761.

Seyed, E. S.; Yalda, S.; Narjess-Sadat, M. "Isolation and identification of ferulic acid

from aerial parts of *Kelussia odoratissima* Mozaff.", *Jundishapur J. Nat. Pharm. Prod*. **2012**, *7(4)*, 159-162.

Shan, H.; Xiaojun, Y. "From resveratrol to its derivatives: New sources of natural antioxidant", *Curr. Med. Chem*. **2013**, *20*, 1005-1017.

Shou-Yuan, W.; Yan-Hui, F.; Qi, Z.; Meng, B.; Guang-Ying, C.; Chang-Ri, H.; Xiao-Ping, S. "Biologically active oligostilbenes from the stems of *Vatica mangachapoi* and chemotaxonomic significance", *Nat. Prod. Res.* **2018**, 1-8.

Shu-Hua, Q. I.; Da-Gang, W. U.; Yun-Bao, M. A.; Xiao-Don, L. U. O. "Chemical constituents of *Ailanthus triphysa*", *Chin. J. Chem*. **2003**, *21*, 200-203.

Sim, L.; Quezada-Calvillo, R.; Sterchi, E. E.; Nichols, B. L.; Rose, D. R. Human Intestinal maltase-glucoamylase: crystal structure of the N-terminal catalytic subunit and basis of inhibition and substrate specificity". *J. Mol. Biol.* **2008**, *375*, 782-792.

Singh, M.; Arseneault, M.; Sanderson, T.; Murthy, V.; Ramassamy, C. "Challenges for research on polyphenols from foods in Alzheimer's disease: bioavailability, metabolism, and cellular and molecular mechanisms". *J. Agric. Food Chem.* **2008**, *56*, 4855-4873.

Singleton, M. V. L.; Rossi, J. A. "Colorimetry of total phenolics with phosphomolybdic-phosphotungstic acid reagent", *Amer. J. Enol. Viticul.* **1965**, *16*, 144-158.

Sivasothya, Y.; Yong, L.-K.; Hoong, L.-K.; Litaudon, M.; Awang, K. "A potent alpha-glucosidase inhibitor from *Myristica cinnamomea* King". *Phytochemistry*, **2016**, *122*, 265-269.

Somwar, R.; Sweeney, G.; Ramlal, T.; Klip, A. "Stimulation of glucose and amino acid transport and activation of the insulin signaling pathways by insulin lisproin L6 skeletal muscle cells". *Clin Ther.* **1998**, *20*, 125-140.

Stone, J. R.; Yang, S. "Hydrogen peroxide: a signaling messenger", *Antioxid. Redox Signal*, **2006**, *8*, 243-270.

Subramaniam, S.; Uvais, M. S. S.; Sivagnanasundram, S.; "Polyphenols from Dipterocarp species: vaticaffinol and ε-viniferin", *J. Chem. Soc. Perkin Trans. I.* **1985**, 159-162.

Sudhanshu, S.; Neerja, P.; Jain, D. C.; Bhakuni, R. S. "Antimalarial agents from plant sources", *Curr. Sci*. **2003**, *85(9)*, 1314-1329.

Sui, X.; Zhang, Y.; Zhou, W. "*In vitro* and *in silico* studies of the inhibition activity of

anthocyanins against porcine pancreatic *α*-amylase". *J. Funct. Foods*, **2016**, *21*, 50-57.

Sultanbawa, M. U. S.; Surendrakumar, S.; Wazeer, M. I. M.; Bladon, P. "Novel resveratrol tetramer, vaticaffinol, from *Vatica affinis* Thw. (Dipterocarpaceae)", *J. Chem. Soc., Chem. Commun*. **1981**, *19*, 1204-1206.

Sun, H.; Wang, D.; Song, X.; Zhang, Y.; Ding, W.; Peng, X.; Zhang, X.; Li, Y.; Ma, Y.; Wang, R.; Yu, P. "Natural prenylchalconaringenins and prenylnaringenins as antidiabetic agents: *α*-Glucosidase and *α*-amylase inhibition and *in vivo* antihyperglycemic and antihyperlipidemic effects". *J. Agric. Food Chem.* **2017**, *65*, 1574-1581.

Suroor, A. K.; Shamsuddin, K.M. "Isolation and structure of 13, 18-dehydroexcelsin, a quassinoid and glaucarubol from *Ailanthus excelsa*", *Phytochemistry*, **1980**, *19*, 2484-2485.

Sweeney, G.; Somwar, R.; Ramlal, T.; Volchuk, A.; Ueyama, A.; Klip, A. "An inhibitor of p38 mitogen-activated protein kinase prevents insulin stimulated glucose transport but not glucose transporter translocation in 3T3-L1 adipocytes and L6 myotubes", *J. Biol. Chem.* **1999**, *274(15)*, 10071–10078.

Syed, M. U. A.; Lin, L.; Akhileshwar, N.; Xiu. J. W.; Xiuwen, T. "Nrf2 signaling pathway: pivotal roles in inflammation", *B.B.A. Mol. Basis Dis.* **2017**, *1863(2)*, 585-597.

Tadeusz, F. M.; Doralyn, S. D.; Sarah, L. L.; Jonel, P. S. "Drug development from marine natural products", *Nat. Rev. Drug Discov*. **2009**, *8*, 69-85.

Talukdar, A. C.; Jain, N.; De, S.; Krishnamoorthy, H. G. "An isoflavone from *Myristica malabarica*", *Phytochemistry*, **2000**, *53*, 155-157.

Tamrakar, A. K.; Jaiswal, N.; Yadav, P. P.; Maurya, R.; Srivastava, A. K. "Pongamol from *Pongamia pinnata* stimulates glucose uptake by increasing surface GLUT4 level in skeletal muscle cells", *Mol. Cell Endocrinol.* **2011**, *339*, 98-104.

Tanaka, T.; Ito, T.; Ido, Y.; Son, T.-K.; Nakaya, K.; Iinuma, M.; Ohyama, M.; Chelladurai, V. "Stilbenoids in the stem bark of *Hopea parviflora*", *Phytochemistry*, **2000**, *53*, 1015-1019.

Tanaka, T.; Ito, T.; Nakaya, K.; Iinuma, M.; Riswan, S. "Oligostilbenoids in stem bark of *Vatica rassak*" , *Phytochemistry*, **2000**, *54*, 63-69.

Taneyama, M.; Yoshida, S.; Kobayashi, M.; Hasegawa, M. "Isolation of norbergenin

from *Saxifraga stolonifera*", *Phytochemistry*, **1983**, *22*, 1053-1054.

Thanesuan, N.; Ruengrit, S.; Tirayut, V.; Khanitha, P. "Dammarane triterpenes from the apical buds of *Gardenia collinsae*", *Phytochem. Lett.* **2011**, *4*, 183-186.

Tomoko, T.; Rieko, N.; Emi, T.; Yukiko, K.; Aya, K.; Michiko, K.; Satoshi, M.; Tetsuro, I.; Munekazu, I.; Yukihiro, A.; Yoshinori, N.; Yuji, A.; Shobu, N.; Hiroyasu, I. "Vaticanol C, a resveratrol tetramer, activates PPARα and PPARβ/δ *in vitro* and *in vivo*", *Nutr. Metab.* **2010**, ***7(46)***, 1-8.

Tong, Y.; Ting, W.; Wei, W.; Nan, J.; , Yan, H. Q.; Ren, X. T.; Hui, M. G. "Polyphenolic acetylcholinesterase inhibitors from *Hopea chinensis*", *Planta Med*. **2012**, *78*, 1015-1019.

Trapero, A.; Llebaria, A. "A prospect for pyrrolidine iminosugars as antidiabetic α-glucosidase inhibitors", *J. Med. Chem.* **2012**, *55*, 10345-10346.

Trong-Tuan, D.; Tien-Lam, T.; Jayeon, K.; Phi-Hung, N.; Eun-Hee, L.; Junsoo, P.; Ik-Soon, J.; Won-Keun, O. "Terpenylated coumarins as SIRT1 activators isolated from *Ailanthus altissima*", *J. Nat. Prod.* **2012**, *75 (7)*, 1332–1338.

Tu, Y. Y.; Ni, M. Y.; Zhong, Y. R.; Li, L. N.; Cui, S. L.; Zhang, M. Q.; Wang, X. Z.; Liang, X. T. "Studies on the constituents of *Artemisia annua* L." *Yao Xue Xue Bao*, **1981**, *16(5)*, 366-370.

Uvais, M. S. S.; Guanasundram, A .S.; Mohamed, I. M. W. "Novel resveratrol tetramer, vaticaffinol, from *Vatica affinis* Thw. (Dipterocarpaceae)", *J.C.S. Chem. Comm.* **1981**, 1204-1206.

Van, C. P.; Akino, J.; Thierry, S.; Bernard, B. "Cytotoxic acylphenols from *Myristica maingayi*, *Tetrahedron*, **2000**, *56*, 1707-1713.

Van, C. P.; Akino, J. Thierry, S.; Bernard, B. "Novel cytotoxic acylphenol dimers of *Myristica gigantea*; enzymatic synthesis of giganteones A and B", *Tetrahedron*, **2002**, *58*, 5709-5714.

Victor, J. N.; John, R. S. "Drug-related hepatotoxicity". *N. Engl. J. Med.* **2006**, *354*, 731-739.

Vincent, C. O. N.; Taiwo, O. A.; Joseph, I. O.; Herbert, L. H. "2-Methoxycanthin-6-one: A new alkaloid from the stem wood of *Quassia amara*", *Planta Med*. **1993**, *59*, 259-261.

Viveka, M. R.; Chandrashekar, K. R. "Antioxidant and antibacterial activities of

Myristica fatua var magnifica (Beddome) Sinclair". *Asian J. Pharm. Clin. Res.* **2016**, *9*, 235-239.

Wan, Z. W. M. Z.; Kamaruzaman, J. "Laevifonol: A unique dimer oligostilbene from the stem bark of *Vatica odorata*", *World Applied Sciences Journal*, **2010**, 8 (9), 1056-1059.

Williams, L. K.; Li, C.; Withers, S. G.; Brayer, G. D. "Order and disorder: differential structural impacts of myricetin and ethyl caffeate on human amylase, an antidiabetic target". *J. Med. Chem.* **2012**, *55*, 10177-10186.

Witek, P.; Korga, A.; Burdan, F.; Ostrowska, M.; Nosowska, B.; Iwan, M.; Dudka, J. "The effect of a number of H9C2 rat cardiomyocytes passage on repeatability of cytotoxicity study results", *Cytotechnology*, **2016**, *68*, 2407-2415.

Xia, G. "Protective effect of *Ailanthus excelsa* Roxb. In myocardial infarction post mesenchymal stem cell transplantation: Study in chronic ischemic rat model", *Afr. J. Tradit. Complement. Altern. Med.* **2016**, *13(6)*, 155-162.

Xiao-Lin, Y.; Yong-Liang, Y.; Dong-Mei, Z.; Fei, L.; Wen-Cai, Y. "Shinjulactone O, a new quassinoid from the root bark of *Ailanthus altissima", Nat. Prod. Res.* **2014**, *28(18)*, 1432-1437.

Xie, M.; Hu, B.; Wang, Y.; Zeng, X. "Grafting of gallic acid onto chitosan enhances antioxidant activities and alters rheological properties of the copolymer", *J. Agric. Food Chem*. **2014**, *62*, 9128-9136.

Xio, Z.; Storms, R.; Tsang, A. "A quantitative starch–iodine method for measuring alpha-amylase and glucoamylase activities". *Anal. Biochem*. **2006**, *351*, 146-148.

Xiong, H.; Zhang, S.; Zhao, Z.; Zhao, P.; Chen, L.; Mei, Z. "Antidiabetic activities of entagenic acid in type 2 diabetic db/db mice and L6 myotubes via AMPK/GLUT4 pathway", *J. Ethnopharmacol.* **2018**, *211*, 366-374.

Yan, H. Q.; Jie, Z.; Jiang, T. C.; Zhi, K. G.; Nan, J.; Ren, X.T.; Hui, M. G. "Oligostilbenes from *Vatica mangachapoi* with xanthine oxidase and acetylcholinesterase inhibitory activities", *RSC Advan*. **2011**, *1*, 135–141.

Yan, W.; Wen-Jing, W.; Chang S.; Dong-Mei, Z.; Li-Peng, X.; Rong-Rong, H.; Lei, W.; Jian, Z.; Xiao-Qi, Z.; Wen-Cai, Y. "Cytotoxic quassinoids from *Ailanthus altissima", Bioorganic Med. Chem. Lett*. **2013**, *23*, 654–657.

Yang, H.; Xiao-Ping, S.; Chang-Ri, H.; Guang-Ying, C.; Shou-Yuan, W.; Wen-Hao, C.

"Resveratrol oligomers from the stem bark of *Vatica mangachapoi"*, *Chem. Nat. Compd.* **2018**, *54(5)*, 981-984.

Yamamoto, K.; Miyake, H.; Kusunoki,M.; Osaki, S. "Crystal structures of isomaltase from *Saccharomyces cerevisiae* and in complex with its competitive inhibitor maltose", *Febs J.* **2010**, *277*, 4205-4214.

Yen, G. C.; Duh, P. D. "Scavenging effect of methanolic extracts of peanut hulls on free-radical and active-oxygen species", *J. Agri. Food Chem*. **1994**, *42*, 629-632.

Yonemoto, R.; Shimada, M.; Gunawan-Puteri, M. D. P. T.; Kato, E.; Kawabata, J. "*α*-Amylase inhibitory triterpene from *Abrus precatorius* leaves". *J. Agric. Food Chem.* **2014**, *62*, 8411-8414.

Yuan, T.; Nahar, P.; Sharma, M.; Liu, K.; Slitt, A.; Aisa, H. A.; Seeram, N. P. "Indazole-type alkaloids from *Nigella sativa* seeds exhibit antihyperglycemic effects via AMPK activation *in vitro*", *J. Nat. Prod.* **2014**, *7(10)*, 2316-2320.

Zghonda, N.; Yoshida, S. Ezaki, S.; Otake, Y.; Murakami, C.; Mliik, A.; Ghorebel, A.; Miyashki, H. "*ε*-Viniferin is more effective than its monomer resveratrol in improving the functions of vascular endothelial cells and the heart", *Bioscien. Biotechnol. Biochem.* **2012**, *76*, 954-960.

Zhang, C.-S.; Li, M.; Ma, T.; Wu, Y. -Q.; Lin, S.-Y.; Lin, S.-C. "Metformin activates AMPK through the lysosomal pathway", *Cell Metab*. **2016**, *24(4)*, 521-522.

Zhang, L.-P; Wang, J.-Y.; Wang, W.; Cui, Y.-X.; Cheng, D.-L. "Two new alkaloidal glycosides from the root bark of *Ailanthus altissima*", *J. Asian Nat. Prod. Res*. **2007,** *9(3)*, 253-259.

Zhang, W. H.; Wang, H. "Nortriptyline protects mitochondria and reduces cerebral ischemia/hypoxia injury", *Stroke*, **2008**, *39*, 455-462.

Zhao, B. "Natural antioxidants protect neurons in Alzheimer's disease and Parkinson's disease", *Neurochem. Res.* **2009**, *34*, 630-638.

Zhi-Lai, H.; Juan, X.; Shi-Biao, W.; Jing-Jing, Z.; Jun-Lin, H.; Yun, Z.; Gang, X.; Jin-Feng, H. "Tetracyclic triterpenoids and terpenylated coumarins from the bark of *Ailanthus altissima* (''Tree of Heaven'')", *Phytochemistry*, **2013**, *86*, 159-167.

Zhu, D.; Zhang, N.; Zhou, X.; Zhang, M.; Liu, Z.; Liu, X. "Cichoric acid regulates the hepatic glucose homeostasis *via* AMPK pathway and activates the antioxidant response in high glucose-induced hepatocyte injury", *RSC Adv*. **2017**, *7*, 1363-1375.

List of Publications

1. Ruthenium catalyzed desymmetrization of diazabicyclic olefins to access heteroaryl substituted cyclopentenes through C–H activation of phenylazoles, P. S. Aparna, **B. Prabha**, P. Prakash, E. Jijy, R. Luxmi Varma, K. V. Radhakrishnan, *Tetrahedron Letters*, **2014**, *55*, 865–868.

2. Comparison of antidiabetic potential of (+) and (-)-Hopeaphenol, a pair of enantiomers isolated from *Ampelocissus indica* (L.) and *Vateria indica* Linn, with respect to inhibition of digestive enzymes and induction of glucose uptake in L6 myotubes**"** P. Sasikumar, **B. Prabha**, T. R Reshmitha , Sheeba Veluthoor, Pradeepkumar, K. R Rohit, B. P Dhanya, V. V Sivan, M.M. Jithin, N. Anil Kumar, I. G. Shibi, P. Nisha and K. V. Radhakrishnan**,** *RSC Adv.* **2016,** *6*, 77075-77082.

3. Lewis acid promoted Regioselective Double Hydro(hetero)arylation of 6,6'-dialkyl Substituted Pentafulvene : A Facile Approach to Bisindole Derivatives, Parameswaran Sasikumar †**,** **Bernard Prabha** †, Sarngadharan Sarath Chand, Maniyamma Aswathy, Murali Madhukrishnan, Preethalayam Preethanuj, Eringathodi Suresh, Florian Jaroschik, and Kokkuvayil Vasu Radhakrishnan, *Eur. J. Org. Chem.* **2017**, 4469-4474. †equally contributed.

4. Antidiabetic potential of phytochemicals isolated from the stem bark of *Myristica fatua* Houtt. *var*. magnifica (Bedd.) Sinclair, **B. Prabha,** S. Neethu, S. Lekshmy Krishnan, D. R. Sherin, M.Madhukrishnan, R.Ananthakrishnan, K. B. Rameshkumar, T. K. Manojkumard, P.Jayamurthy, K. V. Radhakrishnan, *Bioorg. Med. Chem.* **2018**, *26***,** 3461-3467.

5. Dihydro-*β*-agarofuran sesquiterpenoids from the seeds of *Celastrus paniculatus* Willd. and their *α*- glucosidase inhibitory activity, P. Sasikumar, P. Sharathna, **B. Prabha**, Sunil Varughese, N. Anil Kumar, V. V. Sivan, D. R. Sherin, E. Suresh, T. K. Manojkumar, K. V. Radhakrishnan, *Phytochem. Lett.* **2018**, *26*, 1-8.

6. Isolation and characterization of resveratrol oligomers from the stem bark of *Hopea ponga* (Dennst.) Mabb. and their antidiabetic effect by modulation of digestive enzymes, protein glycation and glucose uptake in L6 myocytes, P. Sasikumar, K. Lekshmy, S. Sini,

B. Prabha, N. Anil Kumar,V. V. Sivan, M. M. Jithin, P. Jayamurthy, I.G. Shibi and K. V. Radhakrishnan, *J. Ethnopharmacol*. **2018,** under revision.

7. Antidiabetic properties of apiforol, a potential lead isolated from the seeds of *Musa balbisiana*, Greeshma Gopalan, **B. Prabha**, Alfred Joe, T. R. Reshmitha, D. R. Sherin, M, Sabu, T. K. Manojkumar, K. V. Radhakrishnan, and P. Nisha, *Journal of Science of Food and Agriculture*, **2018**, Accepted.

8. Promalabaricone B from *Myristica fatua* Houtt. var. *magnifica* (Bedd.) Sinclair seeds demonstrate antidiabetic potential by inhibiting carbohydrate hydrolyzing enzymes, protein glycation and modulating glucose uptake via the activation of AMPK in L6 myotubes, **B. Prabha**, S. Sini, D. R. Sherin, S. Neethu,a, d K. B. Rameshkumar, T. K. Manojkumar, P. Jayamurthy, and K. V. Radhakrishnan (To be Submitted)

9. Isolation and characterization of oligostilbenoids from *Vatica chinensis* L. and their ameliorative effect on H_2O_2 induced oxidative stress in H9c2 cardiomyoblasts, **B. Prabha**, T. R. Reshmitha, M. Madhukrishnan, P. Sasikumar, T. Sithara, P. Nisha and K. V. Radhakrishnan (To be Submitted)

10. Dactyloidin from *Myristica fatua* Houtt. var. *magnifica* (Bedd.) Sinclair Seeds Stimulates Glucose Uptake through Translocation of Glucose Transporter-4 via the Activation of AMPK in L6 myotubes, **B. Prabha**, S. Sini, D. R. Sherin, S. Neethu, K. B. Rameshkumar, T. K. Manojkumar, P. Jayamurthy, and K. V. Radhakrishnan (To be Submitted)

11. Naturally occurring quassinoids from the seeds of *Quassia indica* (Gaertn.) Noot. as a potential inhibitors of α-glucosidase enzymes, **B. Prabha**, M. Madhukrishnan, T. R. Reshmitha, D. R. Sherin, T. K. Manojkumar, P. Nisha, and K. V. Radhakrishnan (To be submitted)

12. Anti-inflammatory effects and mechanisms of action of ellagic acid 3, 3', 4-trimethoxy 4'-O-α-L-rhamnopyranoside isolated from *Hopea parviflora* Bedd. in lipopolysaccharide-stimulated RAW 264.7 macrophages, **B. Prabha**, S. Sini, P. Jayamurthy, K. V. Radhakrishnan (To be submitted)

13. Isolation, characterization and antiinflammatory activity of phytochemicals from the stem bark of *Ailanthus excelsa* Roxb. **B. Prabha**, S. Sini, P. Jayamurthy and K. V. Radhakrishnan (Manuscript under preparation)

14. Antidiabetic potential of lignans and neolignans from the mace of *Myristica fragrans*. S. Neethu, **B. Prabha**, S. Lekshmy Krishnan, D. R. Sherin, M. Madhukrishnan, R. Ananthakrishnan, K. B. Rameshkumar, T. K. Manojkumar, P. Jayamurthy, and K. V. Radhakrishnan (Manuscript under preparation)

15. Phytochemicals from the stem bark of *Vatica chinensis* and their antidiabetic effect by modulation of carbohydrate hydrolyzing enzyme, protein glycation and glucose uptake in L6 myotubes. **B. Prabha**, S. Lekshmy Krishnan, P. Sasikumar, D. R. Sherin, T. K. Manojkumar, P. Jayamurthy, and K. V. Radhakrishnan (Manuscript under preparation)

16. Phytochemistry and antidiabetic screening of compounds from *Artocarpus camansi* and *Artocarpus lakoocha* **P. Sasikumar**, T. R Reshmitha, M. Aswathy, B. Prabha, P. Nisha and K. V. Radhakrishnan [To be submitted].

Papers Presented in International/National Conferences

1. Studies on antidiabetic properties of sesquiterpenes and flavonoids of *Zingiber zerumbet* Smith., **B. Prabha**, K. R. Ajish, K. G. Raghu and K. V. Radhakrishnan, Nationl symposium on Transcending Frontiers in Organic Chemistry (**TFOC-2014**), CSIR-NIIST, Thiruvananthapuram. (Poster)

2. Phytochemistry of *Samadera indica*: Reinvestigation and its biological evaluation, **B. Prabha** and K. V. Radhakrishnan. International Symposium on Phytochemistry (ISP-2015) and Prof. Dr. A. Hisham Endowment Award Ceremony, Kerala State Science and Technology Museum, Thiruvananthapuram. **Best Poster Award**

3. Phytochemistry of *Samadera indica*: Re-investigation and Pharmacological Evaluation of Bioactives, **B. Prabha**, P. Nisha and K. V. Radhakrishnan, 11th J-NOST Conference for Research Scholars (J-NOST 2015), School of Chemical Sciences, Bhubaneswar. (Poster)

4. Isolation and characterization of phytochemicals from the stem of *Hopea Parviflora*, **B. Prabha**, C. P. Ummu Jumaila and K. V. Radhakrishnan, International Symposium on Phytochemistry (ISP-2016) and Prof. Dr. A. Hisham Endowment Award Ceremony, Malabar Botanical Garden and Institute for Plant Sciences, Kozhikode. **Best Poster Award**

5. Naturally Occurring Quassinoids from *Samadera indica* and *Ailanthus excelsa* as a potential hyperglycemic agents, Second International Conference on chronic and degenerative diseases. **B. Prabha** and K. V. Radhakrishna (Poster)

6. Antidiabetic potential of phytochemicals from the stem barks of *Myristica fatua* Houtt. Facilitated by inhibition of digestive enzymes, protein glycation and stimulated Glucose uptake in L6 myotubes, **B. Prabha**, S. Neethu, K. Lekshmi, D. R. Sherin, K B. Rameshkumar, T. K. Manojkumar, P. Jayamurthy and K. V. Radhakrishnan, International conference on Advances in degenerative diseases and molecular interventions (ADDMI-2017) (Poster)

7. Phytochemical and pharmacological evaluation of some selected medicinal plants of Kerala-**'PROF. DR. A. HISHAM ENDOWMENT AWARD-2018'**

***